

Modern Analytical Electrochemistry: Fundamentals, Experimental Techniques, and Applications

Guest Editors: Bengi Uslu, Hassan Y. Aboul-Enein, and Sibel A. Ozkan





Modern Analytical Electrochemistry: Fundamentals, Experimental Techniques, and Applications

International Journal of Electrochemistry

Modern Analytical Electrochemistry: Fundamentals, Experimental Techniques, and Applications

Bengi Uslu, Hassan Y. Aboul-Enein, and Sibel A. Ozkan



Copyright © 2011 SAGE-Hindawi Access to Research. All rights reserved.

This is a special issue published in volume 2011 of "International Journal of Electrochemistry." All articles are open access articles distributed under the Creative Commons Attribution License, which permits unrestricted use, distribution, and reproduction in any medium, provided the original work is properly cited.

Editorial Board

Maria Carmen Arévalo, Spain
Shen-Ming Chen, Taiwan
Abel César Chialvo, Argentina
Jean-Paul Chopart, France
A. Rodrigues de Andrade, Brazil
Sergio Ferro, Italy
Gerd-Uwe Flechsig, Germany
Rubin Gulaboski, Germany
Shengshui Hu, China
Mehran Javanbakht, Iran
Jiye Jin, Japan

Emilia Kirowa-Eisner, Israel
Boniface Kokoh, France
Emmanuel Maisondraude, France
Grzegorz Milczarek, Poland
Valentin Mirceski, Macedonia
Mohamed Mohamedi, Canada
Angela Molina, Spain
Davood Nematollahi, Iran
K. I. Ozoemena, South Africa
Mari'a Isabel Pividori, Spain
Miloslav Pravda, Ireland

Manfred Rudolph, Germany
Benjamí'n R. Scharifker, Venezuela
Auro Atsushi Tanaka, Brazil
Germano Tremiliosi-Filho, Brazil
Hamilton Varella, Brazil
Jay D. Wadhawan, UK
Jose H. Zagal, Chile
Sheng S. Zhang, USA
Jiujun Zhang, Canada
Xueji Zhang, USA

Contents

Modern Analytical Electrochemistry: Fundamentals, Experimental Techniques, and Applications, Bengi Uslu, Hassan Y. Aboul-Enein, and Sibel A. Ozkan
Volume 2011, Article ID 196106, 2 pages

A Review of Electroanalytical Techniques for Determination of Anti-HIV Drugs, Burçin Bozal, Bengi Uslu, and Sibel A. Özkan
Volume 2011, Article ID 343947, 17 pages

New Developments in Electrochemical Sensors Based on Poly(3,4-ethylenedioxythiophene)-Modified Electrodes, Stelian Lupu
Volume 2011, Article ID 508126, 8 pages

Design and Development of Biosensors for the Detection of Heavy Metal Toxicity, Graziella L. Turdean
Volume 2011, Article ID 343125, 15 pages

Recent Advances in Electrochemical Glycobiosensing, Germarie Sánchez-Pomales and Rebecca A. Zangmeister
Volume 2011, Article ID 825790, 11 pages

Electrochemical Behavior of Biologically Important Indole Derivatives, Cigdem Karaaslan and Sibel Suzen
Volume 2011, Article ID 154804, 10 pages

Differential Pulse Voltammetric Determination of Fulvestrant in Pharmaceutical Dosage Forms and Serum Samples, Dilek Kul, Burcu Doğan-Topal, Sibel A. Özkan, and Bengi Uslu
Volume 2011, Article ID 941583, 7 pages

Single-Walled-Carbon-Nanotube-Modified Pyrolytic Graphite Electrode Used as a Simple Sensor for the Determination of Salbutamol in Urine, Rajendra N. Goyal, Sunita Bishnoi, and Bharati Agrawal
Volume 2011, Article ID 373498, 8 pages

In Situ Evaluation of Fludarabine-DNA Interaction Using a DNA-Electrochemical Biosensor, H. Eda Satana and Ana Maria Oliveira-Brett
Volume 2011, Article ID 340239, 8 pages

A Biocompatible Nanocomposite for Glucose Sensing, Parvaneh Rahimi, Hedayatollah Ghourchian, Hossain-Ali Rafiee-Pour, Parviz Norouzi, and Mohammad Reza Ganjali
Volume 2011, Article ID 470607, 7 pages

Voltammetric Detection of Dopamine in Presence of Ascorbic Acid and Uric Acid at Poly(Xylenol Orange) Film-Coated Graphite Pencil Electrode, Umesh Chandra, B. E. Kumara Swamy, Ongera Gilbert, and B. S. Sherigara
Volume 2011, Article ID 512692, 8 pages

Electroanalytical Characterisation of Dopa Decarboxylase Inhibitors Carbidopa and Benserazide on Multiwalled Carbon Nanotube and Poly(Nile blue A) Modified Glassy Carbon Electrodes, Dilek Kul and Christopher M. A. Brett
Volume 2011, Article ID 185864, 7 pages

Cyclic Voltammetric Investigation of Dopamine at Poly-(Gabapentin) Modified Carbon Paste Electrode,
M. T. Shreenivas, B. E. Kumara Swamy, Umesh Chandra, and B. S. Sherigara
Volume 2011, Article ID 386987, 5 pages

Anodic Determination of Acetylsalicylic Acid at a Mildly Oxidized Boron-Doped Diamond Electrode in Sodium Sulphate Medium, Codruța Cofan and Ciprian Radovan
Volume 2011, Article ID 451830, 9 pages

Enantioselective Potentiometric Membrane Electrodes Based on Antibiotics for the Determination of L- and D-Glyceric Acids, Raluca-Ioana Stefan-van Staden, R'afat M. Nejem, Jacobus Frederick van Staden, and Hassan Y. Aboul-Enein
Volume 2011, Article ID 427238, 4 pages

Online Monitoring of Electrochemical Degradation of Paracetamol through a Biomimetic Sensor,
Mariana Calora Quintino de Oliveira, Marcos Roberto de Vasconcelos Lanza, José Luis Paz Jara, and Maria Del Pilar Taboada Sotomayor
Volume 2011, Article ID 171389, 11 pages

Scanning Electrochemical Microscopy as a Tool for the Characterization of Dental Erosion,
Pollyana S. Castro, Alex S. Lima, Tiago L. Ferreira, and Mauro Bertotti
Volume 2011, Article ID 952470, 6 pages

Fabrication of Biosensor Based on Polyaniline/Gold Nanorod Composite, Uğur Tamer, Ali İhsan Seçkin, Erhan Temur, and Hilal Torul
Volume 2011, Article ID 869742, 7 pages

Simple Electrochemical Determination of Surface-Active Substances in Natural Waters,
Željka Cvrtković-Karloci, Damir Krznarić, Marijan Šeruga, and Božena Čosović
Volume 2011, Article ID 416834, 7 pages

Solar UV Photooxidation as Pretreatment for Stripping Voltammetric Trace Metal Analysis in River Water, Gelaneh Woldemichael, Taffa Tulu, and Gerd-Uwe Flechsig
Volume 2011, Article ID 481370, 7 pages

Rapid Electrochemical Detection of Radiolysis Products in an Aqueous Solution Exposed to Alpha Particle Beams, J. E. Liedhegner, W. Jennings, and J. Wainright
Volume 2011, Article ID 864126, 9 pages

Cobalt Ferrite Nanocrystallites for Sustainable Hydrogen Production Application, Rajendra S. Gaikwad, Sang-Youn Chae, Rajaram S. Mane, Sung-Hwan Han, and Oh-Shim Joo
Volume 2011, Article ID 729141, 6 pages

Kinetics of Hydrogen Evolution on Copper Electrode Involving Organic Acids as Proton Donors,
A. Survila, S. Kanapeckaitė, J. Pileckienė, and J. Büdienė
Volume 2011, Article ID 160160, 9 pages

Electrochromism and Swelling of Polypyrrole Membranes: An Electrochemical and Ellipsometric Study,
J. O. Zerbino, M. G. Sustersic, C. Falivene, N. Avaca, and A. Maltz
Volume 2011, Article ID 379253, 11 pages

False Oxygen Consumption Effect and Factors Causing It, M. V. Miniaev, M. B. Belyakova, N. V. Kostiuk, and D. V. Leshchenko
Volume 2011, Article ID 376750, 5 pages

Fabrication of Hybrid Diamond and Transparent Conducting Metal Oxide Electrode for Spectroelectrochemistry, Jingping Hu, James Hodge, Arthur J. Boff, and John S. Foord
Volume 2011, Article ID 286458, 7 pages

Editorial

Modern Analytical Electrochemistry: Fundamentals, Experimental Techniques, and Applications

Bengi Uslu,¹ Hassan Y. Aboul-Enein,² and Sibel A. Ozkan¹

¹Department of Analytical Chemistry, Faculty of Pharmacy, Ankara University, Tandoğan, 06100 Ankara, Turkey

²Pharmaceutical and Medicinal Chemistry Department, National Research Centre, Cairo 12311, Egypt

Correspondence should be addressed to Bengi Uslu, buslu@pharmacy.ankara.edu.tr

Received 16 November 2011; Accepted 16 November 2011

Copyright © 2011 Bengi Uslu et al. This is an open access article distributed under the Creative Commons Attribution License, which permits unrestricted use, distribution, and reproduction in any medium, provided the original work is properly cited.

Such use of electrical measurements for analytical purposes has found a vast range of applications, including environmental monitoring, drug and biomedical analysis. Advances in the 1980s and 1990s—including the development of ultramicroelectrodes, the coupling of biological components and electrochemical transducers, the development of ultratrace voltammetric techniques (such as differential pulse voltammetry, square wave voltammetry, stripping voltammetry, etc.) or the use of single-walled and multi-walled carbon nanotubes in scanning probe microscopies, and the microfabrication of molecular devices or efficient flow detectors—have led to a substantial increase in the popularity of electroanalysis and to its expansion into new phases environments.

The use of electrochemical methods to gain key information about drug molecules and their mechanism of action is getting one of the important ways in drug discovery. It should be noticed that many vital physiological processes are depending on oxidoreduction reactions. So, it is easy to find connections between electrochemical and biological reactions regarding electron transfer pathways.

Progress in genomics and particularly in the Human Genome Project in that time stimulated enormous interest in new methods capable to unravel the genetic information stored in the nucleotide sequence of DNA. Only after the construction of DNA chips with optical detection, the attempts to developed DNA chips with electrochemical detection have become popular among electrochemists. Since the middle of 1990s, the electrochemistry of nucleic acids and the development of DNA sensors have become a booming field involving large number of laboratories all over the world. Electrochemical DNA biosensors enable the study

of the interaction of DNA immobilized on the electrode surface with analytes in solution. The investigation based on DNA interactions has great importance in understanding the mechanism of action of many drug compound and complexes, designing of new DNA-drug biosensors, and screening of the drugs *in vitro*. Electrochemical investigations of nucleic acid binding molecules-DNA interactions can provide a useful complement to the spectroscopic techniques and yield information about the mechanism at intercalation and the confirmation of anti-HIV-DNA adduct.

Analytical electrochemists play important roles in monitoring the drug and some metals in their dosage forms, biological samples, and environmental samples. From the viewpoints mentioned above, the title of this special issue “*Modern analytical electrochemistry: fundamentals, experimental techniques, and applications*” was chosen so as to ask electrochemists to appreciate their great roles in chemistry science. This special issue features 5 review and 20 research articles. In this issue: Recent development of electroanalytical techniques such as differential pulse, square wave and their pharmaceutical and environmental applications are presented. It mainly contains current progresses in modified electrodes, DNA biosensors, sensors and their applications to the pharmaceuticals and biological samples, and new electrode materials such as carbon nanotubes and boron-doped diamond.

The recent development of modern analytical chemistry applications, evaluation of electroanalytical methods are focused by key topics in drug and environmental analysis by assessment of the distinguished authors of this special issue. Thus, we expect this special issue will assist readers to find out new information and to encourage them to contribute

more to recent development on drug and environmental analysis using different electroanalytical methods.

The purpose of this special issue will be to serve as a guide to what electroanalytical methods bring to chemistry as well as briefly review their role in drug or environmental samples and the new developments and validation of assay methods of pharmaceutical active components in their dosage forms or in other samples. We hope that the reader will find a number of topics of interest and that additional new ideas will emerge from this special issue.

Acknowledgment

We would like to thank to all of the authors for their excellent contributions and the Editorial Board members of *International Journal of Electrochemistry* for their kind invitations to act as guest editors for this special issue.

*Bengi Uslu
Hassan Y. Aboul-Enein
Sibel A. Ozkan*

Review Article

A Review of Electroanalytical Techniques for Determination of Anti-HIV Drugs

Burçin Bozal, Bengi Uslu, and Sibel A. Özkan

Department of Analytical Chemistry, Faculty of Pharmacy, Ankara University, Tandoğan, 06100 Ankara, Turkey

Correspondence should be addressed to Bengi Uslu, buslu@pharmacy.ankara.edu.tr

Received 19 February 2011; Accepted 21 February 2011

Academic Editor: Hassan Y. Aboul-Enein

Copyright © 2011 Burçin Bozal et al. This is an open access article distributed under the Creative Commons Attribution License, which permits unrestricted use, distribution, and reproduction in any medium, provided the original work is properly cited.

Until now after the human immunodeficiency virus (HIV) was discovered as the then tentative aetiological agent of acquired immune deficiency syndrome (AIDS), exactly 25 anti-HIV compounds have been formally approved for clinical use in the treatment of AIDS. These compounds fall into six categories: nucleoside reverse transcriptase inhibitors (NRTIs: zidovudine, didanosine, zalcitabine, lamivudine, abacavir, stavudine, and emtricitabine), nucleotide reverse transcriptase inhibitors (NtRTIs: tenofovir), nonnucleoside reverse transcriptase inhibitors (NNRTIs: efavirenz, nevirapine, delavirdine, and etravirine), protease inhibitors (PIs: ritonavir, indinavir, saquinavir, nelfinavir, amprenavir, lopinavir, fosamprenavir, atazanavir, tipranavir and darunavir), fusion inhibitors (FIs: enfuvirtide), coreceptor inhibitors (CRIIs: maraviroc), and integrase inhibitors (INIIs: raltegravir). The present paper submitted the use of various electroanalytical techniques for the determination of anti-HIV drugs. This paper covers the time period from 1990 to 2010 including voltammetric techniques that were reported. Presented application concerns analysis of anti-HIV drugs from pharmaceutical dosage forms and biological samples.

1. Introduction

In these early days of anti-HIV drug research, it could hardly be foreseen that within 27 years of the virus being discovered we would now, in 2010, have at hand 25 anti-HIV compounds licensed (thus formally approved) for the treatment of AIDS according to different categories (Table 1).

(a) Nucleoside reverse transcriptase inhibitors (NRTIs): the reverse transcriptase associated with HIV is actually the target for three classes of inhibitors: NRTIs, NtRTIs, and NNRTIs. The NRTIs and NtRTIs interact with the catalytic site of the enzyme, whereas the NNRTIs interact with an allosteric site located at a short distance from catalytic site [1]. There are at present (in 2010) 7 NRTIs that have been formally approved for the treatment of HIV infections: zidovudine, didanosine, zalcitabine, lamivudine, abacavir, stavudine and emtricitabine (Table 1). All the NRTIs could be considered as 2',3'-dideoxynucleoside analogues and act in a similar fashion.

(b) Nucleotide reverse transcriptase inhibitors (NtRTIs): NtRTIs should be clearly distinguished from the NRTIs as they are nucleotide analogues, which means that they only need two phosphorylation steps to be converted to their active form. Also, they contain a phosphonate group that cannot be cleaved by esterases, which would make it more difficult to cleave off these compounds, once incorporated at the 3'-terminal end, compared with their regular nucleotide counterpart. At present, there is only one NtRTI that has been formally approved for the treatment of HIV infections: tenofovir (Table 1).

(c) Nonnucleoside reverse transcriptase inhibitors (NNRTIs): NNRTIs attack the same target enzyme as NRTIs. However, rather than integrating themselves into the transcribed DNA, NNRTIs attach themselves to reverse transcriptase and prevent the enzyme from converting RNA to DNA. Unlike NRTIs, which must be phosphorylated to prevent HIV from infecting the cell, NNRTIs are active in the form administered. The four NNRTIs presently available for the treatment of

- HIV infections are efavirenz, nevirapine, delavirdine, and etravirine [1, 2] (Table 1).
- (d) Protease inhibitors (PIs): during the later stages of the HIV growth cycle, the Gag and Gag-Pol gene products are translated into polyproteins, and these become immature budding particles. Protease is responsible for cleaving these precursor molecules to produce the final structural proteins of the mature virion core. By preventing posttranslational cleavage of the Gag-Pol polyprotein, PIs prevent the processing of viral proteins into functional conformations, resulting in the production of immature, noninfectious viral particles. PIs are active against both HIV-1 and HIV-2; unlike the NRTIs, however, they do not need intracellular activation. The ten PIs currently available for the treatment of HIV infections are ritonavir, indinavir, saquinavir, nelfinavir, amprenavir, lopinavir, fosamprenavir, atazanavir, tipranavir, and darunavir [1–6].
 - (e) Entry inhibitors (fusion inhibitors and coreceptor inhibitors): the process of HIV-1 entry into host cell is complex; each step forms a potential target for inhibition. Viral attachment to the host cell entails binding of the viral envelope glycoprotein complex gp160 to its cellular receptor CD4. At present, there are only two entry inhibitors that have been formally approved for the treatment of HIV infections: enfuvirtide and maraviroc (Table 1) [1–6].
 - (f) Integrase inhibitors (INIs): although integrase has been pursued for many years as a potential target for the development of new anti-HIV compounds, the first integrase inhibitor licensed for clinical use, raltegravir, has only recently been approved. Raltegravir is a pyrimidinone analog that binds integrase, a viral enzyme essential to the replication of both HIV-1 and HIV-2. It is licensed for use in treatment-experienced adult patients infected with strains of HIV-1 resistant to multiple other agents.

In addition, new therapies are continually being sought that exploit new viral targets, have activity against resistant viral strains, have a lower incidence of adverse effects, and offer convenient dosing. New agents of existing classes are currently in advanced stages of clinical development [1–6].

The growing demand for these agents stimulates a search for new even more effective drugs, but also calls for higher level of quality control of these therapeutic substances and preparations, so that they are in the highest possible degree free from any impurities that may come from the production process, as well as from decompositions products of active or auxiliary substances. Therefore, it seems appropriate to develop new analytical methods regarding their qualitative and quantitative analysis. For this aim, different analytical methods are used for determining anti-HIV drugs. One that has been gaining more and more applications is the electroanalytical methods. Electroanalytical methods are widely used in scientific studies and in monitoring of industrial materials, pharmaceutical compounds, biological samples

and the environment. The most widespread electroanalytical methods are voltammetry and polarography. These methods permit the screening and determination of a great number of organic compounds especially pharmaceutical substances with a detection limit of $\sim 10^{-7}$ M. The voltammetric methods used today in analytical chemistry laboratories were made possible by recent advances in instrumentation, by computerized processing of analytical data, and in particular, by innovative electrochemists. Electrochemistry involves in its broad sense a chemical phenomenon associated with charge separation at an electrode surface. As voltammetric methods continue to develop, the range of working electrode materials continues to expand, and the analyst must remain aware of what is available. Both the geometry and composition of the working electrode material must be considered since they will influence the performance of the voltammetric method. Also, the physical form of the working electrode may influence the diffusion process and the electron transfer process involved in the detection of the analyte [7–15]. The voltammetric and polarographic analysis of drugs in pharmaceutical preparations by far is the most common use of electrochemistry for analytical-pharmaceutical problems. As a rule, many of active compounds of the formulations can be readily oxidized or reduced. As has been pointed out, electrochemical techniques are well suited for the determination of drugs in various samples, that is, raw material, pharmaceutical dosage forms even those involving a complex matrix such as syrups, tablets, creams, suppositories, or ointments, or else in biological fluids. The principal advantage of the modern electroanalytical methods is that the excipients do not interfere, and generally the separation and extraction is not necessary. Thus, sample preparation usually consists of dissolving out the active substance from the pharmaceutical dosage form with a suitable solvent and performing direct analysis on an aliquot portion of this solution [16]. Electrochemical techniques are most suitable to investigate the redox properties of a new drug (like new anti-HIV agents); this can give insights into its metabolic fate. Electrochemical data are often correlated to the molecular structure and the pharmacological activity. Also, interactions of drugs with metal ions or with proteins as well as degradation processes occurring on photo- or pH-sensitive drugs may be studied using modern electrochemical techniques [9, 16, 17].

Anti-HIV drugs are the recent developments of drugs and there is a great need to review the analytical work reported so far in the literatures. Efforts have been made to collect the literature from 1990 up to the present. For electroanalytical determinations, CV, LSV, DPV, SWV, and polarography have been used.

2. Electroanalytical Methods for Anti-HIV Drug Determination

2.1. Efavirenz. EFV, (S)-6-chloro-4-(cyclopropylethynyl)-1, 4-dihydro-4-(trifluoromethyl)-2H-3,1-benzoxazin-2-one, is an HIV-1 specific, nonnucleoside reverse transcriptase inhibitor. EFV was approved by the FDA on September 21, 1998, making it the 14th approved antiretroviral drug. It is not

TABLE I: Approved anti-HIV drugs and their structure formulae.

Categories	Generic name	Structure formulae	Brand name	Manufacturer
Nucleoside reverse transcriptase inhibitors (NRTIs)	Zidovudine		Retrovir	GlaxoSmithKline
	Didanosine		Videx (tablet) Videx EC (capsule)	Bristol-Myers Squibb
	Zalcitabine		Hivid	Hoffmann-La Roche
	Stavudine		Zerit	Bristol-Myers Squibb
	Lamivudine		Epivir	GlaxoSmithKline

TABLE I: Continued.

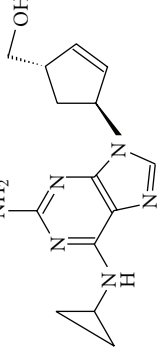
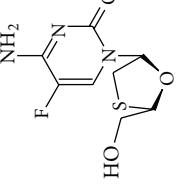
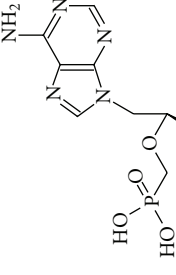
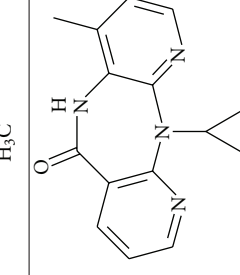
Categories	Generic name	Structure formulae	Brand name	Manufacturer
Nucleotide reverse transcriptase inhibitors (NtRTIs)	Abacavir		Ziagen	GlaxoSmithKline
	Emtricitabine		Emtriva	Gilead Sciences
	Tenofovir		Viread	Gilead Sciences
Nonnucleoside reverse transcriptase inhibitors (NNRTIs)	Nevirapine		Viramune	Boehringer Ingelheim

TABLE I: Continued.

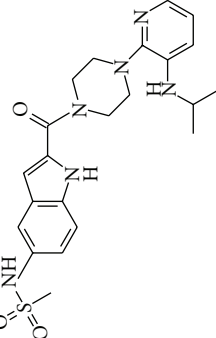
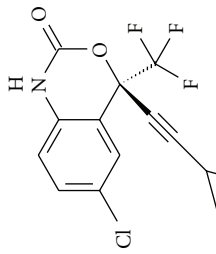
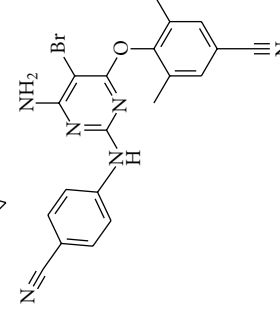
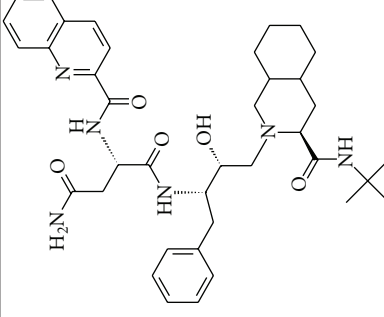
Categories	Generic name	Structure formulae	Brand name	Manufacturer
Delavirdine		Rescriptor	Pfizer	
Efavirenz		Sustiva Stocrin	Bristol-Myers Squibb/Merck	
Etravirine		Intelence	Tibotec Therapeutics	
Saquinavir		Invirase (hard gel capsule) Fortovase (soft gel capsule)	Hoffmann-La Roche Hoffmann-La Roche	
Protease inhibitors (PIs)				

TABLE I: Continued.

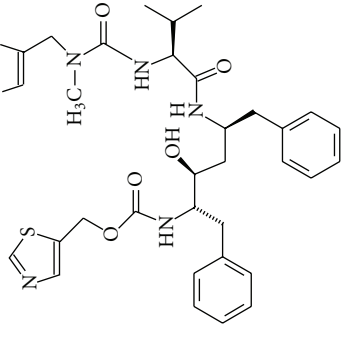
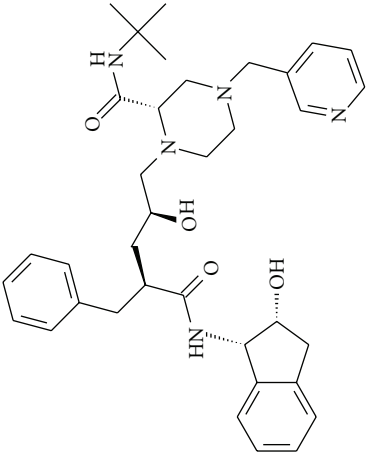
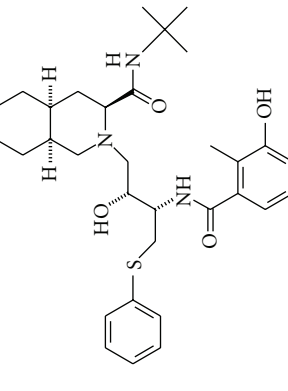
Categories	Generic name	Structure formulae	Brand name	Manufacturer
	Ritonavir		Norvir	Abbott Laboratories
	Indinavir		Crixivan	Merck
	Nelfinavir		Viracept	Agouron Pharmaceuticals

TABLE I: Continued.

Categories	Generic name	Structure formulae	Brand name	Manufacturer
	Amprenavir		Agenerase	GlaxoSmithKline
	Lopinavir (Tritonavir)		Kaletra	Abbott Laboratories
	Atazanavir		Reyataz	Bristol-Myers Squibb
	Fosamprenavir		Lexiva Telzir	GlaxoSmithKline GlaxoSmithKline

TABLE I: Continued.

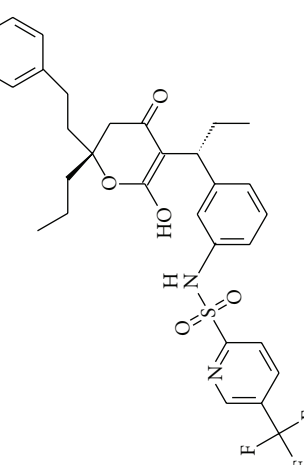
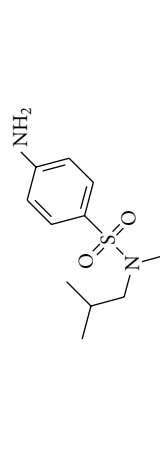
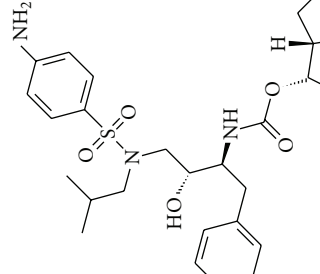
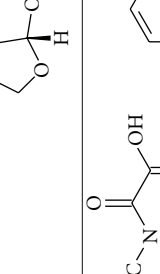
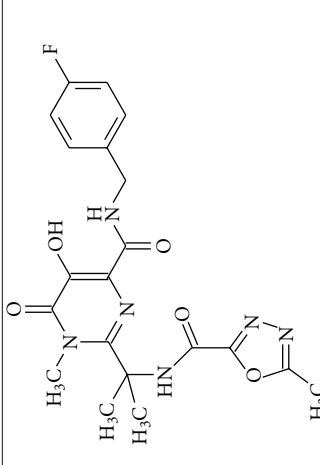
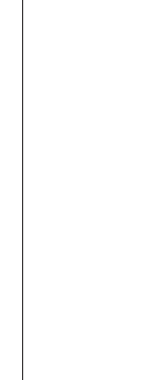
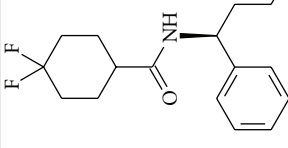
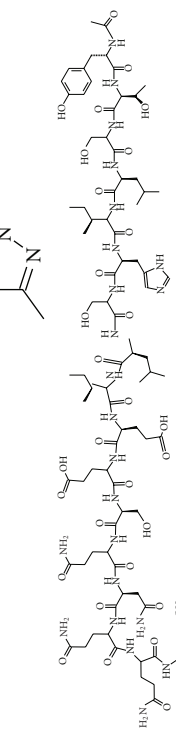
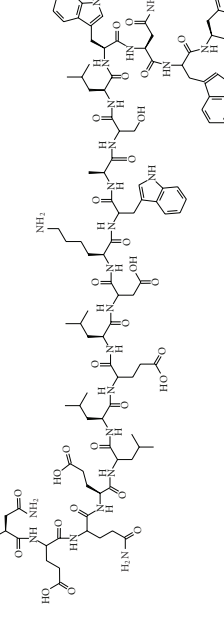
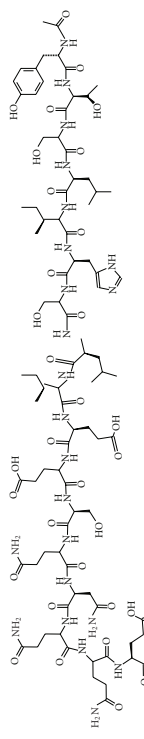
Categories	Generic name	Structure formulae	Brand name	Manufacturer
Tipranavir			Aptivus	Boehringer Ingelheim
Darunavir			Prezista	Tibotec, Inc.
Integrase inhibitors (INIs)			Raltegravir	Merck & Co., Inc.

TABLE I: Continued.

Categories	Generic name	Structure formulae	Brand name	Manufacturer
Cell entry inhibitors and co-receptor inhibitors	Maraviroc	 	Celsentri Selzentry	Pfizer Pfizer
	Enfuvirtide	 	Fuzeon	Hoffmann-La Roche & Trimeris

effective against HIV-2, as the pocket of the HIV-2 reverse transcriptase has a different structure, which confers intrinsic resistance to the NNRTI class. EFV is metabolized in the liver and possesses both inhibitory and including effects on the 3A4 isoform of the cytochrome P450 system. This means EFV may interact with other drugs metabolized in the liver, requiring either increased or decreased dosages [18, 19]. Electrochemical techniques also help for the identification of the redox mechanism of drug compounds and provide important information about DNA-drug interaction [20]. There is only one electroanalytical method for the determination of EFV in dosage forms. Dogan-Topal et al. [20] investigated the voltammetric behavior of EFV at a PGE and presented DNA biosensor. The aim of this study was to establish the experimental conditions such as EFV concentration, its interaction time dsDNA, dsDNA concentration, and the effect of the ionic strength. These results showed that this DNA biosensor could be used for the sensitive, rapid, simple, and cost-effective detection and determination of EFV-dsDNA interaction. The linearity was between 2 and 24 ppm of EFV concentration on guanine signal decreasing curve. This work also aimed to develop a new, selective, simple voltammetric method for the direct determination of EFV in raw material and pharmaceuticals without any time-consuming extraction, evaporation, and separation steps prior to drug assay. Also DPV method was used at bare and dsDNA modified disposable PGE. EFV showed an irreversible oxidation behavior at all pH values, and AdSDPV method was developed for determination of EFV. Under these conditions, the current showed a linear dependence with concentration in the range between 0.018 and 2.56 ppm.

2.2. Abacavir. ABA, {((1S,cis)-4-[2-amino-6-(cyclopropylamino)-9H-purin-9-yl]cyclopent-2-enyl)methanol}, is an NRTI with antiretroviral activity against HIV. It is a carbocyclic synthetic nucleoside analog. ABA is rapidly absorbed following oral administration with a bioavailability of about 80%. It is about 50% bound to plasma proteins. ABA is metabolized into the pharmacological inactive 5'-glucuronide and the 5'-carboxylate.

ABA has been studied and determined using anodic voltammetry by Uslu and Özkan [21]. The goal of this work was the development of new voltammetric methods (DPV and SWV) for the direct determination of ABA in pharmaceutical dosage forms, raw materials, spiked human serum, and urine samples. These two voltammetric techniques for the determination of ABA in Britton-Robinson buffer at pH 2.0, which allows quantitation over the 8×10^{-7} to 2×10^{-4} M range in supporting electrolyte for both methods were proposed. The linear response was obtained in Britton-Robinson buffer in the ranges of 1×10^{-5} to 1×10^{-4} M for spiked urine sample at pH 2.0 and 2×10^{-5} to 2×10^{-4} M for spiked serum samples at pH 3.0 for both techniques.

ABA is electrochemically reduced at the dropping mercury electrode in a four-electron process, similar to structurally related adenine, and adenosine triphosphate [22]. Procedures of analyses of tablets containing ABA were

established and validated, based on peak currents obtained by LSV, DPV, or SWV with an HMDE as indicator electrode. The procedure proved to be more sensitive and more reliable than based on oxidation on a glassy carbon electrode.

2.3. Fosamprenavir. FOS, {(2R, 3S)-1-[N-(2-methylpropyl)(4-aminobenzene)sulfonamido]-3-({[(3S)-oxolan-3-yl]oxy} carbonyl)amino)-4-phenylbutan-2-yl]oxy} phosphonic acid is a prodrug of antiretroviral protease inhibitor amprenavir. Amprenavir is metabolized in the liver by CYP3A4 enzyme system. It is an inhibitor of HIV-1 protease. Amprenavir binds to the active site of HIV-1 protease resulting in the formation of immature noninfectious viral particles [18, 23, 24]. The two major metabolites result from oxidation of the tetrahydrofuran and aniline moieties. Several analytical methods have been published for the determination of amprenavir with other HIV protease inhibitors in biological fluids, based on HPLC with MS detection, with UV detection, and with fluorescence detection. Also there is only one published literature related to electroanalytical studies of amprenavir. In this study, the anodic oxidation of fosamprenavir was investigated using CV and LSV at boron-doped diamond and glassy carbon electrodes. In CV, depending on pH values, FOS showed one sharp irreversible oxidation peak or wave depending on the electrode. The aim of this study was to determine FOS levels in pharmaceutical formulations and biological samples by means of electrochemical methods. DPV and SWV techniques were 0.1 M H_2SO_4 and phosphate buffer at pH 2.0 which allow quantitation over a 4×10^{-6} to 8×10^{-5} M range using boron-doped diamond and 1×10^{-5} to 1×10^{-4} M range using glassy carbon electrodes, respectively, in supporting electrolyte [25].

2.4. Didanosine. 2'-3'-Dideoxyinosine (DDI), 9-[(2R, 5S)-5-(hydroxymethyl)oxolan-2-yl]-6,9-dihydro-3H-purin-6-one, is a dideoxy analogue of the purine nucleoside inosine, which shows high antiretroviral activity against HIV, the agent of AIDS [26]. DDI was approved as a drug in 1991 by the FDA for the treatment of adults and children with advanced HIV infection, who are intolerant or resistant to azidothymidine therapy or whose health has been deteriorated by azidothymidine use [27].

Electroanalytical determination of DDI is possible; however up to now, there is only one published paper. In this study, cobalt (II) phthalocyanine and iron (II) phthalocyanine complexes have been used as an electrocatalysts for the oxidation of DDI [28]. The detection limits were calculated to be 8.80×10^{-7} M for CoPc-CPE with a linear concentration range between 2.0×10^{-6} to -7.0×10^{-4} M, whereas for the FePc-CPE the LOD is 3.50×10^{-7} M with a linear concentration range between 1.0×10^{-6} and 8.0×10^{-4} M in pH 7.4 phosphate buffer solution. Also the main advantage of the proposed method over the other known methods described for DDI is a possibility of its determination directly, without prior separation, with high precision, rapidity, stability, and low consumption of sample and buffer.

2.5. Indinavir. IND, [1(1S,2R),5(S)]-2,3,5-trideoxy-N-(2,3-dihydro-2-hydroxy-1H-inden-1-yl)-5-[2-[(1,1-dimethyl ethyl)-amino] carbonyl]-4-(3-pyridinylmethyl)-1-piperazinyl]-2-phenylmethyl)-D-erythro-pentonamide sulfat is an inhibitor of the HIV protease. IND has a low protein binding ranging from 60 to 70% in species and is extensively metabolized in all species by the cytochrome P450 system. It has been determined by spectrophotometric, capillary electrophoretic, liquid chromatographic methods; however, all the reported methods are laborious, time-consuming and require highly sophisticated instrumentation. Only one paper reported anodic voltammetry using glassy carbon electrode. In this study, pH 6.0 Britton-Robinson buffer solution was selected for analytical medium in which IND exhibited diffusion controlled oxidative peak at +0.89 V. Also the peak current varied linearly with drug concentration in the range between 2.8×10^{-7} and 5.0×10^{-5} M. The proposed DPV and SWV techniques have been applied to the determination of IND in pharmaceutical dosage forms with good recoveries [29]. Besides, there is only one electroanalytical study about the determination and reduction mechanism of IND in bulk form, pharmaceutical dosage forms, and biological fluids. In this study, IND exhibited irreversible cathodic waves over the pH range of 2.0–12.00 in different supporting electrolytes. The current-concentration plot was rectilinear over the range from 8.0×10^{-7} to 8.0×10^{-6} M for DPV and 8.0×10^{-7} – 1.0×10^{-5} M for SWV in Britton-Robinson buffer at pH 10.00. The wave was characterized as being irreversible and diffusion controlled also. The proposed methods were fully validated and successfully applied to the determination of IND in capsules and spiked human serum samples with good recoveries [30]. Ignaszak et al. [31] developed a novel therapeutic biosensor for the determination of IND. An amperometric drug metabolism biosensor consisting of CYP3A4 encapsulated in a didodecyldimethyl ammonium bromide vesicular system on a platinum disk electrode was fabricated. CV, SWV, and pulse voltammetric responses of the bioelectrode showed quasireversible electrochemistry of the $\text{Fe}^{3+}/\text{Fe}^{2+}$ redox species of the heme thiolate CYP3A4 enzyme under aerobic and anaerobic conditions. The new biosensor exhibited excellent response to IND with a detection limit and response time of 6.158×10^{-2} mgL⁻¹ and 40 s, respectively. Also detection limit was well below the plasma concentration of IND (8 h after intake) which ranges from 0.13 to 8.6 mgL⁻¹ [31]. Fizzano et al. [32] developed an HPLC method with electrochemical detection for the quantification of IND in cell culture. For the electrochemical detector, the working parameters were +400 mV for the first electrode and +750 mV for the second; these setting were found to provide optimal detection conditions. The signals generated by the second electrode were used for the quantitation. Also the proposed HPLC assay was utilized to directly evaluate the capability of p-glycoprotein expressing multidrug resistant cells in mediating the transport and efflux of protease inhibitor IND, a basic compound in AIDS care.

2.6. Lamivudine. LAM, 4-amino-1-[(2R,5S)-2-(hydroxymethyl)-1,3-oxathiolan-5-yl]-1,2-dihydro pyrimidin-2-one, is a synthetic nucleoside analogue with activity against HIV-1

and hepatitis B virus. It is an NRTI structurally related to cytosine with activity against retroviruses including HIV. It is used usually in combination with other antiretroviral drugs. Following oral administration, LAM is rapidly absorbed and peak plasma concentrations are achieved in about 1 hour. Binding to plasma protein is reported to be less than 36% [18, 33].

Nowadays, there are two published literatures related to electrochemical study of LAM in pharmaceutical dosage forms. One of them was studied by Dogan et al. [34]. The aim of this study was to determine LAM levels in serum and pharmaceutical formulations, by means of electrochemical methods using HMDE. On this electrode, LAM undergoes irreversible reduction at the peak potential near E_p –1.26 V. Reduction LAM signals were measured DPV and SWV techniques. DPV and SWV techniques for the determination of LAM in acetate buffer at pH 4.5, which allows quantitation over the 4.0×10^{-6} – 1.0×10^{-4} M range for both methods, were proposed. The linear response was obtained in acetate buffer in the ranges of 2.0×10^{-6} to 2.0×10^{-4} M for spiked serum samples at pH 4.5 for both techniques.

Another study was developed by Jain et al. [35]. The electrochemical reduction and adsorption of LAM were studied in a phosphate buffer at pH 3.4 at an HMDE. The reduction was irreversible and exhibited diffusion-controlled adsorption. The responses were evaluated with respect to preconcentration time, pH effect, accumulation potential, accumulation time, and scan rate. The calibration plot of the peak current versus the concentration was found to be linear over the range of 500 ng/mL to 10 μ g/mL for LAM in the SWV method. Also the number of electrons transferred in the reduction process was calculated and the probable reduction mechanism was proposed.

2.7. Zidovudine (Azidothymidine). ZDV, 3'-azido-3'-deoxythymidine, is the cornerstone drug for treatment of patients with HIV-1. ZDV is derived from thymidine where the hydroxyl group at carbon 3 of the sugar moiety is replaced by the azido group. The azido group is responsible not only for the in vivo antiviral activity but also for the electrochemical reduction signal of ZDV on a mercury electrode. The electrochemical properties of ZDV were investigated using CV, DPV, and chronocoulometry [36]. These methods were used to determine the reduction pathway of ZDV and the number of protons and electrons involved in the reduction process. Experiments using a narrow range of moderate scan rates indicate that the electrochemical reduction of ZDV proceeds via a four-electron, two-proton mechanism to a reduced species that undergoes a fast chemical reaction to give a species that precipitates on the electrode surface. The diffusion coefficient for ZDV was calculated to be 4.90×10^{-6} cm²s⁻¹ using the irreversible CV equation and an n value of four electrons. The electrochemical investigation was studied by SWV, LSV, and elimination voltammetry with linear scan using HMDE. This paper explores the possibility of determining ZDV in the presence of native (dsDNA) or denatured calf thymus DNA (ssDNA), and/or same synthetic oligodeoxynucleotides. The detection limit of ZDV in the absence and in the presence of ssDNA (10 μ g/mL) is 1 and

250 nM, respectively. It was found that the signal of ZDV is not substantially affected by the presence of DNA. While ZDV provides an irreversible reduction peak at a potential near -1.1 V, the DNA gives the reduction peak due to adenine and cytosine residues at a potential of ca. -1.4 V [37].

Other similar experiment was developed by Vacek et al. [38]. The aim of this study was to determine ZDV levels in natural samples (urine, serum, whole blood, and cell cultures) without their mineralization and/or purification, by means of electrochemical methods using HMDE. Reduction ZDV signals were measured by CV, DPV, SWV, and constant current chronopotentiometric stripping analysis. In phosphate buffer at pH 8.0, the SWV yielded the best ZDV signal with the detection limit of 1 nM. For monitoring the influence of these compounds, ZDV reduction was performed in the presence of 10 μ g/mL calf thymus ssDNA and/or 100 μ g/mL bovine serum albumin. In these cases, the detection limit increased to 0.25 μ M. The work showed that SWV is a suitable electrochemical method for the determination of ZDV in various biological samples, such as cell cultures and body liquids of HIV-positive patients. Also the SWV method can be recommended as a useful tool for pharmacological and metabolic studies of ZDV.

New simple and direct electroanalytical method was developed for the determination of ZDV in commercial pharmaceutical preparations by Peckova et al. [39]. It is based on DPV at p-AgSAE or m-AgSAE. Achieved LOQs are in the 10^{-7} M concentration range for both amalgam electrodes. This is more than one order of magnitude higher than using HMDE, nevertheless, still attractive for determination of ZDV in pharmaceutical preparations and in biological matrices, especially after a preconcentration step using solid phase or liquid-liquid extraction.

Another DPV method has been described for the quantitative determination of ZDV by Leandro et al. [40]. In this study, the reduction of ZDV at an HMDE was at -0.96 V at pH 8.0 phosphate buffer. Under these optimized conditions, the ZDV peak current varied linearly with its concentration from 0.25 to 1.25 mg/L. Detection and determination limits of 0.0025 and 0.025 mg/L, respectively, and recovery of 99.88% with an RSD of 0.95% were obtained.

Mahmoud and Luong developed highly sensitive screening assay based on electrochemical impedance spectroscopy [41]. The assay format was based on the immobilization of the thiol terminated ferrocene (Fc)-peptatin conjugate on a single-walled carbon nanotube/gold nanoparticle modified gold electrode. This study has demonstrated for the first time the use of nanomaterials in impedance spectroscopy for detecting lopinavir, ritonavir, saquinavir, indinavir, and fosamprenavir at picomolar levels. Thiolated single-walled carbon nanotubes together with gold nanoparticles and a ferrocene conjugate serve as sensitive enhancer tools in this assay format. On the basis of its applicability for evaluation of low-molecular weight compounds, this technique is a definite asset for the expedited development of effective HIV-1 protease inhibitors. This strategy might be extended for the sensing of other interfacial interactions such as enzyme-DNA, antibody-antigen, and cell receptor.

3. Simultaneous Electroanalytical Determination of Analyzed Drugs

Besides the analytical methods for single components, some of the simultaneous determinations are also included in this paper. Lamivudine, didanosine, and saquinavir were simultaneously determined by capillary zone electrophoresis [42]. In this study, the anti-HIV drug mixture of lamivudine, didanosine, and saquinavir was separated and quantitated in human serum with capillary zone electrophoresis. The effects of various factors, such as run buffer type, buffer concentration, and pH on the separation were investigated. All analytes were separated within 10 min with a voltage of +20 kV and a current around 30 μ A in the pH 2.5 phosphate buffer. The method was validated over the range of 0.4–37.8 μ g/mL for lamivudine, 1.4–34.0 μ g/mL for didanosine, and 0.5–24.4 μ g/mL for saquinavir. Baseline separation of lamivudine, didanosine, and saquinavir was achieved with retention times of 4.4, 10.8, and 6.9 min, respectively. The internal standard diltiazem gave a migration time of 5.6 min.

MEKC was used for determination of stavudine, didanosine, saquinavir (mixture A) and stavudine, didanosine, efavirenz (mixture B) in human serum samples [43]. The optimized resolution of both mixture was achieved with a run buffer containing 18 mM sodium dodecylsulfate in 15 mM phosphate and borate buffer (pH 9.0). All analytes were separated within 15 min with a voltage of +15 kV and a current around 30 μ A. The methods were validated over the range of 0.7–35.3 μ g/mL for stavudine, 0.8–18.5 μ g/mL for didanosine, 0.5–12.2 μ g/mL for saquinavir in mixture A and 0.7–35.3 μ g/mL for stavudine, 0.8–18.5 μ g/mL for didanosine, and 0.6–31.9 μ g/mL for efavirenz in mixture B.

Another MEKC method was developed by Fan and Stewart [44]. In this study, the anti-HIV drug mixtures containing zidovudine/didanosine/nevirapine (mixture A) and zidovudine/didanosine/ritonavir (mixture B) were quantitated in human serum samples. All analytes were separated within 14 min with a voltage of +15 kV and a current around 30 μ A. The methods were validated over the range of 0.5–25.0 μ g/mL for zidovudine, 0.8–18.5 μ g/mL for didanosine, 0.5–22.8 μ g/mL for nevirapine in mixture A and the range of 0.5–25.0 μ g/mL for zidovudine, 0.8–18.5 μ g/mL for didanosine, and 1.2–28.8 μ g/mL for ritonavir in mixture B.

4. Validation of the Electroanalytical Methods

Validation of a method is the planned and documented procedure to establish its performance characteristics. Typical parameters that characterize each electroanalytical method include selectivity, specificity, range, linearity, accuracy (recovery), LOD, LOQ, precision, robustness, and ruggedness [45–52]. They define what the method can do under optimized conditions of matrix solution, instrumental settings, active ingredient isolation, and other experimental features.

The electroanalytical procedures presented in this paper have been validated in terms of basic parameters, that is, linearity, LOD, LOQ, precision, and recovery. Validation parameters of the electroanalytical methods used for

TABLE 2: Validation data for analyzed drugs.

Compound	Method	Linear range	LOD	LOQ	Precision (RSD %)	Recovery (%)	Ref.
				Intraday	Interday		
Efavirenz	AdsDPV	2.0–24.00 ppm	0.599 ppm	1.995 ppm	0.96	2.22	101.67 [20]
	DPV	8.0×10^{-7} – 2.0×10^{-4} M	2.20×10^{-7} M	7.34×10^{-7} M	1.02	1.93	99.37 [21]
Abacavir	SWV	8.0×10^{-7} – 2.0×10^{-4} M	1.18×10^{-7} M	3.93×10^{-7} M	0.46	1.76	99.83
	CV	1.0×10^{-7} – 1.0×10^{-5} M	2.11×10^{-8} M	—	0.24	0.87	99.99
Abacavir	DPV	1.0×10^{-7} – 1.0×10^{-5} M	2.41×10^{-8} M	—	0.43	1.17	99.84 [22]
	SWV	1.0×10^{-7} – 1.0×10^{-5} M	2.69×10^{-8} M	—	0.43	1.10	100.21
Fosamprenavir	DPV (BDDE)	4.0×10^{-6} – 1.0×10^{-4} M	2.17×10^{-7} M	6.59×10^{-7} M	0.19	1.40	100.10
	DPV (GCE)	1.0×10^{-5} – 1.0×10^{-4} M	5.05×10^{-7} M	1.53×10^{-6} M	0.58	0.66	99.88 [25]
Didanosine	SWV (BDDE)	4.0×10^{-6} – 1.0×10^{-4} M	2.97×10^{-7} M	9.00×10^{-7} M	1.07	1.85	100.02
	SWV (GCE)	1.0×10^{-5} – 1.0×10^{-4} M	3.78×10^{-7} M	1.16×10^{-6} M	0.47	0.72	100.54
Didanosine	DPV (CoPc-CPE)	2.0×10^{-6} – 7.0×10^{-4} M	8.80×10^{-7} M	—	—	—	99.76 [28]
	DPV (FePc-CPE)	1.0×10^{-6} – 8.0×10^{-4} M	3.50×10^{-7} M	—	—	—	99.79
Indinavir	CV	2.8×10^{-7} – 5.0×10^{-5} M	1.2×10^{-8} M	3.8×10^{-7} M	—	0.35	98.7
	LSV	2.8×10^{-7} – 5.0×10^{-5} M	1.2×10^{-8} M	7.0×10^{-7} M	—	0.46	98.7
Indinavir	DPV	2.8×10^{-7} – 5.0×10^{-5} M	4.4×10^{-8} M	2.7×10^{-7} M	—	0.64	99.0 [29]
	SWV	2.8×10^{-7} – 5.0×10^{-5} M	4.4×10^{-8} M	2.5×10^{-7} M	—	0.86	98.2
Indinavir	DPV	8.0×10^{-7} – 8.0×10^{-6} M	1.26×10^{-7} M	4.21×10^{-7} M	0.55	1.45	100.36 [30]
	SWV	8.0×10^{-7} – 1.0×10^{-5} M	1.57×10^{-7} M	5.23×10^{-7} M	0.44	0.72	100.80
Indinavir	Amperometry	0.13–8.60 mg/L	6.16×10^{-2} mg/L	—	—	—	— [31]
	HPLC (ED)	6–1000 ng/mL	2 ng/mL	4 ng/mL	1.04	3.31	99.99 [32]
Lamivudine	DPV	4.0×10^{-6} – 1.0×10^{-4} M	6.28×10^{-8} M	2.09×10^{-7} M	0.30	0.14	99.45 (tablet) [34]
	SWV	4.0×10^{-6} – 1.0×10^{-4} M	2.02×10^{-8} M	6.72×10^{-8} M	0.32	0.10	99.98 (oral solution) 99.53 (tablet)
Lamivudine	CAdSV	500 ng/mL– $10 \mu\text{g}/\text{mL}$	69 ng/mL	500 ng/mL	0.55	0.72	102.0 [35]
	DPV	$2.5 \mu\text{g}/\text{mL}$ – $40 \mu\text{g}/\text{mL}$	245 ng/mL	2500 ng/mL	0.98	1.5	101.8
Zidovudine	SWV	—	1 nM (absence of ssDNA)	—	—	—	[37]
	SWV	—	250 nM (presence of ssDNA)	—	—	—	[38]
Zidovudine	SWV	500 pM– $1 \mu\text{M}$	1 nM	—	—	—	[38]

TABLE 2: Continued.

Compound	Method	Linear range	LOD	LOQ	Precision (RSD %) Intraday	Precision (RSD %) Interday	Recovery (%)	Ref.
Zidovudine	DPV (m-AgSAE)	0.4–1500 $\mu\text{mol/L}$	0.12 $\mu\text{mol/L}$	0.41 $\mu\text{mol/L}$	1.7	—	101.4	[39]
	DPV (p-AgSAE)	0.6–1500 $\mu\text{mol/L}$	0.20 $\mu\text{mol/L}$	0.67 $\mu\text{mol/L}$	0.3	—	100.3	[39]
	DPV (HMDE)	0.03–1900 $\mu\text{mol/L}$	0.007 $\mu\text{mol/L}$	0.024 $\mu\text{mol/L}$	0.3	—	102.0	[40]
Zidovudine	DPV	0.25–1.25 mg/L	0.0025 mg/L	0.025 mg/L	—	—	99.88	[40]
Lamivudine		0.4–37.8 $\mu\text{g/mL}$	0.2 $\mu\text{g/mL}$	0.4 $\mu\text{g/mL}$	< 13.3	< 13.3	>79.0	[42]
Didanosine	CZE	1.4–34.0 $\mu\text{g/mL}$	0.9 $\mu\text{g/mL}$	1.4 $\mu\text{g/mL}$	—	—	—	[42]
Saquinavir		0.5–24.4 $\mu\text{g/mL}$	0.2 $\mu\text{g/mL}$	0.5 $\mu\text{g/mL}$	—	—	—	[42]
Stavudine		0.7–35.3 $\mu\text{g/mL}$	0.3 $\mu\text{g/mL}$	0.7 $\mu\text{g/mL}$	< 14.5	< 14.5	>77.3	[43]
Didanosine	MEKC	0.8–18.5 $\mu\text{g/mL}$	0.4 $\mu\text{g/mL}$	0.8 $\mu\text{g/mL}$	—	—	—	[43]
Saquinavir		0.5–12.2 $\mu\text{g/mL}$	0.3 $\mu\text{g/mL}$	0.5 $\mu\text{g/mL}$	—	—	—	[43]
Efavirenz		0.6–31.9 $\mu\text{g/mL}$	0.3 $\mu\text{g/mL}$	0.6 $\mu\text{g/mL}$	—	—	—	[43]
Zidovudine		0.5–25.0 $\mu\text{g/mL}$	0.2 $\mu\text{g/mL}$	0.5 $\mu\text{g/mL}$	< 13.9	< 13.9	>75.9	[44]
Didanosine	MEKC	0.8–18.5 $\mu\text{g/mL}$	0.4 $\mu\text{g/mL}$	0.8 $\mu\text{g/mL}$	—	—	—	[44]
Nevirapine		0.2–22.8 $\mu\text{g/mL}$	0.1 $\mu\text{g/mL}$	0.2 $\mu\text{g/mL}$	—	—	—	[44]
Ritonavir		1.2–28.8 $\mu\text{g/mL}$	0.6 $\mu\text{g/mL}$	1.2 $\mu\text{g/mL}$	—	—	—	[44]

the determination of efavirenz, abacavir, fosamprenavir, didanosine, indinavir, lamivudine, zidovudine, saquinavir, stavudine, nevirapine, and ritonavir are presented in Table 2. Comparing validation parameters of already researched techniques, it can be concluded which one of them is more sensitive (low LOD and LOQ values), accurate (precision and recovery) and allows marking in a broad linearity scope.

5. Conclusions

This paper presents electroanalytical methods applied for the determination of anti-HIV drugs between 1990 and 2010. A great number of studies on zidovudine, indinavir, and lamivudine can be noted, whereas for efavirenz, abacavir, fosamprenavir, and didanosine are only a few. Among all of the published methods, DPV and SWV techniques are the most popular techniques which are used both for the analysis of pharmaceutical dosage forms and biological samples. Other techniques, that is, CV, LSV, and amperometry are not so popular. They are used only for understanding redox mechanism. Another technique used for mixture components separation is zone electrophoresis, in which after separation, the individual components can be analyzed in the buffer solution using a spectrophotometric or electrochemical detector. MEKC is a mode of capillary electrophoresis that is capable of separating uncharged compounds. It is viewed as a chromatographic technique in which migrating charged micelles act as a pseudostationary phase. MEKC offers analyte partitioning between micelles formed by a surfactant in the run buffer, such that mixtures of charged and uncharged anti-HIV drugs can be satisfactorily separated. Up to date a lot of new modified electrodes and biosensors were developed for determination of anti-HIV drugs. The ultimate goal is to obtain results with more and more precision and accuracy and at increasingly lower concentration levels of the substances being determined.

Abbreviations

DPV:	Differential pulse voltammetry
SWV:	Square wave voltammetry
CV:	Cyclic voltammetry
LSV:	Linear sweep voltammetry
CoPc-CPE:	Cobalt (II) phthalocyanine carbon paste electrode
FePc-CPE:	Iron (II) phthalocyanine carbon paste electrode
HPLC:	High performance liquid chromatography
HMDE:	Hanging mercury drop electrode
dsDNA:	Double-stranded DNA
ssDNA:	Single-stranded DNA
EFV:	Efavirenz
FDA:	Food and Drug Administration
HIV-1:	Human immunodeficiency virus type 1
HIV-2:	Human immunodeficiency virus type 2
AdsDPV:	Differential pulse adsorptive stripping voltammetry
ABA:	Abacavir

FOS:	Fosamprenavir
MS:	Mass
UV:	Ultraviolet
DDI:	Didanosine
IND:	Indinavir
AIDS:	Acquired immune deficiency syndrome
LAM:	Lamivudine
ZDV:	Zidovudine
p-AgSAE:	Silver solid amalgam electrode with polished surface
m-AgSAE:	Surface modified by mercury meniscus
RSD:	Relative standard deviation
LOD:	Detection limit
LOQ:	Quantitation limit
MEKC:	Micellar electrokinetic chromatography
NRTIs:	Nucleoside reverse transcriptase inhibitors
NtRTIs:	Nucleotide reverse transcriptase inhibitors
NNRTIs:	Nonnucleoside reverse transcriptase inhibitors
PIs:	Protease inhibitors
INIs:	Integrase inhibitors
PGE:	Pencil graphite electrode
CYP3A4:	Cytochrome P450-3A4
GCE:	Glassy carbon electrode
BDDE:	Boron-doped diamond electrode
ED:	Electrochemical detection
CAdSV:	Cathodic adsorptive stripping voltammetry
CZE:	Capillary zone electrophoresis.

References

- [1] E. De Clercq, "Anti-HIV drugs: 25 compounds approved within 25 years after the discovery of HIV," *International Journal of Antimicrobial Agents*, vol. 33, no. 4, pp. 307–320, 2009.
- [2] J. E. Gallant, "Initial therapy of HIV infection," *Journal of Clinical Virology*, vol. 25, no. 3, pp. 317–333, 2002.
- [3] B. G. Kalzung, S. B. Masters, and A. J. Trevor, Eds., *Basic & Clinical Pharmacology*, McGraw Hill Medical, New York, NY, USA, 11th edition, 2010.
- [4] M. R. Sadaie, R. Mayner, and J. Doniger, "A novel approach to develop anti-HIV drugs: adapting non-nucleoside anticancer chemotherapeutics," *Antiviral Research*, vol. 61, no. 1, pp. 1–18, 2004.
- [5] D. J. Back, S. H. Khoo, S. E. Gibbons, H. Reynolds, J. F. Tjia, and C. Merry, "Therapeutic drug monitoring of anti-HIV drugs," *International Congress Series*, vol. 1220, pp. 145–160, 2001.
- [6] X. Tan, C. K. Chu, and F. D. Boudinot, "Development and optimization of anti-HIV nucleoside analogs and prodrugs: a review of their cellular pharmacology, structure-activity relationships and pharmacokinetics," *Advanced Drug Delivery Reviews*, vol. 39, no. 1–3, pp. 117–151, 1999.
- [7] P. T. Kissinger and W. R. Heineman, Eds., *Laboratory Techniques in Electroanalytical Chemistry*, Marcel Dekker, New York, NY, USA, 2nd edition, 1996.
- [8] J. Wang, *Analytical Electrochemistry*, Wiley-VCH, New York, NY, USA, 2000.
- [9] M. R. Smyth and J. G. Vos, *Analytical Voltammetry*, vol. XXVII, Elsevier Science, Amsterdam, The Netherlands, 1992.
- [10] J. P. Hart, Ed., *Electroanalysis of Biologically Important Compounds*, Ellis Harwood, New York, NY, USA, 1990.

- [11] R. Kellner, J. M. Mermet, M. Otto, M. Valcarcel, and H. M. Widmer, Eds., *Analytical Chemistry: A Modern Approach to Analytical Science*, Wiley-VCH, Weinheim, Germany, 2nd edition, 2004.
- [12] J. Wang, Ed., *Electroanalytical Techniques in Clinical Chemistry and Laboratory Medicine*, Wiley-VCH, New York, NY, USA, 1988.
- [13] D. K. Gosser Jr., Ed., *Cyclic Voltammetry: Simulation and Analysis of Reaction Mechanism*, Wiley-VCH, New York, NY, USA, 1993.
- [14] G. Christian, Ed., *Analytical Chemistry*, John Wiley & Sons, Hoboken, NJ, USA, 6th edition, 2004.
- [15] B. Uslu and S. A. Ozkan, "Solid electrodes in electroanalytical chemistry: present applications and prospects for high throughput screening of drug compounds," *Combinatorial Chemistry and High Throughput Screening*, vol. 10, no. 7, pp. 495–513, 2007.
- [16] S. A. Özkan, B. Uslu, and H. Y. Aboul-Enein, "Analysis of pharmaceuticals and biological fluids using modern electroanalytical techniques," *Critical Reviews in Analytical Chemistry*, vol. 33, no. 3, pp. 155–181, 2003.
- [17] B. Uslu and S. A. Ozkan, "Electroanalytical application of carbon based electrodes to the pharmaceuticals," *Analytical Letters*, vol. 40, no. 5, pp. 817–853, 2007.
- [18] S. C. Sweetman, Ed., *Martindale the Complete Drug Reference*, Pharmaceutical Press, 35th edition, 2007.
- [19] K. D. Sanbar, Ed., *Physicians' Desk Reference (PDR)*, Thomson PDR, Montvale, NJ, USA, 61st edition, 2007.
- [20] B. Dogan-Topal, B. Uslu, and S. A. Ozkan, "Voltammetric studies on the HIV-1 inhibitory drug Efavirenz: the interaction between dsDNA and drug using electrochemical DNA biosensor and adsorptive stripping voltammetric determination on disposable pencil graphite electrode," *Biosensors and Bioelectronics*, vol. 24, no. 8, pp. 2358–2364, 2009.
- [21] B. Uslu and S. A. Özkan, "Anodic voltammetry of abacavir and its determination in pharmaceuticals and biological fluids," *Electrochimica Acta*, vol. 49, no. 25, pp. 4321–4329, 2004.
- [22] B. Dogan, B. Uslu, S. A. Ozkan, and P. Zuman, "Electrochemical determination of HIV drug abacavir based on its reduction," *Analytical Chemistry*, vol. 80, no. 1, pp. 209–216, 2008.
- [23] J. Weiss, J. Rose, C. H. Storch et al., "Modulation of human BCRP (ABCG2) activity by anti-HIV drugs," *Journal of Antimicrobial Chemotherapy*, vol. 59, no. 2, pp. 238–245, 2007.
- [24] Lexiva® US prescribing information, GlaxoSmithKline, 2008.
- [25] M. Gumustas and S. A. Ozkan, "Electrochemical evaluation and determination of antiretroviral drug fosamprenavir using boron-doped diamond and glassy carbon electrodes," *Analytical and Bioanalytical Chemistry*, vol. 397, no. 1, pp. 189–203, 2010.
- [26] M. Nasr, C. Litterst, and J. McGowan, "Computer-assisted structure-activity correlations of dideoxynucleoside analogs as potential anti-HIV drugs," *Antiviral Research*, vol. 14, no. 3, pp. 125–148, 1990.
- [27] G. D. Morse, M. J. Shelton, and A. M. O'Donnell, "Comparative pharmacokinetics of antiviral nucleoside analogues," *Clinical Pharmacokinetics*, vol. 24, no. 2, pp. 101–123, 1993.
- [28] K. I. Ozoemena, R. I. Stefan-von Stoden, and T. Nyokong, "Metallophthalocyanina based carbon paste electrodes for the determination of 2'-3'-dideoxyinosine," *Electroanalysis*, vol. 21, pp. 1651–1654, 2009.
- [29] N. Erk, "Voltammetric behavior of indinavir and determination in pharmaceutical dosage forms," *Analytical Letters*, vol. 37, no. 1, pp. 47–63, 2004.
- [30] B. Dogan, D. Canbaz, S. A. Ozkan, and B. Uslu, "Electrochemical methods for determination of the protease inhibitor indinavir sulfate in pharmaceuticals and human serum," *Pharmazie*, vol. 61, no. 5, pp. 409–413, 2006.
- [31] A. Ignaszak, N. Hendricks, T. Waryo et al., "Novel therapeutic biosensor for indinavir—a protease inhibitor antiretroviral drug," *Journal of Pharmaceutical and Biomedical Analysis*, vol. 49, no. 2, pp. 498–501, 2009.
- [32] M. R. Fizzano, L. Valvo, M. L. Dupuis, V. Mennella, and M. Cianfriglia, "LC determination of Indinavir in biological matrices with electrochemical detection," *Journal of Pharmaceutical and Biomedical Analysis*, vol. 22, no. 2, pp. 307–314, 2000.
- [33] PDR®, Electronic Library, Thomson Medical Economics, Mantua, NJ, USA, 2003.
- [34] B. Dogan, B. Uslu, S. Suzen, and S. A. Ozkan, "Electrochemical evaluation of nucleoside analogue lamivudine in pharmaceutical dosage forms and human serum," *Electroanalysis*, vol. 17, no. 20, pp. 1886–1894, 2005.
- [35] R. Jain, N. Jadon, and K. Radhapyari, "Cathodic adsorptive stripping voltammetric studies on lamivudine: an antiretroviral drug," *Journal of Colloid and Interface Science*, vol. 313, no. 1, pp. 254–260, 2007.
- [36] G. C. Barone, H. B. Halsall, and W. R. Heineman, "Electrochemistry of azidothymidine," *Analytica Chimica Acta*, vol. 248, no. 2, pp. 399–407, 1991.
- [37] L. Trnková, R. Kizek, and J. Vacek, "Square wave and elimination voltammetric analysis of azidothymidine in the presence of oligonucleotides and chromosomal DNA," *Bioelectrochemistry*, vol. 63, no. 1-2, pp. 31–36, 2004.
- [38] J. Vacek, Z. Andrysík, L. Trnková, and R. Kizek, "Determination of azidothymidine—an antiproliferative and virostatic drug by square-wave voltammetry," *Electroanalysis*, vol. 16, no. 3, pp. 224–230, 2004.
- [39] K. Pecková, T. Navrátil, B. Yosypchuk, J. C. Moreira, K. C. Leandro, and J. Bareka Jiri, "Voltammetric determination of azidothymidine using silver solid amalgam electrodes," *Electroanalysis*, vol. 21, no. 15, pp. 1750–1757, 2009.
- [40] K. C. Leandro, J. C. Moreira, and P. A. M. Farias, "Determination of zidovudine in pharmaceuticals by differential pulse voltammetry," *Analytical Letters*, vol. 43, no. 12, pp. 1951–1957, 2010.
- [41] K. A. Mahmoud and J. H. T. Luong, "Impedance method for detecting HIV-1 protease and screening for its inhibitors using ferrocene-peptide conjugate/Au nanoparticle/single-walled carbon nanotube modified electrode," *Analytical Chemistry*, vol. 80, no. 18, pp. 7056–7062, 2008.
- [42] B. Fan and J. T. Stewart, "Determination of lamivudine/didanosine/saquinavir in human serum using capillary zone electrophoresis," *Journal of Liquid Chromatography and Related Technologies*, vol. 25, no. 2, pp. 241–249, 2002.
- [43] B. Fan and J. T. Stewart, "Determination of stavudine/didanosine/saquinavir and stavudine/didanosine/efavirenz in human serum by micellar electrokinetic chromatography (MEKC)," *Journal of Liquid Chromatography and Related Technologies*, vol. 25, no. 6, pp. 937–947, 2002.
- [44] B. Fan and J. T. Stewart, "Determinations of zidovudine/didanosine/nevirapine and zidovudine/didanosine/ritonavir in human serum by micellar electrokinetic chromatography," *Journal of Pharmaceutical and Biomedical Analysis*, vol. 30, no. 4, pp. 955–960, 2002.
- [45] ICH Harmonised Tripartite Guideline, ICH Steering Committee, November 1996, Inc. November 2005.

- [46] B. Uslu and S. A. Ozkan, "Solid electrodes in electroanalytical chemistry: present applications and prospects for high throughput screening of drug compounds," *Combinatorial Chemistry and High Throughput Screening*, vol. 10, no. 7, pp. 495–513, 2007.
- [47] B. Bozal, B. Doğan-Topal, B. Uslu, S. A. Özkan, and H. Y. Aboul-Enein, "Quantitative analysis of irbesartan in pharmaceuticals and human biological fluids by voltammetry," *Analytical Letters*, vol. 42, no. 14, pp. 2322–2338, 2009.
- [48] B. Dogan-Topal, B. Bozal, B. Tolga Demircigil, B. Uslu, and S. A. Ozkan, "Electroanalytical studies and simultaneous determination of amlodipine besylate and atorvastatin calcium in binary mixtures using first derivative of the ratio-voltammetric methods," *Electroanalysis*, vol. 21, no. 22, pp. 2427–2439, 2009.
- [49] B. Uslu and D. Canbaz, "Anodic voltammetry of zolmitriptan at boron-doped diamond electrode and its analytical applications," *Pharmazie*, vol. 65, no. 4, pp. 245–250, 2010.
- [50] D. Kul, M. Gumustas, B. Uslu, and S. A. Ozkan, "Electroanalytical characteristics of antipsychotic drug ziprasidone and its determination in pharmaceuticals and serum samples on solid electrodes," *Talanta*, vol. 82, pp. 286–295, 2010.
- [51] Y. Altun, B. Uslu, and S. A. Ozkan, "Electroanalytical characteristics of lercanidipine and its voltammetric determination in pharmaceuticals and human serum on boron-doped diamond electrode," *Analytical Letters*, vol. 43, no. 12, pp. 1958–1975, 2010.
- [52] B. Bozal and B. Uslu, "Applications of carbon based electrodes for voltammetric determination of lornoxicam in pharmaceutical dosage form and human serum," *Combinatorial Chemistry and High Throughput Screening*, vol. 13, no. 7, pp. 599–609, 2010.

Review Article

New Developments in Electrochemical Sensors Based on Poly(3,4-ethylenedioxothiophene)- Modified Electrodes

Stelian Lupu

Department of Analytical Chemistry and Instrumental Analysis, Faculty of Applied Chemistry and Materials Science,
University Politehnica of Bucharest, Polizu 1-7, 011061 Bucharest, Romania

Correspondence should be addressed to Stelian Lupu, stelianl@yahoo.com

Received 2 February 2011; Accepted 14 March 2011

Academic Editor: Bengi Uslu

Copyright © 2011 Stelian Lupu. This is an open access article distributed under the Creative Commons Attribution License, which permits unrestricted use, distribution, and reproduction in any medium, provided the original work is properly cited.

There is a growing demand for continuous, fast, selective, and sensitive monitoring of key analytes and parameters in the control of diseases and health monitoring, foods quality and safety, and quality of the environment. Sensors based on electrochemical transducers represent very promising tools in this context. Conducting polymers (CPs) have drawn considerable interest in recent years because of their potential applications in different fields such as in sensors, electrochemical displays, and in catalysis. Among the organic conducting polymers, poly(3,4-ethylenedioxothiophene) (PEDOT) and its derivatives have attracted particular interest due to their high stability and high conductivity. This paper summarizes mainly the recent developments in the use of PEDOT-based composite materials in electrochemical sensors.

1. Introduction

The improvement of life quality is one of the most important objectives of global research efforts pursued by the international research community. It is a common fact that the quality of life is closely linked to the control of diseases and health monitoring, foods quality and safety, and quality of the environment. A continuous, fast, selective, and sensitive monitoring of key analytes and parameters is required in the above-mentioned fields. Sensors based on electrochemical transducers represent very promising tools in this context. The integration of technological developments, and in particular of a new generation of smart and composite materials interacting with their surrounding, is bringing huge potential for the development of new sensors based on chemically modified electrodes (CMEs), allowing a greater security and safety of the peoples.

2. Electrochemical Transducers

An important application of the CMEs lies in the design of electrochemical (bio)sensors. A (bio)sensor is a device consisting of a (bio)active substance, such as an inorganic or polymeric catalyst, an enzyme, an antibody, a tissue or a microorganism, which can specifically recognize species of

interest, in intimate contact with a transducer. The transducer converts the (bio)chemical signal into an electronic signal. Many forms of transducers have been developed, such as potentiometric and amperometric electrodes, optoelectronic detectors, field-effect transistors, and thermistors. Among these, the electrochemical devices (potentiometric, amperometric, voltammetric, and impedance transducers) have been widely studied. These electrochemical transducers use the powerful features of the corresponding electrochemical methods, for example, potentiometry, amperometry, cyclic voltammetry (CV), and electrochemical impedance spectroscopy (EIS). In the case of potentiometric sensors a local equilibrium is set up at the sensor interface, and the electrode potential is measured. For amperometric sensors, a potential is applied to drive the electrode reaction, and the resulting current is measured. In cyclic voltammetry, the electrode potential is scanned linearly using a triangular potential waveform, and the current is measured. CV provides useful information on the thermodynamics of redox processes, on the kinetics of heterogeneous electron transfer reactions, and on coupled chemical reactions. The measured current is used for the quantification of the analyte. EIS is a nondestructive steady-state technique that provides quantitative information about the relaxation phenomena over a wide range of alternative current (AC) frequencies and the

resistive and capacitive properties of materials. The equivalent circuits fitted to the impedance curves are useful in the characterization of the electrochemical systems. EIS is currently used to investigate the charge transport and adsorption processes in various types of electrochemical sensors.

During the last two decades, the area of electrochemical sensors has greatly benefited from the development of nanotechnology, which has enabled the production of microelectrodes (MEs). MEs have critical dimensions less than the scale of a diffusion layer, and they have enabled the measurements of fast electron transfer kinetics into previously inaccessible domains of time, space, and media [1–3]. MEs can operate at an ionic strength level comparable with that present in real samples. The most used MEs geometries are disk, sphere, hemisphere, and band shapes. MEs can be also wired in parallel with each microelectrode acting diffusional independent, resulting in a signal which is typically thousands of times larger. This device, called array, can contain several MEs in both regular and random distributions [3–8]. The MEs arrays have been proved to be useful in electroanalysis [9]. Recently, a unique design with an arrangement of interdigitated array electrodes (IDEs) has received a lot of attention. In this design, at least one generator electrode is placed closed to a collector electrode. More interesting are arrangements consisting in several generator electrodes placed side by side with collector electrodes in an interdigitated manner. The operation mode of IDEs is based on the generation of electroactive species by a potential excitation at the generator electrodes followed by the diffusion of these species across the thin-layer gap, due to the concentration gradient, to the collector electrodes where they react electrochemically. The reactant species at the collector electrodes can diffuse back to the generator electrodes. This operation mode is called redox cycling and makes the measured currents at both the generator and collector electrodes extremely high. The very small distance between generator and collector electrodes allows a very high percentage of the generated species to be collected at the collector electrodes. Another important feature of these devices is the steady-state current that can be achieved by holding the collector electrodes at a fixed potential while sweeping the potential at the generator electrodes. In the case of a band gap width in the scale of nanometers, it is expected that the device will behave as an electrochemical sensor having the characteristics of both nanoelectrodes and interdigitated array electrodes. The IDEs can detect in this way ultratrace amounts of analytes within a small space [10] and also unstable electrochemical intermediates [11]. Several papers dealing with the characteristic of bare, unmodified, IDEs have appeared in the last decade [12–14]. These studies have provided information on the effect of the electrode size and spacing on the current collection efficiency and redox cycling.

3. Conducting Polymer-Modified Electrodes

The use of electroactive polymers represents an important development in the preparation of modified electrodes. Electroactive polymers present several advantages over monomolecular layers, for example, (i) the electrochemical

responses for polymer films are more clearly observed than those of immobilized monomolecular layers; (ii) multilayer films of polymers can undergo a larger number of oxidation state turnovers than monolayer films, which implies that the redox sites in multilayer films have an enhanced stability; (iii) the presence on the electrode surface of a large number of redox mediator molecules yields a high reaction rate between mediator substrate, resulting in an enhancement of the electrocatalytic efficiency of the modified surface; (iv) the polymer films can incorporate different electroactive species in order to obtain well-defined microstructures on electrode surfaces. Thanks to these advantages and since the electroactive polymers are technically easier to attach at the electrode surfaces than covalently bonded reagents are, polymeric coating has become a popular technique of electrode modification.

The electroactive polymers may be classified into *redox polymers*, *electronically conducting polymers*, and *ion exchange polymers*.

Conducting polymers (CPs) conduct electricity via delocalized metal-like band structures. The interest in CPs has started in the late 1970s, and since then much attention has been devoted to the preparation, characterization, and application of these polymers [15–17]. These polymeric films exhibit good adhesion and electrical contact to the electrode surface. Thin films of CPs deposited on the electrode surface can be electrochemically cycled between the neutral, for example, the insulating state, and the oxidized, for example, the conducting state. Also, thicker films of CPs can be obtained in the oxidized, conducting state and then can be removed from the electrode surface to yield free-standing, electrically conducting films. The oxidation of the insulating polymer is referred to as a “doping” process by analogy with the doping of inorganic semiconductors. The neutral polymer can be converted into an ionic complex that consists of a polymeric cation (or anion) and a counterion, which is the reduced form of the oxidizing agent (or the oxidized form of the reducing agent). The use of an oxidizing agent corresponds to a p-type doping process and that of a reducing agent to an n-type doping process. In the case of oxidation, for example, removal of an electron from the polymeric chain, a so-called “ polaron ” is formed [18]. The polaron is a radical ion (spin 1/2) associated with a lattice distortion. When a second electron is removed from the polymer chain, a so-called “ bipolaron ” is formed. A bipolaron is defined as a pair of charge (spinless) associated with a strong local lattice distortion. This class of polymers includes polypyrrole, polyaniline, polythiophene, and relevant derivatives.

The functioning of a large part of CMEs is based on electrocatalysis. The electrooxidation or reduction of an analyte at a bare electrode surface occurs at much more positive or negative potentials than expected on the basis of thermodynamics, respectively, which means that an overpotential is required by the electrode reaction. In Figure 1 the basic idea of decreasing or eliminating this overpotential by an immobilized mediator catalyst is depicted. The analyte (substrate) diffuses from the bulk of the solution to the electrode surface, where the oxidized form of the mediator (M_{ox}) oxidizes it by a purely chemical reaction. The electrode

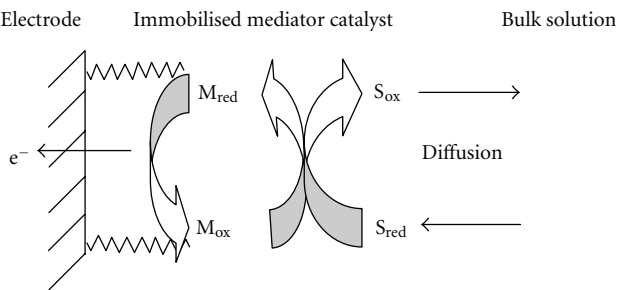


FIGURE 1: Electrocatalysis at modified electrode. M: mediator, S: substrate.

is maintained at a potential positive enough to assure that the oxidized form M_{ox} is the stable state of the mediator. Then, the reduced form M_{red} is rapidly reoxidized to the active form M_{ox} . By this approach, the oxidation of the substrate takes place at a potential that is between the thermodynamic value of the substrate oxidation and that of the redox mediator.

The decrease of the electrode potential at which oxidation or reduction actually occurs may improve the analytical performance. By decreasing the detection potentials, possible improved detection limits and selectivity may be obtained because of the lower noise level. Furthermore, electrode processes that occur at potentials near those of solvent breakdown, or even beyond this limit, can be shifted to a useful potential value.

3.1. PEDOT-Inorganic Composite-Modified Electrodes. In recent years, a considerable progress has been made with developing modified electrodes, for instance, based on redox and conducting polymers [19, 20]. The electrode surface can be deliberately modified by different procedures, such as adsorption, electropolymerization, chemical bonding, and electropolymerization of various chemical species. Modification of the electrode surface can also be an important aid in obtaining greater selectivity and sensibility. Conducting polymers (CPs) have drawn considerable interest in recent years because of their potential applications in different fields such as in sensors, electrochemical displays, and in catalysis [16, 17]. Among the organic conducting polymers, poly(thiophene) and its derivatives, such as poly(3,4-ethylenedioxythiophene), (PEDOT), have attracted particular interest because these compounds appeared to be the most stable organic conducting polymers currently available [21–28]. Conducting polymers can be deposited as dense modifying layers on common electrode substrates, which is of importance to the development of many technologies, including electrochemical sensors technology. Conducting organic polymers also constitute a category of materials showing suitable reversible redox chemistry. On the other hand, considerable interest has been also devoted to the preparation and characterisation of polynuclear transition metal hexacyanoferrates by virtue of their characteristics which include electrochromic properties [29], ability to mediate redox reactions [30–33]. The transition metal hexacyanoferrates represent an important class of insoluble mixed valence compounds. A large number of inorganic films have

been prepared both chemically and electrochemically onto various electrode substrates. However, their low stability, especially in alkaline solutions, remains a central problem for the application of any metal hexacyanoferrate film-modified-electrode in electroanalysis. The extraordinary properties of both CP and metal hexacyanoferrates have been exploited in the preparation of electrodes modified with bilayer structures consisting of conducting polymers and iron(III) hexacyanoferrate (Prussian blue, PB) [34–41]. The presence of organic conducting polymers in the bilayer films increases the stability of PB, resulting in enhanced electrochemical responses. Prussian Blue (iron(III)hexacyanoferrate(II), PB) has been extensively studied for modification of conducting polymers [35, 42–45]. The use of PEDOT and PB for the preparation of the composite materials is based on the appealing properties of each component, such as the excellent stability of the PEDOT layer in aqueous solution and its doped state [46–49], and the electrocatalytic activity of PB [50–52]. It is important to note that, in the potential region where the composite materials are electrochemically active, the PEDOT organic component is in its conducting state, while the PB inorganic component displays its good electrocatalytic activity. As a consequence, a synergistic effect is obtained, and the composite material displays new electrochemical properties. These composite coatings are prepared by a two-step method. In the first step, the organic layer is deposited through the electrochemical polymerization of the corresponding monomer in the presence of the ferric hexacyanoferrates anions. In the second step, the *in situ* formation of PB within the PEDOT matrix is achieved via potentiodynamic methods in Fe^{3+} containing aqueous solution. Both forms of PB, for example, soluble and insoluble, can be deposited by this procedure [53, 54]. Another approach consists in the use of a mixture of ferric and ferrous hexacyanoferrates [55–59] or iron (III) chloride and ferricyanide [60]. These composite materials showed appealing properties for various applications in capacitors and electrochemical sensors. The incorporation of ferric hexacyanoferrates within the PEDOT matrix was also investigated in respect of the development of new electrochemical sensors [61–64].

3.2. PEDOT-Metal-Nanoparticles Composite-Modified Electrodes. Metal nanoparticles-based composite materials have attracted a great deal of interest due to their unique electrochemical, optical, and catalytic properties and their potential use in electrochemical sensors and biosensors [65–72]. Noble metal nanoparticles (NPs) were incorporated into conducting polymers using various preparation procedures in order to improve their analytical performances [73]. To this purpose, chemical and electrochemical methods have been developed for *ex situ* or *in situ* NPs preparation. The incorporation of NPs in conducting polymers has been achieved by self-assembly of chemically synthesized NPs onto self-assembled monolayers (SAMs) [74], electrochemical deposition of chemically pre-synthesized NPs onto previously synthesized polymer films [75], electrochemical polymerization of the appropriate monomer in the presence of chemically pre-synthesized NPs [73], and layer-by-layer intercalation of the inorganic NPs into conducting polymer

composite coatings [67, 76]. In this area, PEDOT has been quite extensively studied for NPs incorporation into polymeric films [77, 78], mainly due to its excellent stability and the possibility to prepare the corresponding PEDOT polymer matrix through electrochemical polymerization of the 3,4-ethylenedioxythiophene (EDOT) monomer in aqueous solution [79–84]. Another approach consists in the use of ultrasounds for NPs preparation [85]. This new preparation procedure resulted in homogeneous size distribution within the range 5–17 nm. The use of ultrasounds in the electropolymerisation of conducting polymers on various substrates and the preparation of sonogel-based electrochemical sensors has been also reported [86–92]. Recently, a great deal of interest has been also devoted to the *in situ* preparation of Pt nanoparticles [93–98]. In this case, the *in situ* preparation of Pt nanoparticles has been achieved via electrochemical methods, and in particular potentiostatic deposition at a fixed potential value which is sufficiently negative to assure reduction of the appropriate precursors to metallic states. However, this latter approach for *in situ* electrodeposition of NPs onto conducting polymers layers has not reached yet the full analytical potential being currently under investigation by various research groups.

4. Conducting Polymers-Modified Microelectrode Arrays

Due to the unique features of the microelectrodes arrays, the modification of the surfaces of these devices has been also the subject of several studies. For instance, the generator-collector operation mode has been exploited in the study of the diffusion of electroactive species within a thin film deposited onto the surface of microelectrodes arrays [99–102]. The modification of interdigitated microelectrodes with conducting polymers allowed the preparation of new miniaturized pH electrochemical sensors [103–106]. Other microelectrodes arrays modified with inorganic films [107], organic polymers [108], inorganic-organic composite materials [109], and enzymes [110] were recently reported. Despite the benefits of the microelectrodes arrays, the modification of these devices with composite organic-inorganic materials has not been fully investigated. Based on the electrochemical properties of microelectrodes and interdigitated microelectrodes arrays as well as the selectivity and electrocatalytic activity of coatings consisting of composite organic-inorganic materials, there is a niche topic of research that can be exploited in order to combine these challenging properties for the design of new electrochemical microsensors.

5. Conclusions

The interest in electrochemical sensors based on PEDOT is still growing thanks especially to the new composite materials that have been recently developed. The composite materials are prepared via *in situ* formation of the inorganic component within the conducting polymer coating. New properties induced by the combination of a conducting polymer and a mixed valence compound were reported.

The electrochemical behavior of these composite materials is based mainly on the redox reaction of the inorganic component. The incorporation of noble metal nanoparticles within conducting polymers matrix can improve the analytical performances of the electrochemical sensors and affords the electrochemical detection of analytes that usually are determined by using enzymes-based biosensors. The electrochemical microsensors based on microelectrode arrays can be used in multianalyte electrochemical sensing of biologically active compounds and potential hazardous compounds, which are key analytes for life quality control. It can be sought that the final application of these new electrochemical sensors will be the *in situ* study of real matrices, which implies only minor manipulation of the matrix. Therefore, the applications of these electrochemical microsensors to biomedical, foods, and environmental analysis are very promising in respect of qualitative and quantitative determination of specific analytes of interest, as well as analytes that, for different reasons, are dangerous to health.

Acknowledgment

Financial support from the Romanian Ministry of Education, Research and Youth (Grant no. 2 CEEX 06-1143/25.07.2006) is gratefully acknowledged.

References

- [1] D. E. Williams, *Microelectrodes: Theory and Applications*, M. I. Montenegro, M. A. Queiros and J. L. Daschbach, Eds., Kluwer Academic Publishers, Dordrecht, The Netherlands, 1991.
- [2] R. M. Wightman and D. O. Wipf, *Electroanalytical Chemistry*, vol. 15 of *A. J. Bard*, Ed., Marcel Dekker, New York, NY, USA, 1989.
- [3] C. Amatore, *Physical Electrochemistry: Principles, Methods and Applications*, I. Rubenstein, Ed., Marcel Dekker, New York, NY, USA, 1995.
- [4] S. Fletcher and M. D. Horne, “Random assemblies of microelectrodes (RAM™ electrodes) for electrochemical studies,” *Electrochemistry Communications*, vol. 1, no. 10, pp. 502–512, 1999.
- [5] M. Pagels, C. E. Hall, N. S. Lawrence et al., “All-diamond microelectrode array device,” *Analytical Chemistry*, vol. 77, no. 11, pp. 3705–3708, 2005.
- [6] B. J. Seddon, Y. Shao, and H. H. Girault, “Printed microelectrode array and amperometric sensor for environmental monitoring,” *Electrochimica Acta*, vol. 39, no. 16, pp. 2377–2386, 1994.
- [7] T. J. Davies, S. Ward-Jones, C. E. Banks et al., “The cyclic and linear sweep voltammetry of regular arrays of microdisc electrodes: fitting of experimental data,” *Journal of Electroanalytical Chemistry*, vol. 585, no. 1, pp. 51–62, 2005.
- [8] T. J. Davies and R. G. Compton, “The cyclic and linear sweep voltammetry of regular and random arrays of microdisc electrodes: theory,” *Journal of Electroanalytical Chemistry*, vol. 585, no. 1, pp. 63–82, 2005.
- [9] O. Ordeig, J. Del Campo, F. X. Muñoz, C. E. Banks, and R. G. Compton, “Electroanalysis utilizing amperometric

- microdisk electrode arrays," *Electroanalysis*, vol. 19, no. 19-20, pp. 1973–1986, 2007.
- [10] P. Ugo, L. M. Moretto, and F. Vezzà, "Ionomer-coated electrodes and nanoelectrode ensembles as electrochemical environmental sensors: recent advances and prospects," *ChemPhysChem*, vol. 3, no. 11, pp. 917–925, 2002.
- [11] M. V. Mirkin, H. Yang, and A. J. Bard, "Borohydride oxidation at a gold electrode," *Journal of the Electrochemical Society*, vol. 139, no. 8, pp. 2212–2216, 1992.
- [12] O. Niwa, M. Morita, and H. Tabei, "Electrochemical behavior of reversible redox species at interdigitated array electrodes with different geometries: consideration of redox cycling and collection efficiency," *Analytical Chemistry*, vol. 62, no. 5, pp. 447–452, 1990.
- [13] M. Paeschke, U. Wollenberger, C. Köhler, T. Liseč, U. Schnakenberg, and R. Hintsche, "Properties of interdigital electrode arrays with different geometries," *Analytica Chimica Acta*, vol. 305, no. 1–3, pp. 126–136, 1995.
- [14] K. Ueno, M. Hayashida, J. Y. Ye, and H. Misawa, "Fabrication and electrochemical characterization of interdigitated nanoelectrode arrays," *Electrochemistry Communications*, vol. 7, no. 2, pp. 161–165, 2005.
- [15] R. J. Waltman and J. Bargon, "Electrically conducting polymers: a review of the electropolymerization reaction, of the effects of chemical structure on polymer film properties, and of applications towards technology," *Canadian Journal of Chemistry*, vol. 64, no. 1, pp. 76–95, 1986.
- [16] J. Roncali, "Conjugated poly(thiophenes): synthesis, functionalization, and applications," *Chemical Reviews*, vol. 92, no. 4, pp. 711–738, 1992.
- [17] J. Roncali, "Synthetic principles for bandgap control in linear π -conjugated systems," *Chemical Reviews*, vol. 97, no. 1, pp. 173–205, 1997.
- [18] J. L. Brédas and G. B. Street, "Polarons, bipolarons, and solitons in conducting polymers," *Accounts of Chemical Research*, vol. 18, no. 10, pp. 309–315, 1985.
- [19] R. W. Murray, "Chemically modified electrodes," in *Electroanalytical Chemistry*, A. J. Bard, Ed., vol. 13, Marcel Dekker, New York, NY, USA, 1984.
- [20] R. W. Murray, Ed., *Molecular Design of Electrode Surfaces*, vol. 22, Wiley, New York, NY, USA, 1992.
- [21] M. Dietrich, J. Heinze, G. Heywang, and F. Jonas, "Electrochemical and spectroscopic characterization of polyalkylenedioxothiophenes," *Journal of Electroanalytical Chemistry*, vol. 369, no. 1-2, pp. 87–92, 1994.
- [22] H. Yamato, M. Ohwa, and W. Wernet, "Stability of polypyrrole and poly(3,4-ethylenedioxothiophene) for biosensor application," *Journal of Electroanalytical Chemistry*, vol. 397, no. 1-2, pp. 163–170, 1995.
- [23] D. Iarossi, A. Mucci, L. Schenetti et al., "Polymerization and characterization of 4,4'-Bis(alkylsulfanyl)-2,2'-bithiophenes," *Macromolecules*, vol. 32, no. 5, pp. 1390–1397, 1999.
- [24] B. Ballarin, F. Costanzo, F. Mori et al., "Electropolymerization and characterization of poly[4,4'-bis(butylsulphanyl)-2,2'-bithiophene]," *Electrochimica Acta*, vol. 46, no. 6, pp. 881–889, 2001.
- [25] B. Ballarin, R. Seeber, D. Tonelli et al., "Electrosynthesis and characterization of alkylester-substituted polythiophenes," *Synthetic Metals*, vol. 88, no. 1, pp. 7–13, 1997.
- [26] B. Ballarin, R. Seeber, L. Tassi, and D. Tonelli, "Electrochemical synthesis and characterisation of polythiophene conducting polymers functionalised by metal-containing porphyrin residue," *Synthetic Metals*, vol. 114, no. 3, pp. 279–285, 2000.
- [27] S. Lupu, A. Mucci, L. Pigani, R. Seeber, and C. Zanardi, "Polythiophene derivative conducting polymer modified electrodes and microelectrodes for determination of ascorbic acid. Effect of possible interferents," *Electroanalysis*, vol. 14, no. 7-8, pp. 519–525, 2002.
- [28] S. Lupu, F. Parenti, L. Pigani, R. Seeber, and C. Zanardi, "Differential pulse techniques on modified conventional-size and microelectrodes. Electroactivity of poly[4,4'-bis(butylsulfanyl)-2,2'-bithiophene] coating towards dopamine and ascorbic acid oxidation," *Electroanalysis*, vol. 15, no. 8, pp. 715–725, 2003.
- [29] P. J. Kulesza, M. A. Malik, M. Berrettoni et al., "Electrochemical charging, counteraction accommodation, and spectrochemical identity of microcrystalline solid cobalt hexacyanoferrate," *Journal of Physical Chemistry B*, vol. 102, no. 11, pp. 1870–1876, 1998.
- [30] D. M. Zhou, H. X. Ju, and H. Y. Chen, "Catalytic oxidation of dopamine at a microdisk platinum electrode modified by electrodeposition of nickel hexacyanoferrate and Nafion®," *Journal of Electroanalytical Chemistry*, vol. 408, no. 1-2, pp. 219–223, 1996.
- [31] A. A. Karyakin, E. E. Karyakina, and LO. Gorton, "On the mechanism of H_2O_2 reduction at Prussian Blue modified electrodes," *Electrochemistry Communications*, vol. 1, no. 2, pp. 78–82, 1999.
- [32] N. Totir, S. Lupu, E. M. Ungureanu, and N. Iftimie, "Electrochemical behaviour of dopamine at a Prussian Blue modified electrode," *Revista de Chimie, (Bucuresti) (English edition)*, vol. 2, no. 1-2, pp. 23–27, 2001.
- [33] N. Totir, S. Lupu, E. M. Ungureanu, M. Giubelan, and A. řtefanescu, "Electrochemical behaviour of ascorbic acid on Prussian Blue modified electrodes," *Revue Roumaine de Chimie*, vol. 46, no. 10, pp. 1091–1096, 2001.
- [34] K. Ogura, N. Endo, M. Nakayama, and H. Ootsuka, "Mediated activation and electroreduction of CO on modified electrodes with conducting polymer and inorganic conductor films," *Journal of the Electrochemical Society*, vol. 142, no. 12, pp. 4026–4032, 1995.
- [35] S. Lupu, C. Mihailciuc, L. Pigani, R. Seeber, N. Totir, and C. Zanardi, "Electrochemical preparation and characterisation of bilayer films composed by Prussian Blue and conducting polymer," *Electrochemistry Communications*, vol. 4, no. 10, pp. 753–758, 2002.
- [36] S. Lupu, "Electrochemical detection of ascorbic acid and dopamine using poly-(3,4-ethylenedioxothiophene)/prussian blue films on platinum," *Revue Roumaine de Chimie*, vol. 50, no. 3, pp. 213–217, 2005.
- [37] S. Lupu, "Electrochemical detection of ascorbic acid using prussian blue/poly-(3,4-ethylenedioxothiophene) films on platinum," *Revue Roumaine de Chimie*, vol. 50, no. 3, pp. 207–211, 2005.
- [38] S. Lupu, "Electrochemical study of prussian blue/poly-(3,4-ethylenedioxothiophene) composite films," *Revue Roumaine de Chimie*, vol. 50, no. 3, pp. 201–205, 2005.
- [39] S. Lupu, C. Lete, M. Marin, and N. Totir, "Electrochemistry of metal hexacyanoferrates and conducting polymers bilayer structures deposited on conventional size electrodes and ultramicroelectrodes. I. conventional size modified electrodes," *Revue Roumaine de Chimie*, vol. 53, no. 7, pp. 539–546, 2008.
- [40] S. Lupu, C. Lete, M. Marin, and N. Totir, "Electrochemistry of metal hexacyanoferrates and conducting polymers bilayer

- structures deposited on conventional size electrodes and ultramicroelectrodes. II. modified ultramicroelectrodes," *Revue Roumaine de Chimie*, vol. 53, no. 7, pp. 547–552, 2008.
- [41] S. Lupu, C. Lete, M. Marin, N. Totir, and P. C. Balaure, "Electrochemical sensors based on platinum electrodes modified with hybrid inorganic-organic coatings for determination of 4-nitrophenol and dopamine," *Electro-chimica Acta*, vol. 54, no. 7, pp. 1932–1938, 2009.
- [42] M. Nakayama, M. Iino, and K. Ogura, "In situ FTIR studies on Prussian blue (PB)-, polyaniline (PAn)- and inner PB—outer PAn film-modified electrodes," *Journal of Electroanalytical Chemistry*, vol. 440, no. 1-2, pp. 125–130, 1997.
- [43] R. Koncki and O. S. Wolfbeis, "Composite films of Prussian Blue and N-substituted polypyrroles: fabrication and application to optical determination of pH," *Analytical Chemistry*, vol. 70, no. 13, pp. 2544–2550, 1998.
- [44] P. J. Kulesza, K. Miecznikowski, M. A. Malik et al., "Electrochemical preparation and characterization of hybrid films composed of Prussian blue type metal hexacyanoferrate and conducting polymer," *Electrochimica Acta*, vol. 46, no. 26-27, pp. 4065–4073, 2001.
- [45] A. Lisowska-Oleksiak, A. P. Nowak, and V. Jasulaitiene, "Poly(3,4-ethylenedioxythiophene)-Prussian Blue hybrid material: evidence of direct chemical interaction between PB and pEDOT," *Electrochemistry Communications*, vol. 8, no. 1, pp. 107–112, 2006.
- [46] S. Zhang, J. Hou, R. Zhang, J. Xu, G. Nie, and S. Pu, "Electrochemical polymerization of 3,4-ethylenedioxythiophene in aqueous solution containing N-dodecyl- β -d-maltoside," *European Polymer Journal*, vol. 42, no. 1, pp. 149–160, 2006.
- [47] C. Kvarnström, H. Neugebauer, S. Blomquist, H. J. Ahonen, J. Kankare, and A. Ivaska, "In situ spectroelectrochemical characterization of poly(3,4-ethylenedioxythiophene)," *Electrochimica Acta*, vol. 44, no. 16, pp. 2739–2750, 1999.
- [48] L. Adamczyk, P. J. Kulesza, K. Miecznikowski, B. Palys, M. Chojak, and D. Krawczyk, "Effective charge transport in poly(3,4-ethylenedioxythiophene) based hybrid films containing polyoxometallate redox centers," *Journal of the Electrochemical Society*, vol. 152, no. 3, pp. E98–E103, 2005.
- [49] N. Rozlosnik, "New directions in medical biosensors employing poly(3,4-ethylenedioxy thiophene) derivative-based electrodes," *Analytical and Bioanalytical Chemistry*, vol. 395, no. 3, pp. 637–645, 2009.
- [50] F. Li and S. Dong, "The electrocatalytic oxidation of ascorbic acid on prussian blue film modified electrodes," *Electrochimica Acta*, vol. 32, no. 10, pp. 1511–1513, 1987.
- [51] R. Koncki, "Chemical sensors and biosensors based on Prussian blues," *Critical Reviews in Analytical Chemistry*, vol. 32, no. 1, pp. 79–96, 2002.
- [52] F. Ricci and G. Palleschi, "Sensor and biosensor preparation, optimisation and applications of Prussian Blue modified electrodes," *Biosensors and Bioelectronics*, vol. 21, no. 3, pp. 389–407, 2005.
- [53] S. Lupu, "In situ electrochemical preparation and characterization of PEDOT-Prussian blue composite materials," *Synthetic Metals*, vol. 161, no. 5-6, pp. 384–390, 2011.
- [54] S. Lupu and N. Totir, "The optimization of the electrochemical preparation of pedot-prussian blue hybrid electrode material and application in electrochemical sensors," *Collection of Czechoslovak Chemical Communications*, vol. 75, no. 8, pp. 835–851, 2010.
- [55] A. Lisowska-Oleksiak and A. P. Nowak, "Metal hexacyanoferrate network synthesized inside polymer matrix for electrochemical capacitors," *Journal of Power Sources*, vol. 173, no. 2, pp. 829–836, 2007.
- [56] A. Lisowska-Oleksiak and A. P. Nowak, "Impedance spectroscopy studies on hybrid materials consisting of poly(3,4-ethylenedioxythiophene) and iron, cobalt and nickel hexacyanoferrate," *Solid State Ionics*, vol. 179, no. 1–6, pp. 72–78, 2008.
- [57] M. Wilamowska and A. Lisowska-Oleksiak, "Hybrid electrodes composed of electroactive polymer and metal hexacyanoferrates in aprotic electrolytes," *Journal of Power Sources*, vol. 194, no. 1, pp. 112–117, 2009.
- [58] A. P. Nowak, M. Wilamowska, and A. Lisowska-Oleksiak, "Spectroelectrochemical characteristics of poly(3,4-ethylenedioxythiophene)/ iron hexacyanoferrate film-modified electrodes," *Journal of Solid State Electrochemistry*, vol. 14, no. 2, pp. 263–270, 2010.
- [59] A. Lisowska-Oleksiak, A. P. Nowak, M. Wilamowska, M. Sikora, W. Szczera, and CZ. Kapusta, "Ex situ XANES, XPS and Raman studies of poly(3,4-ethylenedioxythiophene) modified by iron hexacyanoferrate," *Synthetic Metals*, vol. 160, no. 11-12, pp. 1234–1240, 2010.
- [60] V. Noël, H. Randriamahazaka, and C. Chevrot, "Composite films of iron(III) hexacyanoferrate and poly(3,4-ethylenedioxythiophene): electrosynthesis and properties," *Journal of Electroanalytical Chemistry*, vol. 489, no. 1, pp. 46–54, 2000.
- [61] V. S. Vasantha and S. M. Chen, "Electrochemical preparation and electrocatalytic properties of PEDOT/ferricyanide film-modified electrodes," *Electrochimica Acta*, vol. 51, no. 2, pp. 347–355, 2005.
- [62] A. I. Melato, L. M. Abrantes, and A. M. Botelho do Rego, "Fe(CN) incorporation on Poly(3,4-ethylenedioxythiophene) films: preparation and X-ray Photoelectron Spectroscopy characterization of the modified electrodes," *Thin Solid Films*, vol. 518, no. 8, pp. 1947–1952, 2010.
- [63] A. Michalska, A. Gałuszkiewicz, M. Ogonowska, M. Ocypa, and K. MakSYMiuK, "PEDOT films: multifunctional membranes for electrochemical ion sensing," *Journal of Solid State Electrochemistry*, vol. 8, no. 6, pp. 381–389, 2004.
- [64] M. Ocypa, A. Michalska, and K. MakSYMiuK, "Accumulation of Cu(II) cations in poly(3,4-ethylenedioxythiophene) films doped by hexacyanoferrate anions and its application in Cu²⁺- selective electrodes with PVC based membranes," *Electrochimica Acta*, vol. 51, no. 11, pp. 2298–2305, 2006.
- [65] S. Guo and S. Dong, "Biomolecule-nanoparticle hybrids for electrochemical biosensors," *Trends in Analytical Chemistry*, vol. 28, no. 1, pp. 96–109, 2009.
- [66] I. Willner, B. Willner, and E. Katz, "Biomolecule-nanoparticle hybrid systems for bioelectronic applications," *Bioelectrochemistry*, vol. 70, no. 1, pp. 2–11, 2007.
- [67] C. Zanardi, F. Terzi, B. Zanfragnini et al., "Effective catalytic electrode system based on polyviologen and Au nanoparticles multilayer," *Sensors and Actuators, B*, vol. 144, no. 1, pp. 92–98, 2010.
- [68] S. Xu, G. Tu, B. Peng, and X. Han, "Self-assembling gold nanoparticles on thiol-functionalized poly(styrene-co-acrylic acid) nanospheres for fabrication of a mediatorless biosensor," *Analytica Chimica Acta*, vol. 570, no. 2, pp. 151–157, 2006.
- [69] J. Wang, "Nanoparticle-based electrochemical DNA detection," *Analytica Chimica Acta*, vol. 500, no. 1-2, pp. 247–257, 2003.

- [70] X. Luo, A. Morrin, A. J. Killard, and M. R. Smyth, "Application of nanoparticles in electrochemical sensors and biosensors," *Electroanalysis*, vol. 18, no. 4, pp. 319–326, 2006.
- [71] C. M. Welch and R. G. Compton, "The use of nanoparticles in electroanalysis: a review," *Analytical and Bioanalytical Chemistry*, vol. 384, no. 3, pp. 601–619, 2006.
- [72] F. W. Campbell and R. G. Compton, "The use of nanoparticles in electroanalysis: an updated review," *Analytical and Bioanalytical Chemistry*, vol. 396, no. 1, pp. 241–259, 2010.
- [73] F. Terzi, C. Zanardi, V. Martina, L. Pigani, and R. Seeber, "Electrochemical, spectroscopic and microscopic characterisation of novel poly(3,4-ethylenedioxothiophene)/gold nanoparticles composite materials," *Journal of Electroanalytical Chemistry*, vol. 619-620, no. 1-2, pp. 75–82, 2008.
- [74] L. Zhang and X. Jiang, "Attachment of gold nanoparticles to glassy carbon electrode and its application for the voltammetric resolution of ascorbic acid and dopamine," *Journal of Electroanalytical Chemistry*, vol. 583, no. 2, pp. 292–299, 2005.
- [75] A. Nirmala Grace and K. Pandian, "Pt, Pt-Pd and Pt-Pd/Ru nanoparticles entrapped polyaniline electrodes—a potent electrocatalyst towards the oxidation of glycerol," *Electrochemistry Communications*, vol. 8, no. 8, pp. 1340–1348, 2006.
- [76] K. Karnicka, M. Chojak, K. Miecznikowski et al., "Polyoxometallates as inorganic templates for electrocatalytic network films of ultra-thin conducting polymers and platinum nanoparticles," *Bioelectrochemistry*, vol. 66, no. 1-2, pp. 79–87, 2005.
- [77] S. S. Kumar, J. Mathiyarasu, and K. L. Phani, "Exploration of synergism between a polymer matrix and gold nanoparticles for selective determination of dopamine," *Journal of Electroanalytical Chemistry*, vol. 578, no. 1, pp. 95–103, 2005.
- [78] K. M. Manesh, P. Santhosh, A. Gopalan, and K. P. Lee, "Electrocatalytic oxidation of NADH at gold nanoparticles loaded poly(3,4-ethylenedioxothiophene)-poly(styrene sulfonic acid) film modified electrode and integration of alcohol dehydrogenase for alcohol sensing," *Talanta*, vol. 75, no. 5, pp. 1307–1314, 2008.
- [79] F. Sundfors and J. Bobacka, "EIS study of the redox reaction of $\text{Fe}(\text{CN})_6^{3-}/^{4-}$ at poly(3,4-ethylenedioxothiophene) electrodes: influence of dc potential and $c_{\text{Ox}} : c_{\text{Red}}$ ratio," *Journal of Electroanalytical Chemistry*, vol. 572, no. 2, pp. 309–316, 2004.
- [80] L. Pigani, A. Heras, Á. Colina, R. Seeber, and J. López-Palacios, "Electropolymerisation of 3,4-ethylenedioxothiophene in aqueous solutions," *Electrochemistry Communications*, vol. 6, no. 11, pp. 1192–1198, 2004.
- [81] R. Hass, J. García-Cañadas, and G. García-Belmonte, "Electrochemical impedance analysis of the redox switching hysteresis of poly(3,4-ethylenedioxothiophene) films," *Journal of Electroanalytical Chemistry*, vol. 577, no. 1, pp. 99–105, 2005.
- [82] A. Zykwińska, W. Domagala, B. Pilawa, and M. Lapkowski, "Electrochemical overoxidation of poly(3,4-ethylenedioxothiophene)-PEDOT studied by means of in situ ESR spectroelectrochemistry," *Electrochimica Acta*, vol. 50, no. 7-8, pp. 1625–1633, 2005.
- [83] A. I. Melato, A. S. Viana, and L. M. Abrantes, "Different steps in the electrosynthesis of poly(3,4-ethylenedioxothiophene) on platinum," *Electrochimica Acta*, vol. 54, no. 2, pp. 590–597, 2008.
- [84] L. Chen, C. Yuan, H. Dou, BO. Gao, S. Chen, and X. Zhang, "Synthesis and electrochemical capacitance of core-shell poly (3,4-ethylenedioxothiophene)/poly (sodium 4-styrenesulfonate)-modified multiwalled carbon nanotube nanocomposites," *Electrochimica Acta*, vol. 54, no. 8, pp. 2335–2341, 2009.
- [85] L. M. Cubillana-Aguilera, M. Franco-Romano, M. L. A. Gil, I. Naranjo-Rodríguez, J. L. Hidalgo-Hidalgo De Cisneros, and J. M. Palacios-Santander, "New, fast and green procedure for the synthesis of gold nanoparticles based on sonocatalysis," *Ultrasonics Sonochemistry*, vol. 18, no. 3, pp. 789–794, 2011.
- [86] Y. Wei, Y. Li, N. Zhang, G. Shi, and L. Jin, "Ultrasound-radiated synthesis of PAMAM-Au nanocomposites and its application on glucose biosensor," *Ultrasonics Sonochemistry*, vol. 17, no. 1, pp. 17–20, 2010.
- [87] MA. Del, I. Naranjo-Rodríguez, J. M. Palacios-Santander, L. M. Cubillana-Aguilera, and J. L. Hidalgo-Hidalgo-de-Cisneros, "Study of the responses of a sonogel-carbon electrode towards phenolic compounds," *Electroanalysis*, vol. 17, no. 9, pp. 806–814, 2005.
- [88] J. M. Palacios-Santander, L. M. Cubillana-Aguilera, M. Cocchi et al., "Multicomponent analysis in the wavelet domain of highly overlapped electrochemical signals: resolution of quaternary mixtures of chlorophenols using a peg-modified Sonogel-Carbon electrode," *Chemometrics and Intelligent Laboratory Systems*, vol. 91, no. 2, pp. 110–120, 2008.
- [89] A. Et Taouil, F. Lallemand, J. Y. Hihn, J. M. Melot, V. Blondeau-Patissier, and B. Lakard, "Doping properties of PEDOT films electrosynthesized under high frequency ultrasound irradiation," *Ultrasonics Sonochemistry*, vol. 18, no. 1, pp. 140–148, 2011.
- [90] A. Et Taouil, F. Lallemand, J. Y. Hihn, and V. Blondeau-Patissier, "Electrosynthesis and characterization of conducting polypyrrole elaborated under high frequency ultrasound irradiation," *Ultrasonics Sonochemistry*, vol. 18, no. 4, pp. 907–910, 2011.
- [91] A. Et Taouil, F. Lallemand, L. Hallez, and J.-Y. Hihn, "Electropolymerization of pyrrole on oxidizable metal under high frequency ultrasound irradiation. Application of focused beam to a selective masking technique," *Electrochimica Acta*, vol. 55, no. 28, pp. 9137–9145, 2010.
- [92] B. Lakard, L. Ploux, K. Anselme et al., "Effect of ultrasounds on the electrochemical synthesis of polypyrrole, application to the adhesion and growth of biological cells," *Bioelectrochemistry*, vol. 75, no. 2, pp. 148–157, 2009.
- [93] Y. Liu, M. Yang, Z. Zheng, and B. Zhang, "In situ synthesis of Pt nanoparticles in hyperbranched thin film for electrocatalytic reduction of dioxygen," *Electrochimica Acta*, vol. 51, no. 4, pp. 605–610, 2005.
- [94] F. Maillard, E. R. Savinova, and U. Stimming, "CO monolayer oxidation on Pt nanoparticles: further insights into the particle size effects," *Journal of Electroanalytical Chemistry*, vol. 599, no. 2, pp. 221–232, 2007.
- [95] C. W. Kuo, C. Sivakumar, and T. C. Wen, "Nanoparticles of $\text{Pt}/\text{H}_x\text{MoO}_3$ electrodeposited in poly(3,4-ethylenedioxothiophene)-poly(styrene sulfonic acid) as the electrocatalyst for methanol oxidation," *Journal of Power Sources*, vol. 185, no. 2, pp. 807–814, 2008.
- [96] S. Patra and N. Munichandraiah, "Electrooxidation of methanol on pt-modified conductive polymer PEDOT," *Langmuir*, vol. 25, no. 3, pp. 1732–1738, 2009.

- [97] V. Zin, B. G. Pollet, and M. Dabalà, “Sonoelectrochemical (20 kHz) production of platinum nanoparticles from aqueous solutions,” *Electrochimica Acta*, vol. 54, no. 28, pp. 7201–7206, 2009.
- [98] L. Y. Bian, Y. H. Wang, J. B. Zang, J. K. Yu, and H. Huang, “Electrodeposition of Pt nanoparticles on undoped nanodiamond powder for methanol oxidation electrocatalysts,” *Journal of Electroanalytical Chemistry*, vol. 644, no. 1, pp. 85–88, 2010.
- [99] I. A. Arkoub, C. Amatore, C. Sella, L. Thouin, and J. S. Warkocz, “Diffusion at double microband electrodes operated within a thin film coating. Theory and experimental illustration,” *Journal of Physical Chemistry B*, vol. 105, no. 37, pp. 8694–8703, 2001.
- [100] C. Amatore, C. Sella, and L. Thouin, “Diffusional cross-talk between paired microband electrodes operating within a thin film: theory for redox couples with unequal diffusion coefficients,” *Journal of Physical Chemistry B*, vol. 106, no. 44, pp. 11565–11571, 2002.
- [101] C. Amatore, C. Sella, and L. Thouin, “Effects of chemical environment on diffusivities within thin Nafion® films as monitored from chronoamperometric responses of generator-collector double microband assemblies,” *Journal of Electroanalytical Chemistry*, vol. 547, no. 2, pp. 151–161, 2003.
- [102] S. Lupu, “The electrochemical features of sol-gel monoliths and films incorporating Cu(II)-cyclam complexes,” *Revue Roumaine de Chimie*, vol. 50, no. 11-12, pp. 967–974, 2005.
- [103] B. Lakard, G. Herlem, M. De Labachelerie et al., “Miniatuized pH biosensors based on electrochemically modified electrodes with biocompatible polymers,” *Biosensors and Bioelectronics*, vol. 19, no. 6, pp. 595–606, 2004.
- [104] B. Lakard, O. Segut, S. Lakard, G. Herlem, and T. Gharbi, “Potentiometric miniaturized pH sensors based on polypyrrole films,” *Sensors and Actuators, B*, vol. 122, no. 1, pp. 101–108, 2007.
- [105] O. Segut, B. Lakard, G. Herlem et al., “Development of miniaturized pH biosensors based on electrosynthesized polymer films,” *Analytica Chimica Acta*, vol. 597, no. 2, pp. 313–321, 2007.
- [106] A. E. Musa, F. J. Del Campo, N. Abramova et al., “Disposable miniaturized screen-printed pH and reference electrodes for potentiometric systems,” *Electroanalysis*, vol. 23, no. 1, pp. 115–121, 2011.
- [107] O. Ordeig, C. E. Banks, F. J. Del Campo, F. X. Muñoz, and R. G. Compton, “Electroanalysis of bromate, iodate and chlorate at tungsten oxide modified platinum microelectrode arrays,” *Electroanalysis*, vol. 18, no. 17, pp. 1672–1680, 2006.
- [108] A. Berduque, G. Herzog, Y. E. Watson et al., “Development of surface-modified microelectrode arrays for the electrochemical detection of dihydrogen phosphate,” *Electroanalysis*, vol. 17, no. 5-6, pp. 392–399, 2005.
- [109] S. Lupu, F. J. del Campo, and F. X. Muñoz, “Development of microelectrode arrays modified with inorganic-organic composite materials for dopamine electroanalysis,” *Journal of Electroanalytical Chemistry*, vol. 639, no. 1-2, pp. 147–153, 2010.
- [110] R. Solná, E. Dock, A. Christenson et al., “Amperometric screen-printed biosensor arrays with co-immobilised oxidoreductases and cholinesterases,” *Analytica Chimica Acta*, vol. 528, no. 1, pp. 9–19, 2005.

Review Article

Design and Development of Biosensors for the Detection of Heavy Metal Toxicity

Graziella L. Turdean

Physical Chemistry Department, Babes-Bolyai, University of Cluj-Napoca, 11 Arany Janos Street, 400028 Cluj-Napoca, Romania

Correspondence should be addressed to Graziella L. Turdean, gturdean@chem.ubbcluj.ro

Received 28 February 2011; Accepted 23 March 2011

Academic Editor: Sibel A. Ozkan

Copyright © 2011 Graziella L. Turdean. This is an open access article distributed under the Creative Commons Attribution License, which permits unrestricted use, distribution, and reproduction in any medium, provided the original work is properly cited.

Many compounds (including heavy metals, HMs) used in different fields of industry and/or agriculture act as inhibitors of enzymes, which, as consequence, are unable to bind the substrate. Even if it is not so sensitive, the method for detecting heavy metal traces using biosensors has a dynamic trend and is largely applied for improving the “life quality”, because of biosensor’s sensitivity, selectivity, and simplicity. In the last years, they also become more and more a synergistic combination between biotechnology and microelectronics. Dedicated biosensors were developed for offline and online analysis, and also, their extent and diversity could be called a real “biosensor revolution”. A panel of examples of biosensors: enzyme-, DNA-, immuno-, whole-cell-based biosensors were systematised depending on the reaction type, transduction signal, or analytical performances. The mechanism of enzyme-based biosensor and the kinetic of detection process are described and compared. In this context, is explainable why bioelectronics, nanotechnology, miniaturization, and bioengineering will compete for developing sensitive and selective biosensors able to determine multiple analytes simultaneously and/or integrated in wireless communications systems.

1. Introduction

1.1. About Heavy Metals. Heavy metals (HMs) and their ions are ubiquitous and by definition are metals having atomic weights between 63.5 and 200.6 g mol⁻¹ and a specific gravity greater than 5 g cm⁻³ [1]. Living organisms require small doses of some essential heavy metals, including cobalt, copper, iron, manganese, molybdenum, vanadium, strontium, and zinc. However, in the case of essential metals and very toxic metals, excessive levels and, respectively, even small doses, influence both the ecosystem and human health [2]. Nonessential heavy metals which affect the surface water systems are cadmium, chromium, mercury, lead, arsenic, and antimony.

Because HMs are relatively abundant in the Earth’s crust and are often used in industrial processes and agriculture, consequently they become toxic to humans. These can make important alterations to the biochemical cycles of life. Human activities are adapted and interfered with natural cycles and produced a release to the aquatic and terrestrial

systems. The HMs are transported by runoff water and contaminate water sources downstream from the industrial site. For life, all living (micro)organisms, plants, and animals depend on water, but because heavy metals can bind to the surface of microorganisms, they may be transported inside the cell. There, the HMs can be chemically changed using chemical reactions similarly with those for digesting food [1, 2].

The determination of trace levels (subpart per billion, ppb) of toxic HMs in complex matrices like biological material (serum and cytoplasm of cells) for clinical medicine/toxicology and animal husbandry, natural waters (ocean, sea, rivers), wastewater (from mining, metal processing, tanneries, pharmaceuticals, pesticides, organic chemicals, rubber and plastics, lumber and wood products, etc.), soil and air for chemical oceanography or for environmental monitoring (wastewater treatment or monitoring), for industrial process monitoring has become very important, because these media are vulnerable to this class of pollutants [1, 3–5].

Powerful analytical methods/techniques including atomic absorption and emission spectroscopy, inductively coupled plasma mass spectroscopy, and their combination with chromatographic techniques are widely used and are commercially available. These techniques exhibit high sensitivity, selectivity, reliability, and accuracy, but require sophisticated instrumentation inadequate for use outside the laboratory, skilled personnel, complicated sample collection, pretreatment (pre-concentration), and a long measuring period [3, 6, 7].

Consequently, with the comparable sensitivity and selectivity, the electrochemical methods such as ion-selective electrodes, biosensors, polarography, and other voltammetric techniques are also extensively used as attractive choice to the classical methods, due to their less complex instrumentation and shorter measuring period [7]. Also, simple, inexpensive, and portable instruments are attractive and desirable for real-time sampling/measuring and online and continuous analysis/monitoring/control of natural samples [3].

1.2. What Is a Biosensor? According to the International Union of Pure and Applied Chemistry (IUPAC) (namely Physical Chemistry and Analytical Chemistry Divisions) a biosensor is defined as “a self-contained integrated device that is capable of providing specific quantitative or semi-quantitative analytical information using a biological recognition element (biochemical receptor) which is in direct spatial contact with a transduction element” [8, 9]. A typical biosensor construct has three main features: a recognition element (enzyme, antibody, DNA, etc.), a signal transducing structure (electrical, optical, or thermal), and an amplification/processing element (see Figure 1), same models including also, a permselective membrane which controls transport of analyte to the bioreceptor [10].

As summarized in Table 1, various transduction mechanisms can be used: electrochemical, electrical, optical, thermal, and piezoelectric [8, 11]. Most commonly, in a biosensor, a biorecognition phase (e.g., enzyme, antibody, receptor, and single-stranded DNA) interacts with the analyte to produce a signal, which may be due to (i) a change in proton concentration, (ii) a release or uptake of gases such as ammonia or oxygen, (iii) a release or uptake of electrons, (iv) a light emission, absorption, or reflectance, (v) a heat emission, or (vi) a mass change, and so forth. The function of the transducer is to convert the signal into an appropriate measurable response (e.g., current, potential or temperature change). Through signal processing, this interaction is converted into digital values that relate to the build-up of concentration/activity of the analyte in the environs of the device, which in turn relates to the ambient levels in the bulk investigated sample. A biosensor is not necessarily an individual entity, but is considered as part of a general designed instrumentation [8].

2. Enzyme-Based Biosensor

Adsorption, covalent binding to solid surfaces and supported films, entrapment in polymer hydrogels and

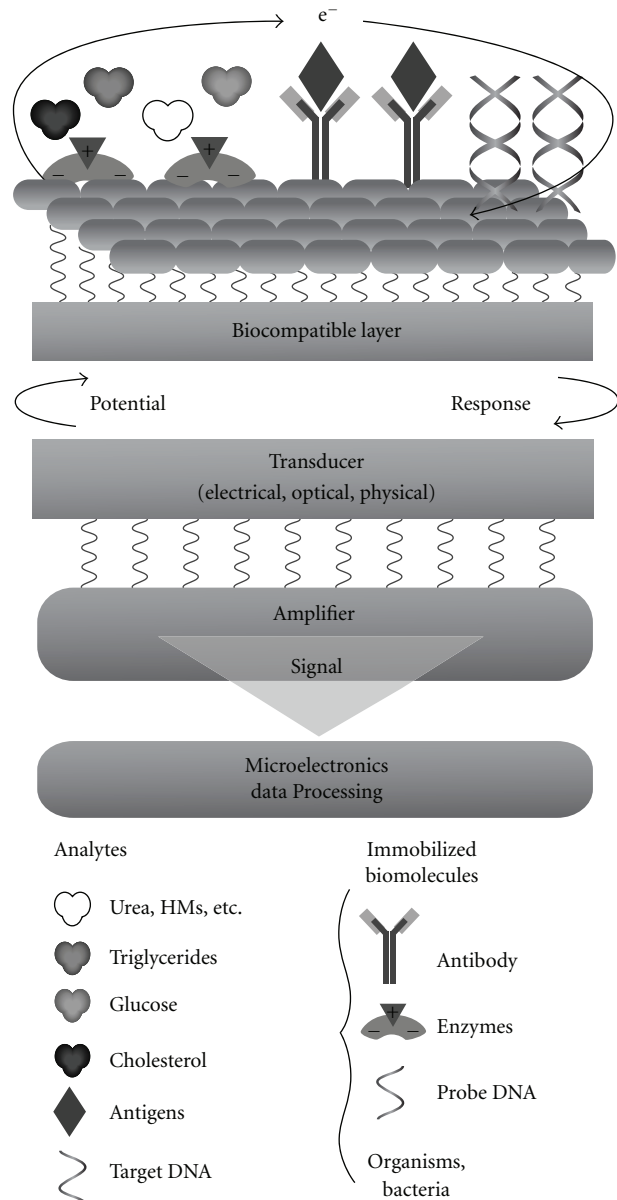


FIGURE 1: Schematic principle of operation of a biosensor.

microencapsulation have been used for a long period to immobilize enzymes [12].

The application of immobilized enzymes has several advantages in comparison with free enzymes [13, 14]:

- (i) thousands times lower consumption of immobilized enzyme;
- (ii) reduction of interferences by the differential mode of operation;
- (iii) unnecessary preincubation;
- (iv) rapid analysis procedure, less than 5 min;
- (v) in the case of reversible inhibition, sometimes the reactivation of enzyme activity is not necessary.

Biosensors have been used for indirect monitoring of organic (e.g., pesticides) or inorganic substances (e.g., heavy

TABLE 1: Principal transduction systems used in biosensors.

Transduction system	Measurement/parameters
Electrochemical	Amperometry/current Potentiometry/voltage at zero current
Electrical	Conductometry/conductance
Optical	Fotometry/luminescence Fotometry/fluorescence Refractometry/refractive index
Thermal	Calorimetry/temperature
Piezoelectric	Mass-quartz crystal microbalances/mass Mass-surface acoustic waves/velocity and so forth.

metals) which inhibit its biocatalytic properties. The problem with biosensors based in enzymatic inhibition is that only a few enzymes are sensitive to heavy metals [12].

Generally, for a bioelectrocatalytical scheme the following reactions it can be written as follows:



where S is a substrate; P is a product; E is a enzyme; M_{ox} , M_{red} are the oxidized and reduced forms of a redox mediator molecules.

The “ping-pong” mechanism is proposed for the enzyme reaction described by a reaction rate (v_s), which at steady state is given by (4). The measured current (I_{app}) reflects v_s , as expressed by the approximate equation [15]:

$$v_s = \frac{k_{cat}[E]}{1 + (K_s/[S]) + (K_M/M_{ox})}, \quad (4)$$

$$I_{app} = FA[M] \sqrt{\frac{2n_S n_M D_M k_{cat}[E]}{2K_M + [M]}}, \quad (5)$$

where k_{cat} = catalytic constant; K_s is Michaelis constant for S; K_M is Michaelis constant for M_{ox} ; E is enzyme concentration; S is substrate concentration; M_{ox} is mediator concentration; F is Faraday's constant; A is electrode surface area; M is bulk concentration of mediator M; D_M is diffusion coefficient of M; n_S and n_M are the number of electrons involved in (1)–(3), respectively.

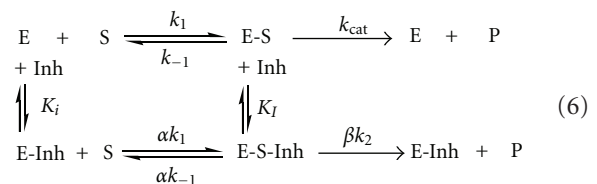
2.1. Enzyme Inhibitor System. The long-term function of enzyme-based biosensors may be severely limited by the powerful of inhibitors which is measured. Because the enzyme-inhibitor reaction is habitually complicated, the inhibition of the enzyme can be either reversible or an irreversible inactivation.

Sometimes the effect of an inhibitor can be reversed by decreasing the concentration of inhibitor (e.g., by dilution or dialysis). It is the case of the reversible inhibition. Once inhibition has occurred and there is no reversal

of inhibition with decreasing the inhibitor concentration, the inhibition is called irreversible. The difference between reversible and irreversible inhibition is not absolute and is difficult to do, if the inhibitor binds very strongly to the enzyme and if it is released very slowly. Reversible inhibitors that work in a way that is difficult to distinguish from irreversible inhibition are called tight-binding inhibitors [16].

2.1.1. Reversible Inhibition. Reversible inhibitors are molecules that bind reversibly to enzymes with rapid association by noncovalent interactions and rapid dissociation rates. This chemical equilibrium between the enzyme and the inhibitor can be displaced in favour of the enzyme and so the activity of the enzyme can be regained, by the removal of the inhibitor by dialysis, gel filtration, and so forth. The removal of the inhibitor restores the enzyme activity to its original value.

The inhibition process of the immobilised enzyme can be described by the following generally kinetic scheme [11, 16–18]:



where: E is immobilised enzyme; S is free substrate; P is product; E-S is enzyme-substrate complex; E-Inh is enzyme-inhibitor complex; E-S-Inh is ternary complex containing enzyme-substrate inhibitor; K_I and K_i are equilibrium dissociation constants of the E-S-Inh complex and the E-Inh complex, respectively.

In function of the binding site, inhibitors can be: competitive, uncompetitive, noncompetitive and mixed, and their effects on the kinetic parameters (K_M and v_{max}) are resumed in Table 2 [19, 20].

From the general scheme 6 the value of equilibrium dissociation constants (K_I , K_i) could be calculated from

TABLE 2: Type of inhibitors.

Inhibitor type	Binding site on enzyme	Kinetic effect
Competitive inhibitor	An inhibitor that is structurally similar to the substrate cannot undergo the catalytic step, so it wastes the enzyme's time by preventing S binding, that is, inhibitor competes with substrate for the enzyme-substrate binding site in a dynamic equilibrium process, thus increasing K_M for substrate. Inhibition is reversible using high concentrations of substrate.	v_{max} is unchanged; K_M is increased.
Uncompetitive inhibitor	Binds only to ES complexes at locations other than the catalytic site. Substrate binding modifies enzyme structure, making inhibitor-binding site available. Inhibition cannot be reversed by substrate.	v_{max} and K_M decreased with the same factor.
Noncompetitive inhibitor	If the inhibitor is not only bound to the E, but also to the E-S complex, at a remote site other than at the catalytic site of the enzyme, thus the active centre is usually deformed and its function is thus impaired, affecting k_{cat} . In this case the substrate and the inhibitor do not compete with each other. Substrate binding is unaltered, but ESI complex cannot form products. Inhibition cannot be reversed by substrate.	K_M appears unaltered; v_{max} is decreased proportionately to inhibitor concentration.
Mixed inhibitor	As the noncompetitive, this inhibitor binds at a site other than the active site (E or ES) and causes changes in the overall 3D shape of the enzyme that leads to a decrease in activity. The inhibitor binds to E and ES with different affinity (K_i not equal to K_I). Mixed inhibition cannot be overcome by high substrate concentration.	v_{max} decrease and K_M either increase or decrease.

the slope and intercept of the linear plot $1/I$ versus $1/[S]$ according to (7) [12, 21]:

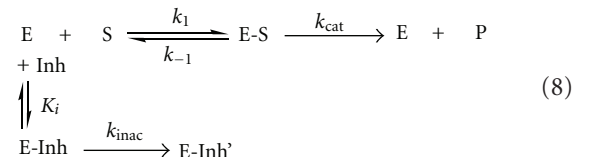
$$\frac{1}{I} = \left(1 + \frac{[Inh]}{K_i}\right) \frac{K_M}{I_{max}[S]} + \left(1 + \frac{[Inh]}{K_I}\right) \frac{1}{I_{max}}. \quad (7)$$

2.1.2. Irreversible Inactivation. The term irreversible inhibitor means that the decomposition of the enzyme-inhibitor complex results in the destruction of enzyme (e.g., its hydrolysis, oxidation, etc.) or modification of an essential aminoacid required for enzyme activity. Frequently, this is due to a covalent bond between the enzyme active site and the inhibitor. These inhibitors are designed to mimic the natural substrate in the recognition phase and to bind to the active site of the enzyme in a second step. Upon binding and some catalytic modification, a highly reactive inhibitor product is formed, that binds irreversibly and consequently inactivates the enzyme [19].

The kinetics of the inhibition depends strongly on the biosensor configuration. Thus, in the case of a thin enzymatic layer, the kinetics observed is similar to that of the enzyme in solution. Also, the inhibition of native enzymes is related directly to the incubation time [19]. An interesting case concerning the inhibition of peroxidise by HM was investigated [7]. The conclusion is that there exists an early

phase of reversible inhibition (5 s), followed by irreversible inhibition. As consequence, it is hard to accomplish the amperometric measurement of remaining activity (v_i) so soon after a reversible inhibition. However, irreversible inhibition or inactivation has to be considered, when longer incubation times were used (1–8 min). Also, HM salts at high concentration (>1 mM) inactivate all enzymes by coprecipitation, while lower concentrations affect only some enzyme activities by interaction with specific protein groups [22].

Knowing that the irreversible inactivation follows the reaction mechanism described by scheme (8) [22]



and supposing that the irreversible inactivation process was a first order versus enzyme concentration [E], according to the literature, the reaction rate is described by equation (9)

$$\frac{d[E]}{dt} = -k_{obs}[E] \quad (9)$$

which become after variable separation:

$$\frac{d[E]}{[E]} = -k_{\text{obs}} dt \quad (10)$$

After integration

$$\ln v_i = -k_{\text{obs}}t + \text{const}, \quad (11)$$

the linear dependence of $\ln v_i$ versus t which can be plotted for each incubation time is obtained.

The experimental slope is

$$k_{\text{obs}} = \frac{k_{\text{inac}}[\text{Inh}]}{[\text{Inh}] + K_i}, \quad (12)$$

where $[\text{Inh}]$ is inactivator concentration, K_i is equilibrium dissociation constant, and k_{inac} is rate constant of inactivation.

(i) For $[\text{Inh}] \ll K_i$, equation (12) became

$$k_{\text{obs}} = \frac{k_{\text{inac}}[\text{Inh}]}{K_i}. \quad (13)$$

Thus the $1/k_{\text{obs}}$ plotted against $1/[\text{Inh}]$ is a straight line with the slope K_i/k_{inac} [7], which permit also the determination of the detection limit and the efficiency of inactivation.

(ii) For $[\text{Inh}]$ around K_i , $1/k_{\text{obs}}$ plotted versus $1/[\text{Inh}]$ permitted the determination of k_i and K_i and calculation of k_i/K_i [22].

Also, when the inhibition reaction 6 is reduced to scheme (8) (i.e., $K_I \rightarrow \infty$, $\alpha k_1 \rightarrow \infty$, $k_2 \rightarrow 0$) the inhibition constant (K_i) value can be determined from the slope and intercept of the linear $1/I$ versus $1/[S]$ plot of the modified equation (7) [12, 21]:

$$\frac{1}{I} = \left(1 + \frac{[\text{Inh}]}{K_i}\right) \frac{K_M}{I_{\max} [S]} + \frac{1}{I_{\max}}. \quad (14)$$

2.1.3. Degree of Inhibition. Irreversible inhibition is usually quantified in terms of the rate of inhibition. In order to investigate the heavy metals inhibition an experimental method is used consisting in recording the bioelectrode amperometric response to successive additions of substrate, before and after its incubation in an inhibitor solution, for a given period of time. Thus, the method allows to calculate the percent of inhibition (% Inh), defined using the formula [23–28]:

$$\% \text{Inh} = \frac{I_0 - I}{I_0} * 100, \quad (15)$$

where I_0 is bioelectrode initial response when the inhibitor was absent; I is bioelectrode response after incubation with the inhibitor.

Also, it was reported that the degree of inhibition depends on the concentration of the inhibitor and on the exposure time (at a defined pH value and at inhibitor concentration which is in excess with respect to enzyme)

[29, 30]. There have been some initial efforts at the development and experimental verification of theoretical models for the inhibition of immobilized enzymes using biosensors. When diffusion phenomenon are taken into account, the model predicts that the percentage of enzyme inhibition (% Inh), after exposure to an inhibitor, is linearly related to both the inhibitor concentration [Inh] and the square root of incubation time ($t^{1/2}$) [19, 31].

2.2. Examples of Enzyme-Based Biosensors for Heavy Metal Detection. For heavy metals detection, different enzymes such as acetylcholinesterase, alkaline phosphatase, urease, invertase, peroxidise, L-lactate dehydrogenase, tyrosinase, and nitrate reductase, have been used. The inhibition of the immobilized enzyme can be detected via electrochemical (amperometric, potentiometric, and conductometric) or optical measurements. The principle of detection is resumed in Table 3 and the analytical parameters of the enzyme-based biosensors are summarized in Table 4.

3. DNA-Based Biosensor

During last years, there has been a huge increase in the use of nucleic acids, as a way in the recognition and monitoring of many toxic compounds of analytical interest, because many of this molecules, and especially HMs, show a high affinity for DNA and they can interact with nucleic acids. The interaction between metal ions and DNA is important in living organisms, because it could have, either favourable, or adverse effects in life science reported to the damage, replication and transcription of DNA in *vivo*, mutation of gene, action mechanism of some synthetic chemical nucleases, and molecular analysis [57], which often lead to the change of the structure and function of genetic materials, by development of malignant tumours [58]. Thus, the ability to monitor and quantify the levels of HMs (such as Pb, Cd, and Ni) that interact with DNA is widely studied [59], because these ions have been detected in different sources: foods, beverages, soil, plants, natural waters, and so forth. Also, the International Agency for Research on Cancer (IARC) lists some HMs (as Pb and Cd) as possible human carcinogens, while the carcinogenic properties of Ni are related to tumour promotion [58].

Usually, for HMs studies, the DNA was native (from *Calf Thymus*, double-stranded DNA, ds-DNA) or denatured (single-stranded DNA, ss-DNA) [59, 60]. The electrochemical techniques (chronopotentiometric or voltammetric methods), especially the pulse techniques, are appropriate for studying the biological systems, and also, for DNA heavy metal interactions, because they improve the selectivity and the signal-to-noise ratio, are fast, of low cost, and have high sensitivity [57, 58].

An electrochemical DNA biosensor is an integrated receptor-transducer device that uses DNA as a biomolecular recognition element to measure specific binding processes with DNA, through electrochemical (especially carbon electrodes) transduction [57]. As for other biosensors, the most important factor for the construction of efficient DNA-based

TABLE 3: Principle of detection using enzyme-based biosensors.

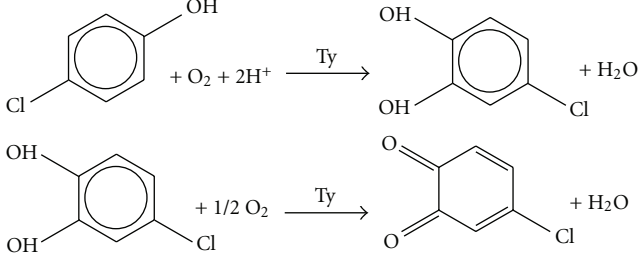
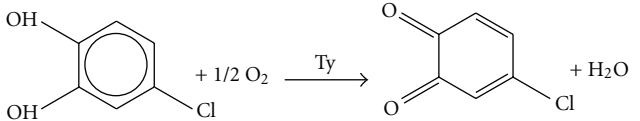
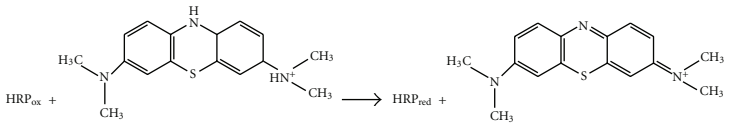
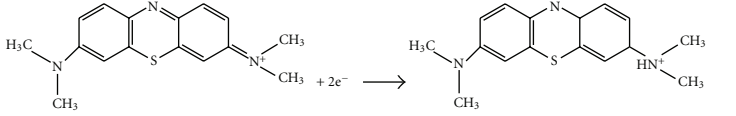
Enzyme (1)	Reaction (2)	Equations (3)	References (4)
Alkaline phosphatase (EC: 3.1.3.1, ALP)	orthophosphoric monoester + H ₂ O $\xrightarrow{\text{ALP}}$ alcohol + H ₃ PO ₄	(16)	[12–14, 32]
Urease (EC: 3.5.1.5)	NH ₂ CONH ₂ + 3 H ₂ O $\xrightarrow{\text{urease}}$ 2 NH ₄ ⁺ + HCO ₃ ⁻ + OH ⁻	(17)	[5, 33–38]
Urease/glutamate dehydrogenase (GLDH)	NH ₂ CONH ₂ + H ₂ O $\xrightarrow{\text{urease}}$ CO ₂ + 2 NH ₃	(18)	[39]
	NH ₃ + α-ketoglutarate + NADH + H ⁺ $\xrightarrow{\text{GLDH}}$ L-glutamate + NAD ⁺	(19)	
Tyrosinase (EC: 1.14.18.1, Ty)		(20)	[40, 41]
		(21)	
Acetylcholinesterase (EC: 3.1.1.7, AChE)	2(CH ₃) ₃ N ⁺ (CH ₂) ₂ SCOCH ₃ + H ₂ O $\xrightarrow{\text{AChE}}$ (CH ₃) ₃ N ⁺ (CH ₂) ₂ SH + CH ₃ COOH	(22)	[42, 43]
	2(CH ₃) ₃ N ⁺ (CH ₂) ₂ SH - 2e ⁻ → (CH ₃) ₃ N ⁺ (CH ₂) ₂ S-S(CH ₂) ₂ N ⁺ (CH ₃) ₃ + 2H ⁺	(23)	
Nitrate reductase (EC: 1.7.1.2, NR or NAD(P)H-NR)	NO ₃ ⁻ + NAD(P)H + H ⁺ $\xrightarrow{\text{NR}}$ NO ₂ ⁻ + NAD(P) ⁺ + H ₂ O	(24)	[44, 45]
PQQ glucose dehydrogenase (EC: 1.1.5.2, PQQ-GDH)	D-glucose + ubiquinone $\xrightarrow{\text{PQQ-GDH}}$ D-glucono-1,5-lactone + ubiquinol	(25)	[15]
Glycerol-(PQQ) 1-oxidoreductase (EC: 1.1.99.22, PQQ-GlyDH)	Glycerol + acceptor (ox) $\xrightarrow{\text{PQQ-GlyDH}}$ glycerine/dihydroxyacetone + acceptor (red)	(26)	[46]
	first generation glucose + Gox(FAD) + H ₂ O ⇌ [glucose-Gox(FAD)] → gluconic acid + Gox(FADH ₂)	(27)	[20, 47]
Glucose oxidase (EC: 1.1.3.4, Gox)	O ₂ + Gox(FADH ₂) ⇌ [O ₂ -Gox(FADH ₂)] → H ₂ O ₂ + Gox(FAD)	(28)	
	second generation glucose + Gox(FAD) + H ₂ O ⇌ [glucose-Gox(FAD)] → gluconic acid + Gox(FADH ₂)	(27)	
	M _{ox} + Gox(FADH ₂) → M _{red} + Gox(FAD) + 2H ⁺	(29)	[48]
	M _{red} → M _{ox} + e ⁻	(30)	
Invertase (EC: 3.2.1.26, Inv)/Gox	Sucrose + H ₂ O $\xrightarrow{\text{Inv}}$ α-D-glucose + D-fructose	(31)	[49]
	α-D-glucose + O ₂ $\xrightarrow{\text{Gox}}$ D-gluconic acid + H ₂ O ₂	(32)	
	Sucrose + H ₂ O $\xrightarrow{\text{Inv}}$ α-D-glucose + D-fructose	(33)	
Invertase/Mutarotase/Gox	α-D-glucose $\xrightarrow{\text{Mutarotase}}$ β-D-glucose	(34)	[50]
	β-D-glucose + O ₂ $\xrightarrow{\text{Gox}}$ D-gluconic acid + H ₂ O ₂	(32)	
	H ₂ O ₂ $\xrightarrow{\text{Pt}}$ O ₂ + 2H ⁺ + 2e ⁻	(35)	
	H ₂ O ₂ + HRP _{red} → H ₂ O + HRP _{ox}	(36)	
Horseradish peroxidase (EC: 1.11.1.7, HRP)		(37)	[7]
		(38)	

TABLE 3: Continued.

Enzyme (1)	Reaction (2)	Equations (3)	References (4)
L-lactate dehydrogenase (EC: 1.1.1.27, LDH)/L-lactate oxidase (EC: 1.13.12.4, LOD)	NADH + H ⁺ + pyruvate $\xrightarrow{\text{LDH}}$ L-lactate + NAD ⁺ L-lactate + O ₂ $\xrightarrow{\text{LOD}}$ pyruvate + H ₂ O ₂	(39) (40)	[22]

TABLE 4: Principle characteristics of enzyme biosensors for heavy metal detection.

Enzyme	Detection; working electrode; applied potential	Limit of detection	References
AChE	Amperometry; G/AChE; 0.80 V versus SCE	10 ⁻¹⁰ M Hg ²⁺	[43]
ALP	Conductometry; Au/ALP-GA-BSA-glycerol;—	0.5 ppm Cd ²⁺ , 2 ppm Zn ²⁺ , 2 ppm Co ²⁺ , 5 ppm Ni ²⁺ , 40 ppm Pb ²⁺	[13]
ALP	Amperometry; SPE/ALP-chitosan; +0.6 versus Ag/AgCl	mg/L Hg ²⁺ , Cd ²⁺ , Ag ⁺ , Zn ²⁺ , Cu ²⁺	[51]
ALP	Fluorescence;—	10.1 μM Ag ⁺	[12]
ALP	Chemiluminescence;—	0.36 ppb Zn ²⁺	[52]
HRP	Amperometry; GCE/MB-HRP-GdA	0.1 ng/mL HgCl ₂ , 0.2 ng/mL Hg ₂ (NO ₃) ₂	[7]
Gox	Amperometry; Pt/PA/Fc/GA/GOx; +0.7 V versus SCE	0.49 μg/L Hg ²⁺ 2.5 μM Hg ²⁺ , 0.05 μM Ag ⁺ , 5.0 μM Cu ²⁺ , 5.0 μM Cd ²⁺ , 12.0 μM Fe ³⁺ , 8.0 μM Co ²⁺ , 4.8 μM Ni ²⁺ , 48 μM CrO ₄ ²⁻	[48]
Gox	Amperometry; Pt/PPD/GOx; +0.7 V versus SCE	5* 10 ⁻¹⁰ M Hg ²⁺ , 3* 10 ⁻⁸ M Pb ²⁺ , 5* 10 ⁻⁸ M Ag ⁺ , 2.5* 10 ⁻⁸ M Cd ²⁺	[20, 47]
Inv Gox	Amperometry; Pt/Inv-Gox-agarose-guar gum; +0.35 versus Ag/AgCl	5* 10 ⁻¹⁰ M Hg ²⁺ , 3* 10 ⁻⁸ M Pb ²⁺ , 5* 10 ⁻⁸ M Ag ⁺ , 2.5* 10 ⁻⁸ M Cd ²⁺	[49]
Inv Mu Gox	Amperometry; Pt/Inv-Mu-Gox-laponite; +0.6 versus Ag/AgCl	3 ppb Hg ²⁺	[50]
LDH LOD	Amperometry; Clark electrode (Pt cathode); -0.7 V versus Ag/AgCl	1 μM HgCl ₂ , 10 μM Cu ²⁺ , 25 μM Zn ²⁺	[22]
NR	Conductometry; Pt/NR-GA-BSA-metyl viologen/ Nafion	0.05 μM Cu ²⁺ , 0.5 μM Zn ²⁺ , 0.1 μM Cd ²⁺ , 1 μM Pb ²⁺	[45]
PQQ-GDH	Amperometry; G/PQQ-GDH-GA; +0.25 versus Ag/AgCl	15* 10 ⁻⁵ M Cd ²⁺ , 15* 10 ⁻⁵ M Pb ²⁺	[15]
Ty	Amperometry; GCE/Ty-pPy; +0.4 versus Ag/AgCl	5 10 ⁻⁷ M Cr ³⁺	[41]
Ty	Conductometry; Ty-GA-BSA/Pt;—	1 ppb Cu ²⁺	[40]
Urease	Amperometry; Pt/PVF/urease; +0.7 V versus SCE	7.4 μM Hg ²⁺	[34]
Urease	Potentiometry; PVC-NH ₂ /Au-NP/urease;—	0.05 μM Hg ²⁺	[53]
Urease	Potentiometry; SPE (RuO ₂ +urease+graphite);—	—	[54]
Urease	Potentiometry; Ir/IrO ₂ /Urease-PVC;—	0.02 μM Hg ²⁺	[5]
Urease	Potentiometry; NH ₄ ⁺ - ENFET;—	0.2 μM Cu ²⁺ , 0.1 μM Hg ²⁺ 0.005 mM Hg ²⁺ , 0.02 mM Cu ²⁺ , 0.1 mM Cd ²⁺ , 0.9 mM Pb ²⁺	[55]
Urease	Conductometry; SPE;—	7.2 μg/L Hg ²⁺ , 8.5 μg/L Cu ²⁺ , 0.3 mg/L Cd ²⁺ , 0.2 mg/L Zn ²⁺	[35]
Urease/GLDH	Amperometry; C-Rh; +0.3 versus Ag/AgCl	—	[56]

ALP = alkaline phosphatase; Au-NP = gold nanoparticles; BSA = bovine serum albumin; C-Rh = rhodinised carbon electrode; ENFET = enzyme field effect transistor; Fc = ferrocene; MB = methylene blue; GA = glutaraldehyde; GdA = glutaric dialdehyde; GCE = glassy carbon electrode; GLDH = glutamate dehydrogenase; Gox = glucose oxidase; Inv = invertase; Mu = mutarotase; NR = nitrate reductase; PA = polyaniline; PPD = poly(*o*-phenylenediamine); pPy = polypyrrole; PQQ-GDH = pyrroloquinoline quinone dependent glucose dehydrogenase; PVC = poly(vinyl chloride); PVC-NH₂ = ethylenediamine poly(vinyl chloride); PVF = poly(vinylferrocenium); SCE = saturated calomel electrode; SPE = screen-printed electrode; Ty = tyrosinase.

TABLE 5: Examples of DNA-based electrodes.

Electrode	Immobilisation technique	Toxic effect	References
GCE/ds-DNA	Deposition	Pb ²⁺ interacts with ds-DNA preferentially at adenine-containing segments, leading to modifications in the double-helical structure.	[58]
SMFE/ss-DNA	Inclusion in a CN membrane	Pb ²⁺ and Cd ²⁺ covalent bind during complexation with ss-DNA. Constants of binding (estimated from Scatchard graphs): $K_{\text{bind}}(\text{Pb}^{2+} - \text{ssDNA}) = (12 \pm 0.3) * 10^5 \text{ M}^{-1}$; $K_{\text{bind}}(\text{Fe}^{3+} - \text{ssDNA}) = (1.4 \pm 0.3) * 10^5 \text{ M}^{-1}$; $K_{\text{bind}}(\text{Cd}^{2+} - \text{ssDNA}) = (0.6 \pm 0.2) * 10^5 \text{ M}^{-1}$. Limits of detection: $10^{-10} \text{ M Pb}^{2+}$, $10^{-9} \text{ M Cd}^{2+}$ and $10^{-7} \text{ M Fe}^{3+}$.	[61]
Au/ss-DNA.	Self assembled method	Cd ²⁺ has the ability to be deposited at underpotential conditions onto gold substrates when it is electrochemically reduced. Constant of binding $K_{\text{bind}}(\text{Cd}^{2+} - \text{ssDNA}) = 8.33 * 10^5 \text{ M}^{-1}$. Limit of detection: 10 pM Cd ²⁺ .	[59]
SPE/ds-DNA and SPE/MWCNT-ds-DNA	Deposition on SPE	Sn ²⁺ and As ³⁺ was studied.	[62]

GCE = glassy carbon electrode; SMFE = stationary mercury-film electrode; CN = cellulose nitrate; MWCNT= multi-wall carbon nanotubes; SPE = screen printed electrode.

TABLE 6: Advantages and disadvantages of whole cell based biosensor.

Advantages	Disadvantages
<ul style="list-style-type: none"> (i) React only to the available fraction of metal ions; (ii) Are fast, less expensive, and less intensive labour; (iii) Are compatible with and comparable to chemical analysis; (iv) Are more sensitive than chemical methods; (v) Produces real-time data and can be applied in field work or in situ analysis; does not involve the bulky, fragile equipment, or specialized training; (vi) They are more tolerant of suboptimal pH and temperatures than purified enzymes; (vii) Are cheaper to use because the active biological component does not have to be isolated and because microorganisms are living, unlimited quantities can be prepared relatively inexpensively; (viii) Can provide information about the bioavailability of the analyte; (xi) May perform multi-step reactions since all reactions are conveniently packaged within the cell and thus, efficiently carried out. 	<ul style="list-style-type: none"> (i) The limited understanding of the biochemistry involved. (ii) Lack of genetic stability and short lifetime (iii) Cells require relatively long incubation time (usually longer than 30 min); (iv) Difficult reversibility of the signal (v) Experimental conditions (temperature, pH, incubation time, buffer, and reagents) can affect the luminescence production and thus the biosensor performances (vi) Less/limited of selectivity

electrochemical biosensors is the immobilization of the DNA or its components (such as nucleotides, nucleosides, purine, and pyrimidine bases) on the electrode surface. Different adsorption immobilization procedures, such as electrostatic adsorption or evaporation, adsorption of a monolayer, or multilayer DNA films have been widely used [58].

Because DNA has four different potential sites for binding of metal ions: (1) the negatively charged phosphate oxygen atoms, (2) the ribose hydroxyls, (3) the base ring nitrogens, and (4) the exocyclic base keto groups [58], in the case of DNA biosensors, there are two possibilities to detect pollutants: one is to detect the hybridization of nucleic

TABLE 7: Examples of recombinant bacteria for specific heavy metal detection.

Promoter/ reporter gene	Biorecognition element Host microorganism	Metal ion/ detection limit	Linear range	Detection method	References
(1)	(2)	(3)	(4)	(6)	(7)
<i>Bacteria</i>					
Ars pR773/ <i>lacZ</i>	<i>Escherichia coli</i>	As ³⁺ /50 μM; Sb ³⁺ /1 fM	μM-mM; fM-μM	Chemiluminescence	[73]
CUP 1/ <i>lacZ</i>	<i>Saccharomyces cerevisiae</i>	Cu ²⁺	16.0–32.0 mg/L	Amperometry/ –0.6 V versus Ag/AgCl	[80]
pMOL 90 + Tn4431/ <i>luxCDABE</i>	<i>Alcaligenes eutrophus</i> (AE1239)	Cu ²⁺ /1 μM	0–250 μM	Bioluminescence	[81]
<i>cadA</i> and <i>cadC/lucFF</i>	<i>Staphylococcus aureus</i> (RN4220)	Cd ²⁺ /10 nM; Pb ²⁺ /33 nM; Sb ²⁺ /1 nM	10 nM–1 μM 33 nM–330 μM 1 nM–330 nM	Bioluminescence	[82]
<i>mer</i> / <i>lux</i>	<i>Escherichia coli</i> (CM 2624)	Hg ²⁺		Bioluminescence	[83]
<i>merR/luxFF</i>	<i>Escherichia coli</i> (S30)	Hg ²⁺		Luminescence	[84]
<i>merR/luxFF</i>	<i>Escherichia coli</i> (MC 1061)	Hg ²⁺		Luminescence	[85]
–/DsRed-GFP	<i>Escherichia coli</i> (DH5α)	Cu ²⁺ /45 nM		Fluorescence	[86]
–/lux	<i>Burkholderia</i> sp (RASC c2)	Zn ²⁺ /1.7 μg/mL Cu ²⁺ /0.09 μg/mL Cd ²⁺ /0.1 nmol/L;		Bioluminescence	[70]
<i>cad/rs-GFP</i>	<i>Escherichia coli</i> (DH5α)	Pb ²⁺ /10 nmol/L; Sb ³⁺ /0.1 nmol/L		Fluorescence	[87]
–/eGFP205C	<i>Escherichia coli</i> (K12), <i>Caenorhabditis elegans</i>	Hg ²⁺		Fluorescence	[88]
copA/lux	<i>Escherichia coli</i> (W3110)	Cu ²⁺ , Ag ⁺ , Au ³⁺		Bioluminescence	[89]
<i>Algae</i>					
<i>Tetraselmis chuii</i> (Prasinophyceae)/CPE		Cu ²⁺ /4.6 10 ⁻¹⁰ M	5 10 ⁻⁸ –10 ⁻⁶ M	Amperometry/ –0.4 V versus Ag/AgCl	[90]
<i>Chlorella vulgaris</i>		Cd ²⁺		Synchronous-scan Spectrofluorimetry	[91]
AlkP from <i>Chlorella vulgaris</i> /Pt		Cd ²⁺ , Zn ²⁺ /10 ppb		Conductometry	[75]
<i>Phormidium</i> sp./CPE		Pb ²⁺ /2.5 10 ⁻⁸ M	5 10 ⁻⁸ –2 10 ⁻⁵ M	CV, DPSV	[92]
<i>Yeast cell</i>					
<i>Rhodotorula mucilaginosa</i> /CPE		Cu ²⁺	10 ⁻⁷ –10 ⁻⁵ M	CV, DPSV	[93]
<i>Fungi</i>					
<i>Rhizopus arrhizus</i> /CPE		Pb ²⁺ /0.5 10 ⁻⁸ M	10 ⁻⁷ –1.25 10 ⁻⁵ M	CV, DPSV	[94]
<i>Metal-binding protein</i>					
Synthetic phytochelatin (EC)/Au		Hg ²⁺ , Cd ²⁺ , Pb ²⁺ , Cu ²⁺	1 fM–10 mM	capacitance	[68]
GST-SmtA/Au		Hg ²⁺		capacitance	[83]
GST-SmtA/Au		Hg ²⁺ , Cd ²⁺ , Cu ²⁺ , Zn ²⁺ /10 ⁻¹⁵ M		capacitance	[6, 95]
MerR/Au		Hg ²⁺ , Cd ²⁺ , Cu ²⁺ , Zn ²⁺ /10 ⁻¹⁵ M		capacitance	[6, 95]
<i>Cytocrom c3</i> from <i>Desulfomicrobium norvegicum</i> /GCE		Cr ⁶⁺ /0.2 mg/L		Amperometry/ –0.53 V versus SCE	[96]

TABLE 7: Continued.

Promoter/ reporter gene	Biorecognition element Host microorganism	Metal ion/detection limit	Linear range	Detection method	References
(1)	(2)	(3)	(4)	(6)	(7)
	<i>Escherichia coli</i> (NCIMB 8277)/SPE	Hg ²⁺ /1 ppm		Conductometry	[78]
	<i>Acidithiobacillus ferrooxidans</i> /O ₂ Clark electrode	Cr ³⁺	2 10 ⁻⁵ –40 10 ⁻⁵ M	Amperometry/—	[97]
	<i>Circinella</i> sp./CPE	Cu ²⁺ /5.4 10 ⁻⁸ M(0.0034 mg/L)	5 10 ⁻⁷ – 1 10 ⁻⁵ M Cu ²⁺ (0.032–0.635 mg/L)	DPSV	[65] [80]
	<i>CUP1</i> gene from <i>Saccharomyces</i>				
	<i>Cerevisiae</i> —fused to <i>lacZ</i> gene from <i>Escherichia coli</i> /O ₂ Clark electrode	Cu ²⁺	16–32 mg/L	Amperometry/–0.6 V versus Ag/AgCl	
	<i>Escherichia coli</i> (K-12)-(PAH-PSS) ₃ —ITO	Hg ²⁺ /10 ⁻¹² M	10 ⁻¹² –10 ⁻³ M	Electrochemical impedance spectroscopy	[98]
	<i>Bacillus sphaericus</i> MTCC 5100/ NH ₄ ⁺ -ISE	Ni ²⁺ /100 ppm or 0.044 ppm in food	0.03–0.68 nM	Potentiometry	[99]

CPE = carbon paste electrode; CV = cyclic voltammetry, DPSV = differential pulse stripping voltammetry, GCE = glassy carbon electrode; ISE = ion selective electrode; ITO = indium-tin-oxide glass electrode; lucFF = firefly luciferase; PAH = poly(allylamine hydrochlorure); PSS = poly(styrene sulfonate); rs-GFP = red-shifted green fluorescent protein; SCE = saturated calomel electrode, SPE = screen-printing electrode.

acid sequences from infectious microorganisms, and the other one is to monitor the interaction of small pollutants with the immobilized DNA (drugs, mutagenic pollutants, etc.) [39]. Most HM ions interact with more than two different sites and their interactions with DNA are more complex. Under chosen conditions, the following methods of metal-DNA interactions are proposed: (i) indirect chelation between the nitrogen N₇ atom of the DNA purine base with the oxygen atom of the DNA phosphate backbone and (ii) direct coordination bond with the nitrogen N₇ of guanine base (rarely of adenine). Two additional models have been identified: (a) intrastrand chelating between N₇ and O₆ atoms of guanine and (b) intrastrand bindings formation with the N₇ guanine atoms of ss-DNA [58, 59, 61].

Several examples and the obtained results/conclusions are synthesised in Table 5.

4. Immunosensors

This type of device attaches the recognition elements (antibody-antigen, Ab–Ag) with a physicochemical transduction element (electrochemical, optical, piezoelectric, and SPR) and generally presents the advantages of sensitivity and selectivity derived from the immunochemical interactions [63]. Important restrictions are the difficulties to regenerate the immune surface and cross-reactivity, while a certain degree of cross-reactivity is often desirable to detect different species of the same class [39].

Antibody-antigen interactions propose an alternative procedure for metal ion detection, based on the availability of antibodies to bind HMs. The KinExA 3000 is an example of an immunodevice based on the high surface area of

beads containing an immobilized capture reagent (protein-thioureido-L-benzyl-chelate–metal) in the flow cell of an instrument. Since the immobilized antigen is in contact for a limited time with the antibody-binding sites, the KinExA is a device more sensitive, with a lower limit of detection, where the antibody binds with higher affinity to the immobilized antigen, than in the soluble case [64].

5. Whole-Cell-Based Biosensors

A whole cell-based biosensor is an analytical device which integrates whole cells—which are responsible for its selectivity—with a physical transducer to generate a measurable signal proportional to the concentration of analytes. These natural receptors, which can specifically bind HMs, are proteins of noncatalytic or nonimmunogenic origin [39] and microorganisms such as: bacteria, mosses, algae [65, 66], yeasts [67], fungi, and lichens [6, 68]. By coupling the cells to a transducer that convert the cellular response into detectable signals it can be express the HM toxicity from a variety of environmental media including soil, sediment, and water [39, 69].

5.1. Bioluminescent-Based Sensor. It is well known that low concentrations of HMs (0.01–0.05 µg/mL) stimulated light output. This stimulation might occur due to (i) the modifications of the composition of fatty acid in cell membrane which affect the synthesis of fatty acids into intracellular media (and therefore alter the biochemical pathway of the light reaction) or to (ii) the interruption in the cell energy production [70]. As consequence, light production from the whole cell depends on the energy derived from the electron transport chain, so that luminescence measuring

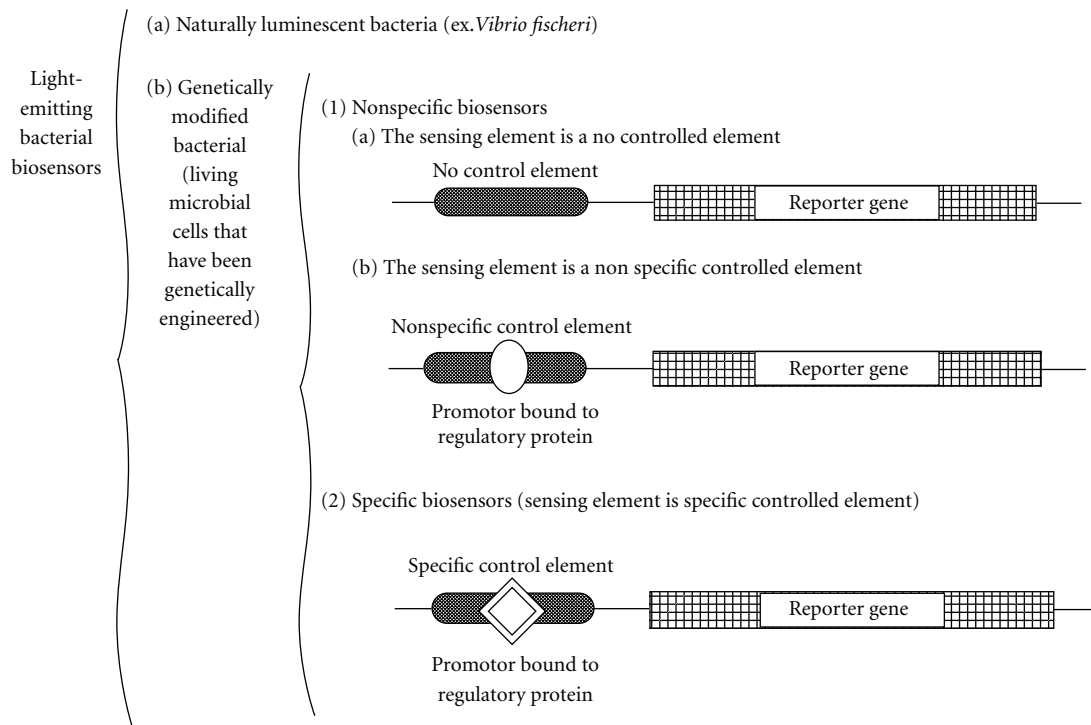


FIGURE 2: Classification of light-emitting bacterial biosensors.

gives information about the metabolic activity. According to the classical definition, the whole cell must be integrated with a transducer (photometer, luminometer, charged-couple device, and liquid-scintillation counter) to function as a true biosensor [67]. As consequence, the principle of biosensor based on bioluminescence is to estimate the toxicity of HMs by measuring the decrease in light output from the bacterium, when it is exposed to environmental samples [71].

The biosensors based on light-emitting bacteria could be classified in function of recognition element as described in Figure 2 [39, 67, 69, 72–74].

For surviving and growing in environments containing levels of toxic metals, the microorganisms have developed a variety of mechanisms, as following [73]:

- (i) exclusion of the metal by the cell membrane;
- (ii) active transport of the metal from the cell;
- (iii) sequestration of the metal inside the cell, so that it is not able to produce its toxic effects;
- (iv) sequestration of the metal in extracellular media, to prevent its entering into the cell;
- (v) chemical transformation of the metal in a compound that is less toxic to the cell.

Certainly, biosensors based on bacterial whole cell have either advantages or disadvantages over conventional methods of detecting contaminants (Table 6) [67–69, 73].

Whole cells/microbial biosensors typically suffer from the poor selectivity because of the nonspecific cellular response to substrates. There are several ways to improve the

selectivity of microbial biosensors: (i) using the biotechnology developments in the field of genetically engineering of cells with specific metabolic pathways upregulated or downregulated; (ii) to develop cell-based sensor arrays which generate a finger-printed response pattern; (iii) using the nanotechnology developments especially in the field of the nanostructured materials which can be coimmobilized with whole cells; (iv) the use of microfabrication, for example, micron-sized electrodes in view to develop single cell-based devices; (v) to build a lab-on-a-chip technique in which the integration of a cells onto a microfluidic chip can develop a biotic-microelectromechanical system; (vi) to develop a simple immobilization method to achieve a cells monolayer with very strong adhesion to a surface and without losing any of its biological function, in view to avoid the limits of the chemical methods (covalent binding and cross-linking) or the poor stability induced by physical methods (adsorption and entrapment).

5.2. Examples of Biosensors Based on Whole Cells for Heavy Metal Detection. Representative examples of biosensors based on whole cells are given in Table 7. As it can be seen, except the optical detection, the change of conductivity [75, 76] or of capacitance [68, 77] at an electrode/solution interface can supply information about conformational changes of the immobilised cells in the presence of HMs. A disposable setup (CellSense TM) is an example of a commercial system that allows up to 32 disposable biosensors to be monitored in a simultaneous manner; using such device a large number of measurements and replicates can be performed rapidly (30 min per assay) [78, 79].

The essential drawbacks (slow response, low sensitivity, and poor selectivity) using whole cells as biosensing element limit the widespread importance of commercial biosensors on the market.

6. Conclusions

Using the main interdisciplinary works from the past decades, the present paper summarises the recent progress in the fabrication and application of biosensors for HMs detection, with an accent on the types of immobilization techniques and the different types of transducers used. The increasing number of published papers has revealed the use of biosensors based on enzymes, DNA, or whole cells—as an easy technique for detections, HMs is in continuous improvement in a wide range of areas and also in the environmental market. Particularly, although the DNA and whole-cell-based biosensors have demonstrated their efficacy in gene discovery and genomics research, in the HMs detection they are more laboratory oriented and engage expensive equipment. The synergism between biotechnology and microelectronics lead developing new opportunities to build “smart” biosensors, highly integrated systems, and test kits applied in the alarm monitoring of environmental pollution, by using as bioreceptor novel enzymes or enzyme sources having a necessary enzyme activity. They will be small in size and high in sensitivity. However, until such biosensor accomplish operational characteristics similar to the simple pH electrode (in terms of durability, selectivity, extended concentration range, and resistance to biofouling), they will probable continue to meet major barriers to extensive acceptance and to be applied for environmental monitoring.

For practical applications, at this time there is a strong need for a really integrated biosensor system that includes probes, samplers, detector as well as amplifier, and logic circuitry. Thus systems have great promise to present several advantages in size, performance, fabrication, analysis, and production cost. The small sizes of the probes (microliter to nanoliter) minimize sample requirement and diminish reagent and waste requirement. Highly integrated systems lead to a decrease in noise and an increase in signal, due to the enhanced efficiency of sample collection and the reduction of interfaces. The capacity of large-scale production using low-cost integrated circuit technology is, also, a significant benefit. The process of assemblage of various components is made by simple integration of some elements on a single chip.

All evolutions in micromachining and nanotechnology and all progresses concerning the selectivity and stability of recognition elements of “smart” sensors, of molecular devices, and of multiparameter sensor arrays are evident to have a main impact on pollution control. Further efforts should be done (i) to the development of new immobilization techniques (that enhance the stability of the biocomponent), (ii) to the design of new electrocatalysts (that facilitate the detection of pollutants), (iii) to address the fouling and degradation of electrochemical sensors during

use, and (iv) to the introduction of multisensor systems for simultaneous monitoring of several priority contaminants.

References

- [1] N. K. Srivastava and C. B. Majumder, “Novel biofiltration methods for the treatment of heavy metals from industrial wastewater,” *Journal of Hazardous Materials*, vol. 151, no. 1, pp. 1–8, 2008.
- [2] I. Oehme and S. Wolfbeis, “Optical sensors for determination of heavy metal ions,” *Mikrochimica Acta*, vol. 126, no. 3–4, pp. 177–192, 1997.
- [3] R. B. Thompson, B. P. Maliwal, V. L. Feliccia, C. A. Fierke, and K. McCall, “Determination of picomolar concentrations of metal ions using fluorescence anisotropy: biosensing with a “reagentless” enzyme transducer,” *Analytical Chemistry*, vol. 70, no. 22, pp. 4717–4723, 1998.
- [4] R. B. Thompson, B. P. Maliwal, and C. A. Fierke, “Selectivity and sensitivity of fluorescence lifetime-based metal ion biosensing using a carbonic anhydrase transducer,” *Analytical Biochemistry*, vol. 267, no. 1, pp. 185–195, 1999.
- [5] T. K. Vel Krawczyk, M. Moszczyńska, and M. Trojanowicz, “Inhibitive determination of mercury and other metal ions by potentiometric urea biosensor,” *Biosensors and Bioelectronics*, vol. 15, no. 11–12, pp. 681–691, 2000.
- [6] I. Bontidean, C. Berggren, G. Johansson et al., “Detection of heavy metal ions at femtomolar levels using protein-based biosensors,” *Analytical Chemistry*, vol. 70, no. 19, pp. 4162–4169, 1998.
- [7] S. Han, M. Zhu, Z. Yuan, and X. Li, “A methylene blue-mediated enzyme electrode for the determination of trace mercury(II), mercury(I), methylmercury, and mercury-glutathione complex,” *Biosensors and Bioelectronics*, vol. 16, no. 1–2, pp. 9–16, 2001.
- [8] J. E. Pearson, A. Gill, and P. Vadgama, “Analytical aspects of biosensors,” *Annals of Clinical Biochemistry*, vol. 37, no. 2, pp. 119–145, 2000.
- [9] D. R. Thévenot, K. Toth, R. A. Durst, and G. S. Wilson, “Electrochemical biosensors: recommended definitions and classification,” *Biosensors and Bioelectronics*, vol. 16, no. 1–2, pp. 121–131, 2001.
- [10] M. N. Velasco-Garcia and T. Mottram, “Biosensor technology addressing agricultural problems,” *Biosystems Engineering*, vol. 84, no. 1, pp. 1–12, 2003.
- [11] G. L. Turdean, S. E. Stanca, and I. C. Popescu, *Biosenzori Amperometrici. Teorie si Aplicatii*, Presa Universitara Clujana, Cluj-Napoca, Romania, 2005.
- [12] F. García Sánchez, A. Navas Díaz, M. C. Ramos Peinado, and C. Belledone, “Free and sol-gel immobilized alkaline phosphatase-based biosensor for the determination of pesticides and inorganic compounds,” *Analytica Chimica Acta*, vol. 484, no. 1, pp. 45–51, 2003.
- [13] A. L. Berezhetskyy, O. F. Sosovska, C. Durrieu, J. M. Chovelon, S. V. Dzyadevych, and C. Tran-Minh, “Alkaline phosphatase conductometric biosensor for heavy-metal ions determination,” *ITBM-RBM*, vol. 29, no. 2–3, pp. 136–140, 2008.
- [14] R. Koncki, K. Rudnicka, and L. Tymecki, “Flow injection system for potentiometric determination of alkaline phosphatase inhibitors,” *Analytica Chimica Acta*, vol. 577, no. 1, pp. 134–139, 2006.
- [15] I. Lapenaite, B. Kurtinaitiene, L. Pliusksys et al., “Application of PQQ-GDH based polymeric layers in design of biosensors for

- detection of heavy metals," *Materials Science (Medžiagotyra)*, vol. 9, no. 4, pp. 431–435, 2003.
- [16] R. A. Copeland, *Enzymes: A Practical Introduction to Structure, Mechanism and Data Analysis*, Wiley-VCH, 2nd edition, 2000.
- [17] G. A. Evtugyn, H. C. Budnikov, and E. B. Nikolskaya, "Sensitivity and selectivity of electrochemical enzyme sensors for inhibitor determination," *Talanta*, vol. 46, no. 4, pp. 465–484, 1998.
- [18] G. A. Evtugyn, H. C. Budnikov, and E. B. Nikolskaya, "Biosensors for the determination of environmental inhibitors of enzymes," *Russian Chemical Reviews*, vol. 68, no. 12, pp. 1041–1064, 1999.
- [19] A. Amine, H. Mohammadi, I. Bourais, and G. Palleschi, "Enzyme inhibition-based biosensors for food safety and environmental monitoring," *Biosensors and Bioelectronics*, vol. 21, no. 8, pp. 1405–1423, 2006.
- [20] C. Malitesta and M. R. Guascito, "Heavy metal determination by biosensors based on enzyme immobilised by electropolymerisation," *Biosensors and Bioelectronics*, vol. 20, no. 8, pp. 1643–1647, 2005.
- [21] J. L. Gelpi, J. J. Avilés, M. Busquets et al., "A theoretical approach to the discrimination and characterization of the different classes of reversible inhibitors," *Concepts in Biochemistry*, vol. 70, no. 10, pp. 805–816, 1993.
- [22] S. Fennouh, V. Casimiri, A. Geloso-Meyer, and C. Burstein, "Kinetic study of heavy metal salt effects on the activity of L-lactate dehydrogenase in solution or immobilized on an oxygen electrode," *Biosensors and Bioelectronics*, vol. 13, no. 7-8, pp. 903–909, 1998.
- [23] M. Albareda-Sirvent, A. Merkoçi, and S. Alegret, "Pesticide determination in tap water and juice samples using disposable amperometric biosensors made using thick-film technology," *Analytica Chimica Acta*, vol. 442, no. 1, pp. 35–44, 2001.
- [24] M. Albareda-Sirvent, A. Merkoçi, and S. Alegret, "Thick-film biosensors for pesticides produced by screen-printing of graphite-epoxy composite and biocomposite pastes," *Sensors and Actuators B*, vol. 79, no. 1, pp. 48–57, 2001.
- [25] E. V. Gogol, G. A. Evtugyn, J. L. Marty, H. C. Budnikov, and V. G. Winter, "Amperometric biosensors based on nafion coated screen-printed electrodes for the determination of cholinesterase inhibitors," *Talanta*, vol. 53, no. 2, pp. 379–389, 2000.
- [26] F. N. Kok, F. Bozoglu, and V. Hasirci, "Construction of an acetylcholinesterase-choline oxidase biosensor for aldicarb determination," *Biosensors and Bioelectronics*, vol. 17, no. 6-7, pp. 531–539, 2002.
- [27] E. Wilkins, M. Carter, J. Voss, and D. Ivnitski, "A quantitative determination of organophosphate pesticides in organic solvents," *Electrochemistry Communications*, vol. 2, no. 11, pp. 786–790, 2000.
- [28] S. Zhang, H. Zhao, and R. John, "Development of a quantitative relationship between inhibition percentage and both incubation time and inhibitor concentration for inhibition biosensors: theoretical and practical considerations," *Biosensors and Bioelectronics*, vol. 16, no. 9, pp. 1119–1126, 2001.
- [29] A. Guerrieri, L. Monaci, M. Quinto, and F. Palmisano, "A disposable amperometric biosensor for rapid screening of anticholinesterase activity in soil extracts," *Analyst*, vol. 127, no. 1, pp. 5–7, 2002.
- [30] T. Neufeld, I. Eshkenazi, E. Cohen, and J. Rishpon, "A micro flow injection electrochemical biosensor for organophosphorus pesticides," *Biosensors and Bioelectronics*, vol. 15, no. 5-6, pp. 323–329, 2000.
- [31] S. Zhang, H. Zhao, and R. John, "A theoretical model for immobilized enzyme inhibition biosensors," *Electroanalysis*, vol. 13, no. 18, pp. 1528–1534, 2001.
- [32] B. Rozum and R. Koncki, "Application of monofluorophosphate/alkaline phosphatase system in flow injection analysis," *Talanta*, vol. 77, no. 2, pp. 507–513, 2008.
- [33] R. Ilangovan, D. Daniel, A. Krastanov, C. Zachariah, and R. Elizabeth, "Enzyme based biosensor for heavy metal ions determination," *Biotechnology and Biotechnological Equipment*, vol. 20, no. 1, pp. 184–189, 2006.
- [34] F. Kuralay, H. Özyörük, and A. Yıldız, "Inhibitive determination of Hg^{2+} ion by an amperometric urea biosensor using poly(vinylferrocenium) film," *Enzyme and Microbial Technology*, vol. 40, no. 5, pp. 1156–1159, 2007.
- [35] S. M. Lee and W. Y. Lee, "Determination of heavy metal ions using conductometric biosensor based on sol-gel-immobilized urease," *Bulletin of the Korean Chemical Society*, vol. 23, no. 8, pp. 1169–1172, 2002.
- [36] N. J. Nepomuscene, D. Daniel, and A. Krastanov, "Biosensor to detect chromium in wastewater," *Biotechnology and Biotechnological Equipment*, vol. 21, no. 3, pp. 377–381, 2007.
- [37] M. Singh, N. Verma, A. K. Garg, and N. Redhu, "Urea biosensors," *Sensors and Actuators B*, vol. 134, no. 1, pp. 345–351, 2008.
- [38] G. A. Zhylyak, S. V. Dzyadevich, Y. I. Korpan, A. P. Soldatkin, and A. V. El'skaya, "Application of urease conductometric biosensor for heavy-metal ion determination," *Sensors and Actuators B*, vol. 24, no. 1–3, pp. 145–148, 1995.
- [39] S. Rodriguez-Mozaz, M. P. Marco, M. J. Lopez De Alda, and D. Barceló, "Biosensors for environmental applications: future development trends," *Pure and Applied Chemistry*, vol. 76, no. 4, pp. 723–752, 2004.
- [40] T. M. Anh, S. V. Dzyadevych, N. Prieur et al., "Detection of toxic compounds in real water samples using a conductometric tyrosinase biosensor," *Materials Science and Engineering C*, vol. 26, no. 2-3, pp. 453–456, 2006.
- [41] O. Domínguez Renedo, M. A. Alonso Lomillo, and M. J. Arcos Martínez, "Optimisation procedure for the inhibitive determination of chromium(III) using an amperometric tyrosinase biosensor," *Analytica Chimica Acta*, vol. 521, no. 2, pp. 215–221, 2004.
- [42] R. Solná, S. Sapelníková, P. Skládal et al., "Multienzyme electrochemical array sensor for determination of phenols and pesticides," *Talanta*, vol. 65, no. 2, pp. 349–357, 2005.
- [43] M. Stoytcheva and V. Sharkova, "Kinetics of the inhibition of immobilized acetylcholinesterase with Hg^{2+} ," *Electroanalysis*, vol. 14, no. 14, pp. 1007–1010, 2002.
- [44] A. M. Aiken, B. M. Peyton, W. A. Apel, and J. N. Petersen, "Heavy metal-induced inhibition of *Aspergillus niger* nitrate reductase: applications for rapid contaminant detection in aqueous samples," *Analytica Chimica Acta*, vol. 480, no. 1, pp. 131–142, 2003.
- [45] X. J. Wang, S. Q. Xia, J. F. Zhao, H. N. Zhao, and N. Renault Jaffrezic, "Inhibitive determination of heavy metal ions by conductometric nitrate reductase biosensor," *Chemical Research in Chinese Universities*, vol. 25, no. 4, pp. 443–445, 2009.
- [46] I. Lapenaite, B. Kurtinaitiene, J. Razumiene et al., "Properties and analytical application of PQQ-dependent glycerol dehydrogenase from *Gluconobacter sp. 33*," *Analytica Chimica Acta*, vol. 549, no. 1-2, pp. 140–150, 2005.
- [47] M. R. Guascito, C. Malitesta, E. Mazzotta, and A. Turco, "Inhibitive determination of metal ions by an amperometric glucose oxidase biosensor: study of the effect of hydrogen

- peroxide decomposition," *Sensors and Actuators B*, vol. 131, no. 2, pp. 394–402, 2008.
- [48] J. X. Liu, X. M. Xu, L. Tang, and G. M. Zeng, "Determination of trace mercury in compost extract by inhibition based glucose oxidase biosensor," *Transactions of Nonferrous Metals Society of China (English Edition)*, vol. 19, no. 1, pp. 235–240, 2009.
- [49] D. Bagal-Kestwal, M. S. Karve, B. Kakade, and V. K. Pillai, "Invertase inhibition based electrochemical sensor for the detection of heavy metal ions in aqueous system: application of ultra-microelectrode to enhance sucrose biosensor's sensitivity," *Biosensors and Bioelectronics*, vol. 24, no. 4, pp. 657–664, 2008.
- [50] H. Mohammadi, A. Amine, S. Cosnier, and C. Mousty, "Mercury—enzyme inhibition assays with an amperometric sucrose biosensor based on a trienzymatic-clay matrix," *Analytica Chimica Acta*, vol. 543, no. 1-2, pp. 143–149, 2005.
- [51] L. K. Shyuan, L. Y. Heng, M. Ahmad, S. A. Aziz, and Z. Ishak, "Evaluation of pesticide and heavy metal toxicity using immobilized enzyme alkaline phosphatase with an electrochemical biosensor," *Asian Journal of Biochemistry*, vol. 3, no. 6, pp. 359–365, 2008.
- [52] S. D. Kamtekar, R. Pande, M. S. Ayyagari et al., "Trace analysis of Zn(II), Be(II), and Bi(III) by enzyme-catalyzed chemiluminescence," *Analytical Chemistry*, vol. 68, no. 1, pp. 216–220, 1996.
- [53] Y. Yang, Z. Wang, M. Yang et al., "Inhibitive determination of mercury ion using a renewable urea biosensor based on self-assembled gold nanoparticles," *Sensors and Actuators B*, vol. 114, no. 1, pp. 1–8, 2006.
- [54] D. Ogonczyk, L. Tymecki, I. Wyzkiewicz, R. Koncki, and S. Glab, "Screen-printed disposable urease-based biosensors for inhibitive detection of heavy metal ions," *Sensors and Actuators B*, vol. 106, no. 1, pp. 450–454, 2005.
- [55] A. Senillou, N. Jaffrezic-Renault, C. Martelet, and S. Cosnier, "A miniaturized urea sensor based on the integration of both ammonium based urea enzyme field effect transistor and a reference field effect transistor in a single chip," *Talanta*, vol. 50, no. 1, pp. 219–226, 1999.
- [56] B. B. Rodriguez, J. A. Bolbot, and I. E. Tothill, "Development of urease and glutamic dehydrogenase amperometric assay for heavy metals screening in polluted samples," *Biosensors and Bioelectronics*, vol. 19, no. 10, pp. 1157–1167, 2004.
- [57] A. M. Tencaliec, S. Laschi, V. Magearu, and M. Mascini, "A comparison study between a disposable electrochemical DNA biosensor and a *Vibrio fischeri*-based luminescent sensor for the detection of toxicants in water samples," *Talanta*, vol. 69, no. 2, pp. 365–369, 2006.
- [58] S. C. B. Oliveira, O. Corduneanu, and A. M. Oliveira-Brett, "In situ evaluation of heavy metal-DNA interactions using an electrochemical DNA biosensor," *Bioelectrochemistry*, vol. 72, no. 1, pp. 53–58, 2008.
- [59] E. L. S. Wong, E. Chow, and J. J. Gooding, "The electrochemical detection of cadmium using surface-immobilized DNA," *Electrochemistry Communications*, vol. 9, no. 4, pp. 845–849, 2007.
- [60] S. S. Babkina, N. A. Ulakhovich, and Y. I. Zyavkina, "Amperometric DNA biosensor for the determination of auto-antibodies using DNA interaction with Pt(II) complex," *Analytica Chimica Acta*, vol. 502, no. 1, pp. 23–30, 2004.
- [61] S. S. Babkina and N. A. Ulakhovich, "Amperometric biosensor based on denatured DNA for the study of heavy metals complexing with DNA and their determination in biological, water and food samples," *Bioelectrochemistry*, vol. 63, no. 1-2, pp. 261–265, 2004.
- [62] A. Ferancová, M. Adamovski, P. Gründler et al., "Interaction of tin(II) and arsenic(III) with DNA at the nanostructure film modified electrodes," *Bioelectrochemistry*, vol. 71, no. 1, pp. 33–37, 2007.
- [63] M. Farré, L. Kantiani, S. Pérez, and D. Barceló, "Sensors and biosensors in support of EU Directives," *Trends in Analytical Chemistry*, vol. 28, no. 2, pp. 170–185, 2009.
- [64] D. A. Blake, R. M. Jones, R. C. Blake, A. R. Pavlov, I. A. Darwish, and H. Yu, "Antibody-based sensors for heavy metal ions," *Biosensors and Bioelectronics*, vol. 16, no. 9–12, pp. 799–809, 2001.
- [65] Ş. Alpat, S. K. Alpat, B. H. Çadirci, I. Yaşa, and A. Telefoncu, "A novel microbial biosensor based on *Circinella* sp. modified carbon paste electrode and its voltammetric application," *Sensors and Actuators B*, vol. 134, no. 1, pp. 175–181, 2008.
- [66] L. E. De-Bashan and Y. Bashan, "Immobilized microalgae for removing pollutants: review of practical aspects," *Bioresource Technology*, vol. 101, no. 6, pp. 1611–1627, 2010.
- [67] J. Castillo, S. Gáspár, S. Leth et al., "Biosensors for life quality—design, development and applications," *Sensors and Actuators B*, vol. 102, no. 2, pp. 179–194, 2004.
- [68] I. Bontidean, J. Ahlvist, A. Mulchandani et al., "Novel synthetic phytochelatin-based capacitive biosensor for heavy metal ion detection," *Biosensors and Bioelectronics*, vol. 18, no. 5–6, pp. 547–553, 2003.
- [69] H. Strosnider, *Whole-cell bacterial biosensors and the detection of bioavailable arsenic*, Ph.D. thesis, National Network of Environmental Management Studies, August 2003.
- [70] F. A. Chinalia, G. I. Paton, and K. S. Killham, "Physiological and toxicological characterization of an engineered whole-cell biosensor," *Bioresource Technology*, vol. 99, no. 4, pp. 714–721, 2008.
- [71] J. J. C. Dawson, C. D. Campbell, W. Towers, C. M. Cameron, and G. I. Paton, "Linking biosensor responses to Cd, Cu and Zn partitioning in soils," *Environmental Pollution*, vol. 142, no. 3, pp. 493–500, 2006.
- [72] J. Bhattacharyya, D. Read, S. Amos, S. Dooley, K. Killham, and G. I. Paton, "Biosensor-based diagnostics of contaminated groundwater: assessment and remediation strategy," *Environmental Pollution*, vol. 134, no. 3, pp. 485–492, 2005.
- [73] S. Ramanathan, M. Ensor, and S. Daunert, "Bacterial biosensors for monitoring toxic metals," *Trends in Biotechnology*, vol. 15, no. 12, pp. 500–506, 1997.
- [74] S. Ripp and G. S. Sayl, "Advanced bioreporter technologies for targeted sensing of chemical and biological agents," <http://www.ceb.utk.edu>.
- [75] C. Chouteau, S. Dzyadevych, C. Durrieu, and J. M. Chovelon, "A bi-enzymatic whole cell conductometric biosensor for heavy metal ions and pesticides detection in water samples," *Biosensors and Bioelectronics*, vol. 21, no. 2, pp. 273–281, 2005.
- [76] N. Jaffrezic-Renault and S. V. Dzyadevych, "Conductometric microbiosensors for environmental monitoring," *Sensors*, vol. 8, no. 4, pp. 2569–2588, 2008.
- [77] C. Berggren, B. Bjarnason, and G. Johansson, "Capacitive biosensors," *Electroanalysis*, vol. 13, no. 3, pp. 173–180, 2001.
- [78] R. Bhatia, J. W. Dilleen, A. L. Atkinson, and D. M. Rawson, "Combined physico-chemical and biological sensing in environmental monitoring," *Biosensors and Bioelectronics*, vol. 18, no. 5–6, pp. 667–674, 2003.
- [79] H. Wang, X. J. Wang, J. F. Zhao, and L. Chen, "Toxicity assessment of heavy metals and organic compounds using

- CellSense biosensor with *E. coli*,” *Chinese Chemical Letters*, vol. 19, no. 2, pp. 211–214, 2008.
- [80] K. Tag, K. Riedel, H. J. Bauer, G. Hanke, K. H. R. Baronian, and G. Kunze, “Amperometric detection of Cu^{2+} by yeast biosensors using flow injection analysis (FIA),” *Sensors and Actuators B*, vol. 122, no. 2, pp. 403–409, 2007.
- [81] S. Leth, S. Maltoni, R. Simkus et al., “Engineered bacteria based biosensors for monitoring bioavailable heavy metals,” *Electroanalysis*, vol. 14, no. 1, pp. 35–42, 2002.
- [82] S. Tauriainen, M. Karp, W. Chang, and M. Virta, “Luminescent bacterial sensor for cadmium and lead,” *Biosensors and Bioelectronics*, vol. 13, no. 9, pp. 931–938, 1998.
- [83] I. Bontidean, A. Mortari, S. Leth et al., “Biosensors for detection of mercury in contaminated soils,” *Environmental Pollution*, vol. 131, no. 2, pp. 255–262, 2004.
- [84] T. Pellinen, T. Huovinen, and M. Karp, “A cell-free biosensor for the detection of transcriptional inducers using firefly luciferase as a reporter,” *Analytical Biochemistry*, vol. 330, no. 1, pp. 52–57, 2004.
- [85] P. R. G. Barrocas, W. M. Landing, and J. M. Hudson, “Assessment of mercury(II) bioavailability using a bioluminescent bacterial biosensor: practical and theoretical challenges,” *Journal of Environmental Sciences*, vol. 22, no. 8, pp. 1137–1143, 2010.
- [86] J. P. Sumner, N. M. Westerberg, A. K. Stoddard et al., “DsRed as a highly sensitive, selective, and reversible fluorescence-based biosensor for both Cu^+ and Cu^{2+} ions,” *Biosensors and Bioelectronics*, vol. 21, no. 7, pp. 1302–1308, 2006.
- [87] V. H. C. Liao, M. T. Chien, Y. Y. Tseng, and K. L. Ou, “Assessment of heavy metal bioavailability in contaminated sediments and soils using green fluorescent protein-based bacterial biosensors,” *Environmental Pollution*, vol. 142, no. 1, pp. 17–23, 2006.
- [88] R. R. Chapleau and M. Sagermann, “Real-time *in vivo* imaging of mercury uptake in *Caenorhabditis elegans* through the foodchain,” *Toxicology*, vol. 261, no. 3, pp. 136–142, 2009.
- [89] J. V. Stoyanov, D. Magnani, and M. Solioz, “Measurement of cytoplasmic copper, silver, and gold with a lux biosensor shows copper and silver, but not gold, efflux by the CopA ATPase of *Escherichia coli*,” *FEBS Letters*, vol. 546, no. 2-3, pp. 391–394, 2003.
- [90] S. K. Alpat, Ş. Alpat, B. Kutlu, Ö. Özbayrak, and H. B. Büyükişik, “Development of biosorption-based algal biosensor for Cu(II) using *Tetraselmis chuii*,” *Sensors and Actuators B*, vol. 128, no. 1, pp. 273–278, 2007.
- [91] H. Nguyen-Ngoc, C. Durrieu, and C. Tran-Minh, “Synchronous-scan fluorescence of algal cells for toxicity assessment of heavy metals and herbicides,” *Ecotoxicology and Environmental Safety*, vol. 72, no. 2, pp. 316–320, 2009.
- [92] M. Yüce, H. Nazir, and G. Dönmez, “An advanced investigation on a new algal sensor determining Pb(II) ions from aqueous media,” *Biosensors and Bioelectronics*, vol. 26, no. 2, pp. 321–326, 2010.
- [93] M. Yüce, H. Nazir, and G. Dönmez, “A voltammetric *Rhodotorula mucilaginosa* modified microbial biosensor for Cu(II) determination,” *Bioelectrochemistry*, vol. 79, no. 1, pp. 66–70, 2010.
- [94] M. Yüce, H. Nazir, and G. Dönmez, “Using of *Rhizopus arrhizus* as a sensor modifying component for determination of Pb(II) in aqueous media by voltammetry,” *Bioresource Technology*, vol. 101, no. 19, pp. 7551–7555, 2010.
- [95] I. Bontidean, J. R. Lloyd, J. L. Hobman et al., “Bacterial metal-resistance proteins and their use in biosensors for the detection of bioavailable heavy metals,” *Journal of Inorganic Biochemistry*, vol. 79, no. 1–4, pp. 225–229, 2000.
- [96] C. Michel, A. Ouerd, F. Battaglia-Brunet et al., “Cr(VI) quantification using an amperometric enzyme-based sensor: interference and physical and chemical factors controlling the biosensor response in ground waters,” *Biosensors and Bioelectronics*, vol. 22, no. 2, pp. 285–290, 2006.
- [97] R. Zlatev, J. P. Magnin, P. Ozil, and M. Stoytcheva, “Bacterial sensors based on *Acidithiobacillus ferrooxidans*: part II. Cr(VI) determination,” *Biosensors and Bioelectronics*, vol. 21, no. 8, pp. 1501–1506, 2006.
- [98] M. Souiri, I. Gammoudia, H. Ben Ouada et al., “*Escherichia coli*-functionalized magnetic nanobeads as an ultrasensitive biosensor for heavy metals,” *Procedia Chemistry*, vol. 1, no. 1, pp. 1027–1030, 2009.
- [99] N. Verma and M. Singh, “A *Bacillus sphaericus* based biosensor for monitoring nickel ions in industrial effluents and foods,” *Journal of Automated Methods and Management in Chemistry*, vol. 2006, Article ID 83427, pp. 1–4, 2006.

Review Article

Recent Advances in Electrochemical Glycobiosensing

Germarie Sánchez-Pomales and Rebecca A. Zangmeister

Bioprocess Measurements Group, Biochemical Science Division, Material Measurement Laboratory,
National Institute of Standards and Technology, 100 Bureau Drive, Gaithersburg, MD 20899, USA

Correspondence should be addressed to Rebecca A. Zangmeister, razang@nist.gov

Received 16 March 2011; Accepted 8 April 2011

Academic Editor: Bengi Uslu

Copyright © 2011 G. Sánchez-Pomales and R. A. Zangmeister. This is an open access article distributed under the Creative Commons Attribution License, which permits unrestricted use, distribution, and reproduction in any medium, provided the original work is properly cited.

Biosensors based on electrochemical transduction mechanisms have recently made advances into the field of glycan analysis. These glyco-biosensors offer simple, rapid, sensitive, and economical approaches to the measurement need for rapid glycan analysis for biomarker detection, cancer and disease diagnostics, and bioprocess monitoring of therapeutic glycoproteins. Although the prevalent methods of glycan analysis (high-performance liquid chromatography, mass spectrometry, and nuclear magnetic resonance spectroscopy) provide detailed identification and structural analysis of glycan species, there are significantly few low-cost, rapid glycan assays available for diagnostic and screening applications. Here we review instances in which glyco-biosensors have been used for glycan analysis using a variety of electrochemical transduction mechanisms (e.g., amperometric, potentiometric, impedimetric, and voltammetric), selective binding agents (e.g., lectins and antibodies), and redox species (e.g., enzyme substrates, inorganic, and nanomaterial).

1. Introduction

Glycosylation is the process by which a glycan (i.e., saccharide or carbohydrate) is added to a nonglycan moiety (e.g., protein) and is the most common posttranslational modification of proteins [1]. The glycoforms (i.e., diverse molecular forms of a glycoprotein, resulting from variable glycan structure and/or glycan attachment site occupancy) of a protein profoundly influence structure, function, stability, and serum half-life, which in turn affects many biological processes. Glycosylation plays a role in cell-cell interactions and has been linked to several disease states, including infection, genetic disorders, and cancer [2–4]. In the case of cancer, abnormal protein glycosylation has been linked to early tumor cell growth and proliferation; therefore, glycan-based biomarkers have been sought for early detection [3, 5–9].

Protein glycans are classified as either N-linked or O-linked (Figure 1). N-linked glycans are attached to the peptide at an Asn-X-Ser/Thr sequence site, where X ≠ proline, and share a common branched trimannosyl core. There are three N-glycan subtypes: *high-mannose* N-glycans which have mannose residues attached to the mannose core,

complex N-glycans that do not contain terminal mannose residues but have complex branching, and *hybrid* N-glycans which contain both mannose residues and complex branching. O-linked glycans tend to be less complex (i.e., linear), they do not share a common single core, and they attach through serine or threonine residues (GalNAc α 1-O-Ser/Thr). The seven monosaccharides found in human glycoprotein are mannose (Man), glucose (Glc), fucose (Fuc), galactose (Gal), N-acetylgalactosamine (GalNAc), N-acetylglucosamine (GlcNAc), and sialic acid (SA) or neuraminic acid (NeuNAc).

The variation in glycosylation has also been shown to influence the biological activity (efficacy) and immunogenicity (safety) of protein therapeutic drug products, the majority of which are glycosylated [10–12]. Glycoanalysis is required for approval and licensing of protein therapeutic drugs and is used for quality control and process change monitoring [12–14]. With the imminent introduction of biosimilars into the marketplace, glycoanalysis will figure prominently in the determination of “sameness” of generic protein therapeutic drugs. The impact on efficacy and safety of a drug product due to a particular glycan structure

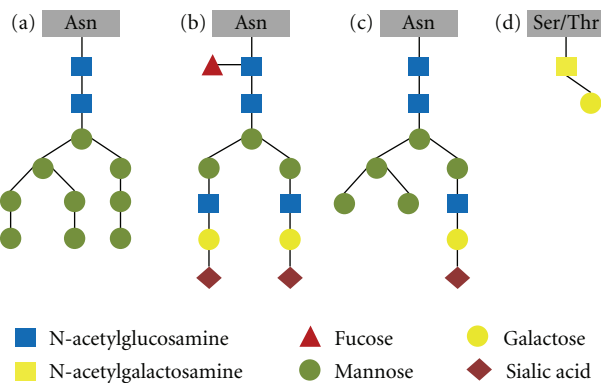


FIGURE 1: Oligosaccharide structure of the most common N-linked (a–c) and O-linked (d) glycans, including (a) high-mannose, (b) complex, and (c) hybrid glycans, and (d) the TF antigen.

or variation in that structure is somewhat unpredictable. Therefore, manufacturers of glycosylated proteins routinely specify and control the observed fractions of glycoforms down to a level dictated by the limit of detection (LOD) and/or limit of quantitation (LOQ) of the glycoanalysis techniques used. One consequence of this is that glycan species representing less than 5% of the total glycan count may be required to be controlled and specified.

This stringent requirement for characterization of glycan content in biomanufacturing and other areas of research has led to the development of sophisticated glycoanalysis techniques. Glycoanalysis is challenging for several reasons [1]. Unlike other areas of modern biology, such as the ability to predict the peptide sequence of a protein from its RNA and DNA sequences, glycosylation is not template driven and is therefore unpredictable. Glycosylation is inherently heterogeneous with variation found in the identity, relative amounts, and linking of the sugar groups of the oligosaccharide examined [14, 15]. The chemical structures of sugar subunits can be very similar, with no difference in molecular weight or charge. Even within a population of monoclonal antibodies produced using a cloned cell expression system, and highly monitored growth conditions, a heterogeneous glycan population can exist due to variation in expression levels [16, 17]. To complicate the analysis further, the glycans can be buried within the protein structure, as is the case for monoclonal antibodies, the largest class of protein therapeutics. Therefore, the glycan is not easily accessible for recognition binding assays and sample preparatory steps must be taken to cleave the glycan off the protein for further chemical and/or structural analysis.

The most common analytical techniques used for complex glycoanalysis include mass spectrometry [19–22], nuclear magnetic resonance spectroscopy [23–26], and separation techniques (e.g., high-performance liquid chromatography and capillary electrophoresis) [27–29]. These methods are well established and are able to provide detailed structural information, making them the most commonly used among nuclear glycoanalysis research centers [30–33]. Although the information gained by these analytical methods is detailed

and rigorous, the time and expertise required to carry out these analyses inhibits the application of these methods as diagnostic or screening assays for quality control monitoring of biomanufactured samples, or biomarker screening for disease or infection.

Complete structural detail may not be required for monitoring, screening, or diagnostic applications [34]. Accurate identification and quantitation of the terminal sugar oligo(saccharides) is all that may be required for these types of applications. Although biosensors cannot provide detailed glycosylation information, the level of selectivity and quantitative information they can provide, through the integrated transduction of a biological recognition event to a measurable signal, may be sufficient for high-throughput glycoanalysis measurements by nonspecialist laboratories [15, 34, 35].

2. Glycobiosensors

Glycobiosensors have recently made advances into this area of measurement science. Although sugar analysis by electrochemical methods has a long history (specifically we refer here to the large amount of literature devoted to glucose analysis by the glucose oxidase enzyme electrode [36–39]), the extension to the analysis of the glycan species of glycoconjugates (e.g., glycoproteins and glycopeptides) or cleaved glycan species is rare in comparison. There are several comprehensive reviews on the applications of biosensors for the study of glycans [34, 40] and carbohydrates in general [41, 42]. These reviews include a range of biosensor designs where the transduction mechanisms include optical (e.g., surface plasmon resonance, SPR), piezoelectric (quartz crystal microbalance, QCM), electrochemical (e.g., electron impedance spectroscopy, EIS or pulsed amperometric detection, PAD), and μ -cantilever deflection. Here we review instances in which glycobiosensors have been used for glycan analysis specifically using a variety of electrochemical transduction mechanisms.

2.1. Electrochemical Glycobiosensors. Electrochemical transduction methods are attractive because they often do not require labeling of the glycan, the physical instrumentation required for electrochemical analysis is often very simple and inexpensive, and the electrode characteristics (e.g., potential window, surface chemistry, and size) can be tailored for specific applications. One of the most widely used applications of electrochemical transduction methods for the analysis of carbohydrates, including cleaved glycans, is the coupling of an efficient separation technique, such as liquid chromatography (LC) or capillary electrophoresis (CE) with PAD. LC-PAD and CE-PAD systems have demonstrated high selectivity for easily oxidized or reduced analytes and limits of detection that rival fluorescence and mass spectrometric techniques [42]. These mature analytical systems have shown significant success over the past few decades. The application of LC, in particular high-performance anion exchange chromatography (HPAEC), and CE with PAD for the determination of oligosaccharide structure and the characterization of potential glycosylation sites has been thoroughly reviewed

by several groups [42–47]. These reviews discuss the analysis of mixtures of oligosaccharides, glycoproteins, glycopeptides and glycoconjugates by LC-PAD and CE-PAD.

Other electrochemical transduction methods used in glycobiosensor design include differential pulse voltammetry (DPV) [48–54], cyclic voltammetry (CV) [50, 54, 55], electrochemical impedance spectroscopy [18, 53, 54, 56–64], potentiometry [65, 66], and square wave voltammetry (SWV) [67, 68]. This review is focused specifically on biosensor technologies applied to glycoanalysis (i.e., a glycobiosensor) that use electrochemical transduction mechanisms, unless otherwise noted [69, 70].

Glycobiosensor designs can be quite complex, due to challenges associated with direct electrochemical analysis of glycans. Although carbohydrates are able to be oxidized using chemical agents, they do not commonly exhibit redox behavior [42]. Similarities in the chemical structure of sugars require the use of a selective binding agent or a separation technique prior to glycoanalysis [42]. The most well-known biosensor design is that of the enzyme electrode applied to the detection of glucose. In this example, the carbohydrate (glucose) is the substrate for the enzyme (glucose oxidase) which is proximal to the electrode surface; the redox active product of the enzymatic reaction is measured at the electrode surface and is proportional to the amount of glucose in solution. This technology was first introduced 50 years ago [36, 38], and there are several comprehensive articles that review the history of research in this field [39, 71–75].

The most common types of glycobiosensor design are presented in Figure 2. All of them use selective binding agents; the most common of which are lectins (carbohydrate-binding proteins), as will be discussed below, and a redox probe combined with one of the electrochemical transduction techniques listed above, the most common being EIS and DPV. Typically when EIS is used (Figure 2(a)), the electrode (planar or modified with a nanomaterial coating) is modified with a glycan-binding agent (lectin), which imparts selectivity and affinity. Changes in the charge transfer resistance at the electrode in the presence of a redox couple (e.g., $[Fe(CN)_6]^{3-/4-}$) are monitored and interpreted as binding of glycans, glycoconjugates, or cell surface carbohydrates. In the case of a lectin biosensor sandwich assay (Figure 2(b)), a surface-bound lectin selectively attracts a glycan target to the electrode surface, and a second redox active lectin conjugate binds to the captured target. Lastly, in the case of cell surface carbohydrate analysis, the cell is often captured at an electrode surface (planar or modified with a nanomaterial coating), and a lectin-enzyme conjugate in the presence of substrate selectively binds to cell surface carbohydrates and provides the electrochemical signature (Figure 2(c)). As will be seen in specific examples from the literature discussed below, nanomaterials are often incorporated into these biosensor designs either to increase the surface area and subsequently the signal generated at the electrode, or as a redox agent.

Lectins are by far the most commonly used selective binding elements for glycobiosensor measurements. Lectins are naturally occurring carbohydrate-binding proteins that exhibit specificity dependent on the identity of the terminal

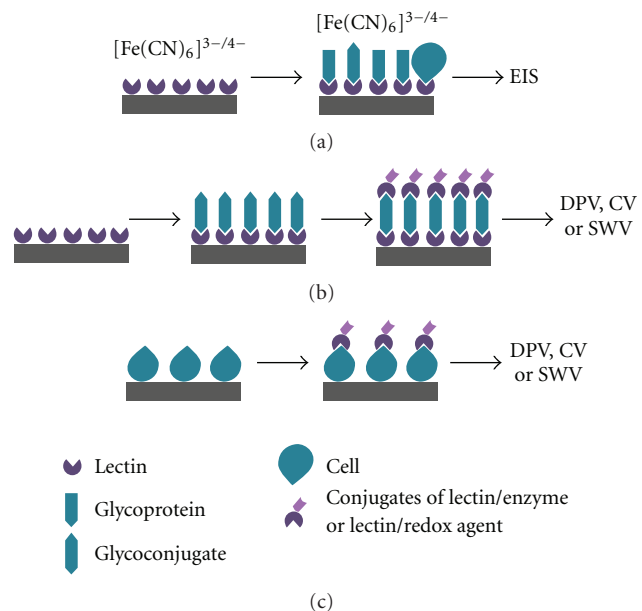


FIGURE 2: Schematic showing the most common types of electrochemical biosensors for glycan analysis: (a) electron impedance spectroscopy-(EIS) based assay; (b) a lectin biosensor sandwich assay using differential pulse voltammetry (DPV), cyclic voltammetry (CV), or square wave voltammetry (SWV) detection; (c) surface cell carbohydrate assay using a binding lectin/enzyme conjugate to provide the electrochemical signature detected by DPV, CV, or SWV.

sugar residue of the analyte. Although the specificity of lectins depends primarily on the terminal sugar group, quantitative differences in the affinity of lectins with various carbohydrate sequences, even in the case when the terminal sugar is the same, have been reported [76, 77]. Lectins are used in many areas of glycomics research including biomarker detection, clinical diagnostics, and the understanding of carbohydrate-protein interactions [35, 77–79].

Table 1 lists the lectins used and the sugar-binding specificity [34] for each instance surveyed here. Con A, a mannose/glucose binding lectin, is most often used as a selective pull-down reagent, bringing glycans, glycoconjugates, or cells to planar electrodes [63, 64] and to nanomaterial coated electrodes [18, 60, 61]. Covalent bonding of an enzyme (e.g., horseradish peroxidase, HRP) to Con A creates a lectin-enzyme conjugate that both binds to the glycan species of interest at the electrode and provides an enzymatically generated redox signal [48, 52]. Con A has also been used in lectin-glycan-lectin sandwich assays [51].

2.1.1. Glycobiosensors Based on Electrochemical Impedance Spectroscopy. Electrochemical impedance spectroscopy (EIS) is an efficient, sensitive, rapid, and inexpensive technique suitable for the characterization of transformations on electrode surfaces and, therefore, is especially suited for the label-free transduction of biosensing events on electrodes [64]. EIS enables rapid, label-free assays, through the analysis of changes in the properties of the electrode interface associated with analyte binding. In the case of glycan analysis, EIS

TABLE 1: Lectins used in glycobiosensor applications noted within this manuscript.

Lectin	Abbreviation	Major specificity	Reference(s)
Concanavalin A	Con A	Man, Glc, GlcNAc	[18, 48, 50–54, 56, 59–61, 63, 64, 82–84]
Peanut agglutinin	PNA	Gal- β (1,3)-GalNAc(O-linked GalNAc)	[18, 48, 58, 67, 83]
Sambucus lectin	SNA I SNA II	Sialic acid- α (2,6)Gal/GalNAc	[51, 57, 58][58]
Horse gram lectin	DBA	GalNAc	[18, 48, 83]
Wheat germ agglutinin	WGA	NeuAc/GlcNAc	[18, 48, 83]
Castor bean lectin	RCA	Gal	[56]
Lentil lectin	LCA	Man, Glc, GlcNAc	[82]
Maackia agglutinin	MAA	Sialic acid- α (2,3)	[57]
Cratylia mollis	Cramoll	Man, Glc	[62]

allows for the interrogation of lectin-glycan binding events by monitoring a change in the system impedance, or more specifically, a change in charge transfer resistance (R_{CT}) in the presence of a redox couple.

EIS measures the impedance of a system over a range of frequencies through the application of a small-amplitude alternating-current signal. EIS can be used to understand electrochemical reaction rates, and to describe interfaces due to its sensitivity to charge transfer processes that occur at the electrode/electrolyte interface. By fitting EIS data to an equivalent circuit, the value for R_{CT} (which models charge transfer across the interface) can be obtained. Binding events at the electrode surface would affect R_{CT} , due to the blocking effect that the immobilized molecules have on the charge transfer process; therefore, R_{CT} (or ΔR_{CT}) can be used as a detection parameter.

Electrochemical impedance spectroscopy, in conjunction with lectins, was used for the first time by La Belle and coworkers for the detection of glycoconjugates on a chip-based biosensor [58]. The plant lectins PNA and SNA (I and II) were covalently attached to a gold electrode previously modified with mercaptohexadecanoic acid, and impedimetric measurements in the presence of the redox couple ferrocyanide/ferricyanide were used to demonstrate binding of artificial and natural glycoconjugates to the lectin-modified gold electrode. An “artificial glycoprotein” construct of gold nanoparticles (AuNP) encapsulated with TF-antigens (Gal β 1-3GalNAc), as well as the glycoprotein asialofetuin (ASF), were rapidly detected on PNA-modified electrodes, whereas the glycoprotein fetuin (FET), the sialylated glycoform of ASF, was detected on SNA-modified electrodes with limits of detection as low as 1×10^{-8} g/L (150 femtomol/L).

Oliveira et al. modified gold electrodes using a sol-gel method with conjugates of lectins and gold nanoparticles and with polyvinyl butyral (PVB) [61]. Using EIS, they studied the interaction between the glycoprotein ovalbumin and the electrodes in the presence of potassium ferrocyanide/ferricyanide in phosphate buffer. The glucose/manose-specific lectins, Con A, and Cramoll bound ovalbumin, as evidenced by an increase in charge transfer resistance after the addition of the glycoprotein to the electrode. Increases in

the concentration of ovalbumin, from 0.025 g/L up to 0.2 g/L, resulted in increases in R_{CT} . These changes were confirmed by cyclic voltammetry.

The AuNP-lectin-PVB electrode prepared by Oliveira and coworkers [61] was also used to create an impedimetric biosensor to detect serum glycoproteins from patients infected by dengue fever (DF) [59]. A large increase in R_{CT} was obtained when the glycan portion of the glycoproteins present in the sera of patients infected with DF was allowed to interact with Con A in the modified gold electrode. A smaller increase in R_{CT} was observed when the serum of healthy patients was analyzed, demonstrating that the specific interaction between Con A and glycans can discriminate between sera from healthy and DF patients. A subsequent report by the same group demonstrated that impedimetric measurements with the AuNP-Con A-PVB electrode discriminate between the sera of patients infected by DF and dengue hemorrhagic fever (DHF), due to a higher expression of glycoproteins in the serum of DHF patients, which results in a larger increase in R_{CT} in comparison to the DF serum [60].

A similar EIS biosensor was fabricated by modifying Fe₃O₄ nanoparticles with the lectin Cramoll, mixing them with PVB and depositing them on a gold electrode [62]. The Fe₃O₄-Cramoll-PVB electrode was exposed to the glycoprotein fetuin and to sera from patients infected by different dengue serotypes, and increases in impedance were subsequently observed, indicating that the electrode can be used to sense lectin-glycan interactions. This biosensor effectively detected the presence of glycoproteins in just minutes, used small sample volumes, and was able to discriminate between different dengue serotypes.

Label-free impedimetric biosensors (Figure 3) have used the interaction between glycans and lectin-modified electrodes as the recognition principle to analyze the glycan expression on living cells [18]. Furthermore, the specificity of the lectin-glycan interaction enabled the detection, and identification of bacteria [64]. For example, rapid, label-free electrochemical detection, identification, and quantification of different bacteria were achieved by monitoring the impedimetric changes caused by the recognition between

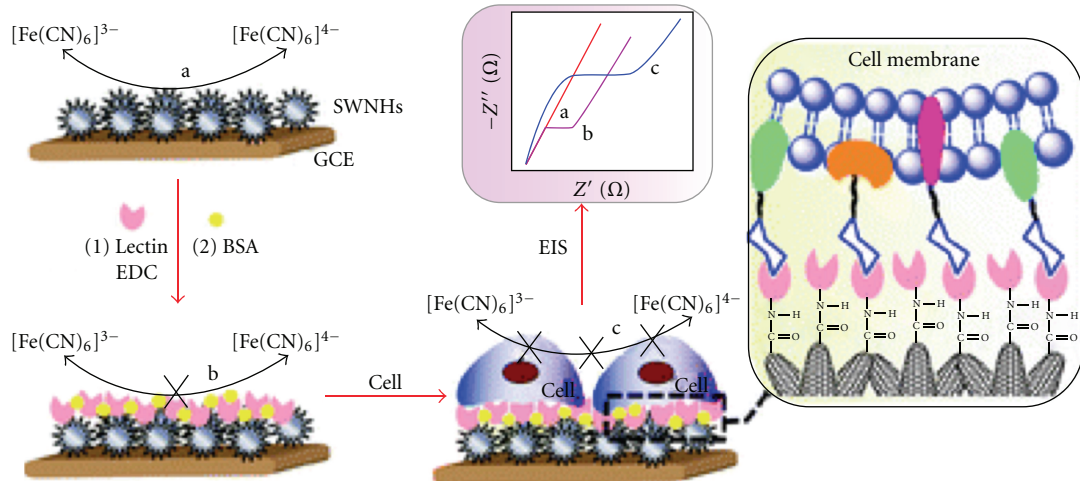


FIGURE 3: Schematic representation of the electrochemical label-free sensor for the analysis of glycan expression on cell surfaces. The sensor was fabricated by modifying a glassy carbon electrode (GCE) with single-walled nanohorns (SWNHs), followed by the covalent attachment of the lectin to the SWNHs, and blocking by bovine serum albumin (BSA). The specific binding between the lectin and the cell membrane carbohydrate was detected by EIS as an increase in charge transfer resistance in the presence of the redox couple $[\text{Fe}(\text{CN})_6]^{3-/4-}$ [18]. Reproduced with the permission of The Royal Society of Chemistry. <http://dx.doi.org/10.1039/B918008G>.

lectins and glycan components of bacteria walls. Nine different biotinylated lectins were mixed with the microorganisms, and subsequently deposited on the gold electrode for analysis. The biosensor detected, identified, and quantified three different bacteria with a detection limit and linear range equal to or better than other electrochemical biosensors. Another advantage is that this impedimetric sensor was able to rapidly monitor the change in charge transfer resistance resulting from the interaction between the lectins and the bacteria at gold electrodes without any preconcentration or preenrichment steps. The sensor showed the capability to discriminate between different types of bacteria by using multiplexed analysis with up to nine lectins (Figure 4).

Wan and coworkers fabricated another lectin-based impedimetric biosensor for the rapid and label-free detection of sulfate-reducing bacteria (SRB) at Con A-modified gold electrodes [63]. Con A was covalently attached to a self-assembled monolayer of 11-mercaptopoundecanoic acid (MPA) on gold and subsequently allowed to interact with SRB in order to determine and monitor the bacterial growth by impedance measurements in $[\text{Fe}(\text{CN})_6]^{3-/4-}$. Several parameters, including solution pH and incubation time, were optimized, and the concentration of SRB was determined from the charge transfer resistance values obtained by EIS. Additionally, the specificity of the biosensor was investigated by analyzing different types of bacteria, and it was reported that equal concentrations of different species of bacteria (e.g., SRB and Gram-negative bacterium *V. anguillarum*) induced different changes in the R_{CT} values (Figure 5). The impedimetric biosensor produced SRB growth curves similar to those obtained with the conventional and time-consuming most probable number (MPN) method, thus, demonstrating that EIS has great potential for the rapid, simple and low-cost detection and monitoring of microbial populations. Furthermore, recent work by Xi et al.

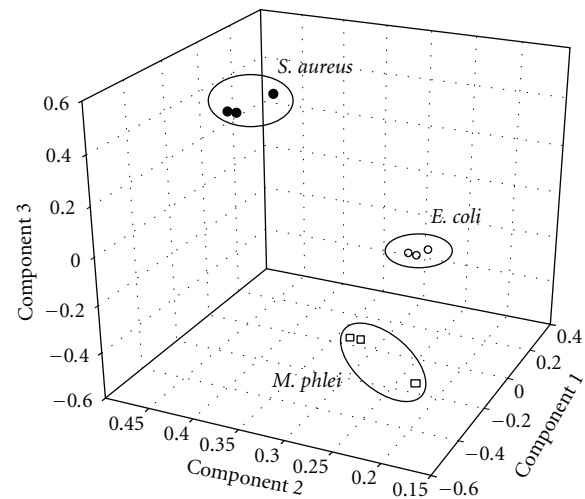


FIGURE 4: Pattern recognition plot obtained from impedimetric measurements using different lectins showing that EIS allows classification and distinction among different types of bacteria. Reprinted from [64], Copyright 2009, with permission from Elsevier.

has shown that a gold electrode modified with lectins by the layer-by-layer self-assembly technique can selectively discriminate Gram-negative bacteria, Gram-positive bacterium, fungus, and mammalian cells by EIS [56].

In related studies, EIS has been used as an effective technique to probe the sugar-binding specificity of lectins using carbohydrate-modified electrodes, composed of boron-doped diamond [80] and gold [81], among others. Furthermore, impedimetric measurements have elucidated the effect of changes in lectin conformation on glucose binding at platinum electrodes [82].

3. Applications: Biomarker and Cell Detection

Cell surface glycans play significant roles in many key biological processes, including cell differentiation, cell adhesion, cell recognition, and microbial pathogenesis [49]. Aberrant glycosylation patterns of cell surface carbohydrates have been linked to various diseases; thus, it is essential to develop sensitive, reliable, and high-throughput techniques to identify and detect cell surface carbohydrates. Due to their high sensitivity, low cost, simplicity, short assay time and ease of miniaturization, glycobiosensors are a promising alternative for glycan biomarker discovery [57]. In the past few years, glycobiosensors based on electrochemical impedance spectroscopy [57], potentiometry [66], and voltammetry [48, 54, 68] have been reported for the detection of cell surface glycans and potential biomarkers. Furthermore, in-situ imaging of membrane glycan motifs of human gastric carcinoma cells (BGC-823) has been performed by scanning electrochemical microscopy (SECM) [83].

One of the simplest glycobiosensor designs for cell surface glycan monitoring combined the specificity of lectin-glycan binding with the electroactive properties of the ferrocenyl group [50]. Ferrocene monocarboxylic acid (FcCOOH) was covalently conjugated to Con A, and the electroactive species-lectin conjugate was allowed to interact with K562 cells. The cell-Fc-Con A conjugates were unable to diffuse freely to the electrode surface, which, therefore, induced a decrease in differential pulse voltammetry (DPV) peak current, as compared to free Fc-Con A. The magnitude of the decrease in current was proportional to the amount of K562 cells, as well as to the expression extent of mannose-presenting glycans on the cell surface. This simple approach achieved cytosensing and cell surface glycan quantification.

A similar principle (i.e., monitoring a decrease in DPV peak current caused by binding of cells to the electrode) was used for the sensitive detection and quantification of intestinal human colon adenocarcinoma (LS180) cells. This novel glycobiosensor was based on a competition between the specific binding of L-selectin to an aptamer, versus specific binding of L-selectin with glycans on the surface of LS180 cells. Binding of LS180 cells effectively blocked electron transfer between the electroactive species (naphthoquinone) and the electrode, causing a decrease in the DPV peak current.

The principle of double layer capacitive measurements was used by Nagaraj and coworkers to identify glycoform variants of fetuin and differences in glycosylation of protein extracts from a human pancreatic cancer cell line [57]. The sensor, named Nanomonitor, consisted of an array of gold electrodes on a silicon chip that were modified with lectins via biotin/streptavidin linker chemistry. Perturbations of the electrical double-layer occurred when glycans interacted with the lectins, and the perturbations were detected with impedimetric measurements. The sensor distinguished between different synthesized glycoforms of fetuin and differences in glycosylation between protein extracts from human cancerous and normal pancreatic cells. In comparison to lectin-based ELISA assays, the Nanomonitor provided rapid, label-free analysis of glycoproteins with higher

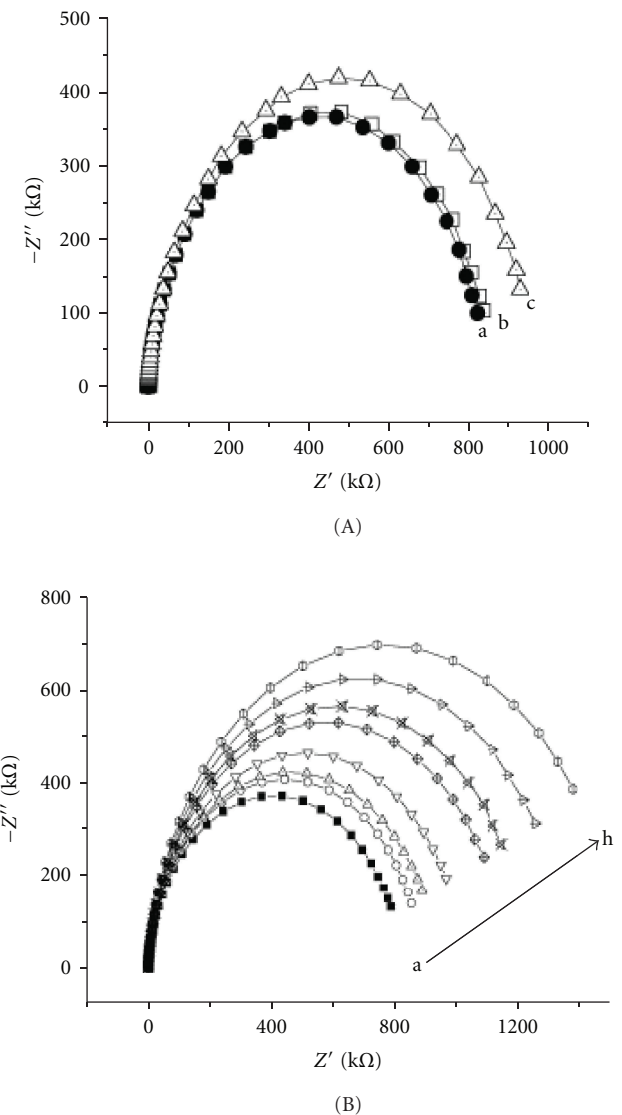


FIGURE 5: Electrochemical impedance spectra obtained on Con A/MPA/Au electrodes before (a) and after incubation with *V. anguillarum*. (b) and SRB (c) culture samples (A), and at different concentrations of SRB ranging from 1.8×10^3 cfu (colony forming units)/L to 1.8×10^{10} cfu/L (B). Reprinted from [63], Copyright 2009, with permission from Elsevier.

sensitivity (five orders of magnitude higher) and a broader dynamic range of glycoprotein concentrations.

Engineered nanomaterials, including nanoparticles [51, 66], nanotubes [48, 52, 54], quantum dots [67, 68, 84], and carbon nanohorns [53], have been used in conjunction with biological binding agents to fabricate glycobiosensors for biomarker detection. For example, single-walled carbon nanotubes functionalized with a short peptide sequence (RGDS, an integrin-binding sequence that inhibits integrin receptor function) were used to capture human leukemic K562 cells on a screen-printed carbon electrode or BGC-823 human gastric carcinoma cells on a glassy carbon electrode

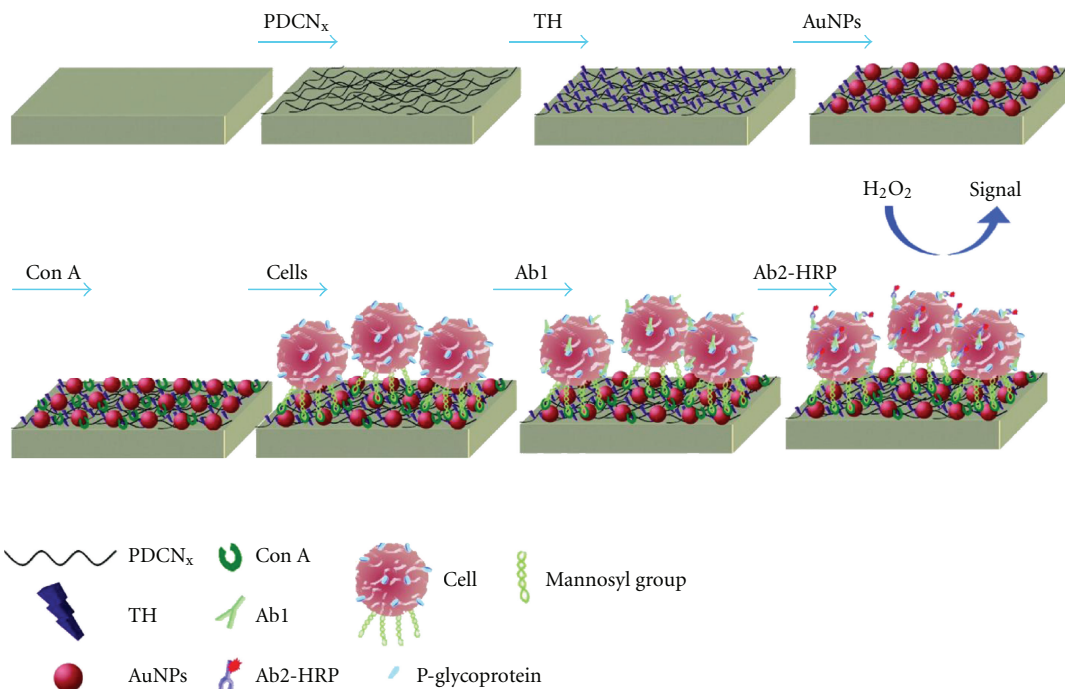


FIGURE 6: Schematic representation of the fabrication of the electrochemical enzyme-linked immunoassay for the detection of cell-surface glycans. Human epithelial carcinoma cells were captured on a glassy carbon electrode modified with nitrogen-doped carbon nanotubes, gold nanoparticles, and Con A. The enzyme HRP was incorporated to the electrode by two-step immunoreactions, and its catalytic reaction towards the oxidation of thionine by H₂O₂ was monitored. Reprinted with permission from [54]. Copyright 2010 American Chemical Society.

[48, 52]. The glycans on the cell wall then captured lectins conjugated to horseradish peroxidase (HRP), and differential pulse voltammetry (DPV) recorded the characteristic electrochemical signal from HRP catalysis in a solution containing H₂O₂ and *o*-phenylenediamine. DPV peak currents quantified the amount of lectins captured, which was directly related to the quantity of glycans on the cell surface. The degree of glycan expression on the cancer cell surface and changes in glycan expression after drug treatment were determined with high sensitivity and reproducibility. A variation of this assay showed enhanced sensitivity for the detection of K562 cell wall carbohydrates by combining single-walled carbon nanohorns and gold nanoparticles modified with Con A and HRP [53].

Zhang and coworkers also developed an electrochemical enzyme-linked immunoassay that relied on DPV for the detection of cell surface carbohydrates and an energy-dependent protein, P-glycoprotein, which can be found on tumor cells [54]. The HRP-catalyzed oxidation of thionine by H₂O₂ was monitored by cyclic voltammetry, EIS, and DPV at a glassy carbon electrode modified with nitrogen-doped carbon nanotubes, gold nanoparticles, and Con A (Figure 6). The specific binding between Con A and cell surface mannose groups captured human epithelial carcinoma cells. Electrocatalytic peak currents obtained from DPV measurements were correlated to the amount of glycans present on the cell surface. The designed cytosensor, while complex, showed good stability and reproducibility, and a wide linear

range and low detection limit for the quantification of P-glycoprotein and cell surface carbohydrates.

Alternatively, the potential shift that occurs when an electrode reacts with an ovarian tumor marker formed the basis for a potentiometric immunoassay for carbohydrate antigen-125 (CA125) [66]. Multifunctional magnetic beads, synthesized using magnetic Fe₃O₄ nanoparticles and poly(amidoamine) dendrimer, were used as an affinity support for the immobilization of anti-CA125 and, with the aid of a magnet, were attached on a carbon paste electrode. The potential shift recorded after CA125 was bound to the electrode allowed for the simple, rapid, and sensitive electrochemical detection of the CA125 tumor marker. The detection of the CA125 mucin-like glycoprotein was also achieved by a sandwich-type electrochemical immunoassay using anti-CA125-coated magnetic beads for CA125 capture and immobilization on the electrode, and anti-CA125-coated nanosilica particles doped with HRP and thionine for signal enhancement [55].

Gu et al. developed another sandwich-type immunoassay to detect the carbohydrate antigen 19-9 (CA 19-9), a marker for pancreatic cancer [68]. Conjugates of ZnO quantum dots and the antibody for CA 19-9 formed a sandwich structure through the immunoreactions with CA 19-9 and a monolayer of CA 19-9 antibody on a silicon wafer. The ZnO quantum dots linked to the substrate were dissolved in acidic media, and the solution containing Zn²⁺ was accumulated at the electrode and analyzed by square wave stripping

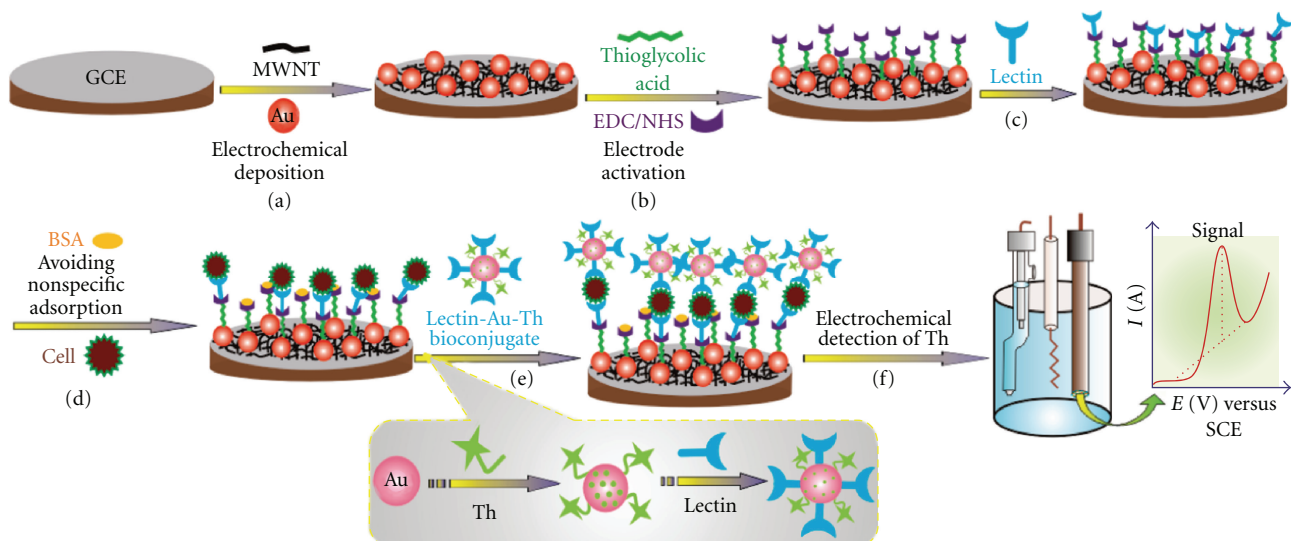


FIGURE 7: Schematic of the sandwich-type lectin-based sensor for electrochemical analysis of glycan expression on cells. A glassy carbon electrode was modified with gold nanoparticles, thioglycolic acid and lectins, and nonspecific adsorption to the electrode was blocked by BSA. Cell-surface glycans were bound to the lectin-modified electrode, and gold nanoparticles modified with lectins and thionine were subsequently bound to the cells to create the sandwich. Thionine was detected electrochemically by DPV. Reprinted with permission from [51]. Copyright 2010 American Chemical Society.

voltammetry (SWSV). This reusable immunosensor presented high sensitivity, stability, selectivity, and good reproducibility. Furthermore, SWSV in conjunction with CdS or CdTe quantum dots has also been used to develop competitive assays for the analysis of K562 cell surface carbohydrates [84], and for the detection of the cancer associated T-antigen [67].

The sandwich format was also used to fabricate a lectin-based sensor for the analysis of sialic acid potential biomarkers for human lung, liver, and prostate cancer [51]. A composite film of gold nanoparticles and multiwalled carbon nanotubes immobilized the lectins (Figure 7). Binding of the glycans on the cell wall surface to the lectin-modified electrode, followed by the attachment of gold nanoparticles labeled with lectins and the electroactive species thionine to the immobilized cells, formed the sandwich. The electrochemical signal of thionine was correlated to the carbohydrate expression levels on the cells, and indirectly to the amount of bound cells, therefore allowing cell quantification. A label-free, potentiometric sensor based on the interaction between phenylboronic acid (PBA) and 1,2- or 1,3-diols was applied to the analysis of altered sialic acid expression on erythrocytes as a model for diabetes diagnosis [65]. The previously described glycobiosensors were capable of detecting enhanced expression of sialic acid in cancer cells as compared to normal ones, and differences in sialic acid content in erythrocytes, thus demonstrating that sialic acid could serve as a potential biomarker for different types of cancer, as well as for diabetes mellitus.

4. Summary

Glycobiosensors offer simple, rapid, sensitive, and economical approaches to the measurement needs associated

with desired rapid glycan analysis for biomarker detection, cancer and disease diagnostics, and bioprocess monitoring of therapeutic glycoproteins. The examples discussed here are generally singular in occurrence, but the successful application of a variety of electrochemical transduction methods, combined with novel redox probes speak to the compatibility of biosensors with glycoanalysis. The high sensitivity and broad dynamic range reported for the Nanomonitor system is one example of how a well-engineered glycobiosensor can offer a rapid and label-free alternative to glycan monitoring by traditional lectin-based ELISA assays. As new information about glycan structure and function is gleaned from glycobiomics researchers, new glycobiosensors can be developed. In addition to lectin binding agents, the integration of aptamer and antibody binding agents into electrochemical glycobiosensors may improve the specificity of these assays. Further advances in the development of these types of glycobiosensors will help to effectively transfer the knowledge gained from specialist glycoanalysis research facilities into practical low-cost assays for high-throughput analysis that will be accessible for use in clinical and biomanufacturing settings.

Acknowledgment

Financial support was received by G. S.-Pomales through the National Research Council-Research Associateship Program/NIST postdoctoral fellowship program.

References

- [1] A. Varki et al., Ed., *Essentials of Glycobiology*, Cold Spring Harbor Press, Cold Spring Harbor, NY, USA, 1999.

- [2] D. H. Dube and C. R. Bertozzi, "Glycans in cancer and inflammation—potential for therapeutics and diagnostics," *Nature Reviews Drug Discovery*, vol. 4, no. 6, pp. 477–488, 2005.
- [3] N. H. Packer, C. W. von der Lieth, K. F. Aoki-Kinoshita et al., "Frontiers in glycomics: bioinformatics and biomarkers in disease: an NIH White Paper prepared from discussions by the focus groups at a workshop on the NIH campus, Bethesda MD (September 11–13, 2006)," *Proteomics*, vol. 8, no. 1, pp. 8–20, 2008.
- [4] H. J. An, S. R. Kronewitter, M. L. A. de Leoz, and C. B. Lebrilla, "Glycomics and disease markers," *Current Opinion in Chemical Biology*, vol. 13, no. 5-6, pp. 601–607, 2009.
- [5] T. Patwa, C. Li, D. M. Simeone et al., "Glycoprotein analysis using protein microarrays and mass spectrometry," *Mass Spectrometry Reviews*, vol. 29, no. 5, pp. 830–844, 2010.
- [6] P. M. Drake, W. Cho, B. Li et al., "Sweetening the pot: adding glycosylation to the biomarker discovery equation," *Clinical Chemistry*, vol. 56, no. 2, pp. 223–236, 2010.
- [7] Y. Qiu, T. H. Patwa, L. Xu et al., "Plasma glycoprotein profiling for colorectal cancer biomarker identification by lectin glycoarray and lectin blot," *Journal of Proteome Research*, vol. 7, no. 4, pp. 1693–1703, 2008.
- [8] K. Ueda, T. Katagiri, T. Shimada et al., "Comparative profiling of serum glycoproteome by sequential purification of glycoproteins and 2-nitrobenzenesulfenyl (NBS) stable isotope labeling: a new approach for the novel biomarker discovery for cancer," *Journal of Proteome Research*, vol. 6, no. 9, pp. 3475–3483, 2007.
- [9] H. J. An, S. Miyamoto, K. S. Lancaster et al., "Profiling of glycans in serum for the discovery of potential biomarkers for ovarian cancer," *Journal of Proteome Research*, vol. 5, no. 7, pp. 1626–1635, 2006.
- [10] P. M. Rudd, T. Elliott, P. Cresswell, I. A. Wilson, and R. A. Dwek, "Glycosylation and the immune system," *Science*, vol. 291, no. 5512, pp. 2370–2376, 2001.
- [11] Y. van Kooyk and G. A. Rabinovich, "Protein-glycan interactions in the control of innate and adaptive immune responses," *Nature Immunology*, vol. 9, no. 6, pp. 593–601, 2008.
- [12] G. Walsh and R. Jefferis, "Post-translational modifications in the context of therapeutic proteins," *Nature Biotechnology*, vol. 24, no. 10, pp. 1241–1252, 2006.
- [13] A. J. Chirino and A. Mire-Sluis, "Characteristics biological products and assessing comparability following manufacturing changes," *Nature Biotechnology*, vol. 22, no. 11, pp. 1383–1391, 2004.
- [14] R. Jefferis, "Glycosylation of recombinant antibody therapeutics," *Biotechnology Progress*, vol. 21, no. 1, pp. 11–16, 2005.
- [15] S. A. Brooks, "Strategies for analysis of the glycosylation of proteins: current status and future perspectives," *Molecular Biotechnology*, vol. 43, no. 1, pp. 76–88, 2009.
- [16] M. Butler, "Optimisation of the cellular metabolism of glycosylation for recombinant proteins produced by mammalian cell systems," *Cytotechnology*, vol. 50, no. 1–3, pp. 57–76, 2006.
- [17] N. Jenkins, R. B. Parekh, and D. C. James, "Getting the glycosylation right: implications for the biotechnology industry," *Nature Biotechnology*, vol. 14, no. 8, pp. 975–981, 1996.
- [18] L. Ding, W. Cheng, X. Wang et al., "A label-free strategy for facile electrochemical analysis of dynamic glycan expression on living cells," *Chemical Communications*, no. 46, pp. 7161–7163, 2009.
- [19] A. Dell and H. R. Morris, "Glycoprotein structure determination by mass spectrometry," *Science*, vol. 291, no. 5512, pp. 2351–2356, 2001.
- [20] N. Kawasaki, M. Ohta, S. Hyuga, O. Hashimoto, and T. Hayakawa, "Analysis of carbohydrate heterogeneity in a glycoprotein using liquid chromatography/mass spectrometry and liquid chromatography with tandem mass spectrometry," *Analytical Biochemistry*, vol. 269, no. 2, pp. 297–303, 1999.
- [21] A. Lim, A. Reed-Boggs, and B. J. Harmon, "Glycosylation profiling of a therapeutic recombinant monoclonal antibody with two N-linked glycosylation sites using liquid chromatography coupled to a hybrid quadrupole time-of-flight mass spectrometer," *Analytical Biochemistry*, vol. 375, no. 2, pp. 163–172, 2008.
- [22] A. Zamfir and J. Peter-Katalinić, "Capillary electrophoresis-mass spectrometry for glycoscreening in biomedical research," *Electrophoresis*, vol. 25, no. 13, pp. 1949–1963, 2004.
- [23] B. Meyer and T. Peters, "NMR spectroscopy techniques for screening and identifying ligand binding to protein receptors," *Angewandte Chemie International Edition*, vol. 42, no. 8, pp. 864–890, 2003.
- [24] H. J. Gabius, H. C. Siebert, S. André, J. Jiménez-Barbero, and H. Rüdiger, "Chemical biology of the sugar code," *ChemBioChem*, vol. 5, no. 6, pp. 740–764, 2004.
- [25] M. R. Wormald, A. J. Petrescu, Y. L. Pao, A. Glithero, T. Elliott, and R. A. Dwek, "Conformational studies of oligosaccharides and glycopeptides: complementarity of NMR, X-ray crystallography, and molecular modelling," *Chemical Reviews*, vol. 102, no. 2, pp. 371–386, 2002.
- [26] J. Ø. Duus, C. H. Gotfredsen, and K. Bock, "Carbohydrate structural determination by NMR spectroscopy: modern methods and limitations," *Chemical Reviews*, vol. 100, no. 12, pp. 4589–4614, 2000.
- [27] N. Blow, "Glycobiology: a spoonful of sugar," *Nature*, vol. 457, no. 7229, pp. 617–620, 2009.
- [28] S. Kamoda and K. Kakehi, "Capillary electrophoresis for the analysis of glycoprotein pharmaceuticals," *Electrophoresis*, vol. 27, no. 12, pp. 2495–2504, 2006.
- [29] P. M. Rudd, H. C. Joao, E. Coghill et al., "Glycoforms modify the dynamic stability and functional activity of an enzyme," *Biochemistry*, vol. 33, no. 1, pp. 17–22, 1994.
- [30] Y. Wada, A. Dell, S. M. Haslam et al., "Comparison of methods for profiling O-glycosylation: human proteome organisation human disease glycomics/proteome initiative multi-institutional study of IgA1," *Molecular & Cellular Proteomics*, vol. 9, no. 4, pp. 719–727, 2010.
- [31] Y. Wada, P. Azadi, C. E. Costello et al., "Comparison of the methods for profiling glycoprotein glycans—HUPO human disease glycomics/proteome initiative multiinstitutional study," *Glycobiology*, vol. 17, no. 4, pp. 411–422, 2007.
- [32] S. Thobhani, C. T. Yuen, M. J. A. Bailey, and C. Jones, "Identification and quantification of N-linked oligosaccharides released from glycoproteins: an inter-laboratory study," *Glycobiology*, vol. 19, no. 3, pp. 201–211, 2009.
- [33] A. Beck, E. Wagner-Rousset, M. C. Bussat et al., "Trends in glycosylation, glycoanalysis and glycoengineering of therapeutic antibodies and Fc-fusion proteins," *Current Pharmaceutical Biotechnology*, vol. 9, no. 6, pp. 482–501, 2008.
- [34] S. Cunningham, J. Q. Gerlach, M. Kane, and L. Joshi, "Glycobioreceptors: recent advances and applications for the detection of free and bound carbohydrates," *Analyst*, vol. 135, no. 10, pp. 2471–2480, 2010.
- [35] J. Hirabayashi, "Lectin-based structural glycomics: glycoproteomics and glycan profiling," *Glycoconjugate Journal*, vol. 21, no. 1–2, pp. 35–40, 2004.

- [36] L. C. Clark and C. Lyons, "Electrode systems for continuous monitoring in cardiovascular surgery," *Annals of the New York Academy of Sciences*, vol. 102, pp. 29–45, 1962.
- [37] J. Wang, "Electrochemical glucose biosensors," *Chemical Reviews*, vol. 108, no. 2, pp. 814–825, 2008.
- [38] S. J. Updike and G. P. Hicks, "The enzyme electrode," *Nature*, vol. 214, no. 5092, pp. 986–988, 1967.
- [39] J. Wang, "Glucose biosensors: 40 years of advances and challenges," *Electroanalysis*, vol. 13, no. 12, pp. 983–988, 2001.
- [40] J. Q. Gerlach, S. Cunningham, M. Kane, and L. Joshi, "Glyco-biomimics and glycobiosensors," *Biochemical Society Transactions*, vol. 38, no. 5, pp. 1333–1336, 2010.
- [41] R. Jelinek and S. Kolusheva, "Carbohydrate biosensors," *Chemical Reviews*, vol. 104, no. 12, pp. 5987–6015, 2004.
- [42] R. P. Baldwin, "Electrochemical determination of carbohydrates: enzyme electrodes and amperometric detection in liquid chromatography and capillary electrophoresis," *Journal of Pharmaceutical and Biomedical Analysis*, vol. 19, no. 1-2, pp. 69–81, 1999.
- [43] T. R. I. Cataldi, C. Campa, and G. E. De Benedetto, "Carbohydrate analysis by high-performance anion-exchange chromatography with pulsed amperometric detection: the potential is still growing," *Fresenius' Journal of Analytical Chemistry*, vol. 368, no. 8, pp. 739–758, 2000.
- [44] P. L. Weber and S. M. Lunte, "Capillary electrophoresis with pulsed amperometric detection of carbohydrates and glycopeptides," *Electrophoresis*, vol. 17, no. 2, pp. 302–309, 1996.
- [45] M. R. Hardy and R. R. Townsend, "Separation of positional isomers of oligosaccharides and glycopeptides by high-performance anion-exchange chromatography with pulsed amperometric detection," *Proceedings of the National Academy of Sciences of the United States of America*, vol. 85, no. 10, pp. 3289–3293, 1988.
- [46] M. W. Spellman, "Carbohydrate characterization of recombinant glycoproteins of pharmaceutical interest," *Analytical Chemistry*, vol. 62, no. 17, pp. 1714–1722, 1990.
- [47] R. R. Townsend, "Analysis of glycoconjugates using high-pH anion-exchange chromatography," in *Carbohydrate Analysis*, Z. El Rassi, Ed., pp. 181–209, Elsevier, Amsterdam, The Netherlands, 1995.
- [48] W. Cheng, L. Ding, S. Ding, Y. Yin, and H. Ju, "A simple electrochemical cytosensor array for dynamic analysis of carcinoma cell surface glycans," *Angewandte Chemie International Edition*, vol. 48, no. 35, pp. 6465–6468, 2009.
- [49] Z. Shao, Y. Li, Q. Yang, J. Wang, and G. Li, "A novel electrochemical method to detect cell surface carbohydrates and target cells," *Analytical and Bioanalytical Chemistry*, vol. 398, no. 7-8, pp. 2963–2967, 2010.
- [50] Y. Xue, L. Ding, J. Lei, and H. Ju, "A simple electrochemical lectin-probe for in situ homogeneous cytosensing and facile evaluation of cell surface glycan," *Biosensors & Bioelectronics*, vol. 26, no. 1, pp. 169–174, 2010.
- [51] X. Zhang, Y. Teng, Y. Fu et al., "Lectin-based biosensor strategy for electrochemical assay of glycan expression on living cancer cells," *Analytical Chemistry*, vol. 82, no. 22, pp. 9455–9460, 2010.
- [52] W. Cheng, L. Ding, J. Lei, S. Ding, and H. Ju, "Effective cell capture with tetrapeptide-functionalized carbon nanotubes and dual signal amplification for cytosensing and evaluation of cell surface carbohydrate," *Analytical Chemistry*, vol. 80, no. 10, pp. 3867–3872, 2008.
- [53] L. Ding, Q. Ji, R. Qian, W. Cheng, and J. Huangxian, "Lectin-based nanoprobe functionalized with enzyme for highly sensitive electrochemical monitoring of dynamic carbohydrate expression on living cells," *Analytical Chemistry*, vol. 82, no. 4, pp. 1292–1298, 2010.
- [54] J. J. Zhang, F. F. Cheng, T. T. Zheng, and J. J. Zhu, "Design and implementation of electrochemical cytosensor for evaluation of cell surface carbohydrate and glycoprotein," *Analytical Chemistry*, vol. 82, no. 9, pp. 3547–3555, 2010.
- [55] D. Tang, B. Su, J. Tang, J. Ren, and G. Chen, "Nanoparticle-based sandwich electrochemical immunoassay for carbohydrate antigen 125 with signal enhancement using enzyme-coated nanometer-sized enzyme-doped silica beads," *Analytical Chemistry*, vol. 82, no. 4, pp. 1527–1534, 2010.
- [56] F. Xi, J. Gao, J. Wang, and Z. Wang, "Discrimination and detection of bacteria with a label-free impedimetric biosensor based on self-assembled lectin monolayer," *Journal of Electroanalytical Chemistry*, vol. 656, no. 1-2, pp. 252–257, 2011.
- [57] V. J. Nagaraj, S. Aithal, S. Eaton, M. Bothara, P. Wiktor, and S. Prasad, "NanoMonitor: a miniature electronic biosensor for glycan biomarker detection," *Nanomedicine*, vol. 5, no. 3, pp. 369–378, 2010.
- [58] J. T. La Belle, J. Q. Gerlach, S. Svarovsky, and L. Joshi, "Label-free impedimetric detection of glycan-lectin interactions," *Analytical Chemistry*, vol. 79, no. 18, pp. 6959–6964, 2007.
- [59] M. D. L. Oliveira, M. T. S. Correia, and F. B. Diniz, "A novel approach to classify serum glycoproteins from patients infected by dengue using electrochemical impedance spectroscopy analysis," *Synthetic Metals*, vol. 159, no. 21-22, pp. 2162–2164, 2009.
- [60] M. D. L. Oliveira, M. T. S. Correia, and F. B. Diniz, "Concanavalin A and polyvinyl butyral use as a potential dengue electrochemical biosensor," *Biosensors & Bioelectronics*, vol. 25, no. 4, pp. 728–732, 2009.
- [61] M. D. L. Oliveira, M. T. S. Correia, L. C. B. B. Coelho, and F. B. Diniz, "Electrochemical evaluation of lectin-sugar interaction on gold electrode modified with colloidal gold and polyvinyl butyral," *Colloids and Surfaces B*, vol. 66, no. 1, pp. 13–19, 2008.
- [62] M. D. L. Oliveira, M. L. Nogueira, M. T. S. Correia, L. C. B. B. Coelho, and C. A. S. Andrade, "Detection of dengue virus serotypes on the surface of gold electrode based on Cratylia mollis lectin affinity," *Sensors and Actuators B*, vol. 155, no. 2, pp. 789–795, 2011.
- [63] Y. Wan, D. Zhang, and B. Hou, "Monitoring microbial populations of sulfate-reducing bacteria using an impedimetric immunosensor based on agglutination assay," *Talanta*, vol. 80, no. 1, pp. 218–223, 2009.
- [64] M. Gamella, S. Campuzano, C. Parrado, A. J. Reviejo, and J. M. Pingarrón, "Microorganisms recognition and quantification by lectin adsorptive affinity impedance," *Talanta*, vol. 78, no. 4-5, pp. 1303–1309, 2009.
- [65] A. Matumoto, N. Sato, H. Cabral, K. Kataoka, and Y. Miyahara, "Label free potentiometric sialic acid detection applicable to living cell diagnosis," in *IEEE Sensors Conference (SENSORS '09)*, pp. 1885–1888, October 2009.
- [66] X. H. Fu, "Poly(amidoamine) dendrimer-functionalized magnetic beads as an immunosensing probe for electrochemical immunoassay for carbohydrate antigen-125 in human serum," *Analytical Letters*, vol. 43, no. 3, pp. 455–465, 2010.
- [67] Z. Dai, A. N. Kawde, Y. Xiang et al., "Nanoparticle-based sensing of glycan-lectin interactions," *Journal of the American Chemical Society*, vol. 128, no. 31, pp. 10018–10019, 2006.

- [68] B. Gu, C. Xu, C. Yang, S. Liu, and M. Wang, “ZnO quantum dot labeled immunosensor for carbohydrate antigen 19-9,” *Biosensors & Bioelectronics*, vol. 26, no. 5, pp. 2720–2723, 2011.
- [69] D. R. Thevenot, K. Toth, R. A. Durst et al., “Electrochemical biosensors: recommended definitions and classification—(technical report),” *Pure and Applied Chemistry*, vol. 71, no. 12, pp. 2333–2348, 1999.
- [70] D. R. Thévenot, K. Toth, R. A. Durst, and G. S. Wilson, “Electrochemical biosensors: recommended definitions and classification,” *Biosensors & Bioelectronics*, vol. 16, no. 1-2, pp. 121–131, 2001.
- [71] E. H. Yoo and S. Y. Lee, “Glucose biosensors: an overview of use in clinical practice,” *Sensors*, vol. 10, no. 5, pp. 4558–4576, 2010.
- [72] A. Heller and B. Feldman, “Electrochemical glucose sensors and their applications in diabetes management,” *Chemical Reviews*, vol. 108, no. 7, pp. 2482–2505, 2008.
- [73] G. S. Wilson and Y. Hu, “Enzyme-based biosensors for in vivo measurements,” *Chemical Reviews*, vol. 100, no. 7, pp. 2693–2704, 2000.
- [74] N. S. Oliver, C. Toumazou, A. E. G. Cass, and D. G. Johnston, “Glucose sensors: a review of current and emerging technology,” *Diabetic Medicine*, vol. 26, no. 3, pp. 197–210, 2009.
- [75] J. D. Newman and A. P. F. Turner, “Home blood glucose biosensors: a commercial perspective,” *Biosensors & Bioelectronics*, vol. 20, no. 12, pp. 2435–2453, 2005.
- [76] A. M. Wu, “Carbohydrate structural units in glycoproteins and polysaccharides as important ligands for Gal and GalNAc reactive lectins,” *Journal of Biomedical Science*, vol. 10, no. 6, pp. 676–688, 2003.
- [77] A. M. Wu, E. Lisowska, M. Duk, and Z. Yang, “Lectins as tools in glycoconjugate research,” *Glycoconjugate Journal*, vol. 26, no. 8, pp. 899–913, 2009.
- [78] D. Mislovičová, P. Gemeiner, A. Kozarova, and T. Kožár, “Lectinomics I. Relevance of exogenous plant lectins in biomedical diagnostics,” *Biologia*, vol. 64, no. 1, pp. 1–19, 2009.
- [79] P. Gemeiner, D. Mislovičová, J. Tkáč et al., “Lectinomics. II. A highway to biomedical/clinical diagnostics,” *Biotechnology Advances*, vol. 27, no. 1, pp. 1–15, 2009.
- [80] S. Szunerits, J. Niedziolka-Jonsson, R. Boukherroub, P. Woisel, J.-S. Baumann, and A. Siriwardena, “Label-free detection of lectins on carbohydrate-modified boron-doped diamond surfaces,” *Analytical Chemistry*, vol. 82, no. 19, pp. 8203–8210, 2010.
- [81] L. Tan, Q. Xie, and S. Yao, “Electrochemical piezoelectric quartz crystal impedance study on the interaction between concanavalin A and glycogen at Au electrodes,” *Bioelectrochemistry*, vol. 70, no. 2, pp. 348–355, 2007.
- [82] R. R. Ueta and F. B. Diniz, “Adsorption of concanavalin A and lentil lectin on platinum electrodes followed by electrochemical impedance spectroscopy: effect of protein state,” *Colloids and Surfaces B*, vol. 61, no. 2, pp. 244–249, 2008.
- [83] Y. Xue, L. Ding, J. Lei, F. Yan, and H. Ju, “In situ electrochemical imaging of membrane glycan expression on micro-patterned adherent single cells,” *Analytical Chemistry*, vol. 82, no. 17, pp. 7112–7118, 2010.
- [84] L. Ding, W. Cheng, X. Wang, S. Ding, and H. Ju, “Carbohydrate monolayer strategy for electrochemical assay of cell surface carbohydrate,” *Journal of the American Chemical Society*, vol. 130, no. 23, pp. 7224–7225, 2008.

Review Article

Electrochemical Behavior of Biologically Important Indole Derivatives

Cigdem Karaaslan and Sibel Suzen

Department of Pharmaceutical Chemistry, Faculty of Pharmacy, Ankara University, Tandoğan 06100, Ankara, Turkey

Correspondence should be addressed to Sibel Suzen, sibel@pharmacy.ankara.edu.tr

Received 11 January 2011; Accepted 21 January 2011

Academic Editor: Bengi Uslu

Copyright © 2011 C. Karaaslan and S. Suzen. This is an open access article distributed under the Creative Commons Attribution License, which permits unrestricted use, distribution, and reproduction in any medium, provided the original work is properly cited.

Voltammetric techniques are most suitable to investigate the redox properties of a new drug. Use of electrochemistry is an important approach in drug discovery and research as well as quality control, drug stability, and determination of physiological activity. The indole nucleus is an essential element of a number of natural and synthetic products with significant biological activity. Indole derivatives are the well-known electroactive compounds that are readily oxidized at carbon-based electrodes, and thus analytical procedures, such as electrochemical detection and voltammetry, have been developed for the determination of biologically important indoles. This paper explains some of the relevant and recent achievements in the electrochemistry processes and parameters mainly related to biologically important indole derivatives in view of drug discovery and analysis.

1. Indoles in Medicinal Chemistry

Indole is an aromatic heterocyclic compound that has a bicyclic structure. It is an accepted constituent of fragrances and the precursor to many pharmaceuticals. One of the oldest and most reliable methods for synthesizing substituted indoles is the Fischer indole synthesis (Scheme 1) developed in 1883 [1].

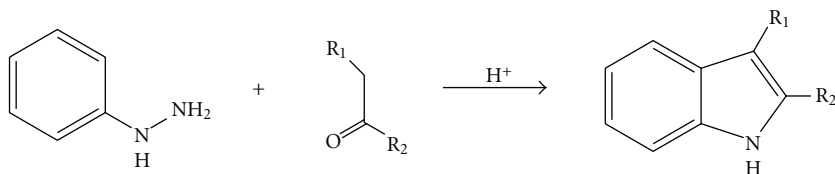
Indoles are present in many important biological compounds. Tryptophan is a significant indole derivative while serotonin and melatonin are biochemically active indole molecules. There are also many indole alkaloid derivatives found in nature. The plant hormone Auxin contains indol-3-acetic acid. Furthermore, there are many important indole derivatives used in treatment. The anti-inflammatory drug indomethacin, the betablocker pindolol, and the naturally occurring hallucinogen dimethyltryptamine are some of the important indole derivatives.

Indole derivatives represent many important classes of therapeutical agents in medicinal chemistry such as anti-cancer [2], antioxidant [3], antirheumatoidal [4], and anti-HIV [5, 6]. Studies showed that some of the 2-phenylindole (2PI) sulfamates are inhibitors of steroid sulfatase with antiproliferative activity in breast cancer cells [7, 8]. Some

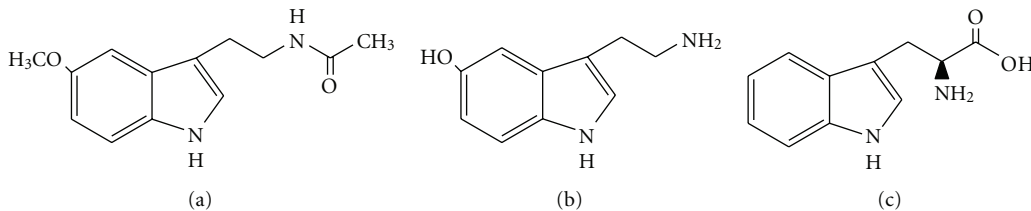
of the sulfur containing 2PI derivatives show *in vivo* anti-neoplastic and antiestrogenic activity [9, 10]. Furthermore, some indole derivatives, such as melatonin and serotonin, influence many important biochemical processes. They act as antioxidant and play an important role in the immune system [11–14].

Melatonin (MLT; Scheme 2(a)), is an indole ring containing hormone produced in the brain by the pineal gland, from the amino acid tryptophan. It has a significant role in the protection of nuclear and mitochondrial DNA. In recent years, many physiological properties of MLT have been described resulting in much attention in the development of synthetic compounds possessing the indole ring. MLT was initially found to function as a mediator of circannual reproductive rhythms and circadian cycles [15]. Furthermore, it has oncostatic effects [16], immune system stimulation [17], and anti-inflammatory functions [18]. MLT was identified as a powerful free radical scavenger and indirect antioxidant [19, 20].

Serotonin (Scheme 2(b)) or 5-Hydroxytryptamine (5-HT) is a monoamine neurotransmitter. Biochemically derived from tryptophan (Scheme 2(c)), serotonin is primarily found in the gastrointestinal tract, platelets, and in the central nervous system of humans and animals. It is a



SCHEME 1: Fischer indole synthesis.



SCHEME 2: Chemical formula of melatonin (a), serotonin (b), and tryptophan (c).

well-known contributor to feelings of well-being; therefore, it is also known as a happiness hormone.

Neurotransmitter serotonin synthesizes from tryptophan and can be converted to neurohormone melatonin via N-acetyltransferase and 5-hydroxyindole-O-methyltransferase activities. Niacin is synthesized from tryptophan as key biosynthetic intermediate.

Indole and its derivatives are well known electroactive compounds that are readily oxidized at carbon-based electrodes, for example, glassy carbon electrode [21]. Voltammetric techniques in general, and differential pulse voltammetry (DPV) in particular, are considered to be useful tools for the determination of indole derivatives [22, 23].

2. Introduction to Electrochemical Studies with Indole Derivatives

Electrochemistry deals with behavior of oxidation and reduction reactions connected by an external electric circuit to understand each process. Redox and electrochemical processes involve electron transfer to/from a molecule. This reaction can occur by the application of a voltage or by the release of chemical energy.

Electrochemical synthesis has shown to be a very useful procedure to obtain organic molecules. The main advantage of the electrochemical synthesis is the lack of oxidant and reducing agents, which makes the workup procedure easier [24–26]. The synthesis of the indole ring is of particular importance in organic, pharmaceutical, and medical chemistry. There is great effort to the improvement of existing methods for indole preparation in the pharmaceutical research. Electrochemistry offers an important alternative to the classical methodologies utilized in the synthesis of chemicals. Procedures in electroanalysis strongly depend on material aspects such as chemical and physical properties of

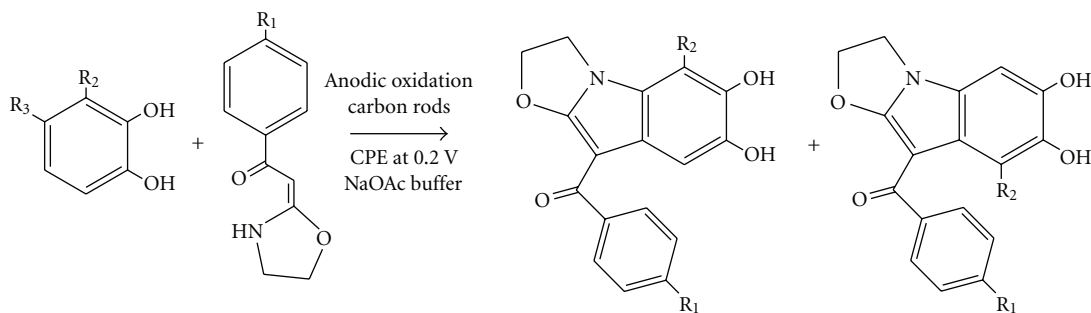
electrode surfaces, the effects of applied potential, adsorption, and coatings applied to the electrode surface to enhance detection [27].

A good electrical conductivity of the electrodes is an important factor. Solid electrodes in general, especially carbon, are easy and practical as mercury for electroanalytical research. A detailed review was published by Uslu and Ozkan [27] including developments and applications of carbon-based electrodes for drug compounds in their dosage forms and in biological samples in the period from 1996 till 2006. Furthermore, compared to other voltammetric techniques, a squarewave voltammetry was presented in a minireview [28]. In the review, the several advantages such as high speed, increased analytical sensitivity, and relative insensitivity to the presence of dissolved oxygen were discussed.

Voltammetry is an electroanalytical method used in pharmaceutical, medicinal, analytical, and organic chemistry as well as various industrial processes. In this method, data about an analyte is obtained by measuring the current as the potential is varied. There are many types of voltammetry including linear sweep voltammetry, staircase voltammetry, squarewave voltammetry (SWV), cyclic voltammetry (CV), anodic stripping voltammetry, cathodic stripping voltammetry, adsorptive stripping voltammetry, alternating current voltammetry, rotated electrode voltammetry, normal pulse voltammetry and DPV.

CV is very suitable to investigate the redox properties of a new drug to give insights to metabolic fate. DPV and SWV voltammetry has been particularly useful for trace measurements of electroactive compounds in body fluids and tissues. SWV is a large amplitude differential technique in which a waveform composed of a symmetrical squarewave, superimposed on a base staircase potential, is applied to the working electrode [29].

2.1. Studies on the Substituted Synthetic Indole Derivatives. It is well known that voltammetric techniques are most suitable



SCHEME 3: Some electrochemically synthesized fused indole derivatives.

to investigate the redox properties of a new drug in order to have more information about drugs metabolic fate [30].

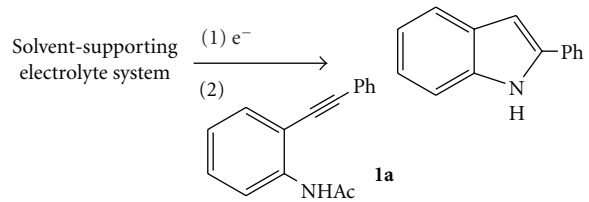
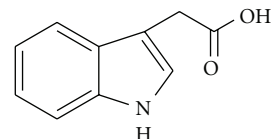
Applications of electrochemistry include the determination of electrode oxidation mechanisms. Knowing that there is a resemblance between electrochemical and biological reactions, it can be considered that the oxidation mechanisms taking place at the electrode and in the body may have similar principles.

A suitable electrochemical approach was described in a study for the synthesis of indole derivatives from catechols and R-oxoheterocyclic ketene N,O-acetals (Scheme 3) [31]. This is an environmentally friendly method to create fused indole derivatives containing active hydroxyls and carbonyl under mild reaction conditions.

The electrochemical-mediated annulation of 2-alkynylanilines to the corresponding indole derivatives proceeds in good yields and under conditions that avoid the use of metal catalysts or classical organic acids and bases (Scheme 4) [32]. A novel preparation of the electrogenerated cyanomethyl anion as an electrogenerated base, in the synthesis of substituted indoles from alkynylanilines was developed. The workup process only requires filtration or flash chromatography of the evaporated reaction mixture. It was reported that this electrochemical approach represents an important alternative to the previous procedures.

The effect of indole and 5-chloroindole on the anodic dissolution of copper in acidic sodium chloride solutions was studied using voltammetry on a rotating disc electrode (RDE) [33]. Both compounds, used at 10^{-3} M concentration act as strong inhibitors on the copper dissolution, but indole exhibits better inhibiting properties. The influence of these organic additives on the electrodeposition of copper on platinum was also investigated using RDE and electrochemical quartz crystal microbalance (EQCM) techniques. The EQCM measurements show that a sparingly soluble layer of the inhibitor is responsible for the protective effects observed in chloride solutions.

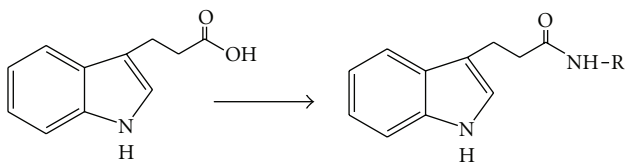
A new voltammetric method was successfully used to detect indole-3-acetic acid (IAA; Scheme 5) in some plant leaves. Sodium dodecyl sulfate (SDS), an anionic surfactant, can strongly adsorb at the surface of a carbon paste electrode (CPE) *via* the hydrophobic interaction. In the presence of SDS, the cationic indole-3-acetic acid was highly accumulated at the CPE surface through the electrostatic

SCHEME 4: Synthesis of 2-phenyl indole derivative by cyclization of **1a** induced by the electrogenerated cyanomethyl anion under different reaction conditions [32].

SCHEME 5: Chemical formula of indole-3-acetic acid.

interaction between the negative-charged head group of SDS and cationic IAA, compared with that in the absence of SDS. The experimental parameters, such as pH, varieties of surfactants, concentration of SDS, and scan rate were optimized for IAA determination [34].

Metabolization usually progressed through the addition or the modification of a substituent; this will give rise to additional waves or to a shift of the main wave due to the metabolites. CV has been used in studying the redox mechanism that is related to antioxidant activity of synthesized indole-3-propionamide (Scheme 6) [21]. Based on this study, a simple, rapid, and sensitive voltammetric method was developed for the determination of the indole derivatives that are readily oxidized at the carbon-based electrodes. The oxidative behavior of the indole derivatives was studied as a function of pH at a glassy carbon electrode. The results showed that the compounds might have profound effects on our understanding of their *in vivo* redox processes and pharmaceutical activity. It was assumed that the oxidation step of indolic compounds is located on the nitrogen atom in the indole ring of the molecule, which is electroactive in both acidic and basic media, leading finally to hydroxylation of benzene ring.



SCHEME 6: Chemical formula of indole-3-propionamides [21].

Electrochemical techniques offer important information about drug molecules and their mechanisms in the body, such as metabolism, which is one of the important actions in drug discovery. Two compounds, namely, 1-methylindole-3-carboxaldehyde isonicotinoyl hydrazone (Scheme 7(a)) and 5-chloro-1H-indole-3-carboxaldehyde isonicotinoyl hydrazone (Scheme 7(b)) were synthesized, characterized, and examined electrochemically using different voltammetric techniques in order to evaluate the possible biological behavior [35]. A linear response was obtained in the different media for the compounds with low detection limits of the synthesized compounds.

Electrochemical behavior of some indolyl-thiohydantoin derivatives (Scheme 8) was studied in order to understand the electrochemical process that occurs on the glassy carbon electrode, both pH and scan rate [36]. For the quantitative determination, differential pulse voltammetric methods were applied. It was assumed that the oxidation steps occur for all the compounds on the nitrogen atom in the indole ring, which is electroactive in both acidic and basic media, leading finally to hydroxylation of the benzene ring. Studies of electrochemical oxidation of indole and some derivatives showed that the indole ring is most likely form dimers and trimers. This technique has been successfully applied to trace measurements of important pharmaceutical compounds.

The use of electrochemistry and combination of this method with other analytical techniques are becoming one of the important approaches in drug discovery. Many physiological processes depend on oxidoreduction reactions in the body. For that reason, it may be possible to find similarities between electrochemical and biochemical reactions. In a review by Suzen and Ozkan [37], the latest developments related to the use of electrochemical techniques in drug research will be surveyed in order to evaluate possible combinations of spectrometric methods with electrochemical techniques, were presented. The use of electrochemistry and combination with spectroscopic techniques are becoming one of the important approaches in drug discovery and research.

In a review published by Greci et al. [38], reactivity of radical cations of primary aromatic amines towards indoles and that of indoles towards primary aromatic amines were studied. It is known that radical cations can be generated from substrates with low oxidation potentials by electrochemical oxidation. For some researchers, many reactions interpreted by an electron transfer process actually occur through an ionic mechanism while others, described by an ionic mechanism, involve an electron transfer

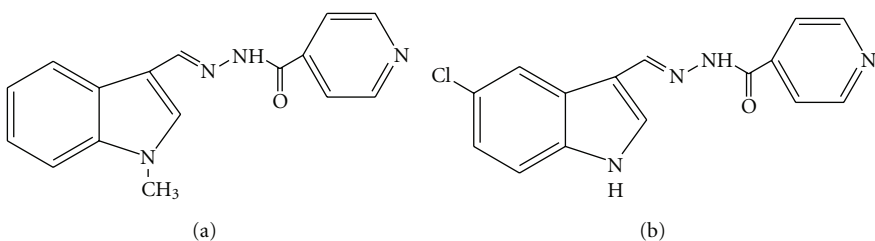
process [38]. Radical cations of primary aromatic amines were unable to attack nucleophiles such as 2-phenyl-1H-indole. The interaction between 2-phenyl-1H-indole, and primary aromatic amines may only occur through coupling of their neutral radicals. The 2-phenyl-1H-indolyl radical cation can dimerise as observed for tetrahydrocarbazoles, but dimerisation is faster when it reacts *via* the indolyl radical. As a result, 2-phenyl-1H-indole reacts with *p*-anisidine, 2-nitro-*p*-anisidine, and 2-nitro-*p*-methylaniline, under anodic oxidation, to give several products, depending on the potential used and on the presence or the absence of oxygen and a deprotonating agent. This study gives new information about the reactivity of radical cations generated by a controlled anodic potential and neutral radicals.

Some 2-phenyl indole (2PI; Scheme 9) derivatives were investigated electroanalytically by voltammetric determination as a function of pH at a glassy carbon and hanging mercury drop electrodes in different buffer media [29]. The studied molecules are extensively metabolized *in vivo*, mainly through oxidative processes in which we assume that the oxidation step of indolic compounds is located on the nitrogen atom in the indole ring of the molecule. Based on this study, simple, rapid, sensitive and validated voltammetric method was developed for the determination and investigation of electrochemical behaviour of the 2PI derivatives.

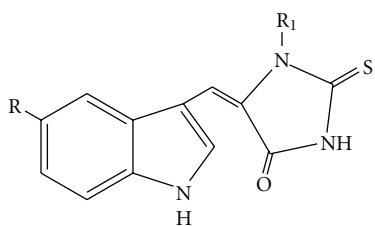
2.2. Studies-Related to Tryptophan Derivatives. The electrochemical behavior of an indole library of compounds that were found to be active free radical scavengers was investigated by Estevão et al. [39]. They used a voltammetric study and the oxidation potentials to make a correlation to the scavenging activity reported for the studied indoles. The study included several tryptophan and tryptamine derivatives. All the compounds showed an oxidation potential peak lower than that observed for indole, but higher than that described for the antioxidant melatonin. The electrochemical behavior showed a high correlation with the scavenging activity of peroxy radical, for selected compounds. It was observed that for some reactive species the scavenging mechanism involves electron transfer while for other species some structural requirements, such as the steric hindrance between the substrate and the bulky oxidant, should be considered when analyzing the scavenging activity.

A method has been developed for the simultaneous determination of MLT and pyridoxine hydrochloride in pharmaceutical dosage forms by DPV, based on the oxidation of both drugs at a glassy carbon electrode [40]. Cyclic and linear scan voltammetry were used to examine the influence of pH, nature of the buffer, scan rate, and concentration. The proposed method was successfully applied to the commercial tablets containing this drug combination without any interference by the excipients.

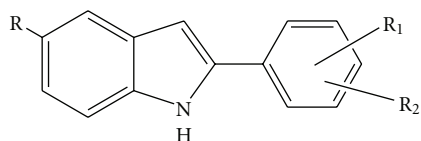
Indole and its metabolites (e.g., tryptamine and serotonin) are of biochemical importance, and analytical procedures have been developed for their determination in mixtures, based on liquid chromatography with electrochemical detection [41] and voltammetry [42, 43].



SCHEME 7: Chemical formula of 1-methylindole-3-carboxaldehyde isonicotinoyl hydrazone (a) and 5-chloro-1H-indole-3-carboxaldehyde isonicotinoyl hydrazone (b).



SCHEME 8: Chemical formula of indolyl-thiohydantoin derivatives.



SCHEME 9: Chemical formula of 2-phenyl indole derivatives.

The electrochemical behavior of tryptophan and its derivatives, such as indole-3-acetic acid, 5-hydroxytryptamine (Scheme 10(a)), 5-hydroxy-indole-3-acetic acid, and glycyl-tryptophan (Scheme 10(b)) peptide at a glassy carbon electrode modified with hemin (natural metalloporphyrin) by electropolymerization have been investigated in detail [44]. The results showed that the hemin/GC electrode would catalyze the electrochemical oxidation of tryptophan and its derivatives, based on which a differential pulse voltammetric procedure. The results indicated that a two-electron and two-proton transfer was involved in the electrode reaction process.

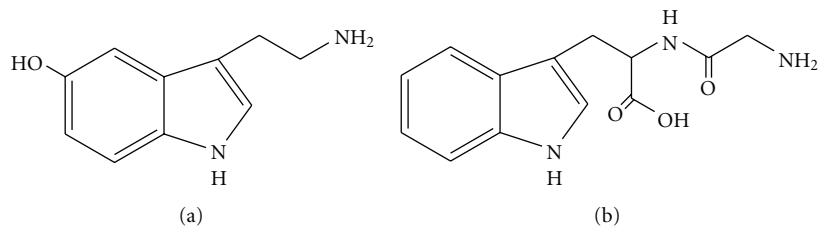
Tryptophan is an essential amino acid for humans and a precursor for serotonin, melatonin, and niacin. It has been implicated as a possible cause of schizophrenia in people who cannot metabolize it properly. Therefore, simple, sensitive, and less expensive detection of tryptophan is of great interest. Concentration of amino acids in biological samples is low; therefore, it is necessary to use a highly sensitive method that provides determination of these analytes at subordinate concentrations. Electroanalytical technique is an attractive method due to simplicity, low expense, high sensitivity, and possibility of miniaturization. In a study [45], a modified carbon paste electrode was prepared by using TiO₂ nanoparticles and ferrocene carboxylic acid (FCCA) in carbon paste matrix. The electrocatalytic oxidation of

glutathione (GSH) and tryptophan is individually and simultaneously investigated at the surface of FCCa-TiO₂ modified electrode using CV and DPV. High sensitivity and selectivity together with very low detection limit of the electrode response make it very suitable for simultaneous and individual determination of trace amounts of GSH and tryptophan in pharmaceutical and clinical preparations.

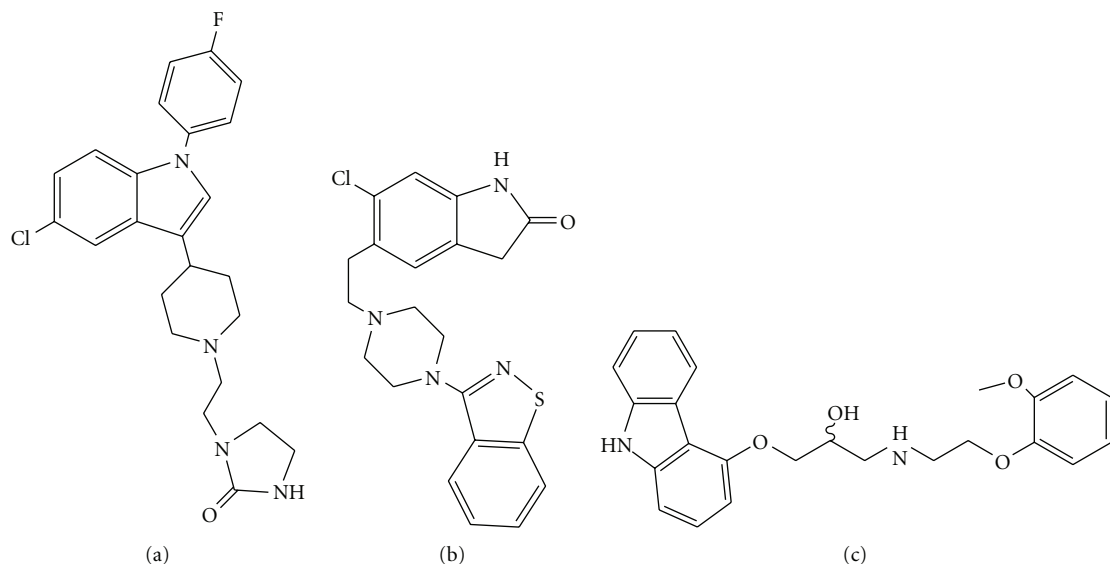
In a study, a modified electrode that was prepared by mixing 10 wt% of multiwalled carbon nanotube (MWCNT) and fine graphite powder with mineral oil (Nujol) and modified with cobalt salophen (CoSal) to applied for the selective determination of tryptophan in the presence of potentially interfering compounds such as cysteine and ascorbic acid [46]. A complete resolution between DPV peak of tryptophan from those of cysteine and ascorbic acid provides a very suitable and effective method for simultaneous determination of tryptophan, cysteine, and ascorbic acid in pharmaceutical and clinical preparations.

2.3. Studies on the Indole Ring Containing Drugs. The electrochemical oxidation of sertindole (Scheme 11(a)), the newer atypical antipsychotic was investigated using cyclic, linear sweep voltammetry at a glassy carbon and boron-doped diamond electrodes [47]. Sertindole levels were determined in serum and pharmaceutical formulations, by means of electrochemical methods. In CV, depending on pH values, sertindole showed one or two irreversible oxidation responses that were found related to the different electroactive part of the molecule. Using second and sharp oxidation peak, two voltammetric methods were described for the determination of sertindole by differential pulse and squarewave voltammetry at the glassy carbon and boron-doped diamond electrodes. To find out the relationship between the oxidative behavior and protonation constant, pK_a value of sertindole was determined. The proposed methods might be alternatives to the LC techniques in therapeutic drug monitoring or the experimental data might be used for the development LC-EC method.

Another psychotropic agent, Ziprasidone (Scheme 11), used for the treatment of schizophrenia was investigated electrochemically at boron-doped diamond and glassy carbon electrodes using cyclic, differential pulse, and squarewave voltammetry [48]. The dependence of the peak current and peak potentials on pH, concentration, nature of the buffer, and scan rate were examined. The proposed methods were



SCHEME 10: Chemical formula of 5-Hydroxytryptamine (a) and Glycyl-tryptophan (b).



SCHEME 11: Sertindole (a), ziprasidone (b), and carvedilol (c).

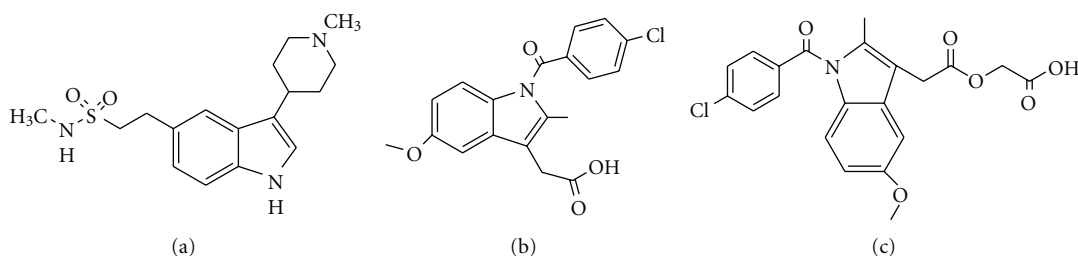
applied for the determination of ziprasidone from pharmaceutical dosage forms and human serum samples without any time-consuming extraction, separation, evaporation, or adsorption steps prior to drug assay except precipitation of the proteins using acetonitrile. The results were statistically compared with those obtained through an established LC-UV technique, no significant differences were found between the voltammetric and LC methods.

Carvedilol (Scheme 11(c)) is a nonselective β -adrenergic blocking agent with α_1 -blocking activity. It is used in the management of hypertension and angina pectoris and as an adjunct to standard therapy in symptomatic heart failure [49]. The electrochemical oxidation of carvedilol was investigated using cyclic, linear sweep voltammetry at a glassy carbon electrode [50]. These methods were successfully applied for the analysis of carvedilol pharmaceutical dosage forms and spiked human serum samples and were found to be rapid, requiring less than 7 min to run a sample. The electrochemical oxidation of carvedilol molecule has two irreversible electrode processes and both of them are pH dependent. No electroactive interferences from the tablet excipients and endogenous substances from biological material were found. These recovery results reveal that the proposed methods had adequate precision and accuracy,

and, consequently, can be applied to the determination of carvedilol without any interference from tablet excipients.

The electrochemical behavior and the analytical application of the selective serotonin agonist naratriptan (N-methyl-3-(1-methyl-4-piperidyl)indole-5-ethanesulfonamide; Scheme 12(a)) was presented by Velasco-Aguirre and Álvarez-Lueje [51]. Naratriptan exhibits an anodic response in aqueous media over a broad pH range (pH 2–12), as determined by DPV and CV using glassy carbon electrodes. This response is irreversible in nature, diffusion controlled, and, probably, caused by the oxidation of the naratriptan indole moiety. Selectivity trials revealed that the oxidation signal of the drug was not disturbed by the presence of excipients or degradation products. It was concluded that the method offered is useful for the quantification of naratriptan in pharmaceutical drugs and that this method requires no separations or extractions. The method was found not to be time consuming and is inexpensive when compared with the Pharmacopoeial HPLC method.

Indomethacin, 1-(p-chlorbenzoyl)5-methoxy-2-methyl-3-indolylacetic acid (Scheme 12(b)) is an important nonsteroidal anti-inflammatory drug, derived from indol, used in the treatment of some forms of inflammatory and degenerative diseases of articulations [52, 53]. A boron-doped diamond electrode was used to examine the possibility of

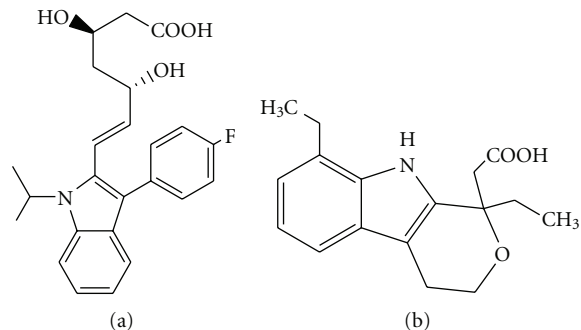


SCHEME 12: Chemical formula of naratriptan (a), indomethacin (b), and acemethacin (c).

anodic detection and determination of indomethacin by CV. The oxidation of this drug exhibited an irreversible character. Very sensitive output signal to low concentrations has been associated with a relative high background current. Scan rate dependencies suggested a diffusion-controlled process complicated by certain surface effects [53]. In another study, procedures for the determination of indomethacin and acemetacin (Scheme 12(c)) by differential pulse adsorptive stripping voltammetry with a mercury electrode have been described and optimized [54]. In a different study, the reduction of acemetacin was established using linear-sweep voltammetry at Hg electrode [55]. Indomethacin and acemetacin in urine were determined with good results and without the need for prior separation. Determination of indomethacin was described by a fully validated squarewave adsorptive cathodic stripping voltammetric procedure [56]. The procedure was based on the reduction of the C=O double bond of the drug molecule after its preconcentration onto the mercury electrode surface. The proposed procedure was successfully applied for determination of the drug in tablets and human serum with good recoveries.

Fluvastatin sodium (Fluvastatin; Scheme 13(a)) is a water-soluble cholesterol-reducing agent which acts by inhibition of 3-hydroxy-3-methylglutaryl-coenzyme A reductase. The oxidation of fluvastatin sodium on a glassy carbon electrode has been studied by use of a variety of voltammetric techniques [43]. Oxidation of fluvastatin sodium was found to be diffusion controlled and irreversible. The best results for the determination of fluvastatin sodium were obtained by using differential pulse and squarewave voltammetric techniques. The proposed methods were successfully applied to the determination of the drug in capsules and biological fluids. Determination of fluvastatin sodium in *Loscol capsule* and the electrochemical behavior of fluvastatin sodium on a glassy carbon electrode were investigated by CV, linear sweep voltammetry, and DPV by Yan [57]. Fluvastatin sodium gave a sensitive oxidation peak under the differential pulse voltammetric mode. The electrochemical analysis method described in the study enables simple and rapid determination of fluvastatin sodium in real samples.

Etodolac [1,8-Diethyl-1,3,4,9-tetrahydropyrano (3,4-b)-indole-1-acetic acid] (Scheme 13(b)) is a nonsteroidal anti-inflammatory drug used in postoperative pain and rheumatoid arthritis and inhibits the activity of prostaglandin synthetase. The drug appears to be uricosuric. The electrochemical oxidation of etodolac was investigated by cyclic, linear



SCHEME 13: Chemical formula of fluvastatin (a) and etodolac (b).

sweep, differential pulse, and squarewave voltammetry using glassy carbon electrode [22]. Based on this study, simple, rapid, selective, and sensitive two voltammetric methods were developed for the determination of the etodolac in tablet dosage form and human serum.

2.4. Studies on the Other Indole Compounds. The indole nucleus is present in a wide range of natural products, and the synthesis of this important structure has been a steady topic of interest for many years. The electrochemical oxidation of catechol has been studied in the presence of indole using CV and controlled-potential coulometry methods [58]. The results revealed that the quinone derived from the oxidation of catechol participates in Michael addition reactions with indole and converts it to the trisindolyl-quinone in a good yield via electrochemical oxidation. In another study, electrochemical behavior of some dihydroxybenzoic acid and catechol derivatives in the presence of indole as a nucleophile using cyclic strategy for the synthesis of some new indolyl derivatives of quinones and catechols was studied [59]. These products were obtained with good yields based on electrochemical oxidation under controlled-potential conditions in aqueous solutions, without toxic reagents and solvents at a carbon electrode, using an environmentally friendly method.

Electrochemical reduction of indole derivatives were studied by mechanism with many researchers [60]. Synthesis and discovery of new potent fluorinated active plant hormones was described [61]. The indirect electrochemical reduction, by means of an aromatic anion mediator,

of perfluoroalkyl halides in the presence of purine and indolyl anions was carried out. The corresponding C-perfluoroalkylated products were obtained in moderate to good yields. It was demonstrated that the electrochemical induction of the SRN₁ mechanism is a useful synthetic tool to obtain new F-alkylated purine and indole derivatives.

The oxidative dehydrocyclization of the 3-(indolizin-2'-yl)-2-oxoquinoxaline, performed either electrochemically or under the action of molecular iodine, affords new redox-active heterocyclophane [62]. The CV study of heterocyclophane showed the three-step oxidation of the indolizine fragments accompanied by the single-electron transfer in each step.

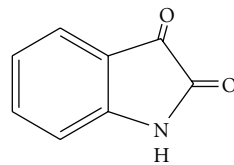
2.5. Studies on the Isatin Derivatives. The indole is known as a potent pharmacodynamic compound. One of the indole derivative, isatin (indole-2,3-dione; Scheme 14), present in mammalian tissues and body fluids, is a modulator of different biochemical processes in the body. This molecule was discovered as an inhibitor of monoamine oxidase (MAO), and subsequently identified as a selective inhibitor of MAO_B. Further investigations have shown that isatin acts as an antagonist of both atrial natriuretic peptide-stimulated and nitric oxide-stimulated guanylate cyclase activity [63]. Concentration of isatin in urine is a diagnostic marker in the clinical studies of Parkinson's disease in humans [64].

In a study with isatin, a molecule with a broad range of applications in synthetic, biological, and clinical activity undergoes oxidation and reduction at a glassy carbon electrode. The oxidation of isatin was found to be pH dependent and the reduction of isatin was irreversible. Using CV, two consecutive electron transfer reactions were identified [63].

The electrochemical behaviors of isatin, monoamine neurotransmitters, and their metabolites at chemically modified electrode were investigated by CV [65]. It was found that the PdHCF chemically modified electrode displayed high sensitivity and stability for determination of monoamine neurotransmitters and could effectively catalyze the oxidation of isatin and increase the sensitivity for determination of monoamine neurotransmitters.

The electrochemical behavior of eosin, isatin, and alloxan on the hanging mercury drop electrode was investigated using the CV and the electrochemical impedance techniques (EIS) [66]. The CV assay showed that the electroreduction of isatin was completely irreversible and a diffusion-controlled process is observed only in aprotic media. EIS data of these compounds is mostly characterized by a semicircle similar to that expected for a purely capacitive response.

Some electrochemical studies were carried out with a series of Schiff bases of 3-[5-phenylpyrazol-3-ylimino]indol-2-ones. The results have been compared with corresponding isatin in dimethylformamide in 0.1 M LiCl using CV at hanging mercury drop electrode [67]. All synthesized Schiff bases exhibit a single irreversible two-electron reduction wave in contrast with the two discrete one-electron transfer reduction waves observed for isatin in this medium. A mechanism for the electroreduction process has been proposed. Kinetic parameters have also been calculated.



SCHEME 14: Chemical formula of isatin.

3. Conclusion

Indole derivatives are certainly very important heterocycles in the drug-discovery studies. They are a very important class of compounds that play a major role in cell physiology and are potential intermediates for many biological reactions. There has been an increasing interest in the use of electrochemical cells to generate oxidation and reduction profiles, drug stability experiments, quantitative analyses, and *in vivo* and *in vitro* experiments of drug candidates.

This paper reviews the current status and the recent studies of how electrochemical techniques are being used to maintain research studies of biologically important indole derivatives. The review is meant to present a general overview of the various research activities in this expanding field.

References

- [1] E. Fischer and F. Jourdan, "Ueber die Hydrazine der Brenztraubensäure," *Berichte der deutschen chemischen Gesellschaft*, vol. 16, no. 2, pp. 2241–2245, 1883.
- [2] I. Chen, S. Safe, and L. Bjeldanes, "Indole-3-carbinol and diindolymethane as aryl hydrocarbon (Ah) receptor agonists and antagonists in T47D human breast cancer cells," *Biochemical Pharmacology*, vol. 51, no. 8, pp. 1069–1076, 1996.
- [3] S. Suzen and E. Buyukbingol, "Anti-cancer activity studies of indolalthiohydantoin (PIT) on certain cancer cell lines," *Il Farmaco*, vol. 55, no. 4, pp. 246–248, 2000.
- [4] G. Giagoudakis and S. L. Markantonis, "Relationships between the concentrations of prostaglandins and the non-steroidal antiinflammatory drugs indomethacin, diclofenac, and ibuprofen," *Pharmacotherapy*, vol. 25, no. 1, pp. 18–25, 2005.
- [5] E. Buyukbingol, S. Suzen, and G. Klopman, "Studies on the synthesis and structure-activity relationships of 5-(3'-indolal)-2-thiohydantoin derivatives as aldose reductase enzyme inhibitors," *Il Farmaco*, vol. 49, no. 6, pp. 443–447, 1994.
- [6] S. Suzen and E. Buyukbingol, "Evaluation of anti-HIV activity of 5-(2-phenyl-3'-indolal)-2 thiohydantoin," *Il Farmaco*, vol. 53, no. 7, pp. 525–527, 1998.
- [7] G. Walter, R. Liebl, and E. von Angerer, "2-phenylindole sulfamates: inhibitors of steroid sulfatase with antiproliferative activity in MCF-7 breast cancer cells," *Journal of Steroid Biochemistry and Molecular Biology*, vol. 88, no. 4–5, pp. 409–420, 2004.
- [8] S. Leichtl and E. von Angerer, "2-phenylbenzo[b]thiophene-based antiestrogens with mammary tumor inhibiting activity," *Archiv der Pharmazie*, vol. 331, no. 9, pp. 283–289, 1998.
- [9] C. Biberger and E. von Angerer, "2-phenylindoles with sulfur containing side chains. Estrogen receptor affinity, antiestrogenic potency, and antitumor activity," *Journal of Steroid*

- Biochemistry and Molecular Biology*, vol. 58, no. 1, pp. 31–43, 1996.
- [10] X. Ge, S. Yannai, G. Rennert, N. Gruener, and F. A. Fares, “3,3'-diindolylmethane induces apoptosis in human cancer cells,” *Biochemical and Biophysical Research Communications*, vol. 228, no. 1, pp. 153–158, 1996.
- [11] M. Valko, H. Morris, and M. T. D. Cronin, “Metals, toxicity and oxidative stress,” *Current Medicinal Chemistry*, vol. 12, no. 10, pp. 1161–1208, 2005.
- [12] A. M. S. Poon, Z. M. Liu, C. S. Pang, G. M. Brown, and S. F. Pang, “Evidence for a direct action of melatonin in the immune system,” *Biological Signals*, vol. 3, no. 2, pp. 107–117, 1994.
- [13] P. M. Liebmann, A. Wölfle, P. Felsner, D. Hofer, and K. Schauenstein, “Melatonin and the immune system,” *International Archives of Allergy and Immunology*, vol. 112, no. 3, pp. 203–211, 1997.
- [14] F. Lezoualc'h, T. Skutella, M. Widmann, and C. Behl, “Melatonin prevents oxidative stress-induced cell death in hippocampal cells,” *NeuroReport*, vol. 7, no. 13, pp. 2071–2077, 1996.
- [15] D. J. Kennaway and H. Wright, “Melatonin and circadian rhythms,” *Current Topics in Medicinal Chemistry*, vol. 2, no. 2, pp. 199–209, 2002.
- [16] D. E. Blask, L. A. Sauer, and R. T. Dauchy, “Melatonin as a chronobiotic/anticancer agent: cellular, biochemical, and molecular mechanisms of action and their implications for circadian-based cancer therapy,” *Current Topics in Medicinal Chemistry*, vol. 2, no. 2, pp. 113–132, 2002.
- [17] J. M. Guerrero and R. J. Reiter, “Melatonin-immune system relationships,” *Current Topics in Medicinal Chemistry*, vol. 2, no. 2, pp. 167–179, 2002.
- [18] S. Cuzzocrea and R. J. Reiter, “Pharmacological actions of melatonin in acute and chronic inflammation,” *Current Topics in Medicinal Chemistry*, vol. 2, no. 2, pp. 153–165, 2002.
- [19] D. X. Tan, R. J. Reiter, L. C. Manchester et al., “Chemical and physical properties and potential mechanisms: melatonin as a broad spectrum antioxidant and free radical scavenger,” *Current Topics in Medicinal Chemistry*, vol. 2, no. 2, pp. 181–197, 2002.
- [20] R. J. Reiter, D. X. Tan, J. C. Mayo, R. M. Sainz, J. Leon, and Z. Czarnocki, “Melatonin as an antioxidant: biochemical mechanisms and pathophysiological implications in humans,” *Acta Biochimica Polonica*, vol. 50, no. 4, pp. 1129–1146, 2003.
- [21] S. Süzen, Z. Ateş-Alagöz, B. T. Demircigil, and S. A. Özkan, “Synthesis and analytical evaluation by voltammetric studies of some new indole-3-propionamide derivatives,” *Il Farmaco*, vol. 56, no. 11, pp. 835–840, 2001.
- [22] S. Yilmaz, B. Uslu, and S. A. Özkan, “Anodic oxidation of etodolac and its square wave and differential pulse voltammetric determination in pharmaceuticals and human serum,” *Talanta*, vol. 54, no. 2, pp. 351–360, 2001.
- [23] N. E. Zoulis, D. P. Nikolelis, and C. E. Efstatithiou, “Pre-concentration of indolic compounds at a carbon paste electrode and indirect determination of (L)-tryptophan in serum by adsorptive stripping voltammetry,” *Analyst*, vol. 115, no. 3, pp. 291–295, 1990.
- [24] M. A. Matthews, “Green electrochemistry. Examples and challenges,” *Pure and Applied Chemistry*, vol. 73, no. 8, pp. 1305–1308, 2001.
- [25] G. Sotgiu, “Easy electrochemical synthesis of 2-amino-4-aryl-3-cyano-5-ethoxycarbonyl-6-methyl-4H-pyrans in the absence of supporting electrolyte,” *Letters in Organic Chemistry*, vol. 5, no. 7, pp. 555–558, 2008.
- [26] J. I. Yoshida, K. Kataoka, R. Horcajada, and A. Nagaki, “Modern strategies in electroorganic synthesis,” *Chemical Reviews*, vol. 108, no. 7, pp. 2265–2299, 2008.
- [27] B. Uslu and S. A. Ozkan, “Electroanalytical application of carbon based electrodes to the pharmaceuticals,” *Analytical Letters*, vol. 40, no. 5, pp. 817–853, 2007.
- [28] B. Dogan-Topal, S. A. Ozkan, and B. Uslu, “The analytical applications of square wave voltammetry on pharmaceutical analysis,” *The Open Chemical and Biomedical Methods Journal*, vol. 3, pp. 56–73, 2010.
- [29] P. Bozkaya, B. Dogan, S. Suzen, D. Nebioğlu, and S. A. Ozkan, “Determination and investigation of electrochemical behaviour of 2-phenylindole derivatives: discussion on possible mechanistic pathways,” *Canadian Journal of Analytical Sciences and Spectroscopy*, vol. 51, no. 3, pp. 125–139, 2006.
- [30] J. C. Vire and J. M. Kauffmann, “Trends in electrochemistry in drug analysis,” *Current Topics in Electrochemistry*, vol. 3, pp. 493–515, 1994.
- [31] C. C. Zeng, F. J. Liu, D. W. Ping, L. M. Hu, Y. L. Cai, and R. G. Zhong, “One-pot electrochemical synthesis of fused indole derivatives containing active hydroxyl groups in aqueous medium,” *Journal of Organic Chemistry*, vol. 74, no. 16, pp. 6386–6389, 2009.
- [32] A. Arcadi, G. Bianchi, A. Inesi, F. Marinelli, and L. Rossi, “Electrochemical-mediated cyclization of 2-alkynylanilines: a clean and safe synthesis of indole derivatives,” *European Journal of Organic Chemistry*, no. 5, pp. 783–787, 2008.
- [33] M. Scendo, D. Poddebska, and J. Malyszko, “Indole and 5-chloroindole as inhibitors of anodic dissolution and cathodic deposition of copper in acidic chloride solutions,” *Journal of Applied Electrochemistry*, vol. 33, no. 3-4, pp. 287–293, 2003.
- [34] S. Zhang and K. Wu, “Square wave voltammetric determination of indole-3-acetic acid based on the enhancement effect of anionic surfactant at the carbon paste electrode,” *Bulletin of the Korean Chemical Society*, vol. 25, no. 9, pp. 1321–1325, 2004.
- [35] H. Shirinzadeh, A. D. Yilmaz, M. Gumustas, S. Suzen, S. Ozden, and S. A. Ozkan, “Electrochemical behavior of indole-3-carboxaldehyde izonicotinoyl hydrazones: discussion on possible biological behavior,” *Combinatorial Chemistry and High Throughput Screening*, vol. 13, no. 7, pp. 619–627, 2010.
- [36] S. Süzen, B. T. Demircigil, E. Buyukbingol, and S. A. Özkan, “Electroanalytical evaluation and determination of 5-(3'-indolyl)-2-thiohydantoin derivatives by voltammetric studies: possible relevance to in vitro metabolism,” *New Journal of Chemistry*, vol. 27, no. 6, pp. 1007–1011, 2003.
- [37] S. Suzen and S. A. Ozkan, “Combination of electrochemical, spectrometric and other analytical techniques for high throughput screening of pharmaceutically active compounds,” *Combinatorial Chemistry and High Throughput Screening*, vol. 13, no. 7, pp. 658–664, 2010.
- [38] L. Greci, G. Tommasi, P. Astolfi et al., “Radical cations: reactions of 2-phenylindole with aromatic amines under anodic oxidation. β-Scission of an amino alkoxyl radical,” *Journal of the Chemical Society. Perkin Transactions 2*, no. 8, pp. 1749–1755, 2000.
- [39] M. S. Estevão, L. C. Carvalho, L. M. Ferreira, E. Fernandes, and M. M. B. Marques, “Analysis of the antioxidant activity of an indole library: cyclic voltammetry versus ROS scavenging activity,” *Tetrahedron Letters*, vol. 52, no. 1, pp. 101–106, 2011.
- [40] B. Uslu, B. T. Demircigil, S. A. Özkan, Z. Şentürk, and H. Y. Aboul-Enein, “Simultaneous determination of melatonin and pyridoxine in tablet formulations by differential pulse voltammetry,” *Pharmazie*, vol. 56, no. 12, pp. 938–942, 2001.

- [41] X. Páez and L. Hernández, "Plasma serotonin monitoring by blood microdialysis coupled to high-performance liquid chromatography with electrochemical detection in humans," *Journal of Chromatography B*, vol. 720, no. 1-2, pp. 33–38, 1998.
- [42] S. Yilmaz, B. Uslu, and S. A. Özkan, "Anodic oxidation of etodolac and its square wave and differential pulse voltammetric determination in pharmaceuticals and human serum," *Talanta*, vol. 54, no. 2, pp. 351–360, 2001.
- [43] S. A. Özkan and B. Uslu, "Electrochemical study of fluvastatin sodium—analytical application to pharmaceutical dosage forms, human serum, and simulated gastric juice," *Analytical and Bioanalytical Chemistry*, vol. 372, no. 4, pp. 582–586, 2002.
- [44] C. G. Nan, Z. Z. Feng, W. X. Li, D. J. Ping, and C. H. Qin, "Electrochemical behavior of tryptophan and its derivatives at a glassy carbon electrode modified with hemin," *Analytica Chimica Acta*, vol. 452, no. 2, pp. 245–254, 2002.
- [45] J. B. Raoof, R. Ojani, and M. Baghayeri, "Simultaneous electrochemical determination of glutathione and tryptophan on a nano-TiO₂/ferrocene carboxylic acid modified carbon paste electrode," *Sensors and Actuators B*, vol. 143, no. 1, pp. 261–269, 2009.
- [46] S. Shahrokhan and L. Fotouhi, "Carbon paste electrode incorporating multi-walled carbon nanotube/cobalt salophen for sensitive voltammetric determination of tryptophan," *Sensors and Actuators B*, vol. 123, no. 2, pp. 942–949, 2007.
- [47] Y. Altun, B. Dogan-Topal, B. Uslu, and S. A. Ozkan, "Anodic behavior of sertindole and its voltammetric determination in pharmaceuticals and human serum using glassy carbon and boron-doped diamond electrodes," *Electrochimica Acta*, vol. 54, no. 6, pp. 1893–1903, 2009.
- [48] D. Kul, M. Gumustas, B. Uslu, and S. A. Ozkan, "Electroanalytical characteristics of antipsychotic drug ziprasidone and its determination in pharmaceuticals and serum samples on solid electrodes," *Talanta*, vol. 82, pp. 286–295, 2010.
- [49] S. C. Sweetman, Ed., *Martindale, the Complete Drug Reference*, Pharmaceutical Press, London, UK, 32th edition, 2002.
- [50] B. Dogan and S. A. Ozkan, "Electrochemical behavior of carvedilol and its adsorptive stripping determination in dosage forms and biological fluids," *Electroanalysis*, vol. 17, no. 22, pp. 2074–2083, 2005.
- [51] C. Velasco-Aguirre and A. Álvarez-Lueje, "Voltammetric behavior of naratriptan and its determination in tablets," *Talanta*, vol. 82, pp. 796–802, 2010.
- [52] C. Reguera, M. Cruz Ortiz, and M. Julia Arcos, "Differential pulse voltammetric simultaneous determination of four anti-inflammatory drugs by using soft modelling," *Electroanalysis*, vol. 14, no. 24, pp. 1699–1706, 2002.
- [53] C. Radovan, D. Dascalu, I. Vlaicu, V. Chiriac, and A. Ciobra, "Determination of indomethacin at a boron doped diamond electrode," in *Proceedings of the 12th Symposium on Analytical and Environmental Problems*, pp. 265–268, Szeged, Hungary, September 2005.
- [54] C. Reguera, M. Julia Arcos, and M. Cruz Ortiz, "An optimization procedure for determination of indomethacin and acemethacin by differential pulse adsorptive stripping voltammetry. Application on urine samples," *Talanta*, vol. 46, no. 6, pp. 1493–1505, 1998.
- [55] H. Y. Gao, H. Huang, and Y. H. Zeng, "Adsorptive voltammetric behavior of acemetacin," *Journal of Analytical Science*, vol. 17, no. 3, pp. 217–220, 2001.
- [56] G. B. El-Hefnawy, I. S. El-Hallag, E. M. Ghoneim, and M. M. Ghoneim, "Square-wave adsorptive cathodic stripping voltammetric determination of anti-inflammatory indomethacin drug in tablets and human serum at a mercury electrode," *Analytical and Bioanalytical Chemistry*, vol. 376, no. 2, pp. 220–225, 2003.
- [57] J.-L. Yan, "Determination of fluvastatin sodium by differential pulse voltammetry," *Pakistan Journal of Biological Sciences*, vol. 9, no. 11, pp. 2156–2158, 2006.
- [58] D. Nematollahi and S. Dehdashtian, "Electrochemical oxidation of catechol in the presence of indole: a facile and one-pot method for the synthesis of trisindolyl-o-benzoquinone," *Tetrahedron Letters*, vol. 49, no. 4, pp. 645–649, 2008.
- [59] D. Nematollahi, S. Dehdashtian, and A. Niazi, "Electrochemical oxidation of some dihydroxybenzene derivatives in the presence of indole," *Journal of Electroanalytical Chemistry*, vol. 616, no. 1-2, pp. 79–86, 2008.
- [60] R. Andruzzi, A. Trazza, L. Greci, and L. Marchetti, "On the electrochemical reduction mechanism of indolinone nitroxide radicals in DMF," *Journal of Electroanalytical Chemistry and Interfacial Electrochemistry*, vol. 107, no. 2, pp. 365–374, 1980.
- [61] M. Medebielle, S. Fujii, and K. Kato, "An electrochemical approach for the synthesis of perfluoroalkylated purine and indole analogues of plant growth regulators," *Tetrahedron*, vol. 56, no. 17, pp. 2655–2664, 2000.
- [62] V. A. Mamedov, A. A. Kalinin, V. V. Yanilkin et al., "Synthesis, structure, and electrochemical properties of 1²,4²-dioxo-2¹,3¹-diphenyl-7,10,13-trioxa-1,4(3,1)-diquinoxalina-2(2,3),3(3,2)-diindolizinacyclopentadecaphane," *Russian Chemical Bulletin*, vol. 56, no. 10, pp. 2060–2073, 2007.
- [63] V. C. Diculescu, S. Kumbhat, and A. M. Oliveira-Brett, "Electrochemical behaviour of isatin at a glassy carbon electrode," *Analytica Chimica Acta*, vol. 575, no. 2, pp. 190–197, 2006.
- [64] A. Medvedev, M. Crumeyrolle-Arias, A. Cardona, M. Sandler, and V. Glover, "Natriuretic peptide interaction with [³H]isatin binding sites in rat brain," *Brain Research*, vol. 1042, no. 2, pp. 119–124, 2005.
- [65] H. Xu, D. Wang, W. Zhang, W. Zhu, K. Yamamoto, and L. Jin, "Determination of isatin and monoamine neurotransmitters in rat brain with liquid chromatography using palladium hexacyanoferrate modified electrode," *Analytica Chimica Acta*, vol. 577, no. 2, pp. 207–213, 2006.
- [66] F. A. Rashwan, "Determination of A.C. impedance spectroscopic and cyclic voltammetric behavior of some heterocarbonyl compounds in both aprotic and aqueous media," *American Journal of Applied Sciences*, vol. 2, no. 7, pp. 1153–1157, 2005.
- [67] A. K. Gupta and R. S. Sindal, "A comparative study of electrochemical reduction of isatin and its synthesized Schiff bases at HMDE," *Journal of Chemical Sciences*, vol. 121, no. 3, pp. 347–351, 2009.

Research Article

Differential Pulse Voltammetric Determination of Fulvestrant in Pharmaceutical Dosage Forms and Serum Samples

Dilek Kul,¹ Burcu Doğan-Topal,² Sibel A. Özkan,² and Bengi Uslu²

¹Faculty of Pharmacy, Karadeniz Technical University, 61080 Trabzon, Turkey

²Department of Analytical Chemistry, Faculty of Pharmacy, Ankara University, Tandoğan, 06100 Ankara, Turkey

Correspondence should be addressed to Bengi Uslu, buslu@pharmacy.ankara.edu.tr

Received 9 November 2010; Accepted 3 December 2010

Academic Editor: Hassan Y. Aboul-Enein

Copyright © 2011 Dilek Kul et al. This is an open access article distributed under the Creative Commons Attribution License, which permits unrestricted use, distribution, and reproduction in any medium, provided the original work is properly cited.

The electrooxidation behavior and determination of fulvestrant at a glassy carbon electrode were investigated. The voltammetric study of the model compounds allowed elucidating the possible oxidation mechanism of fulvestrant. The dependence of the peak current and peak potentials on pH, concentration, nature of the buffer, and scan rate was determined. The oxidation of fulvestrant showed a single and irreversible peak at glassy carbon electrode, and the process was found diffusion controlled. Linear responses were obtained for the concentrations between 4×10^{-6} M and 6×10^{-5} M in standard samples and between 2×10^{-5} M and 1×10^{-4} M in serum samples. The repeatability of the method was found 0.93 RSD%. The repeatability, reproducibility, precision, and accuracy of proposed method were investigated.

1. Introduction

Fulvestrant is a member of a group of drugs called estrogen receptor downregulators. Most breast cancer cells have estrogen receptors on their cell surface. Estrogen stimulates these cells with estrogen receptors to divide without regard to the body's estrogen needs. This is referred to as "estrogen-receptor-positive breast cancer." Fulvestrant works by blocking and destroying the estrogen receptor in the cell so that estrogen cannot bind to it. The action effectively lowers (downregulates) the estrogen receptor activity in the cell so that it acts more like a normal cell [1, 2].

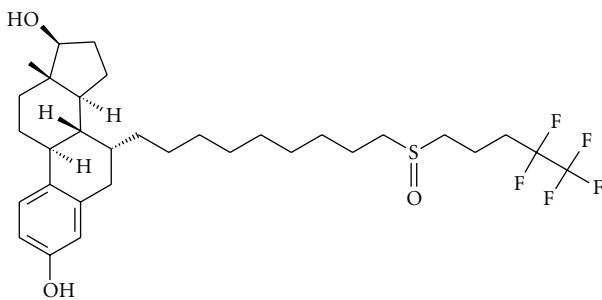
Fulvestrant has a steroid-like structure 7-alpha-(9-((4,4,5,5,5-pentafluoropentyl) sulfinyl) nonyl) estra-1,3,5(10)-triene, 3,7 beta-diol (Scheme 1), which when complexed with oestrogen receptors prevents its dimerisation and renders the receptor transcriptionally inactive [3–6].

There has been no study published on quantitative determination of fulvestrant in pharmaceutical formulations. Moreover, no monograph of fulvestrant has been reported in the official pharmacopoeias as of today.

The widespread use of this compound and the need for clinical and pharmacological studies require fast and sensi-

tive analytical techniques to assay the drug in pharmaceutical dosage forms and biological samples. These may also be used for monitoring patient compliance and establishing relationship between blood concentration and the therapeutic effects, which are not always fully understood.

In the last decades, modern-computer-based voltammetric techniques have been used to realize the determination of organic chemicals in diverse types of samples, especially pharmaceutical fields. The advance in experimental electrochemical techniques in the field of drug analysis is because of their straightforwardness, low cost, and relatively short analysis times no need for derivatizations or time-consuming extraction steps when compared with other analytical techniques [7–12]. Cyclic voltammetry (CV) is the most widely used technique for qualitative information about electrochemical reactions. Conventionally, glassy carbon (GC) is widely used for working electrodes especially for analytical applications because of its relatively wide potential window in comparison with metal electrodes such as Au and Pt. GC is composed almost exclusively of sp^2 -type carbon. The electronic and electrochemical properties of this electrode depend on several factors including surface preparation, microstructure, and presence of carbon-oxygen functional groups.



SCHEME 1: Chemical formula of fulvestrant.

This work is aimed to study the detailed voltammetric oxidation mechanism of fulvestrant at GC electrode using CV. Also, the proposed method has been applied to the determination of electroactive fulvestrant and quantitation of fulvestrant in pharmaceutical dosage form, and human serum samples using differential pulse voltammetry (DPV).

2. Experimental

2.1. Equipment. Voltammetric experiments were performed using a BAS 100 W (Bionalytical System, USA) electrochemical analyzer associated to one-compartment glass electrochemical cell equipped with a three-electrode system consisting of a glassy carbon (GC) electrode (BAS; 3 mm, diameter), working electrode, a platinum wire counter electrode and an Ag/AgCl saturated KCl reference electrode. GC electrode was polished manually with aqueous slurry of alumina powder ($0.01\text{ }\mu\text{m}$, diameter) on a damp smooth polishing cloth (BAS velvet polishing pad) before each experiment.

The pH measurements were completed using a model 538, WTW pH-meter (Austria) with a combined electrode (Glass-reference electrodes) with an accuracy of $\text{pH} \pm 0.05$.

The experimental conditions for differential pulse voltammetry (DPV) were as follows: pulse amplitude of 50 mV, pulse width of 50 ms, and scan rate of 20 mV/s.

2.2. Reagents. Fulvestrant and its pharmaceutical dosage form were kindly supplied by Astra Zeneca (Istanbul, Turkey). Model compounds, levodopa, carbidopa, benserazide, epirubicin, and doxorubicin were kindly supplied from different pharmaceutical companies in Turkey. Other chemicals were reagent grade (Merck or Sigma).

Stock solutions of fulvestrant ($1 \times 10^{-3}\text{ M}$) were prepared in acetonitrile and kept in the dark at 4°C . Fulvestrant working solutions for voltammetric investigations were prepared by dilution of the stock and contained 30% acetonitrile. Four different supporting electrolytes, sulphuric acid solution (0.1 M and 0.5 M), phosphate buffer ($0.2\text{ M H}_3\text{PO}_4$; $0.2\text{ M NaH}_2\text{PO}_4 \cdot 2\text{ H}_2\text{O}$; $0.2\text{ M Na}_2\text{HPO}_4$; pH 2.0–8.0), Britton-Robinson buffer ($0.04\text{ M H}_3\text{BO}_3$; $0.04\text{ M H}_3\text{PO}_4$, and $0.04\text{ M CH}_3\text{COOH}$; pH 2.0–10.0), and acetate buffer ($0.2\text{ M CH}_3\text{COOH}$; pH 3.5–5.5), were used for electrochemical measurements. All the solutions were protected from light

and were used within 24 h to avoid decomposition. All measurements were carried out at the ambient temperature of the laboratory ($23\text{--}27^\circ\text{C}$). The calibration curve for DPV analysis was constructed by plotting the peak current versus the fulvestrant concentration.

The ruggedness and precision were checked at different days. The results were given as repeatability (within day) and reproducibility (between days). Relative standard deviations (RSDs) were calculated to check the ruggedness and precision of the method [9, 13–19].

The accuracy and precision of the developed methods are described in a quantitative fashion by the use of relative errors (Bias%). An example of the Bias% is the accuracy which describes the deviation from the expected results.

2.3. Injectable Solution Assay. 1.21 mL of Faslodex injectable solution, maintained to contain 250 mg fulvestrant per 5 mL of the solution, was dissolved in 100 mL of acetonitrile. An aliquot of this solution was transferred into a 10.0 mL volumetric flask and diluted to the mark with supporting electrolyte, and the voltammogram was recorded.

The nominal content of the injectable solution was determined from corresponding regression equation.

2.4. Analysis of Serum. Drug-free human blood, obtained from healthy volunteers (after obtaining their signed consent), was centrifuged (5000 rpm) for 30 min at room temperature. The separated serum samples were stored frozen until assay. An aliquot volume of the serum sample was fortified with fulvestrant dissolved in acetonitrile to achieve final concentration of $1 \times 10^{-3}\text{ M}$. This solution contained acetonitrile as serum precipitating agent. Acetonitrile removed serum proteins effectively, by the addition of 1 volume to 1.5 volumes of the serum. The mixture was vortexed for 30 s and centrifuged for 10 min at 5000 rpm to remove serum protein residues, and the supernatant was taken carefully. Appropriate volumes of the supernatant were transferred to the volumetric flask and diluted to the chosen volumes with 0.1 M sulphuric acid solution. The concentration of fulvestrant in the prepared solutions was varied in the range of $2 \times 10^{-5}\text{ M}$ – $1 \times 10^{-4}\text{ M}$ using DPV technique with GC electrode in human serum samples.

Quantifications were performed by means of the calibration curve method from the related calibration equation.

3. Results and Discussion

The electrochemical behavior of fulvestrant on the glassy carbon electrode was studied by CV, linear sweep voltammetry (LSV), and differential pulse voltammetry (DPV). Various supporting electrolytes were investigated using CV: phosphate buffer, Britton-Robinson buffer, acetate buffer, and sulphuric acid. The best result was obtained with 0.1 M sulphuric acid; peak oxidation potential 0.83 V versus Ag/AgCl (3.0 mol L^{-1} KCl) was obtained for fulvestrant (Figure 1).

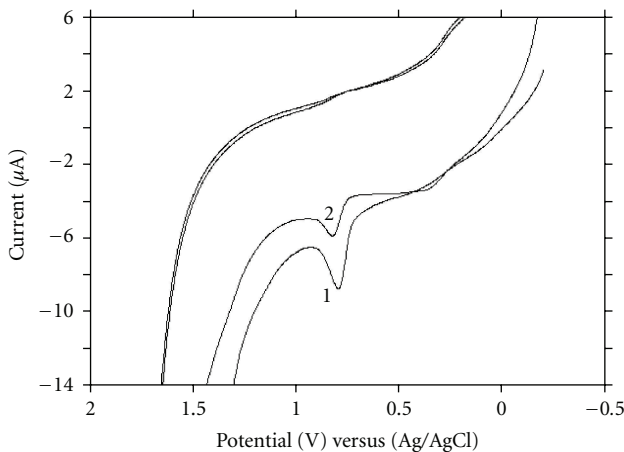


FIGURE 1: (1) First cycle and (2) second cycle of the repetitive voltammograms for 8×10^{-5} M fulvestrant solution in 0.1 M sulphuric acid solution. Curves are from 0 to +1.8 V. Scan rate is 100 mV/s.

Voltammogram obtained for fulvestrant at the GC electrode presented an irreversible chemical behavior in all supporting electrolytes. Cyclic voltammogram of 8×10^{-5} M fulvestrant using GC electrode (sweep rate 100 mV/s) exhibited a single well-defined and irreversible oxidation peak at 0.83 V. No peaks were observed on the reverse scan corresponding to the main anodic peak. This observation confirmed the irreversibility of the oxidation process (Figure 2).

The plot of the peak potential (E_p) versus pH created a straight line (Figure 3(a)) between pH 1.0 and 10.0. The peak potential moved to less positive values by increasing the pH. This can be expressed by the following equation:

$$E_p = 784.05 - 55.81 \text{ pH}; r = 0.994.$$

(SE of intercept: 1.17×10^1 , SE of slope: 1.84)

(Acetate, phosphate, and BR buffer between pH 1.0 and 10.0). (1)

The intersection of the curves was located around pH 10.0 for GC electrode. This value was found similar to the value given in the literature which is 10.03 [20]. The peak potential seemed to be pH independent after a pH value of 10.0.

The effect of pH (within the range of 1.8–12.0) on the peak current of fulvestrant was investigated (Figure 3(b)). The plot of I_p versus pH indicated that the peak current reached a maximum for 0.1 M H₂SO₄. Therefore, 0.1 M H₂SO₄ was chosen as the supporting electrolyte for the quantitative determination part of the study. This supporting electrolyte showed sharp response and better peak shape for the calibration equation of pharmaceutical dosage forms and biological samples.

The peak potential shifted to more positive potentials (about 66 mV) to the anodic direction when the scan rate

was increased for GC electrode which can be expressed by the following equation:

$$\begin{aligned} E_p(\text{mV}) &= 0.34\nu(\text{mV/s}) + 764.13; r = 0.976, \\ n &= 6 \text{ (for 5–100 mV/s)} \end{aligned} \quad (2)$$

(SE of intercept: 2.11, SE of slope: 3.77×10^{-2}).

The rate increased to the observed potential until 100 mV/s and levelled off thereafter.

Scan rate studies were then carried out to understand whether the processes on GC electrode were under diffusion or adsorption control. When the scan rate was varied from 5 to 750 mV/s in 8×10^{-5} M fulvestrant, a linear dependence of the peak intensity I_p (μA) upon the square root of the scan rate ($\nu^{1/2}$) (mV/s) was found, demonstrating a diffusional behavior.

The equation is for GC electrode in 0.1 M H₂SO₄ solution

$$\begin{aligned} I_p(\mu\text{A}) &= 0.31\nu^{1/2}(\text{mV/s}) - 0.51; r = 0.997, n = 8. \\ (\text{SE of intercept: } 1.32 \times 10^{-1}, \text{ SE of slope: } 1.05 \times 10^{-2}) \end{aligned} \quad (3)$$

It followed from the variation of the logarithm of the peak current as a function of the logarithm of the sweep rate in the range of 5–750 mV/s that the process was diffusion controlled since the value of the straight line $\log I_p = f(\log \nu)$ was equal to 0.58. This demonstrated that the process had a diffusive component.

Tafel plot was obtained with a scan rate of 5 mV/s beginning from a steady-state potential in 0.1 M H₂SO₄ from the slope of the linear part. The αn value was 0.33. The exchange current density (I_o) was 1.76×10^{-10} A cm⁻² for this system.

The results showed that oxidation of fulvestrant may be postulated by oxidation of the phenolic hydroxyl group. To investigate this finding, comparative studies on levodopa, carbidopa, benserazide, epirubicin, and doxorubicin related for the hydroxyl group of fulvestrant were carried out by CV on GC electrode as a function of pH in order to identify the other oxidation step of fulvestrant. The cyclic voltammograms of the compounds closely matched the more positive part of the voltammograms of fulvestrant. It was assumed that the oxidation process, via an initial oxidation of two electrons and the conversion of hydroxyl group to quinone, might be occurring on the selected compounds and the hydroxyl group of fulvestrant, which was electroactive in both acidic and basic media.

3.1. Analytical Applications and Validation of the Proposed Method. After the preliminary trials using different percentage of methanol and acetonitrile, 30% of acetonitrile ratio gave the finest response and solubility. The best result with respect to signal enhancement and peak shape accompanied by sharper response was obtained with 0.1 M sulphuric acid with constant amount acetonitrile as 30%. The calibration graph from the standard solution of fulvestrant according to

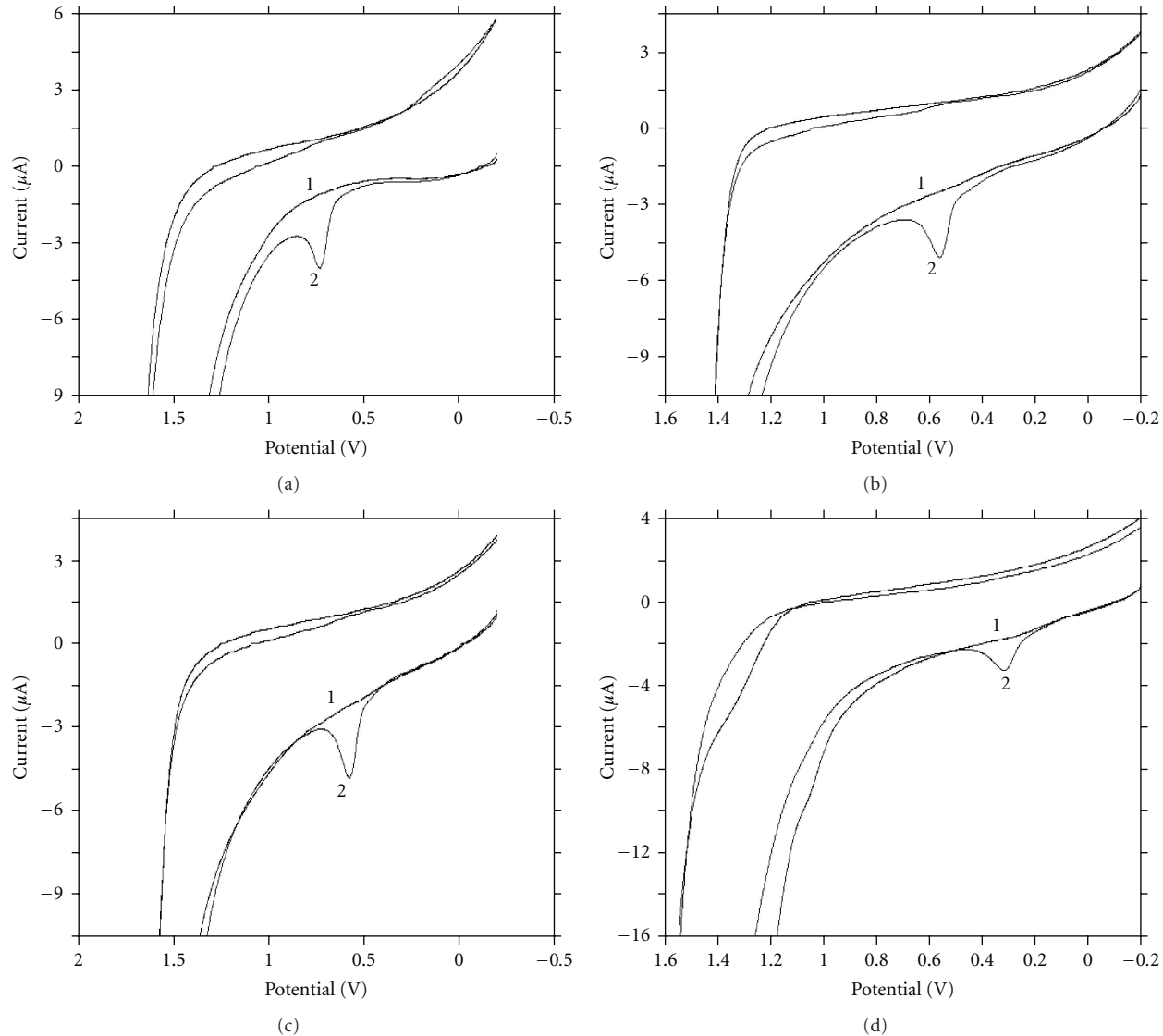


FIGURE 2: Cyclic voltammograms of supporting electrolyte (1) and 8×10^{-5} M fulvestrant (2) on GC electrode. (a) pH 2.0 phosphate buffer; (b) pH 4.5 acetate buffer; (c) pH 5.0 BR buffer; (d) pH 9.0 BR buffer solutions.

the procedures described above was constructed by DPV. A linear relation in the concentration range between 4×10^{-6} M and 6×10^{-5} M was found, indicating that the response was diffusion controlled in this range. The characteristics of the calibration plot are summarized in Table 1.

The limit of detection (LOD) and the limit of quantification (LOQ) were calculated on the peak current using the following equations:

$$\text{LOD} = 3.3 \text{ s/m}; \quad \text{LOQ} = 10 \text{ s/m}, \quad (4)$$

where s is the standard deviation of the peak currents (three runs), and m is the slope of the calibration curve. The LOD and LOQ values were also shown in Table 1.

The low values of SE of slope, the intercept, and a correlation coefficient greater than 0.99 in the supporting electrolyte and human serum samples confirmed the precision of the proposed method.

The stability of the reference substance and sample solutions was checked by analyzing prepared standard solution of fulvestrant in the supporting electrolyte aged at +4°C in the dark against freshly prepared sample. The results demonstrated that the working reference solutions were stable at least for 3 days. The fulvestrant response for the assay reference solutions did not change considerably over 3 days.

The developed techniques were validated according to the ICH guidelines [21]. The results are summarized in Table 1. Accuracy, precision, specificity, selectivity, reproducibility, LOD, and LOQ of the proposed techniques were assessed by performing replicate analysis of the standard solutions in the supporting electrolyte and human serum samples within calibration curves. The selected concentrations were prepared in both media, assayed with the related calibration equations to determine repeatability and

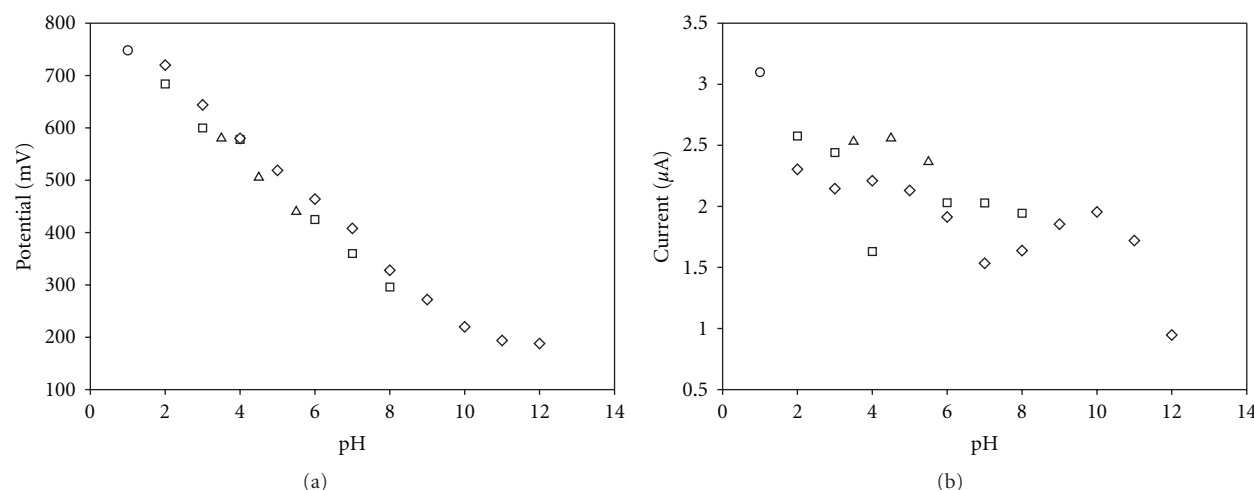


FIGURE 3: Effect of pH on fulvestrant anodic peak potential (a) and peak current (b); fulvestrant concentration: 8×10^{-5} M. (○) 0.1 M sulphuric acid; (□) 0.2 M phosphate; (△) 0.2 M acetate; (◊) 0.04 M BR buffers.

TABLE 1: Regression data of the calibration curve and quantitative determination of fulvestrant by DPV in standard solution and human serum.

	Standard solution	Serum
Measured potential (V)	0.83	0.84
Linearity range (M)	4×10^{-6} – 6×10^{-5}	2×10^{-5} – 1×10^{-4}
Slope ($\mu\text{A M}^{-1}$)	5.34×10^4	8.21×10^3
Intercept (μA)	2.78×10^{-2}	-5.22×10^{-2}
Correlation coefficient	0.998	0.999
SE of slope	1.60×10^3	1.06×10^2
SE of intercept	4.61×10^{-2}	7.00×10^{-3}
LOD (M)	5.40×10^{-7}	1.52×10^{-6}
LOQ (M)	1.80×10^{-6}	5.07×10^{-6}
Repeatability of peak current (RSD%)	0.93	0.51
Repeatability of peak potential (RSD%)	0.26	0.26
Reproducibility of peak current (RSD%)	1.68	0.72
Reproducibility of peak potential (RSD%)	0.26	0.32

reproducibility, and were shown as RSD% values in Table 1. The validation results shown in Table 1 demonstrate good precision, accuracy, and reproducibility.

3.2. Determination of Fulvestrant in Injectable Dosage Forms. On the basis of above results, DPV method was applied to the direct determination of fulvestrant in injectable dosage forms, using related calibration straight line without any sample extraction, evaporation, or filtration other than an adequate dilution step. The mean results were found very close to the confirmed value of 250 mg/5 mL. The results showed that the proposed method was successfully applied for the assay of fulvestrant in its dosage forms (Table 2). There is no official method present in any pharmacopoeias (e.g., USP, BP, or EP) related to pharmaceutical dosage forms or bulk drugs of fulvestrant. For checking the accuracy, precision, and selectivity of the proposed methods and in order to know whether the excipients in pharmaceutical dosage forms show any interference with the analysis,

TABLE 2: Results obtained from the determination and recovery experiments in injectable dosage form.

Labeled claim ($\text{mg } 5 \text{ mL}^{-1}$)	250.00
Amount found ^a	262.96
RSD%	0.70
Bias%	-5.18
Added fulvestrant (mg)	20.00
Found fulvestrant (mg) ^a	19.90
Average recovery%	99.49
RSD% of recovery	0.53
Bias%	0.51

^aEach value means five experiments.

the proposed methods were evaluated by recovery tests after addition of known amounts of pure drug to various preanalyzed formulation of fulvestrant.

TABLE 3: Results obtained from fulvestrant determination from spiked serum.

Added fulvestrant concentration (M)	8.00×10^{-5}
Obtained fulvestrant concentration (M)	7.60×10^{-5}
Number of experiments	5
Average recovery%	94.87
RSD% of recovery	1.56
Bias%	5.13

In order to detect interactions of excipients, the standard addition technique was applied to the same pharmaceutical preparations, which were analyzed by the calibration curve. Recovery experiments using the developed assay procedures further indicated the absence of interference from commonly encountered pharmaceutical excipients used in the selected formulations (Table 2). The results indicated the validity of the proposed techniques for the determination of fulvestrant in injectable dosage form (Table 2).

3.3. Determination of Fulvestrant in Spiked Human Serum. The optimized procedure was successfully applied to the determination of fulvestrant in protein-free spiked human samples. Acetonitrile was used as a serum precipitating agent. The best results were obtained with 5.4 mL of acetonitrile. No extraction or evaporation other than the centrifugal protein separation was required prior to assay for the drug. The measurements of fulvestrant in serum samples were performed as described in Section 2.

The applicability of the proposed method to the human serum samples and the calibration equation were obtained in spiked human serum samples. Calibration equation parameters and essential validation data were shown in Table 1. The recovery results of fulvestrant in serum samples were calculated from the related linear regression equation, which were given in Table 1. Recovery results of spiked human serum samples were given in Table 3.

Analysis of drugs from serum samples usually requires extensive time-consuming sample preparation and use of expensive organic solvents and other chemicals. In this study, the serum proteins and endogenous substances in serum samples were precipitated by the addition of acetonitrile and centrifugation at 5000 rpm. The supernatant was taken and diluted with the supporting electrolyte and directly analyzed. Typical DPV curves of fulvestrant examined in serum samples were shown in Figure 4. There were no oxidation compounds and no extra noise peaks presented in biological material peak occurred in the potential range where the analytical peak appeared.

Stability of serum samples kept in cold (+4°C) was tested with five consecutive analyses of the sample over a period of approximately 5 h. There were no significant changes in the peak currents and potentials between the first and last measurements.

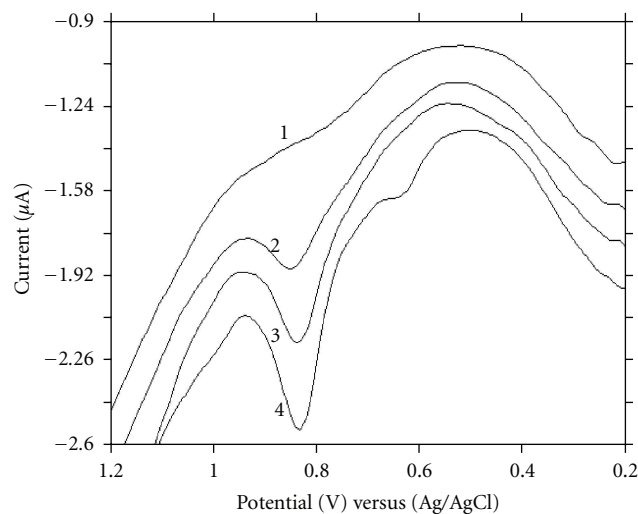


FIGURE 4: DP voltammograms in 0.1 M sulphuric acid for the determination of fulvestrant in spiked human serum samples: (1) blank serum extract, (2) extract containing 4×10^{-5} M, (3) extract containing 6×10^{-5} M, and (4) extract containing 1×10^{-4} M.

4. Conclusion

The electrochemical behavior of fulvestrant was examined for the first time with this study. The voltammetric oxidation steps of fulvestrant in different buffer solutions of pH 0.3–12.0 have been elucidated with glassy carbon electrode. The detailed electrooxidation outcome of fulvestrant at carbon-based electrodes might be used for analytical purposes, particularly as a sensor.

Fully validated, highly selective and sensitive, simple and precise voltammetric procedures were described for determination of fulvestrant in bulk form, pharmaceutical dosage form, and human serum samples without the necessity of sample pretreatment or time-consuming extraction and evaporation steps prior to the analysis.

In this study, possible oxidation pathways were investigated to identify the functional groups responsible from the oxidation. Therefore, the oxidation process of fulvestrant was compared with some model compounds. Comparative studies on levodopa, carbidopa, benserazide, epirubicin, and doxorubicin related for the hydroxyl group of fulvestrant were performed by CV on BDD electrode, as a function of pH, in order to identify the oxidation step of fulvestrant. The oxidation mechanism of fulvestrant found related to the oxidation of the hydroxyl group on the aromatic ring.

Consequently, the above-presented technique is a good analytical alternative for determining fulvestrant in pharmaceutical dosage forms and spiked serum samples. This study only shows the possibility of monitoring this compound that makes the method useful for pharmacokinetic and pharmacodynamic purposes. However, the proposed methods might be alternatives to the HPLC techniques in therapeutic drug monitoring, or the experimental data might be used for the development of HPLC-EC method.

Acknowledgments

This work is produced from Ph.D. thesis of Pharm. Burcu Dogan-Topal (Ankara University, Health Science Institute). This research was supported by a Grant from Ankara University Scientific Project Foundation (Grant no. 20030803043) for Dr. B. Uslu. The authors would like to thank Asta Zeneca (Istanbul, Turkey) for providing standard fulvestrant and pharmaceutical dosage forms for developing the proposed method.

References

- [1] <http://www.cancer.org/Treatment/TreatmentsandSideEffects/index>.
- [2] <http://en.Wikipedia.org/wiki/Fulvestrant>.
- [3] I. Vergote and P. Abram, "Fulvestrant, a new treatment option for advanced breast cancer: tolerability versus existing agents," *Annals of Oncology*, vol. 17, no. 2, pp. 200–204, 2006.
- [4] D. Dodwell and I. Vergote, "A comparison of fulvestrant and the third-generation aromatase inhibitors in the second-line treatment of postmenopausal women with advanced breast cancer," *Cancer Treatment Reviews*, vol. 31, no. 4, pp. 274–282, 2005.
- [5] Physicians Desk Reference (PDR), Published by Thomson PDR, Montvale, p. 653, 2005.
- [6] D. Dodwell, G. Coombes, J. M. Bliss, L. S. Kilburn, and S. Johnston, "Combining fulvestrant (Faslodex™) with continued oestrogen suppression in endocrine-sensitive advanced breast cancer: the SoFEA trial," *Clinical Oncology*, vol. 20, no. 5, pp. 321–324, 2008.
- [7] J. Wang, *Electroanalytical Techniques in Clinical Chemistry and Laboratory Medicine*, VCH, New York, NY, USA, 1988.
- [8] P. T. Kissenger and W. R. Heineman, *Laboratory Techniques in Electroanalytical Chemistry*, Marcel Dekker, New York, NY, USA, 2nd edition, 1996.
- [9] D. K. Gosser, Ed., *Cyclic Voltammetry, Simulation and Analysis of Reaction Mechanism*, VCH, New York, NY, USA, 1993.
- [10] S. A. Özkan, B. Uslu, and H. Y. Aboul-Enein, "Analysis of pharmaceuticals and biological fluids using modern electroanalytical techniques," *Critical Reviews in Analytical Chemistry*, vol. 33, no. 3, pp. 155–181, 2003.
- [11] B. Uslu and S. A. Ozkan, "Solid electrodes in electroanalytical chemistry: present applications and prospects for high throughput screening of drug compounds," *Combinatorial Chemistry and High Throughput Screening*, vol. 10, no. 7, pp. 495–513, 2007.
- [12] B. Uslu and S. A. Ozkan, "Electroanalytical application of carbon based electrodes to the pharmaceuticals," *Analytical Letters*, vol. 40, no. 5, pp. 817–853, 2007.
- [13] C. M. Riley and T. W. Rosanske, *Development and Validation of Analytical Methods*, Elsevier Science, New York, NY, USA, 1996.
- [14] M. E. Swartz and I. S. Krull, *Analytical Method Development and Validation*, Marcell Dekker, New York, NY, USA, 1997.
- [15] J. Ermer and J. H. Miller, Eds., *Method Validation in Pharmaceutical Analysis*, Wiley-VCH, Weinheim, Germany, 2005.
- [16] P. Bievre and H. Günzler, *Validation in Chemical Measurements*, Springer, New York, NY, USA, 2005.
- [17] E. R. Brown, R. F. Large, A. Weissberger, and B. W. Rossiter, Eds., *Physical Methods of Chemistry*, Wiley Interscience, Rochester, NY, USA, 1964.
- [18] R. N. Goyal, V. K. Gupta, M. Oyama, and N. Bachheti, "Differential pulse voltammetric determination of atenolol in pharmaceutical formulations and urine using nanogold modified indium tin oxide electrode," *Electrochemistry Communications*, vol. 8, no. 1, pp. 65–70, 2006.
- [19] R. N. Goyal, N. Jain, and V. Gurnani, "Electrooxidation of chlorpromazine in aqueous and micellar media and spectroscopic studies of the derived cationic free radical and dication species," *Monatshefte für Chemie*, vol. 132, no. 5, pp. 575–585, 2001.
- [20] SciFinder Scholar Programme, American Chemical Society, Version, 2007.
- [21] Expert Working Group (Quality) of the ICH, "ICH-Q2Bn-validation of analytical procedures: methodology," in *International Conference on Harmonization of Technical Requirements for Registration of Pharmaceuticals for Human Use*, Geneva, Switzerland, November 1996.

Research Article

Single-Walled-Carbon-Nanotube-Modified Pyrolytic Graphite Electrode Used as a Simple Sensor for the Determination of Salbutamol in Urine

Rajendra N. Goyal, Sunita Bishnoi, and Bharati Agrawal

Department of Chemistry, Indian Institute of Technology Roorkee, Roorkee 247667, India

Correspondence should be addressed to Rajendra N. Goyal, rncyfcy@iitr.ernet.in

Received 2 December 2010; Accepted 23 December 2010

Academic Editor: Bengi Uslu

Copyright © 2011 Rajendra N. Goyal et al. This is an open access article distributed under the Creative Commons Attribution License, which permits unrestricted use, distribution, and reproduction in any medium, provided the original work is properly cited.

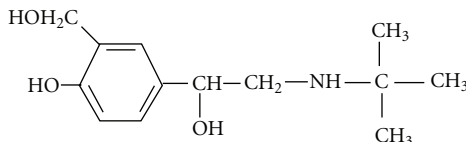
A fast and sensitive voltammetric method has been proposed for the determination of salbutamol at single-walled-carbon-nanotube-modified edge-plane pyrolytic graphite electrode (SWNT/EPPGE) in human urine. The electrochemical response of salbutamol was determined by square wave voltammetry (SWV) in phosphate buffer solution (PBS) at physiological pH 7.2. The modified electrode showed improved voltammetric response towards the oxidation of salbutamol, and a well-defined anodic peak was observed at ~600 mV with enhanced peak current in comparison to the bare electrode. Linear calibration plot using SWNT/EPPGE was obtained in the concentration range of 50 to 2500 ng ml⁻¹ with sensitivity and detection limit of 2.15 nA/ng ml⁻¹ and 4.31 ng ml⁻¹, respectively. The developed method has been successfully applied for the determination of salbutamol in commercial preparations and human body fluids. Fast analysis of salbutamol in human urine makes the proposed method of great interest for doping control purposes at the site of competitive games.

1. Introduction

β_2 -agonists are effective bronchodilators and normally used in symptomatic treatment of asthma and chronic bronchitis [1–3]. Salbutamol (α^1 -[(tert-butylamino) methyl]-4-hydroxy-m-xylene- α,α' -diol) (Scheme 1) is a direct-acting β_2 -agonist with beta-adrenergic activity employed as bronchodilator for the treatment of asthmatic disorders and chronic obstructive pulmonary diseases [4, 5]. It is also used to reduce premature labor in pregnancy [6]. Salbutamol is commonly administrated as pressurized metered dose inhaler and nebulized aerosol [7]. Salbutamol has been pharmacologically proven to be able to increase muscle protein, reduce total body fat, and promote muscle growth, therefore, it is highly abused by athletes to improve muscular strength and in turn improve their performance in sports [8–10]. The list of prohibited substances in sports published by the World Anti-Doping Agency (WADA) specifies that salbutamol can be used only by inhalation. Administration of salbutamol by oral or parenteral route and very large inhaled

dose are forbidden due to strong adrenergic stimulation. The threshold concentration of 1000 ng/mL has been established to suspect for oral administration of salbutamol by the WADA rules [11, 12]. A concentration of salbutamol greater than 1000 ng/mL is considered as an adverse analytical finding of anabolic agent and constitutes a doping violation [13]. In view of the extensive use and misuse of salbutamol in sports, it has been mandatory to analyze salbutamol concentration in pharmaceutical formulations as well as in biological fluids.

Several techniques have been explored for the determination of salbutamol to monitor the therapeutic use as well as to control illegal use. This includes high-performance liquid chromatography [14], capillary electrophoresis with UV detection [15], flow-injection analysis using spectrophotometric method [16], solid-phase extraction method [17], conductometric method [18], and electrogenerated chemiluminescence detection [19]. Although spectrophotometry and chromatography are the most commonly employed techniques, but these involve many derivatization steps and



SCHEME 1

an effective extraction purification approach prior to final analysis which is very time consuming and the demand of expensive and heavy instrumentation. The voltammetric methods have been proven to be advantageous alternative way due to their simplicity, high sensitivity, and rapidness [20, 21]. Hence, the determination of salbutamol at variety of electrodes has been attempted [22–27]. In many of these investigations, biological samples particularly urine have not been analyzed; hence, their usefulness could not be ascertained. In several others, the detection limit was much higher than expected to be present in blood plasma or urine. In the last few years our laboratory has been also trying to develop an efficient sensor for the determination of salbutamol [23]; however, at nanogold-modified electrode, a detection limit of $0.30\text{ }\mu\text{M}$ is achieved. As the preparation of nanogold electrode is tedious and the size of nanoparticles depends on time for which ITO sheet is dipped in the solution for crystal growth [28], pyrolytic graphite modified with carbon nanotubes is used in the present studies. The aim of the present work is to develop a fast and sensitive voltammetric sensor for the direct determination of salbutamol in human body fluids particularly urine as it can easily detect the cases of doping at the site of competitive games. The EPPGE has been proved to be an effective substrate for detecting lower concentration of biomolecules and drugs in comparison to other conventional electrodes [29, 30]. Carbon nanotubes are expected to increase electrochemical performance of electrodes due to their excellent electrical conductivity, nanometer size, and good chemical stability [31–35]. Therefore, the studies have been performed at SWNT/EPPGE. Square wave voltammetry is one of the widely used techniques due to its higher sensitivity, simplicity, and lower limit of detection for drugs and biomolecules [36, 37]; hence, it has been utilized for the sensitive sensing of salbutamol in body fluids and pharmaceutical preparations to monitor clinical and doping cases.

2. Experimental

2.1. Instrumentation. The voltammetric studies were carried out using BAS (Bioanalytical System, West Lafayette, USA) CV-50W voltammetric analyzer. The voltammetric cell used was a single compartment glass cell containing SWNT/EPPGE as working electrode, a platinum wire as counter electrode, and Ag/AgCl (3 M NaCl) as reference electrode (model BAS MF-2052 RB-5B). The edge-plane pyrolytic graphite piece was obtained from Pfizer Inc., New York, USA, and the electrode was prepared as reported

earlier in literature [38]. The pH of the buffer solutions was measured using digital pH meter (Model CP-901), Century India Ltd. All potential are reported with respect to Ag/AgCl reference electrode at an ambient temperature of $27 \pm 2^\circ\text{C}$.

2.2. Chemicals and Reagents. Salbutamol sulphate in powdered form was obtained as a gift sample from Vamsi labs Ltd., Maharashtra, India. SWNTs of purity >98% were purchased from Bucky USA, Houston, Tex, USA. Salbutamol-containing tablets of different companies were purchased from local market. Phosphate buffer solutions (1 M) were prepared according to the method of Christian and Purdy [39]. All chemicals used were of analytical grade and were purchased from Merck. Double-distilled water was used throughout the experiments.

2.3. Preparation of SWNT/EPPGE. Prior to modification, the surface of EPPGE was rubbed on an emery paper followed by cleaning it with double-distilled water and soft touching with tissue paper. Firstly, different concentrations of nanotubes in N,N-dimethylformamide (DMF) were prepared. Then, 0.5 mg/mL was selected as optimum based on the optimum current response of fixed concentration of salbutamol. A 0.5 mg/mL suspension of SWNT was prepared by dispersing 0.5 mg SWNT in 1.0 mL DMF by ultrasonic agitation. A known volume (40 μL) of this suspension was coated onto the surface of the bare EPPGE, and the solvent was allowed to evaporate at room temperature. The modified electrode was now ready for use. The surface morphology of the bare and modified electrodes was characterized by recording FE-SEM using Quanta 200 FE-SEM instrument. A comparison of FE-SEM images of the bare and SWNT-modified electrodes is presented in Figure 1 and clearly indicates the deposition of SWNT on the surface of the electrode. The surface of bare pyrolytic graphite appears to be rough, whereas in the case of modified electrode the deposition of SWNT with some agglomeration is observed in FE-SEM.

2.4. Analytical Procedure. Stock solution of salbutamol (1 mM) was prepared by dissolving the required amount of compound in double-distilled water. A known amount of stock solution was added to 2.0 mL phosphate buffer, and the total volume of 4.0 mL was obtained with double-distilled water. Square wave voltammograms were then recorded at the optimized parameters: initial E : 0 mV, final E : 1200 mV, square wave frequency (f): 15 Hz, square wave amplitude (E_{sw}): 20 mV, and step E : 4 mV. Urine sample of an asthma patient (male, 30 years, 45 kg) undergoing treatment with salbutamol from 8 months and blood plasma samples of healthy volunteers (female, 25 years, 50 kg; male, 30 years, 55 kg) were obtained from the Institute Hospital of IIT Roorkee. Blood sample was ultracentrifuged at a speed of 1000 rpm for 5 min, and supernatant blood plasma was used for the determination of salbutamol. Urine and blood samples were diluted 2 and 4 times, respectively, with phosphate buffer solution of pH 7.2 prior to analysis.

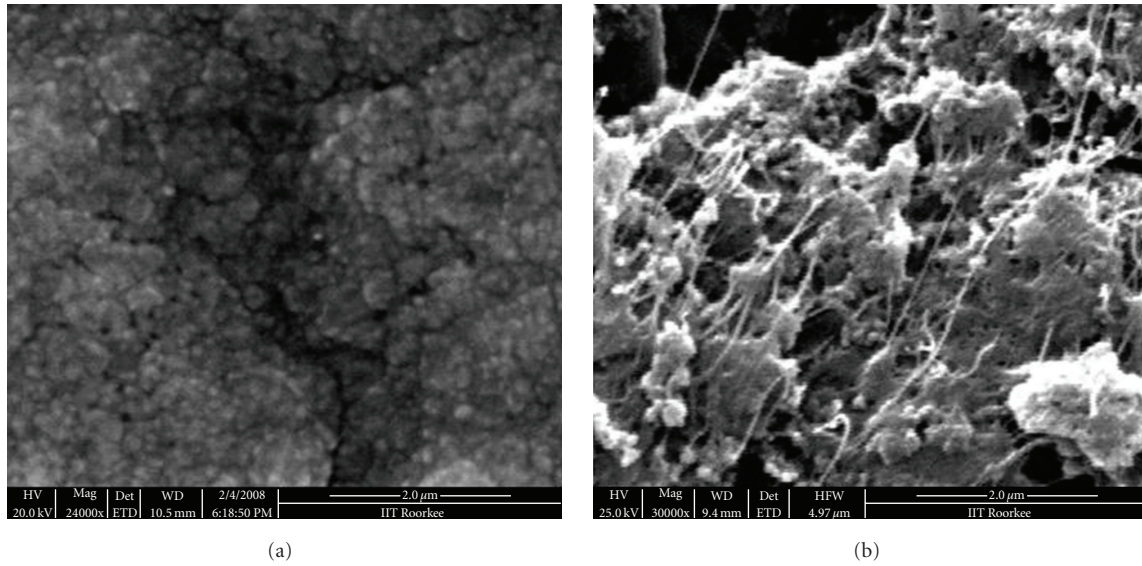


FIGURE 1: Typical FE-SEM images of (a) bare and (b) SWNT/EPPGE.

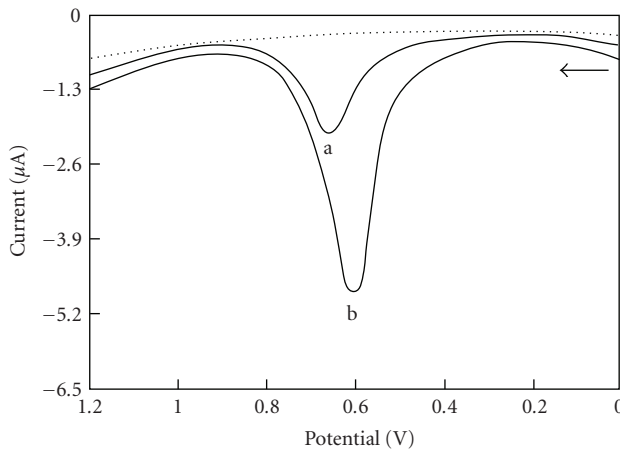


FIGURE 2: Comparison of square wave voltammograms for 2000 ng/mL of salbutamol at bare electrode (peak a) and SWNT-modified electrode (peak b) at pH 7.2 and background PBS (1 M) at SWNT/EPPGE (...).

3. Results and Discussion

3.1. Comparison of Bare and Modified Electrode. Electrochemical properties of salbutamol were demonstrated by using square wave voltammetry at bare and SWNT-modified EPPGE in phosphate buffer solution of pH 7.2. Figure 2 clearly indicates that on scanning the potential from 0 to 1200 mV oxidation peak was noticed at \sim 660 mV (peak a) using the bare electrode while for the modified electrode the oxidation peak appeared at \sim 600 mV (peak b) having marked increment in current value as compared to the bare electrode for 2000 ng/mL salbutamol. The significant improvement in peak current with decreasing potential clearly demonstrates that single-walled carbon nanotubes act as an efficient electron mediator for the oxidation of

salbutamol. The edge-plane-like defects which are present at the open ends of nanotubes and the embedded metal impurities in CNT samples are important reasons responsible for electrocatalytic properties of nanotubes [40, 41]. The modified electrode acts as a better substrate for voltammetric oxidation of salbutamol; therefore, further detailed studies were carried out at SWNT-modified EPPGE.

3.2. Electrochemical Behavior of Salbutamol

3.2.1. Cyclic Voltammetry. Cyclic voltammetry is one of the most widely used techniques which provide considerable information about the electrode reaction. Electrochemical response of salbutamol was determined by recording the cyclic voltammogram of 5000 ng/mL salbutamol at SWNT-modified EPPGE in phosphate buffer of pH 7.2 at scan rate of 20 mV/s. Figure 3 shows that a well-defined anodic peak is observed with peak potential of \sim 657 mV for salbutamol oxidation at SWNT/EPPGE. The absence of any peak in the reverse sweep clearly indicates that salbutamol was oxidized irreversibly at SWNT/EPPGE. Then, to analyze the nature of electrode reaction, cyclic voltammograms of 2000 ng/mL salbutamol were recorded at different scan rates in the range from 20 to 330 mV/s as shown in inset of Figure 3. It was found that peak current increases linearly with the increase in scan rate (v), and the plot of i_p versus $v^{1/2}$ clearly indicated that the reaction occurring at the surface of modified electrode is governed by the diffusion process [42, 43]. The dependence of peak current on scan rate can be expressed by the following relation:

$$i_p (\mu\text{A}) = 1.273v^{1/2} - 3.223, \quad (1)$$

where v is scan rate (mV/s) having a correlation coefficient of 0.997, where v is sweep rate in mV/s. Since SWV is more

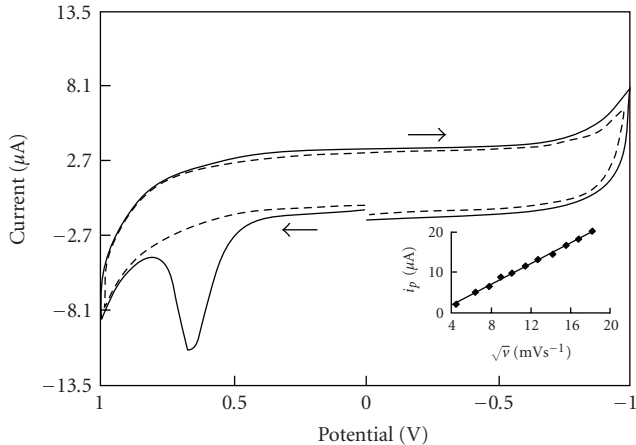


FIGURE 3: Cyclic voltammogram for 5000 ng/mL of salbutamol at SWNT-modified EPPGE (—) and background PBS at SWNT-modified EPPGE (---) at pH 7.2 and scan rate of 20 mV/S. Inset: Effect of scan rate (v) on peak current (i_p) of salbutamol.

sensitive than other voltammetric techniques and has the advantage of suppressing the background current; hence, further studies for the determination of salbutamol in real samples were performed by square wave voltammetry.

3.2.2. Effect of pH. The pH of the supporting electrolyte is one of the variables that strongly affect the redox reaction of analytes. Hence, it is usually important to investigate the effect of pH on electrochemical system. In order to optimize pH, the effect of pH on the oxidation of salbutamol was studied in the range of 2.3 to 9.9 using SWNT/EPPGE. The peak potential (E_p) of salbutamol was found to shift towards the less positive potential with the increase in pH as shown in Figure 4(a). The linear dependence of peak potential on pH can be expressed by the following relations:

$$\begin{aligned} E_p(\text{mV}) \text{ versus } \frac{\text{Ag}}{\text{AgCl}} &= 980.9 - 51.52 \text{ pH} \quad \text{at SWNT} \\ &\quad \text{EPPGE}, \\ E_p(\text{mV}) \text{ versus } \frac{\text{Ag}}{\text{AgCl}} &= 1041.1 - 52.05 \text{ pH} \quad \text{at bare EPPGE}, \end{aligned} \quad (2)$$

having correlation coefficients of 0.995 and 0.992, respectively. The observed slope of $\sim 52 \text{ mV/pH}$ clearly indicates that an equal number of electrons and protons are involved in the electrode reaction [44]. It was found that at pH 6.0 peak current was comparatively higher than at pH 7.0 for salbutamol solution; however, the study was performed in neutral media (pH 7.20) owing to the fact that the pH of human body fluids is almost equal to 7.00 and the determination of salbutamol in human body fluids was the main aim of proposed work.

3.2.3. Study of the Linear Range, Sensitivity, and Detection Limit. Square wave voltammograms of different concentration of salbutamol were recorded in order to plot calibration curves using bare and modified electrodes. A systematic

increase in peak current is observed with an increase in concentration of salbutamol at electrodes surface. The peak current versus concentration plots presents a good linearity for bare and modified electrodes in the concentration range of 500–2500 ng/mL and 50–2500 ng/mL, respectively, as depicted in Figure 4(b). Linear relations between peak current and concentration of salbutamol can be expressed at both electrodes by the following equations:

$$\begin{aligned} i_p(\text{nA}) &= 2.147C + 0.445 \quad \text{at SWNT} \\ &\quad \text{EPPGE}, \\ i_p(\text{nA}) &= 0.830C + 2.125 \quad \text{at bare EPPGE}, \end{aligned} \quad (3)$$

where C is the concentration (ng/mL) of salbutamol having correlation coefficients of 0.996 and 0.995, respectively. Figure 5 illustrates a series of square wave voltammograms obtained for salbutamol at different concentrations in 1 M phosphate buffer solution of pH 7.2 using SWNT/EPPGE. The detection limit for modified electrodes was calculated by using the formula $3\sigma/b$, where σ is the standard deviation and b is the slope of calibration curve, and was found to be 4.31 ng/mL.

3.2.4. Stability and Reproducibility of SWNT/EPPGE. Reproducibility and stability are two important parameters of an electrode for the selective and sensitive quantitative determination. The stability of the modified electrode was examined by measuring the current response at fixed concentration of salbutamol over a period of 15 days. The electrode was used daily and stored in air. The experimental results show that the current intraday responses deviate by 1.28% and interday responses by 1.90%, suggesting thereby that SWNT-modified EPPGE possesses good stability for the determination of salbutamol.

The reproducibility of modified electrode was evaluated by the repetitive measurements ($n = 6$) of salbutamol at a fixed concentration of $10 \mu\text{M}$. The corresponding relative standard deviation of 0.4% confirms that results are satisfactorily reproducible. In order to examine intraday (repeatability) and interday (reproducibility) response, SWVs were recorded for a fixed concentration of salbutamol ($10 \mu\text{M}$) using SWNT/EPPGE. The experimental results show that the current intraday responses deviate by 1.94% and interday responses by 2.40%, suggesting thereby that SWNT/EPPGE possesses adequate reproducibility for the determination of salbutamol. Intra-electrode reproducibility is also an important parameter; hence, to examine electrode-to-electrode variation response, four pyrolytic graphite electrodes ($1 \times 1 \times 3 \text{ mm}^3$) are casted with $40 \mu\text{L}$ of SWNT suspension. It was observed that these electrodes show a variation of $\pm 2.9\%$ in peak current of $10 \mu\text{M}$ salbutamol. Thus, it is concluded that the electrode-to-electrode variation is nonsignificant. Thus, the SWNT-modified EPPGE exhibits a good reproducibility and stability for the determination of salbutamol, and therefore the proposed sensor is also recommended for the determination of similar drugs and biomolecules with good sensitivity and low detection limit.

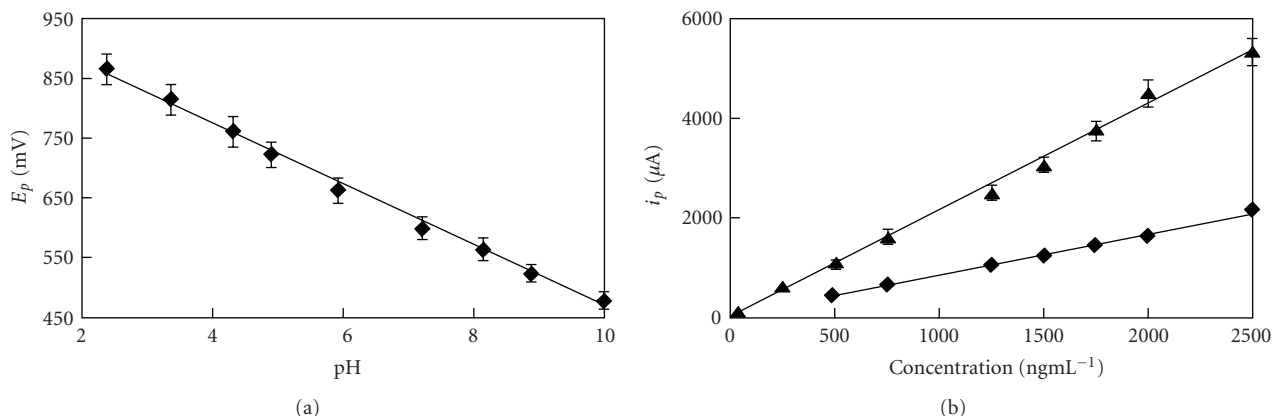


FIGURE 4: (a) Dependence of pH on peak potential of salbutamol at SWNT/EPPGE. (b) Calibration plot of salbutamol at bare (■) and SWNT-modified EPPGE (▲) at pH 7.2.

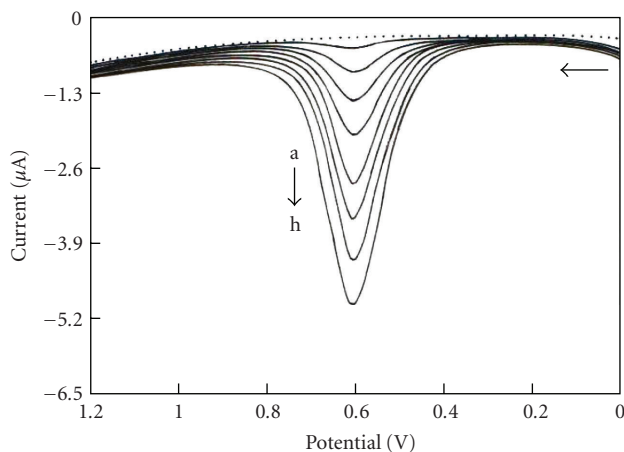


FIGURE 5: Square wave voltammograms of various concentrations of salbutamol at SWNT-modified EPPGE in 1 M phosphate buffer (pH 7.2); [salbutamol]: a = 50, b = 250, c = 500, d = 750, e = 1250, f = 1500, g = 1750, h = 2000 ng/mL.

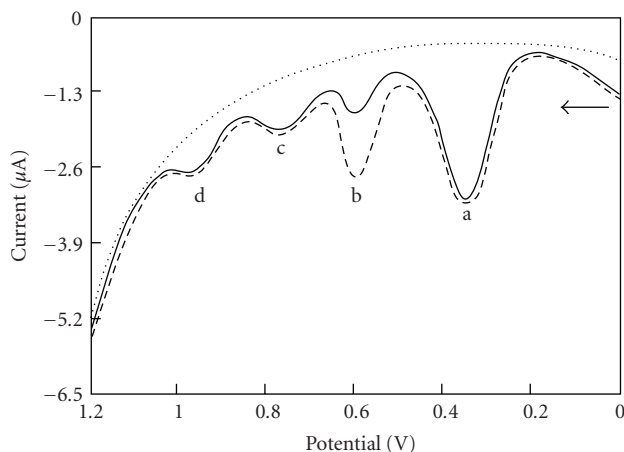


FIGURE 6: Square wave voltammograms for urine sample of asthma patient (—) and urine sample of patient spiked with salbutamol (---) using SWNT/EPPGE. The background PBS at modified electrode is shown as (...).

TABLE 1: Determination of salbutamol in different pharmaceutical preparations using SWNT/EPPGE.

Tablet	Amount labeled (mg)	Amount detected ^a (mg)	Error %
Salbetol-2	2.00	2.05	+2.5%
Asthalin-2	2.00	2.04	+2.0%
Asthalin-4	4.00	3.90	-2.5%
Ventolin-8	8.00	7.99	-0.12%
Eto-Salbetol	2.00	1.99	-0.5%

^aThe RSD value for the determination of salbutamol was less than $\pm 2.2\%$ for $n = 3$.

TABLE 2: Recovery data for salbutamol determination in plasma samples of healthy volunteers at SWNT-modified EPPGE.

Spiked amount (μM)	Detected amount ^a (μM)	Recovery (%)
<i>Sample 1</i>		
0.50	0.50	100.00
1.00	0.99	99.00
1.50	1.49	99.33
<i>Sample 2</i>		
0.50	0.49	98.00
1.00	0.98	98.00
1.50	1.49	99.33

^aThe RSD value for the determination of salbutamol was less than $\pm 3.2\%$ for $n = 3$.

3.3. Analytical Utility

3.3.1. Real Sample Analysis. In order to establish the analytical utility of the proposed method, attempts have been made to analyze the urine sample of an asthma patient undergoing treatment with salbutamol for the last 8 months. Urine sample was collected after oral administration of 2 mg salbutamol tablet (Salbetol-2). Prior to analysis, the urine sample was diluted 2 times with PBS of pH 7.2 in order to minimize interference of matrix. Square wave voltammograms of the urine sample of the patient spiked with known

TABLE 3: A comparison of voltammetric response of SWNT/EPPGE with previously reported methods for the determination of salbutamol.

Sr. no.	Electrode	Concentration range (μM)	Limit of detection (μM)	Sensitivity ($\mu\text{A}/\mu\text{M}$)	Analytical utility real samples	Ref. no.
(1)	Pt electrode	100–1000	80.00	0.012	No	[22]
	GCE	20–1000	10.00	0.066	No	[22]
(2)	NGITO	0.20–8.35	0.31	0.055	Yes	[23]
(3)	GCE	0.80–80.00	0.20	—	No	[24]
(4)	MWNT/GCE	0.80–10.00	0.20	0.620	No	[25]
(5)	C ₆₀ /GCE	0.42–8.35	0.17	0.048	Yes	[26]
(6)	GN/GCE	5–90	0.10	—	No	[27]
(7)	SWNT/EPPGE	0.20–10.45	0.018	0.520	Yes	Proposed method

amount of salbutamol were then recorded under optimized parameters using SWNT-modified EPPGE. Figure 6 clearly shows that a well-defined oxidation peak was observed at ~ 600 mV (peak b) in urine sample of the patient. In order to confirm that this peak is due to the excreted salbutamol in urine, a known amount of authentic salbutamol was spiked in the diluted urine sample of the patient. It was observed that the peak current of peak at ~ 600 mV increased on spiking of salbutamol, indicating thereby that the peak at $E_p \sim 600$ is due to the oxidation of salbutamol excreted in the urine sample of the patient. Some additional peaks were also observed in the urine sample at ~ 300 (a), ~ 780 (c), and ~ 980 mV (d) and were likely to be due to the oxidation of major urinary metabolites, that is, uric acid, xanthine, and hypoxanthine, respectively, although no efforts had been made to analyze them. The concentration of salbutamol in the patient's urine sample was calculated by using calibration plot and found to be $2.00 \mu\text{M}$, which was further confirmed using standard addition method. The RSD for the determination was found to be less than 2.2% for $n = 5$.

3.3.2. Pharmaceutical Analysis. The proposed method was also used to analyze salbutamol-containing tablets to determine their salbutamol content using SWNT-modified EPPGE. The salbutamol content was determined in five common medicinal tablets, that is, Salbetol-2 (Verna industrial estates verna, FDC Ltd., Mfg. Lic no. 656), Asthalin-2 (Mfd. by Cipla Ltd.), Asthalin-4 (Mfd. by Cipla Ltd.), Venterlin-8 (Mfd. by Themis laboratories Pvt. Ltd., Mfg. Lic no. KD-638), and Eto-Salbetol (Mfd. by Kare labs Pvt. Ltd., Mfg. Lic. no. 314). Firstly, tablets were crushed and dissolved in double-distilled water. The solutions obtained by dissolution of tablets were subsequently diluted so that reported salbutamol concentration falls in the range of calibration plot. Square wave voltammograms were then recorded under identical conditions which were used during plotting the calibration plot. The concentration of salbutamol determined by employing the proposed method in different pharmaceutical formulations is compared with labeled concentration of salbutamol and summarized in Table 1. The results show that salbutamol content for all pharmaceutical preparations fall within the claimed amount with error of $\pm 2.5\%$ indicating the adequate accuracy of the proposed method.

3.4. Recovery Study. In order to examine the stability of salbutamol in human body fluids and the accuracy of the developed method, recovery experiments were carried out at SWNT/EPPGE. Square wave voltammograms of plasma samples from two healthy volunteers were recorded for this purpose. Recovery experiments were carried out by standard addition method using SWNT-modified EPPGE. The drug-free plasma samples were spiked with known concentrations of standard solution of salbutamol followed by recording their voltammograms. The concentration of salbutamol was calculated by using regression equation, and the results observed are tabulated in Table 2. The recoveries varied in the range from 98.00% to 100.00% with relative standard deviation (RSD) of $\pm 3.2\%$ indicating good accuracy of the proposed sensor, and adequate stability of salbutamol in body fluids is also recommended.

4. Conclusions

The results presented in this paper indicated that square wave voltammetry associated with the use of SWNT/EPPGE serves as a fast and reliable tool for the analysis of salbutamol in the biological system. SWNT/EPPGE exhibits improved electrocatalytic properties with enhanced peak current and decreased peak potential as compared to bare EPPGE and several other electrodes. The ability to mediate fast electron transfer reaction with salbutamol in solution makes the modified electrode an ideal candidate for its use in electrochemical experiments. The two important analytical parameters for efficient quantitative determination are sensitivity and detection limit. It was found that the sensitivity of salbutamol determination was almost three times higher using the modified electrode as compared to the bare electrode, and detection limit was also low enough at SWNT/EPPGE. Findings of the proposed work prove that the above-described approach can be a desirable pathway for fabrication of sensors based on nanotubes systems. It was also found that detection limit, sensitivity, and practical utility of the proposed method utilizing SWNT/EPPGE are much better than earlier reported methods (Table 3). The detection limit at the proposed electrode is almost ten and sixty times lower than that reported recently at MWNT/GCE and graphite-nanosheet-modified electrodes, respectively [25, 27], and sensitivity is ten times higher

than nanogold-modified ITO [23]. Real sample analysis is an important analytical utility of any sensor; however, no information regarding real sample analysis has been provided in recently reported methods using MWNT/GCE for salbutamol determination. Thus, it is reasonable to conclude that SWNT/EPPGE is a better sensor for the determination of salbutamol in comparison to nanogold-modified ITO or several other conventional electrodes reported earlier (Table 3). The proposed sensor showed a good linear range, low detection limit, good reproducibility, satisfactory recovery results, and high stability making this system a promising example of chemical sensor and interesting alternative for quantification of salbutamol in human body fluids as well as in commercial preparations.

Acknowledgment

The authors (S. Bishnoi and B. Agarwal) are thankful to the Council of Scientific and Industrial Research, New Delhi for awarding them the Senior Research fellowship and the Junior Research fellowship, respectively.

References

- [1] V. M. Balanag, F. Yunus, P. C. Yang, and C. Jorup, "Efficacy and safety of budesonide/formoterol compared with salbutamol in the treatment of acute asthma," *Pulmonary Pharmacology and Therapeutics*, vol. 19, no. 2, pp. 139–147, 2006.
- [2] R. Ventura, L. Damasceno, M. Farré, J. Cardoso, and J. Segura, "Analytical methodology for the detection of β -agonists in urine by gas chromatography-mass spectrometry for application in doping control," *Analytica Chimica Acta*, vol. 418, no. 1, pp. 79–92, 2000.
- [3] S. M. Dennis, S. J. Sharp, M. R. Vickers et al., "Regular inhaled salbutamol and asthma control: the TRUST randomised trial," *Lancet*, vol. 355, no. 9216, pp. 1675–1679, 2000.
- [4] M. R. Ganjali, P. Norouzi, M. Ghorbani, and A. Sepehri, "Fourier transform cyclic voltammetric technique for monitoring ultratrace amounts of salbutamol at gold ultra micro-electrode in flowing solutions," *Talanta*, vol. 66, no. 5, pp. 1225–1233, 2005.
- [5] B. Valenzuela, A. Nácher, V. G. Casabó, and A. Martín-Villodre, "The influence of active secretion processes on intestinal absorption of salbutamol in the rat," *European Journal of Pharmaceutics and Biopharmaceutics*, vol. 52, no. 1, pp. 31–37, 2001.
- [6] I. Dol and M. Knochen, "Flow-injection spectrophotometric determination of salbutamol with 4-aminoantipyrine," *Talanta*, vol. 64, no. 5, pp. 1233–1236, 2004.
- [7] M. Cope and F. Bautista-Parra, "The degradation of salbutamol in ethanolic solutions," *Journal of Pharmaceutical and Biomedical Analysis*, vol. 52, no. 2, pp. 210–215, 2010.
- [8] V. A. Sakkas, P. Calza, C. Medana et al., "Heterogeneous photocatalytic degradation of the pharmaceutical agent salbutamol in aqueous titanium dioxide suspensions," *Applied Catalysis B*, vol. 77, no. 1-2, pp. 135–144, 2007.
- [9] M. Cepero, Y. Pérez-Pertejo, J. C. Cubría et al., "Muscle and serum changes with salbutamol administration in aerobically exercised rats," *Comparative Biochemistry and Physiology C*, vol. 126, no. 1, pp. 45–51, 2000.
- [10] Q. Chen, L.-Y. Fan, W. Zhang, and C.-X. Cao, "Separation and determination of abused drugs clenbuterol and salbutamol from complex extractants in swine feed by capillary zone electrophoresis with simple pretreatment," *Talanta*, vol. 76, no. 2, pp. 282–287, 2008.
- [11] R. Ventura, R. Ramírez, N. Monfort, and J. Segura, "Ultraperformance liquid chromatography tandem mass spectrometric method for direct quantification of salbutamol in urine samples in doping control," *Journal of Pharmaceutical and Biomedical Analysis*, vol. 50, no. 5, pp. 886–890, 2009.
- [12] M.-H. Spyridaki, P. Kioussi, A. Vonaparti et al., "Doping control analysis in human urine by liquid chromatography-electrospray ionization ion trap mass spectrometry for the Olympic Games Athens 2004: determination of corticosteroids and quantification of ephedrines, salbutamol and morphine," *Analytica Chimica Acta*, vol. 573–574, pp. 242–249, 2006.
- [13] J. Zhang, Y. Xu, X. Di, and M. Wu, "Quantitation of salbutamol in human urine by liquid chromatography- electrospray ionization mass spectrometry," *Journal of Chromatography B*, vol. 831, no. 1-2, pp. 328–332, 2006.
- [14] S. H. R. A. Mazhar and H. Chrystyn, "New HPLC assay for urinary salbutamol concentrations in samples collected post-inhalation," *Journal of Pharmaceutical and Biomedical Analysis*, vol. 50, no. 2, pp. 175–182, 2009.
- [15] S. Sirichai and P. Khanatharana, "Rapid analysis of clenbuterol, salbutamol, procaterol, and fenoterol in pharmaceuticals and human urine by capillary electrophoresis," *Talanta*, vol. 76, no. 5, pp. 1194–1198, 2008.
- [16] D. Šatinský, R. Karlíček, and A. Svoboda, "Using on-line solid phase extraction for flow-injection spectrophotometric determination of salbutamol," *Analytica Chimica Acta*, vol. 455, no. 1, pp. 103–109, 2002.
- [17] Y. M. Koh, M. I. Saleh, and S. C. Tan, "Selective extraction of salbutamol from human plasma with the use of phenylboronic acid," *Journal of Chromatography A*, vol. 987, no. 1-2, pp. 257–267, 2003.
- [18] Y. M. Issa, A. F. Shoukry, and R. M. El-Nashar, "Conductimetric determination of reproterol HCl and pipazethate HCl and salbutamol sulphate in their pharmaceutical formulations," *Journal of Pharmaceutical and Biomedical Analysis*, vol. 26, no. 3, pp. 379–386, 2001.
- [19] C. A. Lindino and L. O. S. Bulhões, "Determination of fenoterol and salbutamol in pharmaceutical formulations by electrogenerated chemiluminescence," *Talanta*, vol. 72, no. 5, pp. 1746–1751, 2007.
- [20] V. Pedrosa, S. Machado, and L. Avaca, "Application of a deconvolutive procedure to analyze several chlorophenol species in natural waters by square-wave voltammetry on the boron-doped diamond electrode," *Analytical Letters*, vol. 39, no. 9, pp. 1955–1965, 2006.
- [21] R. N. Goyal and S. Bishnoi, "Simultaneous voltammetric determination of prednisone and prednisolone in human body fluids," *Talanta*, vol. 79, no. 3, pp. 768–774, 2009.
- [22] N. Yilmaz, S. A. Özkan, B. Uslu, Z. Şentürk, and I. Biryol, "Voltammetric determination of salbutamol based on electrochemical oxidation at platinum and glassy carbon electrodes," *Turkish Journal of Chemistry*, vol. 22, no. 2, pp. 175–182, 1998.
- [23] R. N. Goyal, M. Oyama, and S. P. Singh, "Fast determination of salbutamol, abused by athletes for doping, in pharmaceuticals and human biological fluids by square wave voltammetry," *Journal of Electroanalytical Chemistry*, vol. 611, no. 1-2, pp. 140–148, 2007.

- [24] K. A. Sagar, M. R. Smyth, and R. Munden, "Voltammetric study of salbutamol and application to its determination in a tablet dosage form and dissolution profiles for the dosage form," *Journal of Pharmaceutical and Biomedical Analysis*, vol. 11, no. 7, pp. 533–540, 1993.
- [25] Y. Wei, Q. Zhang, C. Shao, C. Li, L. Zhang, and X. Li, "Voltammetric determination of salbutamol on a glassy carbon electrode coated with a nanomaterial thin film," *Journal of Analytical Chemistry*, vol. 65, no. 4, pp. 398–403, 2010.
- [26] R. N. Goyal, D. Kaur, S. P. Singh, and A. K. Pandey, "Effect of graphite and metallic impurities of C fullerene on determination of salbutamol in biological fluids," *Talanta*, vol. 75, no. 1, pp. 63–69, 2008.
- [27] LI. Shen, Z. Li, and P. He, "Electrochemical behavior of β -agonists at graphite nanosheet modified electrodes," *Electrochemistry Communications*, vol. 12, pp. 876–881, 2010.
- [28] R. N. Goyal, A. Aliumar, and M. Oyama, "Comparison of spherical nanogold particles and nanogold plates for the oxidation of dopamine and ascorbic acid," *Journal of Electroanalytical Chemistry*, vol. 631, no. 1-2, pp. 58–61, 2009.
- [29] D. S. Shishmarev, N. V. Rees, and R. G. Compton, "Full paper enhanced performance of edge-plane pyrolytic graphite (EPPG) electrodes over glassy carbon (GC) electrodes in the presence of surfactants: application to the stripping voltammetry of copper," *Electroanalysis*, vol. 22, no. 1, pp. 31–34, 2010.
- [30] R. T. Kachoosangi and R. G. Compton, "A simple electroanalytical methodology for the simultaneous determination of dopamine, serotonin and ascorbic acid using an unmodified edge plane pyrolytic graphite electrode," *Analytical and Bioanalytical Chemistry*, vol. 387, no. 8, pp. 2793–2800, 2007.
- [31] W. Yue-Rong, H. Ping, L. Qiong-Lin, L. Guo, and W. Yi-Ming, "Application of carbon nanotube modified electrode in bioelectroanalysis," *Chinese Journal of Analytical Chemistry*, vol. 36, no. 8, pp. 1011–1016, 2008.
- [32] F. Valentini, S. Orlanducci, M. L. Terranova, A. Amine, and G. Palleschi, "Carbon nanotubes as electrode materials for the assembling of new electrochemical biosensors," *Sensors and Actuators B*, vol. 100, no. 1-2, pp. 117–125, 2004.
- [33] R. Antiochia and L. Gorton, "Development of a carbon nanotube paste electrode osmium polymer-mediated biosensor for determination of glucose in alcoholic beverages," *Biosensors and Bioelectronics*, vol. 22, no. 11, pp. 2611–2617, 2007.
- [34] A. Curulli, F. Valentini, G. Padeletti, M. Viticoli, D. Caschera, and G. Palleschi, "Smart (Nano) materials: TiO nanostructured films to modify electrodes for assembling of new electrochemical probes," *Sensors and Actuators B*, vol. 111-112, pp. 441–449, 2005.
- [35] A. Merkoçi, M. Pumera, X. Llopis, B. Pérez, M. Del Valle, and S. Alegret, "New materials for electrochemical sensing VI: carbon nanotubes," *Trends in Analytical Chemistry*, vol. 24, no. 9, pp. 826–838, 2005.
- [36] D. Abd El-Hady, M. I. Abdel-Hamid, M. M. Seliem, V. Andrisano, and N. Abo El-Maali, "Osteryoung square wave stripping voltammetry at mercury film electrode for monitoring ultra trace levels of Tarabine PFS and its interaction with ssDNA," *Journal of Pharmaceutical and Biomedical Analysis*, vol. 34, no. 5, pp. 879–890, 2004.
- [37] R. A. De Toledo, M. Castilho, and L. H. Mazo, "Determination of dipyridamole in pharmaceutical preparations using square wave voltammetry," *Journal of Pharmaceutical and Biomedical Analysis*, vol. 36, no. 5, pp. 1113–1117, 2005.
- [38] R. N. Goyal, M. Oyama, and A. Tyagi, "Fullerene-C₆₀-modified edge plane pyrolytic graphite electrode for the determination of dexamethasone in pharmaceutical formulations and human biological fluids," *Biosensors and Bioelectronics*, vol. 581, pp. 32–36, 2007.
- [39] G. D. Christian and W. C. Purdy, "The residual current in orthophosphate medium," *Journal of Electroanalytical Chemistry*, vol. 3, no. 6, pp. 363–373, 1962.
- [40] C. E. Banks, M. R. Moore, T. J. Davies, and R. G. Compton, "Investigation of modified basal plane pyrolytic graphite electrodes: definitive evidence for the electrocatalytic properties of the ends of carbon nanotubes," *Chemical Communications*, vol. 10, no. 16, pp. 1804–1805, 2004.
- [41] X. Liu, V. Gurel, D. Morris et al., "Bioavailability of nickel in single-wall carbon nanotubes," *Advanced Materials*, vol. 19, no. 19, pp. 2790–2796, 2007.
- [42] R. H. Wopschall and I. Shain, "Adsorption characteristics of the methylene blue system using stationary electrode polarography," *Analytical Chemistry*, vol. 39, no. 13, pp. 1527–1534, 1967.
- [43] F. Quente and C. Elleouet, "Square-wave voltammetry of molybdenum-fulvic acid complex," *Electroanalysis*, vol. 13, no. 12, pp. 1030–1035, 2001.
- [44] X. Jiang and X. Lin, "Overoxidized polypyrrole film directed DNA immobilization for construction of electrochemical micro-biosensors and simultaneous determination of serotonin and dopamine," *Analytica Chimica Acta*, vol. 537, no. 1-2, pp. 145–151, 2005.

Research Article

In Situ Evaluation of Fludarabine-DNA Interaction Using a DNA-Electrochemical Biosensor

H. Eda Satana^{1,2} and Ana Maria Oliveira-Brett¹

¹Departamento de Química, Faculdade de Ciências e Tecnologia, Universidade de Coimbra, 3004-535 Coimbra, Portugal

²Department of Analytical Chemistry, Faculty of Pharmacy, Gazi University, Etiler, 06330 Ankara, Turkey

Correspondence should be addressed to Ana Maria Oliveira-Brett, brett@ci.uc.pt

Received 25 January 2011; Accepted 23 February 2011

Academic Editor: Bengi Uslu

Copyright © 2011 H. Eda Satana and A. M. Oliveira-Brett. This is an open access article distributed under the Creative Commons Attribution License, which permits unrestricted use, distribution, and reproduction in any medium, provided the original work is properly cited.

Fludarabine, 9-β-D-arabinosyl-2-fluoroadenine, the nucleoside analog, represents a highly effective treatment for hairy cell leukemia. The electrochemical behaviour of fludarabine is an irreversible diffusion controlled oxidation mechanism and was investigated at a glassy carbon electrode in different supporting electrolytes using cyclic, differential pulse, and square wave voltammetry. The diffusion coefficient of fludarabine was calculated to be $D_{FLU} = 1.71 \times 10^{-6} \text{ cm}^2 \text{ s}^{-1}$ in pH 7.0 0.1 M phosphate buffer. The oxidation mechanism of fludarabine occurs with the transfer of one proton and one electron and the formation of a hydroxylated species. The interaction of fludarabine with DNA was investigated, by differential pulse voltammetry, in incubated solutions and using dsDNA- and polyhomonucleotides-, poly[G] and poly[A], electrochemical biosensors. The results showed that fludarabine interacts with DNA causing changes in the DNA structure.

1. Introduction

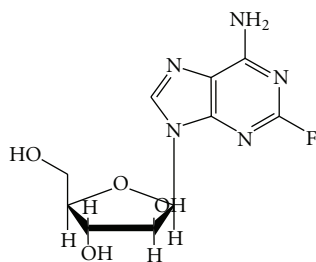
Nucleotides are essential components of the signal transduction system and energy providers such as adenosine triphosphate (ATP). Nucleoside analogs are antimetabolites used in cellular and molecular biology research, as well as in the treatment of some diseases as antiviral or anticancer drugs. These analogs are metabolized to pharmacologically active derivatives in cells and compete with natural products.

The nucleoside analog fludarabine (FLU, 9-β-D-arabinosyl-2-fluoroadenine), Scheme 1, represents a highly effective treatment for hairy cell leukemia, chronic lymphocytic leukaemia, and other several hematopoietic malignancies [1]. The introduction of a fluorine atom in the nucleoside group has improved the pharmacological properties of the molecule with minor stereochemistry changes. Unlike the former nucleoside analogs, FLU is resistant to deamination by adenosine deaminase. After entering the cells by means of specific nucleoside transporters, FLU is activated to its phosphorylated derivative by intracellular kinase. Its active metabolite competes with deoxy-ATP for incorporation into the growing nucleic acid chain causing disruption of nucleic

acid synthesis. In the same way, this metabolite interrupts the elongation of the RNA primer strand [2].

To improve treatment results in patients, individualization of FLU dosing is important. This individualization must be depended on correlations between dosing and plasma concentration of drug and its derivatives. Furthermore, the determination of cellular concentrations of FLU could provide valuable information for understanding the mechanisms of DNA damage and cell death. Therefore, some methods based on high performance liquid chromatographic and voltammetric techniques were developed for the determination of FLU especially in biological samples. FLU and its triphosphate derivative were determined by liquid chromatography with UV detection [3–7] and with tandem mass spectrometry [8] in human cells, urine, plasma, and pharmaceuticals, and the electrochemical behaviour of FLU was also investigated using pyrolytic graphite electrode [9].

Most studies were related with the pharmacological character and effects of FLU on biological molecules, carried out in cell lines, and several studies indicated that FLU is an agent that causes disruption or breakages in the genetic material.



SCHEME 1: Chemical structure of fludarabine.

Deoxyribonucleic acid (DNA) is the genetic material and has important biological roles including transcription of the genetic information, signalling, and metabolic regulation. Formation of DNA strand breaks causes chromosome aberrations and accumulation of these mutations and other DNA damages increase carcinogenic or teratogenic risks. Finally, these events may result in a malignant transformation or cell death. Due to their important biological and genetic roles, nucleic acids have been intensively studied and a number of different techniques have been developed to elucidate various aspects of DNA and RNA structures and properties. Electrochemical methods including DNA-electrochemical biosensors comprise an important group of these techniques. Compared with optical devices, electrochemical sensors have some advantages such as their high sensitivity, simplicity, low cost, and fast response time [10–13].

A DNA-electrochemical biosensor consists of an electrode with DNA immobilized on the surface. Interaction of a damaging agent with DNA causes changing of electrochemical properties of the DNA recognition layer. This effect is turned to measurable electrical signals and DNA damage and interaction caused by hazardous compounds, such as metals or pharmaceutical drugs, can be determined.

In this study, the electrochemical oxidation of FLU and the mechanism of FLU-dsDNA and polyhomonucleotides, poly[G] and poly[A], interaction were carried out using cyclic, square wave and differential pulse voltammetry at a glassy carbon electrode. The results will contribute to the clarification of the mechanism by which FLU can cause direct *in vivo* DNA damage.

2. Experimental

2.1. Materials and Reagents. Fludarabine, double stranded (dsDNA), polyadenylic acid (Poly[A]), and polyguanylic acid (Poly[G]) were obtained from Sigma and used without further purification. A stock solution of 1 mM FLU was prepared in deionized water and stored at 5°C.

Solutions of different concentrations of FLU were prepared by dilution of the appropriate quantity in supporting electrolyte. Stock solutions of 186 µg mL⁻¹ dsDNA, 477 µg mL⁻¹ Poly[G], and 587 µg mL⁻¹ Poly[A] were prepared in deionized water and diluted to the desired concentrations in pH 4.5 0.1 M acetate buffer.

TABLE 1: Supporting electrolyte buffer solutions.

pH	Composition
2.1	HCl + KCl
3.4	HAcO + NaAcO
4.3	HAcO + NaAcO
4.5	HAcO + NaAcO
5.4	HAcO + NaAcO
6.1	NaH ₂ PO ₄ + Na ₂ HPO ₄
7.0	NaH ₂ PO ₄ + Na ₂ HPO ₄
8.0	NaH ₂ PO ₄ + Na ₂ HPO ₄
9.2	NH ₃ + NH ₄ Cl
10.5	NH ₃ + NH ₄ Cl
12.0	NaOH + KCl

All supporting electrolyte solutions (Table 1) were prepared using analytical grade reagents and purified water from a Millipore Milli-Q system (conductivity ≤ 0.1 µS cm⁻¹).

2.2. Apparatus. Voltammetric experiments were carried out using a µ Autolab running with GPES 4.9 software, Eco-Chemie, Utrecht, The Netherlands. Measurements were carried out using a three-electrode system in a 0.5 mL one-compartment electrochemical cell (Cypress System Inc., USA). Glassy carbon electrode (GCE, *d* = 1.5 mm) was the working electrode, Pt wire the counter electrode, and Ag/AgCl (3 M KCl) the reference electrode.

The pH measurements were carried out with a Crison micropH 2001 pH-meter with an Ingold combined glass electrode. All experiments were done at room temperature (25 ± 1°C) and, microvolumes were measured using EP-10 and EP-100 Plus Motorized Microliter Pippettes (Rainin Instrument Co. Inc., Woburn, USA).

The experimental conditions for differential pulse (DP) voltammetry were: pulse amplitude 50 mV, pulse width 70 ms, and scan rate 5 mV s⁻¹. For square wave (SW) voltammetry, a frequency of 50 Hz and a potential increment of 2 mV, corresponding to an effective scan rate of 100 mV s⁻¹ were used.

The GCE was polished using diamond spray (particle size 3 µm) (Kemet, UK) before each electrochemical experiment. After polishing, it was rinsed thoroughly with Milli-Q water. Following this mechanical treatment, the GCE was placed in buffer supporting electrolyte and voltammograms were recorded until a steady-state baseline voltammogram was obtained. This procedure ensured very reproducible experimental results.

2.3. Acquisition and Presentation of Voltammetric Data. All the voltammograms presented were background-subtracted and baseline-corrected using the moving average application with a step window of 5 mV included in GPES version 4.9 software. This mathematical treatment improves the visualization and identification of peaks over the baseline without introducing any artifact, although the peak intensity is, in some cases, reduced (<10%) relative to that of the

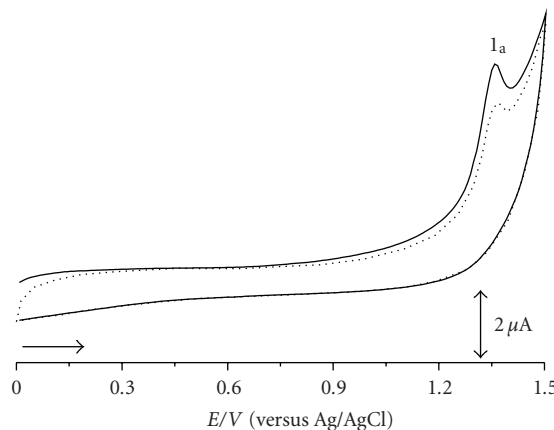


FIGURE 1: Cyclic voltammograms of $100 \mu\text{M}$ FLU in pH 6.1 0.1 M phosphate buffer solution, N_2 saturated; “solid line” first scan, “dotted line” second scan, and $\nu = 100 \text{ mV s}^{-1}$.

untreated curve. Nevertheless, this mathematical treatment of the original voltammograms was used in the presentation of all experimental voltammograms for a better and clearer identification of the peaks. The values for peak current presented in all plots were determined from the original untreated voltammograms after subtraction of the baseline.

2.4. Incubation Procedure and DNA-Electrochemical Biosensor Preparation. In order to perform the incubation procedure in pH 4.5 0.1 M acetate buffer, $100 \mu\text{g mL}^{-1}$ dsDNA were mixed with $2 \mu\text{M}$ FLU and $100 \mu\text{g mL}^{-1}$ Poly[G] or Poly[A] were mixed with $5 \mu\text{M}$ FLU, and then incubated during different periods at room temperature. Control solutions of FLU, dsDNA, Poly[G], and Poly[A] in pH 4.5 0.1 M acetate buffer were also prepared and stored during the same periods in similar conditions as the FLU-dsDNA, FLU-Poly[G], and FLU-Poly[A] incubated solutions.

The thin layer dsDNA-modified electrode was prepared with three drops of $5 \mu\text{L}$ each containing $50 \mu\text{g mL}^{-1}$ dsDNA. After setting each drop on the electrode surface, the biosensor was allowed to dry under the constant flux of N_2 . The dsDNA-electrochemical biosensor was incubated in $50 \mu\text{M}$ FLU solution during different times. Then, in order to remove unbound FLU molecules from the surface, the electrode was carefully rinsed with deionized water and transferred to supporting electrolyte. After each measurement, the dsDNA film was removed from the electrode surface and a new biosensor was prepared for each experiment.

Poly[G]- and Poly[A]-electrochemical biosensors were prepared placing three drops of $5 \mu\text{L}$ each containing $25 \mu\text{g mL}^{-1}$ of each polyhomonucleotide on the electrode surface.

3. Results and Discussion

The electrochemical behaviour of FLU was investigated using the glassy carbon electrode (GCE) and cyclic (CV), differential pulse (DP), and square wave (SW) voltammetry.

Systematic studies to explain the mechanism of interaction of FLU with dsDNA, Poly[A], and Poly[G] were carried out, with the multilayer modified electrodes or in incubated solutions, using the GCE and DP voltammetry. DP voltammetry, due of its high sensitivity, enabled the detection of minor changes on the DNA double helical structure and DNA oxidative damage.

3.1. Electro-Oxidation of Fludarabine

3.1.1. Cyclic Voltammetry. The CV of $100 \mu\text{M}$ FLU at a GCE, in pH 6.1 0.1 M phosphate buffer, showed one anodic peak 1_a , at $E_{pa}^1 = +1.36 \text{ V}$, Figure 1. Reversing the potential no reduction peak was observed, indicating that the oxidation process was irreversible, and peak 1_a current decreased with increasing number of scans due to FLU and/or its oxidation product adsorption on the GCE surface.

The effect of pH on the electrochemical oxidation behaviour of FLU was investigated in aqueous buffered solutions in the range $2 < \text{pH} < 12$. CVs showed that in strong acidic buffer solutions, $\text{pH} \leq 2$, no FLU oxidation peak was observed. For $\text{pH} > 2$, the CVs showed irreversible peak 1_a . The oxidation process was pH-dependent, and the peak potentials of FLU shifted, with increasing pH.

The effect of the scan rate in a $100 \mu\text{M}$ FLU solution, in N_2 saturated pH 6.1 0.1 M phosphate buffer, between 5 and 500 mV s^{-1} was also investigated. Increasing the scan rate, the peak 1_a potential was slightly shifted to more positive potentials, and $|E_{pa} - E_{p/2a}| \sim 33 \text{ mV}$. Since for a diffusion-controlled irreversible system $|E_{pa} - E_{p/2a}| = 47.7/(\alpha_a n')$ where α_a is the charge transfer coefficient and n' the number of electrons in the rate-determining step [14], it was calculated the value of $\alpha_a n' = 1.8$.

Increasing the scan rate the peak 1_a current increased linearly with square root of ν , indicating a diffusion controlled behaviour of FLU. The peak current for a diffusion-controlled irreversible system is given by $I_{pa}(A) = -2.99 \times 10^5 n(\alpha_a n')^{1/2} A [O]_\infty D_O^{1/2} \nu^{1/2}$ where n is the number of the electrons transferred during the oxidation of FLU ($n = 1$ as shown Section 3.1.2), A is the electrode area in cm^2 , D_O is the diffusion coefficient in $\text{cm}^2 \text{ s}^{-1}$, $[O]_\infty$ is the concentration in mol cm^{-3} , and ν is in V s^{-1} [14]. The GCE electroactive area of $A = 0.00691 \text{ cm}^2$ was determined as described elsewhere [15]. By plotting I_{pc} versus $\nu^{1/2}$, the value of D_O was obtained from the slope $-3.04 \times 10^{-7} \text{ A} (\text{V s}^{-1})^{-1/2}$. The diffusion coefficient of FLU was calculated to be $D_{FLU} = 1.71 \times 10^{-6} \text{ cm}^2 \text{ s}^{-1}$.

3.1.2. Differential Pulse Voltammetry. DP voltammetry was used to investigate the effect of pH on the electrochemical oxidation of $100 \mu\text{M}$ FLU, and peak 1_a , in aqueous supporting electrolytes over a pH range from 2.0 to 12.0, Figure 2(a). As already found by CV, in strong acidic buffer solution, no FLU oxidation peak was observed.

The peak 1_a potential shifted linearly with pH towards more negative values and peak current increased up to pH 6.1 and afterwards decreased with increasing pH, Figure 2(b). The relationship was linear following the equation

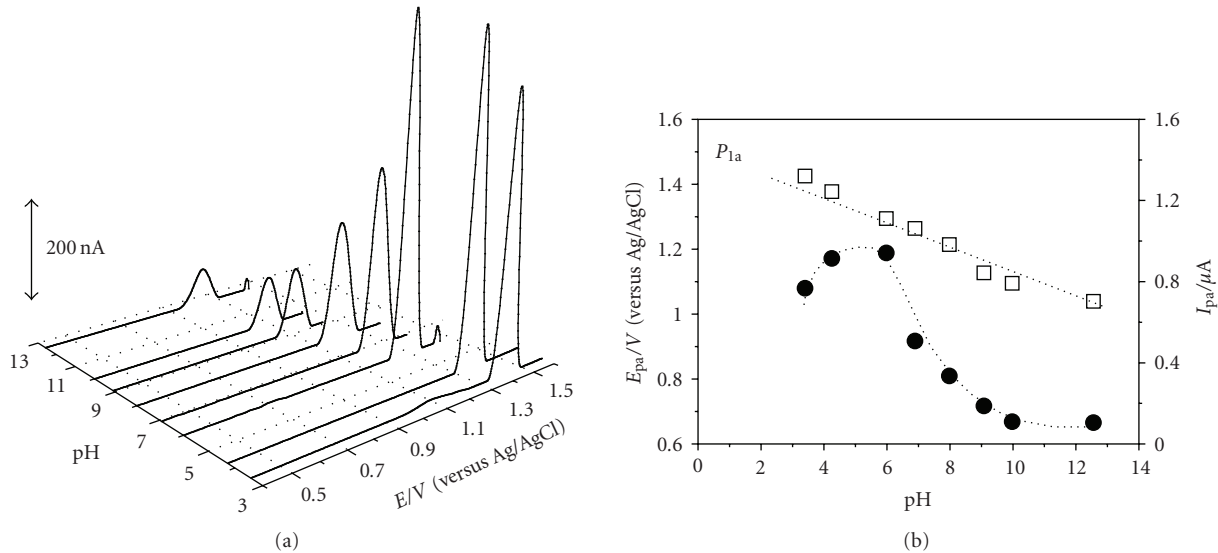


FIGURE 2: (a) 3D plots of baseline corrected DP voltammograms in $100 \mu\text{M}$ FLU (b) Plot of peak 1_a : (\square) E_{pa} and (\bullet) I_{pa} versus pH. Dotted line corresponds to 59 mV per pH unit.

E_{pa} (mV) = $1.48 - 0.06 \text{ pH}$, Figure 2(b). The slope of the line, -59 mV per pH unit, shows that the mechanism of oxidation involves the same number of electrons and protons. The number of electrons transferred, n , was determined by the peak width at half height, $W_{1/2} \sim 75 \text{ mV}$ and is close to the theoretical value of 90 mV , corresponding to an electrochemical reaction involving the transfer of one electron.

According to these results, the oxidation of FLU occurs with a transfer of one electron and one proton to produce a finally hydroxylated product. Since FLU is an adenine analogue, the irreversible oxidation mechanism is similar to adenine.

Successive scans in the same solution, without cleaning the electrode, showed the decrease of peak 1_a current and the occurrence of oxidation peak 2_a , at $E_p = +0.33 \text{ V}$, corresponding to the oxidation of FLU oxidation product.

The effect of pH on the electrochemical oxidation behaviour of peak 2_a showed that with increasing pH, peak 2_a shifted to less positive potentials, and a linear relationship, with the slope of the E_{pa} versus pH of -59 mV per pH unit, was found corresponding to the transfer of the same number of electron and proton in aqueous buffer solution.

3.1.3. Square Wave Voltammetry. The electrochemical behaviour of FLU was also investigated using SW voltammetry due to its advantages such as fast analysis time, lower blocking of electrode surface by the species, and less consumption of analyte. This method enables to detect during only one scan whether the electron transfer reaction is reversible or not. Due to the sampling of current values in both positive and negative going pulses, peaks belonging to the oxidation and reduction of the species at the electrode surface can be obtained simultaneously.

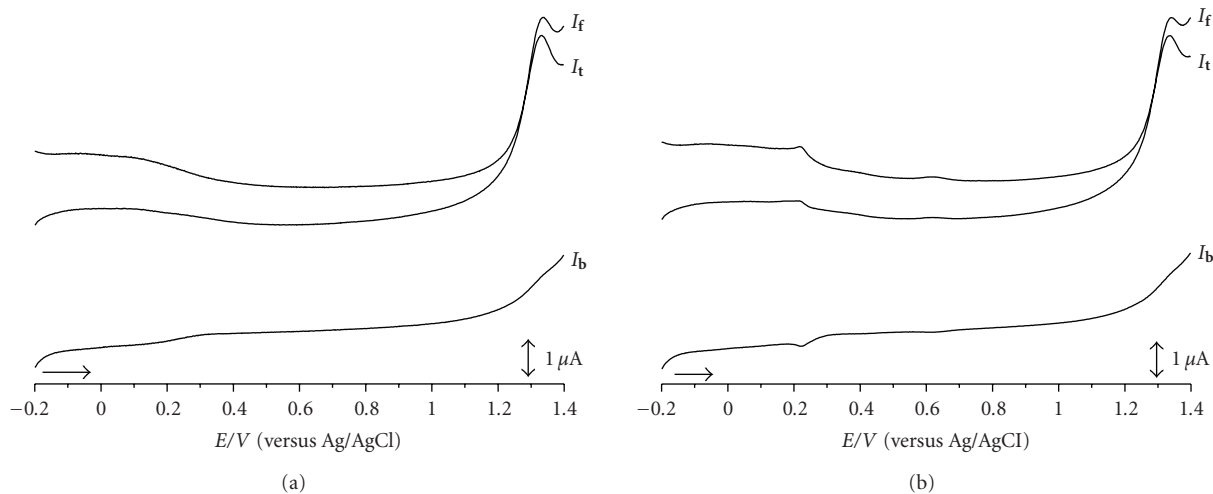
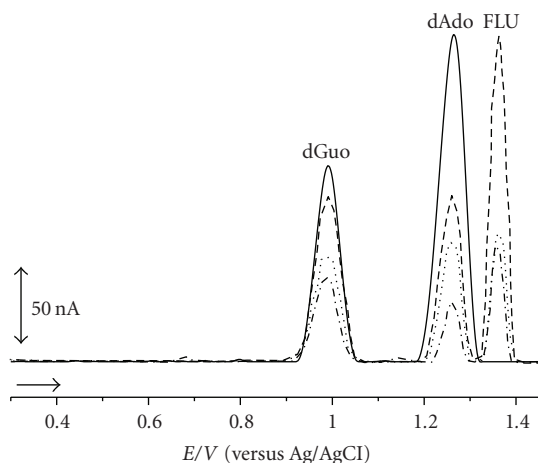
SW voltammetric experiments were carried out in the same pH range as CV and DP voltammetry. The oxidation peak 1_a was observed in all buffer solutions, and its irreversibility was confirmed by plotting the forward and backward components of the total current obtained in solutions of $100 \mu\text{M}$ FLU in pH 6.1 0.1 M phosphate buffer, Figure 3(a). The results obtained on the second and subsequent scans in the same solution without cleaning electrode showed the second oxidation peak 2_a , at $E_{\text{pa}} = +0.33 \text{ V}$, related to the oxidation of FLU oxidation product, Figure 3(b). Since reduction and oxidation currents were equal, the reversibility of the second peak was confirmed.

3.1.4. Analytical Determination of Fludarabine. DP voltammetry was used for the electroanalytical determination of FLU due to its advantages such as good discrimination, low detection limit, and short analysis time. According to Figure 2, the best pH was pH 6.1 0.1 M phosphate buffer and linearity range was achieved between 0.99 and $14.8 \mu\text{M}$ FLU, Table 2. Above this range, due to the adsorption of FLU or its oxidation product on the GCE surface, a loss of linearity was observed. In order to ensure a clean electrode surface and to avoid the adsorption of FLU and/or its oxidation product, the GCE surface was always cleaned between each measurement. The detection limit (LOD) and quantification limit (LOQ) were calculated according to the $3 s/m$ and $10 s/m$, [16, 17], where s is the standard deviation of the peak current, m is slope of calibration curve, and $\text{LOD} = 0.28 \mu\text{M}$ and $\text{LOQ} = 0.94 \mu\text{M}$ were found, Table 2.

3.2. DNA-Fludarabine Interaction. FLU was synthesized as an adenosine nucleoside analogue and used in the treatment of leukemia. After intravenous infusion, FLU is transported to cell by means of transporters, inhibits DNA synthesis,

TABLE 2: Regression and validation data of calibration line of fludarabine.

Potential	Linearity range (μM)	Slope	Intercept	Correlation coefficient	LOD (μM)	LOQ (μM)	Repeatability of peak current (RSD%)	Repeatability of peak potential (RSD%)
1.28	1.6–14.8	1.56×10^{-8}	1.29×10^{-8}	0.9993	0.28	0.94	1.55	0.09

FIGURE 3: SW voltammograms of $100 \mu\text{M}$ FLU in pH 6.1 0.1 M phosphate buffer: (a) first scan, (b) second scan, $f = 50 \text{ Hz}$, $\Delta E_s = 2 \text{ mV}$, $^1\text{pulse amplitude } 100 \text{ mV}$, I_t —total, I_f —forward and I_b —backward, and $v_{\text{effective}} = 100 \text{ mV s}^{-1}$.FIGURE 4: DP voltammograms baseline corrected in pH 4.5 0.1 M acetate buffer of: (solid line) $100 \mu\text{g mL}^{-1}$ dsDNA and incubated solutions during (dashed line) 0 h, (dotted line) 1 h, and (dash-dotted line) 3 h of $100 \mu\text{g mL}^{-1}$ DNA with $2 \mu\text{M}$ FLU. Pulse amplitude-50 mV, pulse width-70 ms, and $v = 5 \text{ mV s}^{-1}$.

and causes DNA disruption or breakages. Therefore, the investigation and clarification of the interaction mechanism between FLU and DNA is very important.

The mechanism of interaction of FLU with dsDNA, Poly[A] and Poly[G], in incubated solutions or with the multilayer GCE modified as described in the Experimental (Section 2.4), was investigated.

3.2.1. DNA-Fludarabine Interaction in Incubated Solutions. In order to investigate the interaction between FLU and dsDNA, Figure 4, presents the DP voltammograms obtained, in pH 4.5 0.1 M acetate buffer, for FLU, one oxidation peak 1_a , at $E_{\text{pa}} = +1.35 \text{ V}$, and for dsDNA, two well-defined and separated peaks corresponding to the oxidation of desoxyguanosine (dGuo), at $E_{\text{pa}} = +0.98 \text{ V}$, and desoxyadenosine (dAdo), at $E_{\text{pa}} = +1.25 \text{ V}$, Figure 4.

The interaction between FLU and dsDNA was studied in incubated solutions of $2 \mu\text{M}$ FLU and $100 \mu\text{g mL}^{-1}$ dsDNA, in pH 4.5 0.1 M acetate buffer, and DP voltammograms recorded for different incubation times. Control solutions of $2 \mu\text{M}$ FLU and $100 \mu\text{g mL}^{-1}$ dsDNA, in pH 4.5 0.1 M acetate buffer, were also prepared, and DP voltammograms recorded for the same incubation times. The GCE surface was cleaned between each measurement to avoid the blocking of the GCE surface by adsorption of the FLU and dsDNA.

The DP voltammograms obtained immediately after addition of FLU to dsDNA solution, showed three peaks corresponding to the oxidation of dsDNA purinic bases, dGuo, at $E_{\text{pa}} = +0.98 \text{ V}$, dAdo, at $E_{\text{pa}} = +1.25 \text{ V}$, and FLU, at $E_{\text{pa}} = +1.35 \text{ V}$, Figure 4. Increasing the incubation time, the peak current of dGuo and dAdo decreased, indicating that dsDNA structure was modified due to the interaction FLU-dsDNA by condensation and/or aggregation, which makes more difficult the access of the dsDNA bases to the electrode surface hindering their oxidation. However, no dsDNA oxidative damage caused by FLU occurred, as no peaks corresponding to the oxidation of 8-oxoGua or 2,8-oxoAde, the oxidation products of dsDNA purinic bases, were observed in the DP voltammograms, Figure 4.

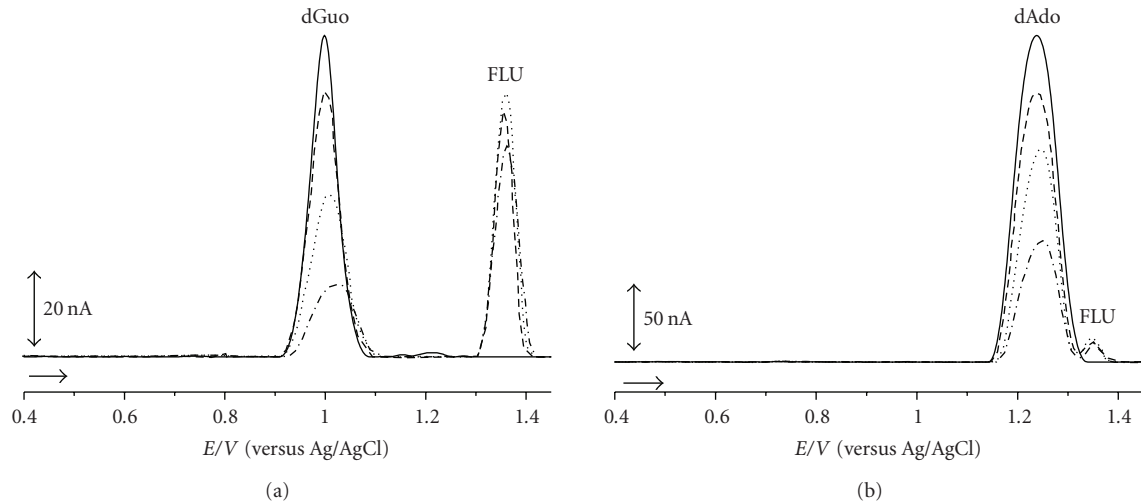


FIGURE 5: DP voltammograms baseline corrected in pH 4.5 0.1 M acetate buffer of $100 \mu\text{g mL}^{-1}$: (a) Poly[G] and (b) Poly[A] (solid line) before and after incubation with $5 \mu\text{M}$ FLU during (dashed line) 0 h, (dotted line) 1 h, and (dash-dotted line) 3 h. Pulse amplitude-50 mV, pulse width-70 ms, and $\nu = 5 \text{ mV s}^{-1}$.

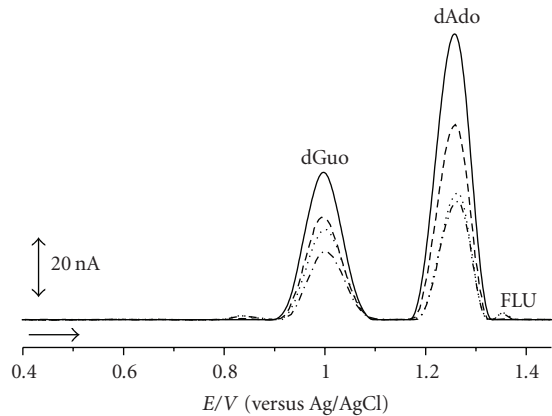


FIGURE 6: DP voltammograms baseline corrected in pH 4.5 0.1 M acetate buffer with dsDNA-electrochemical biosensors (solid line) before and after incubation during (dashed line) 5 min, (dotted line) 10 min, and (dash dotted line) 15 min in a solution of $50 \mu\text{M}$ FLU. Pulse amplitude-50 mV, pulse width-70 ms, and scan rate $\nu = 5 \text{ mV s}^{-1}$.

To clarify the interaction of FLU and dsDNA, experiments were also carried out in incubated solutions of $5 \mu\text{M}$ FLU and $100 \mu\text{g mL}^{-1}$ purinic base solutions, poly[G] or poly[A], in pH 4.5 0.1 M acetate buffer, Figure 5. DP voltammograms showed similar results as with dsDNA, confirming the decrease of the oxidation peaks of dGuo and dAdo and no oxidative damage, as no peaks corresponding to the oxidation products of guanine, 8-oxoGua, and adenine, 2,8-oxoAde, occurred.

3.2.2. *In Situ* DNA-Fludarabine Interaction. Multilayer dsDNA-, Poly[G]-, and Poly[A]-electrochemical biosensors

were prepared and used to investigate the *in situ* DNA-fludarabine interaction. The electrochemical biosensor surface was covered by a multilayer to make sure that the undesired adsorption of FLU on GCE could not occur. The dsDNA-, Poly[G]-, and Poly[A]-electrochemical biosensors enable the identification of the *in situ* interaction with time, besides the advantage of low cost, fast response time, simple design, and high detection limit.

The dsDNA-electrochemical biosensor was prepared, Section 2.4, incubated in $50 \mu\text{M}$ FLU solution for different times, 5, 10, and 15 min, and transferred to supporting electrolyte buffer solution. In order to remove unbounded FLU, the dsDNA-electrochemical biosensor was carefully washed with deionized water before being transferred to pH 4.5 0.1 M acetate buffer where the DP voltammograms were recorded, Figure 6. In this way, the observed peaks in the DP voltammograms can only be caused by the interaction between dsDNA and FLU. As expected, dGuo and dAdo, and a very small FLU oxidation peaks were also obtained, Figure 6. After each measurement, the dsDNA film was removed from the electrode surface and the experiments were always performed with a newly prepared biosensor. The results showed that dGuo and dAdo oxidation peaks decreased with increasing incubation time in the FLU solution. This is caused by modifications in the dsDNA morphological structure and strand breaks, due to the interaction with FLU. No oxidation peaks for 8-oxoGua and 2,8-oxoA, the dsDNA purinic bases oxidation products, were observed, so there was no DNA oxidative damage.

Polynucleotides biosensors, Poly[G]- and Poly[A]-electrochemical biosensors, were prepared, Section 2.4, and incubated in $50 \mu\text{M}$ FLU in pH 4.5 0.1 M acetate buffer for different times, in order to shine more information on the interaction between dsDNA and FLU, Figure 7.

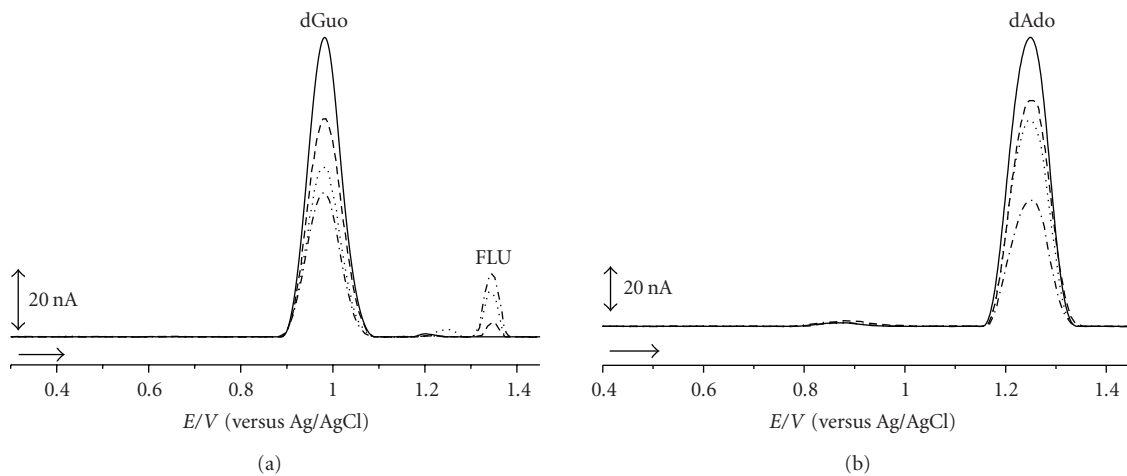


FIGURE 7: DP voltammograms baseline corrected in pH 4.5 0.1 M acetate buffer with (a) Poly[G]- and (b) Poly[A]-electrochemical biosensors (solid line) before and incubation during (dashed line) 5 min, (dotted line) 10 min, and (dash-dotted line) 15 min in a solution of $50 \mu\text{M}$ FLU. Pulse amplitude-50 mV, pulse width-70 ms and scan rate $\nu = 5 \text{ mV s}^{-1}$.

Poly[G]-electrochemical biosensor, after being transferred to pH 4.5 0.1 M acetate buffer, showed two peaks one for FLU and the other for poly[G], corresponding the oxidation of dGuo, at $E_{pa} = +0.98 \text{ V}$, which decreased with increasing incubation time, and no oxidation peak for 8-oxoGua was observed, Figure 7(a).

Poly[A]-electrochemical biosensor, after being transferred to pH 4.5 0.1 M acetate buffer, showed two peaks one for FLU and the other for poly[A], corresponding the oxidation of dAdo, at $E_{pa} = +1.25 \text{ V}$, which decreased with increasing incubation time, and no oxidation peak for 2,8-oxoA was observed, Figure 7(b).

These experiments using polyhomopurinenucleotide single-stranded sequences, poly[G]- and poly[A]-electrochemical biosensors, confirm the results obtained using the dsDNA-electrochemical biosensor.

4. Conclusion

The electrochemical behaviour of fludarabine was investigated on the GCE in different aqueous buffer solutions using CV, DP, and SW voltammetry. The oxidation mechanism of fludarabine is irreversible, pH dependent and occurs with one electrode and one proton transfer. The diffusion coefficient $D_{FLU} = 1.71 \times 10^{-6} \text{ cm}^2 \text{ s}^{-1} \cdot 10^{-6} \text{ cm}^2 \text{ s}^{-1}$ was determined. In the electroanalytical determination of FLU, the values of LOD = $0.28 \mu\text{M}$ and LOQ = $0.94 \mu\text{M}$ were found.

The mechanism of interaction of FLU with dsDNA, poly[A] and poly[G], in incubated solutions or with multilayer GC modified electrodes, clearly showed, using the concentrations chosen, that fludarabine-DNA interaction caused morphological changes and strand breaks in the dsDNA structure in a time-dependent manner, but no DNA oxidative damage.

Acknowledgments

Financial support from Fundação para a Ciência e Tecnologia (FCT), Projects PTDC/QUI/65732/2006 and PTDC/QUI/098562/2008, POCI (cofinanced by the European Community Fund FEDER), CEMUC-R (Research Unit 285), and The Scientific and Technological Research Council of Turkey (TUBITAK)—International Postdoctoral Research Fellowship Programme (BIDEB) (H.E.S.) are gratefully acknowledged.

References

- [1] C. Tondini, M. Balzarotti, I. Raminelli et al., "Fludarabine and cladribine in relapsed/refractory low-grade non-Hodgkin's lymphoma: a phase II randomized study," *Annals of Oncology*, vol. 11, no. 2, pp. 231–233, 2000.
- [2] S. J. Wright, L. E. Robertson, S. O'Brien, W. Plunkett, and M. J. Keating, "The role of fludarabine in hematological malignancies," *Blood Reviews*, vol. 8, no. 3, pp. 125–134, 1994.
- [3] C. O. Rodriguez Jr., W. Plunkett, M. T. Paff et al., "High-performance liquid chromatography method for the determination and quantitation of arabinosylguanine triphosphate and fludarabine triphosphate in human cells," *Journal of Chromatography B*, vol. 745, no. 2, pp. 421–430, 2000.
- [4] T. Yamauchi and T. Ueda, "Simple and sensitive method for quantification of fludarabine triphosphate intracellular concentration in leukemic cells using isocratic liquid chromatography," *Journal of Chromatography B*, vol. 799, no. 1, pp. 81–86, 2004.
- [5] A. Kemeny, M. Fernandez, J. Bauman, M. Keating, and W. Plunkett, "A sensitive fluorescence assay for quantitation of fludarabine and metabolites in biological fluids," *Clinica Chimica Acta*, vol. 200, no. 2-3, pp. 95–106, 1991.
- [6] G. Misztal and B. Paw, "Determination of fludarabine phosphate in human plasma using reversed phase high-performance liquid chromatography," *Pharmazie*, vol. 51, no. 10, pp. 733–734, 1996.

- [7] R. Ficarra, M. L. Calabrò, S. Tommasini et al., "Determination of fludarabine in a pharmaceutical formulation by LC," *Journal of Pharmaceutical and Biomedical Analysis*, vol. 21, no. 5, pp. 1077–1081, 1999.
- [8] L. D. Vainchtein, H. Rosing, J. H. M. Schellens, and J. H. Beijnen, "A new, validated HPLC-MS/MS method for the simultaneous determination of the anti-cancer agent capecitabine and its metabolites: 5'-deoxy-5-fluorocytidine, 5'-deoxy-5-fluorouridine, 5-fluorouracil and 5-fluorodihydrouracil, in human plasma," *Biomedical Chromatography*, vol. 24, no. 4, pp. 374–386, 2010.
- [9] N. De-Los-Santos-Álvarez, M. J. Lobo-Castañón, A. J. Miranda-Ordieres, and P. Tuñón-Blanco, "Electrocatalytic adsorptive voltammetry for fludarabine determination in urine," *Analytica Chimica Acta*, vol. 504, no. 2, pp. 271–277, 2004.
- [10] F. Jelen, M. Fojta, and E. Paleček, "Voltammetry of native double-stranded, denatured and degraded DNAs," *Journal of Electroanalytical Chemistry*, vol. 427, no. 1-2, pp. 49–56, 1997.
- [11] A. M. Oliveira-Brett, J. A. P. Piedade, L. A. Silva, and V. C. Diculescu, "Voltammetric determination of all DNA nucleotides," *Analytical Biochemistry*, vol. 332, no. 2, pp. 321–329, 2004.
- [12] X. Cai, G. Rivas, H. Shirashi et al., "Electrochemical analysis of formation of polynucleotide complexes in solution and at electrode surfaces," *Analytica Chimica Acta*, vol. 344, no. 1-2, pp. 65–76, 1997.
- [13] A. M. Chiorcea-Paquim, O. Corduneanu, S. C. B. Oliveira, V. C. Diculescu, and A. M. Oliveira-Brett, "Electrochemical and AFM evaluation of hazard compounds-DNA interaction," *Electrochimica Acta*, vol. 54, no. 7, pp. 1978–1985, 2009.
- [14] C. M. A. Brett and A. M. Oliveira-Brett, *Electrochemistry, Principles, Methods and Applications*, Oxford University Press, Oxford, UK, 1993.
- [15] 2010, <http://www.hbcpnetbase.com/HandbookofChemistry-andPhysics>.
- [16] C. M. Riley and T. W. Rosanske, *Development and Validation of Analytical Methods*, Elsevier Science, New York, NY, USA, 1996.
- [17] M. E. Swartz and I. S. Krull, *Analytical Method Development and Validation*, Marcel Dekker, New York, NY, USA, 1997.

Research Article

A Biocompatible Nanocomposite for Glucose Sensing

Parvaneh Rahimi,^{1,2} Hedayatollah Ghourchian,¹ Hossain-Ali Rafiee-Pour,¹ Parviz Norouzi,² and Mohammad Reza Ganjali²

¹ Laboratory of Microanalysis, Institute of Biochemistry and Biophysics, University of Tehran, Tehran 1417614411, Iran

² Center of Excellence in Electrochemistry, Faculty of Chemistry, University of Tehran, Tehran 1417614411, Iran

Correspondence should be addressed to Hedayatollah Ghourchian, hadi@ibb.ut.ac.ir

Received 7 February 2011; Accepted 28 February 2011

Academic Editor: Sibel A. Ozkan

Copyright © 2011 Parvaneh Rahimi et al. This is an open access article distributed under the Creative Commons Attribution License, which permits unrestricted use, distribution, and reproduction in any medium, provided the original work is properly cited.

A nanocomposite containing amine functionalized multiwalled carbon nanotubes and a room temperature ionic liquid (1-butyl-3-methylimidazolium tetrafluoroborate) was prepared and applied for glucose oxidase (GOx) immobilization on glassy carbon electrode. The proposed nanocomposite provided a favorable microenvironment to preserve the bioactivity of GOx. It could also effectively facilitate the enzyme direct electron transfer to the electrode. This brought about a remarkable improvement in the sensitivity of the glucose biosensor. Under the optimum experimental conditions, the formal potential of GOx was about -467.5 mV . Moreover, the sensitivity and response time of the biosensor toward glucose were $1277\text{ }\mu\text{A mM}^{-1}\text{ cm}^{-2}$ and 6 s, respectively. The biosensor provided a linear dynamic response between 0.1 and $43\text{ }\mu\text{M}$ with a very low detection limit of 63 nM . Also, the values for apparent Michaelis-Menten constant and maximum current were obtained as $18\text{ }\mu\text{M}$ and $2.7\text{ }\mu\text{A}$, respectively.

1. Introduction

Nanoscale materials have been considerably contributing to biosensor design in recent years. Carbon nanotubes (CNTs) as an example of nanoscale material are broadly used for the fabrication of electrochemical biosensor owing to their outstanding properties [1]. Wang and Musameh [2] reported the first CNTs/enzyme electrodes for glucose and ethanol by incorporating glucose oxidase (GOx) and alcohol dehydrogenase within a three-dimensional CNTs/Teflon matrix. The electrocatalytic properties of CNTs and their ability to promote direct electron transfer between redox proteins and electrode surface were explained by Compton's group [3].

Room temperature ionic liquids (RTILs) are a new class of nonaqueous solvent that consist of an organic cation and either an organic or an inorganic anion. They have unique characteristics such as high conductivity, nonvolatile nature, low toxicity, large electrochemical window, strong electrostatic field, and good electrochemical stability [4]. Because of special properties of RTILs, their applications are

increasing in different fields [5] especially for improvement in enzyme electron transfer rate and stability [4, 6, 7].

By combination of CNTs and RTILs, attractive nanocomposites could be obtained which are useful for the study of protein direct electrochemistry [8–10]. These nanocomposites show high sensitivity and good biocompatibility. Different methods have been developed for fabricating CNTs/RTILs nanocomposite-based biosensors including electrode modification by RTIL/CNTs/polymer, layer-by-layer self-assembly, CNTs/RTIL pastes, or dispersion of RTIL/CNTs [8].

So far, different types of CNTs/RTIL/GOx nanocomposites have been used for the development of glucose biosensors [11–13]; nevertheless, in the present study we designed a new nanocomposite based on the amine functionalized MWCNTs ($\text{NH}_2\text{-MWCNTs}$). This nanocomposite consists of a typical RTIL, $\text{NH}_2\text{-MWCNTs}$, and GOx. The proposed nanocomposite not only provided a favorable microenvironment to preserve the bioactivity of GOx but also could effectively facilitate the enzyme direct electron transfer to the

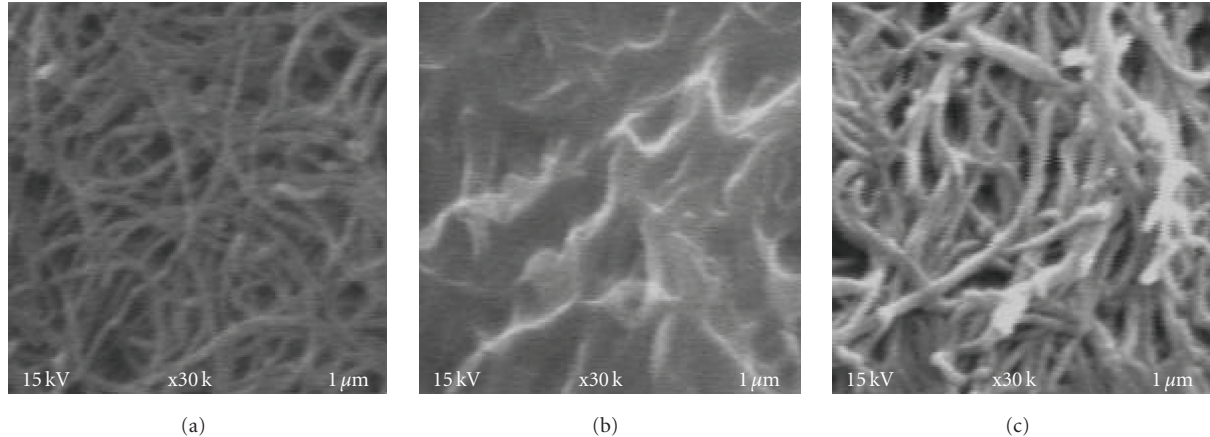


FIGURE 1: FESEM images of $\text{NH}_2\text{-MWCNTs}/\text{GC}$ (a), $\text{RTIL}/\text{NH}_2\text{-MWCNTs}/\text{GC}$ (b) and $\text{GOx}/\text{RTIL}/\text{NH}_2\text{-MWCNTs}/\text{GC}$ (c) electrodes.

electrode. The fast and easy electron transfer brought about a remarkable improvement in sensitivity of the biosensor toward glucose.

2. Experimental

2.1. Materials and Methods. GOx type X-S from *Aspergillus niger* (EC 1.1.3.4.), $\beta\text{-D}(+)\text{glucose}$, and 1-butyl-3-methylimidazolium tetrafluoroborate ($[\text{BMIM}] \text{BF}_4^-$) as a typical RTIL were purchased from Sigma (U.S.A) and used without further purification. Multiwall carbon nanotubes (MWCNTs), prepared by chemical vapor deposition, were supplied by Timesnano. Co. (China). $\text{K}_4[\text{Fe}(\text{CN})_6]$, $\text{K}_3[\text{Fe}(\text{CN})_6]$, KCl , KH_2PO_4 , K_2HPO_4 , and $\text{C}_2\text{H}_4[\text{NH}_2]_2$ were purchased from Merck. Thionyl chloride (SOCl_2) was supplied by Acros Organics (Belgium). $\beta\text{-D}-\text{glucose}$ solutions were stand overnight to allow equilibration of the monomers. All solutions were prepared in double-distilled deionized water.

Electrochemical studies were carried out using an electrochemical system (EG&G model 263A potentiostat/galvanostat) controlled by a PowerSuite software package and a GPIB interface. All electrochemical studies were carried out using a conventional three-electrode cell. It was equipped with a modified glassy carbon (GC) electrode (bare or modified with nanocomposites film, from Azar Electrode, Uromia, Iran), a saturated Ag/AgCl (3 M KCl solution) reference electrode (from Metrohm), and a platinum wire counter electrode. Field emission scanning electron microscopic (FESEM) images were obtained using an FESEM model S4160, Hitachi, Japan. Electrochemical impedance measurements were carried out on a PGSTAT30/FRA2 system (Autolab, Netherlands) in 2 mM $\text{K}_3[\text{Fe}(\text{CN})_6]/\text{K}_4[\text{Fe}(\text{CN})_6]$ and the frequency range from 10^{-2} to 10^5 Hz.

2.2. Immobilization of Enzyme. The GC electrode (2 mm in diameter) was first polished mechanically with 0.3 and $0.05\ \mu\text{m}$ alumina slurry, respectively, and sonicated in water and ethanol, successively.

MWCNTs were amine functionalized based on the method described in our previous work [14]. For GOx

immobilization, first 1 mg of $\text{NH}_2\text{-MWCNTs}$ was dispersed in 1 mL of dimethylformamide using an ultrasonic bath to give a black suspension. Then, $2.5\ \mu\text{L}$ of the suspension was transferred onto the cleaned GC electrode and dried in air. The $\text{NH}_2\text{-MWCNT/GC}$ electrode was immersed in pure $[\text{BMIM}] \text{BF}_4^-$ solution for 10 hrs at 4°C to adsorb a layer of RTIL. At this time, a 6 mg/mL solution of GOx was prepared in phosphate buffer solution (PBS), 0.1 M, pH 7.0. Finally, the modified electrode was immersed in GOx solution for 10 hrs at 4°C . Thereafter, the modified electrode (denoted as $\text{GOx}/\text{RTIL}/\text{NH}_2\text{-MWCNT/GC}$) was rinsed with PBS and stored at 4°C when not in use.

3. Results and Discussion

3.1. Characterization of Immobilized Enzyme on Modified Electrode. Figure 1 shows the FESEM images of (a) $\text{NH}_2\text{-MWCNTs}/\text{GC}$, (b) $\text{RTIL}/\text{NH}_2\text{-MWCNTs}/\text{GC}$, and (c) $\text{GOx}/\text{RTIL}/\text{NH}_2\text{-MWCNTs}/\text{GC}$ modified electrodes. Figure 1(a) represents the image of $\text{NH}_2\text{-MWCNTs}$ as bundles, which are entangled with one another. A mass of RTIL are embedded into the gaps of the formed $\text{NH}_2\text{-MWCNTs}$ network structure (Figure 1(b)). These FESEM images are similar to those obtained by previous workers for MWCNTs/GC and RTIL/MWCNTs/GC electrodes [9]. Figure 1(c) shows the image of the $\text{RTIL}/\text{NH}_2\text{-MWCNT}/\text{GC}$ electrode after addition of GOx solution and rinsing the uninteracted materials. Therefore, as shown, the bundles were untangled and uniformly covered the surface of GC electrode. This could be an evidence for successful enzyme immobilization.

The electrochemical impedance spectroscopy can provide useful information on the interfacial changes at the electrode surfaces during the fabrication process. In order to illustrate the role of $\text{RTIL}/\text{NH}_2\text{-MWCNTs}$ nanocomposite in electron transferring of GOx , the Nyquist plots for different modified electrodes were recorded (Figure 2). Before GOx immobilization, the bare GC (curve a), $\text{NH}_2\text{-MWCNTs}/\text{GC}$ (curve b), and $\text{RTIL}/\text{NH}_2\text{-MWCNTs}/\text{GC}$ (curve c) electrodes showed no resistance. But, in the presence of GOx , due to hindered pathway of electron transfer, the

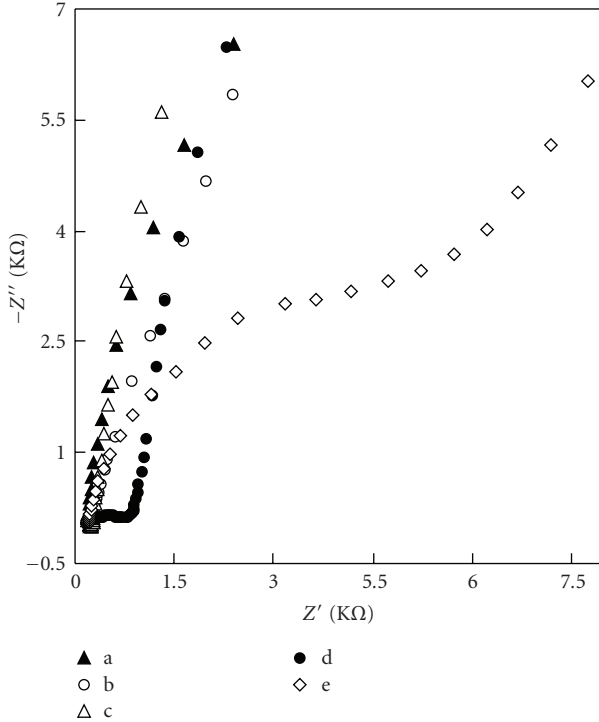


FIGURE 2: Electrochemical impedance spectra of (a) bare GC, (b) $\text{NH}_2\text{-MWCNTs}/\text{GC}$, (c) $\text{RTIL}/\text{NH}_2\text{-MWCNTs}/\text{GC}$, (d) $\text{GOx}/\text{RTIL}/\text{NH}_2\text{-MWCNTs}/\text{GC}$, and (e) GOx/GC electrodes in 0.1 M KCl solution containing 2 mM $\text{K}_3[\text{Fe}(\text{CN})_6]/\text{K}_4[\text{Fe}(\text{CN})_6]$.

resistance increased as expected for protein immobilized layer. As shown in Figure 2, the interfacial resistance of the $\text{GOx}/\text{RTIL}/\text{NH}_2\text{-MWCNTs}/\text{GC}$ electrode was $\sim 1000 \Omega$ (curve d), while the resistance value of GOx/GC electrode increased to $\sim 5000 \Omega$ (curve e). This result indicates that the RTIL/ $\text{NH}_2\text{-MWCNTs}$ nanocomposite accelerates the electron transfer between GOx active site and the GC electrode surface.

3.2. Electrochemical Behavior of GOx on $\text{RTIL}/\text{NH}_2\text{-MWCNT}/\text{GC}$. To consider the electrochemical behavior of GOx immobilized on $\text{RTIL}/\text{NH}_2\text{-MWCNTs}$ nanocomposite, cyclic voltammetry was used. Figure 3 shows the cyclic voltammograms (CVs) of different electrodes in 0.1 M N_2 -saturated PBS, pH 7.0 at the scan rate of 0.1 V/s. As seen at the GOx/GC electrode (curve a), no obvious electrochemical redox peak is observed. It is well known that flavin adenine dinucleotide (FAD) is deeply embedded in a protective protein shell, which makes the direct electron communication with electrodes extremely difficult. Also, the $\text{NH}_2\text{-MWCNT}/\text{GC}$ electrode (curve b) and $\text{RTIL}/\text{NH}_2\text{-MWCNT}/\text{GC}$ electrode (curve c) did not show any response because they contain no electroactive species. But when GOx was immobilized on the $\text{NH}_2\text{-MWCNT}/\text{GC}$ electrode regarding the role of CNTs in facilitating the electron transfer process between the enzyme and electrode surface, a couple of broad redox peaks emerged (curve d). The peaks could be attributed to the FAD/FADH₂ redox couple located in

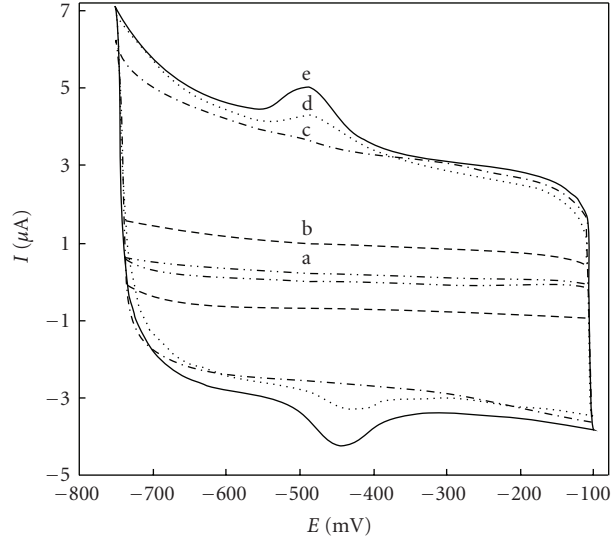


FIGURE 3: CVs of different modified electrodes: (a) GOx/GC , (b) $\text{NH}_2\text{-MWCNTs}/\text{GC}$, (c) $\text{RTIL}/\text{NH}_2\text{-MWCNTs}/\text{GC}$, (d) $\text{GOx}/\text{NH}_2\text{-MWCNTs}/\text{GC}$, and (e) $\text{GOx}/\text{RTIL}/\text{NH}_2\text{-MWCNTs}/\text{GC}$. The results were obtained in 0.1 M N_2 -saturated PBS, pH 7.0, at the scan rate of 0.1 V/s.

the protein shell. The observed redox response coincided with previously reported CVs for GOx immobilized on CNTs [15, 16]. However, the $\text{GOx}/\text{RTIL}/\text{NH}_2\text{-MWCNT}/\text{GC}$ electrode exhibited a well-defined couple of anodic peaks at -440 and cathodic peak at -495 mV (versus Ag/AgCl). The formal potential (E°) for GOx modified electrode as a mean value of anodic (E_{pa}) and cathodic (E_{pc}) peak potentials was calculated to be -467.5 mV (versus Ag/AgCl). The peak-to-peak separation, ΔE_p , was measured to be 60 mV, indicating a fast electron transfer reaction. This is the sign that the RTIL/ $\text{NH}_2\text{-MWCNT}$ nanocomposite is able to provide a microenvironment and also to establish an excellent electronic communication between GOx and GC electrode (curve e). Wu et al. [17] have investigated the effect of RTILs as electrolyte on the conformation and electrocatalytic activity of GOx . Their experimental results indicated that $[\text{BMIM}] \text{BF}_4^-$ did not affect on GOx conformation, but the enzyme electrocatalytic current decreased in the presence of RTIL. In the present work, combination of the RTIL and $\text{NH}_2\text{-MWCNT}$ produced a biocompatible nanocomposite by which not only the electrocatalytic activity of GOx did not reduce but also it showed a nearly symmetric redox peak (curve e). As reported previously [9, 10], MWCNTs interact with RTILs through $\pi\text{-}\pi$, $\pi\text{-cationic}$ (the positively charged imidazolium ions) and/or hydrophobic-hydrophobic interactions. In addition, according to Wei et al. [9], RTIL can bind to protein through ionic interaction. As known, at pH 7.0 the net charge of GOx is negative, and therefore, the anionic functional groups of GOx may show affinity to both the NH_2 groups of MWCNTs and the positively charged imidazolium ions of RTIL. Consequently, it seems that these ionic interactions are helpful for adsorption of GOx on the $\text{RTIL}/\text{NH}_2\text{-MWCNTs}$ nanocomposite. Moreover, the nanocomposite

led to a relatively fast electronic communication between the enzyme and the modified electrode as shown by curve e.

Figure 4 represents the CVs of GOx/RTIL/NH₂-MWCNTs/GC electrode in N₂-saturated PBS at different scan rates. Both the anodic and cathodic peak currents of GOx are linearly proportional to the scan rate (Figure 4(a)). This suggests that the electrode reaction corresponds to a typical surface-controlled electrochemical process as expected for immobilized systems. The linear regression equation for cathodic (I_{pc}) and anodic (I_{pa}) peak currents are $I_{pc} = 0.036 \log \nu + 0.3834$ (mV s⁻¹, $r^2 = 0.9998$) and $I_{pa} = -0.0327 \log \nu - 0.0908$ (mV s⁻¹, $r^2 = 0.9991$), respectively. The ratio of I_{pc}/I_{pa} was found to be close to the theoretical value of one, as expected for thin-layer electrochemical behavior [18].

As specified by the plot of $E_p = f(\log \nu)$ (Figure 4(b)) at scan rates below 500 mV s⁻¹, the peak separations are almost independent of the potential scan rate indicating a facile charge transfer kinetic over the range of applied sweep rate. But at scan rates above 750 mV s⁻¹, the peak separations begin to increase, indicating the limitation arising from charge transfer kinetics. The kinetic parameters of charge transfer coefficient (α) and apparent charge transfer rate constant (k_s) were calculated using Laviron's equation [19]

$$\log k_s = \alpha \log(1 - \alpha) + (1 - \alpha) \log \alpha - \log \left(\frac{RT}{nF\nu} \right) - \frac{\alpha(1 - \alpha)nF\Delta E_p}{2.3RT}, \quad (1)$$

α can be calculated using the plot of peak potentials (E_p) versus logarithm of scan rate ($\log \nu$). At scan rates above 750 mV s⁻¹, both E_{pc} and E_{pa} depend linearly on $\log \nu$. The graph of $E_p = f(\log \nu)$ yields two straight lines with slopes of $-2.3RT/\alpha nF$ and $2.3RT/(1 - \alpha)nF$ for the cathodic and anodic peaks, respectively, where n is the number of electron and R , T , and F have their usual meanings ($R = 8.314 \text{ J mol}^{-1} \text{ K}^{-1}$, $T = 298^\circ \text{K}$, $F = 96483 \text{ C mol}^{-1}$). Following these equations, the charge transfer coefficient (α) and the apparent charge transfer rate constant (k_s) for GOx on nanocomposite layer can be calculated to be 0.49 and 2.35 s^{-1} , respectively.

Based on the slope of peak current versus scan rate (Figure 4(a)) and (2), the surface concentration of electroactive proteins on nanocomposite layer (Γ_c) was estimated as $2.7 \times 10^{-10} \text{ mol cm}^{-2}$. These values are comparable to those reported in the literature [11]

$$I_p = \frac{n^2 F^2 \nu A \Gamma_c}{4RT}, \quad (2)$$

where n , F , and A represent the electron transfer number, the Faraday's constant, and the electrode area, respectively [20].

The operational stability of immobilized GOx on RTIL/NH₂-MWCNTs/GC electrode was evaluated by cyclic voltammetry. The current of redox peak decreased 10% after 90 cycles at the scan rate of 0.1 V/s. The biocompatibility of RTIL/NH₂-MWCNTs also was considered as the ability of nanocomposite to preserve the GOx storage stability. By

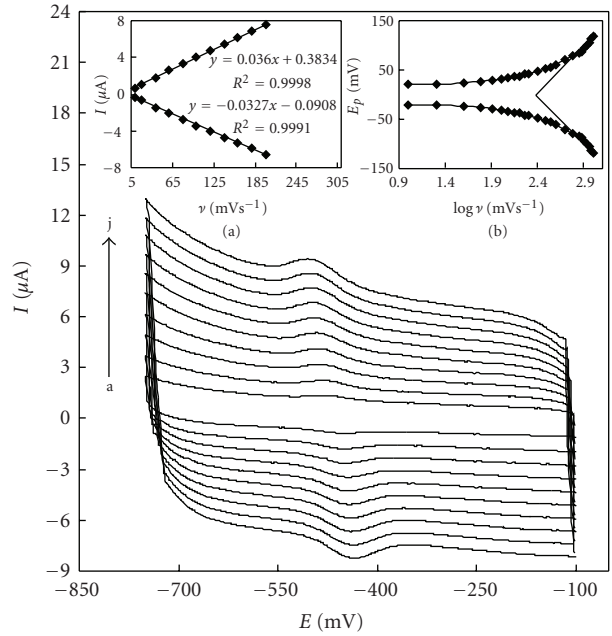


FIGURE 4: CVs of GOx/RTIL/NH₂-MWCNTs/GCE in 0.1 M N₂-saturated PBS, pH 7.0 at various scan rates of 20, 40, 60, 80, 100, 120, 140, 160, 180, and 200 mVs⁻¹ from a to j, respectively. Insets represent the plots of I_p versus ν (a) and E_p versus $\log \nu$ (b).

storing the prepared enzyme electrode in PBS at 4°C for a period of 10 days, 7% of the current response was lost.

3.3. pH Effect. To control the effect of pH on the electrochemical behavior of immobilized GOx, a series of experiments were carried out. Figure 5 shows peak currents of the electrode in N₂-saturated PBS at various pH ranging from 6.2 to 8.2. By increasing the pH, a negative shift was observed in both the reduction and oxidation peak potentials. As illustrated in Figure 5(a), the cathodic peak current increased with the pH change from 6.2 to 7.0, then it decreased up to pH 8.2. According to this plot, pH 7.0 was chosen as the optimal pH for next experiments. As seen in Figure 5(b), within the pH range from 6.2 to 8.2, the slope of E^o versus pH is 61.7 mV/pH with the regression equation of $y = -0.061 \text{ pH} - 0.038$. This slope is close to the theoretical value of 0.059 V/pH, as expected for a reversible 2-proton and 2-electron transfer process at 25°C.

3.4. Catalytic Activity of Immobilized GOx. The electrocatalytic activity of GOx on RTIL/NH₂-MWCNTs/GC electrode toward glucose was also studied. Figure 6 shows the CVs of the electrode in O₂-saturated PBS containing various concentration of glucose. As known, the electrochemical characteristics of GOx modified electrodes are influenced by oxygen [21]. In oxygenated PBS and in the absence of glucose, the enzyme prosthetic group (FAD) is in oxidized form [21, 22]. Therefore, comparing with Figure 3(e), the oxidation peak height is decreased, while the cathodic peak height is increased. Oxygen molecules can also be reduced at RTIL/NH₂-MWCNTs/GC electrode in the same potential

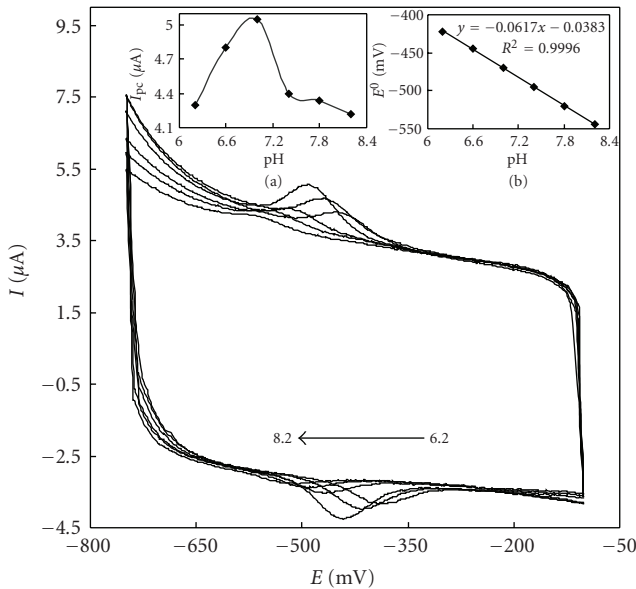


FIGURE 5: CVs of GOx/RTIL/NH₂-MWCNTs/GCE in 0.1 M N₂-saturated PBS at pH 6.2, 6.6, 7.0, 7.4, 7.8, and 8.2 from right to left, respectively. Insets show the plot of I_{pc} versus pH (a) and E° versus pH (b).

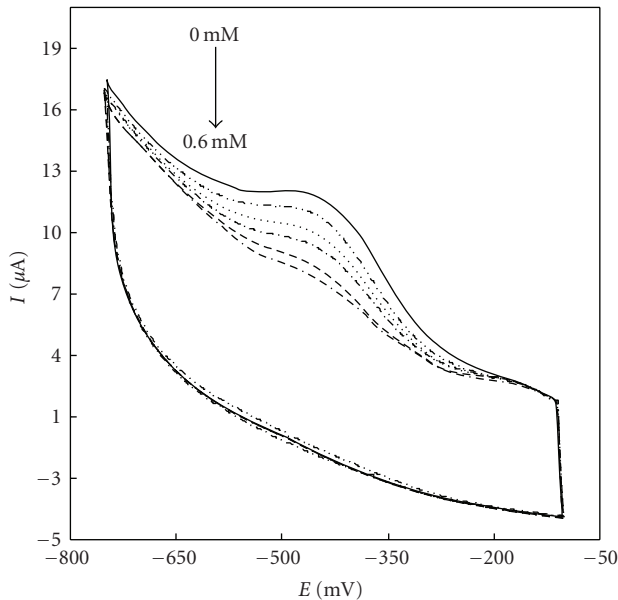
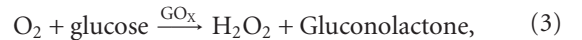


FIGURE 6: CVs of GOx/RTIL/NH₂-MWCNTs/GC electrode in 0.1 M O₂-saturated PBS, pH 7.0, containing (from outer to inner) 0, 0.042, 0.13, 0.22, 0.33, and 0.6 mM glucose at a scan rate of 0.1 V/s.

window as FAD. Therefore, it seems that both reduction processes of FAD prosthetic group and molecular oxygen contribute to the cathodic peak of Figure 6 (solid curve). By addition of glucose to the PBS, the cathodic peak current height is decreased. As shown in reactions 1 and 2, glucose as the substrate of GOx plays a bifunctional role in decreasing the cathodic peak. By changing the FAD into FADH₂, the

FAD (oxidized form) concentration is lessened, and the dissolved oxygen at the electrode surface is also consumed



According to these results, it is obvious that the RTIL/NH₂-MWCNTs nanocomposite film not only makes an intimate electronic relationship between enzyme and electrode but also could preserve the electrocatalytic activity of GOx towards glucose oxidation.

3.5. Amperometric Detection of Glucose. To consider the role of ionic liquid in the biosensor efficiency, two modified enzyme electrodes (A and B) were developed, and their analytical parameters were compared. The composition of electrode A was GOx/RTIL/NH₂-MWCNTs/GC and that of B was GOx/NH₂-MWCNTs/GC. Figure 7 illustrates the current time plots of the electrodes at a detection potential of -510 mV (versus Ag/AgCl) on successive addition of glucose concentrations. The response time (the time during which the electrode current response reaches to a steady state) for the electrodes A and B were 6 and 10 s, respectively. Comparison of these values obviously reveals the role of RTIL in electrode response time enhancement. Interestingly, the amperometric response at each glucose addition step for electrode A is higher than that for the electrode B. Also, the calibration curves of both electrodes are shown in the insets of Figure 7. The analytical parameters extracted from the calibration curves were listed in last two rows of Table 1. The current sensitivity was $40.1 \mu\text{A mM}^{-1}$ ($1277 \mu\text{A mM}^{-1} \text{cm}^{-2}$) for electrode A and $13 \mu\text{A mM}^{-1}$ ($414 \mu\text{A mM}^{-1} \text{cm}^{-2}$) for electrode B. These values are much higher than those reported in the literature (Table 1). At a signal-to-noise ratio of 3 ($S/N = 3$), the detection limits were estimated to be 63 and 393 nM for electrodes A and B, respectively. These values were lower than the values obtained with the GOx/CHIT/IL/GNPs ($1.5 \mu\text{M}$) [23], the GOx/IL/GNP/IL/SWNTs ($0.8 \mu\text{M}$) [11], and the GOx/MWCNTs/PSS/Au-IL ($25 \mu\text{M}$) [12] (The abbreviations used here are as follows: CHIT: chitosan, GNPs: gold nano particles, SWNTs: single-walled carbon nanotubes, and PSS: poly[sodium 4-styrene-sulfonate]). The results depicted in Table 1 showed that the analytical parameters such as detection limit, sensitivity, and k_s were improved by the present research. Also, comparison of the electrode (A and B) responses revealed that the RTIL could enhance the sensitivity and detection limit by 3 and 7 folds, respectively.

The relationship between catalytic current and the concentration of glucose was considered based on the electrochemical version of Michaelis-Menten plot. The enzyme kinetic parameters of apparent Michaelis-Menten constant (K_m^{ap}) and maximum current (I_{max}) measured under substrate saturated concentration can be calculated based on Lineweaver-Burk (5) [24]

$$\frac{1}{I_{ss}} = \frac{1}{I_{max}} + \frac{K_m^{ap}}{I_{max} C}, \quad (5)$$

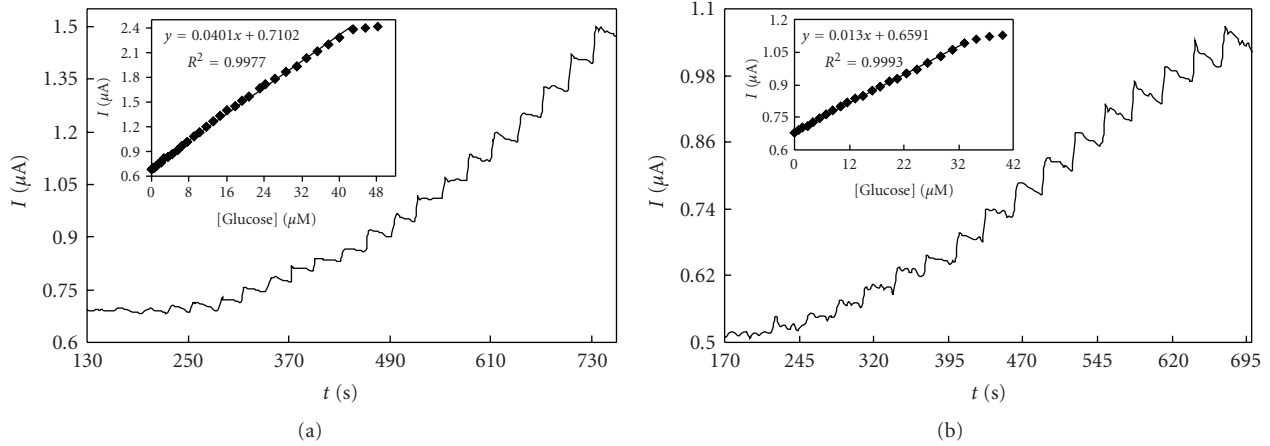


FIGURE 7: Amperometric response of GOx/RTIL/NH₂-MWCNTs/GC (a) and GOx/NH₂-MWCNTs/GC (b) electrodes to glucose. The electrodes were held at -0.51 V (versus Ag/AgCl), while its rotation speed was 500 rpm in 0.1 M PBS, pH 7.0. The final concentration of glucose after each successive addition was 0.10, 0.25, 0.50, 0.87, 1.36, 2.0, 2.7, 3.5, 4.4, 5.4, 6.5, 7.7, 9.0, 10.3, 11.7, 13.1, 14.6, 16.1, 17.7, 19.3, 20.9, 22.5, 24.3, 26.4, 28.8, 31.0, 33, 35.3, 37.6, 40, 43, 45.6, and 48.3 μM , respectively. Inset shows the calibration plot for glucose.

TABLE 1: Comparison between the analytical parameters of the proposed electrodes and other reported GOx/ionic liquids/nanoparticles based biosensors.

GOx-based electrode	Linear range (M)	Detection limit (μM)	Sensitivity ($\mu\text{A mM}^{-1}$)	K_m^{ap} (mM)	K_s (s^{-1})	Reference
CHIT/IL/AuNPs	3×10^{-6} – 9×10^{-3}	1.50	0.450	7.800	—	[19]
IL-GNP-IL-SWNT	2×10^{-6} – 5×10^{-5}	0.80	—	0.022	2.12	[8]
MWCNTs/PSS/Au-IL	0 – 2×10^{-2}	25.00	—	—	—	[9]
Au/CS-ILMWNT(SH)	1×10^{-3} – 1×10^{-2}	—	4.10	—	—	[10]
(A) RTIL/NH ₂ MWCNTs	1.2×10^{-7} – 4.3×10^{-5}	0.06	40.10	0.018	2.35	This work
(B) NH ₂ -MWCNTs	2×10^{-6} – 3.3×10^{-5}	0.39	13.00	0.024	2.20	

where I_{ss} stands for steady state current. From the slope and intercept of the plot, the values of K_m^{ap} and I_{\max} for electrode A were estimated to be $18 \mu\text{M}$ and $2.7 \mu\text{A}$, respectively. The obtained K_m^{ap} value is much smaller than those reported in the literature [11, 23, 25, 26]. Such a low K_m^{ap} value could be the sign of higher biological affinity of the biosensor to glucose. Also, comparison of the electrode responses revealed that the RTIL could enhance the K_m^{ap} value for the electrode A (Table 1).

The reproducibility at $10 \mu\text{M}$ glucose concentration was examined between three different electrodes, and the relative standard deviation was calculated to be 3.4 and 6.3% for electrode A and B, respectively.

4. Conclusion

The results obtained in present research showed that the nanocomposite of RTIL/NH₂-MWCNTs/GC could prepare a biocompatible microenvironment to immobilize GOx on modified GC electrode and maintain its activity while facilitate the direct electron transfer between enzyme and electrode surface. The prepared electrode, relative to the similar electrodes reported in the literature, exhibited an extra biocatalytic activity toward glucose with high sensitivity,

low detection limit, fast amperometric response, and small value of K_m^{ap} . The comparison of the results obtained by the electrode A with those attained by electrode B revealed that the ionic liquid [BMIM]BF₄ could enhance the sensitivity, detection limit, and K_s and K_m^{ap} values of the biosensor.

Acknowledgment

Financial supports provided by the Research Council of the University of Tehran and Iran National Science Foundation (INSF) are gratefully appreciated.

References

- [1] M. Pumera, S. Sánchez, I. Ichinose, and J. Tang, “Electrochemical nanobiosensors,” *Sensors and Actuators B*, vol. 123, no. 2, pp. 1195–1205, 2007.
- [2] J. Wang and M. Musameh, “Carbon nanotube/Teflon composite electrochemical sensors and biosensors,” *Analytical Chemistry*, vol. 75, no. 9, pp. 2075–2079, 2003.
- [3] C. E. Banks, T. J. Davies, G. G. Wildgoose, and R. G. Compton, “Electrocatalysis at graphite and carbon nanotube modified electrodes: edge-plane sites and tube ends are the reactive sites,” *Chemical Communications*, no. 7, pp. 829–841, 2005.

- [4] F. Zhao, X. Wu, M. Wang, Y. Liu, L. Gao, and S. Dong, "Electrochemical and bioelectrochemistry properties of room-temperature ionic liquids and carbon composite materials," *Analytical Chemistry*, vol. 76, no. 17, pp. 4960–4967, 2004.
- [5] S. Hu and C. Hu, "Carbon nanotube-based electrochemical sensors: principles and applications in biomedical systems," *Journal of Sensors*, vol. 2009, Article ID 187615, 40 pages, 2009.
- [6] U. Kragl, M. Eckstein, and N. Kaftzik, "Enzyme catalysis in ionic liquids," *Current Opinion in Biotechnology*, vol. 13, no. 6, pp. 565–571, 2002.
- [7] S. Park and R. J. Kazlauskas, "Biocatalysis in ionic liquids—advantages beyond green technology," *Current Opinion in Biotechnology*, vol. 14, no. 4, pp. 432–437, 2003.
- [8] R. T. Kachoosangi, M. M. Musameh, I. Abu-Yousef et al., "Carbon nanotube-ionic liquid composite sensors and biosensors," *Analytical Chemistry*, vol. 81, no. 1, pp. 435–442, 2009.
- [9] W. Wei, H. H. Jin, and G. C. Zhao, "A reagentless nitrite biosensor based on direct electron transfer of hemoglobin on a room temperature ionic liquid/carbon nanotube-modified electrode," *Microchimica Acta*, vol. 164, no. 1-2, pp. 167–171, 2009.
- [10] Q. Zhao, D. Zhan, H. Ma et al., "Direct proteins electrochemistry based on ionic liquid mediated carbon nanotube modified glassy carbon electrode," *Frontiers in Bioscience*, vol. 10, no. 1, pp. 326–334, 2005.
- [11] R. Gao and J. Zheng, "Amine-terminated ionic liquid functionalized carbon nanotube-gold nanoparticles for investigating the direct electron transfer of glucose oxidase," *Electrochemistry Communications*, vol. 11, no. 3, pp. 608–611, 2009.
- [12] F. Li, Z. Wang, C. Shan, J. Song, D. Han, and L. I. Niu, "Preparation of gold nanoparticles/functionalized multiwalled carbon nanotube nanocomposites and its glucose biosensing application," *Biosensors and Bioelectronics*, vol. 24, no. 6, pp. 1765–1770, 2009.
- [13] D. Ragupathy, A. I. Gopalan, and K. P. Lee, "Synergistic contributions of multiwall carbon nanotubes and gold nanoparticles in a chitosan-ionic liquid matrix towards improved performance for a glucose sensor," *Electrochemistry Communications*, vol. 11, no. 2, pp. 397–401, 2009.
- [14] P. Rahimi, H. A. Rafiee-Pour, H. Ghouchian, P. Norouzi, and M. R. Ganjali, "Ionic-liquid/NH-MWCNTs as a highly sensitive nano-composite for catalase direct electrochemistry," *Biosensors and Bioelectronics*, vol. 25, no. 6, pp. 1301–1306, 2010.
- [15] C. Cai and J. Chen, "Direct electron transfer of glucose oxidase promoted by carbon nanotubes," *Analytical Biochemistry*, vol. 332, no. 1, pp. 75–83, 2004.
- [16] Y. Liu, M. Wang, F. Zhao, Z. Xu, and S. Dong, "The direct electron transfer of glucose oxidase and glucose biosensor based on carbon nanotubes/chitosan matrix," *Biosensors and Bioelectronics*, vol. 21, no. 6, pp. 984–988, 2005.
- [17] X. Wu, P. Du, P. Wu, and C. Cai, "Effects of 1-butyl-3-methylimidazolium tetrafluoroborate on the oxidation of glucose catalyzed by glucose oxidase," *Electrochimica Acta*, vol. 54, no. 2, pp. 738–743, 2008.
- [18] A. J. Bard and L. Faulkner, *Electrochemical Methods: Fundamentals and Applications*, John Wiley & Sons, New York, NY, USA, 1980.
- [19] E. Laviron, "General expression of the linear potential sweep voltammogram in the case of diffusionless electrochemical systems," *Journal of Electroanalytical Chemistry*, vol. 101, no. 1, pp. 19–28, 1979.
- [20] E. Laviron, "The use of linear potential sweep voltammetry and of a.c. voltammetry for the study of the surface electrochemical reaction of strongly adsorbed systems and of redox modified electrodes," *Journal of Electroanalytical Chemistry*, vol. 100, no. 1-2, pp. 263–270, 1979.
- [21] D. Wang and L. Chen, "Facile direct electron transfer in glucose oxidase modified electrodes," *Electrochimica Acta*, vol. 54, no. 18, pp. 4316–4320, 2009.
- [22] X. Wu, F. Zhao, J. R. Varcoe, A. E. Thumser, C. Avignone-Rossa, and R. C. T. Slade, "Direct electron transfer of glucose oxidase immobilized in an ionic liquid reconstituted cellulose-carbon nanotube matrix," *Bioelectrochemistry*, vol. 77, no. 1, pp. 64–68, 2009.
- [23] X. Zeng, X. Li, L. Xing et al., "Electrodeposition of chitosan-ionic liquid-glucose oxidase biocomposite onto nano-gold electrode for amperometric glucose sensing," *Biosensors and Bioelectronics*, vol. 24, no. 9, pp. 2898–2903, 2009.
- [24] J. Li, S. N. Tan, and H. Ge, "Silica sol-gel immobilized amperometric biosensor for hydrogen peroxide," *Analytica Chimica Acta*, vol. 335, no. 1-2, pp. 137–145, 1996.
- [25] Y. T. Wang, L. Yu, Z. Q. Zhu, J. Zhang, J. Z. Zhu, and C. H. Fan, "Improved enzyme immobilization for enhanced bioelectrocatalytic activity of glucose sensor," *Sensors and Actuators B*, vol. 136, no. 2, pp. 332–337, 2009.
- [26] Y. Zou, L. X. Sun, and F. Xu, "Biosensor based on polyaniline-Prussian Blue/multi-walled carbon nanotubes hybrid composites," *Biosensors and Bioelectronics*, vol. 22, no. 11, pp. 2669–2674, 2007.

Research Article

Voltammetric Detection of Dopamine in Presence of Ascorbic Acid and Uric Acid at Poly (Xylenol Orange) Film-Coated Graphite Pencil Electrode

Umesh Chandra, B. E. Kumara Swamy, Ongera Gilbert, and B. S. Sherigara

Department of P. G. Studies and Research in Industrial Chemistry, Jnana Sahyadri, Kuvempu University, Shankaraghatta-577 451, Shimoga, Karnataka (S), India

Correspondence should be addressed to B. E. Kumara Swamy, kumaraswamy21@yahoo.com

Received 17 February 2011; Accepted 6 April 2011

Academic Editor: Bengi Uslu

Copyright © 2011 Umesh Chandra et al. This is an open access article distributed under the Creative Commons Attribution License, which permits unrestricted use, distribution, and reproduction in any medium, provided the original work is properly cited.

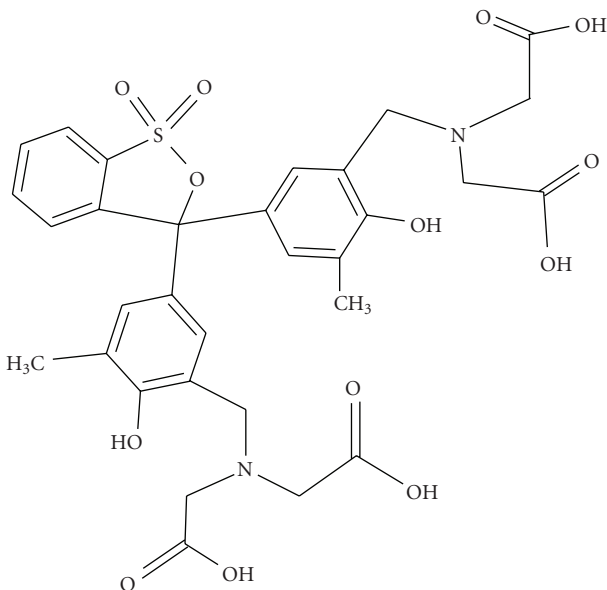
Poly (xylenol orange) film-coated graphite pencil electrode was fabricated for the detection of dopamine in the presence of ascorbic acid and uric acid in phosphate buffer solution of pH 7. The redox peaks obtained at modified electrode shows a good enhancement. The scan rate effect was found to be a diffusion-controlled electrode process. The electrochemical oxidation of dopamine was depended on pH, and the limit of detection was found to be 9.1×10^{-8} M. The simultaneous study gave and excellent result with great potential difference between dopamine and other bioactive organic molecules by using both cyclic voltammetric and differential pulse voltammetric techniques. The present modified graphite electrode was applied to the detection of dopamine in the injection samples, and the recovery obtained was satisfactory.

1. Introduction

The graphite pencil electrode (GPE) has been successfully acting as a biosensor in modern electroanalytical field. A porous composite is consisting of graphite particles, polymeric binder and other additives such as clay. Due to high electrochemical reactivity, high electrical conductivity, good mechanical rigidity, low cost, low technology, high electrochemical reactivity, ease of modification, renewal, low background current, and miniaturization, the GPE has good application in analysis of neurotransmitter and in the detection of traces of metal ions [1–4]. GPE has a larger active electrode surface area and is therefore able to detect low concentrations and/or volume of the analyt [5]. This type of electrode has been successfully applied to design various biosensors [6–9].

In recent days the electropolymer modified carbon paste electrode works with very much excellent effort in acting as a sensor for dopamine [10–12]. Especially, the electropolymer film-coated electrodes with dyes have good stability, reproducibility, more active sites, homogeneity in

electrochemical deposition [13, 14]. The electropolymerisation generally results in polymer film which is uniform and strongly adherent to the electrode surface. In addition the polymer film can be deposited onto the small area with high degree of geometrical conformity and controllable thickness. Several redox dyes are known to artificial electron donors [15]. Such dyes are able to undergo electropolymerisation from aqueous solution producing stable redox active layer [16, 17]. Dopamine (DA) is a well-known biogenic amine acting as a neurotransmitter in the brain. It has received considerable attention because of its suspected role in a variety of neuropsychiatric disorders such as Parkinson's disease and Schizophrenia [18–21]. It has been found that the dopamine possesses very strong electrochemical activity by giving dopamine-*o*-quinone as oxidation product. However the determination remains a challenge because of the presence of large excess of ascorbic acid (AA) and uric acid (UA). It is generally believed that direct redox reactions of these species at bare electrode are irreversible and therefore requires high over potential [22]. Moreover the direct redox reactions of these species at bare electrodes take place at



SCHEME 1: Structure of xylenol orange.

very similar potential and often suffer from a fouling effect, which results in rather poor selectivity and reproducibility. The ability to determine DA, UA, and AA selectively has been a major goal of electroanalytical research [23]. Development of both sensitivity and selectivity are of equal importance in voltammetric procedure and also this would help in the prevention and treatment of several neurodegenerative diseases [24].

The aim of our work was to fabricate stable electrode by electropolymerising xylenol orange (The structure of xylenol orange was shown in Scheme 1) on the surface of graphite pencil electrode to achieve the challenge of simultaneous determination of DA in the presence of AA, and UA in physiological pH. In this investigation electrochemical method was chosen for the detection of DA because, the electrochemical methods have proved to be selective, sensitive, reliable, and cost effective [25]. Although no examination of the detection of dopamine in the presence of both ascorbic acid and uric acid in physiological pH at poly(xylenol orange) film-coated graphite pencil (poly(XO)/GPE) electrode has been reported. This work discussed about sensitivity, selectivity and reproducibility of neurotransmitter at poly(XO)/GPE at physiological pH.

2. Experimental

2.1. Materials. The pencil-lead rods were (HB 0.5 mm in diameter and 6 cm length) purchased from local bookstore. 25×10^{-3} M xylenol orange stock solution was prepared in double-distilled water. 10×10^{-5} M DA stock solution was prepared in 0.1 M perchloric acid solution. 10×10^{-3} M UA stock solution was prepared in 0.1 M NaOH and 10×10^{-3} M AA was prepared in double-distilled water. Buffer used was 0.2 M phosphate buffer solution (PBS) and chemicals

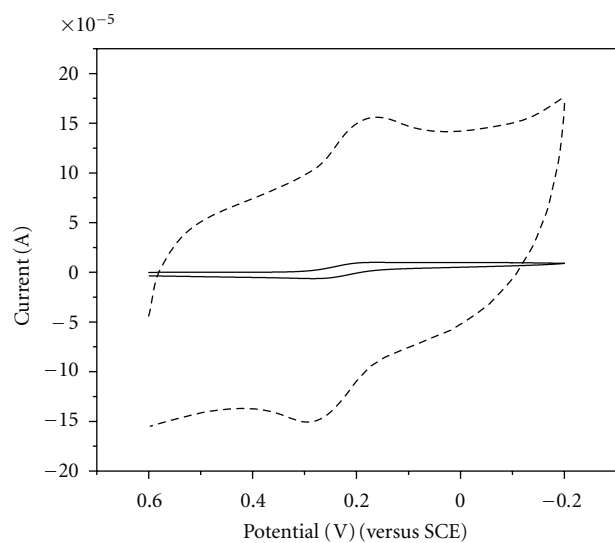


FIGURE 1: Cyclic voltammogram of 1 mM potassium ferricyanide at BGPE (solid line) and at poly(XO)/GPE (dashed line) in 1 M potassium chloride at scan rate of 50 mV s^{-1} .

mentioned above were all analytical grade used without purification.

2.2. Apparatus. The electrochemical experiments were carried out using a model-201 electroanalyser (EA-201 chemilink system). The electrode system contained the working electrodes were bare graphite pencil electrode (0.5 mm in diameter), platinum counter electrode and saturated calomel reference electrode.

2.3. Preparation of Poly(XO)/GPE. The poly(XO)/GPE was prepared by placing 5×10^{-4} M XO with 0.2 M PBS at pH = 10 as supporting electrolyte in an electrochemical cell. The potential was maintained between -400 mV to 2000 mV with 10 multiple cycles at scan rate of 100 mV s^{-1} . The poly(XO) film could be formed uniformly on the surface of GPE. After that, the electrode was rinsed with double-distilled water and kept in the 0.2 M PBS at pH 7.

3. Results and Discussion

3.1. Electrochemical Characterization of Poly(XO)/GPE Using Standard Potassium Ferricyanide System. The freshly prepared 1×10^{-3} M potassium ferricyanide and 1 M potassium chloride solutions were placed in the electrochemical cell. Figure 1 shows the cyclic voltammograms recorded for the 1×10^{-3} M potassium ferricyanide at both BGPE (solid line) and at poly(XO)/GPE (dashed line) at scan rate of 50 mV s^{-1} . The low redox current signals were observed at BGPE. The anodic and cathodic peak potentials were located at 171 mV and 283 mV. The redox peak potentials difference (ΔE_p) was 112 mV. But the poly(XO)/GPE showed significant improvement in the redox peak current signals. The anodic and cathodic peak potentials were found at 169 mV and

289 mV. The ΔE_p was 120 mV. This shows the electrocatalytic property of poly(XO)/GPE.

3.2. Electrocatalytic Response of DA at Poly(XO)/GPE. Figure 2(a) explains the cyclic voltammogram of 0.5×10^{-5} M DA in 0.2 M PBS at pH 7 at BGPE and poly(XO)/GPE at 50 mV s^{-1} sweep rate. The poor electrochemical response was observed at BGPE (solid line). The oxidation peak potential (E_{pa}) was located at 240 mV and reduction peak potential (E_{pc}) response at 110 mV were observed at BGPE. The potential difference (ΔE_p) was found to be 130 mV. However the strong improvement and reversible redox peaks current were observed at poly(XO)/GPE. During the first cycle (dashed line) the E_{pa1} and E_{pc1} were located at 200 mV and 160 mV, respectively, and another reduction peak E_{pc2} was found at -250 mV. The ΔE_p (E_{pa1} and E_{pc1}) was 40 mV. This is the clear evidence that our electrode has better electrocatalytic activity by exposing large surface area for electrochemical oxidation of DA. In the same condition, the poly(XO)/GPE was scanned again. The resultant voltammogram (dotted line) shows another anodic peak E_{pa2} at -200 mV. The oxidation mechanism of DA at poly(XO)/GPE could be explained as shown in Scheme 2. During the first scan the DA was oxidized and converted to dopa-o-quinone (E_{pa1}) in forward scan. While in reverse scan this was reduced to DA (E_{pc1}). The E_{pc2} was appeared by next to the E_{pc1} . This is because, the electron-rich nitrogen atom becomes deprotonated leads to formation of cyclized product known as lucodopachrome. By applying the second scan E_{pa2} appeared because of the lucodopachrome oxidized to dopachrome [9, 26–30].

To understand whether the E_{pc2} and E_{pa2} were exist or not, the experiment was carried out at poly(XO)/GPE by applying successive multiple cycle in the same above mentioned solution and condition. The voltammogram was recorded for 20 multiple cycles (Figure 2(b)). The voltammogram shows negligible decrease for second and third cycles and almost constant for further cycles and the results shows E_{pc2} and E_{pa2} were existing strongly. This confirms that DA was undergoing ring cyclization, that is, lucodopachrome and that was oxidizing to dopachrome.

3.3. Effect of Scan Rate towards the Electro-Oxidation of DA at Poly(XO)/GPE. To study the scan rate effect at poly(XO)/GPE the voltammograms were recorded for different scan rate. The cyclic voltammogram recorded for 0.5×10^{-5} M DA in 0.2 M PBS at pH 7.4 at different scan rates at poly(XO)/GPE, respectively. The redox peak currents were increased with increase in the scan rate from 50 to 400 mV s^{-1} . The graph of redox peak current versus square root of scan rate was plotted (Figure 3). The graphs shows linear relations ships between redox peak currents and scan rates. The correlation coefficient occurred was $r^2 = 0.999$ suggested diffusion-controlled electrode process. Further the graph of E_p versus $\ln \nu$ was plotted to calculate the heterogeneous rate constant and number of electron transferred in the electrochemical oxidation of DA. These

parameters were calculated by using the equation given below [31, 32]

$$E_{pa} = E^0 + m \left[0.78 + \ln \left(\frac{D^{1/2}}{k^0} \right) - 0.5 \ln m \right] + 0.5m \ln \nu, \quad (1)$$

$$m = \frac{RT}{[(1-\alpha)nF]}, \quad (2)$$

$$E_{pc} = E^0 - m' \left[0.78 + \ln \left(\frac{D^{1/2}}{k^0} \right) - 0.5 \ln m' \right] - 0.5m \ln \nu, \quad (3)$$

$$m' = \frac{RT}{[\alpha nF]}, \quad (4)$$

where E^0 is the formal potential, D is the diffusion coefficient, k^0 is the heterogeneous rate constant, α is the energy transferred coefficient and n is the number of electrons transferred. R , T , and F are the universal gas constant, absolute temperature and Faraday constant, respectively.

The k^0 was calculated from the above equation and it was found to be 0.0055 cm s^{-1} for forward electrochemical reaction and 0.0048 cm s^{-1} for backward electrochemical reaction at poly(XO)/GPE. The average k^0 was $0.00515 \text{ cm s}^{-1}$. This calculated rate constant was higher when compared to the rate constant for BGPE 0.0005 cm s^{-1} . The graph of $\ln I_p$ versus $(E_p - E^0)$ were plotted for the poly(XO)/GPE. The slope values from the above graph were used to calculate the energy transfer coefficient (α) using the equation (5) [31, 32]

$$I_p = 0.227FAC_0k^0 \exp[-\alpha f(E_p - E^0)], \quad (5)$$

where A is the surface area of the electrode, C_0 is the concentration of DA and $f = F/RT$.

The calculated average energy transfer coefficients were 0.662 for BGPE and 0.635 for poly(XO)/GPE. From this energy transfer coefficients the number of electrons transferred in the electrochemical redox process for DA were calculated using (2) and (4).

In our case the number of electrons transferred were $n_a = 1.93$ for anodic peak and $n_c = 1.75$ for cathodic peak when working electrode used was poly(XO)/GPE. Hence from this evidence this was confirmed that the electrochemical redox process of DA at poly(XO)/GPE was carried by transferring the two electrons.

3.4. Effect of Solution pH. The electrochemical response of DA at poly(XO)/GPE was generally pH dependent. The both redox peak potentials of DA were shifted to less positive side with increasing in the pH values. The anodic peak potential of DA shifted from 300 mV to 90 mV with respect the pH from 4 to 10. The potential diagram was constructed by plotting the graph of E_{pa} versus pH of the solution (Figure 4). The graph has good linearity with a slope of 54 mV/pH suggested, equal number of electron and proton transfer reactions [33–35].

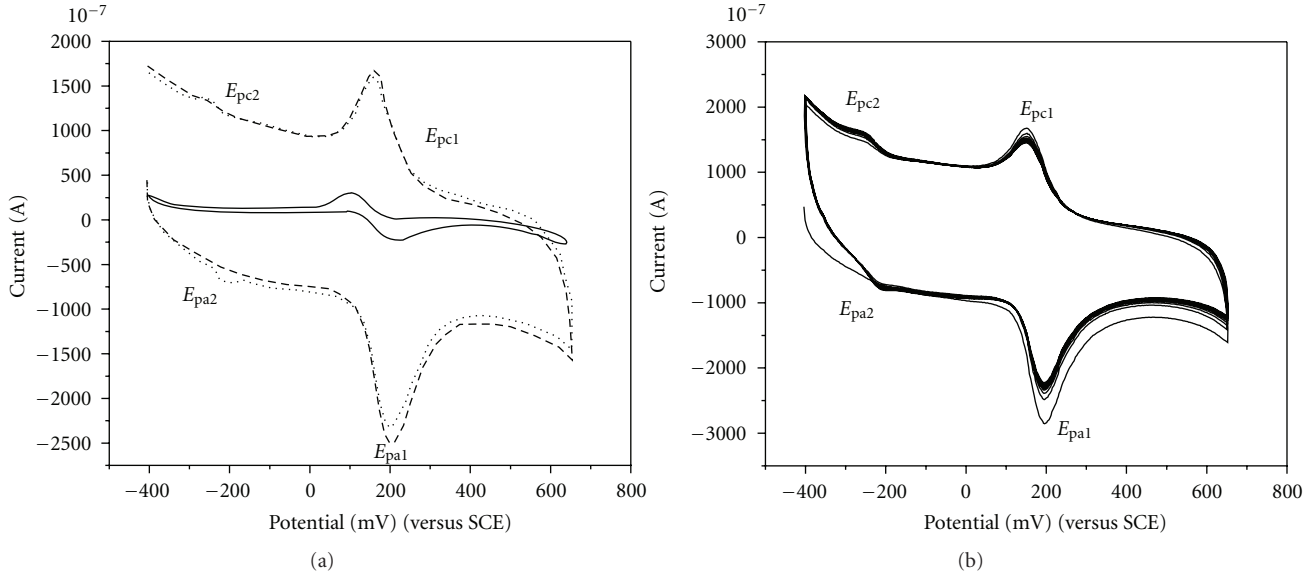
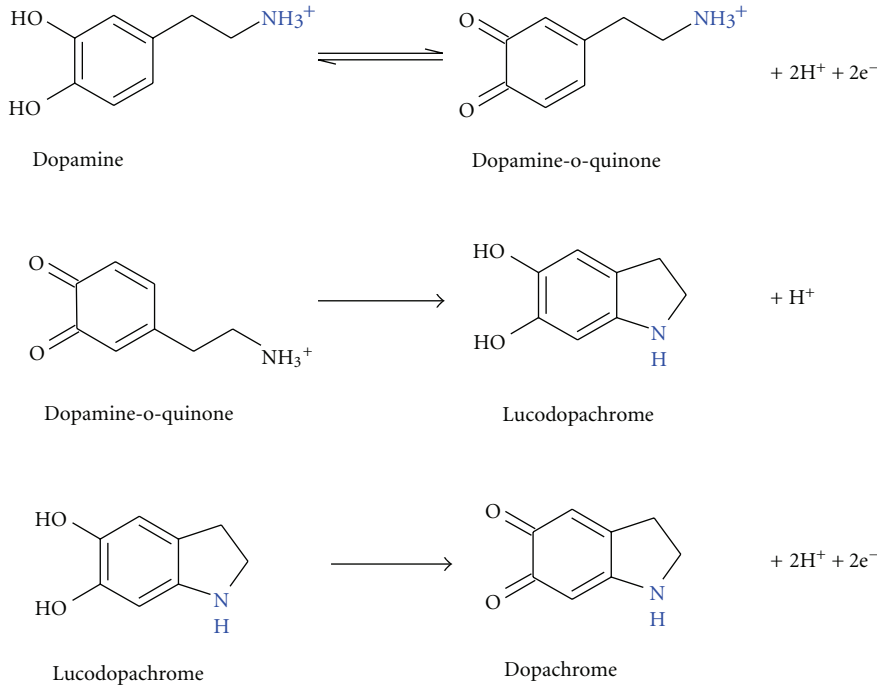


FIGURE 2: (a) Cyclic voltammograms of 0.5×10^{-5} M dopamine at BGPE (solid line) and at poly(XO)/GPE; First cycle (dashed line) and Second Cycle (dotted line) in 0.2 M PBS of pH 7 at sweep rate 50 mV s^{-1} . (b) Cyclic voltammograms of 0.5×10^{-5} M dopamine for 20 multiple cycles in 0.2 M PBS at poly(XO)/GPE at sweep rate 50 mV s^{-1} .



SCHEME 2: Electrocatalytic oxidation mechanism of DA at the poly(XO) GPE surface.

3.5. Simultaneous Determination of DA, AA, and UA. Further our poly(XO)/GPE was introduced for analysis of DA in the mixture containing large excess of AA and UA. As shown in Figure 5(a), the cyclic voltammogram at BGPE (solid line) appear the seriously overlapped peak at around 240 mV was observed for the mixture containing 0.5×10^{-5} M DA, 1×10^{-4} M AA, and 5×10^{-5} M UA in 0.2 M PBS at pH

7. However, resolved voltammetric peaks were obtained at poly(XO)/GPE (dashed line) with great enhancement in current signals. The anodic peak potentials (E_{pa1} and E_{pa2}) of DA were found at 205 and -205 mV. The corresponding E_{pc1} and E_{pc2} were located at 160 and -250 , respectively. The anodic peak potentials of AA and UA were found at 10 mV and 350 mV, respectively. The difference of anodic

TABLE 1: Comparison of different modified electrodes for DA determination.

Electrode	Detection limit ($\mu\text{mol/L}$)	Method	Reference
Triazole Self-Assembled Monolayer-Modified Gold Electrode	0.5	DPV	[36]
Metallothioneins self-assembled gold electrode	6	CV	[37]
IL-CPE	0.7	CV	[41]
Poly(L-methionine) Modified Electrode	0.42	CV	[38]
P-pTSA modified electrode	0.6	DPV	[39]
poly(XO)/GPE	0.091	DPV	This work

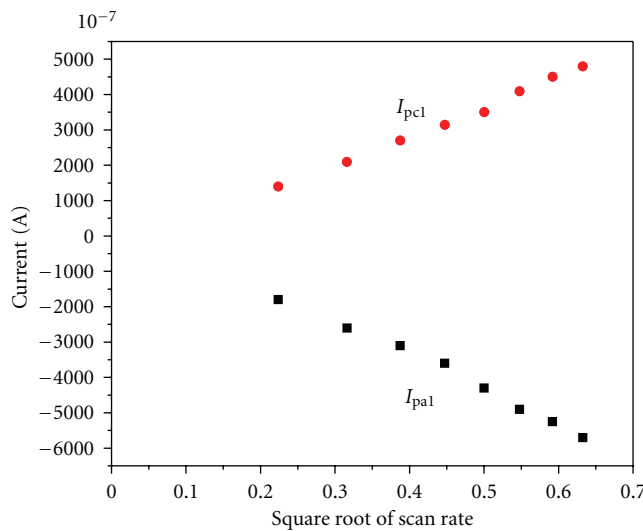
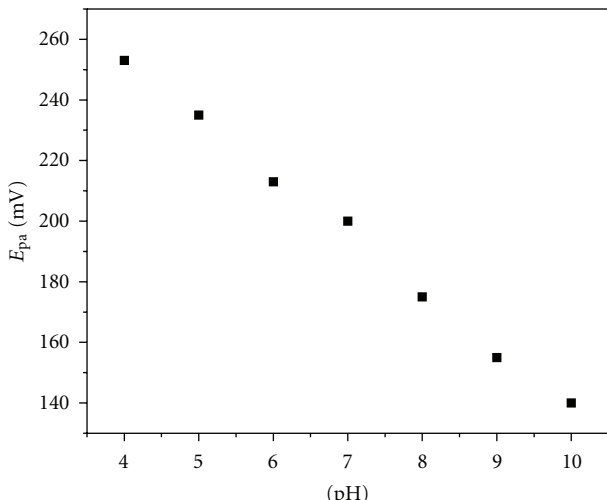


FIGURE 3: Graph of redox peak current of DA versus different scan rate.

FIGURE 4: Graph of anodic peak potential (E_{pa1}) of DA versus different pH.

peak potential between DA (E_{pa1})-AA was 195 mV and to that of UA-DA (E_{pa1}) was 145 mV by CV technique.

DPV technique was used for the determination of DA, AA, and UA at both BGPE and poly(XO)/GPE because to get higher current sensitivity and better resolution. Figure 5(b)

shows the DPVs recorded for the mixture of the same samples and condition mentioned above. The DPV recorded at BGPE shows a single and broad peak (solid line) and well-separated three anodic peaks of DA, AA, and UA were occurred at poly(XO)/GPE. The oxidation peaks of DA, AA, and UA were located at 190 mV, -20 mV and 360 mV, respectively. The anodic peak potential differences between DA-AA and UA-DA were 210 mV and 170 mV, respectively. The peak separation were greater when comparing to peak separation occurred by CV.

3.6. Calibration of DA Concentration. The incorporation study of DA was carried out in its mixture at poly(XO)/GPE when the concentration of DA was increased whereas the concentration of AA and UA were keep constant. From Figure 6(a), it can be seen that the concentration of DA was increased from 0.2×10^{-5} M to 0.9×10^{-5} M when keeping the concentration of UA 5×10^{-5} M and AA 1×10^{-4} M. The anodic peak current was proportional to concentration of DA and there were no change in the peak current and peak potential occurred for AA and UA. The graph of anodic peak current of DA was plotted against its concentration (Figure 6(b)). The correlation coefficient was found to be 0.9989. The linear regression equation was $I_{\text{pa}} (\mu\text{A}) = 47.416(\mu\text{M/L}) + 23.833$. The limit of detection and limit of quantification were calculated by using the equations given below (6) and (7), respectively, [18, 40]. The limit of detection and quantification were 9.1×10^{-8} M and 3.03×10^{-7} M, respectively, and this was compared with the other literatures [36–39, 41] (Table 1)

$$\text{LOD} = 3 \frac{S}{M}, \quad (6)$$

$$\text{LOQ} = 10 \frac{S}{M}, \quad (7)$$

where S is standard deviation and M is the slope of calibration plot.

3.7. Analytical Application. The modified electrode was applied to the determination of dopamine hydrochloride injection. The DA injection sample purchased from Sterile Specialities India Private Ltd with a specified content of DA of 40.0 mg/mL. The sample was used after suitable dilution using 0.2 M PBS. The recovery and R.S.D. were acceptable ($n = 5$), showing that the proposed methods could be efficiently used for the determination of DA in injections with recovery in the range 98.5–100.05% (Table 2).

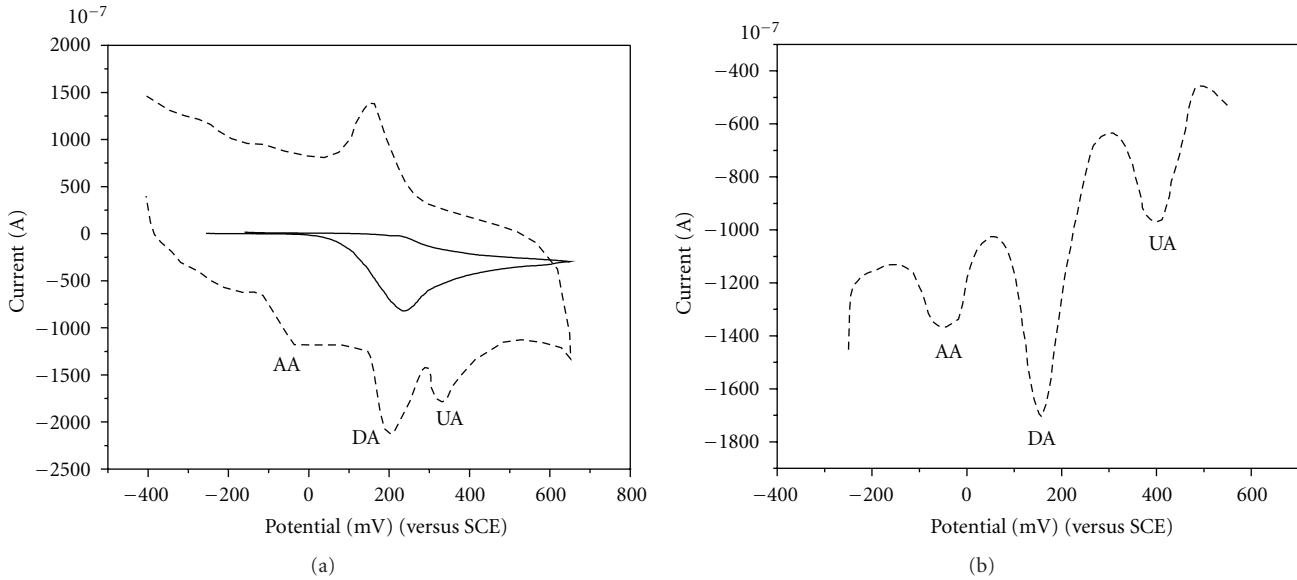


FIGURE 5: (a) Simultaneous detection of 0.5×10^{-5} M DA, 1×10^{-4} M AA, and 5×10^{-5} M UA at BGPE (solid line) and at poly(XO)/GPE (dashed line) by CV at scan rate of 50 mV s^{-1} . (b) Simultaneous detection of 0.5×10^{-5} M DA, 1×10^{-4} M AA, and 5×10^{-5} M UA at BGPE (solid line) and at poly(XO)/GPE (dashed line) by DPV at scan rate of 20 mV s^{-1} .

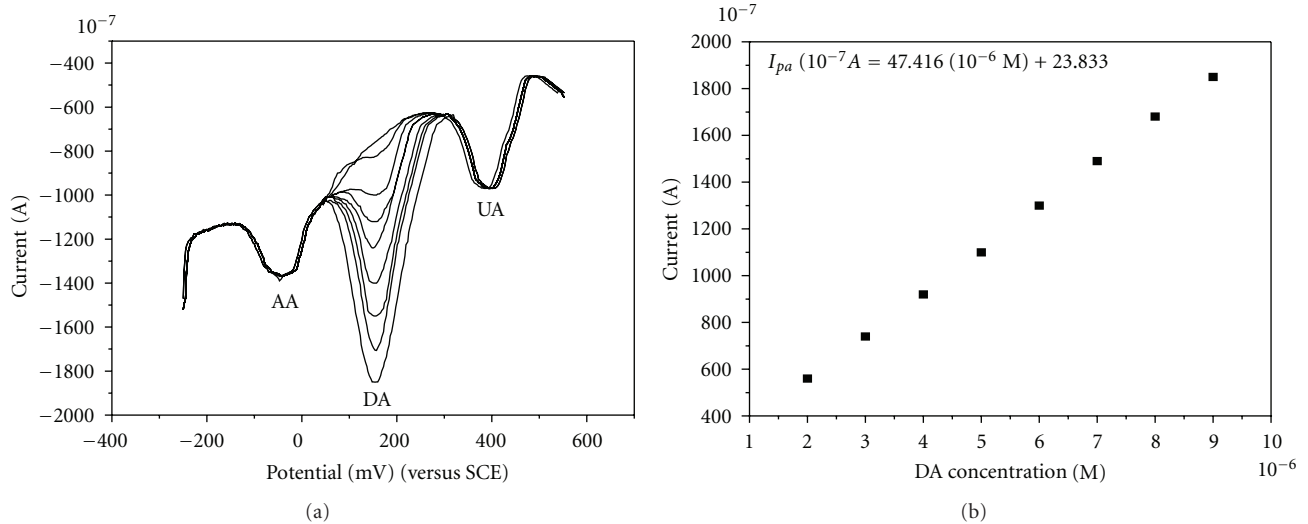


FIGURE 6: (a) Differential pulse voltammograms of different concentration of DA (a-g; $0.2, 0.3, 0.4, 0.5, 0.5, 0.6, 0.7, 0.8$ and 0.9×10^{-5} M in 0.2 M phosphate buffer solution of pH 7.0 in the presence of 1×10^{-3} M AA, and 5×10^{-4} M UA at poly(XO)/GPE. (b) Graph of anodic peak current versus different concentration of DA.

TABLE 2: Detection of DA in injection samples ($n = 5$).

Sample	Content (mg/mL)	Found (mg/mL)	RSD (%)	Recovery (%)
1	4.0	3.94	2.4	98.5
2	4.0	3.968	2.0	99.2
3	4.0	4.002	2.2	100.05

4. Conclusion

DA can be detected electrochemically in mixture of solution, at physiological pH, containing large excess of AA and UA at

poly(XO)/GPE. The prepared modified electrode detection limit was 9.1×10^{-8} M and it has excellent sensitivity, selectivity and antifouling properties. The proposed methods can be applied to the detection of DA in injection. This approach can readily be applied to the development of electrochemical sensors for dopamine and related neurotransmitters.

Acknowledgment

The authors are very thankful to the Department of Science and Technology, Government of India, New Delhi for the funding given through project no. DST/TSG/ME/2007/44.

References

- [1] W. Gao, J. Song, and N. Wu, "Voltammetric behavior and square-wave voltammetric determination of trepibutone at a pencil graphite electrode," *Journal of Electroanalytical Chemistry*, vol. 576, no. 1, pp. 1–7, 2005.
- [2] D. Demetriadis, A. Economou, and A. Voulgaropoulos, "A study of pencil-lead bismuth-film electrodes for the determination of trace metals by anodic stripping voltammetry," *Analytica Chimica Acta*, vol. 519, no. 2, pp. 167–172, 2004.
- [3] H. Karadeniz, B. Gulmez, F. Sahinci et al., "Disposable electrochemical biosensor for the detection of the interaction between DNA and lycorine based on guanine and adenine signals," *Journal of Pharmaceutical and Biomedical Analysis*, vol. 33, no. 2, pp. 295–302, 2003.
- [4] A. Levent, Y. Yardim, and Z. Senturk, "Voltammetric behavior of nicotine at pencil graphite electrode and its enhancement determination in the presence of anionic surfactant," *Electrochimica Acta*, vol. 55, no. 1, pp. 190–195, 2009.
- [5] M. Vestergaard, K. Kerman, and E. Tamiya, "An electrochemical approach for detecting copper-chelating properties of flavonoids using disposable pencil graphite electrodes: possible implications in copper-mediated illnesses," *Analytica Chimica Acta*, vol. 538, no. 1–2, pp. 273–281, 2005.
- [6] A. Erdem, P. Papakonstantinou, and H. Murphy, "Direct DNA hybridization at disposable graphite electrodes modified with carbon nanotubes," *Analytical Chemistry*, vol. 78, no. 18, pp. 6656–6659, 2006.
- [7] M. Ozsoz, A. Erdem, K. Kerman et al., "Electrochemical genosensor based on colloidal gold nanoparticles for the detection of factor V leiden mutation using disposable pencil graphite electrodes," *Analytical Chemistry*, vol. 75, no. 9, pp. 2181–2187, 2003.
- [8] J. Wang, A. N. Kawde, and E. Sahlin, "Renewable pencil electrodes for highly sensitive stripping potentiometric measurements of DNA and RNA," *Analyst*, vol. 125, no. 1, pp. 5–7, 2000.
- [9] U. Chandra, B. E. Kumara Swamy, O. Gilbert et al., "Poly (amaranth) film based sensor for resolution of dopamine in the presence of uric acid: a voltammetric study," *Chinese Chemical Letters*, vol. 21, no. 12, pp. 1490–1492, 2010.
- [10] O. Gilbert, U. Chandra, B. E. K. Swamy, M. PandurangaChar, C. Nagaraj, and B. S. Sherigara, "Poly (alanine) modified carbon paste electrode for simultaneous detection of dopamine and ascorbic acid," *International Journal of Electrochemical Science*, vol. 3, pp. 1186–1195, 2008.
- [11] M. Pandurangachar, B. E. K. Swamy, U. Chandra, and B. S. Sherigara, "Simultaneous determination of dopamine, ascorbic acid and uric acid at poly(pattan and reeder's) modified carbon paste electrode," *International Journal of Electrochemical Science*, vol. 4, no. 5, pp. 672–683, 2009.
- [12] O. Gilbert, B. E. K. Swamy, U. Chandra, and B. S. Sherigara, "Electrocatalytic oxidation of dopamine and ascorbic acid at poly (eriochrome black-T) modified carbon paste electrode," *International Journal of Electrochemical Science*, vol. 4, no. 4, pp. 582–591, 2009.
- [13] Y. Ohnuki, H. Matsuda, T. Ohsaka, and N. Oyama, "Permelectivity of films prepared by electrochemical oxidation of phenol and amino-aromatic compounds," *Journal of Electroanalytical Chemistry*, vol. 158, no. 1, pp. 55–67, 1983.
- [14] A. Volkov, G. Tourillon, P. C. Lacaze, and J. E. Dubois, "Electrochemical polymerization of aromatic amines. IR, XPS and PMT study of thin film formation on a Pt electrode," *Journal of Electroanalytical Chemistry*, vol. 115, no. 2, pp. 279–291, 1980.
- [15] C. X. Cai and K. H. Xue, "Electrochemical characterization of electropolymerized film of naphthol green B and its electrocatalytic activity toward NADH oxidation," *Microchemical Journal*, vol. 58, no. 2, pp. 197–208, 1998.
- [16] A. A. Karyakin, O. A. Bobrova, and E. E. Karyakina, "Electroreduction of NAD⁺ to enzymatically active NADH at poly(neutral red) modified electrodes," *Journal of Electroanalytical Chemistry*, vol. 399, no. 1–2, pp. 179–184, 1995.
- [17] A. A. Karyakin, A. K. Strakhova, E. E. Karyakina, S. D. Verfolomeyev, and A. K. Yatsimirsky, "The electrochemical polymerization of methylene blue and bioelectrochemical activity of the resulting film," *Bioelectrochemistry and Bioenergetics*, vol. 32, no. 1, pp. 35–43, 1993.
- [18] U. Chandra, B. E. Kumara Swamy, O. Gilbert, and B. S. Sherigara, "Voltammetric resolution of dopamine in the presence of ascorbic acid and uric acid at poly (calmagite) film coated carbon paste electrode," *Electrochimica Acta*, vol. 55, no. 24, pp. 7166–7174, 2010.
- [19] O. Gilbert, B. E. Kumara Swamy, U. Chandra, and B. S. Sherigara, "Simultaneous detection of dopamine and ascorbic acid using polyglycine modified carbon paste electrode: a cyclic voltammetric study," *Journal of Electroanalytical Chemistry*, vol. 636, no. 1–2, pp. 80–85, 2009.
- [20] U. Chandra, B. E. Kumara Swamy, O. Gilbert, M. Pandurangachar, and B. S. Sherigara, "Voltammetric resolution of dopamine in presence of ascorbic acid at polyvinyl alcohol modified carbon paste electrode," *International Journal of Electrochemical Science*, vol. 4, no. 10, pp. 1479–1488, 2009.
- [21] U. Chandra, B. E. Kumara Swamy, O. Gilbert, and B. S. Sherigara, "Determination of dopamine in presence of ascorbic acid at eriochrome black T modified carbon paste electrode: a voltammetric study," *International Journal of Electrochemical Science*, vol. 5, no. 10, pp. 1475–1483, 2010.
- [22] R. N. Adams, "Probing brain chemistry with electroanalytical techniques," *Analytical Chemistry*, vol. 48, no. 14, pp. 1126A–1138A, 1976.
- [23] R. R. Naik, B. E. K. Swamy, U. Chandra, E. Niranjana, B. S. Sherigara, and H. Jayadevappa, "Separation of ascorbic acid, dopamine and uric acid by acetone/water modified carbon paste electrode: a cyclic voltammetric study," *International Journal of Electrochemical Science*, vol. 4, no. 6, pp. 855–862, 2009.
- [24] G. Alarcón-Angeles, S. Corona-Avendaño, M. Palomar-Pardavé, A. Rojas-Hernández, M. Romero-Romo, and M. T. Ramírez-Silva, "Selective electrochemical determination of dopamine in the presence of ascorbic acid using sodium dodecyl sulfate micelles as masking agent," *Electrochimica Acta*, vol. 53, no. 6, pp. 3013–3020, 2008.
- [25] S. Corona-Avendaño, G. Alarcón-Ángeles, M. T. Ramírez-Silva, M. Romero-Romo, A. Cuán, and M. Palomar-Pardavé, "Simultaneous electrochemical determination of adrenaline and ascorbic acid: influence of [CTAB]," *Journal of the Electrochemical Society*, vol. 156, no. 12, pp. J375–J381, 2009.
- [26] Y. Zhang, G. Jin, Y. Wang, and Z. Yang, "Determination of dopamine in the presence of ascorbic acid using poly

- (acridine red) modified glassy carbon electrode," *Sensors*, vol. 3, no. 10, pp. 443–450, 2003.
- [27] E. S. Forzani, G. A. Rivas, and V. M. Solís, "Amperometric determination of dopamine on vegetal-tissue enzymatic electrodes. Analysis of interferers and enzymatic selectivity," *Journal of Electroanalytical Chemistry*, vol. 435, no. 1–2, pp. 77–84, 1997.
- [28] A. Ciszewski and G. Milczarek, "Polyeugenol-modified platinum electrode for selective detection of dopamine in the presence of ascorbic acid," *Analytical Chemistry*, vol. 71, no. 5, pp. 1055–1061, 1999.
- [29] Y. Zhang, G. Jin, Z. Yang, and H. Zhao, "Determination of dopamine in the presence of ascorbic acid using a poly(amidosulfonic acid) modified glassy carbon electrode," *Microchimica Acta*, vol. 147, no. 4, pp. 225–230, 2004.
- [30] Y. Zhang, G. Jin, W. Cheng, and S. Li, "Poly (O-aminobenzoic acid) modified glassy carbon electrode for electrochemical detection of dopamine in the presence of ascorbic acid," *Frontiers in Bioscience*, vol. 10, no. 1, pp. 23–29, 2005.
- [31] S. Corona-Avendaño, M. T. Ramírez-Silva, M. Palomar-Pardavé, L. Hernández-Martínez, M. Romero-Romo, and G. Alarcón-Ángeles, "Influence of CTAB on the electrochemical behavior of dopamine and on its analytic determination in the presence of ascorbic acid," *Journal of Applied Electrochemistry*, vol. 40, no. 2, pp. 463–474, 2010.
- [32] S. Corona-Avendaño, G. Alarcón-Ángeles, M. T. Ramírez-Silva, G. Rosquete-Pina, M. Romero-Romo, and M. Palomar-Pardavé, "On the electrochemistry of dopamine in aqueous solution. Part I: the role of [SDS] on the voltammetric behavior of dopamine on a carbon paste electrode," *Journal of Electroanalytical Chemistry*, vol. 609, no. 1, pp. 17–26, 2007.
- [33] B. D. Jones and J. D. Ingle Jr., "Evaluation of immobilized redox indicators as reversible, in situ redox sensors for determining Fe(III)-reducing conditions in environmental samples," *Talanta*, vol. 55, no. 4, pp. 699–714, 2001.
- [34] S. M. Chen, G. H. Chuang, and V. S. Vasantha, "Preparation and electrocatalytic properties of the TBO/nafion chemically-modified electrodes," *Journal of Electroanalytical Chemistry*, vol. 588, no. 2, pp. 235–243, 2006.
- [35] X. Wang, N. Yang, Q. Wan, and X. Wang, "Catalytic capability of poly(malachite green) films based electrochemical sensor for oxidation of dopamine," *Sensors and Actuators, B*, vol. 128, no. 1, pp. 83–90, 2007.
- [36] S. Yixin and S. F. Wang, "Simultaneous determination of dopamine and ascorbic acid at a triazole self-assembled monolayer-modified gold electrode," *Microchimica Acta*, vol. 154, no. 1–2, pp. 115–121, 2006.
- [37] Q. Wang, N. Li, and W. Wang, "Electrocatalytic response of dopamine at a metallothioneins self-assembled gold electrode," *Analytical Sciences*, vol. 18, no. 6, pp. 635–639, 2002.
- [38] W. Ma and D. M. Sun, "The electrochemical properties of dopamine, epinephrine and their simultaneous determination at a poly(L-methionine) modified electrode," *Russian Journal of Electrochemistry*, vol. 43, no. 12, pp. 1382–1389, 2007.
- [39] P. F. Huang, L. Wang, J. Y. Bai, H. J. Wang, Y. Q. Zhao, and S. D. Fan, "Simultaneous electrochemical detection of dopamine and ascorbic acid at a poly(*p*-toluene sulfonic acid) modified electrode," *Microchimica Acta*, vol. 157, no. 1–2, pp. 41–47, 2007.
- [40] R. N. Hegde, B. E. Kumara Swamy, N. P. Shetti, and S. T. Nandibewoor, "Electro-oxidation and determination of gabapentin at gold electrode," *Journal of Electroanalytical Chemistry*, vol. 635, no. 1, pp. 51–57, 2009.
- [41] W. Sun, M. Yang, and K. Jiao, "Electrocatalytic oxidation of dopamine at an ionic liquid modified carbon paste electrode and its analytical application," *Analytical and Bioanalytical Chemistry*, vol. 389, no. 4, pp. 1283–1291, 2007.

Research Article

Electroanalytical Characterisation of Dopa Decarboxylase Inhibitors Carbidopa and Benserazide on Multiwalled Carbon Nanotube and Poly(Nile blue A) Modified Glassy Carbon Electrodes

Dilek Kul^{1,2} and Christopher M. A. Brett¹

¹ Departamento de Química, Faculdade de Ciências e Tecnologia Universidade de Coimbra, 3004-535 Coimbra, Portugal

² Faculty of Pharmacy, Karadeniz Technical University, 61080 Trabzon, Turkey

Correspondence should be addressed to Christopher M. A. Brett, cbrett@ci.uc.pt

Received 1 March 2011; Accepted 22 March 2011

Academic Editor: Bengi Uslu

Copyright © 2011 D. Kul and C. M. A. Brett. This is an open access article distributed under the Creative Commons Attribution License, which permits unrestricted use, distribution, and reproduction in any medium, provided the original work is properly cited.

Modified glassy carbon electrodes have been made by deposition of functionalised multiwalled carbon nanotubes (MWCNTs) followed by formation of poly(Nile blue) (PNB) films by electropolymerisation, using potential cycling in 0.1 M phosphate buffer solution (PBS) at pH 6.0. The electrochemical oxidation of carbidopa (CD) and benserazide (BS) on these MWCNTs/PNB-modified electrodes was investigated using cyclic and differential pulse voltammetry in 0.1 M PBS at different values of pH between 5.0 and 8.0; both CD and BS gave one diffusion-controlled irreversible oxidation peak in cyclic voltammetry. Analytical characterisation of CD and BS was carried out in 0.1 M PBS, pH 5.0. Peak currents in differential pulse voltammetry were linear over the concentration range of 1×10^{-5} to 1×10^{-4} M for CD and 4×10^{-6} to 4×10^{-5} M for BS. The repeatability, precision, and accuracy of the method were also investigated. Higher sensitivities and lower detection limits, of $1.17 \mu\text{M}$ for CD and $0.50 \mu\text{M}$ for BS, were obtained with this new modified electrode compared with previous studies reported in the literature.

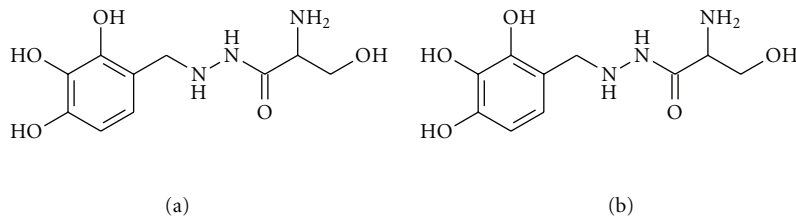
1. Introduction

Dopa decarboxylase inhibitors are used as part of the treatment for Parkinson's disease. Parkinson's disease (PD) is a degenerative disorder of the central nervous system that affects movement, muscle control, balance, and other functions. The most obvious symptoms are motor related such as tremor, rigidity, slowness of movement, and postural instability [1, 2]. There is currently no cure for Parkinson's disease. However, medications are used to increase levels of dopamine in the brain of patients with PD and in this way slow down the progression of the disease, since motor symptoms are produced by a lack of dopamine. The main drugs used for Parkinson's disease are levodopa, dopamine agonists, and MAO-B inhibitors [3].

Treatment using levodopa involves it being transformed into dopamine and increasing its level in the central nervous

system. However, only 5–10% of levodopa crosses the blood-brain barrier, and the rest is decarboxylated to dopamine in the metabolism before it reaches the brain, causing various side effects. Carbidopa, (2S)-3-(3,4-dihydroxyphenyl)-2-hydrazino-2-methylpropanoic acid, and benserazide, 2-amino-3-hydroxy-N'-(2,3,4-trihydroxybenzyl) propanehydrazide, (Scheme 1) are decarboxylase inhibitors of levodopa which are unable to cross the blood-brain barrier themselves and used in combination with levodopa for the treatment of PD. They prevent the carboxylation of levodopa before it reaches the brain and reduce the side effects when high doses of levodopa are used [4, 5].

Polymers of dyes such as phenothiazines, phenazines, and phenoxazines have recently been found to be attractive as redox mediators on the surface of solid electrodes [6, 7]. These dyes can be electropolymerised from aqueous solutions to obtain electrochemically active polymers. The



SCHEME 1: Structures of (a) carbidopa and (b) benserazide.

resulting polymers have many advantages such as simple one-step preparation, high stability, and reproducibility. Thus, they can be used as sensors and biosensors for the investigation of the electrochemical characteristics of some carboxylic acids [8] and NADH [9, 10].

Nile blue A (NB), one of the phenoxyazine dyes, is a well-known water-soluble electroactive molecule. Electrochemical polymerisation of NB gives a semiconducting poly(Nile blue) (PNB) film. PNB has been used as a mediator for the electrocatalytic oxidation of the nicotinamide coenzymes NADH and NADPH [11, 12] and also used in biofuel cells [13].

Single- (SWCNT) and multiwalled (MWCNT) carbon nanotubes have a great interest due to their properties such as high electrical conductivity, chemical stability, high surface area, and insolubility in all solvents [14, 15]. The unique and one-dimensional structures of carbon nanotubes lead them to be used in sensors and biosensors [16–19]. CNTs have also been used with conducting polymers as redox mediators to obtain new modified electrodes having good electrical and mechanical properties [20, 21].

The goal of this work is to carry out investigation and analytical measurement of carbidopa (CD) and benserazide (BS), which are anti-Parkinsonian agents, with modified glassy carbon (GC) electrodes by using cyclic voltammetry (CV) and differential pulse voltammetry (DPV). Modification was achieved first with functionalised multiwalled carbon nanotubes on the surface of GC electrodes. Nile blue A was then electropolymerised onto MWCNT-modified electrodes by cyclic voltammetry. The analytical measurement of CD and BS was carried out at MWCNT/PNB-modified electrodes in the selected supporting electrolyte. The results obtained for CD and BS were compared.

2. Experimental

2.1. Reagents. Nile blue A and N,N-dimethylformamide (DMF) were purchased from Fluka (Switzerland). Carbidopa (CD, ≥98%, M_w : 226.23 g/mol) and benserazide (BS, ≥98%, M_w : 293.70 g/mol) were from Sigma (USA), and nitric acid was from Riedel-de Haën (Germany). They were used without further purification.

Multiwalled carbon nanotubes were from NanoLab, USA, with ~95% purity, 30 ± 10 nm diameter and 1–5 μm length. For carboxylate functionalisation, 120 mg of MWCNT was stirred in 10 mL of a 3 M nitric acid for 24 h at room temperature. The solid product was filtered, then

washed with nanopure water until the filtrate became close to neutral ($\text{pH} \approx 7$), and dried at 80°C for 24 h.

Phosphate buffer solutions (PBSs), ionic strength 0.1 M, with different pH values were used both for electropolymerisation of NB and as supporting electrolyte for CD and BS. They were prepared from sodium di-hydrogenphosphate and di-sodium hydrogenphosphate (Riedel-de-Haën, Germany), and the pH was then adjusted with 5 M NaOH (Riedel-de Haën, Germany) solution.

Stock solutions of CD and BS (1×10^{-3} M) were prepared in nanopure water and stored in the dark and at +4°C. Working solutions of CD and BS for the voltammetric experiments were prepared by direct dilution of the stock solution with the selected supporting electrolyte just before use.

Millipore Milli-Q nanopure water (resistivity $\geq 18 \text{ M}\Omega \text{ cm}$) and analytical reagents were used for preparation of all solutions.

2.2. Instrumentation. A three-electrode electrochemical cell was used for voltammetric experiments. It contained a glassy carbon (GC) working electrode with a diameter of 5.5 mm, a platinum foil as counter electrode, and a saturated calomel electrode (SCE) as reference. Measurements were performed using a computer-controlled μ -Autolab Type II potentiostat/galvanostat with GPES 4.9 software (Metrohm-Autolab, the Netherlands).

The pH measurements were carried out with a CRISON 2001 micro-pH meter at room temperature.

2.3. Modification of GC Electrodes with MWCNT and PNB. Modification of GC electrodes was achieved with functionalised MWCNT and PNB films. Before modification, the GC electrode was polished with diamond spray (Kemet International Ltd., UK) down to 1 μm particle size, then sonicated in Milli-Q nanopure water and rinsed with nanopure water.

The functionalised MWCNTs were dispersed in DMF with loading 0.2% ($\text{mg}/\mu\text{L}$) and sonicated for 4 h to obtain a homogeneous mixture. Then, 20 μL of the 0.2% MWCNT/DMF dispersion was dropped directly on the surface of the GC electrode using a micropipette and dried overnight at room temperature.

NB was electropolymerised onto MWCNT coatings (denoted as MWCNT/PNB) by cycling in the potential region from -0.6 to +1.2 V versus SCE at a scan rate of 50 mV s^{-1} in 0.1 M PBS at pH 6.0 containing 0.5 mM of NB. The optimum number of cycles for electropolymerisation of NB

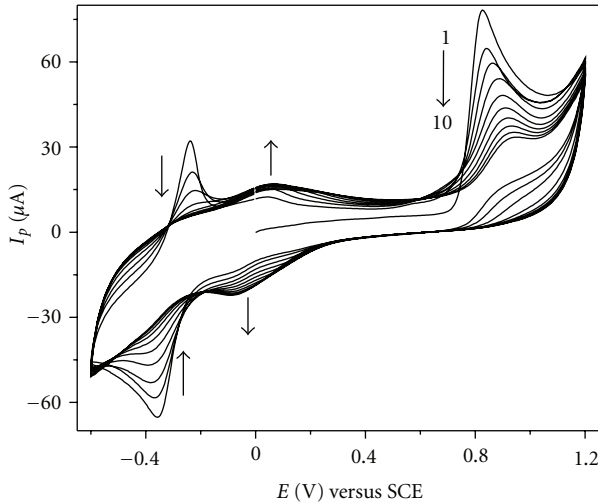


FIGURE 1: Cyclic voltammograms during potential cycling electro-polymerisation of 0.5 mM NB in 0.1 M PBS at pH 6.0. Scan rate 50 mV s^{-1} .

was found to be 5. After polymerisation, MWCNT/PNB-modified electrodes were dried for 24 h at room temperature.

2.4. Analytical Procedures. For analytical assays, all solutions were freshly prepared before the experiments and protected from the light. Measurements were carried out using differential pulse voltammetry (DPV) at room temperature ($25 \pm 1^\circ\text{C}$). The calibration equations for the DPV technique were constructed by plotting the peak current against CD or BS concentration.

Validation of the studied method was carried out with regard to ruggedness, precision, and accuracy by assaying five replicate samples [22, 23].

3. Results and Discussion

3.1. Electrochemical Polymerisation of Nile Blue. Electropolymerisation of NB was carried out in 0.1 M PBS at pH 6.0 containing 0.5 mM of NB by potential cycling on the MWCNT-modified electrodes. These polymerisation conditions were chosen according to a detailed study between pH 5–8, which showed that these conditions led to the polymer with the best electrochemical behaviour, with the most well-defined voltammetric peaks and the most stable PNB film [24]. Five cycles were used for the polymerisation of NB, since thicker PNB films, obtained with more than 5 cycles, onto MWCNTs coatings, led to unstable surface modifier films [24].

Cyclic voltammograms during and after NB polymerisation gave two redox couples: oxidation/reduction peaks for NB monomer and PNB polymer at around -0.4 V and 0.0 V , respectively. The irreversible oxidation peak at $\sim 0.9 \text{ V}$ is due to formation of the monomer radical (Figure 1). Peak currents for the electropolymerisation of NB onto MWCNT coatings were much higher than those of on the surface of the GC electrode, since modification by MWCNT leads to a larger electroactive surface area [15, 24, 25].

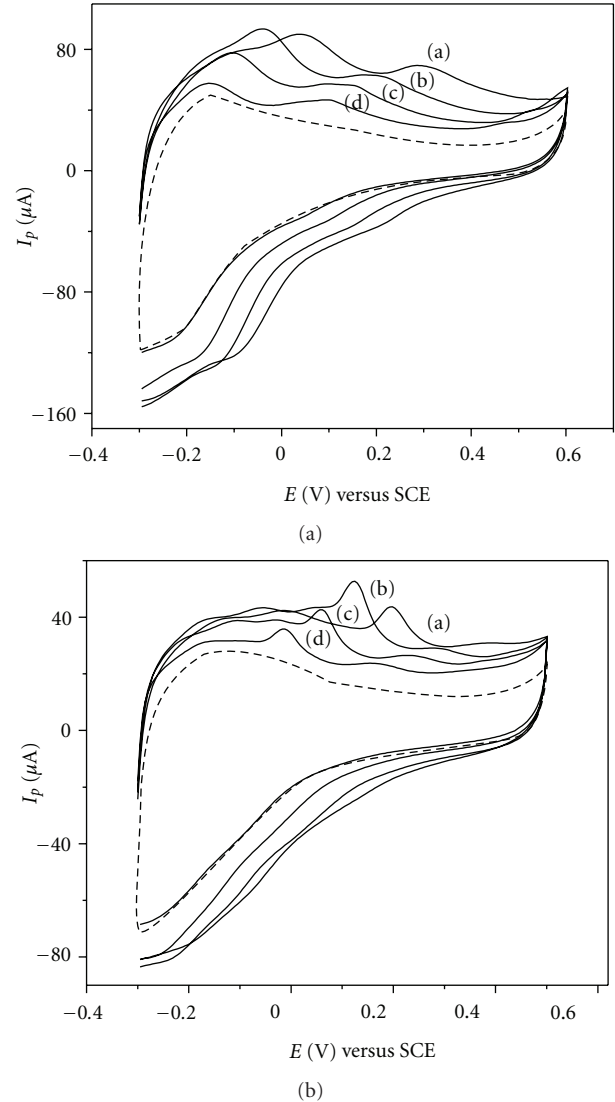
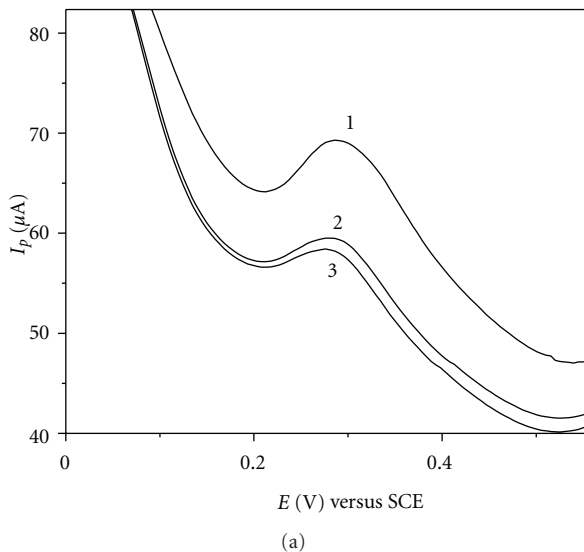


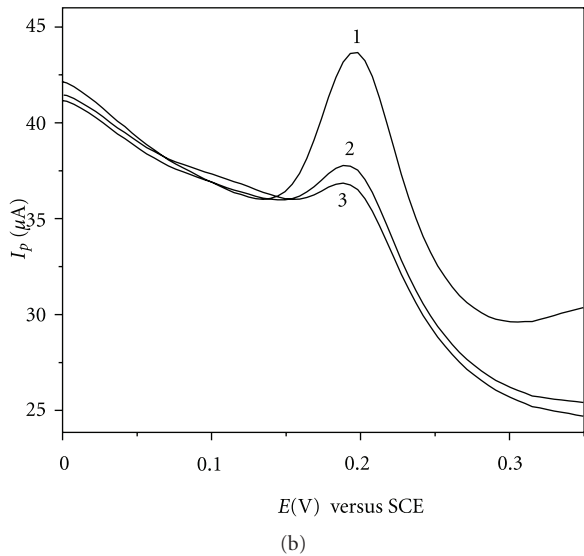
FIGURE 2: Cyclic voltammograms of (A) CD and (B) BS in 0.1 M PBS at pH (a) 5.0, (b) 6.0, (c) 7.0, and (d) 8.0 with MWCNTs/PNB-modified electrode. Dashed lines: 0.1 M PBS at pH 8.0. CD and BS concentrations: $100 \mu\text{M}$. Scan rate 50 mV s^{-1} .

3.2. Electrochemical Behaviour of CD and BS with Modified Electrodes. The electrochemical oxidation behaviour of CD and BS was investigated using cyclic voltammetry (CV) with MWCNTs/PNB-modified electrodes in 0.1 M PBS at different pH values between 5.0 and 8.0. More acidic buffer solutions were not used, since PNB films were unstable in media more acidic than pH 5.0 and media of pH > 8.0 cause decomposition of CD and BS.

CV measurements were made in the region between -0.3 V and 0.5 V , scanning in the positive direction at a scan rate of 50 mV s^{-1} in 0.1 M PBS at pH 5.0, 6.0, 7.0, and 8.0 containing $100 \mu\text{M}$ CD or BS; typical cyclic voltammograms are shown in Figure 2. Both CD and BS gave a single broad oxidation peak for all pH values tested. The oxidation peaks of CD and BS were at 286 and 198 mV versus SCE in 0.1 M



(a)



(b)

FIGURE 3: (1) First cycle, (2) second cycle, and (3) third cycle of the anodic responses of 1×10^{-4} M (a) CD and (b) BS from repetitive voltammograms in 0.1 M PBS at pH 5.0 with MWCNTs/PNB-modified electrode. Scan rate 50 mV s^{-1} .

PBS at pH 5.0. A very small cathodic response on sweep inversion was observed at around 210 mV for CD but only in pH 5.0 buffer solution. No reduction corresponding to the oxidation of BS was observed on the negative scan. These results demonstrate the irreversible nature of the CD and BS oxidation processes. The peaks of CD and BS decreased in the second and later cycles, due to blocking adsorption on the surface of the modified electrodes (Figure 3).

The effect of pH on the peak potential and peak current was investigated at pH 5.0, 6.0, 7.0, and 8.0 using both CV and DPV. Since the variations with pH seen by CV were similar to those with DPV, only the results obtained with DPV are shown in Figure 4. Both techniques showed that the peak potential of the anodic process moved to less positive potentials with increasing pH for both CD and BS.

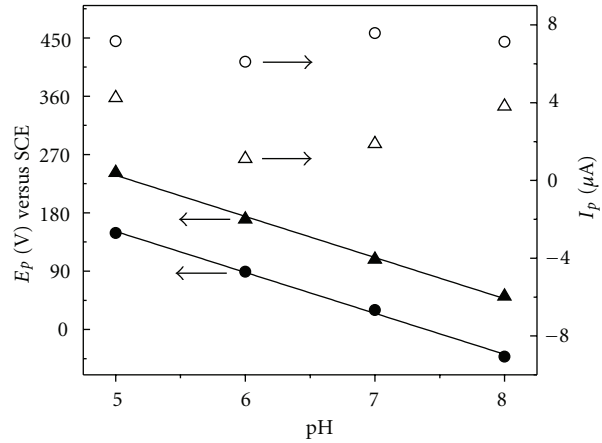


FIGURE 4: Plots of peak potential, E_p , and peak current, I_p , versus pH from DP voltammograms of CD and BS (concentrations $100 \mu\text{M}$) in 0.1 M PBS at MWCNT/PNB-modified electrodes. Triangles indicate CD and circles BS; filled symbols refer to E_p and unfilled ones to I_p .

Anodic peak potentials gave a linear dependence on pH with a negative slope of 63.5 mV/pH (correlation coefficient 0.996) and 63.2 mV/pH (correlation coefficient 0.997) for CD and BS, respectively, Figure 4. These slope values are close to the theoretical value of 59 mV/pH , obtained if the numbers of protons and electrons involved in the oxidation process are equal [6, 26]. The relationship between pH and peak current of CD and BS was also investigated. The maximum peak current and the better peak shape were obtained in 0.1 M PBS at pH 5.0 for CD and pH 7.0 for BS. However, BS was not stable at pH 7.0 for sufficient time to complete all of the studies. Thus, phosphate buffer at pH 5.0 was used as supporting electrolyte for the analytical characterisation of both CD and BS.

Scan rate studies were carried out in the range between 5 and 200 mV s^{-1} by CV to further assess the electrochemical oxidation of CD and BS. The oxidation peak potentials shifted to more positive potentials by about 132 mV for CD and 127 mV for BS when the scan rate was increased. Linear plots were not observed over this range neither from the plots of anodic peak current versus scan rate nor versus the square rate of scan rate, suggesting a more complex behavior. For this reason, plots of logarithm of peak current, $\log(I_p)$ versus logarithm of scan rate, $\log(\nu)$, for CD and BS were constructed, where a slope of 0.5 means a diffusion-controlled process and of 1.0 signifies an adsorption-controlled or surface-confined electrode process [27]. These plots showed the same tendencies for both CD and BS. At lower scan rates, $\leq 50 \text{ mV s}^{-1}$, the slope of the plot of $\log(I_p)$ versus $\log(\nu)$ was close to 0.5, indicative of diffusion control, and then began to increase, indicating that adsorption or thin-layer effects were beginning to have an influence on the observed behaviour. This can be explained taking into account the porous nature of the modifier layer into which the analyte will diffuse: the response is due to oxidation of species diffusing from bulk solution and to

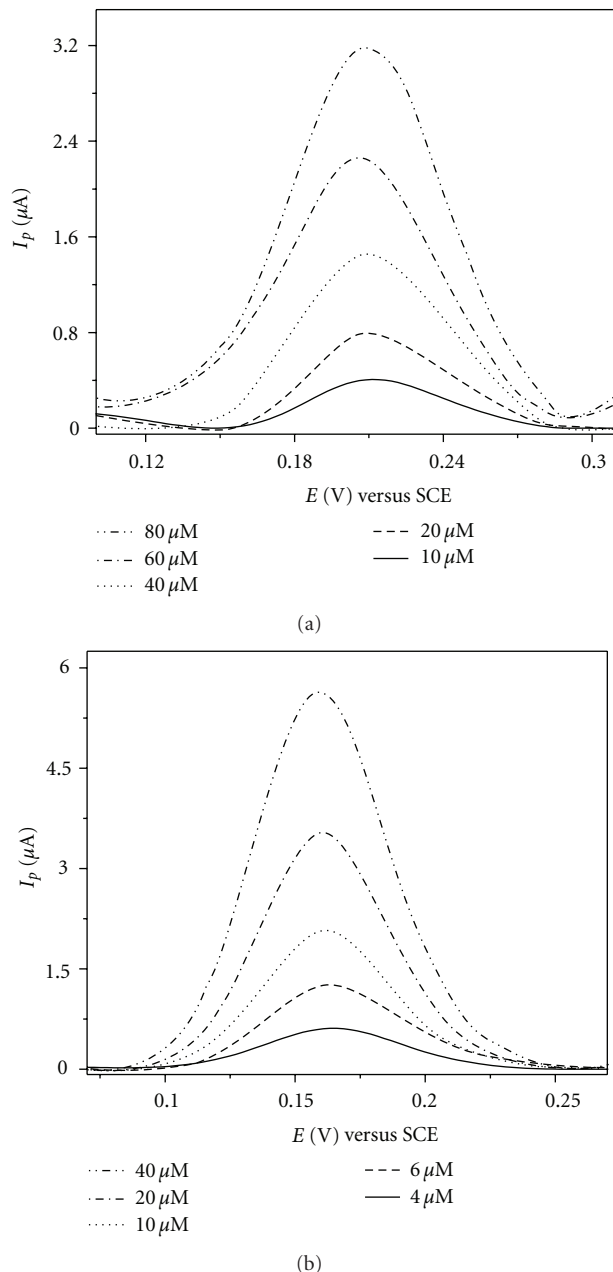


FIGURE 5: Baseline-subtracted differential pulse voltammograms of (a) CD and (b) BS at different concentrations in 0.1 M PBS at pH 5.0, using a MWCNT/PNB-modified electrode.

these species within the porous structure (similar to surface-confined species). As the scan rate increases, the timescale for diffusion decreases and the contribution of the latter becomes proportionally more important.

Tafel plots ($\log I$ versus E) were drawn for the scan rate of 5 mV s^{-1} beginning at a steady-state potential in 0.1 M PBS at pH 5.0 for both CD and BS [27]. The intercepts of the $\log I - f(E)$ plots gave the exchange current density (I_0) values, which were $9.73 \times 10^{-13} \mu\text{A cm}^{-2}$ and $4.48 \times 10^{-13} \mu\text{A cm}^{-2}$ for CD and BS, respectively. These values

TABLE 1: Data from the calibration plots for the analytical characterisation of CD and BS in 0.1 M PBS, pH 5.0 by DPV at the MWCNTs/PNB-modified electrode.

	Carbidopa	Benserazide
Peak potential (mV versus SCE)	210	160
Linearity range (μM)	10–100	4–40
Slope ($\mu\text{A } \mu\text{M}^{-1}$)	0.43 ± 0.001	0.15 ± 0.001
Intercept (μA)	0.49 ± 0.07	-0.32 ± 0.02
Correlation coefficient	0.997	0.999
LOD (μM)	1.17	0.50
LOQ (μM)	3.56	1.53
Repeatability of peak potential (RSD%)	0.50	0.56
Repeatability of peak current (RSD%)	0.96	0.44

confirmed the irreversibility of the oxidation reaction for both CD and BS.

3.3. Validation of the Analytical Methods. Differential pulse voltammetry (DPV) is an effective, selective, and sensitive technique which is suitable for the determination of organic drug compounds at low detection limits [28–30]. In this work, DPV was used for the quantitative evaluation of CD and BS, based on the linear correlation between oxidation peak current and concentration in 0.1 M PBS at pH 5.0 for both CD and BS, since the best response (regarding peak shape, peak current sensitivity, and reproducibility) and the best stability of CD and BS were obtained in this buffer. All solutions used for the analytical experiments were freshly prepared to ensure the stability of the analyte in the solutions.

Calibration plots under the selected conditions and using standard solutions of CD and BS are shown in Figure 5. The linear range was 1×10^{-5} to 1×10^{-4} M for CD and 4×10^{-6} to 4×10^{-5} M for BS; higher concentrations of CD and BS led to the loss of linearity and saturation effects that can be attributed to the effect of adsorption of species on the surface of MWCNT/PNB-modified electrode. The characteristics of the calibration lines and their related validation parameters are summarized in Table 1. Low values of standard error of the slopes and intercepts and correlation coefficients greater than 0.996 for both CD and BS confirmed the precision of the proposed method at MWCNT/PNB-modified electrodes.

The method was validated according to standard procedures [22, 31]. Accuracy, precision, and ruggedness were assessed by performing replicate analysis of the standard solutions in the supporting electrolyte. Limits of detection (LOD), limits of quantification (LOQ), repeatability (within day), precision, and selectivity were evaluated for both CD and BS [23, 29]. The LOD and LOQ were calculated from the peak currents using $\text{LOD} = 3 \text{ s/m}$ and $\text{LOQ} = 10 \text{ s/m}$, where s is the standard deviation of the peak currents (three runs) and m is the slope of the related calibration equation [32]. Also, these results indicated the reliability of the proposed voltammetric technique for the trace assay of CD and BS.

The precision of the method was calculated from five replicate experiments in different solutions having the same

concentration of CD or BS within the same day (repeatability) using DPV at the MWCNT/PNB-modified electrode. The concentrations of CD and BS for these studies were 8×10^{-5} M and 6×10^{-5} M, respectively. The precision and accuracy were determined as R.S.D.% (Table 1). These results demonstrate a good precision, accuracy, and sensitivity.

Electroanalytical studies of carbidopa and benserazide can also be found in the literature, which use differential pulse voltammetry. In [33], linear ranges between $31 \mu\text{M}$ and $470 \mu\text{M}$ with current sensitivity of $0.028 \mu\text{A} \mu\text{M}^{-1}$ and an LOD value of $2.16 \mu\text{M}$ were determined for CD and linear range $31 \mu\text{M}$ to $620 \mu\text{M}$ with current sensitivity $0.054 \mu\text{A} \mu\text{M}^{-1}$ and LOD of $2.77 \mu\text{M}$ for BS at GC electrodes. In another study [34], quantitative analysis of CD was carried out by DPV in the linear range from $5 \mu\text{M}$ to $600 \mu\text{M}$ with $3.6 \mu\text{M}$ of LOD and a current sensitivity of $0.041 \mu\text{A} \mu\text{M}^{-1}$ using ferrocene-modified carbon nanotube paste electrodes. In this work using MWCNTs/PNB-modified electrodes, as shown in Table 1, the sensitivity is significantly higher and the LOD lower than in the articles mentioned above.

4. Conclusions

Glassy carbon electrodes have been modified by coating with MWCNT and then poly(Nile blue), by drop coating with $20 \mu\text{L}$ of 0.2% MWCNT/DMF and then polymerising NB electrochemically in 0.1 M PBS at pH 6.0.

The MWCNT/PNB-modified electrode was used to investigate the electrochemical behaviour of the anti-Parkinsonian agents carbidopa and benserazide. Cyclic voltammetric measurements showed an irreversible behaviour in 0.1 M PBS at all pH values for both CD and BS. From the relationship of pH and peak currents and shapes, 0.1 M PBS at pH 5.0 was selected as supporting electrolyte for further studies. Scan rate studies showed that the process of MWCNT/PNB-modified electrodes was diffusion controlled with some evidence of thin-layer behaviour at high scan rate.

Analytical characterisation of CD and BS was achieved using DPV as a rapid, selective, sensitive, cheap, and simple technique. Linear calibration curves were obtained for both CD and BS. It was shown that the DPV method used gave good precision, accuracy, and sensitivity for CD and BS.

Acknowledgments

Financial support from Fundação para a Ciência e a Tecnologia (FCT), PTDC/QUI/65255/2006 and PTDC/QUI/65732/2006, POCI 2010 (cofinanced by the European Community Fund FEDER) and CEMUC (Research Unit 285), Portugal, is gratefully acknowledged. D. Kul thanks T.C., the Council of Higher Education (YÖK, Turkey) for a Postdoctoral research fellowship and Karadeniz Technical University (Turkey).

References

- [1] J. Jankovic, "Parkinson's disease: clinical features and diagnosis," *Journal of Neurology, Neurosurgery and Psychiatry*, vol. 79, no. 4, pp. 368–376, 2008.
- [2] C. A. Davie, "A review of Parkinson's disease," *British Medical Bulletin*, vol. 86, no. 1, pp. 19–127, 2008.
- [3] S. Fahn, "The history of dopamine and levodopa in the treatment of Parkinson's disease," *Movement Disorders*, vol. 23, no. 3, pp. 497–508, 2008.
- [4] The National Collaborating Centre for Chronic Conditions, "Symptomatic pharmacological therapy in Parkinson's disease," in *Parkinson's Disease*, pp. 59–100, Royal College of Physicians, London, UK, 2006.
- [5] J. Goole and K. Amighi, "Levodopa delivery systems for the treatment of Parkinson's disease: an overview," *International Journal of Pharmaceutics*, vol. 380, no. 1-2, pp. 1–15, 2009.
- [6] M. E. Ghica and C. M. A. Brett, "Poly(brilliant cresyl blue) modified glassy carbon electrodes: electrosynthesis, characterisation and application in biosensors," *Journal of Electroanalytical Chemistry*, vol. 629, no. 1-2, pp. 35–42, 2009.
- [7] R. Pauliukaite, M. E. Ghica, M. M. Barsan, and C. M. A. Brett, "Phenazines and polyphenazines in electrochemical sensors and biosensors," *Analytical Letters*, vol. 43, no. 10-11, pp. 1588–1608, 2010.
- [8] R. Pauliukaite, M. E. Ghica, M. Barsan, and C. M. A. Brett, "Characterisation of poly(neutral red) modified carbon film electrodes; Application as a redox mediator for biosensors," *Journal of Solid State Electrochemistry*, vol. 11, no. 7, pp. 899–908, 2007.
- [9] D. Dicu, L. Muresan, I. C. Popescu, C. Cristea, L. A. Silberg, and P. Brouant, "Modified electrodes with new phenothiazine derivatives for electrocatalytic oxidation of NADH," *Electrochimica Acta*, vol. 45, no. 24, pp. 3951–3957, 2000.
- [10] M. E. Ghica, R. Pauliukaite, N. Marchand, E. Devic, and C. M. A. Brett, "An improved biosensor for acetaldehyde determination using a bienzymatic strategy at poly(neutral red) modified carbon film electrodes," *Analytica Chimica Acta*, vol. 591, no. 1, pp. 80–86, 2007.
- [11] A. S. Santos, L. Gorton, and L. T. Kubota, "Nile blue adsorbed onto silica gel modified with niobium oxide for electrocatalytic oxidation of NADH," *Electrochimica Acta*, vol. 47, no. 20, pp. 3351–3360, 2002.
- [12] P. Du, P. Wu, and C. Cai, "A glucose biosensor based on electrocatalytic oxidation of NADPH at single-walled carbon nanotubes functionalized with poly(Nile blue A)," *Journal of Electroanalytical Chemistry*, vol. 624, no. 1-2, pp. 21–26, 2008.
- [13] Y. M. Yan, O. Yehezkel, and I. Willner, "Integrated, electrically contacted NAD(P)-dependent enzyme-carbon nanotube electrodes for biosensors and biofuel cell applications," *Chemistry: A European Journal*, vol. 13, no. 36, pp. 10168–10175, 2007.
- [14] G. A. Rivas, M. D. Rubianes, M. C. Rodríguez et al., "Carbon nanotubes for electrochemical biosensing," *Talanta*, vol. 74, no. 3, pp. 291–307, 2007.
- [15] Q. Gao, M. Sun, P. Peng, H. Qi, and C. Zhang, "Electro-oxidative polymerization of phenothiazine dyes into a multilayer-containing carbon nanotube on a glassy carbon electrode for the sensitive and low-potential detection of NADH," *Microchimica Acta*, vol. 168, no. 3, pp. 299–307, 2010.
- [16] M. E. Ghica, R. Pauliukaite, O. Fatibello-Filho, and C. M. A. Brett, "Application of functionalised carbon nanotubes immobilised into chitosan films in amperometric enzyme biosensors," *Sensors and Actuators B*, vol. 142, no. 1, pp. 308–315, 2009.
- [17] A. I. Gopalan, K. P. Lee, and D. Ragupathy, "Development of a stable cholesterol biosensor based on multi-walled carbon nanotubes-gold nanoparticles composite covered with a layer of chitosan-room-temperature ionic liquid network,"

- Biosensors and Bioelectronics*, vol. 24, no. 7, pp. 2211–2217, 2009.
- [18] P. Yanez-Sedeno, J. Riu, J. M. Pingarron, and F. X. Rius, “Electrochemical sensing based on carbon nanotubes,” *Trends in Analytical Chemistry*, vol. 29, pp. 939–953, 2010.
- [19] Y. Zhang, J. Wang, and M. Xu, “A sensitive DNA biosensor fabricated with gold nanoparticles/poly (p-aminobenzoic acid)/carbon nanotubes modified electrode,” *Colloids and Surfaces B*, vol. 75, no. 1, pp. 179–185, 2010.
- [20] P. Du, B. O. Zhou, and C. Cai, “Development of an amperometric biosensor for glucose based on electrocatalytic reduction of hydrogen peroxide at the single-walled carbon nanotube/Nile blue A nanocomposite modified electrode,” *Journal of Electroanalytical Chemistry*, vol. 614, no. 1-2, pp. 149–156, 2008.
- [21] G.M. Nascimento, R. C. Oliveira, N. A. Pradie et al., “Single-wall carbon nanotubes modified with organic dyes: synthesis, characterization and potential cytotoxic effects,” *Journal of Photochemistry and Photobiology A*, vol. 211, no. 2-3, pp. 99–107, 2010.
- [22] J. Ermer and J. H. Miller, Eds., *Method Validation in Pharmaceutical Analysis*, Wiley-VCH, Weinheim, Germany, 2005.
- [23] P. Bievre and H. Günzler, *Validation in Chemical Measurements*, Springer, New York, NY, USA, 2005.
- [24] D. Kul, R. Pauliukaite, and C. M. A. Brett, “Electrosynthesis and characterisation of poly(Nile blue) films,” submitted.
- [25] X. Chen, F. Wang, and Z. Chen, “An electropolymerized Nile blue sensing film-based nitrite sensor and application in food analysis,” *Analytica Chimica Acta*, vol. 623, no. 2, pp. 213–220, 2008.
- [26] M. S. Maia Quintino, M. Yamashita, and L. Angnes, “Voltammetric studies and determination of levodopa and carbidopa in pharmaceutical products,” *Electroanalysis*, vol. 18, no. 7, pp. 655–661, 2006.
- [27] E. Laviron, L. Roullier, and C. Degrand, “A multilayer model for the study of space distributed redox modified electrodes. Part II. Theory and application of linear potential sweep voltammetry for a simple reaction,” *Journal of Electroanalytical Chemistry*, vol. 112, no. 1, pp. 11–23, 1980.
- [28] B. Dogan, A. Golcu, M. Dolaz, and S. A. Ozkan, “Electrochemical behaviour of the bactericidal cefoperazone and its selective voltammetric determination in pharmaceutical dosage forms and human serum,” *Current Pharmaceutical Analysis*, vol. 5, no. 2, pp. 179–189, 2009.
- [29] D. Kul, M. Gumustas, B. Uslu, and S. A. Ozkan, “Electroanalytical characteristics of antipsychotic drug ziprasidone and its determination in pharmaceuticals and serum samples on solid electrodes,” *Talanta*, vol. 82, no. 1, pp. 286–295, 2010.
- [30] D. Kul, B. Uslu, and S. A. Ozkan, “Electrochemical determination of anti-hyperlipidemic drug ezetimibe based on its oxidation on solid electrodes,” *Analytical Letters*. In press.
- [31] B. Uslu, B. D. Topal, and S. A. Ozkan, “Electroanalytical investigation and determination of pefloxacin in pharmaceuticals and serum at boron-doped diamond and glassy carbon electrodes,” *Talanta*, vol. 74, no. 5, pp. 1191–1200, 2008.
- [32] I. R. Berry and D. Harpaz, *Validation of Active Pharmaceutical Ingredients*, CRC Press, Washington, DC, USA, 2nd edition, 2001.
- [33] C. Zapata-Urzua, M. Perez-Ortiz, M. Bravo, A. C. Olivieri, and A. Lueje, “Simultaneous voltammetric determination of levodopa, carbidopa and benserazide in pharmaceuticals using multivariate calibration,” *Talanta*, vol. 82, no. 3, pp. 962–968, 2010.
- [34] H. Yaghoubian, H. Karimi-Maleh, M. A. Khalilzadeh, and F. Karimi, “Electrochemical detection of carbidopa using a ferrocene-modified carbon nanotube paste electrode,” *Journal of the Serbian Chemical Society*, vol. 74, no. 12, pp. 1443–1453, 2009.

Research Article

Cyclic Voltammetric Investigation of Dopamine at Poly-(Gabapentin) Modified Carbon Paste Electrode

M. T. Shreenivas, B. E. Kumara Swamy, Umesh Chandra, and B. S. Sherigara

Department of P.G. Studies and Research in Industrial Chemistry, Kuvempu University, Jnana Sahyadri, Shankaraghata, Shimoga(D), Karnataka (S) 577451, India

Correspondence should be addressed to B. E. Kumara Swamy, kumaraswamy21@yahoo.com

Received 7 March 2011; Accepted 9 April 2011

Academic Editor: Bengi Uslu

Copyright © 2011 M. T. Shreenivas et al. This is an open access article distributed under the Creative Commons Attribution License, which permits unrestricted use, distribution, and reproduction in any medium, provided the original work is properly cited.

The poly (gabapentin) film was prepared on the surface of carbon paste electrode by electrochemical method using cyclic voltammetric technique. The poly (gabapentin) film-modified carbon paste electrode was calibrated with standard potassium ferrocyanide solution in 1 M KCl as a supporting electrolyte. The prepared poly (gabapentin) film-coated electrode exhibits excellent electrocatalytic activity towards the detection of dopamine at physiological pH. The scan rate effect was found to be diffusion-controlled electrode process. The concentration effect of dopamine was studied, and the redox peak potentials of dopamine were dependant on pH.

1. Introduction

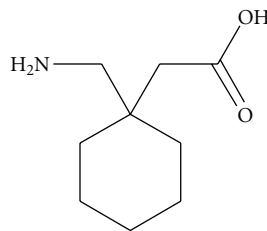
Dopamine (DA) is one of the most important neurotransmitters and plays a significant role in the functioning of central nervous system. A serious disease such as Schizophrenia and Parkinsonism may result from the loss of DA-containing neurons [1, 2], and patients with this disease show a low concentration of DA. Therefore, it is significant to develop sensitive and simple methods for the determination of DA. Many methods were introduced to determine DA, such as spectroscopy, chromatography, and electrochemistry [3–6]. Since DA is an oxidizable compound, it can be easily detectable by electrochemistry methods based on anodic oxidation. Carbon paste electrode was very much attracted towards the determination of biologically active molecules because of the easy preparation of modified electrode, renewability, low background current, and fast response. A number of modified carbon electrodes were developed for the determination of DA by using voltammetric techniques [7–10]. Modified carbon paste electrode can be prepared by adding different types of modifiers. Modification can be done by grinding in an agate mortar [11–13], by electropolymerisation [14–16], and also by immobilization method [17, 18]. The modified electrode has good electrocatalytic activity

such as sensitivity, selectivity, and also low detection limit when compared to traditional carbon paste electrode.

In the present work, the modification was carried out by preparing poly gabapentin for electrochemical investigation of DA by using cyclic voltammetry. Gabapentin, (1-(aminomethyl)cyclohexane-acetic acid; Gpn) (Scheme 1) is extensively used for the treatment of convulsive-type cerebral disorders, such as epilepsy, hypokinesia, and cranial trachoma [19]. It is sometimes prescribed for the management of neuralgia [20] and prescribed usually in combination with other medications for the prevention of seizure in people suffering from seizure disorders. Gabapentin was initially synthesized to mimic the chemical structure of the neurotransmitter gamma-aminobutyric acid (GABA) and used for the treatment of partial seizures in adults and children [21]. It has also been shown to be effective for neuropathic pain [22].

2. Experimental

2.1. Reagent and Chemicals. Gabapentin was obtained as a gift sample from AET Laboratories Pvt Ltd., Hyderabad. Graphite powder (50 micrometer particle size) was purchased from Merck, and silicon oil was purchased from



SCHEME 1: Structure of gabapentin.

Himedia. Potassium ferricyanide [$K_3Fe(CN)_6$] stock solution was prepared by dissolving in double-distilled water. DA stock solution was prepared by dissolving in 0.1 M perchloric acid ($HClO_4$) solution. 1 M potassium chloride (KCl) was used as a supporting electrolyte for the investigation of [$K_3Fe(CN)_6$], and the 0.2 M phosphate buffer solution was used as a supporting electrolyte for DA. Chemicals mentioned above were all purchased from Fluka were analytical grade.

2.2. Apparatus. The electrochemical experiments were carried out using a model-660 electrochemical workstation (CHI660C). All experiments were carried out in a conventional three-electrode system. The electrode system contained a working carbon paste electrode, home-made cavity of 3 mm diameter, a platinum wire as a counterelectrode, and a saturated calomel electrode as a reference electrode.

2.3. Preparation of Bare Carbon Paste Electrode. The bare carbon paste electrode was prepared by mixing 70% of graphite powder and 30% of silicon oil in an agate mortar by hand mixing for about 30 minutes to get homogenous carbon paste. The paste was packed into the cavity and smoothened on weighing paper.

2.4. Preparation of Poly (Gabapentin) Film-Coated Carbon Paste Electrode. The 0.5 mM aqueous gabapentin was placed in the electrochemical cell along with 0.2 M phosphate buffer solution at pH 10 to maintain basic condition to oxidize the monomer (gabapentin). The CPE was scanned 10 multiple cycles between the potential ranges from -0.4 to 1.8 V at 0.1 Vs^{-1} scan rate. After this process, the electrode was immersed in 0.2 M phosphate buffer solution of pH 7.0 until use.

3. Results and Discussion

3.1. Electrochemical Characterization of Poly (Gabapentin) Film-Coated Carbon Paste Electrode. The electrochemical characterization of poly (gabapentin) film-coated carbon paste electrode was done by using standard potassium ferri cyanide in order to check its enhancement property. Figure 1 shows the cyclic voltammogram of 1 mM $K_3Fe(CN)_6$ at bare CPE and poly (gabapentin) film-coated carbon paste electrode in the potential range from -200 to 600 mV at 0.1 Vs^{-1} scan rate in 1 M KCl supporting electrolyte. The cyclic voltammogram of 1 mM $K_3Fe(CN)_6$ at both bare CPE

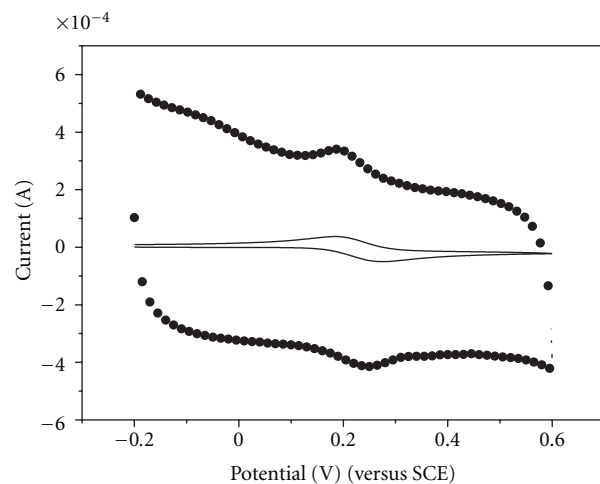


FIGURE 1: Cyclic voltammogram of 1 mM $K_3Fe(CN)_6$ at bare CPE (solid line) and poly (gabapentin) film-coated carbon paste electrode (dotted line) at 0.1 Vs^{-1} scan rate.

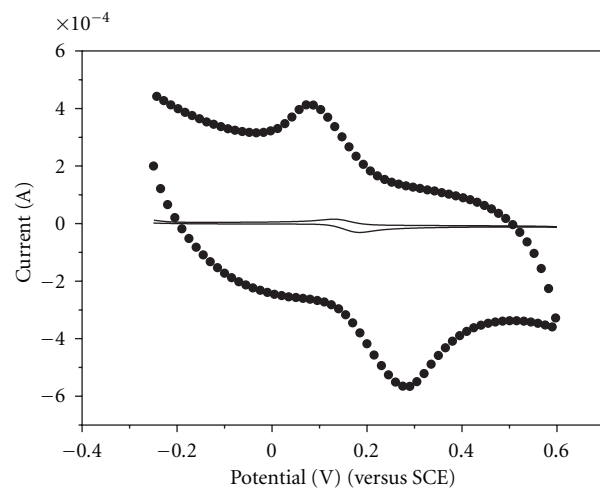
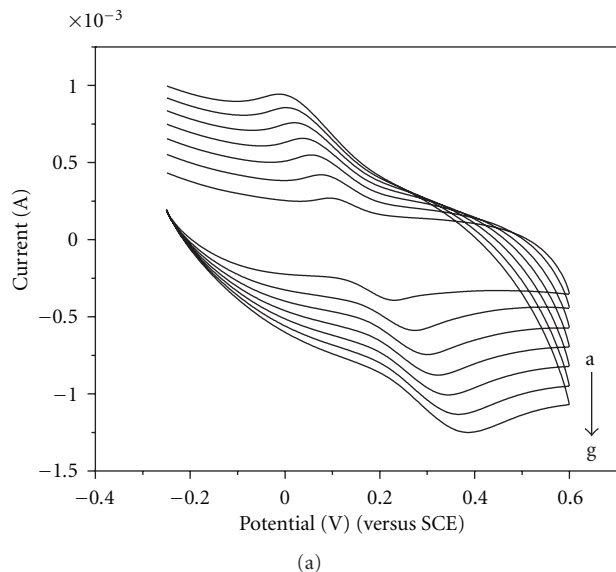


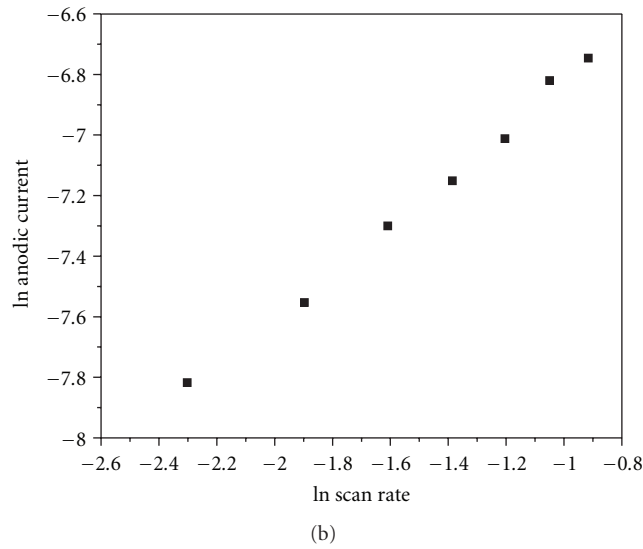
FIGURE 2: Cyclic voltammogram of 5×10^{-5} M DA in 0.2 M phosphate buffer solution at bare CPE (dashed line) and poly (gabapentin) film-coated carbon paste electrode (solid line) at 0.1 Vs^{-1} scan rate.

and poly (gabapentin) film-coated carbon paste electrode showed identical reversible cycles. The poly (gabapentin) film-coated carbon paste electrode showed very good electrochemical response when compared to bare CPE. The solid line shows the electrochemical response of bare CPE having the cathodic peak potential (E_{pc}) 0.2 V and anodic peak potential (E_{pa}) 0.28 V with less current sensitivity. After modification with poly (gabapentin) film, the electrode showed improvement in current signal enhancement of both electrochemical anodic and cathodic peak current; this was shown in dotted line. The E_{pc} and E_{pa} were found at 0.2 V and 0.25 V, respectively.

3.2. Electrocatalytic Response of DA at Poly (Gabapentin) Film-Coated Carbon Paste Electrode. Detection of DA was



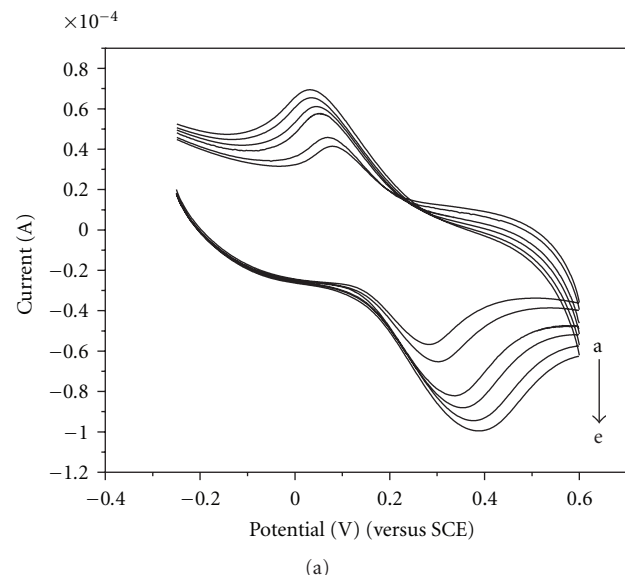
(a)



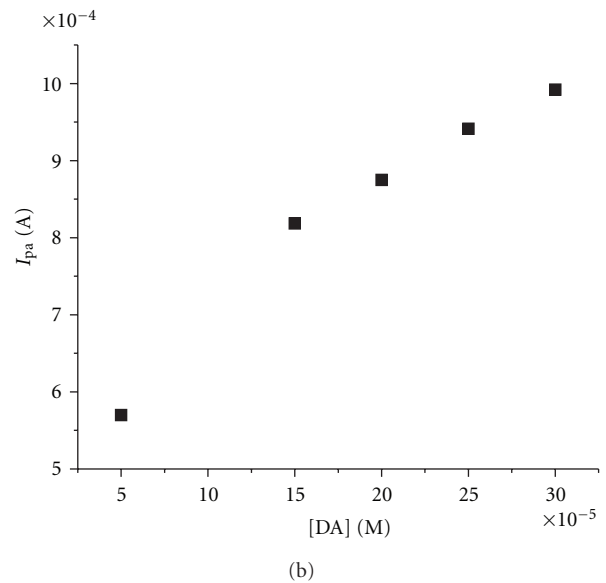
(b)

FIGURE 3: (a) Cyclic voltammogram of 5×10^{-5} M DA in 0.2 M phosphate buffer solution at different scan rate (a–g; 0.1 Vs^{-1} , 0.15 Vs^{-1} , 0.2 Vs^{-1} , 0.25 Vs^{-1} , 0.3 Vs^{-1} , 0.35 Vs^{-1} , and 0.4 Vs^{-1}). (b) Graph of current versus square root of scan rate.

very essential because it plays a very important role in the central nervous system and neurological disorders. DA being an easily oxidizable catecholamine, its voltammogram was recorded in the potential range from -0.25 to 0.6 V using 0.2 M phosphate buffer solution as a supporting electrolyte at 0.1 Vs^{-1} scan rate. Figure 2 showed a pair of redox peaks for 5×10^{-5} M DA at bare CPE (solid line) with E_{pa} at 0.2 V and E_{pc} 0.13 V (versus SCE) in 0.2 M phosphate buffer solution as a supporting electrolyte. The peak-to-peak separation (ΔE_p) was found to be 0.07 V. However, for the poly (gabapentin) film-coated carbon paste electrode, a pair of redox peaks was obtained with strong increase in both anodic and cathodic peak currents (dotted line). The E_{pa} was located at 0.28 V, and the corresponding cathodic peak potential was located



(a)



(b)

FIGURE 4: (a) Cyclic voltammogram for different concentrations of DA: (a) 5×10^{-5} M, (b) 15×10^{-5} M, (c) 20×10^{-5} M, (d) 25×10^{-5} M, and (e) 30×10^{-5} M at poly (gabapentin) film-coated carbon paste electrode with scan rate 0.1 Vs^{-1} . (b) Graph of current versus concentration of DA.

at 0.09 V (versus SCE). The peak-to-peak separation was calculated as 0.19 V. The cyclic voltammogram obtained for poly (gabapentin) film-coated carbon paste electrode was also quasireversible with good improvement in current signal of oxidation and reduction peaks.

3.3. Effect of Scan Rate. The scan rate effect was studied to understand the electrode process. Hence, the voltammogram of DA was recorded by varying the scan rate at poly (gabapentin) film-coated carbon paste electrode. The cyclic voltammogram showed an increase in both anodic and cathodic peak currents of DA with an increase of scan rate

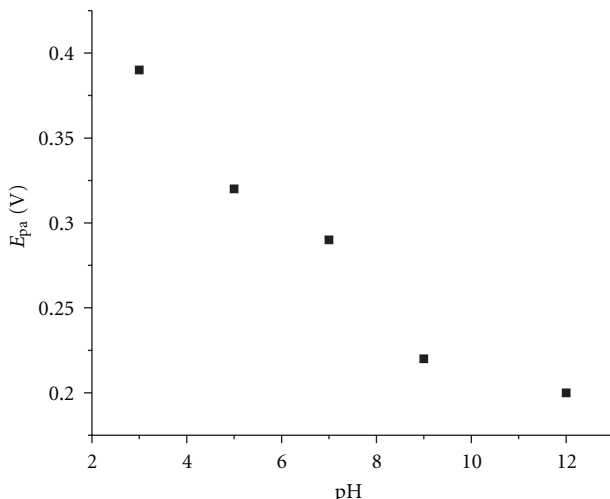


FIGURE 5: Graph of E_{pa} versus pH.

(Figure 3(a)) at the poly (gabapentin) film-coated carbon paste electrode in the range from 0.1 to 0.4 Vs⁻¹. The graph of current ($\ln I_{pa}$) versus $\ln v$ was plotted and the graph obtained was nearly straight line (Figure 3(b)). The slope was found to be 0.738 which lies in the middle of 0.5 and 1.0. Hence, the electrode transfer reaction was controlled by both adsorption and diffusion.

3.4. Effect of DA Concentration. The electrocatalytic oxidation of DA was carried out by varying the concentration at poly (gabapentin) film-coated carbon paste electrode (Figure 4(a)). With the increasing concentration of DA, both the I_{pa} and I_{pc} also increase, and the DA concentration was varied from 5×10^{-5} M to 30×10^{-5} M. The graph of I_{pa} versus concentration of DA shows an increase in electrochemical peak current (Figure 4(b)). The increase of concentration of DA is linearly proportion. The detection limit was calculated as reported in literature [23] and it was found to be 3.5×10^{-7} M.

3.5. Effect of pH. The electrochemical redox reaction of DA was generally dependent on pH. The effect of pH from 3 to 12 on the electrocatalytic oxidation of dopamine at poly (gabapentin) film-coated carbon paste electrode was studied. The current signals obtained for DA were dependant on pH. However, the better shape of the voltammogram of the redox peak obtained at pH 7 suggested it as an optimal pH value. We further studied the relationship between the anodic peak potential of dopamine and pH. Figure 5 shows the graph of E_{pa} versus pH. From the graph, it was found that the anodic peak potential negatively shifted with the increase in pH with slope 0.051 V indicating that equal number of protons and electrons take part in the reactions [23].

4. Conclusion

In this work, we chose gabapentin as a modifier to study the electrochemical response of an interesting neurotransmitter

DA. The fabricated poly (gabapentin) film-coated carbon paste electrode successfully enhanced both anodic and cathodic peak currents of DA when compared to bare carbon paste electrode. The increase in the concentration of DA results in an increase of electrochemical anodic and cathodic peak currents. The detection limit was found to be 3.5×10^{-7} M. We believe that this approach can readily be applied to the development of electrochemical sensors for other neurotransmitters.

References

- [1] M. T. Shreenivas, B. E. Kumara Swamy, U. Chandra, S. Sharath Shankar, J. G. Manjunatha, and B. S. Sherigara, "Electrochemical investigations of dopamine at chemically modified losartan carbon paste electrode: a cyclic voltammetric study," *International Journal of Electrochemical Science*, vol. 5, no. 6, pp. 774–781, 2010.
- [2] C. N. Lin, H. C. Liu, S. J. Tsai, T. Y. Liu, and C. J. Hong, "Association study for Parkinson's disease and a dopamine transporter gene polymorphism (1215A/G)," *European Neurology*, vol. 48, no. 4, pp. 207–209, 2002.
- [3] S. Sarre, Y. Michotte, P. Herregods, D. Deleu, N. De Klippe, and G. Ebinger, "High-performance liquid chromatography with electrochemical detection for the determination of levodopa, catecholamines and their metabolites in rat brain dialysates," *Journal of Chromatography*, vol. 575, no. 2, pp. 207–212, 1992.
- [4] C. L. Guan, J. Ouyang, Q. L. Li, B. H. Liu, and W. R. G. Baeyens, "Simultaneous determination of catecholamines by ion chromatography with direct conductivity detection," *Talanta*, vol. 50, no. 6, pp. 1197–1203, 2000.
- [5] F. B. Salem, "Spectrophotometric and titrimetric determination of catecholamines," *Talanta*, vol. 34, no. 9, pp. 810–812, 1987.
- [6] T. F. Kang, G. L. Shen, and R. Q. Yu, "Voltammetric behaviour of dopamine at nickel phthalocyanine polymer modified electrodes and analytical applications," *Analytica Chimica Acta*, vol. 354, no. 1–3, pp. 343–349, 1997.
- [7] C. R. Raj, K. Tokuda, and T. Ohsaka, "Electroanalytical applications of cationic self-assembled monolayers: square-wave voltammetric determination of dopamine and ascorbate," *Bioelectrochemistry*, vol. 53, no. 2, pp. 183–191, 2001.
- [8] R. N. Hegde, B. E. Kumara Swamy, N. P. Shetti, and S. T. Nandibewoor, "Electro-oxidation and determination of gabapentin at gold electrode," *Journal of Electroanalytical Chemistry*, vol. 635, no. 1, pp. 51–57, 2009.
- [9] A. J. Downard, A. D. Roddick, and A. M. Bond, "Covalent modification of carbon electrodes for voltammetric differentiation of dopamine and ascorbic acid," *Analytica Chimica Acta*, vol. 317, no. 1–3, pp. 303–310, 1995.
- [10] P. Zhang, F. H. Wu, G. C. Zhao, and X. W. Wei, "Selective response of dopamine in the presence of ascorbic acid at multi-walled carbon nanotube modified gold electrode," *Bioelectrochemistry*, vol. 67, no. 1, pp. 109–114, 2005.
- [11] U. Chandra, B. E. Kumara Swamy, O. Gilbert, M. Pandurangachar, and B. S. Sherigara, "Voltammetric resolution of dopamine in presence of ascorbic acid at polyvinyl alcohol modified carbon paste electrode," *International Journal of Electrochemical Science*, vol. 4, no. 10, pp. 1479–1488, 2009.
- [12] S. Reddy, B. E. Kumara Swamy, U. Chandra, B. S. Sherigara, and H. Jayadevappa, "Synthesis of CdO nanoparticles and

- their modified carbon paste electrode for determination of dopamine and ascorbic acid by using cyclic voltammetry technique," *International Journal of Electrochemical Science*, vol. 5, no. 1, pp. 10–17, 2010.
- [13] Rekha, B. E. K. Swamy, R. Deepa et al., "Electrochemical investigations of dopamine at chemically modified alcian blue carbon paste electrode: a cyclic voltammetric study," *International Journal of Electrochemical Science*, vol. 4, no. 6, pp. 832–845, 2009.
- [14] M. Pandurangachar, B. E. K. Swamy, U. Chandra, O. Gilbert, and B. S. Sherigara, "Simultaneous determination of dopamine, ascorbic acid and uric acid at poly(Patton and Reeder's) modified carbon paste electrode," *International Journal of Electrochemical Science*, vol. 4, no. 5, pp. 672–683, 2009.
- [15] O. Gilbert, U. Chandra, B. E. Kumara Swamy et al., "Poly (Alanine) modified carbon paste electrode for simultaneous detection of dopamine and ascorbic acid," *International Journal of Electrochemical Science*, vol. 3, pp. 1186–1195, 2008.
- [16] O. Gilbert, B. E. K. Swamy, U. Chandra, and B. S. Sherigara, "Electrocatalytic oxidation of dopamine and ascorbic acid at poly (Eriochrome Black-T) modified carbon paste electrode," *International Journal of Electrochemical Science*, vol. 4, no. 4, pp. 582–591, 2009.
- [17] S. S. Shankar, B. E. K. Swamy, U. Chandra, J. G. Manjunatha, and B. S. Sherigara, "Simultaneous determination of dopamine, uric acid and ascorbic acid with CTAB modified carbon paste electrode," *International Journal of Electrochemical Science*, vol. 4, no. 4, pp. 592–601, 2009.
- [18] R. R. Naik, B. E. K. Swamy, U. Chandra, E. Niranjana, B. S. Sherigara, and H. Jayadevappa, "Separation of ascorbic acid, dopamine and uric acid by acetone/water modified carbon paste electrode: a cyclic voltammetric study," *International Journal of Electrochemical Science*, vol. 4, no. 6, pp. 855–862, 2009.
- [19] M. J. McLean and B. E. Gidal, "Gabapentin dosing in the treatment of epilepsy," *Clinical Therapeutics*, vol. 25, no. 5, pp. 1382–1406, 2003.
- [20] A. A. Jensen, J. Mosbacher, S. Elg et al., "The anticonvulsant gabapentin (Neurontin) does not act through γ -aminobutyric acid-B receptors," *Molecular Pharmacology*, vol. 61, no. 6, pp. 1377–1384, 2002.
- [21] M. C. Walker and P. N. Patsalos, "Clinical pharmacokinetics of new antiepileptic drugs," *Pharmacology and Therapeutics*, vol. 67, no. 3, pp. 351–384, 1995.
- [22] N. B. Finnerup, H. Gottrup, and T. S. Jensen, "Anticonvulsants in central pain," *Expert Opinion on Pharmacotherapy*, vol. 3, no. 10, pp. 1411–1420, 2002.
- [23] U. Chandra, B. E. Kumara Swamy, O. Gilbert, and B. S. Sherigara, "Voltammetric resolution of dopamine in the presence of ascorbic acid and uric acid at poly (calmagite) film coated carbon paste electrode," *Electrochimica Acta*, vol. 55, no. 24, pp. 7166–7174, 2010.

Research Article

Anodic Determination of Acetylsalicylic Acid at a Mildly Oxidized Boron-Doped Diamond Electrode in Sodium Sulphate Medium

Codruța Cofan¹ and Ciprian Radovan²

¹Department of Chemistry, School of Pharmacy, University of Medicine and Pharmacy "Victor Babes" Timisoara, Piata E. Murgu, no. 2, 300041 Timisoara, Romania

²Laboratory of Electrochemistry, West University of Timisoara, Pestalozzi Street, no. 16, 300115 Timisoara, Romania

Correspondence should be addressed to Codruța Cofan, cofancodruta@umft.ro

Received 11 March 2011; Accepted 6 April 2011

Academic Editor: Bengi Uslu

Copyright © 2011 C. Cofan and C. Radovan. This is an open access article distributed under the Creative Commons Attribution License, which permits unrestricted use, distribution, and reproduction in any medium, provided the original work is properly cited.

Differential pulse voltammetry (DPV) and chronoamperometry (CA) were used to detect and determine acetylsalicylic acid (ASA) at a mildly oxidized boron-doped diamond (BDD) electrode in a neutral sodium sulphate solution as supporting electrolyte. ASA determination in unbuffered medium was achieved using neutralized standard and real samples. Over the concentration range of 0.01 mM–0.1 mM, linear calibration plots of anodic current peaks in DPV and anodic currents in CA experiments versus concentration were obtained with very high correlation coefficients and good sensitivity values. The limits of detection were situated around 1 μ M. The association of DPV and CA techniques with standard addition method represented a suitable option for the determination of ASA in real samples such as pharmaceutical formulations.

1. Introduction

Acetylsalicylic acid (ASA) or aspirin, the world's oldest and best known nonsteroidal anti-inflammatory drug, continues to receive special attention due to its clinical effects on inflammation, fever, renal function, and platelet aggregation [1, 2]. Recent studies have shown that administrated in specific dosages, aspirin has the ability to prevent cardiovascular events and different types of cancer and to reduce even the incidence of Alzheimer's disease occurrence [3–5]. ASA has also an antioxidant effect. In contrast, evidence proves that it induces formation of free-radicals which are involved in gastrointestinal damage and development of gastroduodenal ulcer [6–9]. After entering the bloodstream, acetylsalicylic acid is rapidly metabolized in salicylic acid (SA), the compound known to be primarily responsible for the pharmacological activity of ASA [1, 4, 10, 11]. The therapeutic action and the toxic effects of this widely consumed active substance promote ASA as a drug continuously subjected to extensive research.

A survey in the literature indicates a variety of analytical techniques used for the detection and determination of ace-

tylsalicylic acid. Generally, ASA is indirectly determined after the conversion to salicylic acid, its main hydrolysis product [4, 10]. The conventional "back-titration" method specified by British Pharmacopoeia and the Trinder reaction are methods of reference for the determination of ASA and salicylates, respectively [12–14]. In time, "back-titration" and Trinder reaction have been replaced by methods such as spectroscopy, mass spectrometry, UV-VIS spectrophotometry, spectrofluorimetry, gas chromatography, different types of liquid chromatography, and capillary electrophoresis. The latter methods, used independently or coupled with various detection modes, were applied for ASA investigation in biological fluids, pharmaceutical preparations, and even waste waters [4, 5, 10, 13, 15, 16]. The detection and determination of aspirin using the above-mentioned techniques have been achieved in both single [13, 15, 17, 18] and multicomponent systems [10, 19–29].

Acting as electroactive substance through salicylic acid, aspirin's main hydrolysis product, ASA has also been electrochemically studied from a mechanistic or analytical perspective, using a range of methods, electrode types, and, supporting electrolytes [12, 30–48].

Boron-doped diamond (BDD) is a very important material for electroanalysis, since it exhibits several electrochemically valuable properties such as its very wide electrochemical window in aqueous solutions resulting from the high overpotentials of the oxygen and hydrogen evolution reactions, low and stable voltammetric and amperometric background current, its excellent chemical and electrochemical stability in aggressive conditions, and its good responsiveness to a range of analytes without any conventional pretreatment [49–59].

Several important studies reported the determination of ASA in pharmaceutical formulations based on its hydrolysis to salicylate at controlled temperature conditions, using unmodified or modified graphite [30, 46], carbon paste [30] and glassy carbon [32, 33, 36, 37, 39, 47] electrodes, and different supporting electrolytes, some of them having the inconvenience of methanol [30, 33, 36], diethylether, or ethanol-diethylether [37] content.

Published data reports the use of a boron-doped diamond (BDD) electrode for the electrochemical evaluation of salicylic acid in acidic media [34]. At the same time, the voltammetric study of SA electrochemical oxidation at BDD electrode is merely presented. Mineralization of salicylic acid in acidic aqueous solution by electrochemical advanced oxidation processes using a BDD electrode as anode has also been explored [45]. Only one published paper [48] describes the determination of acetylsalicylic acid from pharmaceutical products by square-wave voltammetric data, using a specially treated boron-doped diamond electrode with very high overpotential for ASA oxidation in an H_2SO_4 medium and without a preliminary hydrolysis step.

This paper presents the cyclic voltammetry (CV) investigation and the determination of acetylsalicylic acid by anodic differential pulse voltammetry (DPV) and chronoamperometry (CA), using a stationary mildly oxidized unmodified BDDE and a very simple and easy accessible supporting electrolyte, a neutral sodium sulphate solution. The actual report continues by outlining specific applications of DPV and CA techniques explored at a BDD electrode coupled with standard addition method to the analysis of two commercialized pharmaceutical formulations.

2. Experimental

The electrochemical data were obtained from CV, DPV, and CA measurements. A Metrohm three-electrode cell equipped with a stabilized BDDE working electrode as a 3 mm diameter stationary disc embedded in a PEEK (PolyEtherEtherKetone) rod, a platinum foil counter-electrode, and a saturated calomel reference electrode (SCE), was used to perform the electrochemical measurements. The unmodified commercial boron-doped diamond electrode supplied by Windsor Scientific Ltd. for electroanalytical use was a mirror-polished doped polycrystalline industrial diamond (microcrystalline, doping degree cca. 0.1% boron) prestabilized in our laboratory by mild electrochemical oxidation at +2 V versus SCE in neutral and alkaline media and several hundreds repeated alternate polarization cycles between -1 and +2 V

versus SCE in acidic and neutral media. All voltammograms were collected using an Autolab PGstat 20 EcoChemie system controlled by a PC running GPES Software version 4.9. The CV measurements obtained corresponded to restricted potential limits ranged between 0 V and +1.25 V versus SCE and a scan rate between 0.005 and 0.03 Vs^{-1} , usually of 0.03 Vs^{-1} . Working parameters for the exemplified differential pulse voltammograms involved a modulation time of 0.05 s, an interval time of 0.25 s, an initial potential of 0 V, an end potential of 1.25 V, a step potential of 0.00405 V, a modulation amplitude of 0.02502 V, and a scan rate of 0.0162 Vs^{-1} . CVs, DPVs, and CAs were recorded at stationary electrode in quiescent solutions, in a controlled argon atmosphere, and at room temperature ($23 \pm 1^\circ\text{C}$).

Before starting each series of electrochemical measurements, the working electrode was carefully cleaned, degreased, and treated to remove fouling by polishing with alumina aqueous suspension, and finally thoroughly washed with double-distilled water. Each determination was repeated three times with good reproducibility of the practically stabilized state of electrode surface recovered by simple means of cleaning of the electrode, short resting period, and brief stirring of the solution between the successive measurements.

The supporting electrolyte was a 0.1 M Na_2SO_4 unbuffered solution, pH practically 7. The substances used were analytical grade Merck reagents. Acetylsalicylic acid standard solutions were freshly prepared at room temperature ($23 \pm 1^\circ\text{C}$), by addition of an NaOH diluted solution in order to transform the target substance into freely water-soluble salt. The explored concentrations of ASA for determination of a coherent electroanalytical method ranged between 0.01 and 0.1 mM in DPV exploration and between 0.01 and 0.09 mM in CA experiments. The higher investigated concentration ranges had no relevance for electroanalytical purpose, and a distinct access to a low limit of detection is being desirable.

The electroanalytical application of DPV and CA methods associated with standard addition method for detection and determination of acetylsalicylic acid was verified using *Aspirin* tablets (BAYER) and *Acid Acetilsalicilic* tablets (SICOMED). The real samples from pharmaceutical formulations were aqueous solutions freshly prepared by dissolution of *Aspirin* tablets and *Acid Acetilsalicilic* tablets, respectively. 250 mL as stock solutions were made up from a single *Aspirin* or *Acid Acetilsalicilic* tablet, under similar conditions as standard solutions. Very small volumes of the standard solutions were added to obtain the desired additional concentrations while maintaining a practically constant solution volume in the cell. The final working solution volume in the cell was 50 mL. All the dilutions of the investigated standard and real sample solutions were made using the simple, easy accessible, unbuffered sodium sulphate supporting electrolyte.

3. Results and Discussion

A series of cyclic voltammetry data recorded in a neutral unbuffered sodium sulphate solution used as supporting

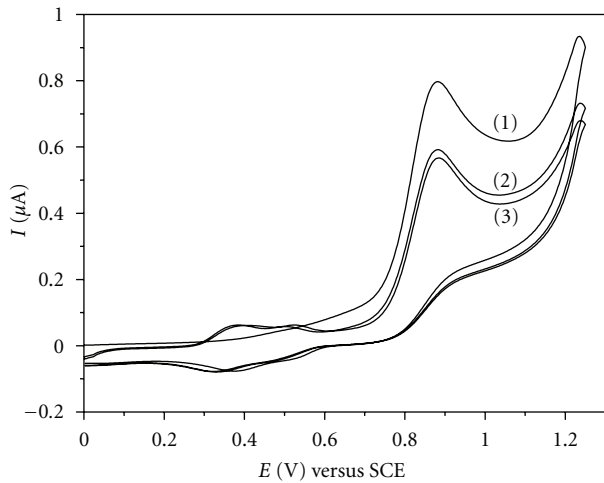


FIGURE 1: Cyclic voltammograms of 0.03 mM ASA. Supporting electrolyte: 0.1 M Na_2SO_4 pH 7; starting potential: 0 V versus SCE; potential range: 0 V \rightarrow +1.25 V \rightarrow 0 V versus SCE; scan rate: 0.03 Vs^{-1} ; (1)–(3): scan 1–scan 3.

electrolyte represented the starting point in evaluating the electrochemical behavior of ASA at an unmodified BDDE. Figure 1 depicts typical examples of anodic cyclic voltammetric responses corresponding to electrochemical oxidation of 0.03 mM ASA at an unmodified BDDE in a neutral 0.1 M Na_2SO_4 solution. The CV successive scans were collected in the potential range between 0 V versus SCE and +1.25 V versus SCE, starting in the positive direction from 0 V versus SCE, at a scan rate of 0.03 Vs^{-1} . On the forward branch of the first scan, a well-defined anodic current peak attributable to anodic oxidation of ASA disposed around +0.9 V versus SCE.

The practical overlapping of second and third scans disposed below the first one corresponded to a stationary state of diffusively controlled anodic process. Voltammograms for ASA solutions, with anodic and cathodic branches (obtained but not presented here in the figures), corresponded to an irreversible electrochemical behavior of the studied compound at an unmodified BDDE. Our work relates only to the analytically oriented investigations without any consideration of the mechanistic aspects.

The influence of the scan rate on ASA anodic oxidation at BDDE in unbuffered 0.1 M Na_2SO_4 solution (pH 7) has been investigated for 0.03 mM ASA final concentration in the electrochemical cell, under cyclic voltammetric conditions. CV scans (see Figure 2) initiated by potential sweep in the positive direction starting from 0 V versus SCE were recorded for scan rates between 0.005 and 0.03 Vs^{-1} . A progressive increase of current peaks manifested around +0.9 V versus SCE and corresponding to ASA anodic oxidation was remarked while increasing scan rate.

The diffusively controlled anodic oxidation process of ASA at BDDE and the absence of adsorbed reaction products on electrode surface were confirmed by the linear dependency and zero intercept of anodic current peak, I , versus

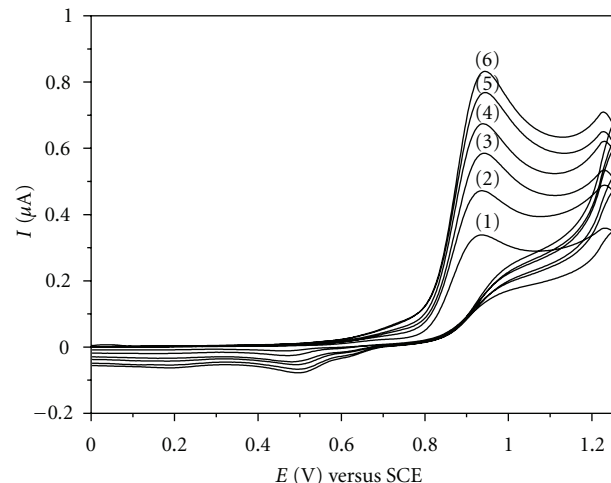


FIGURE 2: Cyclic voltammograms of 0.03 mM ASA. Effect of scan rate: (1) 0.005 Vs^{-1} , (2) 0.01 Vs^{-1} , (3) 0.015 Vs^{-1} , (4) 0.02 Vs^{-1} , (5) 0.025 Vs^{-1} , (6) 0.03 Vs^{-1} ; supporting electrolyte: 0.1 M Na_2SO_4 pH 7; starting potential: 0 V versus SCE; potential range: 0 V \rightarrow +1.25 V \rightarrow 0 V versus SCE.

square root of scan rate, $v^{1/2}$ ($I = 4.82v^{1/2}$, where I (μA), v (Vs^{-1})) obtained with very good values of determination parameter ($R^2 = 0.999$).

In addition, besides the good reproducibility and the detailed aspect regarding the control of anodic process by diffusion, the less positive potential of current peaks comparatively with literature data obtained at a strong oxidized BDD electrode [48] can be mentioned.

ASA concentration effect (not presented here) on the optimum anodic response in CV exploration at an unmodified BDDE using a neutral sodium sulphate solution as supporting electrolyte was also evaluated. The series of CVs obtained for ASA standard solution were recorded over the concentration range of 0.01 mM–0.08 mM. Calibration plot data of anodic current peaks versus concentration of ASA exhibited good linearity and sensitivity (see Table 1). LOD value of 1.02 μM has been calculated according to $3\sigma/\text{slope}$ criterion, where σ was estimated as the standard deviation applied to the net amperometric signal measured for the lowest analyte concentration corresponding to calibration plot and RSD ranged between 2 and 3%.

After this preliminary discussion of cyclic voltammetry data, and confirmation of a diffusively controlled anodic process, more detailed investigations with electroanalytical application purposes were conducted using two other different techniques, differential pulse voltammetry, and chronoamperometry.

3.1. Differential Pulse Voltammetry Data. A series of anodic DPVs presented in Figure 3 involving ASA concentration effect at an unmodified BDDE in a 0.1 M Na_2SO_4 (pH 7) supporting electrolyte were recorded over the concentration range of 0.01 mM–0.1 mM and using ASA standard solution.

Under conditions of the applied parameters of differential pulse voltammetry technique, sharp and well-defined

TABLE 1: Parameters of calibration plots ($I = aC + b$; I (μ A); a (μ A mM $^{-1}$); C (mM); b (μ A)), determination coefficient, and LOD values for acetylsalicylic acid (ASA) determination using CV, DPV, and CA methods.

Figure	Method	Concentration range (mM)	Regression equation of linear calibration plot	Sensitivity (μ A mM $^{-1}$)	R^2	LOD (μ M)
—	CV	0.01–0.08	$I = 24.175C + 0.039$	24.175	0.998	1.02
Figure 3	DPV	0.01–0.1	$I = 12.86C + 0.041$	12.86	0.998	1.03
Figure 5	CA	0.01–0.09	$I = 5.684C - 0.009$	5.684	0.997	1.03
Figure 6	CA ^a	0.01–0.08	$I = 21.397C + 0.034$	21.397	0.998	1.08

^a Continuous addition, stirred solution.

current peaks corresponding to ASA oxidation manifested around +0.9 V versus SCE.

Calibration plot (for calibration data, see Table 1) of anodic current peak, I , versus ASA concentration showed a satisfactory high sensitivity of $12.86 \mu\text{A mM}^{-1}$ and a very good linearity with a determination coefficient, $R^2 = 0.998$. LOD value of $1.03 \mu\text{M}$, very close to that one obtained when using CV technique, was calculated according to the same $3\sigma/\text{slope}$ criterion previously mentioned.

The potential usefulness of DPV method at the determination of ASA content in real sample solutions was verified using aqueous solutions from tablets of *Aspirin* (BAYER) and *Acid Acetilsalicilic* (SICOMED), respectively.

Figure 4(a) depicts a series of DPVs as an example involving ASA determination in an *Aspirin* real sample solution. The exemplified tested real sample was prepared under the conditions mentioned in the experimental part and using a 0.5953 g *Aspirin* tablet. 0.2 mL *Aspirin* initial solution was diluted to 50 mL final volume in 0.1 M Na_2SO_4 (pH 7) supporting electrolyte (0.2/50 dilution), and very small volumes of ASA standard solution were then added. ASA final supplementary concentrations in the tested real sample were 0.01 mM and 0.02 mM, respectively. Value of 473.9 mg ASA/tablet represented the average content determined using anodic DPV technique at BDDE associated with standard addition method. The investigation of 5 *Aspirin* tablets with an average weight of 0.5946 g led to a value of 471.2 mg ASA/tablet. According to the general BAYER product specification, each single tablet should contain 500 mg ASA.

A similar evaluation, Figure 4(b), corresponding to ASA determination was conducted using an aqueous real sample prepared from a 0.5925 g *Acid Acetilsalicilic* tablet. Practical results following application of DPV associated with standard addition method gave a content of 477.1 mg ASA/tablet. An average content of 472.2 mg ASA/tablet was obtained when investigating 5 *Acid Acetilsalicilic* tablets with 0.5917 g average weight. ASA content value in *Acid Acetilsalicilic* tablets indicated by the SICOMED supplier was 500 mg/tablet.

The matrix effects, which can be attributed to particular ingredients present in the tablets, were insignificant in their impact on quantitative evaluation of ASA in real samples.

3.2. Chronoamperometry Data. The preliminary evaluation of cyclic voltammetric data for the detection and determination of acetylsalicylic acid at an unmodified BDDE using as supporting electrolyte a neutral unbuffered sodium sulphate

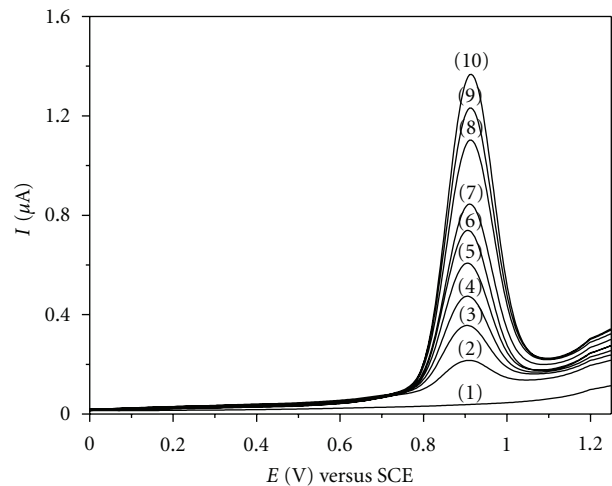


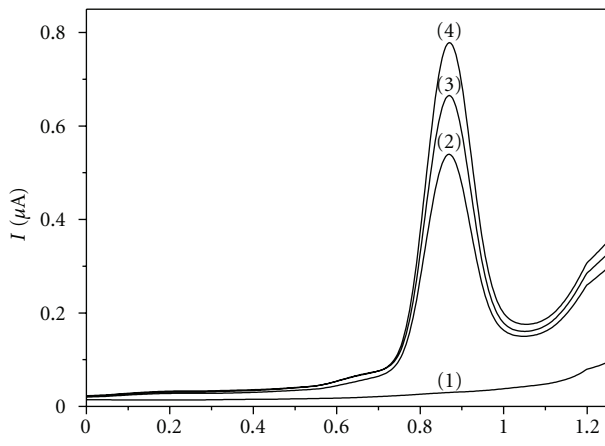
FIGURE 3: Differential Pulse Voltammograms. Effect of ASA concentration: (1) supporting electrolyte, (2) 0.01 mM, (3) 0.02 mM, (4) 0.03 mM, (5) 0.04 mM, (6) 0.05 mM, (7) 0.06 mM, (8) 0.08 mM, (9) 0.09 mM, (10) 0.1 mM; supporting electrolyte: 0.1 M Na_2SO_4 pH 7.

solution, constituted, as already mentioned, a basis for the chronoamperometric study of ASA electrochemical behavior at the same working electrode.

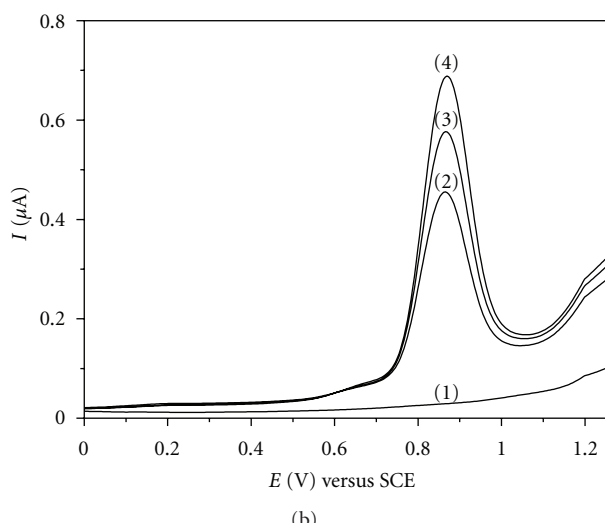
The detailed investigation using the chronoamperometry (CA) method, similar to our former study [57] at a fixed potential and sufficient time for a conventionally quasistationary state, was conducted to establish several working conditions and calibration plots data available as support for applications in practical analytical purposes, that is, the determination of ASA content in real samples obtained from pharmaceutical formulations.

Figure 5 shows a series of chronoamperograms regarding the effect of ASA concentration on the useful anodic response at unmodified BDDE, using standard solutions in 0.1 M Na_2SO_4 (pH 7) supporting electrolyte.

The tested analyte was added in increasing concentration, from 0.01 mM to 0.09 mM, and chronoamperograms were recorded at one potential level, +0.9 V versus SCE, which corresponded to optimum ASA anodic amperometric signal. Calibration plot of anodic currents read at 120 s (a sufficient time period for obtaining a conventional steady state) versus ASA concentration (see Table 1) was linear, presenting a very good determination parameter ($R^2 = 0.997$) and a satisfactory sensitivity value ($5.68 \mu\text{A mM}^{-1}$). Under these conditions



(a)



(b)

FIGURE 4: (a) Differential pulse voltammograms. (1) supporting electrolyte; (2) 0.2/50 dilution of *Aspirin* initial solution in supporting electrolyte; (3) 0.2/50 dilution of *Aspirin* initial solution in supporting electrolyte and ASA addition, 0.01 mM ASA final supplementary concentration; (4) 0.2/50 dilution of *Aspirin* initial solution in supporting electrolyte and ASA addition, 0.02 mM ASA final supplementary concentration; supporting electrolyte: 0.1 M Na_2SO_4 pH 7. (b) Differential pulse voltammograms. (1) supporting electrolyte; (2) 0.2/50 dilution of *Acid Acetilsalicilic* initial solution in supporting electrolyte; (3) 0.2/50 dilution of *Acid Acetilsalicilic* initial solution in supporting electrolyte and ASA addition, 0.01 mM ASA final supplementary concentration; (4) 0.2/50 dilution of *Acid Acetilsalicilic* initial solution in supporting electrolyte and ASA addition, 0.02 mM ASA final supplementary concentration; supporting electrolyte: 0.1 M Na_2SO_4 pH 7.

and according to $3\sigma/\text{slope}$ criterion, the calculated LOD was $1.03 \mu\text{M}$.

A continuous chronoamperogram (see Figure 6) recorded at one potential level, +0.9 V versus SCE, and over the concentration range of 0.01 mM–0.08 mM, was obtained under the conditions of progressive addition, in a stepwise fashion, of an ASA standard solution to the stirred solution of

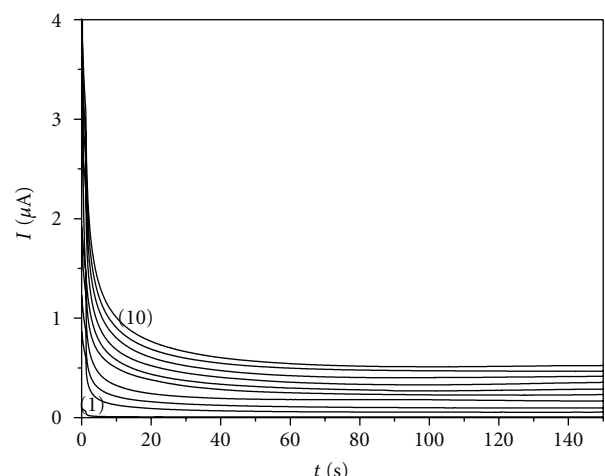


FIGURE 5: Chronoamperograms. Effect of ASA concentration at one potential level, +0.9 V versus SCE, around the corresponding current peak potential from CVs. (1) supporting electrolyte, (2) 0.01 mM, (3) 0.02 mM, (4) 0.03 mM, (5) 0.04 mM, (6) 0.05 mM, (7) 0.06 mM, (8) 0.07 mM, (9) 0.08 mM, (10) 0.09 mM; supporting electrolyte: 0.1 M Na_2SO_4 pH 7.

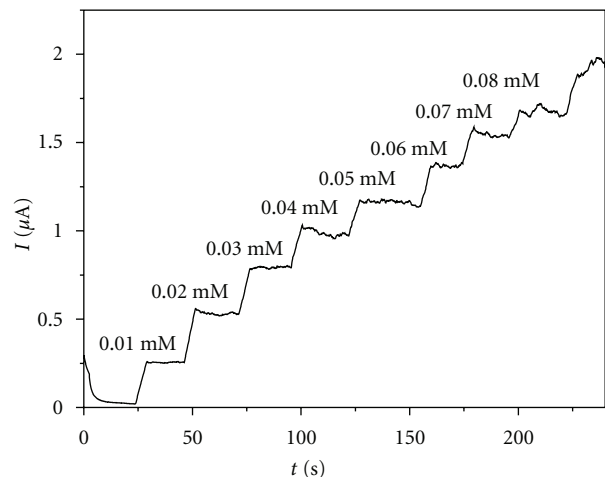


FIGURE 6: Continuous chronoamperogram at one potential level, +0.9 V versus SCE, around the corresponding current peak potential from CVs; progressive addition of ASA in the concentration range of 0.01 mM–0.08 mM; supporting electrolyte: 0.1 M Na_2SO_4 pH 7; stirred solution.

0.1 M Na_2SO_4 supporting electrolyte. No fouling of electrode surface occurred over the above-mentioned concentration range, characteristic aspect which suggested the further application of a BDD electrode as sensor for continuous ASA determination.

Linear plot (for calibration data, see also Table 1) of anodic currents read at 25 s, 50 s, 75 s, ..., and 225 s, respectively, versus ASA concentration presented a high sensitivity of $21.397 \mu\text{A mM}^{-1}$ and a very good determination coefficient ($R^2 = 0.998$), and a $1.08 \mu\text{M}$ LOD value was determined.

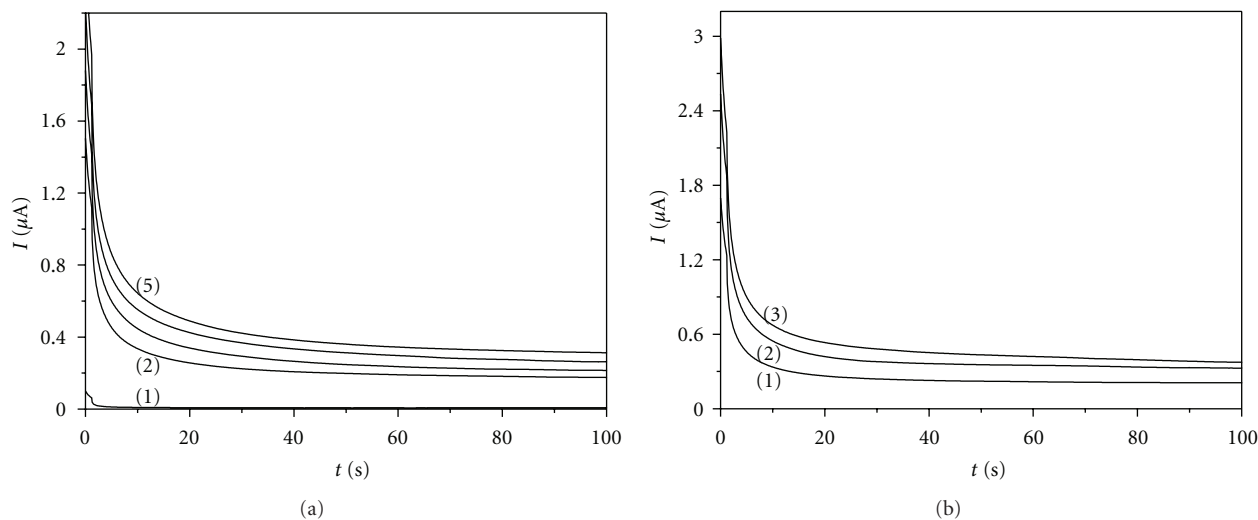


FIGURE 7: (a) Chronoamperograms, at one potential level, +0.9 V versus SCE. (1) supporting electrolyte; (2) 0.2/50 dilution of *Aspirin* initial solution in supporting electrolyte; (3) 0.2/50 dilution of *Aspirin* initial solution in supporting electrolyte and ASA addition, 0.01 mM ASA final supplementary concentration; (4) 0.2/50 dilution of *Aspirin* initial solution in supporting electrolyte and ASA addition, 0.02 mM ASA final supplementary concentration; (5) 0.2/50 dilution of *Aspirin* initial solution in supporting electrolyte and ASA addition, 0.03 mM ASA final supplementary concentration; supporting electrolyte: 0.1 M Na_2SO_4 pH 7; currents read at 100 s. (b) Chronoamperograms, at one potential level, +0.9 V versus SCE. (1) 0.2/50 dilution of *Acid Acetilsalicilic* initial solution in supporting electrolyte; (2) 0.2/50 dilution of *Acid Acetilsalicilic* initial solution in supporting electrolyte and ASA addition, 0.02 mM ASA final supplementary concentration; (3) 0.2/50 dilution of *Acid Acetilsalicilic* initial solution in supporting electrolyte and ASA addition, 0.03 mM ASA final supplementary concentration; supporting electrolyte: 0.1 M Na_2SO_4 pH 7; currents read at 100 s.

The utility of chronoamperometric method for the assessment of ASA in single component systems was suggested by the relatively high sensitivities, RSD values between 2 and 3%, and also by low values of limit of detection. Thus, the potential usefulness of the elaborated method was then verified by practical data of chronoamperometry associated with standard addition method obtained from ASA determination in real samples of *Aspirin* (BAYER) and *Acid Acetilsalicilic* (SICOMED).

Figure 7(a) illustrates an example of chronoamperograms recorded at one potential level, +0.9 V versus SCE, for a real sample of *Aspirin*, and for the mixture of real sample with ASA standard solution added to ensure 0.01 mM, 0.02 mM, and 0.03 mM ASA final supplementary concentrations in the system. In order to prepare the aqueous solution of real sample, a 0.5954 g *Aspirin* tablet was used according to the protocol described in the experimental section. A 0.2 mL *Aspirin* initial solution diluted to 50 mL volume with supporting electrolyte constituted the final volume of the real sample. Using CA technique coupled with standard addition method, the ASA average content in *Aspirin* real sample was 494.4 mg/tablet. It should be noted that the 491.7 mg ASA per tablet represented the average content determined when 5 *Aspirin* tablets with an average weight of 0.5951 g were investigated. According to the BAYER product specification, one *Aspirin* tablet contains 500 mg acetylsalicylic acid.

The other example of ASA determination in pharmaceutical formulations refers to using of an *Acid Acetilsalicilic* (SICOMED) aqueous solution. The initial solution of

real sample was prepared by solubilization of a 0.5847 g *Acid Acetilsalicilic* tablet using the volume control regime described in the experimental part. The real sample solution resulted from 0.2 mL *Acid Acetilsalicilic* initial solution diluted to 50 mL final volume with sodium sulphate supporting electrolyte (0.2/50 dilution). Very small volumes corresponding to final concentrations of 0.02 mM and 0.03 mM ASA standard solutions were added in the real sample and chronoamperograms at the same one potential level, +0.9 V versus SCE, were recorded (see Figure 7(b)). Thus, for the chosen example, the determined average content was 467.9 mg ASA/tablet. ASA content value in *Acid Acetilsalicilic* tablets indicated by the SICOMED supplier was 500 mg ASA per tablet. The investigation of 5 *Acid Acetilsalicilic* tablets with an average weight of 0.5842 g gave an average content of 466.3 mg ASA/tablet.

The association of differential pulse voltammetry, and chronoamperometry techniques with standard addition method proved to be very useful in analytical evaluation of both ASA-containing pharmaceutical products, *Aspirin* (BAYER) and *Acid Acetilsalicilic* (SICOMED). The matrix effects which can be attributed to the presence of adjacent inactive ingredients in pharmaceutical formulations were relatively minor and did not significantly perturb ASA determination. The average analytical data obtained for both pharmaceutical preparations corresponded to very good degrees of component recovery.

Linear calibration data and LOD values obtained are summarized in Table 1.

4. Conclusions

The detection and determination of acetylsalicylic acid by differential pulse voltammetry and chronoamperometry using a mildly oxidized boron-doped diamond electrode and an easily accessible, simple unbuffered sodium sulphate solution as supporting electrolyte has been achieved.

Very good linearities of the calibration plots of anodic current peaks and anodic currents, respectively, versus ASA concentration resulted from DPV and CA data. Adjacent analytical data regarding RSD, LOD, and sensitivities were obtained.

The association of differential pulse voltammetric and chronoamperometric methods with standard addition method has been successfully used for a fast analytical evaluation of pharmaceutical formulations which contain acetylsalicylic acid without significant matrix effects. The average content of ASA in BAYER and SICOMED tablets, explored as real samples, was measured in good accordance with those indicated by the suppliers.

References

- [1] Y. Ding and C. D. Garcia, "Determination of nonsteroidal anti-inflammatory drugs in serum by microchip capillary electrophoresis with electrochemical detection," *Electroanalysis*, vol. 18, no. 22, pp. 2202–2209, 2006.
- [2] M. Farré, M. Petrovic, and D. Barceló, "Recently developed GC/MS and LC/MS methods for determining NSAIDs in water samples," *Analytical and Bioanalytical Chemistry*, vol. 387, no. 4, pp. 1203–1214, 2007.
- [3] I. Farinelli and P. Martelletti, "Aspirin and tension-type headache," *Journal of Headache and Pain*, vol. 8, no. 1, pp. 49–55, 2007.
- [4] A. Battezzati, G. Fiorillo, A. Spadafranca, S. Bertoli, and G. Testolin, "Measurement of salicylic acid in human serum using stable isotope dilution and gas chromatography-mass spectrometry," *Analytical Biochemistry*, vol. 354, no. 2, pp. 274–278, 2006.
- [5] M. J. Scotter, D. P. T. Roberts, L. A. Wilson, F. A. C. Howard, J. Davis, and N. Mansell, "Free salicylic acid and acetylsalicylic acid content of foods using gas chromatography-mass spectrometry," *Food Chemistry*, vol. 105, p. 273, 2007.
- [6] L. Campanella, A. Bonanni, D. Bellantoni, G. Favero, and M. Tomassetti, "Comparison of fluorimetric, voltammetric and biosensor methods for the determination of total antioxidant capacity of drug products containing acetylsalicylic acid," *Journal of Pharmaceutical and Biomedical Analysis*, vol. 36, no. 1, pp. 91–99, 2004.
- [7] A. Guerrero, J. A. González-Correa, M. M. Arrebola, J. Muñoz-Marín, F. Sánchez De La Cuesta, and J. P. De La Cruz, "Antioxidant effects of a single dose of acetylsalicylic acid and salicylic acid in rat brain slices subjected to oxygen-glucose deprivation in relation with its antiplatelet effect," *Neuroscience Letters*, vol. 358, no. 3, pp. 153–156, 2004.
- [8] G. Şener-MuratoGlu, K. PaskaloGlu, S. Arbak, C. HürdaG, and G. AyanoGlu-Dülger, "Protective effect of famotidine, omeprazole, and melatonin against acetylsalicylic acid-induced gastric damage in rats," *Digestive Diseases and Sciences*, vol. 46, no. 2, pp. 318–330, 2001.
- [9] A. Polat and M. H. Emre, "Effects of melatonin or acetylsalicylic acid on gastric oxidative stress after bile duct ligation in rats," *Journal of Gastroenterology*, vol. 41, no. 5, pp. 433–439, 2006.
- [10] J. A. Murillo Pulgarín, A. Alañón Molina, P. Fernández López, and I. Sánchez-Ferrer Robles, "Direct determination of closely overlapping drug mixtures of diflunisal and salicylic acid in serum by means of derivative matrix isopotential synchronous fluorescence spectrometry," *Analytica Chimica Acta*, vol. 583, no. 1, pp. 55–62, 2007.
- [11] M. M. Karim, H. S. Lee, Y. S. Kim, H. S. Bae, and S. H. Lee, "Analysis of salicylic acid based on the fluorescence enhancement of the As(III)-salicylic acid system," *Analytica Chimica Acta*, vol. 576, no. 1, pp. 136–139, 2006.
- [12] M. S. M. Quintino, D. Corbo, M. Bertotti, and L. Angnes, "Amperometric determination of acetylsalicylic acid in drugs by batch injection analysis at a copper electrode in alkaline solutions," *Talanta*, vol. 58, no. 5, pp. 943–949, 2002.
- [13] A. V. Pereira, C. Aniceto, and O. Fatibello-Filho, "Flow injection spectrophotometric determination of acetylsalicylic acid in tablets after on-line microwave-assisted alkaline hydrolysis," *Analyst*, vol. 123, no. 5, pp. 1011–1015, 1998.
- [14] J. M. García, A. I. Jiménez, F. Jiménez, and J. J. Arias, "Simultaneous determination of salicylamide, acetylsalicylic acid and salicylic acid by multi-wavelength spectrophotometric methods," *Analytical Letters*, vol. 29, no. 2, pp. 249–263, 1996.
- [15] A. B. Moreira, I. L. T. Dias, G. O. Neto, E. A. G. Zagatto, and L. T. Kubota, "Solid-phase fluorescence spectroscopy for the determination of acetylsalicylic acid in powdered pharmaceutical samples," *Analytica Chimica Acta*, vol. 523, no. 1, pp. 49–52, 2004.
- [16] M. M. Sena, M. G. Trevisan, and R. J. Poppi, "Combining standard addition method and second-order advantage for direct determination of salicylate in undiluted human plasma by spectrofluorimetry," *Talanta*, vol. 68, no. 5, pp. 1707–1712, 2006.
- [17] S. O. Algar, N. R. Martos, and A. M. Díaz, "Fast and single solid phase fluorescence spectroscopic batch procedure for (acetyl) salicylic acid determination in drug formulations," *Journal of Pharmaceutical and Biomedical Analysis*, vol. 31, no. 3, pp. 439–446, 2003.
- [18] A. Ruiz-Medina, M. L. Fernández-de Córdova, P. Ortega-Barrales, and A. Molina-Díaz, "Flow-through UV spectrophotometric sensor for determination of (acetyl)salicylic acid in pharmaceutical preparations," *International Journal of Pharmaceutics*, vol. 216, no. 1-2, pp. 95–104, 2001.
- [19] E. Mikami, T. Goto, T. Ohno, H. Matsumoto, and M. Nishida, "Simultaneous analysis of dehydroacetic acid, benzoic acid, sorbic acid and salicylic acid in cosmetic products by solid-phase extraction and high-performance liquid chromatography," *Journal of Pharmaceutical and Biomedical Analysis*, vol. 28, no. 2, pp. 261–267, 2002.
- [20] Z. Kokot and K. Burda, "Simultaneous determination of salicylic acid and acetylsalicylic acid in aspirin delayed-release tablet formulations by second-derivative UV spectrophotometry," *Journal of Pharmaceutical and Biomedical Analysis*, vol. 18, no. 4-5, pp. 871–875, 1998.
- [21] M. M. Karim, C. W. Jeon, H. S. Lee et al., "Simultaneous determination of acetylsalicylic acid and caffeine in pharmaceutical formulation by first derivative synchronous fluorimetric method," *Journal of Fluorescence*, vol. 16, no. 5, pp. 713–721, 2006.
- [22] Z. Bouhsain, S. Garrigues, and M. De La Guardia, "PLS-UV spectrophotometric method for the simultaneous determination of paracetamol, acetylsalicylic acid and caffeine in

- pharmaceutical formulations," *Fresenius' Journal of Analytical Chemistry*, vol. 357, no. 7, pp. 973–976, 1997.
- [23] A. Navalón, R. Blanc, M. Del Olmo, and J. L. Vilchez, "Simultaneous determination of naproxen, salicylic acid and acetylsalicylic acid by spectrofluorimetry using partial least-squares (PLS) multivariate calibration," *Talanta*, vol. 48, no. 2, pp. 469–475, 1999.
 - [24] M. R. Gomez, R. A. Olsina, L. D. Martínez, and M. F. Silva, "Simultaneous determination of cloramphenicol, salicylic acid and resorcinol by capillary zone electrophoresis and its application to pharmaceutical dosage forms," *Talanta*, vol. 61, no. 2, pp. 233–238, 2003.
 - [25] M. L. Altun, T. Ceyhan, M. Kartal, T. Atay, N. Ozdemir, and S. Cevheroglu, "LC method for the analysis of acetylsalicylic acid, caffeine and codeine phosphate in pharmaceutical preparations," *Journal of Pharmaceutical and Biomedical Analysis*, vol. 25, no. 1, pp. 93–101, 2001.
 - [26] S. T. Eberhart, A. Hatzis, and R. Rothchild, "Quantitative NMR assay for aspirin, phenacetin, and caffeine mixtures with 1,3,5-trioxane as internal standard," *Journal of Pharmaceutical and Biomedical Analysis*, vol. 4, no. 2, pp. 147–154, 1986.
 - [27] E. R. Montgomery, S. Taylor, J. Segretario, E. Engler, and D. Sebastian, "Development and validation of a reversed-phase liquid chromatographic method for analysis of aspirin and warfarin in a combination tablet formulation," *Journal of Pharmaceutical and Biomedical Analysis*, vol. 15, no. 1, pp. 73–82, 1996.
 - [28] F. A. El-Yazbi, H. H. Hammud, and S. A. Assi, "Derivative-ratio spectrophotometric method for the determination of ternary mixture of aspirin, paracetamol and salicylic acid," *Spectrochimica Acta. Part A*, vol. 68, no. 2, pp. 275–278, 2007.
 - [29] V. Pucci, R. Mandrioli, M. A. Raggi, and S. Fanali, "Reversed-phase capillary electrochromatography for the simultaneous determination of acetylsalicylic acid, paracetamol, and caffeine in analgesic tablets," *Electrophoresis*, vol. 25, no. 4-5, pp. 615–621, 2004.
 - [30] V. Supalkova, J. Petrek, L. Havel et al., "Electrochemical sensors for detection of acetylsalicylic acid," *Sensors*, vol. 6, no. 11, pp. 1483–1497, 2006.
 - [31] K. Selinger and W. C. Purdy, "The determination of salicylic acid and its metabolites in blood plasma by high-performance liquid chromatography with amperometric detection," *Analytica Chimica Acta*, vol. 149, pp. 343–347, 1983.
 - [32] J. M. P. J. Garrido, J. L. F. C. Lima, and C. D. Matos, "Flow injection determination of acetylsalicylic acid in pharmaceutical preparations with an amperometric detector," *Collection of Czechoslovak Chemical Communications*, vol. 65, no. 6, pp. 954–962, 2000.
 - [33] A. A. J. Torriero, J. M. Luco, L. Sereno, and J. Raba, "Voltammetric determination of salicylic acid in pharmaceuticals formulations of acetylsalicylic acid," *Talanta*, vol. 62, no. 2, pp. 247–254, 2004.
 - [34] B. Louhichi, N. Bensalash, and A. Gadri, "Electrochemical oxidation of benzoic acid derivatives on boron doped diamond: voltammetric study and galvanostatic electrolyses," *Chemical Engineering and Technology*, vol. 29, no. 8, pp. 944–950, 2006.
 - [35] F. Montilla, P. A. Michaud, E. Morallón, J. L. Vázquez, and C. Comninellis, "Electrochemical oxidation of benzoic acid at boron-doped diamond electrodes," *Electrochimica Acta*, vol. 47, no. 21, pp. 3509–3513, 2002.
 - [36] D. Evans, J. P. Hart, and G. Rees, "Voltammetric behaviour of salicylic acid at a glassy carbon electrode and its determination in serum using liquid chromatography with amperometric detection," *Analyst*, vol. 116, no. 8, pp. 803–806, 1991.
 - [37] Y. S. Fung and S. F. Luk, "Determination of salicylic acid in pharmaceutical formulations and foods by differential-pulse voltammetry using a glassy carbon electrode," *Analyst*, vol. 114, no. 8, pp. 943–945, 1989.
 - [38] J. C. B. Fernandes, C. A. B. Garcia, L. A. Grandin, G. De Oliveira Neto, and O. E. S. Godinho, "Determination of acetylsalicylic acid in tablets with salicylate ion selective electrode in a batch injection analysis system," *Journal of the Brazilian Chemical Society*, vol. 9, no. 3, pp. 249–251, 1998.
 - [39] B. Muralidharan, G. Gopu, C. Vedhi, and P. Manisankar, "Voltammetric determination of analgesics using a montmorillonite modified electrode," *Applied Clay Science*, vol. 42, no. 1-2, pp. 206–213, 2008.
 - [40] B. G. Milagres, G. De Oliveira Neto, L. T. Kubota, and H. Yamanaka, "A new amperometric biosensor for salicylate based on salicylate hydroxylase immobilized on polypyrrole film doped with hexacyanoferrate," *Analytica Chimica Acta*, vol. 347, no. 1-2, pp. 35–41, 1997.
 - [41] H. Paseková, M. G. Sales, M. C. Montenegro, A. N. Araújo, and M. Polášek, "Potentiometric determination of acetylsalicylic acid by sequential injection analysis (SIA) using a tubular salicylate-selective electrode," *Journal of Pharmaceutical and Biomedical Analysis*, vol. 24, no. 5-6, pp. 1027–1036, 2001.
 - [42] V. J. F. Ferreira, A. C. V. Cavalheiro, E. Fagnani et al., "An electrode of the second kind for aspirin determination in tablet formulations," *Analytical Sciences*, vol. 15, no. 3, pp. 249–253, 1999.
 - [43] M. Neumayr, O. Friedrich, G. Sontag, and F. Pittner, "Flow-injection analysis with electrochemical detection for determination of salicylic acid in pharmaceutical preparations," *Analytica Chimica Acta*, vol. 273, no. 1-2, pp. 469–475, 1993.
 - [44] S. Majdi, A. Jabbari, and H. Heli, "A study of the electrocatalytic oxidation of aspirin on a nickel hydroxide-modified nickel electrode," *Journal of Solid State Electrochemistry*, vol. 11, no. 5, pp. 601–607, 2007.
 - [45] E. Guinea, C. Arias, P. L. Cabot et al., "Mineralization of salicylic acid in acidic aqueous medium by electrochemical advanced oxidation processes using platinum and boron-doped diamond as anode and cathodically generated hydrogen peroxide," *Water Research*, vol. 42, no. 1-2, pp. 499–511, 2008.
 - [46] C. Batchelor-McAuley and G. G. Wildgoose, "The influence of substrate effects when investigating new nanoparticle modified electrodes exemplified by the electroanalytical determination of aspirin on NiO nanoparticles supported on graphite," *Electrochemistry Communications*, vol. 10, no. 8, pp. 1129–1131, 2008.
 - [47] M. Houshmand, A. Jabbari, H. Heli, M. Hajjizadeh, and A. A. Moosavi-Movahedi, "Electrocatalytic oxidation of aspirin and acetaminophen on a cobalt hydroxide nanoparticles modified glassy carbon electrode," *Journal of Solid State Electrochemistry*, vol. 12, no. 9, pp. 1117–1128, 2008.
 - [48] E. R. Sartori, R. A. Medeiros, R. C. Rocha-Filho, and O. Fatibello-Filho, "Square-wave voltammetric determination of acetylsalicylic acid in pharmaceutical formulations using a boron-doped diamond electrode without the need of previous alkaline hydrolysis step," *Journal of the Brazilian Chemical Society*, vol. 20, no. 2, pp. 360–366, 2009.
 - [49] S. E. Coe and R. S. Sussmann, "Optical, thermal and mechanical properties of CVD diamond," *Diamond and Related Materials*, vol. 9, no. 9-10, pp. 1726–1729, 2000.
 - [50] M. Witek, J. Wang, J. Stotter et al., "Summary of recent progress with diamond electrodes in electroanalysis, spectroelectrochemistry and electrocatalysis," *Journal of Wide Bandgap Materials*, vol. 8, no. 3-4, pp. 171–188, 2001.

- [51] Y. V. Pleskov, "Electrochemistry of diamond," *Russian Journal of Electrochemistry*, vol. 38, no. 12, pp. 1275–1291, 2002.
- [52] M. C. Granger, J. Xu, J. W. Strojek, and G. M. Swain, "Polycrystalline diamond electrodes: basic properties and applications as amperometric detectors in flow injection analysis and liquid chromatography," *Analytica Chimica Acta*, vol. 397, no. 1–3, pp. 145–161, 1999.
- [53] R. G. Compton, J. S. Foord, and F. Marken, "Electroanalysis at diamond-like and doped-diamond electrodes," *Electroanalysis*, vol. 15, no. 17, pp. 1349–1363, 2003.
- [54] A. Kraft, "Doped diamond: a compact review on a versatile electrode material," *International Journal of Electrochemical Science*, vol. 2, p. 355, 2007.
- [55] C. Radovan and F. Manea, "Determination of sodium diethyldithiocarbamate in water by anodic voltammetry using a boron-doped diamond electrode," *Electroanalysis*, vol. 19, no. 1, pp. 91–95, 2007.
- [56] C. Radovan, C. Cofan, and D. Cinghiță, "Simultaneous determination of acetaminophen and ascorbic acid at an unmodified boron-doped diamond electrode by differential pulse voltammetry in buffered media," *Electroanalysis*, vol. 20, no. 12, pp. 1346–1353, 2008.
- [57] C. Cofan and C. Radovan, "Simultaneous chronoamperometric sensing of ascorbic acid and acetaminophen at a boron-doped diamond electrode," *Sensors*, vol. 8, no. 6, pp. 3952–3969, 2008.
- [58] C. Radovan, D. Cinghiță, F. Manea, M. Mincea, C. Cofan, and V. Ostafe, "Electrochemical sensing and assessment of parabens in hydro-alcoholic solutions and water using a boron-doped diamond electrode," *Sensors*, vol. 8, no. 7, pp. 4330–4349, 2008.
- [59] C. Cofan, C. Radovan, and D. Cinghiță, "Simultaneous anodic assessment of ascorbic acid and acetaminophen in unbuffered solutions," *Revista de Chimie*, vol. 60, no. 4, pp. 368–372, 2009.

Research Article

Enantioselective Potentiometric Membrane Electrodes Based on Antibiotics for the Determination of L- and D-Glyceric Acids

Raluca-Ioana Stefan-van Staden,¹ R'afat M. Nejem,² Jacobus Frederick van Staden,¹ and Hassan Y. Aboul-Enein³

¹ Laboratory of Electrochemistry and PATLAB Bucharest, National Institute of Research for Electrochemistry and Condensed Matter, 202 Splaiul Independentei Strada, 060021 Bucharest, Romania

² Department of Chemistry, Al-Aqsa University, Gaza, Palestine

³ The Pharmaceutical and Drug Industries Research Division, Pharmaceutical and Medicinal Chemistry Department, National Research Centre, Dokki, Cairo 12311, Egypt

Correspondence should be addressed to Raluca-Ioana Stefan-van Staden, iustinavanstaden@yahoo.com

Received 9 February 2011; Accepted 16 March 2011

Academic Editor: Bengi Uslu

Copyright © 2011 Raluca-Ioana Stefan-van Staden et al. This is an open access article distributed under the Creative Commons Attribution License, which permits unrestricted use, distribution, and reproduction in any medium, provided the original work is properly cited.

Glyceric acid (GA) is a human metabolite existing in L- and D-configurations, which are considered the markers for the diseases L- and D-glyceric aciduria/academia, respectively. Enantioselective, potentiometric membrane electrodes based on carbon paste modified with antibiotics as chiral selectors, vancomycin, and teicoplanin were designed for the assay of L- and D-GA, respectively, in the concentration ranges of 10^{-9} – 10^{-7} and 10^{-4} – 10^{-2} mol/L with very low detection limits (1.5×10^{-10} mol/L for L-GA and 1.6×10^{-4} mol/L for D-GA, resp.). The surface of the electrodes can be regenerated simply by polishing in order to obtain a fresh surface ready to be used in a new assay. The proposed electrodes can be successfully applied for the enantioanalysis of L- and D-glyceric acids in serum samples.

1. Introduction

The enantiomers of the urinary organic acids are important markers for inborn errors of metabolism. Accordingly, there is a growing demand for determining the metabolic products in human blood (academia) and urine (aciduria). Different enantiomers may originate from separate metabolic pathway, due to enzyme deficiency.

Glyceric acid (2,3-dihydroxypropionic acid, GA) is a human metabolite existing in L- and D-configurations. These two enantiomers are vital biological markers for the diagnosis of two different metabolic diseases, primary hyperoxaluria type II (L-glyceric aciduria, PH2) and D-glyceric aciduria [1–6]. Therefore, enantioselective analysis of glyceric acid is necessary to differentiate between the two inherited metabolic diseases.

Up to date, the assay of GA was done using capillary gas chromatography [7–10], liquid chromatography [11],

high-performance liquid chromatography [12], capillary electrophoresis [13], polarimetry [14], and colorimetric methods [15].

Enantioselective, potentiometric membrane electrodes (EPMEs) proved to be very reliable for the enantioanalysis of pharmaceutical compounds as well as of compounds of clinical importance [16]. Macro cyclic antibiotics represent a new class of chiral selectors used in the design of EPME, offering a high selectivity and enantioselectivity [17]. The macrocyclic antibiotics contain stereogenic centers and functional groups, which allow them to interact with chiral molecules by hydrophobic, dipole-dipole, π - π interactions, hydrogen bonding, steric repulsion [18, 19], and charge-to-charge repulsions [20–22].

This paper describes the design, response characteristics, (enantio) selectivity, and applications of two EPMEs based on vancomycin and teicoplanin for the enantioanalysis of GA.

TABLE 1: Response characteristics of enantioselective, potentiometric membrane electrodes for L- and D-glyceric acids^a.

EPME based on	Slope (mV/decade of concentration)	Parameters	Linear range (moL/L)	Detection limit (moL/L)
		Intercept, E ^o (mV)		
Vancomycin	58.6	574.6	10 ⁻⁹ –10 ⁻⁷	1.56 × 10 ⁻¹⁰
Teicoplanin	50.0	206.0	10 ⁻⁴ –10 ⁻²	7.60 × 10 ⁻⁵

^aAll measurements were made at 25°C; all values are the average of ten determinations.

2. Experimental

2.1. Electrode Design. Paraffin oil and graphite powder were mixed in a ratio of 1 : 4 (w/w) to form the carbon paste. The modified carbon pastes were obtained by the addition of the aqueous solutions of vancomycin (pH = 4) or teicoplanin (pH = 6) (10⁻³ moL/L) (100 µL chiral selector solution to 100 mg carbon paste) to the carbon paste. The unmodified carbon paste was filled into a plastic pipette peak leaving a space of 3-4 mm into the top to be filled with the modified carbon paste.

The diameter of the proposed EPMEs was 3 mm. Electric contact was obtained by inserting an Ag/AgCl wire into the carbon paste. 0.1 moL/L KCl was used as internal solution. All the sensors tips were gently rubbed on fine abrasive paper to produce a flat surface. The surface of the sensors was wetted with deionized water and then polished with an alumina paper (polished strips 30144-011, Orion) before use. When not in use, the electrodes were immersed in 10⁻³ moL/L of L- or D-glyceric acid solution, respectively.

2.2. Apparatus. A 663 VA Stand (Metrohm, Herisau, Switzerland) connected to a PGSTAT 100 and software (Eco Chemie version 4.9) was used for all potentiometric measurements. An Ag/AgCl (0.1 moL/L KCl) electrode was used as reference electrode in the cell.

2.3. Reagents and Materials. L- and D-glyceric acids, vancomycin, and teicoplanin were purchased from Sigma-Aldrich (USA). Graphite powder (1-2 µm) was purchased from Aldrich (Milwaukee, WI, USA); paraffin oil was purchased from Fluka (Buchs, Switzerland), and phosphate buffer (pH = 3.5) from Merck (Darmstadt, Germany).

Deionized water from a Modulab system (Continental Water Systems, San Antonio, Tex, USA) was used for all solutions preparation. L- and D-glyceric acid solutions were prepared from standard L- and D-GA solutions (1 × 10⁻¹ moL/L) by serial dilutions. Serum and urine samples were buffered with phosphate buffer (pH = 3.5), sample:buffer = 1 : 1.

2.4. Recommended Procedure. Direct potentiometry was used for potential determination of each standard solution (10⁻¹⁰–10⁻² moL/L). All measurements were performed at 25°C. The electrodes were placed in stirred standard solutions. Calibration graphs were obtained by plotting

E(mV) versus pL-GA or pD-GA, respectively. The unknown concentrations were determined from the calibration graphs.

3. Results and Discussion

3.1. EPMEs Response Characteristics. The response characteristics of the EPMEs were determined at pH = 3.5 (phosphate buffer) using the potentiometric method. The response obtained for L-GA was linear and near-Nernstian only for the EPME based on vancomycin, while the response obtained for D-GA was linear and near-Nernstian only for the EPME based on teicoplanin. The following are the equations of calibration for the EPMEs based on vancomycin and teicoplanin:

$$\begin{aligned} \text{L-GA: } E &= 574.6 - 58.6 \text{ pL-GA}, \quad r = 0.9957, \\ \text{D-GA: } E &= 206.0 - 50.0 \text{ pD-GA}, \quad r = 0.9988, \end{aligned} \quad (1)$$

where E (mV) is the potential of the electrochemical cell, pL-GA = $-\log[\text{L-GA}]$, pD-GA = $-\log[\text{D-GA}]$, and *r* is the correlation coefficient. The response characteristics of the EPMEs are shown in Table 1. A very low detection limit was recorded for the assay of L-GA: 10⁻¹⁰ moL/L magnitude order. The electrodes responses displayed a good stability and reproducibility for the tests performed for 3 months, when daily used for measurements (RSD < 1.0%).

The response time recorded for the assay of the D-enantiomer was 2 min while the response time recorded for the assay of the L-enantiomer was 30 s.

3.2. The Influence of pH on the Responses of the Electrodes. The effect of pH on the response of the electrodes was determined by recording the emf of the cell containing solutions of L- or D-GA of different pH values. The pHs of the solutions of the enantiomers were adjusted using small volumes of HCl (0.1 moL/L) or NaOH (0.1 moL/L) solutions. E (mV) versus pH plots (Figure 1) show that the emf is not depending on the pH in the ranges of 4–9 and 3–8 for vancomycin- and teicoplanin-based EPME, respectively.

3.3. Selectivity of the Electrode. The selectivity of both electrodes was checked using the mixed solutions method proposed by Ren [23], over L- or D-GA, creatine, and creatinine. The ratios between the concentrations of analyte and interferent were 1 : 10. The potentiometric selectivity coefficients (Table 2) obtained for EPMEs proved their

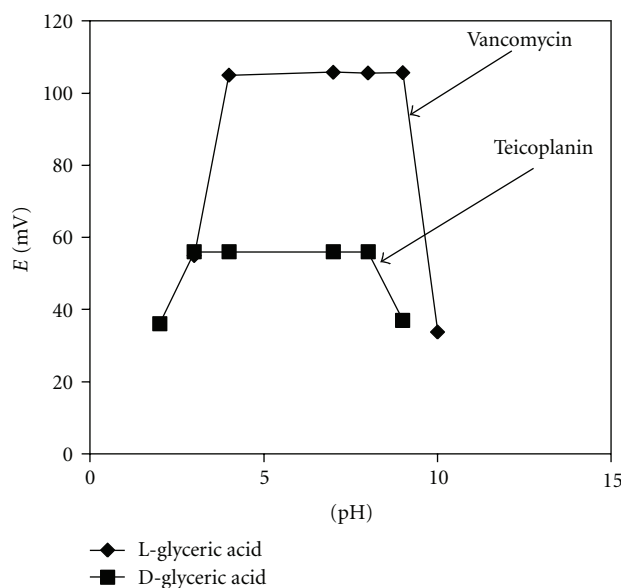


FIGURE 1: Effect of pH on the response of the EPMEs to L-glyceric acid (10^{-8} mol/L L-GA) and D-glyceric acid (10^{-3} mol/L) solutions. (I) Vancomycin-based EPME; (II) teicoplanin-based EPME.

TABLE 2: Potentiometric selectivity coefficients for the electrodes proposed for the assay of L- and D-glyceric acids^a.

Interference species (J)	$pK_{\text{sel}}^{\text{pot}}$	
	EPME based on Vancomycin	Teicoplanin
L-GA	—	2.39
D-GA	2.41	—
Creatine	2.09	2.08
Creatinine	2.41	2.39

^aAll measurements were made at 25°C; all values are the average of ten determinations.

TABLE 3: The results obtained for the determination of L-glyceric acid in the presence of D-glyceric acid^a.

L:D (mol/mol)	Recovery, %	
	Vancomycin-based EPME	Teicoplanin-based EPME
2:1	99.25 ± 0.01	—
1:1	99.75 ± 0.02	—
1:2	99.26 ± 0.06	—
1:4	99.30 ± 0.04	—
1:9	99.67 ± 0.06	—

^aAll measurements were made at 25°C; all values are the average of ten determinations.

enantioselectivity as well as their selectivity over creatine and creatinine. Inorganic cations such Na^+ , K^+ , and Ca^{2+} do not interfere in the analysis of L- and D-GA.

3.4. Analytical Applications. Solutions containing L- and D-GA in different ratios were prepared to test the recovery

TABLE 4: The results obtained for the determination of D-glyceric acid in the presence of L-glyceric acid^a.

D:L (mol/mol)	Recovery, %
2:1	99.96 ± 0.04
1:1	99.57 ± 0.03
1:2	99.99 ± 0.03
1:4	99.95 ± 0.02
1:9	99.93 ± 0.03

^aAll measurements were made at 25°C; all values are the average of ten determinations.

TABLE 5: Recovery of L-glyceric acid in serum and urine samples, (%)^a.

Type of sample	Sample no.	% Recovery, L-GA	
		Standard method [24]	EPMEs
Serum samples	1	98.47	98.52 ± 0.04
	2	98.15	98.08 ± 0.08
	3	98.02	98.00 ± 0.06
	4	99.30	99.25 ± 0.02
	5	99.50	99.49 ± 0.03
Urine samples	6	99.45	99.50 ± 0.03
	7	99.86	99.87 ± 0.02
	8	99.12	99.13 ± 0.01
	9	99.89	99.99 ± 0.02

^aAll measurements were made at 25°C; all values are the average of ten determinations.

TABLE 6: Recovery of D-glyceric acid in serum and urine samples, (%)^a.

Type of sample	Sample no.	% Recovery, D-GA	
		Standard method [24]	EPMEs
Serum samples	10	97.20	97.23 ± 0.02
	11	96.70	96.65 ± 0.03
	12	97.70	97.21 ± 0.08
Urine samples	13	99.20	99.18 ± 0.02
	14	99.50	99.48 ± 0.01
	15	99.93	100.00 ± 0.02
	16	99.43	99.40 ± 0.03
	17	99.15	99.12 ± 0.02
	18	99.11	99.13 ± 0.02

^aAll measurements were made at 25°C; all values are the average of ten determinations.

for each enantiomer in the presence of its antipode and the suitability of the EPMEs for the enantioanalysis of L- and D-GA in serum and urine samples. The recovery tests (Tables 3 and 4) obtained for each enantiomer proved the suitability of the electrodes for enantioanalysis. No significant differences in the recovery values were recorded for the ratios between L:D or D:L enantiomers varying from 1:9 to 1:99.99.

The results obtained for the analysis of L-glyceric and D-glyceric acid in serum and urine samples are shown in Tables 5 and 6, respectively. Different serum samples and urine samples were collected from different patients suspected of L-glyceric academia (1–3) or aciduria (4–9) and D-glyceric academia (10–12) or aciduria (13–18) for the recovery of L- and D-glyceric acid. All the serum and urine samples were buffered with phosphate buffer pH = 3.5. The results obtained using the proposed EPMEs are in good concordance with those obtained using the standard method, which is an HPLC technique [24]. The advantage of the proposed method over the standard one was the high reliability measured through low values of RSD (%), short time of analysis, and low cost of the enantioanalysis.

4. Conclusions

The macrocyclic antibiotics vancomycin and teicoplanin proved to be viable chiral selectors for the design of EPMEs. The enantioselective, potentiometric membranes electrodes proposed can be reliably used for the enantioselective analyses of L- and D-glyceric acids in serum and urine samples. Accordingly, they can be used for the fast and reliable diagnosis of L- or D-glyceric academia/aciduria. The construction of the electrodes is simple, fast, and reproducible. The serum and urine samples need only to be buffered with phosphate buffer of pH of 3.5 before L- and D-glyceric acids were determined.

References

- [1] H. E. Williams and L. H. Smith Jr., "L-glyceric aciduria. A new genetic variant of primary hyperoxaluria," *The New England Journal of Medicine*, vol. 278, no. 5, pp. 233–238, 1968.
- [2] E. Van Schaftingen, "D-Glycerate kinase deficiency as a cause of D-glyceric aciduria," *The FEBS Letters*, vol. 243, no. 2, pp. 127–131, 1989.
- [3] S. K. Wadman, M. Duran, and D. Ketting, "D glyceric acidemia in a patient with chronic metabolic acidosis," *Clinica Chimica Acta*, vol. 71, no. 3, pp. 477–484, 1976.
- [4] N. J. Brandt, S. Brandt, K. Rasmussen, and F. Schnoheyder, "Letter: hyperglycericacidaemia with hyperglycinemia: a new inborn error of metabolism," *British Medical Journal*, vol. 4, no. 5940, pp. 344–347, 1974.
- [5] E. Van Schaftingen, J. P. Draye, and F. Van Hoof, "Coenzyme specificity of mammalian liver D-glycerate dehydrogenase," *European Journal of Biochemistry*, vol. 186, no. 1-2, pp. 355–359, 1989.
- [6] P. D. Dawkins and F. Dickens, "The oxidation of d- and l-glycerate by rat liver," *The Biochemical Journal*, vol. 94, pp. 353–367, 1965.
- [7] A. Kaunzinger, A. Rechner, T. Beck, A. Mosandl, A. C. Sewell, and H. Böhles, "Chiral compounds as indicators of inherited metabolic disease: simultaneous stereodifferentiation of lactic-, 2-hydroxyglutaric- and glyceric acid by enantioselective cGC," *Enantiomer*, vol. 1, no. 3, pp. 177–182, 1996.
- [8] J. P. Kamerling, G. J. Gerwig, J. F. G. Vliegenthart, M. Duran, D. Ketting, and S. K. Wadman, "Determination of the configurations of lactic and glyceric acids from human serum and urine by capillary gas-liquid chromatography," *Journal of Chromatography B*, vol. 143, no. 2, pp. 117–123, 1977.
- [9] D. J. Dietzen, T. R. Wilhite, D. N. Kenagy, D. S. Milliner, C. H. Smith, and M. Landt, "Extraction of glyceric and glycolic acids from urine with tetrahydrofuran: utility in detection of primary hyperoxaluria," *Clinical Chemistry*, vol. 43, no. 8, pp. 1315–1320, 1997.
- [10] M. Petrarulo, C. Vitale, P. Facchini, and M. Marangella, "Biochemical approach to diagnosis and differentiation of primary hyperoxalurias: an update," *Journal of Nephrology*, vol. 11, supplement 1, pp. 23–28, 1998.
- [11] M. S. Rashed, H. Y. Aboul-Enein, M. Alamoudi et al., "Chiral liquid chromatography tandem mass spectrometry in the determination of the configuration of glyceric acid in urine of patients with D-glyceric and L-glyceric acidurias," *Biomedical Chromatography*, vol. 16, no. 3, pp. 191–198, 2002.
- [12] M. Petrarulo, M. Marangella, D. Cosseddu, and F. Linari, "High-performance liquid chromatographic assay for L-glyceric acid in body fluids. Application in primary hyperoxaluria type 2," *Clinica Chimica Acta*, vol. 211, no. 3, pp. 143–153, 1992.
- [13] A. García, M. Muros, and C. Barbas, "Measurement of nephrolithiasis urinary markers by capillary electrophoresis," *Journal of Chromatography B*, vol. 755, no. 1-2, pp. 287–295, 2001.
- [14] M. Fontaine, N. Porchet, C. Largilliere et al., "Biochemical contribution to diagnosis and study of a new case of D-glyceric acidemia/aciduria," *Clinical Chemistry*, vol. 35, no. 10, pp. 2148–2151, 1989.
- [15] G. R. Bartlett, "Human red cell glycolytic intermediates," *The Journal of Biological Chemistry*, vol. 234, no. 3, pp. 449–458, 1959.
- [16] R. I. Stefan, J. F. van Staden, and H. Y. Aboul-Enein, *Electrochemical Sensors in Bioanalysis*, Marcel Dekker, New York, NY, USA, 2001.
- [17] Armstrong D. W., "A new class of chiral selectors for enantiomeric separations by LC, TLC, GC, CE and SFC," in *Proceedings of the Pittsburg Conference Abstracts*, p. 572, Pittcon, 1994.
- [18] D. W. Armstrong and U. B. Nair, "Capillary electrophoretic enantioseparations using macrocyclic antibiotics as chiral selectors," *Electrophoresis*, vol. 18, no. 12-13, pp. 2331–2342, 1997.
- [19] T. J. Ward and T. M. Oswald, "Enantioselectivity in capillary electrophoresis using the macrocyclic antibiotics," *Journal of Chromatography A*, vol. 792, no. 1-2, pp. 309–325, 1997.
- [20] M. P. Gasper, A. Berthod, U. B. Nair, and D. W. Armstrong, "Comparison and modeling study of vancomycin, ristocetin A, and teicoplanin for CE enantioseparations," *Analytical Chemistry*, vol. 68, no. 15, pp. 2501–2514, 1996.
- [21] T. J. Ward, C. Dann, and A. Blaylock, "Enantiomeric resolution using the macrocyclic antibiotics rifamycin B and rifamycin SV as chiral selectors for capillary electrophoresis," *Journal of Chromatography A*, vol. 715, no. 2, pp. 337–344, 1995.
- [22] T. J. Ward, "Macrocyclic antibiotics—the newest class of chiral selectors," *LC GC*, vol. 14, no. 10, pp. 886–894, 1996.
- [23] K. Ren, "Selectivity problems of membrane ion-selective electrodes: a method alternative to the IUPAC recommendation and its application to the selectivity mechanism investigation," *Fresenius' Journal of Analytical Chemistry*, vol. 365, no. 5, pp. 389–397, 1999.
- [24] I. D. P. Wootton, *Micro-Analysis in Medical Biochemistry*, J. A. Churchill Ltd., London, UK, 4th edition, 1964.

Research Article

Online Monitoring of Electrochemical Degradation of Paracetamol through a Biomimetic Sensor

Mariana Calora Quintino de Oliveira,¹ Marcos Roberto de Vasconcelos Lanza,²
José Luis Paz Jara,³ and Maria Del Pilar Taboada Sotomayor¹

¹Departamento de Química Analítica, IQ, Universidade Estadual Paulista, 14801-970 Araraquara, SP, Brazil

²Departamento de Química e Física Molecular, IQSC, Universidade de São Paulo, 13560-970 São Carlos, SP, Brazil

³Instituto de Química, Universidade Estadual de Campinas, 13083-970 Campinas, SP, Brazil

Correspondence should be addressed to Maria Del Pilar Taboada Sotomayor, mpilar@iq.unesp.br

Received 22 February 2011; Accepted 19 March 2011

Academic Editor: Bengi Uslu

Copyright © 2011 Mariana Calora Quintino de Oliveira et al. This is an open access article distributed under the Creative Commons Attribution License, which permits unrestricted use, distribution, and reproduction in any medium, provided the original work is properly cited.

This paper reports, for the first time, the online monitoring to the electrochemical degradation of the paracetamol using a biomimetic sensor coupled to a Flow Injection Analysis (FIA) system. The electrochemical degradation of the drug was carried out in aqueous medium using a flow-by reactor with a DSA anode. The process efficiency was monitored at real time by the biomimetic sensor constructed by modifying a glassy carbon electrode with a Nafion membrane doped with iron tetraphenylporphyrin (FeTPyPz). Simultaneously, we carried out off-line analysis by liquid chromatography (HPLC) during the experiments in order to validate the proposed system. In addition, to investigate the degradation products of the paracetamol electrolysis, we used the techniques of UPLC/MS and GC/MS.

1. Introduction

The environmental sciences have an enormous progress in recent years. The need for planning the rational use of energy resources and water provided a challenge for the applied sciences and engineering to develop new technologies, new processes, and new materials for the prevention and control of pollution. This is also a consequence of the increase of legal pressure that is forcing the industry to accept responsibility for waste treatment or storage, in an attempt to minimize pollution [1].

Oxidative conventional treatments, which may be chemical or biological, of aqueous solution containing organic compounds, are often effective in enforcement. However, this action is not enough nowadays, when environmental considerations should be considered. The conventional technology for wastewater treatment requires chemical storage and handling of hazardous chemicals and leads to the generation of toxic waste. Moreover, biological treatment is time consuming and performed in large physical areas, which

also leads to the generation of soluble non-biodegradable waste. In addition, compounds with high molecular weight of fractions present in some types of aqueous effluents tend to be resistant to biodegradation [2].

In this field, the electrochemical and photochemical technologies may offer an efficient way for pollution controls, providing the degradation of organic pollutants without the disadvantages observed with conventional treatments. Electrolysis, heterogeneous photocatalysis, and photoassisted electrolysis can be used as primary or additional treatment at reduction of the organic matter. In fact, electrons and photons are the unique reagents added to the treatment process that basically does not generate subproducts [3].

The electrolytic process is probably the best tool in the treatment of aqueous effluent, ideal for the present, where environmental considerations are always ahead [2].

The literature outlines the principles and mechanisms for electrochemical treatment of aqueous solutions containing organic compounds with simultaneous oxygen evolution [4, 5]. The key to efficient electrolytic treatment is strongly based

on the choice of anodic material. The high resistance to corrosion of the anode and physical and chemical stability under high applied potentials are the main requirements for an efficient process. When the above properties are required, dimensionally stable anodes (DSAs) are the natural candidates. This designation denotes a class of electrodes thermally prepared where a titanium substrate is covered by metallic oxides. Coatings include TiO_2 , IrO_2 , RuO_2 , and Ta_2O_5 . Combinations such as $\text{TiO}_2/\text{RuO}_2$ are indicated for the alkaline medium, while $\text{IrO}_2/\text{Ta}_2\text{O}_5$ usually shows longer useful life in acid electrolytes. Moreover, some DSA electrodes may receive addition of SnO_2 and Sb_2O_5 in concentrations ranging appropriately, aiming to increase lifetime and eventually their catalytic power and selectivity [6, 7]. Currently, are commercialized some DSA anodes, between them is the DSA- Cl_2 that is composed for a mixture of 70% of TiO_2 and 30% of RuO_2 and was used in the electrochemical degradation of paracetamol in this work.

On the other hand, biomimetic sensors are a recent experimental strategy that has been used to get chemical sensors more stables and durable than the conventional biosensors, that are based on the use of biological materials, such as enzymes or antibodies. These devices aim at to overcome the limitations of the enzymatic biosensors such as availability, cost, and instability of enzymes as well as to promote improvement in the electronic transfer between electrode/active site (biomimetic catalyst)/substrate, since that in the biomimetic sensors the “active site” is free, differently from in the enzymes, where the active site is surrounded by a dense layer of residual aminoacids [8, 9]. However, a condition to mimic or to choose an enzyme for the construction of biomimetic sensors is that the chemistry of the enzymatic reaction catalysis and the structure of its active site should be very well known, and in this sense the P450 enzymes are perfectly fitted in these conditions [9].

In previous papers [10, 11] were described the studies carried out to develop an amperometric sensor based on the use of iron tetrapyridinoporphyrazine (FeTPyPz), a biomimetic catalysts of the P450 enzyme, and its coupling and application satisfactory in the paracetamol detection in an FIA system. Due to the excellent characteristics shown by this FIA system using the biomimetic sensor as detector, and being recognized the importance of the degradation of organic compounds by means electrochemistry, this paper intends to demonstrate the viability of the use of sensors highly selective, stable, and durable, in monitoring online and in real-time of the paracetamol electrochemical degradation, as an alternative tool to existing methods for the offline monitoring, that may be time consuming, expensive, pollutants, and often not selective, as are the cases of the chemical oxygen demand and total organic carbon (TOC). Thus, this paper shows the promising junction of two areas of recent and increasing concern, the electrochemical and electroanalysis.

2. Experimental

2.1. Chemicals and Solutions. All chemicals used in the construction and application of the sensor were analytical

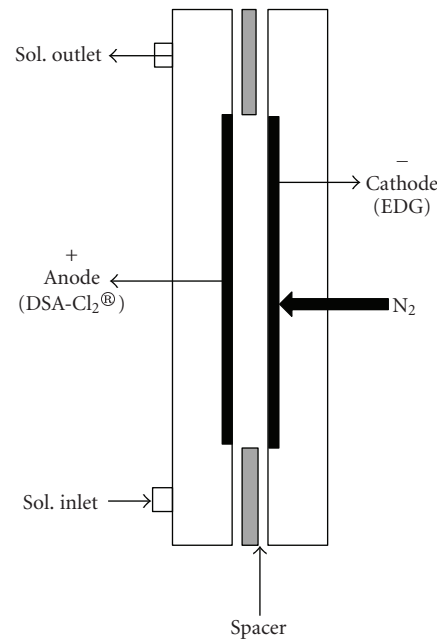


FIGURE 1: Representative scheme of the electrochemical reactor used in this work.

grade reagents. All chemicals used in the chromatographic experiments were high-performance liquid chromatography (HPLC) grade reagents. The biomimetic complex, iron (III) tetrapyridinoporphyrazine (FeTPyPz), was prepared and purified as previously described [12]. Acetic acid and *N,N*-dimethylformamide (DMF) were acquired from Synth (São Paulo, Brazil). Paracetamol (acetaminophen) was obtained from Sigma (St. Louis, USA). 5% (m/v) Nafion solution was from Aldrich (Milwaukee, USA). Sodium acetate was acquired from Merck (Darmstadt, Germany), and all HPLC grade solvents were from Tedia (Rio de Janeiro, Brazil). Paracetamol and acetate buffer solutions were prepared with water purified in a Millipore Milli-Q system, and the pH was determined using Thermo Scientific pH-meter (Orion 3 Star, Benchtop).

2.2. Electroanalytical Flow System. The biomimetic sensor was constructed as previously described [10, 11]. First, a solution containing 5 mg mL⁻¹ of the FeTPyPz in DMF was prepared. Then, the surface of a glassy carbon (GC) electrode (Metrohm, Switzerland), with a geometrical area of 0.126 cm², was cleaned according to the procedure described in the literature [13]. After cleaning the electrode, 100 µL of FeTPyPz solution was mixed with 50 µL of 5% (m/v) Nafion solution, and an aliquot of 50 µL of this mixture was placed on the surface of the electrode. Finally, the solvent was evaporated at room temperature during 6 hours, forming a thin green film.

The biomimetic sensor was inserted into a flow-through wall-jet amperometric cell and used as the working electrode (WE in Figure 2). An Ag | AgCl (KCl sat) electrode was the reference (RE), and a platinum wire was the auxiliary electrode (AE). The electrodes were connected to a potentiostat (Palm-sense, Palm Instruments BV, The Netherlands)

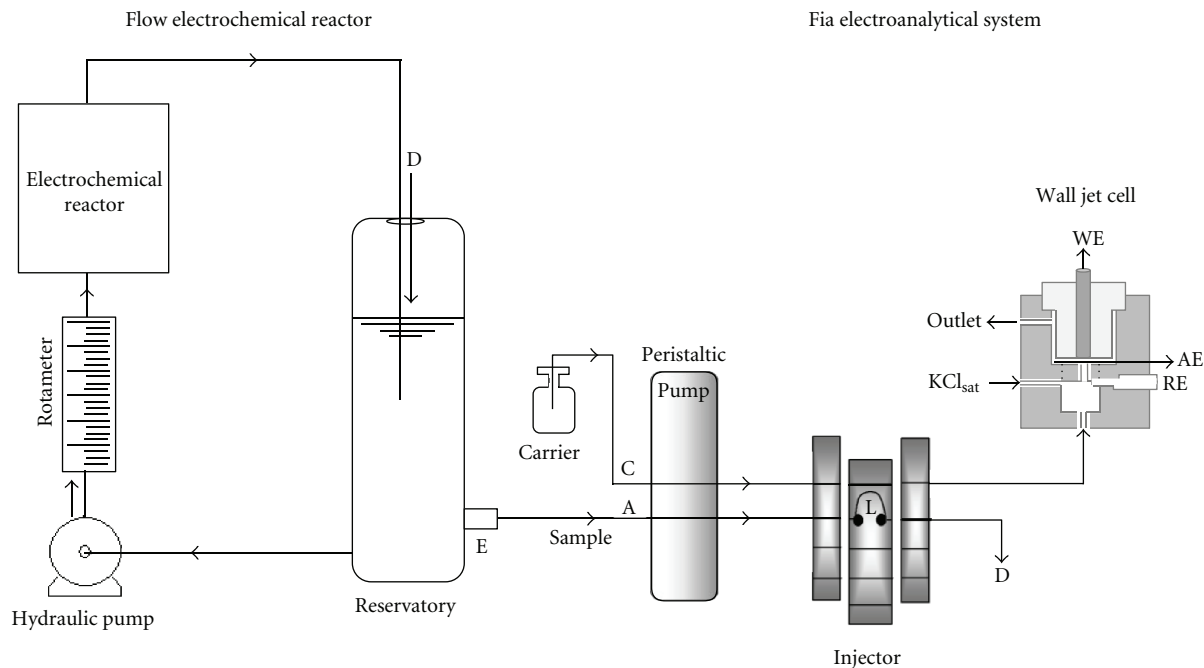


FIGURE 2: Scheme of the coupling of the reactor with the FIA system. WE is the biomimetic sensor, AE represents the counter electrode, RE is the reference electrode. The D channel is used for the return of the electrolysis solution (sample) from the injector to the reservoir of the reactor, allowing maintain-sink condition in the experiments without loss of volume and thus avoiding errors in the calculation of the concentration of paracetamol, since the injected volume is only 75 μL in each sampling.

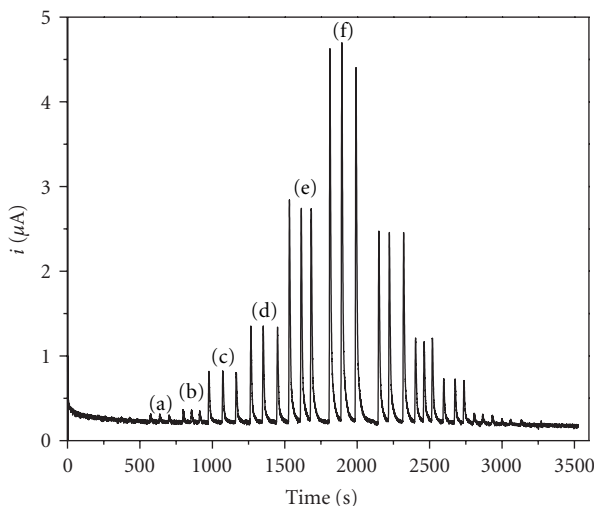


FIGURE 3: FIA signals obtained using the electrolyte solution as carrier stream, consisting of 0.1 mol L⁻¹ K₂SO₄ and 5.0 \times 10⁻⁴ mol L⁻¹ FeSO₄ · 7H₂O. The concentrations evaluated were: (a) 5.0 \times 10⁻⁵ mol L⁻¹ (b) 5.0 \times 10⁻⁴ mol L⁻¹ (c) 1.0 \times 10⁻³ mol L⁻¹; (d) 1.0 \times 10⁻² mol L⁻¹ (e) 2.5 \times 10⁻² mol L⁻¹ and (f) 5.0 \times 10⁻² mol L⁻¹.

interfaced to a microcomputer for potential control and data acquisition.

A peristaltic pump (Ismatec) was used to provide the flow of the 0.1 mol L⁻¹ K₂SO₄ and 5.0 \times 10⁻⁴ mol L⁻¹ FeSO₄ · 7H₂O carrier solution at 1.25 mL min⁻¹. The standards and samples containing paracetamol were injected (loop = 75 μL)

into the carrier using a sliding central bar sampling valve (injector) [14].

2.3. Electrochemical Degradation System. To carry out the electrolysis, was used a flow-by electrochemical reactor with a compartment constructed with PVC plates mounted in the form of a filter press, designed to be coupled to a reservoir with a capacity of 2.5 L [15, 16]. The reactor used a gas diffusion electrode (GDE) containing 20% (w/w) polytetrafluoroethylene (PTFE) acting as a carbon cathode with geometric area of 20 cm² and a commercial anode of DSA-Cl₂ by De Nora do Brazil Ltda [17] (with a geometrical area of 20 cm²). Between the two PVC plates, anodic and cathodic, was placed a rubber spacer, providing a distance of 3 mm, allowing the passage of the solution (Figure 1). The reactor was connected to a recirculation system consisting of a reservoir, a hydraulic pump, and a rotameter to measure the flow of solution in the system (Figure 2). In all experiments, the reactor system operated in the recirculation mode.

To perform the electrochemical degradation of paracetamol was used the electrolysis at constant current through the coupling of a power supply (Tectrol TC 20-05) to the electrochemical reactor system. In this work were used the current densities of 5 and 100 mA cm⁻². The flow of the degradation system was set at 50 L h⁻¹ which presents a laminar regime (Reynolds number) of approximately 500. The electrolyte volume was 2.0 L, consisting of 0.1 mol L⁻¹ K₂SO₄ and 5.0 \times 10⁻⁴ mol L⁻¹ FeSO₄ · 7H₂O containing 2041.2 mg L⁻¹ (1.35 \times 10⁻² mol L⁻¹) of paracetamol. In all tests was applied a positive flow of N₂ (0.2 bar) to GDE by means of the external chamber of the cathode in order to avoid the

formation of H_2O_2 from the cathodic reaction of O_2 , and that could affect the sensor response [18].

2.4. On-Line Monitoring System: FIA and Reactor Coupling. The FIA/sensor system was coupled to the electrochemical system of degradation (Figure 2), by the reservoir, precisely in the region of sampling of the reactor (E in Figure 2), where the aliquots are usually collected to perform the analyzes of monitoring *via* off-line. The electrochemical degradation system was refrigerated to maintain a constant temperature at 25°C. Figure 2 shows the diagram of the coupling of the two systems, electrochemical and electroanalytical for the monitoring on-line and at real-time of the paracetamol degradation. The solution/sample from the flow-by electrochemical reactor was injected directly into the analytical system *via* the sample valve at time intervals pre-established. Prior to filling the sampling loop (75 μL) trapping-bubbles had to be inserted into system to prevent the large number of bubbles formed during the degradation process to entering in the FIA system, which would harm the measurements repeatability. This solution, which leaves the degradation system, travels through the FIA system passing by the injector until it reaches the wall jet cell, where it enters into contact with the biomimetic sensor selective for paracetamol, where are performed amperometric measurements, which is the electroanalytical technique, used to register the FIAgrams. The analyte that is not injected into the electrochemical cell returns to the degradation system by means of the D channel (Figure 2). Thus, keeping a continuous flow of analyte is possible to determine at real-time the amount to paracetamol which is degraded over time.

2.5. HPLC Measurements. In order to validate the results obtained using the proposed on-line system, they were compared to those obtained using the official chromatographic method based on HPLC [19]. Chromatographic analyses were performed using a Shimadzu Model 20A liquid chromatograph coupled to a UV/V detector (SPD-20A), autosampler (SIL-20A), and a degasser DGU-20A5, controlled by a personal computer. A C18 column (250 × 4.6 mm, Shim-Pack CLC-ODS) was used, inside an oven (Shimadzu CTO-10AS) maintained at 30°C. The mobile phase was a mixture of methanol and water in a ratio of 13:87 (v/v) with apparent pH of 4.9. The flow rate was 1.0 mL min^{-1} , the sample injection volume 20 μL , and the detector absorption wavelength 254 nm.

The analytical curve was constructed under the same conditions of the degradation. For this, were prepared standard solutions of paracetamol in the electrolyte of degradation ($0.1 \text{ mol L}^{-1} \text{ K}_2\text{SO}_4$ and $5.0 \times 10^{-4} \text{ mol L}^{-1} \text{ FeSO}_4 \cdot 7\text{H}_2\text{O}$) contained between $1.0 \times 10^{-4} \text{ mol L}^{-1}$ (15.2 mg mL^{-1}) and $5.0 \times 10^{-2} \text{ mol L}^{-1}$ (7560 mg mL^{-1}). The equation of the analytical curve was used to calculate the concentration in the samples collected from the electrochemical reactor at different pre-established times of electrolysis.

The samples were collected from the reactor at the same periods of sampling realized in the on-line system and

immediately frozen until the realization of the chromatographic experiments. Samples collected from degradation at 5 mA cm^{-2} were analyzed by HPLC two days after the electrolysis, and the samples at 100 mA cm^{-2} were examined five days after the electrolysis, becoming an obvious disadvantage of this method.

2.6. UPLC/MS Measurements. For these studies, aliquots of the degradation using the DSA-Cl₂ electrode were collected at 0, 30, 60, and 90 minutes and were immediately analyzed on a Waters UltraAcquity chromatograph, equipped with a binary pump, a C18 reversed phase column Acquity UPLC-BEH (2.1 × 50 mm and 1.7 μm particle size) maintained at 37°C, and a degasser.

Previously, in order to obtain the highest signal and the lowest retention time, the UPLC/MS conditions were optimized. For this, firstly was optimized the ionization process (conversion of the analyte in solution to the gas phase directly in the ionization source), which should preferably take place without occurring of fragmentation, in order to obtain information on the molar mass of the compounds analyzed. Thus, was carried out the direct injection of 500 μL of solution of paracetamol in the electrospray source at a flow rate of 20 $\mu\text{L min}^{-1}$. Additionally, the following chromatographic conditions were also optimized, in order to obtain the best process of separation with the lowest retention time the flow rate and mobile phase in the gradient mode.

Thus, with all parameters optimized the chromatographic analysis was performed at 0.350 mL min^{-1} in the gradient mode, using different mixtures of 0.1% (v/v) formic acid in water (solvent A) and 0.1% (v/v) formic acid in acetonitrile (solvent B), with the programation described follow as: initially between 0 and 4 min, 70% (a) and 30% (b); 4–6 min, 30% (a) and 70% (b); and in last minute (6-7 min) 95% (a) and 5% until reaching the initial proportions of 70% (a) and 30% (b), respectively. Although the chromatographic run was performed for 7 minutes, in order to explore a long period of time and check if other substances would be generated during the electrolysis of paracetamol, the only peaks appeared during the first minute of running, as will be shown in Figure 7.

Additionally, the experimental conditions of the mass detector were as follows: (i) polarity: positive, ES + mode; (ii) capillarity to 1.00 kV; (iii) cone voltage: 30 V; (iv) supply temperature: 120°C; (v) desolvation temperature: 350°C; (v) Gas used in the cone and desolvation: N₂ and the gas flow on the cone: 100 L Hr^{-1} ; (vi) desolvation gas flow 800 L Hr^{-1} ; and (vii) photomultiplier voltage: 650 V.

For analysis of the degradation samples, they were diluted 500 times, in order to avoid saturation of the detector. In the case of the sample collected before starting the electrolysis (t_0), the initial concentration was 4.08 $\mu\text{g mL}^{-1}$. The concentration of standard solution of paracetamol was 1.0 $\mu\text{g mL}^{-1}$.

2.7. GC/MS Measurements. For these studies, aliquots of the degradation at 0, 30, and 60 minutes of electrolysis

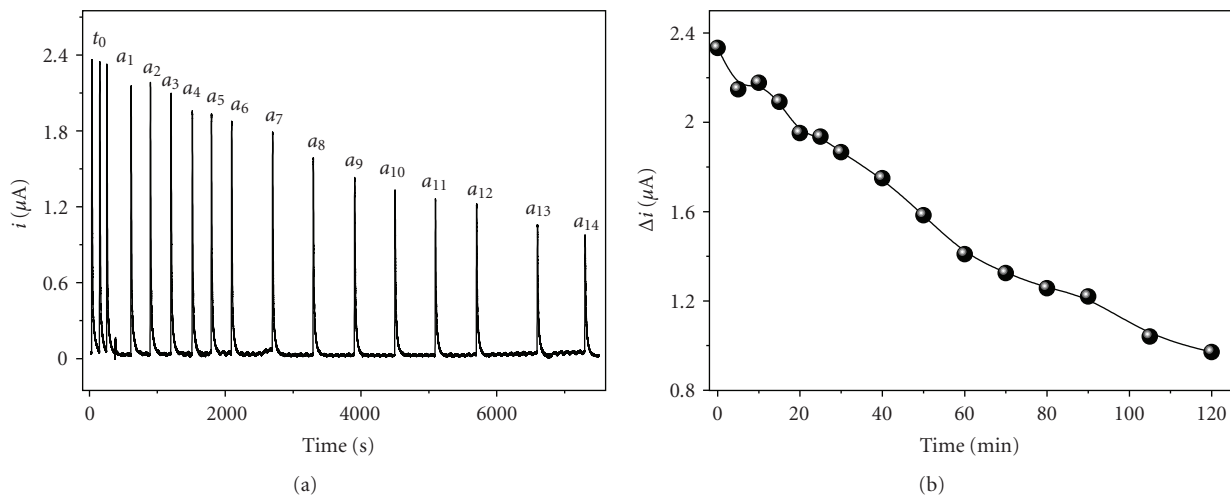


FIGURE 4: (a) Signals obtained at real-time as a function of the degradation time. t_0 : no current is applied. a_1 – a_6 : samples injected every 5 min; a_7 – a_{12} : aliquots of samples injected at 40, 50, 60, 70, 80, and 90 minutes after the electrolysis; a_{13} and a_{14} : aliquots injected at 105 and 120 minutes of electrolysis, respectively. [Paracetamol]₀ = 1.35×10^{-2} mol L⁻¹ (2041.2 mol L⁻¹). (b) Response profile at real-time for the electrochemical degradation of paracetamol.

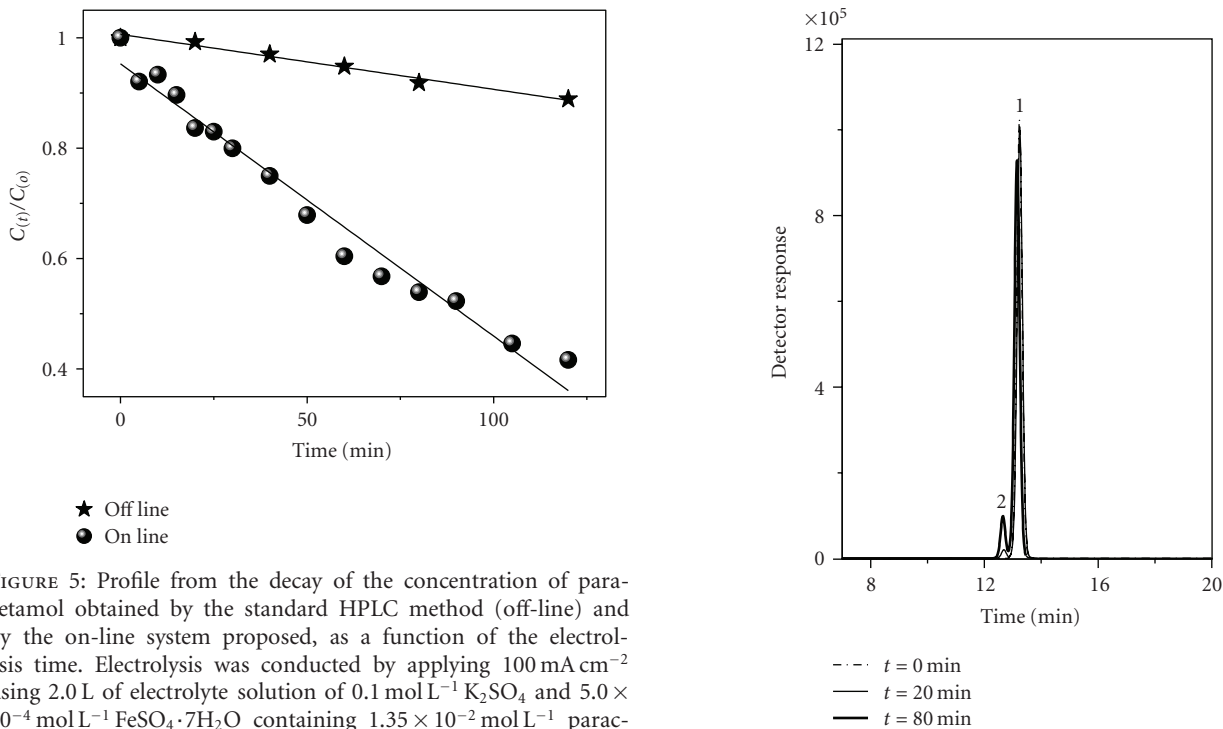


FIGURE 5: Profile from the decay of the concentration of paracetamol obtained by the standard HPLC method (off-line) and by the on-line system proposed, as a function of the electrolysis time. Electrolysis was conducted by applying 100 mA cm⁻² using 2.0 L of electrolyte solution of 0.1 mol L⁻¹ K₂SO₄ and 5.0 × 10⁻⁴ mol L⁻¹ FeSO₄ · 7H₂O containing 1.35×10^{-2} mol L⁻¹ paracetamol.

were taken from the reactor and after a process of liquid-liquid extraction were analyzed by a gas chromatograph model CP-3800 Varian coupled to an ion trap mass spectrometer Varian model Saturn 2100D and using a column of 30 m × 0.25 mm × 0.25 μm , whose stationary phase consisted to a mixture to diphenyl (5%)-dimethyl (95%)-polysiloxane (CP-Sil CB8, Low Bleed).

The experimental conditions were as follows: (i) injector at 260°C in split mode of 1 : 25 and flow of 1.0 mL min⁻¹; and (ii) Programation of the oven: 80°C (1.0 minutes), ramp heating 10°C min⁻¹ up to 280°C, and maintained at that temperature for 5 minutes. Total time to run: 26 minutes. (iii) Detector: Ion Trap MS type, 70 eV, solvent delay 2.5 min, scan range 40–450 Da.

FIGURE 6: HPLC chromatograms obtained from samples of degradation of paracetamol collected at different times.

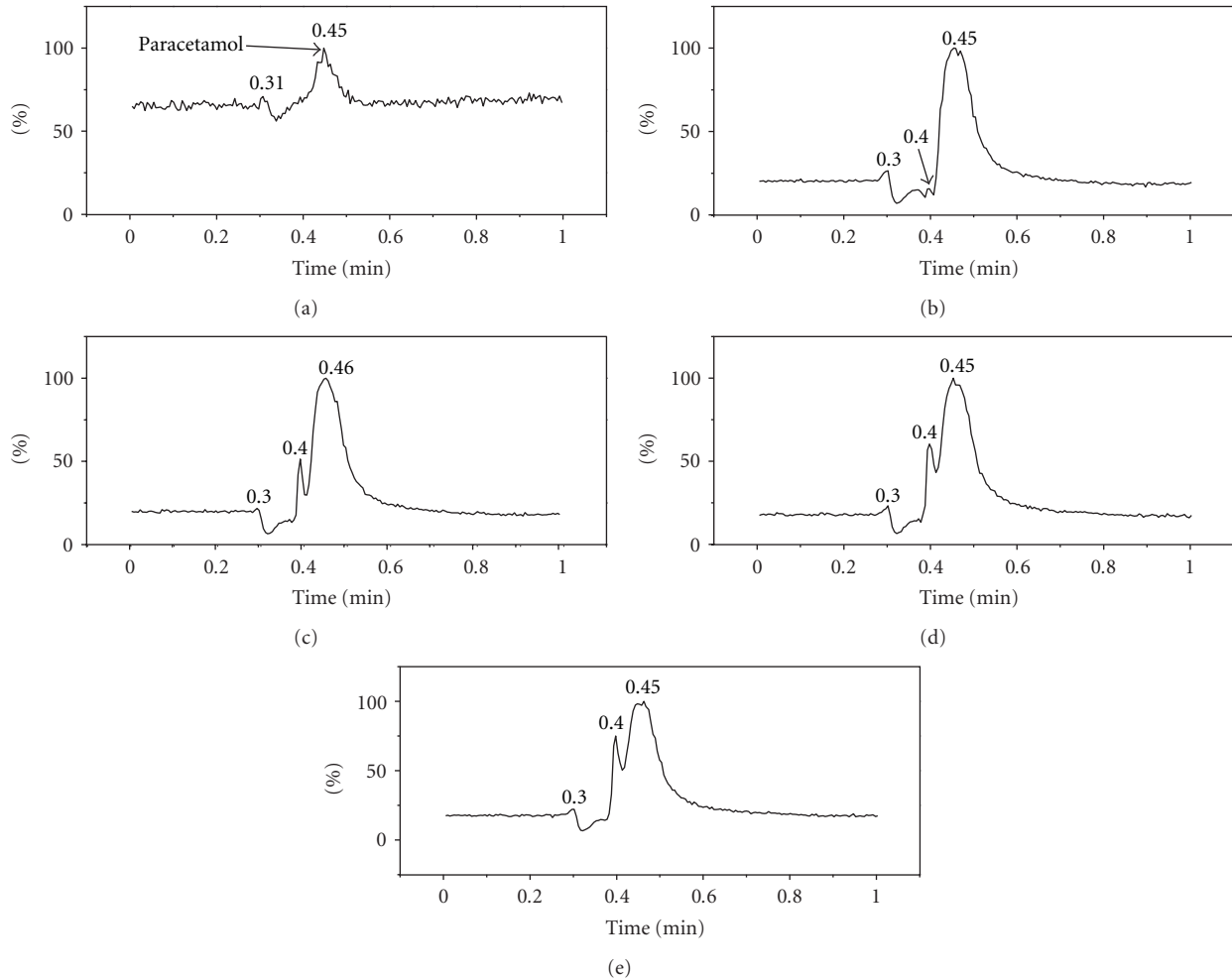


FIGURE 7: UPLC chromatograms obtained for (a) a standard solution of 0.1 mg mL^{-1} paracetamol, and for samples collected from the electrochemical reactor at (b) 0, (c) 30, (d) 60, and (e) 90 minutes.

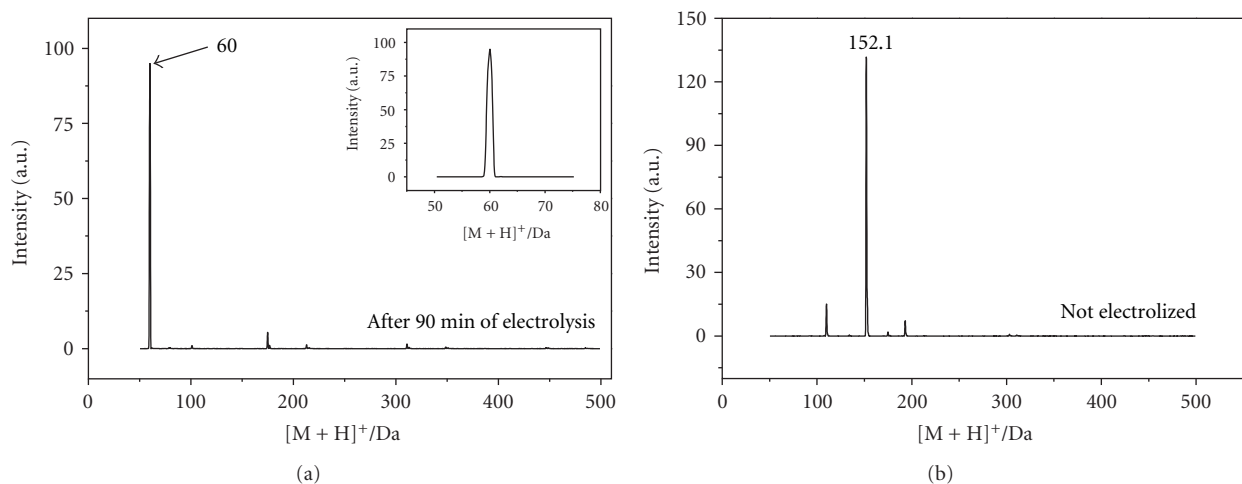


FIGURE 8: (a) Mass spectrum of the UPLC chromatographic peak corresponding to the retention time of 0.40 minutes in Figure 7(e). The inset shows a better view of the value of the $[M + H]^+$, which suggests that the compound is acetamide. (b) Mass spectra of the UPLC chromatographic peak at retention time of 0.45 min, corresponding to paracetamol for samples collected before the electrolysis.

For the analysis by GC/MS the samples were extracted in 500 μL of dichloromethane. For each sample, six successive extractions were performed to each aqueous extract in an Eppendorf of 2 mL. After the extraction performed, the organic phase was dried with MgSO_4 and then injected 0.6 μL into equipment. For comparative studies was prepared a solution of paracetamol in dichloromethane (0.2 mg mL^{-1}) and injected 0.6 μL into equipment.

3. Results and Discussion

3.1. Analytical Profile of the FIA/Sensor System. Firstly, before coupling the sensor to the system of electrochemical degradation, the analytical conditions had to be adjusted in order to obtain results more reliable and reproducible, since in this case the samples from the electrochemical reactor were in 0.1 mol L^{-1} K_2SO_4 and 5.0×10^{-4} mol L^{-1} $\text{FeSO}_4 \cdot 7\text{H}_2\text{O}$ (degradation electrolyte). In this way, was evaluated the response of the system FIA/sensor in this electrolyte, and thus to continue with the studies of the on line coupling of the electrochemical and electroanalytical systems. The results obtained are shown in Figure 3, in which are present the FIA signals as a function of paracetamol concentration using the degradation electrolyte like carrier solution.

Although the sensitivity of the system has decreased when compared to the optimized FIA system, that uses 0.1 mol L^{-1} acetate buffer at pH 3.6 as carrier [12], the response of the FIA/sensor system under this new adjusted condition was also reproducible and sufficiently sensitive for this application proposed. The data presented in Figure 3 were linearly adjusted to a straight line, whose linear regression, in direction of increasing concentration, is shown in (1):

$$\Delta i(\mu\text{A}) = 0.03(\pm 0.01) + 111.6(\pm 2.1) [\text{Paracetamol}] (\text{mol L}^{-1}) \quad (1)$$

3.2. The Paracetamol Degradation Used a Flow-By Electrochemical Reactor. The degradation of paracetamol in the electrochemical reactor is based on the oxidation process of the drug on the surface of the anode $\text{DSA}-\text{Cl}_2$. The use of a GDE as cathode aimed to compose the electric circuit in the reactor without interference in the process of degradation of the organic matter present in the electrolyte.

In this work was carried out electrolysis at current densities at two extreme values (5 and 100 mA cm^{-2}) using as electrolyte the solution of K_2SO_4 0.1 mol L^{-1} and $\text{FeSO}_4 \cdot 7\text{H}_2\text{O}$ 5.0×10^{-4} mol L^{-1} , aiming to allow the complete oxidation of the paracetamol.

The results obtained at 5 mA cm^{-2} practically does not present significant variation of the paracetamol concentration after the first 20 minutes of the electrochemical degradation begin, monitored via FIA/sensor and HPLC (Table 1). On the other hand, as expected, results more relevant were obtained when was applied a current density of 100 mA cm^{-2} , and in this work will be presented the results obtained in this condition.

TABLE 1: Values of the concentration of paracetamol in the electrochemical degradation with $\text{DSA}-\text{Cl}_2$ anode at 5 A cm^{-2} , obtained through the method FIA with amperometric detector (biomimetic sensor) and chromatography (reference).

Electrolysis time/min	[Paracetamol]/mol L^{-1}	
	FIA/sensor	HPLC
0	0.0135	0.0135
20	0.0094	0.0131
40	0.0089	0.0132
60	0.0095	0.0130
80	0.0090	0.0124
90	0.0088	n.a.
120	0.0097	0.0125

n.a.: not analyzed.

3.3. Coupling of FIA/Sensor to the Flow-By Electrochemical Reactor. To evaluate the performance of the flow injection system with biomimetic detection in the on-line monitoring of the paracetamol degradation performed in an electrochemical reactor at pilot scale, both systems were coupled as described in Section 2.4 (Figure 2).

In this case, the measurements were performed injected directly into the FIA system (flow rate of 1.25 mL min^{-1}) 75 μL of the solution/sample from the electrochemical degradation system. Figure 4(a) shows the signals obtained at real-time by the FIA system for the paracetamol degradation at 100 A cm^{-2} . Figure 4(b) shows the corresponding graph of the current variation (Δi) at function of time. The three initial injections correspond to the signals obtained before the start of electrolysis (t_0) and served to verify the stability of the on-line system. With the data shown in Figure 4(b) and using (1), we could verify that the graph $\ln[\text{Paracetamol}]$ versus time shows a linear adjustment ($R = 0.9963$, $n = 15$) whose equation is given as follows (2), suggesting that the kinetics of electrochemical degradation of paracetamol follows a behavior of *pseudo-first* order [20]:

$$\ln[\text{Paracetamol}] = -4.32 - 7.4 \times 10^{-3}/\text{min}^{-1}. \quad (2)$$

In (2) it is verified that the linear coefficient corresponds to $\ln[\text{Paracetamol}]_0$ providing the value of 0.0133 mol L^{-1} of paracetamol, initially added in the electrochemical reactor. The slope corresponds to an apparent constant of the *pseudo-first* order of 7.4 min^{-1} . A great advantage of this proposed on-line system is that a great number of points can be monitored in comparison with the chromatographic off-line method, and thus all constants found for the electrochemical degradation will be more accurate, because they will be based on a larger number of data.

3.4. Quantification of Paracetamol Employed the Official Method of Analysis (Off-Line) in the Electrolysis Performed in the Flow-By Electrochemical Reactor. Analyses were performed to quantify paracetamol using the official method of analysis based on high-performance liquid chromatography (HPLC), with the purpose of comparing the results obtained

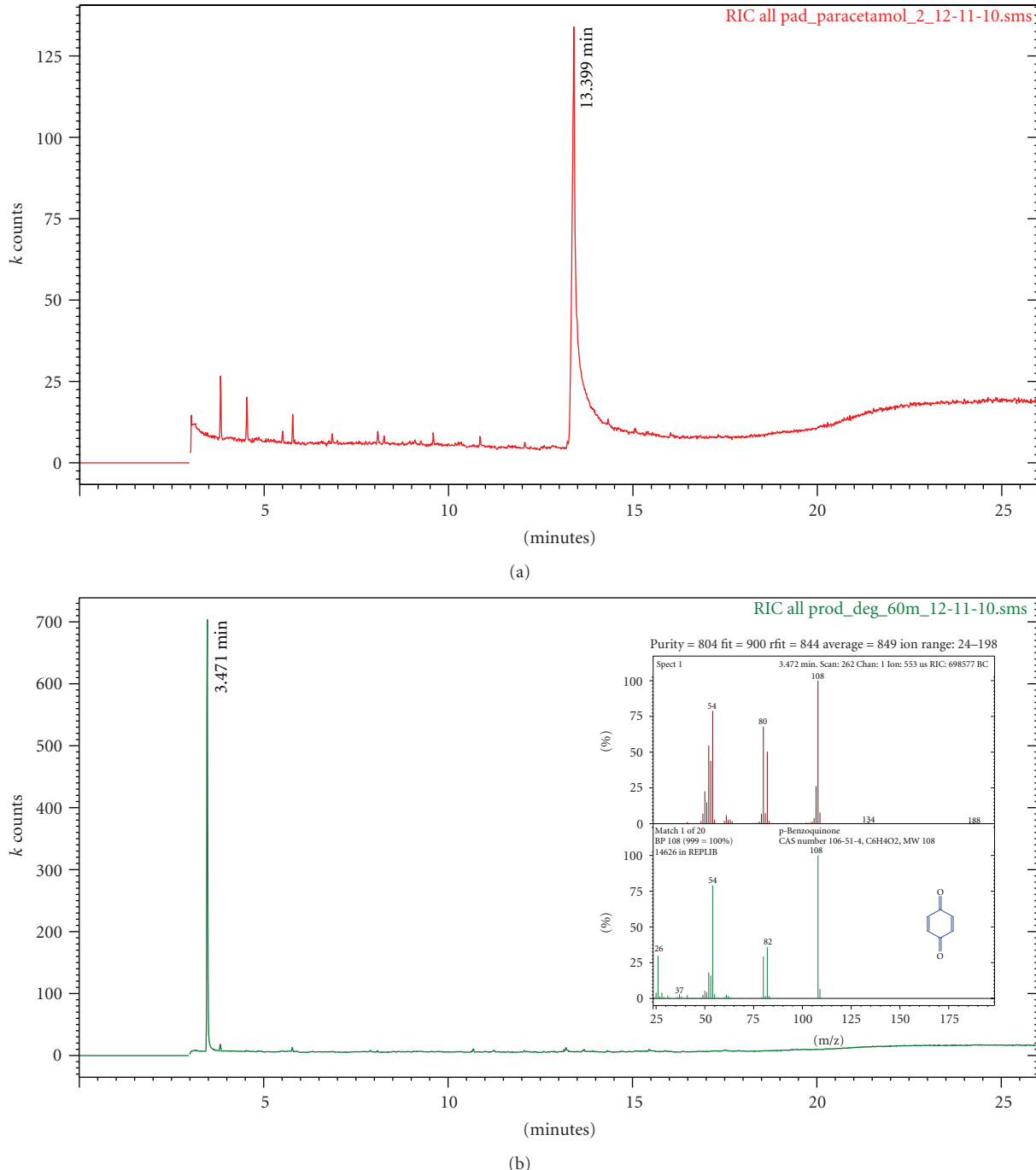


FIGURE 9: (a) GC chromatogram obtained for standard paracetamol solution in dichloromethane. $C_{\text{paracetamol}} = 0.2 \text{ mg mL}^{-1}$. (b) GC chromatogram obtained for the electrochemical degradation product of paracetamol after dichloromethane extraction of the sample collected after 60 minutes of electrolysis. Inset: comparison of the mass spectra obtained experimentally with one shown by the library NIST 2005.

with the proposed online system. Figure 5 shows the decay profiles of normalized concentrations of paracetamol as a function of electrolysis time, obtained by the two methodologies here used, HPLC (off-line) and the proposed (online). In Table 2, also are shown some paracetamol concentrations obtained through the two methodologies used. Based on these results, is evident a great difference between the methodologies.

The difference can be explained if we consider that the samples analyzed by the off-line method were carried out only five days after the collect. In addition, if we observed the chromatograms obtained for the degradation samples at different periods (Figure 6) a formation of a second peak at 12.6 min (2 in Figure 6) very close to the retention time of paracetamol at 13.2 min (1 in Figure 6), causes the calculation of peak area of paracetamol to be wrong,

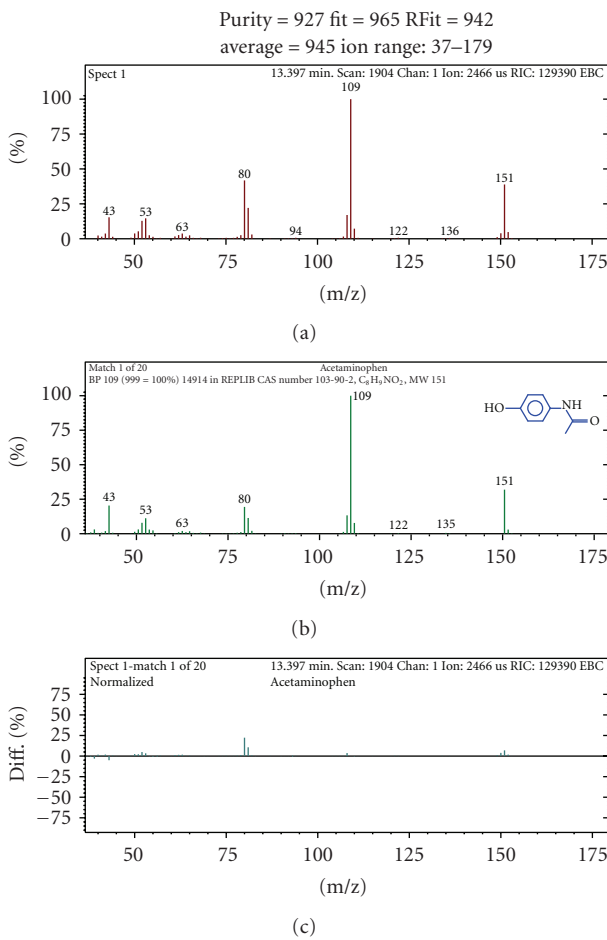


FIGURE 10: (a) Mass spectrum of the chromatographic peak corresponding to the retention time of 13.4 min of Figure 9(a) for a paracetamol concentration of 0.2 mg mL^{-1} , (b) MS recorded by the NIST library, and (c) difference of the spectra (a) and (b), attesting that the compound is paracetamol.

TABLE 2: Values of the concentration of paracetamol in the electrochemical degradation with DSA-Cl₂ anode at 100 A cm^{-2} , obtained through the method FIA with amperometric detector (biomimetic sensor) and chromatography (reference).

Electrolysis time/min	[Paracetamol]/mol L ⁻¹	
	FIA/sensor	HPLC
0	0.0135	0.0135
20	0.0113	0.0131
40	0.0101	0.0131
60	0.0081	0.0128
80	0.0076	0.0124
90	0.0073	n.a.
120	0.0069	0.0119

n.a.: not analyzed.

providing a value greater concentration and thus giving an inexact profile of the degradation.

On the other hand, it should be emphasized that the on-line system is not influenced by the presence of degradation

product **2** (Figure 6) or others, due to the high selectivity shown by the biomimetic sensor used as the detector in the electroanalytical system [10, 12]. At the same time, the results of electrochemical degradation of paracetamol are obtained and recorded in real-time just after the output of reactor, avoiding sample contamination and parallel reactions occur in the collected samples.

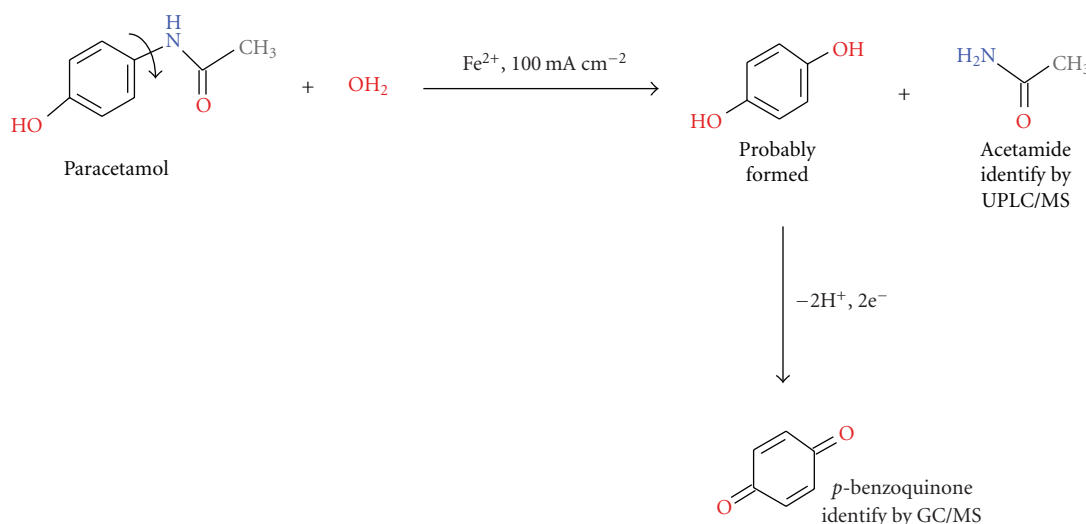
In this way, the advantages offered by this on-line system proposed to monitor degradation experiments are evident, opening a new alternative for the conventional and off-line monitoring methodologies.

3.5. Identification of Products Formed in the Paracetamol Degradation Using Hyphenated Techniques: UPLC/MS and GC/MS. In order to identify the degradation products of paracetamol at 100 A cm^{-2} and, consequently, to show the sensor selectivity used as the detector in the FIA system, was initially used the Ultra performance liquid chromatography (UPLC) coupled to mass spectrometry (Figures 7 and 8).

In Figure 7 are shown the chromatograms obtained for a standard solution of 1.0 mg mL^{-1} paracetamol (Figure 7(a)) and from samples collected at 0 min (Figure 7(b)), 30 min (Figure 7(c)), 60 min (Figure 7(d)), and 90 min (Figure 7(e)) of degradation. It is again possible to observe the two peaks in the degradation samples at 0.40 and 0.45 minutes (Figures 7(c)–7(e)). The first peak increases with electrolysis time, such expected (the degradation compound formed), and the second peak corresponds to paracetamol, as verified by Figures 7(a), 7(b), and 8(b).

Analyzing the peak at 0.40 min (Figure 8(a)) using electrospray mass spectrometry in positive mode (ESI+) shows that this corresponds to the acetamide compound ($[\text{M} + \text{H}]^+ = 60$), which is consistent with the loss of this group on the molecule of paracetamol (Scheme 1). For comparison purposes, is shown in Figure 8(b), the mass spectrum for the paracetamol (at 0.45 min). Comparing both figures one can see clearly the difference in the mass spectra corresponding to each one these molecules. In this way, the results obtained by UPLC/MS suggest that acetamide is a product in the electrochemical degradation, which, being detected by liquid chromatography, causes errors in the calculation of the area, and consequently in the estimated concentration for paracetamol.

Moreover, in order to verify what would be the additional degradation product, corresponding to the remaining portion of the paracetamol molecule, experiments were performed using GC/MS, due to that in liquid chromatography was not possible to identify other molecules formed (Figures 6 and 7). Thus, using gas chromatography, after performing successive extractions in dichloromethane in the sample of 60 min of electrolysis, was observed a peak at the retention time of 3.471 min (Figure 9(b)) which is different from the retention time observed for the standard solution of paracetamol, which occurs at 13.4 min (Figure 9(a)). To identify the product that is formed, was analyzed the peak in Figure 9(b) by mass spectrometry and identified according to the library NIST 2005 as *p*-benzoquinone, such as shown in Figure 9(b). Already for comparison purposes was



SCHEME 1: Proposed route of the electrochemical degradation of paracetamol by DSA- Cl_2 anode, in which the degradation products were identified by hyphenated chromatographic techniques with mass spectrometry.

also analyzed the peak corresponding to paracetamol, and the corresponding mass spectrum is shown in Figure 10.

In Scheme 1 a mechanism for the degradation of the paracetamol based on experimental evidences obtained by chromatographic methods coupled to mass spectrometry is proposed. The experiments suggested the presence of p -benzoquinone and acetamide, on the collected samples after 60 and 90 min of electrolysis, respectively. The mechanism suggests that initially is promoted a cleavage of the molecule of paracetamol releasing acetamide ($[\text{M} + \text{H}]^+ = 60$) and probably generated the p -hydroquinone molecule that is immediately oxidized to p -benzoquinone ($m/z = 108$, inset Figure 9(b)).

It should be emphasized that the proposed sensor does not detect the presence of acetamide or hydroquinone and p -benzoquinone during electroanalytical measurements, which makes it, in fact, an alternative tool to the traditional methods monitor the degradation processes, and that which can lead to obtain erroneous results, for example, in the profile of degradation, in calculation of some constant, and even in the current or potential of electrolysis that should be applied to obtain satisfactory results.

4. Conclusions

It should be emphasized that this study used as a model system the degradation of paracetamol only to demonstrate and/or evaluate the feasibility and benefits of the on-line coupling of a highly selective FIA system to a system of electrochemical degradation, which can be extended to other pollutants and other degradation processes.

The system offers the advantage of monitoring the drug concentrations in real-time, when compared to the reference method. Lastly, commonly the monitoring analyses are performed off-line and sometimes several days after that the

electrolyses were performed, not reflecting the actual values obtained. In the proposed system, really reliable results are obtained once has been used a selective sensor, robust and easily constructed, that allowed obtaining a cheap, fast, and environmentally friendly method for real-time monitoring of electrochemical degradation of paracetamol.

Acknowledgments

The authors gratefully acknowledge financial support from FAPESP (Proc. 2008/00303-5). MCQO is indebted to FAPESP for a fellowship (Proc. 2008/05899-3).

References

- [1] R. Bertazzoli, C. A. Rodrigues, E. J. Dallan et al., "Mass transport properties of a flow-through electrolytic reactor using a porous electrode: performance and figures of merit for Pb(II) removal," *Brazilian Journal of Chemical Engineering*, vol. 15, no. 4, pp. 396–405, 1998.
- [2] R. L. Pelegrino, R. A. Di Iglia, C. G. Sanches, L. A. Avaca, and R. Bertazzoli, "Comparative study of commercial oxide electrodes performance in electrochemical degradation of organics in aqueous solutions," *Journal of the Brazilian Chemical Society*, vol. 13, no. 1, pp. 60–65, 2002.
- [3] R. T. Pelegrini, R. S. Freire, N. Duran, and R. Bertazzoli, "Photoassisted electrochemical degradation of organic pollutants on a DSA type oxide electrode: process test for a phenol synthetic solution and its application for the E1 bleach Kraft mill effluent," *Environmental Science and Technology*, vol. 35, no. 13, pp. 2849–2853, 2001.
- [4] A. Savall, "Electrochemical treatment of industrial organic effluents," *Chimia*, vol. 49, pp. 23–27, 1995.
- [5] C. A. C. Sequeira and C. Cominellis, "Electrochemical oxidation of organic pollutants for wastewater treatment," in *Environmental Oriented Electrochemistry*, pp. 77–101, Elsevier, Amsterdam, The Netherlands, 1994.

- [6] L. Lipp and D. Pletcher, "The preparation and characterization of tin dioxide coated titanium electrodes," *Electrochimica Acta*, vol. 42, no. 7, pp. 1091–1099, 1997.
- [7] B. Correa-Lozano, C. Comminellis, and A. De Battisti, "Service life of Ti/SnO₂-Sb₂O₅ anodes," *Journal of Applied Electrochemistry*, vol. 27, no. 8, pp. 970–974, 1997.
- [8] M. D. P. T. Sotomayor and L. T. Kubota, "Enzymeless biosensors: a novel area for the development of amperometric sensors," *Química Nova*, vol. 25, no. 1, pp. 123–128, 2002.
- [9] M. D. P. T. Sotomayor, A. A. Tanaka, R. S. Freire, and L. T. Kubota, "Amperometric sensors based on biomimetic catalysts," in *Encyclopedia of Sensors*, vol. 1, pp. 195–210, American Scientific, Stevenson Ranch, Calif, USA, 2006.
- [10] M. D. P. T. Sotomayor, A. Sigoli, M. R. V. Lanza, A. A. Tanaka, and L. T. Kubota, "Construction and application of an electrochemical sensor for paracetamol determination based on iron tetrapyrindinoporphyrazine as a biomimetic catalyst of P450 enzyme," *Journal of the Brazilian Chemical Society*, vol. 19, no. 4, pp. 734–743, 2008.
- [11] M. C. Q. Oliveira, M. R. V. Lanza, A. A. Tanaka, and M. D. P. T. Sotomayor, "Flow injection analysis of paracetamol using a biomimetic sensor as a sensitive and selective amperometric detector," *Analytical Methods*, vol. 2, no. 5, pp. 507–512, 2010.
- [12] A. A. Tanaka, C. Fierro, D. A. Scherson, and E. Yeager, "Oxygen reduction on adsorbed iron tetrapyrindinoporphyrazine," *Materials Chemistry and Physics*, vol. 22, no. 3-4, pp. 431–456, 1989.
- [13] P. Calvo-Marzal, S. S. Rosatto, P. A. Granjeiro, H. Aoyama, and L. T. Kubota, "Electroanalytical determination of acid phosphatase activity by monitoring p-nitrophenol," *Analytica Chimica Acta*, vol. 441, no. 2, pp. 207–214, 2001.
- [14] H. Bergamin, J. X. Medeiros, B. F. Reis, and E. A. G. Zagatto, "Solvent extraction in continuous flow injection analysis. Determination of molybdenum in plant material," *Analytica Chimica Acta*, vol. 101, no. 1, pp. 9–16, 1978.
- [15] R. S. Rocha, A. A. G. F. Beati, J. G. Oliveira, and M. R. V. Lanza, "Evaluation of the degradation of sodium diclofenac using H₂O₂/fenton in electrochemical reactor," *Química Nova*, vol. 32, no. 2, pp. 354–358, 2009.
- [16] A. A. G. F. Beati, R. S. Rocha, J. G. Oliveira, and M. R. V. Lanza, "Study of the ranitidine degradation by H₂O₂ electrogenerated/fenton in a electrochemical reactor with gas diffusion electrode," *Química Nova*, vol. 32, no. 1, pp. 125–130, 2009.
- [17] O. De Nora, A. Nidola, G. Trisoglio, and G. Bianchi, Br. Patent no. 1 399 576, 1973.
- [18] L. G. P. Rezende, V. M. Do Prado, R. S. Rocha, A. A. G. F. Beati, M. D. P. T. Sotomayor, and M. R. V. Lanza, "Degradação Eletroquímica do cloranfenicol em reator de fluxo," *Química Nova*, vol. 33, no. 5, pp. 1088–1092, 2010.
- [19] G. Lunn, *HPLC-Methods for Pharmaceutical Analysis*, Vol. 1, John Wiley & Sons, New York, NY, USA, 2000.
- [20] P. Atkins and L. Jones, "Principios de Química: Questionando a vida e o meio ambiente, traduction for Bookman," Porto Alegre, pp. 654, 2001.

Research Article

Scanning Electrochemical Microscopy as a Tool for the Characterization of Dental Erosion

Pollyana S. Castro,¹ Alex S. Lima,¹ Tiago L. Ferreira,² and Mauro Bertotti¹

¹ Instituto de Química, Universidade de São Paulo (USP), 05508-900 São Paulo, SP, Brazil

² Instituto de Ciências Ambientais, Químicas e Farmacêuticas, Universidade Federal de São Paulo (UNIFESP), Campus Diadema, 09972-270 Diadema, SP, Brazil

Correspondence should be addressed to Mauro Bertotti, mbertott@iq.usp.br

Received 9 February 2011; Accepted 11 March 2011

Academic Editor: Sibel A. Ozkan

Copyright © 2011 Pollyana S. Castro et al. This is an open access article distributed under the Creative Commons Attribution License, which permits unrestricted use, distribution, and reproduction in any medium, provided the original work is properly cited.

When the tooth is exposed to acidic environments, an irreversible loss of dental hard tissue occurs in a process called dental erosion. In this work, the scanning electrochemical microscopy (SECM) was used to probe the consumption of protons at the vicinity of a tooth surface with a platinum microelectrode fixed at -0.5 (V) versus Ag/AgCl/KCl_(sat). SECM approach curves were recorded to assess the extent of diffusion in the solution close to the tooth substrate. SECM images clearly demonstrated that the acid erosion process is very fast at solution pH values in the range between 3 and 4.

1. Introduction

The last decades have witnessed major advances in dental medicine and oral health. One of these breakthroughs was the improvement in oral hygiene and the practice of healthier diets, which are the main factors contributing to greater longevity of the dentition. However, more people are consuming high-acid food and drinks, hence exposing their teeth to the risk of erosion. These acid substances slowly soften the tooth surface, making it more susceptible to abrasion and contributing to the loss of the chemical structure. Erosion is the loss of tooth enamel, the hard, protective coating of the tooth, composed of impure calcium hydroxyapatite, $\text{Ca}_{10}(\text{PO}_4)_6(\text{OH})_2$ [1]. The process is caused by acid attack that does not involve bacteria and results in tooth wear of dentin hypersensitivity, loss of form and color of the tooth, which may require restorative complex interventions [2]. When the enamel is worn away, the dentine underneath is exposed, which may lead to pain and sensitivity.

The deterioration of the tooth structure has been investigated by several methods. Xu et al. showed changes in the microstructure of dentin and its composition by using

electrochemical impedance spectroscopy and other surface analysis techniques assisted in the chemical and structural characterization of the investigated material [3]; Cheng et al. used scanning electron microscopy and atomic force microscopy aiming to improve the understanding of the erosion process and obtained qualitative and quantitative information on the morphology and structure of enamel before and after exposure to acid solutions [4]. Atomic force microscopy was used by Quartarone et al. in an in vitro study, where the surface roughness of teeth samples kept in contact with acid drinks was evaluated and the results showed deep holes in the structure of enamel [5]. Heurich et al. using confocal laser scanning microscopy, a technique widely used to quantitatively analyze enamel surfaces eroded by acidic solution, obtained quickly and accurately single 3D image topographic differences between an eroded enamel surface and a given reference area [6].

Scanning Electrochemical Microscopy (SECM) is an attractive technique to get localized information about the nature and properties of a sample surface [7–11]. The probe is a microelectrode electrically biased, and the current is monitored as the sensor is scanned precisely in the x , y , and z directions. The technique can be used, for instance, to obtain

images that show consumption of an electroactive species in a microscopic scale, such as in the investigation of oxygen consumption by a cyclic-tetrameric copper(II) complex immobilized on the surface of a glassy carbon electrode [12]. SECM has already been used to probe localized fluxes of electroactive species diffusing through dentinal tubules [13–16]. Accordingly, the aim of this paper is to demonstrate that SECM can be used to provide interesting *in situ* information on the chemical dissolution of bovine dental enamel by acidic solutions with low pH values. The high-resolution capability of the technique offers the possibility for monitoring different products against enamel and dental erosion in a rapid and simple experiment.

2. Experimental

2.1. Materials. All reagents were of analytical grade and supplied by Merck (Darmstadt, Germany). Deionized water processed through a Nanopure Infinity purification system ($18 \text{ M}\Omega \text{ cm}^{-1}$) (Barnstead, Dubuque, IA, USA) was used to prepare the solutions.

2.2. Electrochemical Measurements. An Autolab PGSTAT 30 (Eco Chemie) bipotentiostat with data acquisition software made available by the manufacturer (GPES 4.8 version) was used for electrochemical measurements. A platinum disc microelectrode was used as working electrode, and a homemade Ag/AgCl (saturated KCl) and a platinum wire were used as reference and counter electrodes, respectively.

2.3. Microelectrode Fabrication. A cleaned $25 \mu\text{m}$ diameter platinum fiber (Alfa Aesar, Massachusetts, USA) was connected to an Ni/Cr wire with silver ink conductive paint (Joint Metal Comércio LTDA, São Paulo, Brazil), inserted into a glass capillary and vacuum-sealed with the P-97 Flaming/Brown Micropipette Puller (Sutter Instrument Company, USA). In order to ensure reproducible measurements, the microelectrode surface was polished with sandpaper (no. 400) and alumina slurry ($1 \mu\text{m}$, Alfa Aesar, Massachusetts, USA). Then, the microelectrode surface was rinsed with water and sonicated for 5 minutes in distilled water. The radius of the microelectrode was determined by measuring the steady-state current in a $10 \text{ mmol L}^{-1} \text{ K}_3\text{Fe}(\text{CN})_6$ solution containing $0.1 \text{ mol L}^{-1} \text{ KCl}$ as supporting electrolyte [17].

2.4. SECM Experiments. Scanning Electrochemical Microscopy (SECM) experiments were performed using a Sensolytics Base SECM (Sensolytics, Bochum, Germany) instrument with option High-Res. The SECM tip was a $25 \mu\text{m}$ diameter platinum disc microelectrode ($\text{RG} = rg/a = 10$, where rg is the radius of the electrode plus surrounding insulator and a is the radius of the disc microelectrode). A homemade Ag/AgCl (saturated KCl) and a platinum wire were used as reference and counter electrodes, respectively. The tip positioning in the z -axis was accomplished by using oxygen as redox mediator in experiments, where the microelectrode was polarized at -0.8 (V) versus Ag/AgCl/KCl_(sat)

[18]. The steady-state current was monitored by moving the tip from the bulk solution toward the substrate surface at a constant scan rate of $2.5 \mu\text{m s}^{-1}$. A touch of the tip to the insulating surface could be usually detected by a sharp decrease of the current because of the hindering effect (negative feedback). The approach curve and SECM images involving the evaluation of localized pH changes were obtained by measuring the diffusion-limiting current for reduction of H^+ with the microelectrode biased at -0.5 (V) versus Ag/AgCl/KCl_(sat). Current data displayed either in the approach curves or SECM images were normalized for the diffusion-limiting current determined experimentally with the tip located in the bulk solution. In order to avoid the loss of activity of the platinum microelectrode tip during the acquisition of SECM images, its surface was cleaned by an electrochemical procedure. Accordingly, the tip had its potential biased at 0.2 (V) versus Ag/AgCl/KCl_(sat) for 10 s between each experiment [12].

2.5. Teeth Samples Preparation. Bovine mandibular incisor teeth were extracted without visible fractures, and the soft tissue was removed by using a periodontal instrument. The samples were subjected to prophylaxis with pumice paste and water and stored in a disinfectant solution (0.5% chloramine T) at 4°C to prevent unwanted bacterial growth. $5 \times 5 \times 5 \text{ mm}$ cross-sections of the teeth were obtained by using a cutting machine (Extec Labcut 1010). The enamel surface was polished using sandpaper (nos. 220, 320, and 600), followed by a $1 \mu\text{m}$ alumina paste (Alfa Aesar, Massachusetts, USA), and then cleaned by ultrasonication to remove residues from polishing. The samples were washed and stored in deionized water at room temperature prior to SECM experiments.

3. Results and Discussion

3.1. Microelectrode Response to H^+ . The monitoring of pH changes at the vicinity of the tooth during acid erosion was carried out by using a platinum microelectrode. Preliminary experiments to assess the behavior of the probe were performed by recording cyclic voltammograms in $0.1 \text{ mol L}^{-1} \text{ KCl}$ solutions containing H^+ at concentrations varying from 0.05 to 0.8 mmol L^{-1} . In this paper, for the sake of simplicity we shall assume that protons concentration is the same as their activity; hence, pH is a measurement of the H^+ concentration. Figure 1 shows a typical voltammogram recorded at 20 mV s^{-1} , a characteristic sigmoidal wave both on the forward and the backward scan being obtained [19]. The limiting current was linear in H^+ concentration according to the following equation: $I(\text{nA}) = -4.1 + 0.14 [\text{H}_2\text{SO}_4] \text{ mmol L}^{-1}$, $r = 0.9968$.

3.2. Concentration Profiles. The protons consumption at the teeth surface was first investigated by performing a SECM approach curve experiment in a solution of $\text{pH} = 3.4$. The tip was biased at -0.5 (V) versus Ag/AgCl/KCl_(sat), where the reduction of solvated protons is mass-transport controlled. As the tip was moved close to an insulating surface

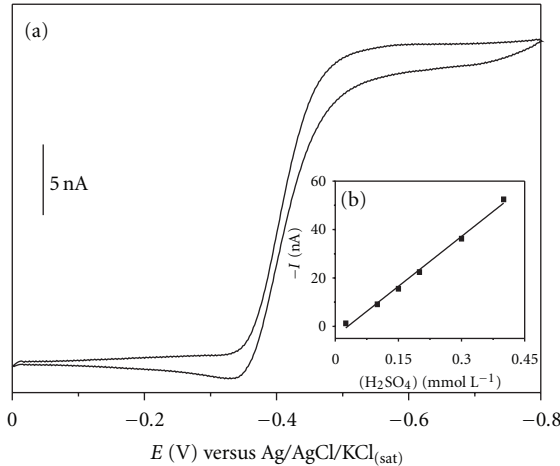
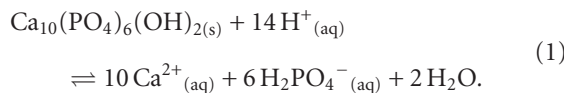


FIGURE 1: Cyclic voltammogram recorded with a platinum micro-electrode in a 0.2 mmol L⁻¹ H₂SO₄ + 0.1 mol L⁻¹ KCl solution (pH = 3.4) (a) and calibration plot (b) Scan rate = 20 mV s⁻¹.

(curve A in Figure 2), the steady-state current decreased because of hindered diffusion. In this case, the negative feedback effect is expected to appear only when the distance between substrate and tip is around a few L units (L = ratio between tip-substrate distance and microelectrode radius) [20]. No hysteresis between forward and back approaches was noticed, hence, this experiment was not time dependent. On the other hand, a clear difference is noticed when the experiment is repeated using a tooth sample as substrate (curve B in Figure 2). In this case, the current decrease starts at regions very far from the substrate surface (around 2000 μ m), which is an indication of the chemical consumption of protons and the development of a concentration gradient. The process involving the enamel dissolution is time dependent, which explains the significant hysteresis observed in the reverse scan. Figure 3 shows a schematic picture of the processes occurring at the tip microelectrode (proton sensing) and the tooth surface (enamel acid erosion).

3.3. SECM Images. The current at the probe is proportional to the concentration of H⁺ in solution. The local proton concentration may change in the gap between the positioned microelectrode and the tooth surface owing to the acid erosion of the enamel, according to the following equation:



Scanning in a rastered pattern was performed at a constant substrate-tip separation above the tooth sample (10 μ m). All the images presented in this paper relate to a 300 μ m × 300 μ m area of the substrate. The SECM images in Figure 4 correspond to a 2D representation of the local tip current. Since the tooth surface is flat, the current changes indicate variations in the proton concentration at this point in the space. A previous experiment was performed by scanning the tip over an insulating substrate

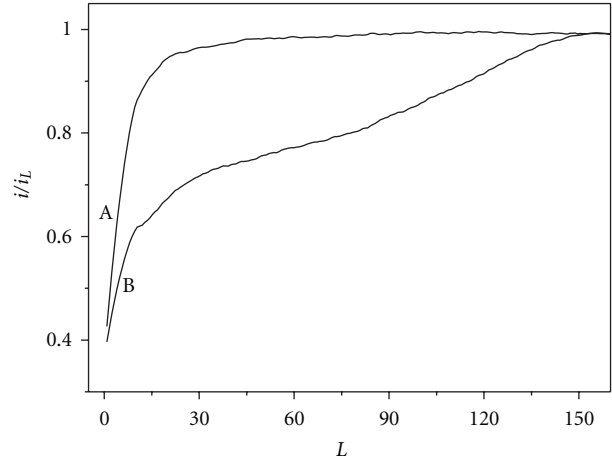


FIGURE 2: Approach curves obtained with a platinum microelectrode ($r = 12.5 \mu\text{m}$) in a 0.2 mmol L⁻¹ H₂SO₄ + 0.1 mol L⁻¹ KCl solution (pH = 3.4) for an insulating substrate (A) and a teeth sample (B), L = ratio between tip-substrate distance and microelectrode radius. Scan rate = 10 $\mu\text{m s}^{-1}$.

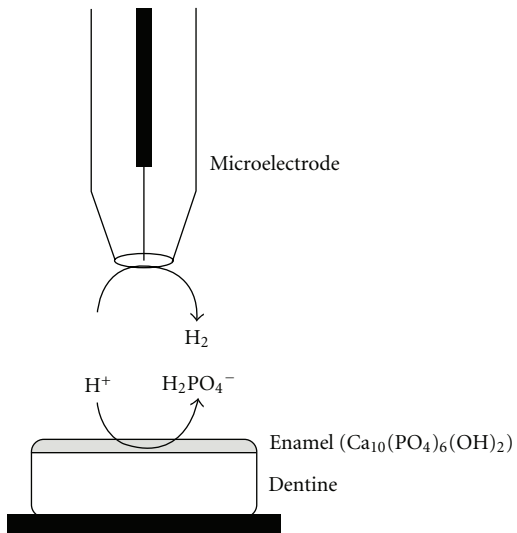


FIGURE 3: Schematic representation of the SECM experiment.

that is inert towards H⁺ reaction. The obtained image (a) reveals no significant change, which indicates the good and reproducible response of the probe and the flatness of the surface and also that no convective effects caused by the tip movement or solution stirring during the scan are noticed.

A noticeable difference is seen when the same experiment was repeated using the tooth as substrate (image (b)). By comparing images (a) and (b) in Figure 4, one can conclude that the results observed in this study clearly demonstrate the protons consumption due to the enamel erosion and that the remarkable current changes are not a consequence of convection due to tip displacement. By taking into account the time required for obtaining one image (around 5 minutes) at the experimental conditions used in this work (scan rate = 20 $\mu\text{m s}^{-1}$), it is possible to conclude that the

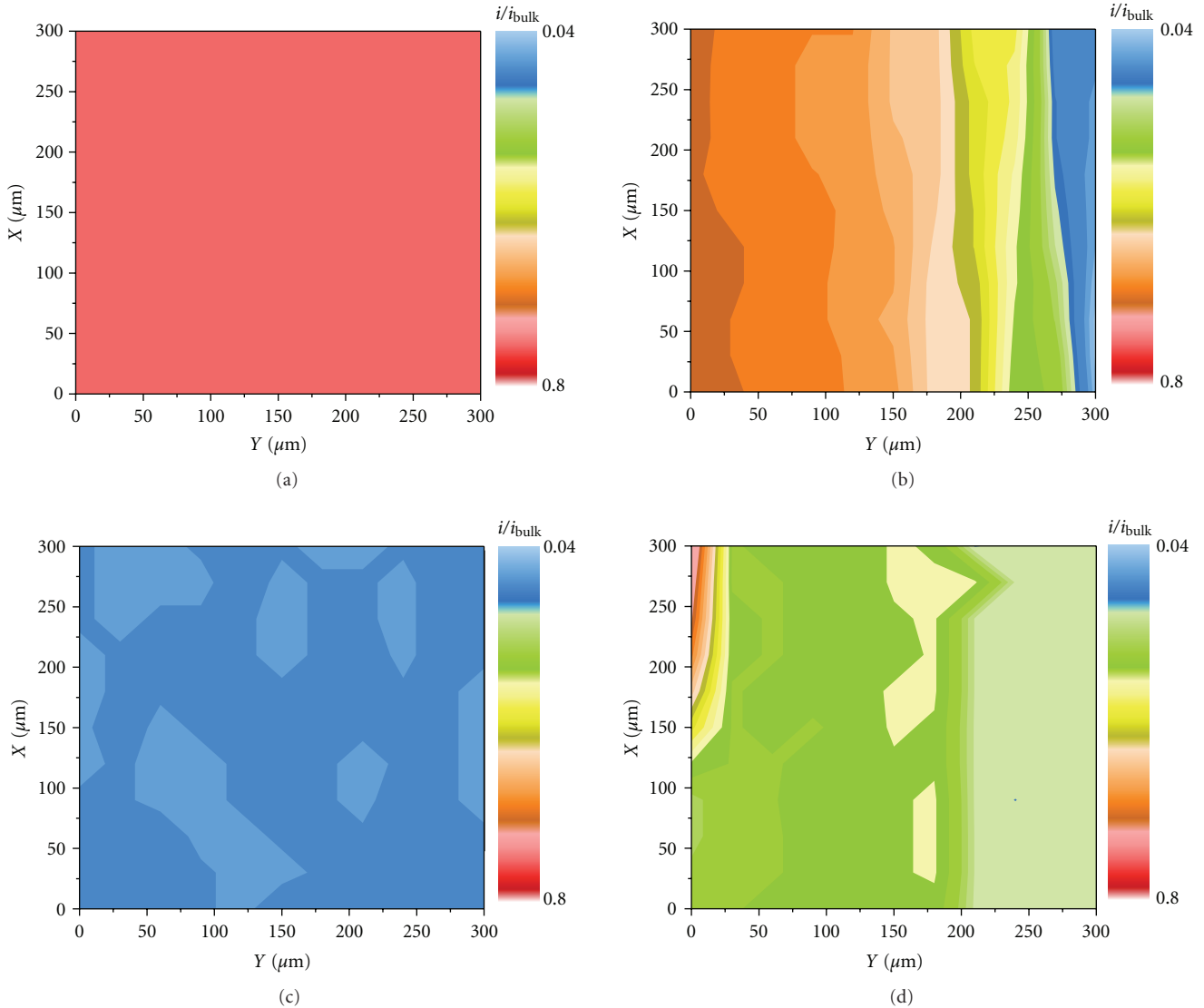


FIGURE 4: SECM 2D images obtained with a platinum microelectrode ($r = 12.5 \mu\text{m}$) in a $0.2 \text{ mmol L}^{-1} \text{ H}_2\text{SO}_4 + 0.1 \text{ mol L}^{-1} \text{ KCl}$ solution ($\text{pH} = 3.4$) for an insulating substrate (a) and a tooth sample at different times: 0 minutes (b), 60 minutes (c), and 70 minutes (d). Image (d) was recorded after solution stirring. Scan rate = $20 \mu\text{m s}^{-1}$.

erosion process is fast. This is in agreement with results of kinetic studies on the chemical dissolution of calcium hydroxyapatite at pH values in the range 3.7 to 6.5 [21] and acid-induced dissolution experiments using SECM [22].

A new image (c) was obtained after one hour, and no significant change during the scan was observed. On the other hand, a different situation was noticed when the solution was stirred for homogenization prior to the acquisition of a new image (d). In the beginning of this experiment the current is similar to the one obtained in the bulk solution, but its decay is very fast probably because of the removal of the chemical resistant enamel outer layer [6, 23]. A final experiment (image not shown) was carried out using an acetate buffer solution of the same $\text{pH} = 3.4$. The current values were almost the same during the whole scan, indicating that the pH is maintained at a constant value because protons are efficiently supplied by the buffer.

4. Conclusions

The dissolution rate of enamel during acid erosion is dependent on some chemical parameters such as pH and calcium and phosphate-containing salts concentration [23]. From the results shown in this work, one can suggest that the enamel dissolution is a relatively fast process that causes the proton diffusion layer to extend to a large distance into the bulk solution.

The dissolution mechanism is controlled by intrinsic interfacial phenomena, and it is well known that in the presence of some ions, such as fluoride, the rate of erosion of calcium hydroxyapatite is greatly reduced. Moreover, SECM can be easily employed as a powerful tool to investigate the complex chemical reactions responsible for acid erosion as well as in the elucidation of the mechanism of protection by inhibiting ions. Another possibility to prevent dental

erosive demineralization is the use of TiF_4 or NaF varnishes, whose protective effect is attributed to the formation of acid-resistant blocking layers [24, 25]. The enamel erosion has been typically monitored by ex-situ contact profilometry [26, 27] and the effectiveness of such treatments can be also easily assessed through a series of simple and fast SECM experiments.

Acknowledgments

The authors are thankful to FAPESP (Fundação de Amparo à Pesquisa do Estado de São Paulo) and CNPq (Conselho Nacional de Desenvolvimento Científico e Tecnológico) for the financial support. The authors are also thankful to Dr. Carlos Eduardo Francci and Alexander C. Nishida for making available to us the teeth used in this work and to Gabriel N. Meloni for helping with the microelectrode images.

References

- [1] M. E. Barbour, D. M. Parker, and K. D. Jandt, "Enamel dissolution as a function of solution degree of saturation with respect to hydroxyapatite: a nanoindentation study," *Journal of Colloid and Interface Science*, vol. 265, no. 1, pp. 9–14, 2003.
- [2] R. Cheng, H. Yang, M. Y. Shao, T. Hu, and X. D. Zhou, "Dental erosion and severe tooth decay related to soft drinks: a case report and literature review," *Journal of Zhejiang University: Science B*, vol. 10, no. 5, pp. 395–399, 2009.
- [3] Z. Xu, K. G. Neoh, and A. Kishen, "Monitoring acid-demineralization of human dentine by electrochemical impedance spectroscopy (EIS)," *Journal of Dentistry*, vol. 36, no. 12, pp. 1005–1012, 2008.
- [4] Z. J. Cheng, X. M. Wang, F. Z. Cui, J. Ge, and J. X. Yan, "The enamel softening and loss during early erosion studied by AFM, SEM and nanoindentation," *Biomedical Materials*, vol. 4, no. 1, Article ID 015020, 2009.
- [5] E. Quartarone, P. Mustarelli, C. Poggio, and M. Lombardini, "Surface kinetic roughening caused by dental erosion: an atomic force microscopy study," *Journal of Applied Physics*, vol. 103, no. 10, Article ID 104702, 2008.
- [6] E. Heurich, M. Beyer, K. D. Jandt et al., "Quantification of dental erosion—a comparison of stylus profilometry and confocal laser scanning microscopy (CLSM)," *Dental Materials*, vol. 26, no. 4, pp. 326–336, 2010.
- [7] M. A. Edwards, S. Martin, A. L. Whitworth, J. V. Macpherson, and P. R. Unwin, "Scanning electrochemical microscopy: principles and applications to biophysical systems," *Physiological Measurement*, vol. 27, no. 12, article R01, 2006.
- [8] A. J. Bard, F.-R. Fan, and M. V. Mirkin, *Scanning Electrochemical Microscopy in Electroanalytical Chemistry*, Marcel Dekker, New York, NY, USA, 1994.
- [9] M. V. Mirkin, "Recent advances in scanning electrochemical microscopy," *Analytical Chemistry*, vol. 68, no. 5, pp. A177–A182, 1996.
- [10] A. L. Barker, M. Gonsalves, J. V. MacPherson, C. J. Slevin, and P. R. Unwin, "Scanning electrochemical microscopy: beyond the solid/liquid interface," *Analytica Chimica Acta*, vol. 385, no. 1–3, pp. 223–240, 1999.
- [11] A. J. Bard and M. V. Mirkin, *Scanning Electrochemical Microscopy*, John Wiley & Sons, New York, NY, USA, 2001.
- [12] I. O. Matos, T. L. Ferreira, T. R. L. C. Paixão, A. S. Lima, M. Bertotti, and W. A. Alves, "Approaches for multicopper oxidases in the design of electrochemical sensors for analytical applications," *Electrochimica Acta*, vol. 55, no. 18, pp. 5223–5229, 2010.
- [13] S. Nugues and G. Denuault, "Scanning electrochemical microscopy: amperometric probing of diffusional ion fluxes through porous membranes and human dentine," *Journal of Electroanalytical Chemistry*, vol. 408, no. 1–2, pp. 125–140, 1996.
- [14] J. V. Macpherson and P. R. Unwin, "Scanning electrochemical microscopy as an in vitro technique for measuring convective flow rates across dentine and the efficacy of surface blocking treatments," *Electroanalysis*, vol. 17, no. 3, pp. 197–204, 2005.
- [15] J. V. Macpherson, M. A. Beeston, P. R. Unwin, N. P. Hughes, and D. Littlewood, "Imaging the action of fluid flow blocking agents on dentinal surfaces using a scanning electrochemical microscope," *Langmuir*, vol. 11, no. 10, pp. 3959–3963, 1995.
- [16] J. V. MacPherson, M. A. Beeston, P. R. Unwin, N. P. Hughes, and D. Littlewood, "Scanning electrochemical microscopy as a probe of local fluid flow through porous solids," *Journal of the Chemical Society, Faraday Transactions*, vol. 91, no. 9, pp. 1407–1410, 1995.
- [17] T. R. L. C. Paixão and M. Bertotti, "Methods for fabrication of microelectrodes towards detection in microenvironments," *Química Nova*, vol. 32, no. 5, pp. 1306–1314, 2009.
- [18] R. M. Souto, L. Fernández-Mérida, and S. González, "Secm imaging of interfacial processes in defective organic coatings applied on metallic substrates using oxygen as redox mediator," *Electroanalysis*, vol. 21, no. 24, pp. 2640–2646, 2009.
- [19] S. Daniele, I. Lavagnini, M. A. Baldo, and F. Magno, "Steady state voltammetry at microelectrodes for the hydrogen evolution from strong and weak acids under pseudo-first and second order kinetic conditions," *Journal of Electroanalytical Chemistry*, vol. 404, no. 1, pp. 105–111, 1996.
- [20] A. J. Bard, F. R. F. Fan, J. Kwak, and O. Lev, "Scanning electrochemical microscopy. Introduction and principles," *Analytical Chemistry*, vol. 61, no. 2, pp. 132–138, 1989.
- [21] J. M. Thomann, J. C. Voegel, and P. Gramain, "Kinetics of dissolution of calcium hydroxyapatite powder IV. Interfacial calcium diffusion controlled process," *Colloids and Surfaces*, vol. 54, no. C, pp. 145–159, 1991.
- [22] C.-A. McGeouch, M. A. Edwards, M. M. Mbogoro, C. Parkinson, and P. R. Unwin, "Scanning electrochemical microscopy as a quantitative probe of acid-induced dissolution: theory and application to dental enamel," *Analytical Chemistry*, vol. 82, no. 22, pp. 9322–9328, 2010.
- [23] M. E. Barbour, D. M. Parker, G. C. Allen, and K. D. Jandt, "Human enamel erosion in constant composition citric acid solutions as a function of degree of saturation with respect to hydroxyapatite," *Journal of Oral Rehabilitation*, vol. 32, no. 1, pp. 16–21, 2005.
- [24] A. C. Magalhães, F. M. Levy, D. Rios, and M. A. R. Buzalaf, "Effect of a single application of TiF_4 and NaF varnishes and solutions on dentin erosion in vitro," *Journal of Dentistry*, vol. 38, no. 2, pp. 153–157, 2010.
- [25] A. C. Magalhães, M. T. Kato, D. Rios, A. Wiegand, T. Attin, and M. A. R. Buzalaf, "The effect of an experimental 4% TiF_4 varnish compared to NaF varnishes and 4% TiF_4 solution on dental erosion in vitro," *Caries Research*, vol. 42, no. 4, pp. 269–274, 2008.

- [26] M. T. Kato, A. L. Leite, A. R. Hannas et al., "Effect of iron on matrix metalloproteinase inhibition and on the prevention of dentine erosion," *Caries Research*, vol. 44, no. 3, pp. 309–316, 2010.
- [27] A. J. White, C. Yorath, V. ten Hengel, S. D. Leary, M.-C. D. N. J. M. Huysmans, and M. E. Barbour, "Human and bovine enamel erosion under 'single-drink' conditions," *European Journal of Oral Sciences*, vol. 118, no. 6, pp. 604–609, 2010.

Research Article

Fabrication of Biosensor Based on Polyaniline/Gold Nanorod Composite

Uğur Tamer, Ali İhsan Seçkin, Erhan Temur, and Hilal Torul

Department of Analytical Chemistry, Faculty of Pharmacy, Gazi University, 06330 Ankara, Turkey

Correspondence should be addressed to Uğur Tamer, utamer@gazi.edu.tr

Received 15 February 2011; Accepted 22 March 2011

Academic Editor: Bengi Uslu

Copyright © 2011 Uğur Tamer et al. This is an open access article distributed under the Creative Commons Attribution License, which permits unrestricted use, distribution, and reproduction in any medium, provided the original work is properly cited.

This present paper describes a new approach to fabricate a new amperometric sensor for the determination of glucose. Polyaniline (PANI) film doped with colloidal gold nanorod particles has been used to immobilize glucose oxidase by glutaraldehyde. The polyaniline/gold nanorod composite structure gave an excellent matrix for enzyme immobilization due to the large specific surface area and higher electroactivity. The composite has been characterized by cyclic voltammetry (CV), scanning electron microscopy (SEM), and surface-enhanced Raman spectroscopy (SERS). The SERS spectrum of the surface-immobilized glucose oxidase and the spectrum of the native enzyme indicate that the main feature of the native structure of glucose oxidase was conserved after being immobilized on the polymer matrix. The amperometric response was measured as a function of concentration of glucose at a potential of 0.6 V versus Ag/AgCl in 0.1 M phosphate buffer at pH 6.4. Linear range of the calibration curve was from $17.6 \mu\text{M}$ to 1 mM with a sensitivity of $13.8 \mu\text{A} \cdot \text{mM}^{-1} \cdot \text{cm}^{-2}$ and a limit of detection (LOD) of $5.8 \mu\text{M}$. The apparent Michaelis-Menten constant K_M was calculated as 1.0 mM and the response time was less than 3 seconds.

1. Introduction

Quantitative determination of glucose has attracted wide interest for biomedical applications due to the high demand for blood glucose monitoring [1]. Numerous analytical techniques are available for glucose quantification especially those that are based on spectroscopy [2, 3] and electrochemical sensing strategies [4]. The simplicity of electrochemical methods makes them highly attractive approaches for the detection of glucose [5]. Application of electrochemical methods at solid electrodes provides new approaches to the detection of glucose regarding controlling the surface properties of electrode so that to improve selectivity and sensitivity. For glucose monitoring, different strategies can be used to endow electrode surfaces with sensing abilities. As a new class of electrode materials, conducting polymers provide a suitable platform for the detection of biological analytes [6].

Conducting polymers have been proven to be suitable host matrices for dispersing metallic particles. Composites of conducting polymers and metal nanoparticles permit a facile flow of electronic charges across the polymer matrix during

electrochemical processes. Conducting polymer plays an additional role in the electrochemical processes. In addition, metallic nanoparticles can also be dispersed well into the matrix of these polymers [7]. Gold nanoparticles have unique optoelectronic properties [8]. Therefore, through a suitable combination of conducting polymers and gold nanoparticles, newly modified surfaces can be generated with higher surface area and enhanced catalytical/electrocatalytic activities [9].

PANI has been of scientific and technological interest [10]. Different biomolecules such as enzymes, proteins, and DNA have been successfully immobilized on PANI modified electrodes and showed excellent performance [11, 12]. However, PANI has low electroactivities and conductivities in neutral solutions due to the slow electron transfer and diffusivities of proteins [13, 14]. The electrochemical and electrocatalytic activities of PANI can be greatly increased if PANI is combined with gold nanoparticles [15]. For example, gold nanoparticles, functionalized with a sulfonate group, were incorporated into a polyaniline film by electropolymerization, and the resulting film was used for biocatalysis [16]. Spherical gold nanoparticles have

also been adsorbed onto the surface of core-shell structured polystyrene/polyaniline, resulting in the formation of PS/PANI/Au nanocomposite, and glucose oxidase was entrapped into the nanocomposite-modified glassy carbon electrode [17]. A large surface area of PANI nanofiber was prepared using HAuCl₄ as an oxidizing agent to immobilize glucose oxidase, and a glucose biosensor was developed [18]. This paper did not show any evidence as to what type of gold nanoparticle exists in the polymer matrix. To the best of our knowledge, there is only one report on using the colloidal gold nanorod particle which is embedded in the cellulose acetate membrane to fabricate the glucose biosensor [19]. Ren et al. worked with cellulose acetate to fabricate glucose biosensor, and they firstly compiled gold nanorod and GOx mixed solution on electrode surface after drying procedure. Then, enzyme was crosslinked by glutaraldehyde. At last point, the electrode was immersed into gold nanorod-cellulose acetate mixture. In our study, firstly, PANI-gold nanorod polymer film was formed electrochemically on electrode surface. Then enzyme was crosslinked by glutaraldehyde as GOx.

In this present paper, we propose a new approach to fabricate a new amperometric sensor for the determination of glucose. PANI film doped with colloidal gold nanorod particles has been used to immobilize glucose oxidase by glutaraldehyde. The polyaniline/gold nanorod composite structure gave an excellent matrix for enzyme immobilization due to the large specific surface area and higher electroactivity. The detailed electrochemical investigation and spectroscopic characterization of film electrode were performed. The composite has been characterized by cyclic voltammetry (CV), scanning electron microscopy (SEM), and surface enhanced Raman spectroscopy (SERS). For the determination of the optimum working conditions of the enzyme electrode, the effect of thickness of the polymeric film, pH, and applied potential on the measured current values have been investigated. The stability of the enzyme electrode and the influence of possible interferences were also examined. The analytical performance of the obtained PANI/gold nanorod/enzyme electrodes with respect to linear range, reproducibility, response time, and stability is presented and discussed.

2. Experimental

2.1. Chemicals. Hydrogen tetrachloroaurate (HAuCl₄), hexadecyltrimethyl-ammonium bromide (CTAB), L-ascorbic acid (AA), and poly(sodium 4-styrenesulfonate) 25 wt% solution in water were obtained from Sigma-Aldrich (Taufkirchen, Germany). Silver nitrate (AgNO₃) and sodium borohydride (NaBH₄) were obtained from Merck (Darmstadt, Germany). Glutaraldehyde and glucose oxidase were purchased from Sigma and all the other chemicals were of analytical grades and were used as received. All solutions were prepared using deionized water, 18.2 MΩ cm free from organic matter, which was obtained from a Millipore purification system and was deaerated with argon to remove the oxygen present.

2.2. Instrumentation. Electrochemical experiments were performed with a Gamry potentiostat (model Reference 600, USA). Polymer film formation was achieved in a conventional one-compartment three-electrode cell under argon atmosphere. SERS experiments were performed with a Delta Nu Examiner Raman Microscopy system with a 785 nm Laser source. A motorized microscope stage sample holder and a charge-coupled device (CCD) detector were used. Instrument parameters were as follows: 20x objective, 30 μm spot size, 60 second acquisition time and baseline correction was performed for all measurements. Before SERS experiments, the fully reduced PANI/gold nanorod films were prepared by reducing the oxidized films in an aqueous solution containing 0.1 M LiClO₄ at a constant cathodic potential of 0 V versus Ag/AgCl until the current leveled off. The working electrode, a platinum disk (0.022 cm²), was cleaned by polishing with Al₂O₃ slurry for the cyclic voltammetric studies. The macrosamples of polymer films were prepared on a Pt macroelectrode (1.0 cm²) which was cleaned by holding it in a flame for a few minutes. All data points reported in this work represent the average of three replicates. All experiments were run at room temperature.

The morphologies of the films were examined by scanning electron microscopy (SEM). Scanning electron micrographs were obtained by a JSM-6400 electron microscope (JEOL), equipped with NORAN System 6 X-ray Microanalysis System and Semafore Digitizer.

2.3. Synthesis of Gold Nanorods and Surface Modification. Gold nanorods were prepared by the seed-mediated growth technique with slight modification [20]. The seed solution was prepared by mixing 7.5 mL of 0.1 M CTAB solution with 250 μL of 0.01 M HAuCl₄ solution. Once mixed, 600 μL of 0.01 M ice-cold NaBH₄ was added to the resulting solution and allowed to stand for 5 min to form seed solution. To prepare rod-shaped gold nanoparticle, 4.75 mL of 0.1 M CTAB, 1 mL of 0.01 M HAuCl₄, and 60 μL of 4 × 10⁻³ M AgNO₃ were mixed, respectively. After that, 250 μL of 0.1 M ascorbic acid was added drop-wise to the resulting solution. Then, 5 μL seed solution was added to the stock solution. This final mixture was stirred for 10 seconds and was allowed to stay for 3 hours at room temperature.

Before electropolymerization, the surface of gold nanorods was modified by poly(sodium 4-styrenesulfonate) (PSS) through electrostatic interaction between the positively charged surface of gold nanorod and the negatively charged PSS. Gold nanorod solution was centrifuged to remove any excess of CTAB from the surface of gold nanorod. The aqueous solution of PSS (200 μL 0.1 M) was added to 5 mL gold nanorod solution to form a mixture. After stirring for one hour in a sonicator, the precipitate was centrifuged and washed with deionized water and the procedure was repeated four times. The resulting particles were dispersed in a 5 mL electrochemical cell.

2.4. Fabrication of PANI-Gold Nanorod Electrode. In order to obtain a PANI/gold nanorod film, 0.1 M aniline was added to 0.1 M sulphuric acid and 0.1 M Na₂SO₄ aqueous solution

containing 5 mL as synthesized PSS-CTAB-modified gold nanorod. The electropolymerization was carried out by applying seven potential cycles between -0.2 and 1.2 V versus Ag/AgCl. The obtained films were deposited onto platinum working electrodes by applying a program of successive voltammetric cycles. Following the synthesis process, the electrodes coated with the polymeric films were rinsed with water and were immersed in the background electrolyte.

Amperometric measurements were performed using a three-electrode cell consisting of PANI/nanorod working electrode, platinum wire counter electrode and Ag/AgCl reference electrode. Measurements were conducted in a 5 mL 0.1 M phosphate buffer at pH 6.4. A potential of $+0.6$ V was applied to the electrochemical cell and solutions having different concentrations of glucose were added to the cell.

2.5. Immobilization of Glucose Oxidase on PANI-Gold Nanorod Electrode. Covalent coupling of glucose oxidase to the conducting polymer electrode was performed using glutaraldehyde in phosphate buffer solution with a pH of 7.4. For immobilizing the glucose oxidase enzyme, first $10\ \mu\text{L}$ of 0.1% glutaraldehyde were spread onto a PANI/gold nanorod film and was allowed to dry and to remove the unbound glutaraldehyde molecules, film electrode was again rinsed with deionized water. Then, the glucose oxidase was prepared by dissolving $3\ \text{mg}$ of glucose oxidase in $1\ \text{mL}$ of 0.1 M phosphate buffer and $30\ \mu\text{L}$ of this solution were added to the PANI/gold nanorod film electrode and kept for four hours. After that, PANI/gold nanorod film electrode was rinsed with deionized water to remove unreacted enzyme and was stored at 4°C when not in use.

3. Results and Discussion

3.1. Characterization of PANI/Gold Nanorod Electrode. Aqueous colloids of gold nanorods were synthesized through the reduction of chloroauric acid by means of ascorbic acid in the presence of the surfactant CTAB. Throughout the growth, CTAB forms micelles and a positively charged bilayer around the gold nanorods [21]. Figure 1 displays SEM images of the resulting gold nanorods. The obtained gold nanorods have uniform morphology with average diameter and length of 15 nm and 45 nm , respectively (aspect ratio of 3). To immobilize the gold nanorods to the PANI film, the surface of gold nanorod particles is modified with PSS in order to form the negative charges. The presence of the negatively charged sulfonate-containing groups was proven by zeta potential measurements. Zeta potential values of CTAB modified gold nanorods and PSS-CTAB-modified gold nanorods were found to be $+0.46\text{ mV}$ and -2.92 mV , respectively. Negatively charged PSS-gold nanorod particles were introduced into polymer chain in the doping process of electrochemical polymerization.

Gold nanorod particles have good biocompatibility and the experimental results indicated that the enzyme electrode containing gold nanorods substantially enhances the response current. The increased electrocatalytic activity of

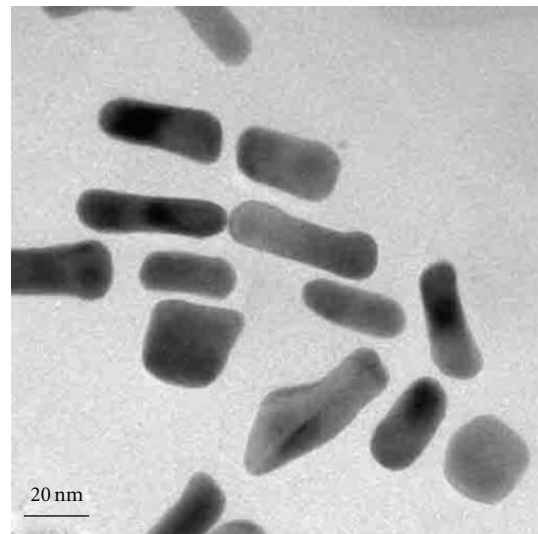


FIGURE 1: SEM image of gold nanorods.

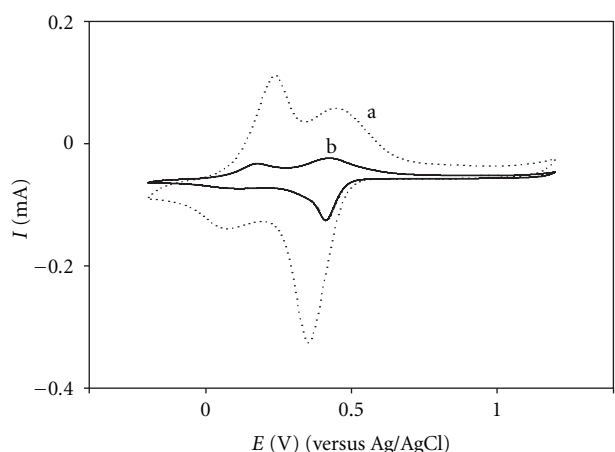


FIGURE 2: Cyclic voltammograms of (a) PANI/gold nanorod and (b) PANI film at 100 mV/s scan rate at $+0.6\text{ V}$ in stirred 0.1 M sulphuric acid and 0.1 M Na_2SO_4 solution.

the electrode containing gold nanorods over the spherical-shaped gold nanoparticle was attributed to the different shape and different oxidation state between gold nanorod and spherical-shaped gold nanoparticle. The surface of the gold nanorod may be partially oxidized to form Au^+ and Au^{+3} during the synthesis and the oxide of the gold could be served as the mediator [22]. Figure 2 shows cyclic voltammograms of PANI in a 0.1 M phosphate buffer solution (pH 7) with and without gold nanorods. The redox peaks observed in the phosphate buffer at pH 7 were the overlap of two redox processes for PANI under acidic conditions [17]. The reason for that gold nanorod with large specific surface area and good conductivity can provide conduction centers in the neutral solution. Therefore, the PANI-gold nanorod composite could also provide an excellent biocompatible environment for enzyme immobilization.

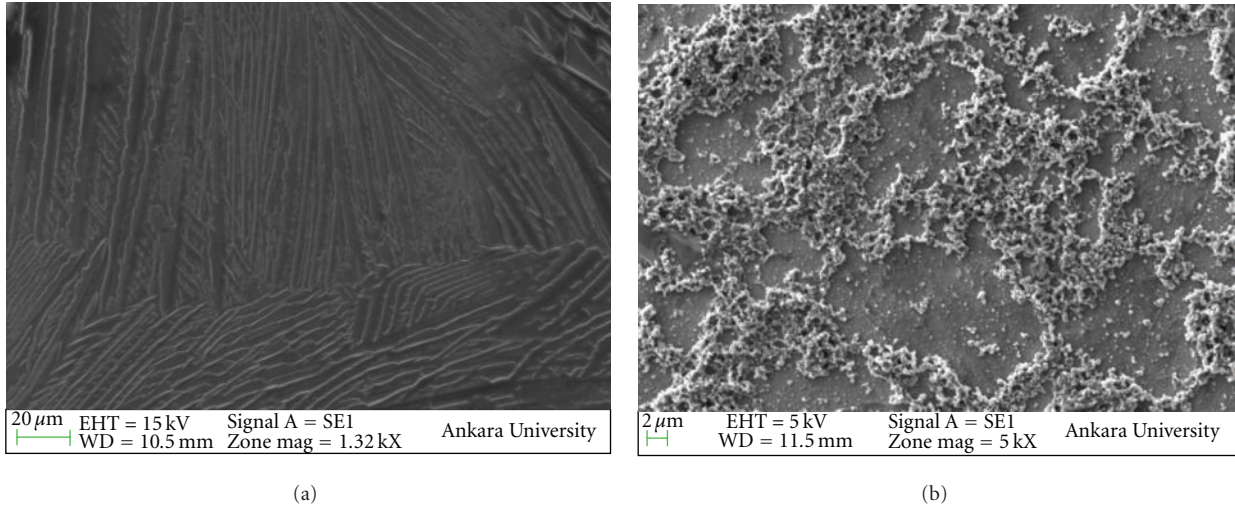


FIGURE 3: SEM images of (a) PANI and (b) PANI/gold nanorod composite electrode.

The nature of the PSS-gold nanorod composite was further examined by SEM. The morphologies of PANI films obtained in the presence and in the absence of gold nanorod were found to be quite different as shown in Figure 3. While PANI prepared in the presence of gold nanorod resulted only in granular morphology, the other gave wrinkled texture as shown in Figure 3(a). This indicated that the morphology of electrochemically synthesized PANI is strongly affected by PSS-CTAB-modified gold nanorods.

3.2. Immobilization of Enzyme on PANI/Gold Nanorod Electrode. Covalent coupling of enzyme to the resulting polymer electrode was performed using glutaraldehyde which is known to be a bifunctional compound mainly used in modification of proteins. A large number of free NH₂ groups are available at the end of each polyaniline chain which bind with the NH₂ groups of enzymes with glutaraldehyde as a crosslinker [23]. To verify and confirm the presence of enzyme in the polymer film, SERS measurements were performed. SERS was used for illustrating the detailed structural information of the conducting polymer film. Figure 4 shows (dotted line) a typical SERS spectrum within the range of 300–2000 cm⁻¹ of PANI film doped with PSS modified gold nanorod. A strong band at 1173 cm⁻¹ is assigned to CH in-plane bending mode of quinoid and semiquinoid rings. The band at 1248 cm⁻¹ can be assigned to CN stretching mode of polaronic units and in-plane deformation quinone ring. The strong band at 1497 cm⁻¹ is assigned to C=N stretching mode which is indicating of quinone diimine structure. Raman bands at 1592 and 1606 cm⁻¹ are attributed to the C=C stretching vibration of benzene rings and C=C stretching of bipolarons, respectively [24–26]. In the SERS spectrum (Figure 4, solid line) recorded after immobilization of glucose oxidase onto the PANI film, several new bands appeared at 1710, 1377, 1075, 1030, 972, 931, 724, and 643 cm⁻¹ which are typical for glucose oxidase, indicating immobilization of glucose oxidase on the polymer surface. The strong band at 1030 cm⁻¹ can

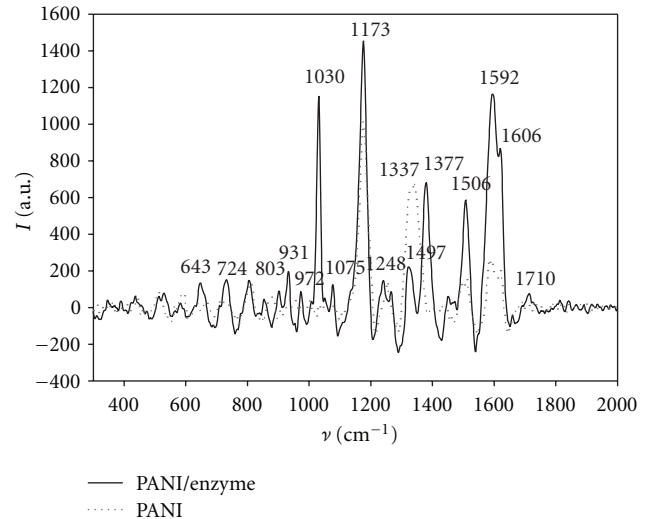


FIGURE 4: SERS spectrum within the range of 300–2000 cm⁻¹ of PANI film doped with PSS-modified gold nanorod (dotted line) and after immobilization of glucose oxidase (solid line).

be assigned to stretching vibrations of N=N bonds and quinone fragment [27]. The bands at 931 and 1377 cm⁻¹ are due to the C-COO⁻ stretching and COO⁻ symmetric stretching vibration modes, respectively [28, 29]. The main characteristic peaks of native glucose oxidase can also be observed in the SERS spectrum as shown in Figure 5. The obtained result agrees with the reported SERS spectrum of the enzyme [30]. The similarity between the SERS spectrum of the surface-immobilized glucose oxidase and the spectrum of the native enzyme indicates that the main feature of the native structure of glucose oxidase was conserved after being immobilized on the polymer matrix.

The thickness of the film is related to the number of cycles in the potential domain selected in cyclic voltammetry. The biosensor performance for different film thicknesses was

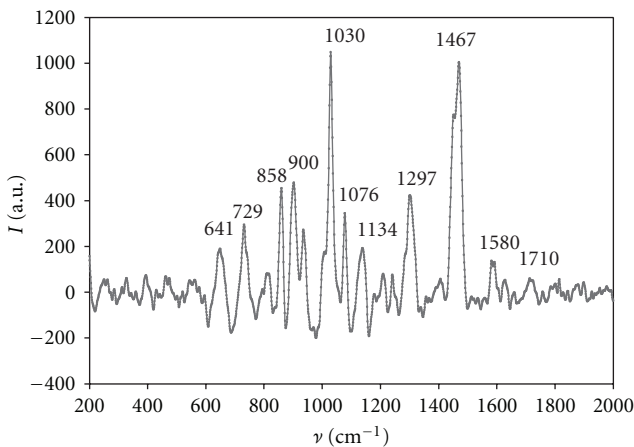


FIGURE 5: SERS spectrum of native glucose oxidase.

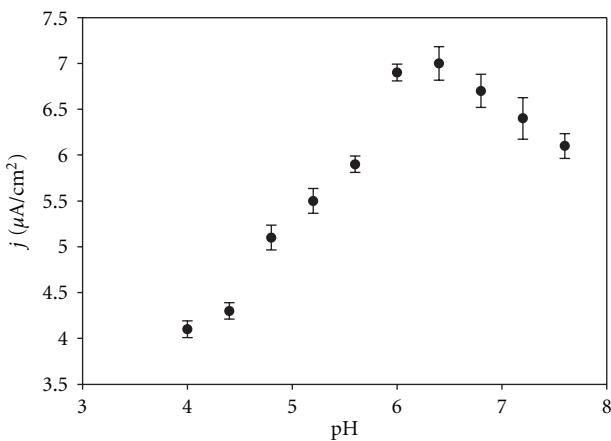
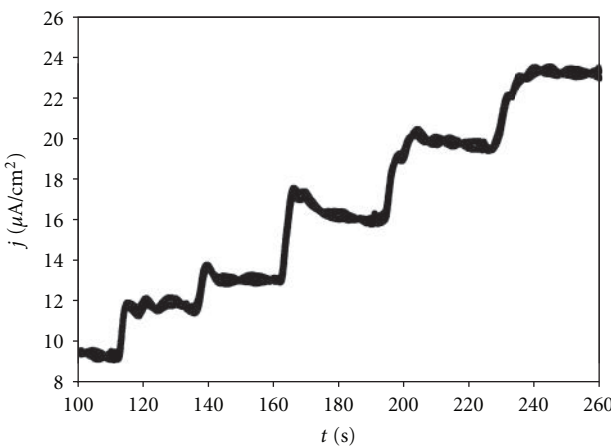


FIGURE 6: The effect of pH on the measured response of PANI-gold nanorod-enzyme film by amperometric detection of 0.5 mM glucose in 0.1 M phosphate buffer in the range of 4.0–8.0.

FIGURE 7: A typical amperometric response of the PANI-gold nanorod-enzyme biosensor after successive additions of 50 μM concentrations of glucose at +0.6 V versus Ag/AgCl in stirred Phosphate buffered saline (PBS) of pH 6.4. (Glucose concentrations were prepared for the final concentrations to be 50, 100, 150, 200, and 250 μM).

evaluated by amperometric detection of 0.5 mM H_2O_2 at 0.6 V versus Ag/AgCl. By increasing the number of cycles, the biosensor response became higher with a maximum of seven cycles, and then the response decreased again. It has been found that PANI-gold nanorod-enzyme electrode with seven deposition cycles showed the desired response characteristics. The effect of pH was also investigated by amperometric detection of 0.5 mM glucose in 0.1 M phosphate buffer in the range of 4.0–8.0. As shown in Figure 6, the highest current intensity was obtained at pH 6.4. Each assay was repeated three times per each pH value. The pH 6.4 was selected for the biosensor response.

3.3. Performance of the Biosensor. Performance of the PANI-gold nanorod-enzyme biosensor was evaluated at room temperature. Figure 7 displays a typical amperometric response of the PANI-gold nanorod-enzyme biosensor upon successive additions of 50 μM concentrations of glucose at +0.6 V versus Ag/AgCl in phosphate buffer of pH 6.4. So glucose concentrations were prepared for the final concentrations to be 50, 100, 150, 200, and 250 μM . With successively increasing the concentration of glucose, a well-defined increase in the current was observed.

The biosensor also shows rapid response to the change of glucose concentration. The response time for the electrode is less than three seconds under optimum conditions. A linear relationship is obtained in the concentration range from 17 μM to 1 mM with a sensitivity of $13.8 \mu\text{A} \cdot \text{mM}^{-1} \cdot \text{cm}^{-2}$ and a limit of detection (LOD) of 5.8 μM . Reproducibility of the biosensor was evaluated from the response for 10 mM glucose at six different biosensors and an RSD value of 2.4% was observed. The enzyme electrode was found to be stable over one week when it was stored at 5°C as dry. The apparent Michaelis-Menten constant K_M indicates the enzyme-substrate kinetics. It was used for evaluating the biological activity of the immobilized enzyme. K_M was calculated as 1 mM according to the Lineweaver-Burk equation which indicated maximal catalytic activity of the enzyme at low substrate concentrations.

The analytical performance of PANI/gold nanorod/Glucose Oxidase (GOD) enzyme electrode was also compared with PANI/GOD electrode; the results are given in Table 1. As it can be inferred from this table, an amperometric signal in the presence of gold nanorods was higher by three orders of magnitude as compared with signals obtained in the absence of the particles. This difference can be related to the different diffusion properties of PANI/gold nanorod/GOD electrode.

In a real matrix, some electroactive species such as ascorbic acid, and uric acid may be involved in the electrochemical reaction and may therefore affect the biosensor response. The main contribution of the presence of a carboxylate group in the polymer structure is the exclusion of these matrix effects. The effect of these interfering substances was tested at their normal physiological concentrations. The addition of 0.05 mM ascorbic acid and 0.2 mM uric acid exhibited no effect on the response of the PANI-gold nanorod-enzyme biosensor as shown in Figure 8.

TABLE 1: Comparison of analytical performance of PANI and PANI-gold nanorod-enzyme film.

	LOD ^a (mol/L)	LOQ ^b (mol/L)	Linear range (mmol/L)	Michaelis-Menten constant (mmol/L)
PANI/GOD	1.08×10^{-3}	3.24×10^{-3}	3.24–12	4.62
PANI/Au/GOD	5.86×10^{-6}	0.0176×10^{-3}	0.0176–1	1

^a: Limit of detection, ^b: Limit of quantification.

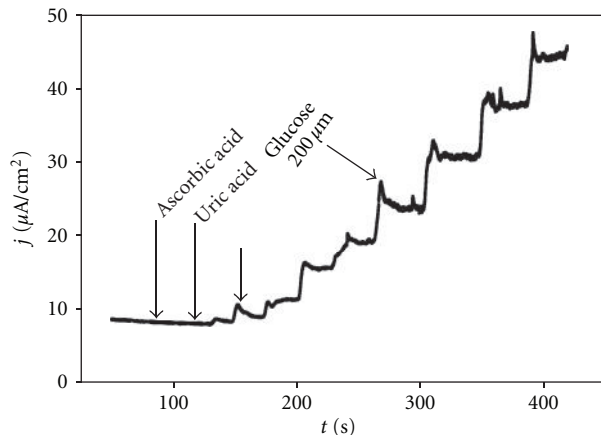


FIGURE 8: A typical amperometric response of the PANI-gold nanorod-enzyme biosensor after addition of 0.05 mM ascorbic acid, 0.2 mM uric acid, and glucose at +0.6 V versus Ag/AgCl in stirred PBS of pH 6.4.

When the developed method was compared with other works, there are some advantages. For instance, a study that is based on SPR system consisted of polypyrrole and GOx on sensor chip could detect range of 1–100 μM glucose concentration. Tian et al. used two steps for this detection procedure as electrochemical technique for modifying chip sensor and optical technique for detecting glucose. On the other hand, our previous study showed that glucose sensor, which developed with 3-aminophenylboronic acid, has had lack ability for six times than ability of fructose, and SPR calibration was linear in the concentration range of 10–120 mM. Here, electrochemically organized glucose sensor prevails to SPR one in terms of preparation and detection limit. Also, Chu et al. designed a biocompatible glucose sensor. This sensor linearly corresponded to glucose concentration over a range of 0.05–4 mM. Our sensor has an advantage and a disadvantage when detection limit and biocompatible property thought. For suitably biocompatible sensor, some application must be required. As for the time required for detection, our sensor is quite rapid according to SPR, but almost similar to other sensors which work with electrochemical and optical techniques [31–33].

The developed sensor is fairly cheap because the chemicals were low amounts for fabrication PANI-gold nanorod electrode.

4. Conclusion

It can be concluded that PANI-gold nanorod is a suitable candidate for enzyme immobilization and detection of

biological compounds. The SERS spectrum of the surface-immobilized glucose oxidase and the spectrum of the native enzyme indicate that the main feature of the native structure of glucose oxidase was conserved after being immobilized on the polymer matrix. Advantages of this biosensor over the previously developed sensors include ease of preparation and rapid response time. An amperometric signal in the presence of gold nanorods was higher by three orders of magnitude as compared with signals obtained in the absence of the particles. Also, the influence of some potential interference such as ascorbic acid and uric acid on the measured current value was not observed. The PANI-gold nanorod may offer a broad potential range for electroanalytical applications.

Acknowledgment

This research was supported by Gazi University, Research Fund through Grants no. 02/2007-06 and no. 02/2005-20.

References

- [1] N. S. Oliver, C. Toumazou, A. E.G. Cass, and D. G. Johnston, “Glucose sensors: a review of current and emerging technology,” *Diabetic Medicine*, vol. 26, no. 3, pp. 197–210, 2009.
- [2] T. W. Siegel, S. R. Smith, C. A. Ellery, J. R. Williamson, and P. J. Oates, “An enzymatic fluorometric assay for fructose,” *Analytical Biochemistry*, vol. 280, no. 2, pp. 329–331, 2000.
- [3] L. Cao, J. Ye, L. Tong, and B. Tang, “A new route to the considerable enhancement of glucose oxidase (GOx) activity: the simple assembly of a complex from CdTe quantum dots and GOx, and its glucose sensing,” *Chemistry: A European Journal*, vol. 14, no. 31, pp. 9633–9640, 2008.
- [4] H. Mugurumia, Y. Kase, N. Murata, and K. Matsumura, “Adsorption of glucose oxidase onto plasma-polymerized film characterized by atomic force microscopy, quartz crystal microbalance, and electrochemical measurement,” *Journal of Physical Chemistry B*, vol. 110, no. 51, pp. 26033–26039, 2006.
- [5] M. Gerard, A. Chaubey, and B. D. Malhotra, “Application of conducting polymers to biosensors,” *Biosensors and Bioelectronics*, vol. 17, no. 5, pp. 345–359, 2002.
- [6] S. Cosnier, “Affinity biosensors based on electropolymerized films,” *Electroanalysis*, vol. 17, no. 19, pp. 1701–1715, 2005.
- [7] P. Santhosh, A. Gopalan, and K.-P. Lee, “Gold nanoparticles dispersed polyaniline grafted multiwall carbon nanotubes as newer electrocatalysts: preparation and performances for methanol oxidation,” *Journal of Catalysis*, vol. 238, no. 1, pp. 177–185, 2006.
- [8] C. A. Foss Jr., M. J. Tierney, and C. R. Martin, “Template synthesis of infrared-transparent metal microcylinders: comparison of optical properties with the predictions of effective medium theory,” *Journal of Physical Chemistry*, vol. 96, no. 22, pp. 9001–9007, 1992.

- [9] Z. Wang, J. Yuan, M. Li et al., "Electropolymerization and catalysis of well-dispersed polyaniline/carbon nanotube/gold composite," *Journal of Electroanalytical Chemistry*, vol. 599, no. 1, pp. 121–126, 2007.
- [10] Md. A. Rahman, P. Kumar, D. S. Park, and Y. Shim, "Electrochemical sensors based on organic conjugated polymers," *Sensors*, vol. 8, no. 1, pp. 118–141, 2008.
- [11] A. Morrin, O. Ngamna, A. J. Killard, S. E. Moulton, M. R. Smyth, and G. G. Wallace, "An amperometric enzyme biosensor fabricated from polyainine nanoparticles," *Electroanalysis*, vol. 17, no. 5-6, pp. 423–430, 2005.
- [12] S. Virji, J. Huang, R. B. Kaner, and B. H. Weiller, "Polyaniline nanofiber gas sensors: examination of response mechanisms," *Nano Letters*, vol. 4, no. 3, pp. 491–496, 2004.
- [13] M. Zhang, A. Yamaguchi, K. Morita, and N. Teramae, "Electrochemical synthesis of Au/polyaniline-poly(4-styrenesulfonate) hybrid nanoarray for sensitive biosensor design," *Electrochemistry Communications*, vol. 10, no. 7, pp. 1090–1093, 2008.
- [14] S. I. Cho, D. H. Choi, S. H. Kim, and S. B. Lee, "Electrochemical synthesis and fast electrochromics of poly(3,4-ethylenedithiophene) nanotubes in flexible substrate," *Chemistry of Materials*, vol. 17, no. 18, pp. 4564–4566, 2005.
- [15] T. K. Sarma, D. Chowdhury, A. Paul, and A. Chattopadhyay, "Synthesis of Au nanoparticle-conductive polyaniline composite using H_2O_2 as oxidising as well as reducing agent," *Chemical Communications*, vol. 10, pp. 1048–1049, 2002.
- [16] E. Granot, E. Katz, B. Basnar, and I. Willner, "Enhanced biocatalysis using Au-nanoparticle/polyaniline hybrid systems in thin films and microstructured rods assembled on electrodes," *Chemistry of Materials*, vol. 17, no. 18, pp. 4600–4609, 2005.
- [17] Y. Liu, X. Feng, J. Shen, J. J. Zhu, and W. Hou, "Fabrication of a novel glucose biosensor based on a highly electroactive polystyrene/polyaniline/Au nanocomposite," *Journal of Physical Chemistry B*, vol. 112, no. 30, pp. 9237–9242, 2008.
- [18] Y. Xian, Y. Hu, F. Liu, Y. Xian, H. Wang, and L. Jin, "Glucose biosensor based on Au nanoparticles-conductive polyaniline nanocomposite," *Biosensors and Bioelectronics*, vol. 21, no. 10, pp. 1996–2000, 2006.
- [19] X. Ren, D. Chen, X. Meng, F. Tang, A. Du, and L. Zhang, "Amperometric glucose biosensor based on a gold nanorods/cellulose acetate composite film as immobilization matrix," *Colloids and Surfaces B*, vol. 72, no. 2, pp. 188–192, 2009.
- [20] B. Nikoobakht and M. A. El-Sayed, "Preparation and growth mechanism of gold nanorods (NRs) using seed-mediated growth method," *Chemistry of Materials*, vol. 15, no. 10, pp. 1957–1962, 2003.
- [21] C. J. Orendorff, A. Gole, T. K. Sau, and C. J. Murphy, "Surface-enhanced Raman spectroscopy of self-assembled monolayers: sandwich architecture and nanoparticle shape dependence," *Analytical Chemistry*, vol. 77, no. 10, pp. 3261–3266, 2005.
- [22] Z. Jia, J. Liu, and Y. Shen, "Fabrication of a template-synthesized gold nanorod-modified electrode for the detection of dopamine in the presence of ascorbic acid," *Electrochemistry Communications*, vol. 9, no. 12, pp. 2739–2743, 2007.
- [23] S. Singh, P. R. Solanki, M. K. Pandey, and B. D. Malhotra, "Covalent immobilization of cholesterol esterase and cholesterol oxidase on polyaniline films for application to cholesterol biosensor," *Analytica Chimica Acta*, vol. 568, no. 1-2, pp. 126–132, 2006.
- [24] L. S. Jiao, Z. Wang, L. Niu et al., "In situ electrochemical SERS studies on electrodeposition of aniline on 4-ATP/Au surface," *Journal of Solid State Electrochemistry*, vol. 10, no. 11, pp. 886–893, 2006.
- [25] M. Baibarac, L. Mihut, G. Louarn et al., "Interfacial chemical effect evidenced on SERS spectra of polyaniline thin films deposited on rough metallic supports," *Journal of Raman Spectroscopy*, vol. 30, no. 12, pp. 1105–1113, 1999.
- [26] C. Liu, J. Zhang, G. Shi, and F. Chen, "Doping level change of polyaniline film during its electrochemical growth process," *Journal of Applied Polymer Science*, vol. 92, no. 1, pp. 171–177, 2004.
- [27] M. Mazur, P. Krysiński, A. Michota-Kamińska, J. Bukowska, J. Rogalski, and G. J. Blanchard, "Immobilization of laccase on gold, silver and indium tin oxide by zirconium-phosphonate-carboxylate (ZPC) coordination chemistry," *Bioelectrochemistry*, vol. 71, no. 1, pp. 15–22, 2007.
- [28] K. S. Kyu, K. M. Soo, and S. Won, "Surface-enhanced raman scattering (SERS) of aromatic amino acids and their glycyl dipeptides in silver sol," *Journal of Raman Spectroscopy*, vol. 18, pp. 171–175, 1987.
- [29] A. Kudelski, "Raman study on the structure of 3-mercaptopropionic acid monolayers on silver," *Surface Science*, vol. 502–503, pp. 219–223, 2002.
- [30] R. E. Holt and T. M. Cotton, "Free flavin interference in surface enhanced resonance raman spectroscopy of glucose oxidase," *Journal of the American Chemical Society*, vol. 109, pp. 1841–1845, 1987.
- [31] Ö. Torun, F. C. Dudak, D. Baş, U. Tamer, and İ. H. Boyacı, "Thermodynamic analysis of the interaction between 3-aminophenylboronic acid and monosaccharides for development of biosensor," *Sensors and Actuators B*, vol. 140, no. 2, pp. 597–602, 2009.
- [32] L. Tian, J. Qiu, Y.-C. Zhou, and S.-G. Sun, "Application of polypyrrole/GOx film to glucose biosensor based on electrochemical-surface plasmon resonance technique," *Microrhimica Acta*, vol. 169, no. 3, pp. 269–275, 2010.
- [33] Y. Hiranuma, H. Hiramatsu, M. X. Chu et al., "Flexible glucose sensor with biocompatible polymer substrate," *Journal of Advanced Science*, vol. 22, pp. 9–10, 2010.

Research Article

Simple Electrochemical Determination of Surface-Active Substances in Natural Waters

Željka Cvrković-Karloci,^{1,2} Damir Krznarić,¹ Marijan Šeruga,² and Božena Čosović¹

¹Division for Marine and Environmental Research, Rudjer Bošković Institute, Bijenička 54, 10000 Zagreb, Croatia

²Faculty of Food Technology, University J.J. Strossmayer, F. Kuhača 18, 31000 Osijek, Croatia

Correspondence should be addressed to Božena Čosović, cosovic@irb.hr

Received 7 March 2011; Revised 19 April 2011; Accepted 19 April 2011

Academic Editor: Sibel A. Ozkan

Copyright © 2011 Željka Cvrković-Karloci et al. This is an open access article distributed under the Creative Commons Attribution License, which permits unrestricted use, distribution, and reproduction in any medium, provided the original work is properly cited.

A simple electrochemical determination of surface-active substances by using time-dependent variation of the capacitive current in a.c. voltammetry at the HMDE is described. Surface-active substances were accumulated by stirring solution at the deposition potential of -0.6 V versus Ag/AgCl (sat. NaCl). The capacitive current was recorded for different deposition times in the range 0–120 s, wherefrom the linear calibration plot is constructed. The proposed method was verified for model surfactant TritonX-100 in the concentration range 0.02–0.25 mg/L and for humic acid in the concentration range 1.65–20 mg/L. The application of the method was demonstrated for freshwater samples of the Drava river, Danube river, and the wetland Kopački Rit, Croatia. The shape of the i_{ac} - E curves as well as the obtained concentrations of surface-active substances by using humic acid as the calibration substance are quite well describing the type and the nature of organic matter in the freshwater samples.

1. Introduction

Organic substances with surface-active properties represent a significant part of dissolved organic matter in natural aquatic systems [1, 2]. Those substances are either naturally present or products of man's activities. The latter are very often, especially in the case of commercial tensides, less abundant in mass while on the contrary they may represent the most surface-active organic material in a particular sample [2].

Although organic surface-active substances are usually electroinactive, that is, those chemical species do not undergo electroreduction or electrooxidation within the available potential window, they can be analyzed by electrochemical methods on the basis of their influence upon the electrode double-layer structure when they get adsorbed at the electrode surface. Surface-active substances were most extensively investigated by electrochemical methods in the sea [3–7], particularly in the thin layer at the sea surface [8–10], in estuarine [11], and river water systems [12, 13], and recently in the atmospheric precipitation samples [14]. Adsorption study at the electrode-solution interface may allow quantification of surface-active substances by measuring the extent of adsorption. In the case of a mixture

of adsorbable substances, the adsorption effect is expressed by using the convenient calibrating substance.

The application of the adsorption study for the analysis of organic surface-active substances has been developing in two main directions: (a) by introducing new or improvement of already existing techniques of measurement [15–17], (b) by using electrochemical method for molecular characterization of the complex mixture of naturally occurring organic adsorbable substances. The latter can be done through comparison of the electrochemical behaviour of the organic matter in the natural sample with the behaviour of the selected model substances and/or by using a complex methodological approach where different analytical techniques are combined with the electrochemical measurement [18, 19].

So far, a.c. voltammetry, particularly tensammetric method with adsorptive preconcentration based on recording either capacitive current or double layer capacity versus potential curves, has been most widely and successfully used for the determination of surface-active substances in aquatic systems. For quantification of the content of surface-active substances, a calibration plot of a selected standard is used, which is in fact the apparent adsorption isotherm for the selected substance at a selected accumulation time. Recently,

a quick and simple tensammetric method was proposed that makes use of a variation in the differential capacity of double layer in relation to the time of accumulation by means of the controlled growth mercury electrode (CGME) [16]. The application of the method was illustrated on two model substances and in the determination of surface-active substances of the river water samples.

While investigating the organic matter content and the chemical composition of real natural water samples, one has to be aware of the fact that the parameters of organic matter could be changed in time and during sample treatment. Therefore, it is a great advantage if one can use simple, direct, and nondestructive analytical methods, possible in the field work and/or on board of a ship. Here, we have used a simple, portable electrochemical instrument in field measurement of surface-active substances in the river water samples. The tensammetric method of determination is modified by means of the time-dependent variation of capacitive current at the HMDE wherefrom the calibration plot was constructed.

2. Experimental

Surface-active substances were analyzed electrochemically by a.c. voltammetry using PalmSens portable instrument (Palm Instruments BV, Netherlands). Three electrode system was used: hanging mercury drop electrode (HMDE WK 2, Institute of Physical Chemistry, Polish Academy of Sciences, Warsaw, Poland) as a working electrode, Ag/AgCl (sat. NaCl) as the reference electrode, and platinum wire as the counter electrode. The potential of $E = -0.6$ V was applied for accumulation of surface-active substances at different accumulation times with stirring. An applied alternating voltage of 10 mV and the frequency of 75 Hz were used. The measurements were carried out in a constant-temperature room at ambient temperature (293+1 K) in the cell open to air, without any sample deaeration. Freshwater samples and model substances were analyzed by addition of sat. NaCl to obtain 0.55 mol/L NaCl solution.

For calibration, the nonionic surfactant polyethoxyethylene-t-octylphenol (Triton-X-100) from Rohm and Haas, Milan, Italy and humic acid from Aldrich (former EGA-Chemie), Germany were used. This is a peat humic acid of molecular weight distribution of two pronounced peaks, one for a molecular mass of 1000 Da and the other for 5000 Da as reported earlier [20].

Freshwater samples were collected from the Drava river near Osijek, Croatia and the Danube river near Batina at the state border between Croatia and Hungary, as well as in the wetland of the Kopački Rit, Croatia.

Dissolved organic carbon (DOC) content of the freshwater samples was determined by using a high-temperature catalytic oxidation analyzer (TOC-5000 Model, Shimadzu, Japan).

3. Results

3.1. Principles of Time-Dependent Tensammetric Determination. It is well known that in a stirred solution, a layer of

thickness δ (Nernst diffusion layer), in which no motion of the solution occurs, exists at the electrode. The concentration of electroactive species within this diffusion layer vary linearly with distance from the electrode [21]. Presuming a fast reaction, concentration of reactant on the electrode surface is practically zero.

In our investigations, the reactant is not a species undergoing a redox process but instead is adsorbed on the electrode. In the case of a strong adsorption and relatively short time, that is, low coverage of the electrode surface, the surface concentration of the surfactant, Γ , is defined as:

$$\Gamma = \frac{M}{A} = \frac{Dc_0 t}{\delta}, \quad (1)$$

where M is number of moles of surfactant, A is the electrode area, D diffusion coefficient, c_0 bulk concentration of surfactant, and t adsorption time.

At a constant potential, differential capacity of the electrode double layer can be expressed as [22]:

$$C_d = C_{\Theta=0}(1 - \Theta) + C_{\Theta=1}\Theta, \quad (2)$$

where $C_{\Theta=0}$ is the differential capacity of a free electrode surface, $C_{\Theta=1}\Theta$ is the differential capacity on a completely covered surface and Θ is the relative surface coverage,

$$\Theta = \frac{\Gamma}{\Gamma_m}, \quad (3)$$

where Γ_m is Surface concentration at maximal coverage.

From (2) and (3):

$$C_d = C_{\Theta=0} - (C_{\Theta=0} - C_{\Theta=1}) \frac{\Gamma}{\Gamma_m}, \quad (4)$$

$$C_d = C_{\Theta=0} - K_1 \Gamma,$$

where K_1 is the constant since $C_{\Theta=0}$, $C_{\Theta=1}$, and Γ_m are constants for a given surfactant.

In the tensammetric measurements, C_d is proportional to a.c. current, i_{ac} , and therefore:

$$i_{ac} = K_2 C_d = K_2 (C_{\Theta=0} - K_1 \Gamma). \quad (5)$$

From (5) and (1),

$$i_{ac} = K_2 \left(C_{\Theta=0} - K_1 \frac{Dc_0 t}{\delta} \right). \quad (6)$$

With constant speed of solution stirring and surfactant concentration,

$$i_{ac} = K_2 C_{\Theta=0} - K_3 t, \quad (7)$$

where

$$K_3 = \frac{K_1 K_2 D c_0}{\delta}. \quad (8)$$

Therefore, the dependence of a.c. current, i_{ac} , on time of deposition, t , is a straight line with negative slope and intercept on i_{ac} axis.

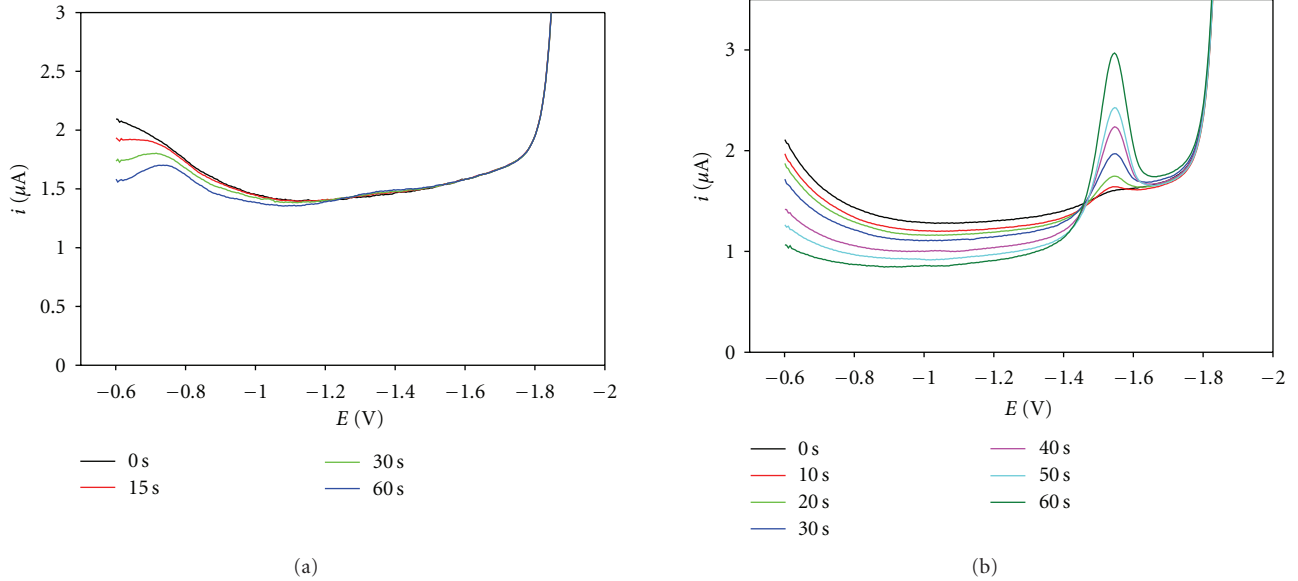


FIGURE 1: i_{ac} - E curves for (a) humic acid, 25.85 mg/L, and (b) Triton-X-100, 0.143 mg/L, recorded for increasing deposition times in 0.55 M NaCl solution. Deposition potential was -0.6 V, amplitude 10 mV, and frequency 75 Hz.

With higher concentrations of surfactants it might be more favourable to measure under diffusion conditions. Diffusion current can be expressed by Cottrell equation [23]

$$i_d = \frac{nFADc_0}{\sqrt{\pi Dt}}. \quad (9)$$

In order to develop the equation for the dependence of a.c. current on surfactant concentration, we start with (9) and proceed in the same manner as above. The final dependence of a.c. current on time is

$$i_{ac} = K_2 C_{\Theta=0} - K_3 \sqrt{t}, \quad (10)$$

where

$$K_3 = K_1 K_2 \frac{c_0 \sqrt{D}}{\sqrt{\pi}}. \quad (11)$$

Thus, under diffusion conditions, current is proportional to the square root of time of deposition.

3.2. Application of the Method: Model Substances and Natural Samples. In order to test our experimental conditions, two model surfactants were used, T-X-100 and humic acid. In Figures 1(a) and 1(b), the dependence of a.c. current on potential for the two surfactants are given. At the potential of -0.6 V, which is close to the potential of electrocapillary zero, both surfactants are strongly adsorbed. Decrease of i_{ac} with t was measured by registering i_{ac} at 0, 15, 30, and 60 s of deposition, each time on a fresh Hg drop, and with stirring of solution. A series of straight lines was obtained for T-X-100 and humic acid (Figures 2(a) and 2(b)) as expected from (7). It would have been more appropriate to measure continuously the change of current with time for

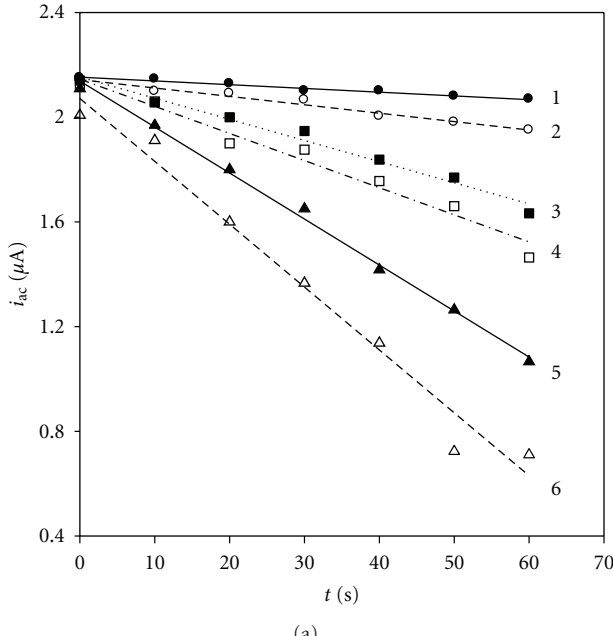
TABLE 1: Determination of surface-active substances in freshwater samples by electrochemical method. Concentrations are expressed in equivalent amounts of two different standards (Triton-X-100 and humic acid). Concentrations of dissolved organic carbon (DOC) in the samples are given too. Samples were collected and analyzed on March 3, 2006.

Freshwater samples	DOC mg C/L	SAS equiv. T-X-100, mg/L	SAS equiv. Humic a., mg/L
Drava River, Osijek	4.91	0.067	15.97
Danube River, Batina	4.21	0.079	18.78
Kopački Rit, Wetland	10.13	0.077	18.47

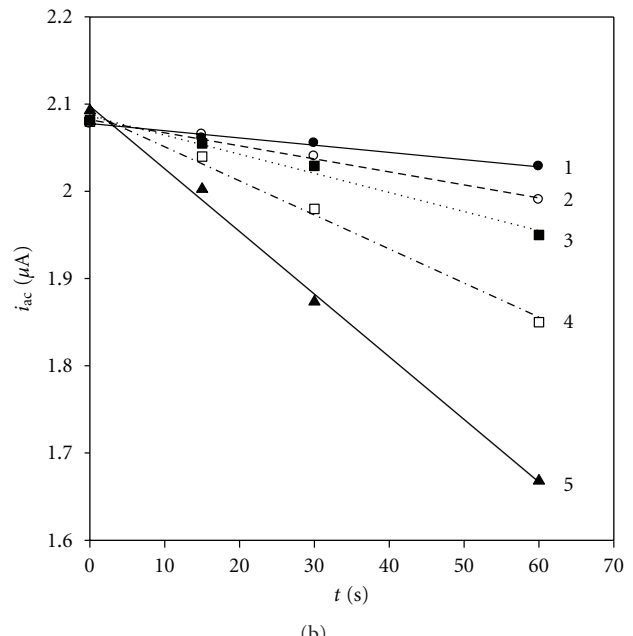
each concentration, but, unfortunately, the instrument used for the field measurements had no such possibilities.

Since field measurements are often done in a span of several days or even months and with different HMDE, the electrode surface areas could vary somewhat. In order to minimize such errors, the lines in Figure 2 were plotted as relative currents by dividing all values with the intercept of the line for supporting electrolyte, which was 0.55 mol L⁻¹ NaCl (Figures 3(a) and 3(b)). Supporting electrolyte was recorded before every set of measurements.

For each surfactant, the relative slope K_3 of i_{ac} - t lines was plotted against bulk concentration of the surfactant. Good, straight lines, with intercept equal to zero, were obtained in both cases (Figures 4(a) and 4(b)). The concentrations of the mixture of the unknown surfactants from natural waters were always measured using these two calibration lines, that is, they were reported as equivalent to a certain concentration of T-X-100 and humic acid.

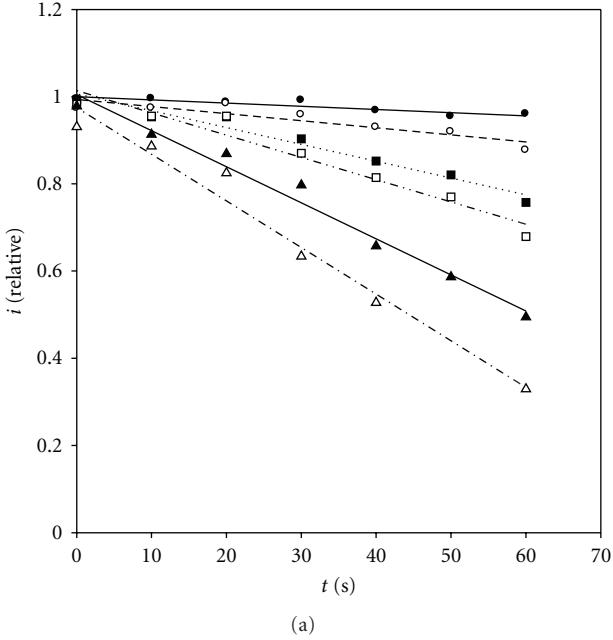


(a)

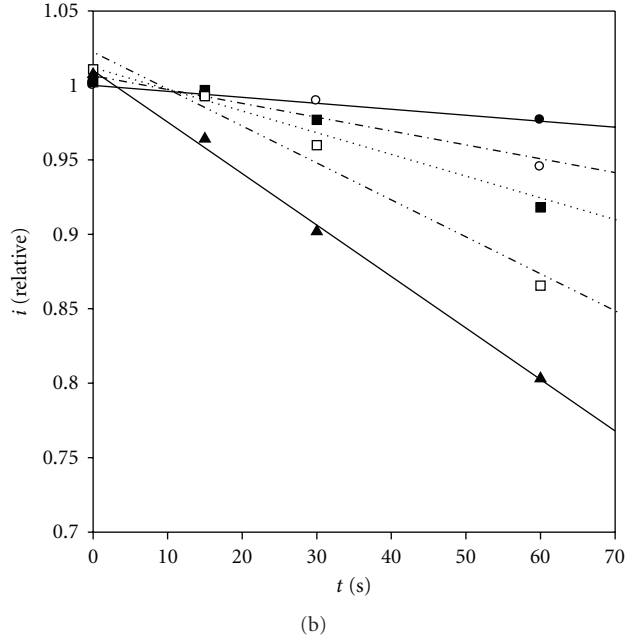


(b)

FIGURE 2: i_{ac} - t curves for different concentrations of (a) T-X-100: (1) 0 mgL^{-1} , (2) 0.0237 mgL^{-1} , (3) 0.0594 mgL^{-1} , (4) 0.0951 mgL^{-1} , (5) 0.143 mgL^{-1} , and (6) 0.190 mgL^{-1} and (b) humic acid: (1) 1.65 mgL^{-1} , (2) 4.4 mgL^{-1} , (3) 6.6 mgL^{-1} , (4) 10.45 mgL^{-1} , and (5) 16.5 mgL^{-1} . Supporting electrolyte: 0.55 M NaCl . Peak-to-peak amplitude 10 mV , frequency 75 Hz . Each point represents a freshly formed Hg drop.



(a)



(b)

FIGURE 3: i_{ac} (relative)- t curves obtained by dividing the results in Figure 2 by the value for supporting electrolyte at $t = 0 \text{ s}$.

The linear calibration plot represents an improvement of the tensammetric method in comparison with the use of the calibration plot which is the apparent adsorption isotherm for a selected model surfactant at one selected adsorption time. The calibration plot obtained at one selected accumulation time can be used only in a narrow

concentration range, that is, below surface saturation [5, 24]. When surface-active substances are determined in different aquatic samples, sometimes they need to be measured at different accumulation times in order to extend the concentration range. In comparison to the use of several adsorption isotherms, each for the selected accumulation

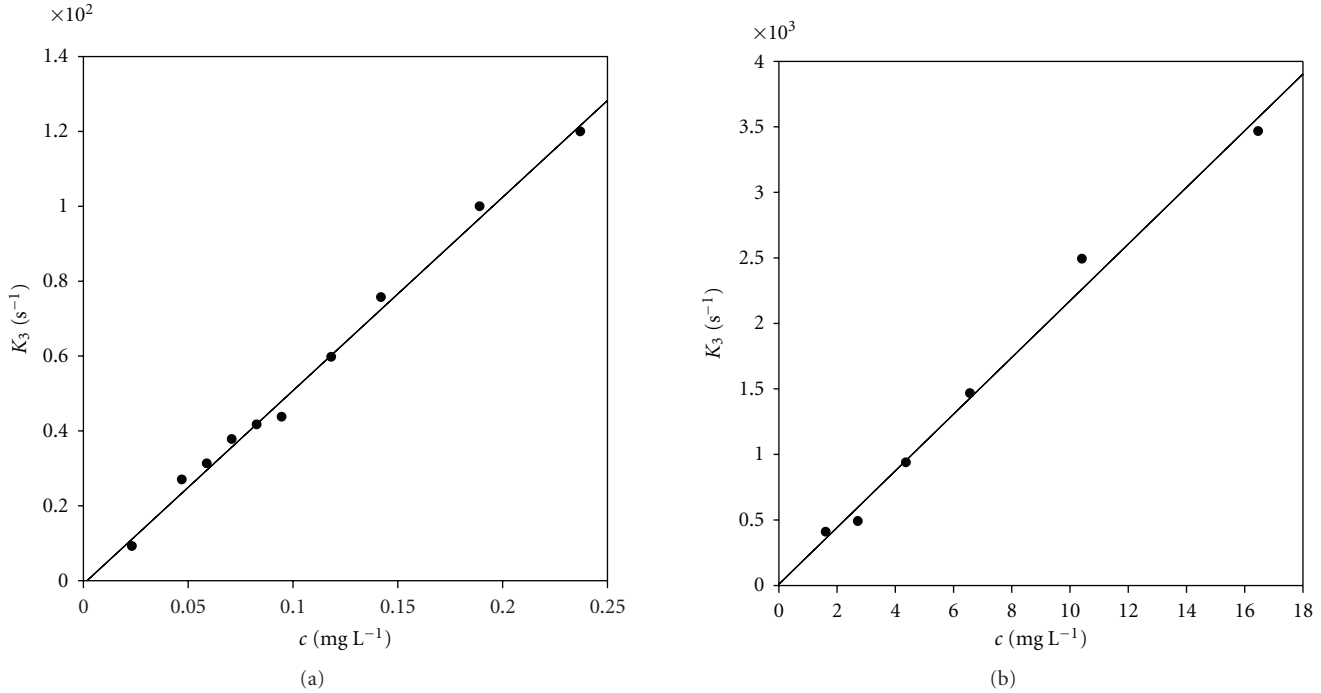


FIGURE 4: The calibration curves for (a) T-X-100 and (b) humic acid constructed by plotting the slopes from i_{ac} (relative)- t lines against concentrations. All conditions as in Figures 2 and 3.

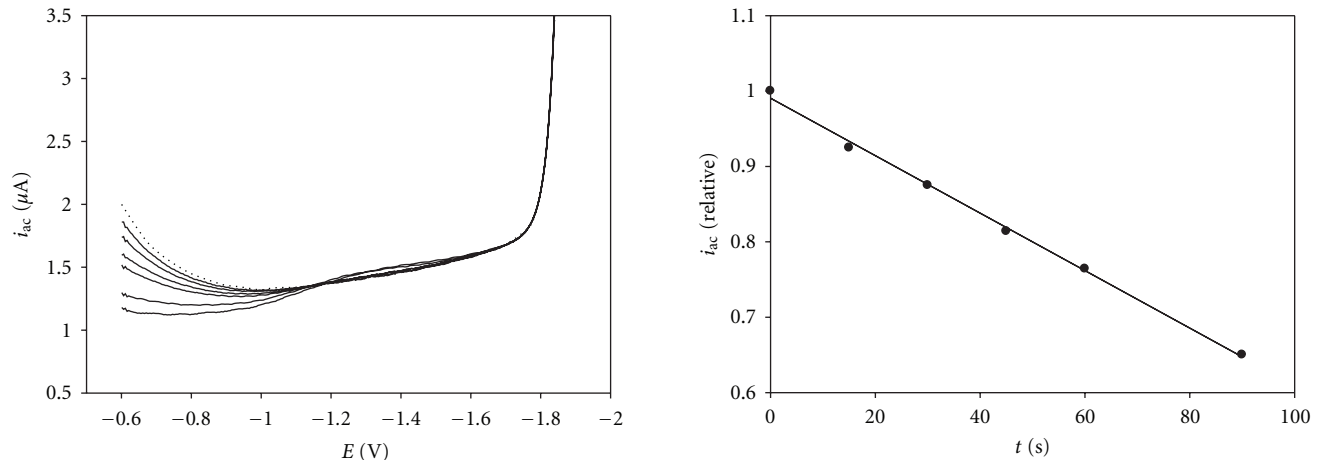


FIGURE 5: i_{ac} - E curves for a sample of Drava river with increasing deposition times from 0 s (dotted line) to 120 s. Deposition potential was -0.6 V, amplitude 10 mV, frequency 75 Hz. 0.55 M NaCl was added to the sample.

time, the advantage of the proposed method is based on the fact that in the time-dependent variation of the capacitive current, all data for different accumulation times are used in one plot, and the concentration of surface-active substances is determined from the linear calibration plot.

The application of the method for the surfactant analysis in a natural water sample is illustrated in Figures 5 and 6.

In Figure 5 are given i_{ac} - E curves for a sample of Drava river in Croatia. Deposition was done at -0.6 V with stirring

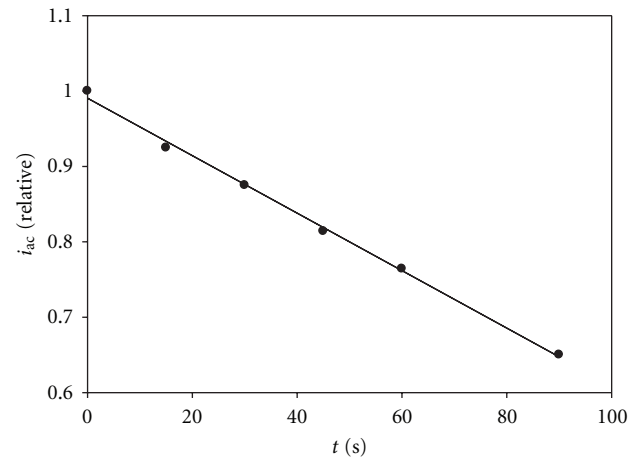


FIGURE 6: i_{ac} (relative)- t curve constructed from the results in Figure 5. i_{ac} current was recorded at -0.6 V. The slope was calculated from the first 5 points on the curve.

of solution. From the shape of the curves, it follows that the surfactants present in that sample behave more like humic acid than T-X-100. No well-defined desorption peaks at negative potentials were observed as in the case of T-X-100. Instead, a low and extended hump around -1.2 V to -1.6 V suggests a partial desorption of segments in the surfactant molecule similar to humic acid. The relative currents at -0.6 V were plotted against deposition time. A good straight line was obtained whose slope was $3.83 \times 10^{-3} \text{ s}^{-1}$ (Figure 6).

It was well within the range of both calibration curves in Figure 4. The concentration of unknown surfactant in the sample corresponds to 0.0759 mg L^{-1} TX-100 or 17.66 mg L^{-1} humic acid.

In Table 1 are presented data for surface-active substances of three freshwater systems as determined by the described electrochemical method. For comparison, the concentrations of dissolved organic carbon for the same samples are given too. As shown, the concentrations of organic matter are relatively high, 4.91 and 4.21 mg C/L for river water samples and 10.13 mg C/L for the wetland sample.

Neither of the calibration substances used, TritonX-100 or humic acid, can completely describe the composition and behaviour of naturally occurring organic surface-active substances in the investigated samples. It is important to mention that K_3 values in the (8), which are linearly proportional to the concentration of surfactant, at the same time depend on the characteristics of the adsorbed surface-active substances, both the naturally occurring and the calibration substances. Those characteristics are the diffusion coefficients, as well as the adsorption parameters, Γ_m and the differential capacities, which are included in the constant K_1 .

The relative standard deviation obtained for multiple analyses of the same solution containing surfactant such that TX-100 at the level $100 \mu\text{g L}^{-1}$ was 5%, which is fairly good. When concentrations of the mixture of the unknown surfactants from natural waters are measured, the choice of the calibration substance is relevant as mentioned in our previous papers [5, 24].

The advantage of TritonX-100 is that because it is widely used as standard, it allows comparison of different natural water samples. For example, the concentrations of surface-active substances, expressed in equivalent of TritonX-100, for samples in Table 1 are relatively low, as compared with other freshwater systems as determined by a.c. voltammetry [12, 13, 25] in spite of the fact that the concentrations of dissolved organic matter, in particular freshwater samples are high (Table 1).

If we compare the shape of the a.c. voltammetric curves of natural freshwater samples with those of model substances, it becomes clear that natural samples fit better to the humic-type substances. Taking into account the elemental composition of humic substances (corresponding to about 50% of organic carbon), it comes out that the concentration of surface-active substances of natural freshwater samples, when expressed in equivalents of humic substance, reveal quite well the chemical nature and behaviour of naturally occurring organic matter in the investigated samples. These are in accordance with our previous investigation of freshwater systems [12].

Acknowledgments

Financial support of the Ministry of Science, Education, and Sports of Republic of Croatia for the project "Nature of organic matter, interaction with traces and surfaces in environment" is gratefully acknowledged.

References

- [1] K. A. Hunter and P. S. Liss, "Polarographic measurement of surface-active material in natural waters," *Water Research*, vol. 15, no. 2, pp. 203–215, 1981.
- [2] B. Čosović, "Aqueous surface chemistry. Adsorption characteristics of organic solutes. Electrochemical evaluation," in *Chemical Processes in Lakes*, W. Stumm, Ed., pp. 55–80, Wiley, New York, NY, USA, 1985.
- [3] B. Čosović and V. Vojvodić, "The application of a.c. polarography to the determination of surface active substances in seawater," *Limnology and Oceanography*, vol. 27, pp. 361–369, 1982.
- [4] B. Čosović and I. Ciglenečki, "Surface active substances in the Eastern Mediterranean," *Croatica Chemica Acta*, vol. 70, no. 1, pp. 361–371, 1997.
- [5] B. Čosović and V. Vojvodić, "Voltammetric analysis of surface active substances in natural seawater," *Electroanalysis*, vol. 10, no. 6, pp. 429–434, 1998.
- [6] B. Gašparović and B. Čosović, "Distribution of surface-active substances in the northern Adriatic Sea," *Marine Chemistry*, vol. 75, no. 4, pp. 301–313, 2001.
- [7] B. Gašparović, M. Plavšić, N. Bošković, B. Čosović, and M. Reigstad, "Organic matter characterization in Barents Sea and eastern Arctic Ocean during summer," *Marine Chemistry*, vol. 105, no. 1-2, pp. 151–165, 2007.
- [8] B. Čosović, V. Žutić, V. Vojvodic, and T. Pleše, "Determination of surfactant activity and anionic detergents in seawater and surface microlayer in the Mediterranean," *Marine Chemistry*, vol. 17, no. 2, pp. 127–139, 1985.
- [9] B. Gašparović, M. Plavšić, B. Čosović, and A. Saliot, "Organic matter characterization in the sea surface microlayers in the subarctic Norwegian fjords region," *Marine Chemistry*, vol. 105, no. 1-2, pp. 1–14, 2007.
- [10] S. Frka, Z. Kozarac, and B. Čosović, "Characterization and seasonal variations of surface active substances in the natural sea surface micro-layers of the coastal Middle Adriatic stations," *Estuarine, Coastal and Shelf Science*, vol. 85, no. 4, pp. 555–564, 2009.
- [11] V. Vojvodić and B. Čosović, "The hydrophobic fraction of organic matter in the Krka River estuary," *Marine Chemistry*, vol. 39, no. 4, pp. 251–267, 1992.
- [12] B. Čosović, V. Vojvodić, and T. Pleše, "Electrochemical determination and characterization of surface active substances in freshwaters," *Water Research*, vol. 19, no. 2, pp. 175–183, 1985.
- [13] E. Bednarkiewicz, M. Donten, and Z. Kublik, "Determination of traces of surfactants in distilled, potable and untreated waters and in supporting electrolytes by tensammetry with accumulation on the HMDE," *Journal of Electroanalytical Chemistry*, vol. 127, pp. 241–253, 1981.
- [14] B. Čosović, P. O. Leko, and Z. Kozarac, "Rainwater dissolved organic carbon: characterization of surface active substances by electrochemical method," *Electroanalysis*, vol. 19, no. 19–20, pp. 2077–2084, 2007.
- [15] D. Krznarić, T. Goričnik, and B. Čosović, "Electrochemical determination of organic surface active substances in model and natural sea water with Au(III) monocrystal electrode," *Croatica Chemica Acta*, vol. 73, no. 1, pp. 247–261, 2000.
- [16] B. Baś and M. Jakubowska, "Estimation of non-ionic, surface-active substances in aqueous solutions by means of the Controlled Growth Mercury Electrode," *Analytica Chimica Acta*, vol. 592, no. 2, pp. 218–225, 2007.
- [17] J. Morchalo, R. Rydlichowski, A. Szymanski, B. Wyrwas, and Z. Lukaszewski, "PTFE capillary trap as a tool to monitor

- non-ionic surfactants in the aquatic environment," *Analytica Chimica Acta*, vol. 540, no. 1, pp. 9–15, 2005.
- [18] V. Vojvodić and B. Čosović, "Fractionation of surface active substances on the XAD-8 resin: Adriatic Sea samples and phytoplankton culture media," *Marine Chemistry*, vol. 54, no. 1-2, pp. 119–133, 1996.
- [19] Z. Kozarac, B. Čosović, S. Frka, D. Möbius, and S. Hacke, "Complex methodological approach to the studies of natural microlayers at the air/water interface," *Colloids and Surfaces A*, vol. 219, pp. 173–186, 2003.
- [20] M. Ochs, B. Čosović, and W. Stumm, "Coordinative and hydrophobic interaction of humic substances with hydrophilic Al_2O_3 and hydrophobic mercury surfaces," *Geochimica et Cosmochimica Acta*, vol. 58, no. 2, pp. 639–650, 1994.
- [21] W. Davison, "Defining the electroanalytically measured species in a natural water sample," *Journal of Electroanalytical Chemistry*, vol. 87, no. 3, pp. 395–404, 1978.
- [22] B. B. Damaskin, O. A. Petrii, and V. V. Batrakov, *Adsorption of Organic Compounds on Electrodes*, Plenum Press, New York, NY, USA, 1971.
- [23] R. G. Compton and C. E. Banks, *Understanding Voltammetry*, World Scientific, Singapore, 2007.
- [24] B. Čosović and V. Vojvodić, "Direct determination of surface active substances in natural waters," *Marine Chemistry*, vol. 22, pp. 363–373, 1987.
- [25] B. Čosović, D. Hršak, V. Vojvodić, and D. Krznarić, "Transformation of organic matter and bank filtration from a polluted stream," *Water Research*, vol. 30, no. 12, pp. 2921–2928, 1996.

Research Article

Solar UV Photooxidation as Pretreatment for Stripping Voltammetric Trace Metal Analysis in River Water

Gelaneh Woldemichael,¹ Taffa Tulu,¹ and Gerd-Uwe Flechsig^{2,3}

¹ School of Humanities and Natural Sciences, Adama University, P.O. Box 1888, Adama, Ethiopia

² Department of Chemistry, University of Rostock, 18051 Rostock, Germany

³ Gensoric GmbH, Schillingallee 68, 18057 Rostock, Germany

Correspondence should be addressed to Gerd-Uwe Flechsig, gerd-uwe.flechsig@uni-rostock.de

Received 21 March 2011; Accepted 18 April 2011

Academic Editor: Sibel A. Ozkan

Copyright © 2011 Gelaneh Woldemichael et al. This is an open access article distributed under the Creative Commons Attribution License, which permits unrestricted use, distribution, and reproduction in any medium, provided the original work is properly cited.

The application of solar ultraviolet radiation as sample pretreatment or preparation step in stripping voltammetric analysis of trace metals in presence of low levels of dissolved organic carbon (DOC) natural water samples (river water) was studied. River water samples were collected from downstream of Warnow river (Germany) and acidified to pH of 2 ± 0.2 (by addition of 1 mL of ultrapure 65% HNO_3 per liter sample). Furthermore, 100 $\mu\text{L/L}$ of hydrogen peroxide solution (ultrapure, 30% H_2O_2) was added to the samples as photochemical reaction initiator. The samples were transferred to polyethylene terephthalate (PET) bottles and irradiated with solar radiation of UV-A intensity of 3.6 mW/m^2 for six hours, and the concentrations of Zn, Cd, Pb, and Cu were determined by differential pulse anodic stripping voltammetry (DPASV). The comparison of the values with the results obtained for the original untreated sample and artificial UV-treated one proved that solar UV radiation can be applied to the digestion of dissolved organic carbon in trace metal analysis in natural waters like river water, lake waters, well waters, and so forth.

1. Introduction

The determination of the concentration of trace elements requires homogeneous samples which are free of organic matter that might interact with the electrode materials by adsorbing to the electrode and reducing the active surface area of the electrode. It also complexes with the metals ions, can increase background current or shift the peak potential disturbing the signal and making the determination impossible [1]. The determination of the metal ions by adsorptive stripping voltammetric (AdSV) method is applied for metal ions that do not form amalgams with mercury and in the absence of dissolved organic matter (DOM) that interacts with the electrodes or the metal ions. Methods like wet digestion and dry ashing have been introduced long ago in the mineralization of organic matter for both liquid and solid samples. Application of these methods is associated with high risk of contamination of the sample due to the addition of different acidic agents like mineral acid, bisulfate ions, and others. To avoid the problem of contamination

of the samples, an alternative clean and efficient method of sample treatment by UV irradiation has been developed long ago [2, 3]. The method is considered environmentally friendly, effective and minimizes the risks of contamination or loss of sample through evaporation [3]. Commercially, there are several UV sources designed for general and specific purposes to be used in science laboratories, industries water and wastewater treatment plants, and so forth. Nowadays, heavy metals in liquid samples are determined by the use of sample preparation methods of these commercially available UV digesters. The most common ones contain mercury lamps and electrodeless cadmium lamps. Numerous publications deal with determination of metals in UV-digested natural water samples such as copper, lead, cadmium and zinc [4, 5], copper and mercury [6], chromium, iron [7], arsenic [8], and antimony and bismuth [9]. Until now, irradiation with powerful UV lamps is considered essential to ensure complete digestion of the organic sample matrix. However, this prevents mobile or remote application in the environment.

The main natural source of UV is the sun. Extreme UV, UVC, and UVB constitute 99% of the total UV radiation reaching the planet Earth and are absorbed in the upper atmosphere by ozone, oxygen, and nitrogen. The atmosphere is transparent to UVA (315–400 nm), and 99% of the total UV-radiation reaching the earth's crust is UVA. This radiation may reach the ground scattered, diffused, or reflected. Its intensity is also dependent on the cloudiness, latitude, season, altitude, elevation of the sun, and so forth. Transmittance is also dependent on the optical property of the transparent object, or it is a function of the type, thickness, angle of incidence, and specific wavelength [10]. Identification and optimization of the transmittance of large number of materials has been investigated. Pyrex glass (borosilicate type) has maximum transmission level at 340 nm and beyond [11]. Transparent plastic materials include Lucite and Plexiglass [12], polyethylene [13], and polyethylene terephthalate (PET) [14]. In case of water, transmittance depends on the water depth and turbidity, which internally depends on the presence or absence of light-absorbing and coloring materials, and mineral salts, humates, as well as wavelength of the radiation [15–18]. Solar UV is increasingly investigated in the areas of photochemistry and biophotochemistry because of its prominent ecological and environmental roles. In addition to biological activities, solar UV is the most important element in natural disintegration of most organic compounds in soil, water, and air [19]. Surface waters such as river waters contain complex organic substances like humic acids, fulvic acids, glycolic acid, peptides, proteins, aminoacids, lipids, and polysaccharides [20]. Humic acids contain negatively charged ions due to the dissociation of carboxylic acid and hydroxyl functional groups and also possess amphipathic character owing to the presence of both hydrophobic and hydrophilic moieties [21]. They are the most important sunlight absorbers in natural waters that can photosensitize the oxidation of certain aquatic pollutants and biologically important substances [22]. The UV irradiation of such samples produces reactive intermediates like excited states of DOM, hydrogen peroxide [23], singlet oxygen [24], hydrated electrons, superoxide ions [25], organoperoxy radicals, hydroxyl radicals, and halogen radicals [23]. These intermediates react with dissolved organic matters, and some of them are nonselectively decomposing organic compounds to carbon dioxide, N₂, and phosphate. The use of certain inorganic peroxides (hydrogen peroxide and sodium persulphate) remarkably enhances the rate of degradation of organic contaminants because they trap the photogenerated electrons more efficiently than O₂ [26].

Solar UV radiation in combination with TiO₂ photocatalysts was tested for its application to the disinfection of water and destruction of pathogens and mineralization of organic compounds [26, 27]. In the above investigations, several parameters such as the intensity of UV radiation, the water depth, latitude, water temperature, and angle of incidence were also tested. The result of this experiment showed that almost all human pathogens were killed or deactivated. Following this investigation, the idea of solar water disinfection (SODIS) is promoted as one of the remedies to provide safe water to people living in developing nations.

In the present investigation, the application of solar UV radiation as a sample preparation step in voltammetric determination of trace metals (Zn, Cd, Pb, and Cu) in low DOC surface waters (river water) is tested. The solar UV irradiation took place in the mid summer at mid latitude (54°05'N, 12°07'E, Rostock, Germany). The results are compared with the results obtained from the undigested original sample and artificial UV irradiated sample. The nature of labile metal ions in the original, solar UV-irradiated and artificial UV-irradiated sample is studied by applying the pseudopolarographic method.

Pseudopolarography had been introduced some decades ago to allow for speciation of complexed metal ions at the trace level [28–31].

2. Experimental

2.1. Instrumentation and Operating Conditions. A μ Autolab potentiostat (Ecochemie) with General Purpose Electrochemical System (GPES) 4.9 software package connected to a Metrohm 663 VA Stand electrolysis cell with a three-electrode system consisting of a HMDE as working electrode, a glassy carbon counter electrode, and Ag/AgCl (3 M KCl) reference electrode was used for the determination of the concentration and pseudopolarographic analysis of the metals. Differential pulse anodic stripping voltammetric (DPASV) method is used for the measurement of both the concentration and pseudopolarography (Table 1).

2.2. Reagents. All reagents used for this experiment were obtained from certified manufacturers (Merck, Fluka) and were ultrapure grades. The stock solutions of Zn²⁺, Cd²⁺, Pb²⁺, and Cu²⁺ (1000 mg/L) were diluted with water as needed. All stock solutions were acidified containing 0.5% HNO₃. Sodium acetate buffer containing 0.1 M KCl (pH = 4.6) was used as supporting electrolyte. All dilutions were made using ultrapure water (>18.2 MΩ, TOC < 2 ppb). Ultrapure nitric acid (65%) was used to acidify the water sample at the spot of sampling to avoid adsorption of the metal ions to the walls of the containers and to hinder biological activities. H₂O₂ (30%) was added as supporting oxidizing agent while amidosulfonic acid and hydroxysulfonic acids were used to remove excess hydrogen peroxide prior to the determination. Humic acid (20% ash) was used for preparation of “artificial river water” containing approximate concentration of the acid as in natural river water.

2.3. Sample Collection, Preparation, and Preservation. River water samples were collected based on the river water sampling protocols (EPA guidelines for regulatory monitoring and testing water and waste water) from the downstream of Warnow river (Rostock, Germany). Plastic bottles were used as sample containers, and the samples were acidified with ultra pure HNO₃, to pH of 2 ± 0.2 (1 mL of 65% HNO₃ per liter of sample water). After taking the samples to the laboratory, they were filtered through a 0.45 μ m pore size cellulose acetate membrane filter inserted in a Millipore filtration glass assembly and, then, 100 μ mol/L of ultrapure

TABLE 1: Instrument operating parameters for simultaneous analysis of Zn(II), Cd(II), Pb(II), and Cu(II) in river water by differential pulse voltammetry.

1	Working electrode	HMDE
2	Calibration	Standard addition
3	Mode	DP
4	Purging time (s)	10 to 600 as stated in the text
5	Deposition potential (V)	-1.15
6	Deposition time (s)	120
7	Equilibration time (s)	10
8	Modulation time (s)	0.05
9	Interval time (s)	0.5
10	Start potential (V)	-1.15
11	End potential (V)	0.05
12	Scan rate (V/s)	0.01

30% H₂O₂, was added. The samples were then divided into three aliquots designated as *Original Sample*, *SoUV Sample*, and *UV Sample*. The *Original Sample* was stored in refrigerator at 4°C until determination took place and was used as control sample. The *SoUV Sample* was transferred to a UVA-transparent (330–450 nm) polyethylene terephthalate (PET) bottles and exposed to solar radiation of UVA intensity of 3.6 mW/cm² for 6 hours. The *UV Sample* was transferred to a UV-transparent (at 254 nm) quartz glass tube and irradiated by artificial UV lamp of 30 W and 254 nm for similar hours. The solar irradiation time was chosen between 10:00 AM. and 4:00 PM. to obtain maximum efficiency of solar radiation as a result of increase of the incident angle of the radiation. In addition to this, using an aluminum solar collector increased the solar radiation intensity. This also increased the infrared intensity of the incident radiation enhancing the synergetic effect of elevated water temperature and UV radiation [32]. All the three samples were stored in a refrigerator at 4°C until determination. Artificial water containing 1.0 mg/L and 0.1 mg/L of humic acid was prepared to compare and estimate the concentration of humic acid in the original Warnow river water by UV-VIS spectrophotometer.

2.4. Procedure. For the determinations of the concentrations of Zn, Cd, Pb, and Cu, 20 mL of the river water samples (Warnow river), 2 mL of 0.1 M KCl and 2 mL of sodium acetate buffer (pH = 4.6) were taken into the voltammetric cell. After the deaeration by purging with nitrogen for 10 minutes, all 4 heavy metals were analyzed simultaneously under the given operating conditions and three replicate measurements were taken for all the three samples of the specified procedures. Standard addition method was used to determine the concentrations of the metal ions in the samples.

Pseudopolarographic data was measured by differential pulse anodic stripping voltammetry (DPASV) with HMDE as working electrode and a supporting electrolyte of acetate buffer containing 0.1 M KCl at pH of 4.5. Accumulation potential (E_{acc}) was scanned between -1.20 V and -0.60 V for Zn and -1.2 V and 0.10 V for Cu with scan increment

(E_{sc.Inc}) of 0.05 V. The time interval (t_{int}) was 0.5 s at scan rate (E_{sc.rate}) of 0.01 V/s. Three replicate measurements were taken for each metal of the three sample types.

To estimate the concentration of humic acid in the original river water sample, UV-VIS spectra was taken for 1000 and 100 times diluted original Warnow river water sample and compared with 1 mg/L and 0.1 mg/L of artificially prepared humic acid solution.

3. Results and Discussions

In this study, the concentrations of the zinc, cadmium, lead, and copper metal ions in the river water of all the sample's categories have been successfully determined by DPASV technique. Voltammograms are presented in Figures 1(a), 1(b), and 1(c). The concentrations of the metal ions Zn, Cd, Pb, and Cu in the *Original Sample*, the *SoUV Sample* and the *UV Sample* were determined by standard addition (i.e., extrapolation of the calibration curve). The standard additions are depicted in Figures 2–5, and the according numbers are given in Table 2.

According to these measurements, the concentration of zinc was found to be 17 ± 0.43, 22.86 ± 0.41, and 26 ± 0.40 ppb, for *Original Sample*, *SoUV Sample*, and *UV Sample*, respectively. In similar procedures, the concentrations of cadmium in the three sample types were obtained as 0.03 ± 0.001, 0.05 ± 0.003, and 0.05 ± 0.005 ppb. In the case of lead, the *Original Sample*, *SoUV Sample*, and *UV Sample* contained 4.36 ± 0.05, 7.07 ± 0.02, and 7.50 ± 0.01 ppb, respectively. Copper concentration in the same river water samples was determined as 32.20 ± 0.34, 58.85 ± 0.31, and 71.57 ± 0.28 ppb as depicted in Figure 3. These results show that solar irradiation over 6 hours has a significant effect upon analysis results of the 4 tested heavy metals. The effect is largest in case of lead, where we found almost the same concentration as compared to the *UV Sample*, which served as the reference. The effect of 6 hours of solar irradiation was smaller for zinc and copper. However, even here, the results were much better than in case of the *Original Sample*. These findings can probably be addressed to matrix components that form complexes with these 3 metal ions. The irradiation effect was smallest for cadmium, which seems to be less prone to complexation by components present in this river water matrix.

The recovery rates were calculated by adding known concentrations of the metal ions to the three different sample categories in the very beginning. This experiment was used to evaluate the data obtained by means of stripping voltammetry in the various sample treatment procedures under consideration. The results obtained in this experiment are given in Table 2. For all 4 metals tested, the worst recovery rate was found for the *Original Sample*, that is, without any irradiation pretreatment. In case of zinc, the best recovery rate was obtained by solar irradiation treatment.

Interestingly, the recovery rate for copper was above 100% for all three kinds of samples. This corresponds to the observed decrease in slope of the standard addition function (Figure 3). Seemingly, the sensitivity in presence of

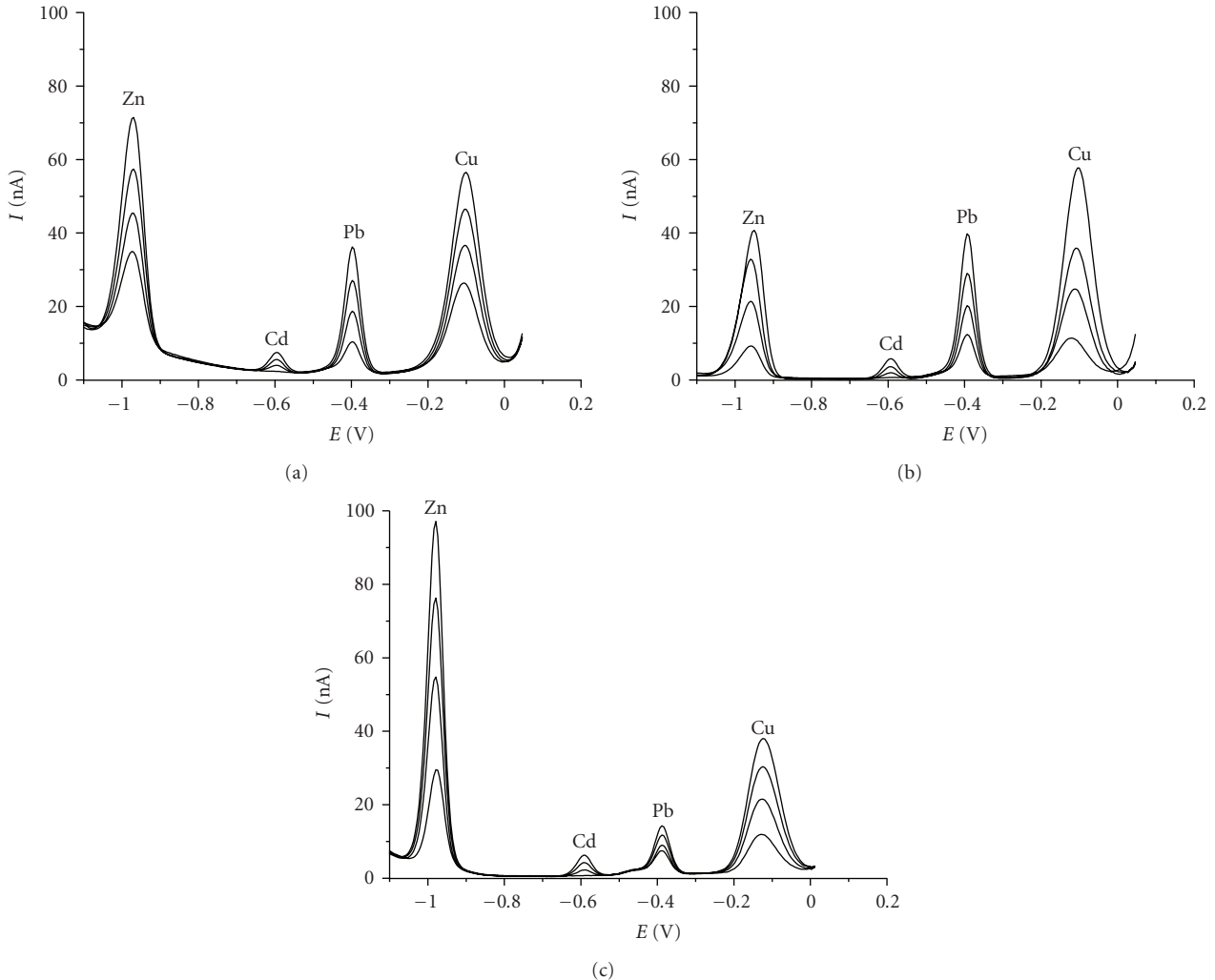


FIGURE 1: DP stripping voltammograms recorded for (a) the *Original Sample*, (b) the *SoUV Sample*, and (c) the *UV Sample*, with additions of 10, 20, 30 ppb for Zn and Cu, 3, 6, and 9 ppb for Pb, and 1, 2, and 3 ppb for Cd.

TABLE 2: Concentration and recovery rates measured for Zn, Cd, Pb, and Cu in *Original Sample*, *SoUV Sample* and *UV Sample* of Warnow River.

Element	Concentration (ppb)			Recovery rate		
	Original sample	SoUV sample	UV sample	Original sample	SoUV sample	UV sample(%)
Zinc	17.17 ± 0.43	22.86 ± 0.41	26.67 ± 0.40	88.81 ± 0.20	95.91 ± 0.13	92.90 ± 0.21
Cadmium	0.03 ± 0.001	0.05 ± 0.003	0.05 ± 0.005	75.32 ± 0.15	87.11 ± 0.22	93.66 ± 0.11
Lead	4.36 ± 0.05	7.07 ± 0.02	7.50 ± 0.01	84.21 ± 0.32	90.32	94.14 ± 0.31
Copper	32.20 ± 0.34	58.85 ± 0.31	73.57 ± 0.28	133.59 ± 0.42	112.75 ± 0.37	104.16 ± 0.35

organic river water matrix is slightly higher compared with both irradiation-treated samples. This would mean that the complexing matrix components lead to increased stripping signals, which on the other hand, leads to incorrect analysis results. The absolute stripping signals are, however, larger for the irradiated samples. The unusual recovery rate of 133.6% for the *Original Sample* in case of copper may also have to do with the considerable complexing effects. The latter is confirmed by pseudopolarographic studies as described below and in Figure 7.

The nature of matrix-complexed zinc and copper ions was studied by means of pseudopolarography of the three different kinds of samples. Figure 6 exhibits such pseudopolarograms for zinc. The main effect of irradiation treatment is a significant increase in peak currents that are plotted here versus deposition potentials. This means that after UV or solar irradiation, more metal ions are available for reduction during the deposition step. Obviously, the irradiative digestion treatment is more complete for artificial UV light; however, also solar irradiation reveals remarkable release of

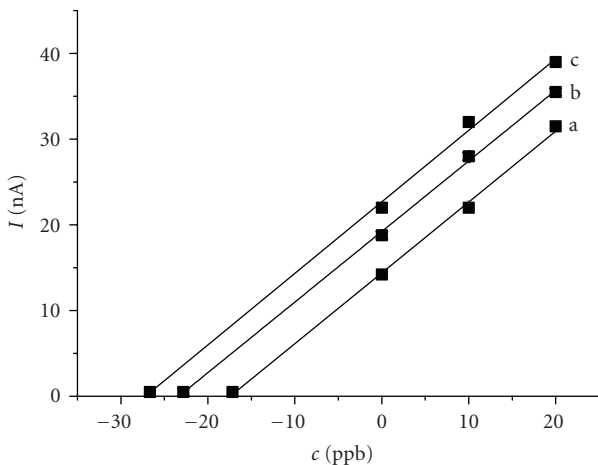


FIGURE 2: Standard addition for zinc in (a) *Original Sample*, (b) *SoUV Sample*, and (c) *UV Sample*.

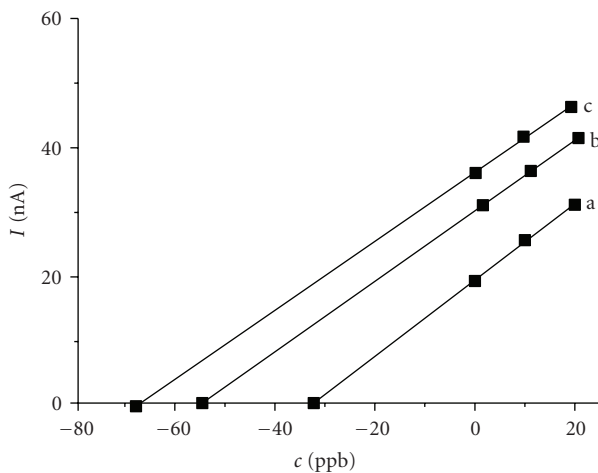


FIGURE 3: Standard addition for copper in (a) *Original Sample*, (b) *SoUV Sample*, and (c) *UV Sample*.

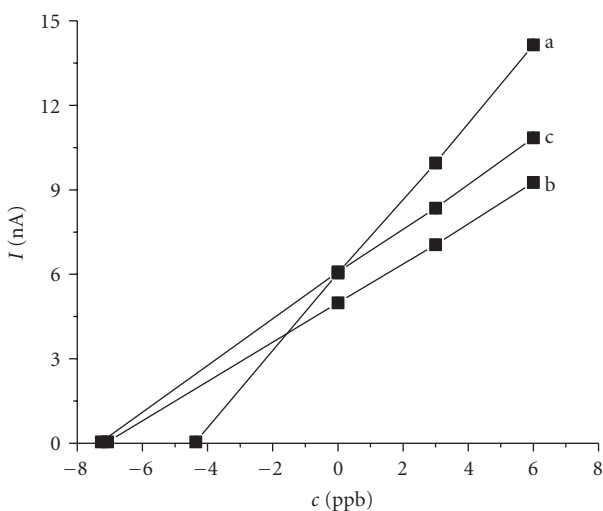


FIGURE 4: Standard addition calibration curve for lead in (a) *Original Sample*, (b) *SoUV Sample*, and (c) *UV Sample*.

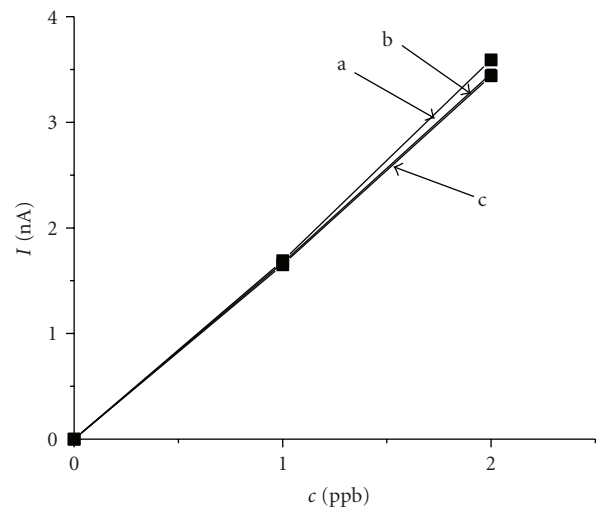


FIGURE 5: Calibration curve for cadmium in (a) *Original Sample*, (b) *SoUV Sample*, and (c) *UV Sample*.

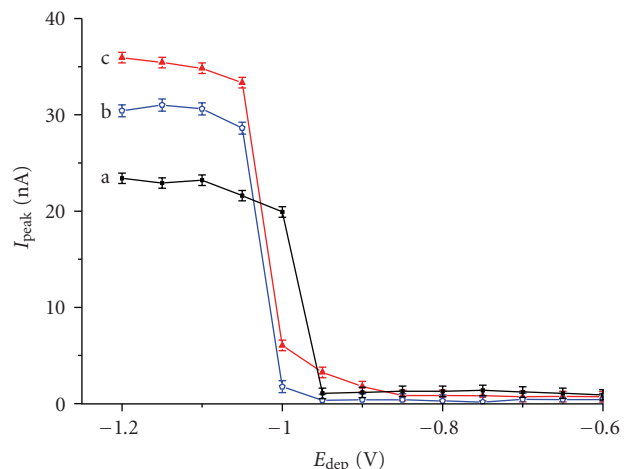


FIGURE 6: Pseudopolarograms of 10 ppb zinc in (a) *Original Sample*, (b) *SoUV Sample*, and (c) *UV Sample*; DPASV at HMDE, accumulation time 240 s, initial potential -1.2 V, final potential -0.70 V, scan increment 0.05 V, interval time 0.5 s, scan rate 10 mV/s, and 0.1 M acetate buffer containing 0.1 M KCl (pH = 4.6).

zinc ions from the matrix complexes by destruction of the organic ligands.

Figure 7 illustrates in case of copper the dramatic effect of both irradiation treatment methods tested in this study. Both the pseudopolarographic half-wave potential and the step height change considerably after treatment with either solar or artificial UV light.

It can be estimated from Figure 8 that more than 1000 ppm humic acids (in a wide sense) have been present in the river water samples. For this estimation, UV/Vis spectra were taken for 1000- and 100-fold diluted original Warnow river water samples and then compared with 1 mg/L and 0.1 mg/L of an artificially prepared humic acid solution. This method was used to estimate the concentration of the most abundant UV/Vis-active organic matter (among them humic

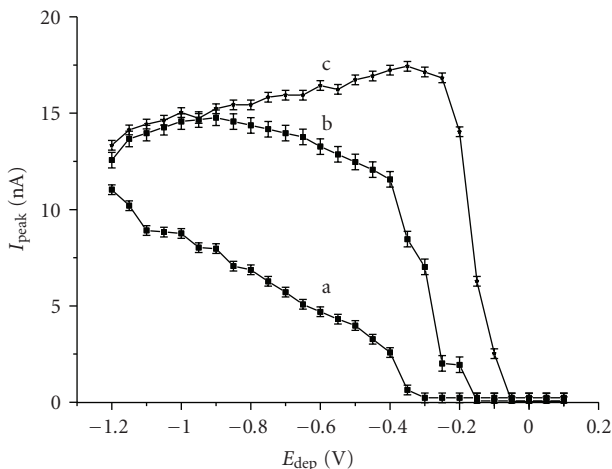


FIGURE 7: Pseudopolarograms of 10 ppb copper in (a) Original Sample, (b) SoUV Sample, and (c) UV Sample; DPASV at HMDE, accumulation time 240 s, initial potential -1.2 V, final potential 0.10 V, scan increment 0.05 mV, interval time 0.5 s, scan rate 10 mV/s, and 0.1 M acetate buffer with 0.1 M KCl ($\text{pH} = 4.5$).

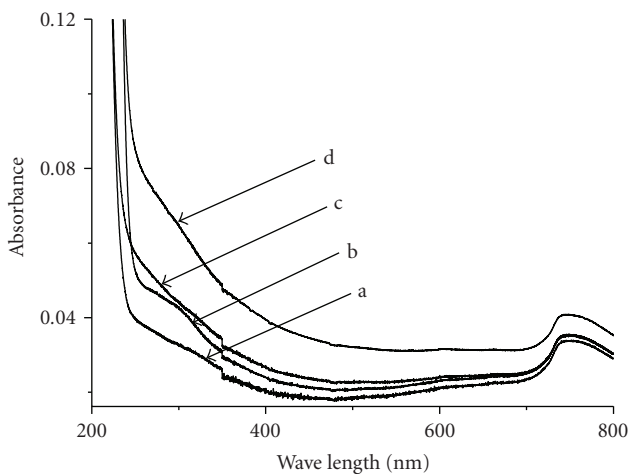


FIGURE 8: UV-VIS spectra of (a) 0.1 mg/L humic acid, (b) 1 mg/L humic acid, (c) Warnow river sample $1:1000$ diluted, and (d) Warnow river sample $1:100$ diluted.

acid) in the used water sample from river Warnow. The high level of organic matter explains the great effect of irradiation treatment.

4. Conclusions

This study demonstrates that solar irradiation assisted by low pH and addition of hydrogen peroxide can serve as a means for water sample digestion. All what is needed includes a few hours of solar irradiation, an aluminum reflector, and a PET plastic bottle. The presented protocol can be recommended for trace determinations of copper and zinc in river water at remote places in the environment or otherwise, where electric high-power UV lamps or commercial UV digestion units cannot be used. The method also works for lead and

cadmium; however, in these cases, 6 hours of sun irradiation seem too short to finish the process.

Acknowledgments

The authors are grateful to the German Research Foundation (DFG, FL 384/7-1, Heisenberg Fellowship) and the German Academic Exchange Service (DAAD) for financial support.

References

- [1] J. Golimowski and K. Golimowska, "UV-photooxidation as pretreatment step in inorganic analysis of environmental samples," *Analytica Chimica Acta*, vol. 325, no. 3, pp. 111–133, 1996.
- [2] F. A. J. Armstrong, P. M. Williams, and J. D. H. Strickland, "Photo-oxidation of organic matter in sea water by ultra-violet radiation, analytical and other applications," *Nature*, vol. 211, no. 5048, pp. 481–483, 1966.
- [3] E. P. Achterberg and C. M. G. Van den Berg, "In-line ultraviolet-digestion of natural water samples for trace metal determination using an automated voltammetric system," *Analytica Chimica Acta*, vol. 291, no. 3, pp. 213–232, 1994.
- [4] J. Labuda, D. Saur, and R. Neeb, "Anodic stripping voltammetric determination of heavy metals in solutions containing humic acids," *Fresenius' Journal of Analytical Chemistry*, vol. 348, no. 4, pp. 312–316, 1994.
- [5] M. Kolb, P. Rach, J. Schäfer, and A. Wild, "Investigations of oxidative UV photolysis - I. Sample preparation for the voltammetric determination of Zn, Cd, Pb, Cu, Ni and Co in waters," *Fresenius' Journal of Analytical Chemistry*, vol. 342, no. 4-5, pp. 341–349, 1992.
- [6] L. Sipos, J. Golimowski, P. Valenta, and H. W. Nurnberg, "New voltammetric procedure for the simultaneous determination of copper and mercury in environmental samples," *Fresenius Zeitschrift für Analytische Chemie Labor und Betriebsverfahren*, vol. 298, no. 1, pp. 1–8, 1979.
- [7] J. Golimowski, "Trace analysis of iron in environmental water and snow samples from Poland," *Analytical Letters*, vol. 22, no. 2, pp. 481–492, 1989.
- [8] R. H. Atallah and D. A. Kalman, "On-line photo-oxidation for the determination of organoarsenic compounds by atomic-absorption spectrometry with continuous arsine generation," *Talanta*, vol. 38, no. 2, pp. 167–173, 1991.
- [9] A. Postupolski and J. Golimowski, "Trace determination of antimony and bismuth in snow and water samples by stripping voltammetry," *Electroanalysis*, vol. 3, no. 8, pp. 793–797, 1991.
- [10] A. Acra, A. Ashkar, and Z. Raffoul, "Environmental health conditions," in *Beirut 1984—A Population and Health Profile*, H. K. Armenian and H. C. Zurayk, Eds., pp. 69–90, American University of Beirut, Beirut, Lebanon, 1985.
- [11] A. Acra, Y. Karahagopian, Z. Raffoul, and R. Dajani, "Disinfection of oral rehydration solutions by sunlight," *Lancet*, vol. 2, no. 8206, pp. 1257–1258, 1980.
- [12] A. G. Dietz, "Diathermanous materials and properties of surfaces," in *Introduction to the Utilization of Solar Energy*, A. M. Zarem and D. Erway, Eds., pp. 59–86, McGraw-Hill, New York, NY, USA, 1963.
- [13] R. S. Fujioka and O. T. Narikawa, "Effect of sunlight on enumeration of indicator bacteria under field conditions," *Applied and Environmental Microbiology*, vol. 44, no. 2, pp. 395–401, 1982.

- [14] M. Wegelin, S. Canonica, C. Alder et al., "Does sunlight change the material and content of polyethylene terephthalate (PTA) bottles?" *Journal of Water Supply: Research and Technology - AQUA*, vol. 50, no. 3, pp. 125–133, 2001.
- [15] J. Calkins, "A preliminary assessment of the effects of UV irradiation on aquatic microorganisms and their ecosystems," in *Proceedings of the 3rd Conference on CIAP*, p. 550, 1974.
- [16] A. L. H. Gameson and J. R. Saxon, "Field studies on effect of daylight on mortality of coliform bacteria," *Water Research*, vol. 1, no. 4, pp. 279–295, 1967.
- [17] N. Ogura, "Ultraviolet absorbing materials in natural waters," *Nippon Kagaku Zasshi*, vol. 90, pp. 601–611, 1969 (Japanese).
- [18] R. G. Qualls, M. P. Flynn, and J. D. Johnson, "The role of suspended particles in ultraviolet disinfection," *Journal of the Water Pollution Control Federation*, vol. 55, no. 10, pp. 1280–1285, 1983.
- [19] R. Al-Rasheed and D. J. Cardin, "Photocatalytic degradation of humic acid in saline waters. Part 1. Artificial seawater: influence of TiO₂, temperature, pH, and air-flow," *Chemosphere*, vol. 51, no. 9, pp. 925–933, 2003.
- [20] C. S. Uyguner and M. Bekbolet, "Evaluation of humic acid photocatalytic degradation by UV-vis and fluorescence spectroscopy," *Catalysis Today*, vol. 101, no. 3-4, pp. 267–274, 2005.
- [21] B. R. Eggins, F. L. Palmer, and J. A. Byrne, "Photocatalytic treatment of humic substances, in drinking water," *Water Research*, vol. 31, no. 5, pp. 1223–1226, 1997.
- [22] C. S. Uyguner and M. Bekbolet, "Photocatalytic degradation of natural organic matter: kinetic considerations and light intensity dependence," *International Journal of Photoenergy*, vol. 6, no. 2, pp. 73–80, 2004.
- [23] X. Zhou and K. Mopper, "Determination of photochemically produced hydroxyl radicals in seawater and freshwater," *Marine Chemistry*, vol. 30, pp. 71–88, 1990.
- [24] P. B. Merkel and D. R. Kearns, "Radiationless decay of singlet molecular oxygen in solution. An experimental and theoretical study of electronic-to-vibrational energy transfer," *Journal of the American Chemical Society*, vol. 94, no. 21, pp. 7244–7253, 1972.
- [25] R. M. Baxter and J. H. Carey, "Evidence for photochemical generation of superoxide ion in humic waters," *Nature*, vol. 306, no. 5943, pp. 575–576, 1983.
- [26] C. Minero, E. Pelizzetti, S. Malato, and J. Blanco, "Large solar plant photocatalytic water decontamination: effect of operational parameters," *Solar Energy*, vol. 56, no. 5, pp. 421–428, 1996.
- [27] D. Robert and S. Malato, "Solar photocatalysis: a clean process for water detoxification," *Science of the Total Environment*, vol. 291, no. 1–3, pp. 85–97, 2002.
- [28] S. Bubic and M. Branica, "Voltammetric characterization of ionic state of cadmium present in seawater," *Thalassia Jugoslavica*, vol. 9, pp. 47–53, 1973.
- [29] M. Branica, D. M. Novak, and S. Bubić, "Application of anodic stripping voltammetry to determination of the state of complexation of traces of metal ions at low concentration levels," *Croatica Chemica Acta*, vol. 49, no. 3, pp. 539–547, 1977.
- [30] M. Branica, I. Pižeta, and I. Marić, "Application of ASV for trace metal speciation. Part VI. A computerized pseudopolarographic system," *Journal of Electroanalytical Chemistry*, vol. 214, no. 1-2, pp. 95–102, 1986.
- [31] M. S. Shuman, "Pseudopolarograms: applied potential-anodic stripping peak current relationships," *Analytical Chemistry*, vol. 51, no. 9, pp. 1546–1550, 1979.
- [32] O. A. McLoughlin, S. C. Kehoe, K. G. McGuigan et al., "Solar disinfection of contaminated water: a comparison of three small-scale reactors," *Solar Energy*, vol. 77, no. 5, pp. 657–664, 2004.

Research Article

Rapid Electrochemical Detection of Radiolysis Products in an Aqueous Solution Exposed to Alpha Particle Beams

J. E. Liedhegner,¹ W. Jennings,² and J. Wainright¹

¹Department of Chemical Engineering, Case Western Reserve University, 10900 Euclid Avenue, Cleveland, OH 44106, USA

²Department of Materials Science and Engineering, Case Western Reserve University, 10900 Euclid Avenue, Cleveland, OH 44106, USA

Correspondence should be addressed to J. Wainright, jesse.wainright@case.edu

Received 20 January 2011; Accepted 23 February 2011

Academic Editor: Sibel A. Ozkan

Copyright © 2011 J. E. Liedhegner et al. This is an open access article distributed under the Creative Commons Attribution License, which permits unrestricted use, distribution, and reproduction in any medium, provided the original work is properly cited.

An electrochemical cell has been developed that allows for the rapid and exhaustive detection of oxygen and/or hydrogen peroxide produced during the radiolysis of aqueous solutions by alpha particle or proton beams. Short, 10–100 s, exposures were sufficient to yield steady-state electrochemical currents proportional to the radiolysis G-factor. The use of thin SiC windows provided a robust means of separating the vacuum environment of the ion-beam accelerator from the aqueous solution at atmospheric pressure with minimal energy loss.

1. Introduction

Radiolysis of water, the production of hydrogen and oxygen from the splitting of water by the decay products of radioactive materials, has primarily been studied from the point of view of radioactive waste management [1]. Water is often in contact with radioactive waste, and the obvious hazards associated with potentially explosive (from H₂/O₂ mixtures) or corrosive (H₂O₂ is often also produced in the radiolysis process) situations required study of the radiolysis process. Concurrently, the possibilities for the commercial production of hydrogen via radiolysis have been considered [2]. In this scenario, electrical energy production is the end goal, with the hydrogen produced by radiolysis being intended as fuel for an electrochemical fuel cell.

Utilizing radioisotopes to generate electrochemical cell reactants is not a new concept. Extensive research has been conducted in radiation chemistry, analyzing the production of chemical species through radiolytic interactions [3–5]. During the 1950s and 1960s, research was conducted utilizing radiochemical means to power fuel cells. These systems were designed to utilize radioactive waste to produce power on a large scale. Not only was the water cycle studied, as is investigated here, but so were the ferric ion and ozone cycles

[3]. In these systems, chemical intermediates produced *via* radiolysis were separated and fed to fuel cells in a normal fashion. The overall efficiency of these units was <1% and would require significant improvements to become a cost effective means of large-scale power generation. Recently however, advances in microfabrication have been employed to take a fresh look at power generation *via* radiolysis.

Using these same radiolysis principles in conjunction with microfabrication, it may be possible to develop a micropower source capable of continuous power output for several years [6, 7]. The idea is to convert nuclear energy into electrical energy *via* a chemical intermediate. Exposure to radiation results in the radiolytic decomposition of water, producing chemical intermediates H₂, O₂, and H₂O₂ [4]. The H₂, O₂, and H₂O₂ can then be used to power a mixed reactant fuel cell. The system is regenerative since the H₂, O₂, and H₂O₂ produced by radiolysis are converted back to water by the fuel cell reaction, closing the cycle. The regenerative cell is then capable of producing electricity for the life of the radioisotope. This closed cycle is illustrated in Figure 1.

The efficiency of chemical production *via* radiolysis can differ greatly from one type of radiation to another. This is especially apparent when comparing radiation with high

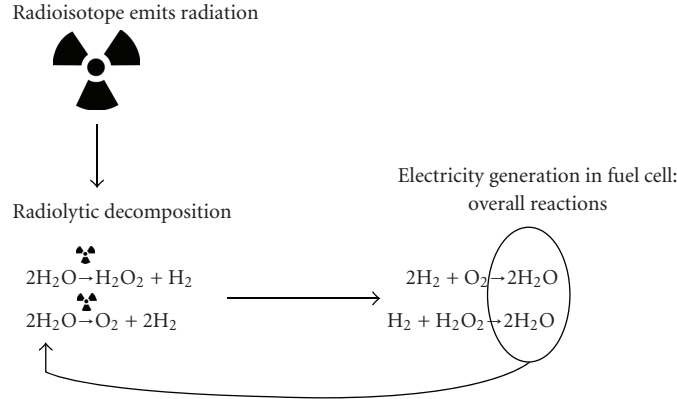
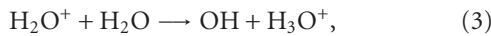
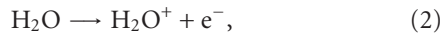
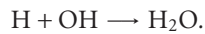
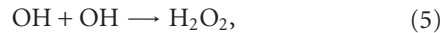
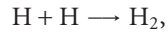


FIGURE 1: Regenerative cycle for radiolytically powered fuel cell.

linear energy transfer (LET), such as alpha (He^{++} particles), and those with low LET, such as beta and gamma. Low LET radiation interacts with water molecules in isolated events that can be far from one another. A majority of the ions and radicals created during these separate events then diffuse into the bulk where they can react, resulting in low chemical yields. In the case of high LET radiation, interactions with water molecules are more constant, and large channels of ions and radicals (spurs) are created. The ions and radicals then react with one another within the spur and very little diffuses into the bulk, resulting in higher chemical yields. The exact mechanism by which molecular species are formed is still under some debate [8]. However, an overview of molecular production, including some of those mechanisms proposed in the literature, can be useful. The process starts with the production of H and OH radicals either by direct cleavage of the H-OH bond or loss of an electron and subsequent decomposition (2)–(4):

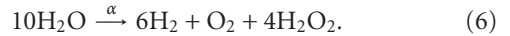


The H and OH radicals then combine to form molecular products:



The production of O_2 is also widely reported in the literature, but it is not clear whether O_2 is produced directly from radical combination, or through the decomposition of H_2O_2 . Some theory suggests possible formation of O radicals which could combine to form O_2 , but this is still under discussion [4, 8].

The chemical yield is generally reported as a G factor, or the number of molecules formed per 100 eV of energy deposited. In the case of pure water, if $G(H_2) = 1$, then ~2.5% of the energy deposited was used to split water and produce H_2 and H_2O_2/O_2 . Literature tells us that $G(H_2) < 1.7$ for radiolysis of pure water by any form of radiation [4, 5]. The other products simply recombine to form water. In the case of alpha emission, the generation of H_2 is about 6–10x that of O_2 [9]. The balance is then hydrogen peroxide. In the case of 6x production of H_2 , the net reaction is



In literature studies of alpha radiolysis yield, typically samples are enclosed in a glass vial and irradiated. The irradiated vial was then crushed [1, 10] or extracted *via* syringe [2, 11] and its contents injected into a gas chromatograph or mass spectrometer. Using this method, throughput of samples is relatively slow, and there is the possibility of significant error. Thus, in order to measure radiolysis yield, a novel experimental method has been developed. The experimental cell developed for this study allows for rapid evaluation of radiolysis yield and considerably higher throughput of samples.

2. Experimental

The cell shown in Figure 2 was coupled to one of the beam lines on the NEC 5SDH accelerator in the Department of Materials Science and Engineering at CWRU. The cell is fabricated in the form of a 2.75" Conflat flange. Since the electrochemical cell has to be nonconductive and stable to chemical attack by the electrolytes used, the blank flange was machined out of a solid block of chlorinated-polyvinyl chloride (CPVC). Machined into the same block as the electrochemical cell were recesses for a quartz window to visualize the ion beam spot and a Faraday cup to measure beam current. These were sealed into the block using high vacuum epoxy.

The NEC accelerator is capable of producing an alpha particle beam up to 5.1 MeV and with beam currents of up to 100 nA. Proton beams of up to 3.4 MeV can also be

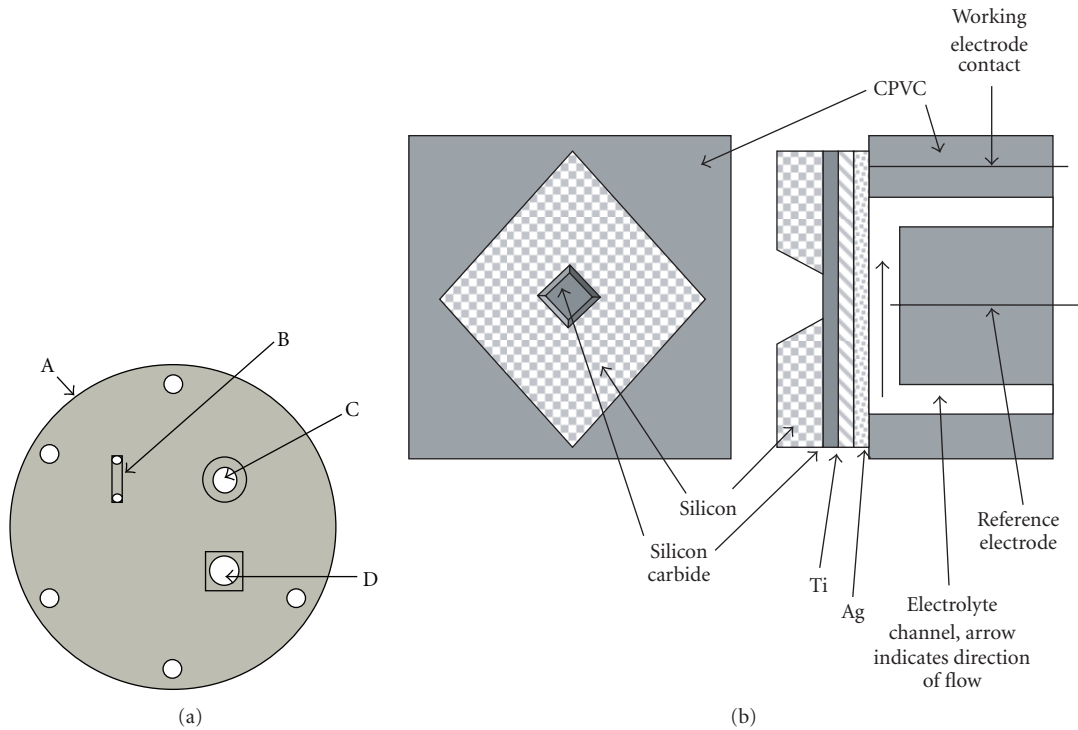


FIGURE 2: (a) Electrochemical cell for radiolysis measurements. A: 2.75" Conflat blank flange, machined from CPVC block. B: electrolyte channel—1 cm long, 2 mm wide, 2 mm deep. C: recess for Faraday cup. D: recess for quartz window. (b) Detailed view of Electrochemical cell for radiolysis measurements. Drawing not to scale.

generated. The focused alpha beam had a typical diameter of 1 mm and a current of 1–5 nA. The ion beam current measured by the Faraday cup corresponds to $2e^-$ per He^{++} or $1e^-$ per H^+ . The beam current was typically measured before and after a series of four radiolysis exposures. A beam current measurement consisted of the average value of thirty current measurements made at a 1 Hz sampling rate.

The radiolysis solution is separated from the accelerator vacuum by a 3 μm thick film of silicon carbide, (SiC) with an unsupported area of $2.5 \text{ mm} \times 2.5 \text{ mm}$ square centered in a $1 \text{ cm} \times 1 \text{ cm}$ Si chip as shown in Figure 2(b). To prepare these windows, a film of SiC is grown by an atmospheric pressure CVD process on one face of a silicon wafer. On the back side of the wafer, a mask is applied, and the Si substrate is removed using a KOH etch to expose a region of the SiC film [12]. The SiC film is completely impervious to the KOH etch. For the SiC unsupported area and thickness used in these experiments, a pressure differential across the SiC film of $>207 \text{ kPa}$ was found to be necessary to break the SiC film. This provided a generous 2 : 1 safety margin when operating the electrochemical cell at atmospheric pressure. The Si chip with the SiC window was mounted to the cell with vacuum epoxy. The cell is mounted on an X-Y positioning stage on the end of the beam line that allows the beam to be centered on the SiC window, or on the quartz window or the Faraday cup. A shutter within the beam line is used to control the exposure time when the electrochemical cell was irradiated. On the solution side of the SiC film were a 3 nm thick Ti adhesion layer and a 100 nm thick silver film that was used

as the working electrode. Both of these films were applied by vacuum deposition. When the Si/SiC chip was affixed to the cell, an electrical connection to the working electrode (Ag film) was made with silver epoxy to a Ag wire imbedded in the CVPC block.

After passing through the thin SiC, Ti, and Ag films, the alpha particles enter the aqueous solution, and radiolysis occurs close to the working electrode. In this arrangement, O_2 and/or H_2O_2 that are radiolytically generated are detected by being electrochemically reduced at the silver film. In alkaline solutions, the reference electrode was a silver wire on which a thin Ag_2O film had been grown. As the silver working electrode has a wide potential range ($\sim 0 \text{ V}$ to 0.7 V versus a reversible hydrogen electrode (RHE); see Figure 3) over which O_2 and H_2O_2 reduction is the only reaction that occurs, exacting potential control is not required, and the $\text{Ag}/\text{Ag}_2\text{O}$ reference electrode provides a sufficiently stable potential of $\sim 1.15 \text{ V}$ versus RHE. For measurements in hydrochloric acid solutions, a thin film of AgCl was electrochemically formed on the Ag wire, creating a reference electrode with a stable potential based on the $\text{Ag}/\text{AgCl}/\text{Cl}^-$ couple. The counter electrode was a Pt wire $\approx 1 \text{ cm}$ from the working electrode which minimized any disturbances resulting from the counter electrode reaction. All solutions were deaerated with bubbling argon for at least 30 minutes prior to being pumped into cell. During the radiolysis experiments, the solution was not circulated, but was stagnant within the cell. All electrochemical measurements were made with a Solartron 1280B potentiostat.

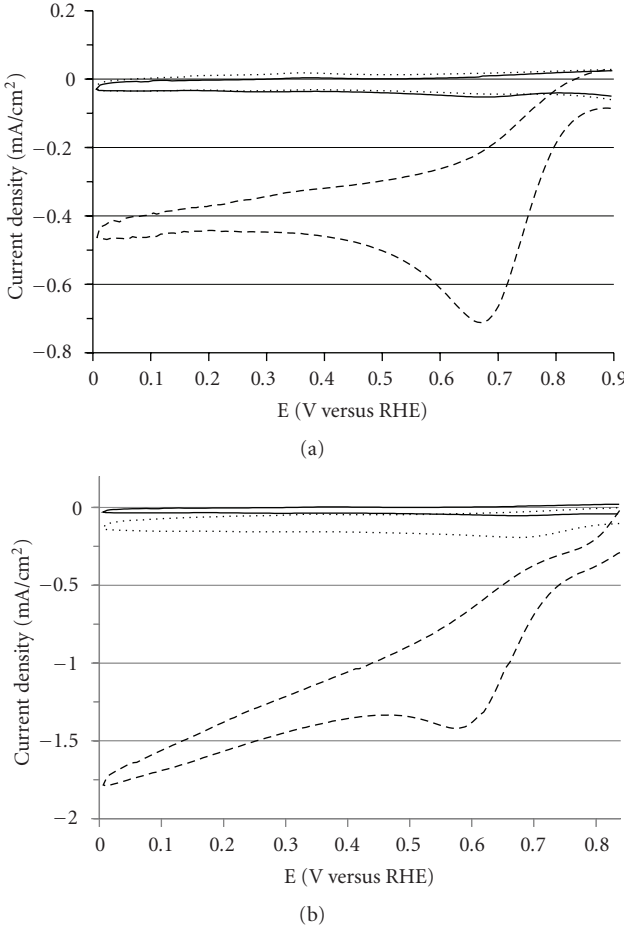


FIGURE 3: (a) Cyclic voltammetry of Ag electrode (1.6 mm diameter disk) in 0.1 M NaOH electrolyte. Solid: N₂ purge, dotted: H₂ purge, and dashed: O₂ purge. Voltammograms were conducted under saturated conditions at 50 mV/sec over a voltage range of 0.0–1.4 V versus RHE. (b) Cyclic voltammetry of Ag electrode (1.6 mm diameter disk) in 0.1 M NaOH electrolyte. Solid: N₂ purge, dotted: xM H₂O₂ with N₂ purge, and dashed: 10 xM H₂O₂ with N₂ purge. Exact concentrations were unknown due to H₂O₂ degradation, but were on the order of 1 mM and 10 mM H₂O₂. Scans were conducted under saturated conditions at 50 mV/sec over a voltage range of 0.0–1.4 V versus RHE.

3. Results and Analysis

3.1. Verification of the Electrochemical Technique. To demonstrate that silver is electrochemically active for the reduction of oxygen and hydrogen peroxide, but not for the oxidation of hydrogen, cyclic voltammetry was conducted over a range of 0.0–1.4 V (versus RHE) at 50 mV/s in solutions of varying pH that were saturated with nitrogen (base case), oxygen, or hydrogen, or that had 1 or 10 mM H₂O₂ added. Typical results are illustrated in Figures 3(a) and 3(b).

At potentials less than 0.8 V versus RHE, Ag exhibits excellent O₂ reduction, on par with Pt. In addition, Ag shows essentially no activity for H₂ oxidation. Ag is also an excellent electrocatalyst for H₂O₂ reduction and results in similar electrochemistry to that obtained for the oxygen saturated

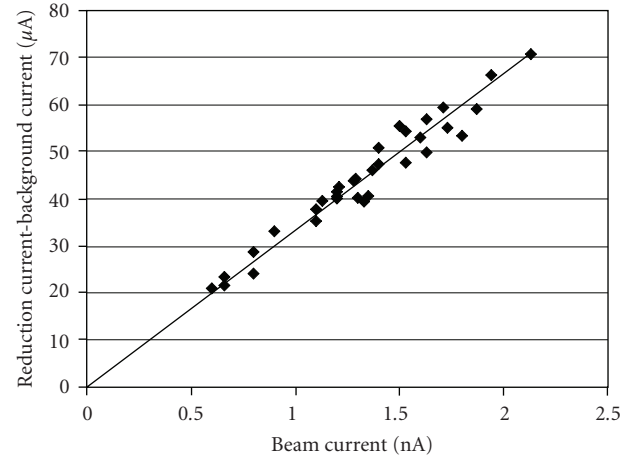


FIGURE 4: Steady-state electrochemical response of 0.01 M KOH exposed to an alpha beam of various beam currents.

solution. Since Ag and Ag₂O are not electrochemically active for H₂ oxidation as shown, the H₂ that is radiolytically generated simply remains in the electrolyte. In alkaline solutions, the Ag/Ag₂O couple is ≈1.15 V versus RHE. As a result, for radiolysis experiments in alkaline solutions, the potential of the silver electrode was held at −1.0 V versus Ag/Ag₂O, equivalent to +0.15 V versus RHE for reference to Figure 3.

For the radiolysis experiments conducted in this study, a 4.5 MeV alpha beam was used. After traveling through the SiC window, the Ti film (negligible energy loss), and the Ag film, the incident energy on the electrolyte was 3.7 MeV. With an incident energy of 3.7 MeV, alpha particles travel ~25 μm through water, losing their energy in a nearly linear fashion. Radiation penetration depths and energy losses were calculated using stopping powers provided by The National Institute of Standards and Technology (NIST) [13].

The current observed during beam exposure is on the order of μA and is due to electrochemical reaction and not due to the beam itself (the beam current is on the order of 1 nA). As is illustrated by Figure 4, a plot of reduction current versus beam current is linear through the origin with little variation. If the beam itself had some direct impact on the electrochemical current, one would expect a nonlinear response with respect to beam current, which is not the case.

This experimental setup and method allow for rapid detection of radiolysis products at the working electrode and for minimization of losses due to diffusion. O₂ and H₂O₂ are generated within 25 μm of the working electrode, which is operated at the limiting current. This proximity allows for efficient capture of essentially all of the radiolytically generated O₂ and/or H₂O₂. The efficient collection of O₂/H₂O₂ can be proved in several ways. First, transient, one-dimensional concentration profiles within the cell during operation were simulated based on Fick's second law with generation:

$$\frac{\partial C_A}{\partial t} - D_A \frac{\partial^2 C_A}{\partial x^2} = R_g, \quad (7)$$

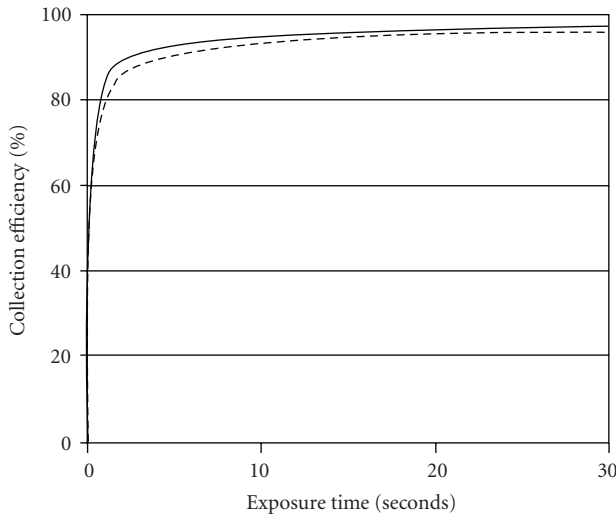


FIGURE 5: Simulated collection efficiency of the radiolytic yield measurement cell with respect to time exposed to the alpha particle beam; Solid: H_2O_2 , dashed: O_2 .

where R_g [$\text{mol cm}^{-3} \text{s}^{-1}$] is the volumetric generation of component A, D_A [cm^2/s] is the diffusivity of component A, t [sec] is time, and C_A [mol/cm^3] is the concentration of component A. Details of the simulation procedure can be found in [7]. Results of such a simulation give an estimation of the system's collection efficiency with respect to exposure time as illustrated in Figure 5.

Generation of O_2 and H_2O_2 occurs nearly uniformly in the $25 \mu\text{m}$ nearest to the working electrode (the radiolysis zone). The working electrode always operates at limiting current, that is, the concentration at the electrode surface is zero, so there is a competition between diffusion toward the working electrode and diffusion into the bulk liquid, where the concentration is also zero. Initially, the concentration of these products is very low, and although the working electrode is operating at limiting current, the driving force for diffusion toward the working electrode is relatively low, and only a small percentage of the O_2 and H_2O_2 generated is collected by the working electrode. As exposure to the alpha beam continues, the concentration of O_2 and H_2O_2 quickly rises in the radiolysis zone, with peak concentration occurring at the edge of the radiolysis zone. As the working electrode continues to operate at limiting current, the concentration gradient grows, increasing the driving force for diffusion towards the working electrode, which increases the percentage of O_2 and H_2O_2 collected by the working electrode. This process occurs rapidly, and high collection efficiencies are quickly established. In our simulations, after just three seconds of exposure, collection efficiency is already $>87\%$, after ten seconds of exposure, collection efficiency is $>93\%$, and at longer times, the efficiency is $>95\%$. Evolution of the H_2O_2 concentration profile over the first thirty seconds of alpha beam exposure is illustrated in Figure 6. Evolution of the O_2 concentration profile is qualitatively similar.

High collection efficiency can also be observed in the experimental results. The result of a 58-second exposure of

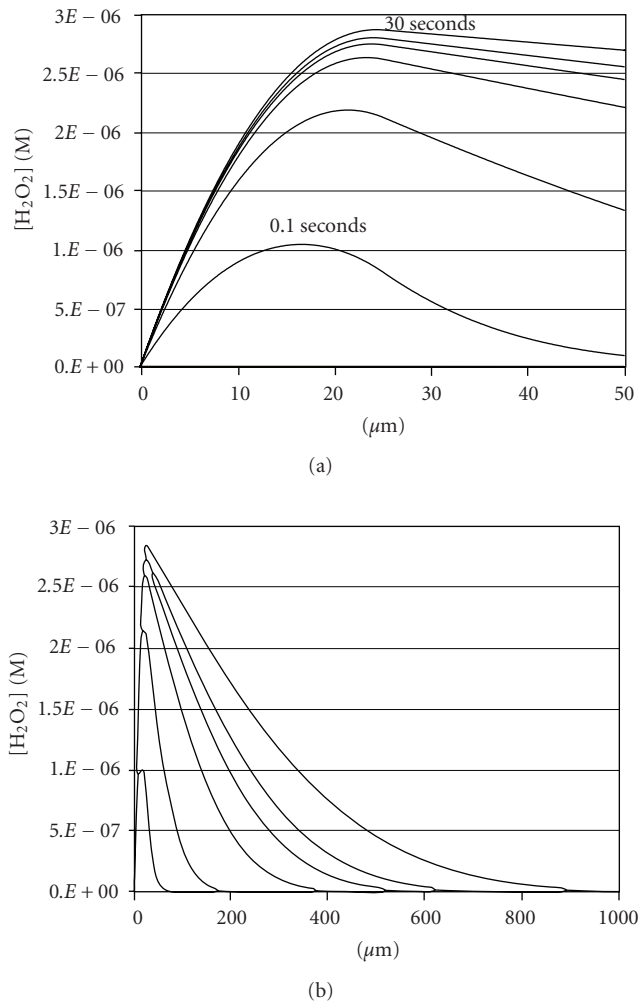


FIGURE 6: Simulated H_2O_2 concentration profile with respect to exposure time (0.1, 1, 5, 10, 15, and 30 seconds) for exposure to a 2 nA, 1 mm diameter alpha beam with $G(\text{H}_2) = 1.5$, dictated by (6).

0.01 M KOH to a 1.28 nA alpha beam is shown in Figure 7. When the shutter was opened at approximately 8.5 seconds, the response to the exposure was nearly instantaneous and steady-state was quickly achieved, in good agreement with the simulations. The small variations in the electrochemical current at steady-state were due to variations in the alpha beam current. When the shutter was closed, the electrochemical response quickly returned to the baseline. The small "tail" after exposure resulted from the collection of a small amount of radiolysis product that had diffused a short distance away from the working electrode. The fast onset of steady-state and insignificant tail after exposure imply very high collection efficiency.

Further experimental proof of high collection efficiency is presented when comparing the tail after exposures of different duration as shown in Figure 8. Since the ion beam current varied over the course of these measurements, the results are presented with the electrochemical current normalized to the ion beam current.

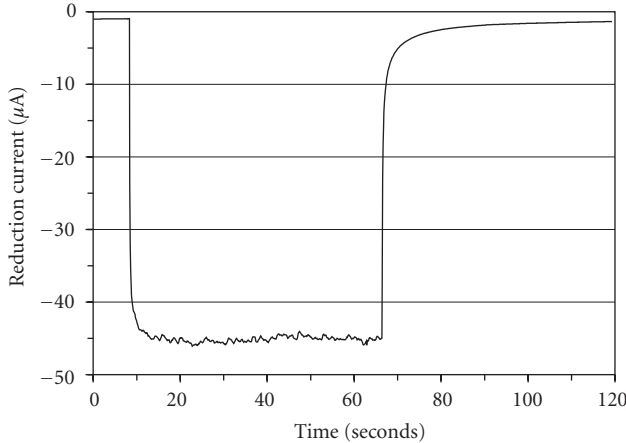


FIGURE 7: Electrochemical response of a solution of 0.01 M KOH exposed to a 1.28 nA alpha beam for 58 seconds.

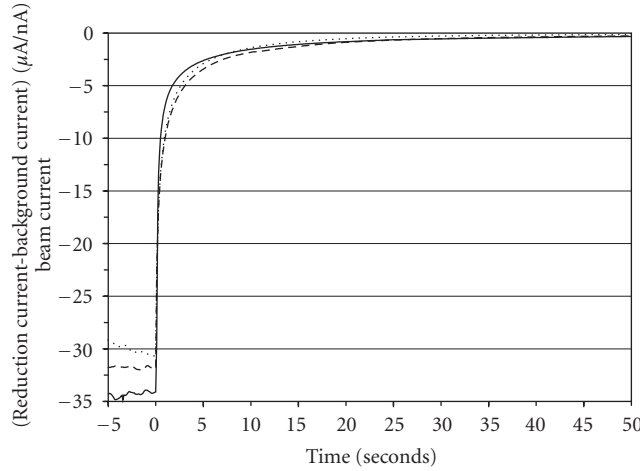


FIGURE 8: Electrochemical current “tails” after exposure of a 0.01 M KOH to alpha radiation indicating collection of O_2/H_2O_2 that has diffused away from the electrode after exposures of different durations. Dotted: 10 sec exposure, dashed: 30 seconds, and solid: 58 seconds.

There is no significant difference between the diffusion tails illustrated in Figure 8. If the collection efficiency were not extremely high, there would be an accumulation of O_2 and H_2O_2 away from the electrode that would increase with increasing exposure to the alpha beam. This would result in a tail that would increase in size with increasing exposure duration. However, there is no appreciable increase in the diffusion tail size with increasing exposure time for this system, confirming that collection efficiency of O_2 and H_2O_2 is extremely high.

It should be noted that if the penetration depth were much greater than $25\ \mu m$, the collection efficiency would be lower and a more pronounced diffusion tail would be seen. For example, consider the electrochemical responses to a 3.0 MeV proton beam versus a 1.2 MeV proton beam as shown in Figure 9. The 3.0 MeV proton beam was calculated to have a penetration depth of $\sim 149\ \mu m$ while the 1.2 MeV

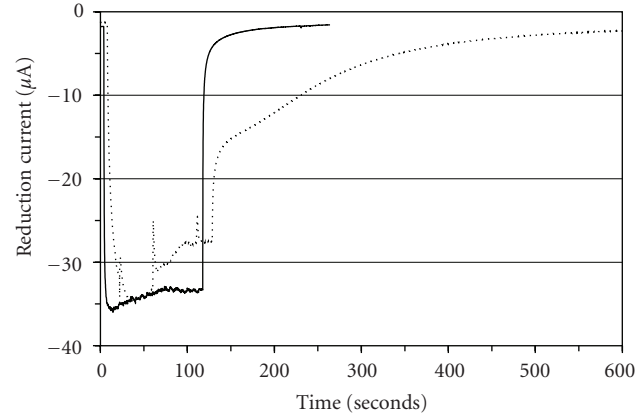


FIGURE 9: Comparison of diffusion tails for 3.0 MeV protons (dotted) and 1.2 MeV protons (solid).

proton beam would have a penetration depth of $\sim 26\ \mu m$, similar to that of 3.7 MeV alpha particles. From Figure 9, it is clear that a significant diffusion tail is present when the radiation penetration depth is large, indicating low collection efficiency by the working electrode. On the other hand, when the penetration depth is smaller ($\approx 26\ \mu m$), the response shows very little diffusion tail, indicating very high collection efficiency.

Since the collection efficiency of O_2/H_2O_2 is very high, the steady-state current achieved during exposure to the alpha beam translates directly to the radiolysis yield of O_2/H_2O_2 . The balance of the O_2/H_2O_2 reaction is H_2 as given by (7), making the calculation of $G(H_2)$ trivial. It should be noted that the relative yield of O_2 or H_2O_2 is immaterial to the calculation of the hydrogen yield, as one H_2 molecule was produced for every two electrons detected in the electrochemical current, regardless of whether O_2 or H_2O_2 was reduced. In addition, two electrons are required to neutralize one He^{++} in the measurement of the beam current, so that the G -factor can be calculated using the following equation assuming perfect collection efficiency:

$$G(H_2) = 100 * \frac{(\text{Steady - state Electrochemical current})}{(\text{Incident Beam Energy} * \text{Beam Current})}, \quad (8)$$

where G is in molecules $H_2/100\text{ eV}$ deposited energy and the electrochemical current has been corrected for the small background current present before radiolysis.

3.2. Radiolysis Yield of Solutions of KOH, NaOH, and HCl. In order to examine the effect of pH on the behavior of the electrochemical cell and the radiolysis yield, experiments were conducted to measure the yield for solutions of HCl, and KOH or NaOH of various ionic strength. The error calculated for all experimental data is based on a 95% confidence interval:

$$CI_{0.95} = \pm 1.96\sigma, \quad (9)$$

where $CI_{0.95}$ is the 95% confidence interval and σ is the standard deviation. Typically, 20 to 30 separate exposures were

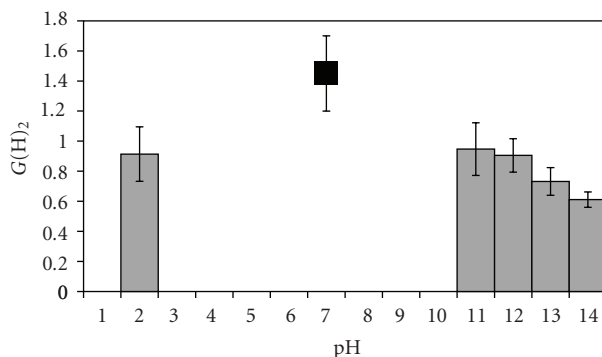


FIGURE 10: Experimentally measured pH dependence of $G(H_2)$, including reported literature values for distilled, deaerated water, shown at pH = 7. Error bars on experimental results indicate 95% confidence interval.

used to generate the average yield and standard deviation. It is important to note that the standard deviation and not the standard error was used to calculate the confidence interval. This means that the confidence interval applies for individual measurements and not for averages.

Solutions of pH = 11, 12, 13, and 14 (0.001, 0.01, 0.1, and 1 M) were prepared with NaOH and KOH. It was found that there was no statistical difference in the radiolysis yield between KOH and NaOH solutions of equal concentration. When exposed to the alpha beam, solutions of pH = 14 (1 M) exhibited a fairly sharp response and achieved steady-state in \approx 8 seconds. This response was not as sharp as was observed with solutions of pH = 13 or 12. This is believed to be due to somewhat lower diffusivities of O_2 and H_2O_2 in the more concentrated alkaline solution.

When exposed to the alpha beam, solutions of pH = 12 and 13 exhibited a sharp response and quickly (<5 seconds) achieved steady-state.

Solutions of pH = 11 (1 mM) exhibited a somewhat sluggish response and achieved steady-state in 15–20 seconds. The sluggish response is due to the low conductivity of 1 mM KOH (or NaOH) solutions. In this system, the primary carriers of ionic current are the cation and OH^- . At low concentrations, it takes some time for the ionic current carrying species to achieve appropriate concentration profiles to sustain higher currents, resulting in the sluggish response. However, once these concentration profiles are established, the steady-state current still corresponds with the generation rate of O_2 and H_2O_2 . The O_2 and H_2O_2 that were able to diffuse away during the initial sluggish response are recaptured after exposure in the diffusion tail. For this solution, optimal results were obtained with relatively low beam currents (\approx 1 nA) that minimized the electrochemical current. This in turn minimized the voltage drop resulting from the flow of current between the working electrode and the counter electrode across the solution resistance between those electrodes. At higher beam currents, the electrochemical current and resulting voltage loss were sufficiently large that the 30 V compliance limit of the potentiostat was

reached, and the working electrode potential could not be maintained at the desired value.

Solutions of pH = 2 (10 mM) were prepared with HCl. When exposed to the alpha beam, the electrochemical response from solutions of pH = 2 are very similar to those of pH = 12 (also 10 mM), and exhibited a sharp response and quickly achieved steady-state. This is not surprising since the ionic conductivities and oxygen diffusion coefficients are very similar for pH = 2 and pH = 12. For 0.01 M HCl solutions, the working electrode was potentiostated at -0.4 V versus $Ag/AgCl/Cl^-$ which gave a similar overpotential for peroxide reduction as was employed in alkaline solutions.

From the results obtained with pH = 2, 11, 12, 13, and 14, the dependence of $G(H_2)$ on pH is shown in Figure 10. It is clear that increases in pH beyond 11 results in lower and lower radiolysis yield. The reason for this lower yield is not clear, nor is it the aim of this work to explain the mechanism. However, this effect may be due to greater radical scavenging by the ions present in solution.

The radiolysis yield appears to level off closer to neutral pH, and low total ion concentration is approached. The data indicates that for a pure water solution, the radiolysis yield would likely be $G(H_2) \sim 1$. Considering the high end of the 95% confidence intervals, this result is consistent with the lower end of reported literature values for pure water, which are shown in Figure 10 as the point at pH 7. Furthermore, the G factors reported here were calculated assuming 100% collection efficiency while the simulations suggest that, at steady-state, the true collection efficiency is slightly lower, on the order of 97%. Correcting for the collection efficiency would raise the calculated G -factor slightly closer to literature values.

4. Discussion

This new method of detecting radiolysis yield has many advantages over the method of irradiating vials described in the literature. With the previous method, relatively long exposures, on the order of hours, may be required in order to build up sufficient hydrogen for analysis by gas chromatograph. This method achieves rapid detection of radiolysis products that is both accurate and efficient. There is inherently a realtime evaluation of radiolysis yield. This could be useful if, for instance, the electrolyte contains scavenging species that are depleted during exposure. The method also provides a very accurate measure of beam stability and can easily see events such as the beam “winking” off and on, beam fluctuation, or beam decay. New electrolytes and solutions of interest can be easily pumped through the cell, allowing for rapid screening. It should be noted that solutions containing suspensions of dispersed nanoparticles can be evaluated using this method [7]. With gamma-ray radiation, such suspensions have been reported to increase the radiolysis yield [1, 2, 11, 14–16].

There are certain drawbacks associated with this method. The system illustrated in Figure 2 is optimally employed with alkaline solutions because of our initial choice of reference electrode (Ag/Ag_2O) and the general stability of the Ag

working electrode in an alkaline environment. However, this system has been used to test chloride containing acidic solutions using the Ag/AgCl internal reference. In this case, potential control of the working electrode must be maintained at all times to prevent corrosion and dissolution of the thin Ag layer. This method is also unable to handle nonconductive solutions, such as pure water, due to the basic limitations of an electrochemically based system. The results obtained with 1 mM KOH illustrate this limitation, as the voltage drop resulting from using a solution of low ionic conductivity became significant. For solutions of lower ionic strength/lower conductivity, the voltage drop in solution would have to be further reduced. The voltage drop in solution could be furthered lowered by either (1) moving the counter electrode closer to the working electrode and/or (2) increasing the diameter of the flow channel. Both of these options were considered but rejected for the following reasons. Since the working electrode is being used to reduce oxygen or peroxide, the most likely counter electrode reaction is the oxidation of water to produce oxygen. Therefore, it is desirable to keep the counter electrode well separated from the working electrode to prevent oxygen generated at the counter electrode from reaching the working electrode via diffusion. Also, it is desirable to keep the cell volume small, to minimize the amount of solution needed for a measurement, and in the unlikely event of a window failure, to minimize the potential damage to the vacuum system and the accelerator.

Another limitation on solutions to be studied is that, ideally, no species (other than those generated radiolytically) in the solution should be reactive on the Ag electrode at the potential of interest. This limitation provides a low, well-defined background current. In the presence of other electroactive species, it would be necessary to hold the working electrode at the potential of interest for some period of time prior to ion-beam exposure. In the unstirred environment inside the cell, the diffusion limited current for any other electrochemically active species would diminish to a low enough value to allow for subsequent sensing of radiolytically derived reactants, but the sensitivity of the method would be lowered. Lastly, since only O₂ and H₂O₂ are being detected, there is a lack of a closed mass balance. Here, the H₂ yield is simply calculated based on the O₂ and H₂O₂ yields, but these calculations could be verified if H₂ production was independently measured. This could be remedied by circulating the electrolyte and using some means of hydrogen sensing external to the radiolysis cell. However, in this case, the analysis may be considerably more difficult depending on the sensitivity and response time of the hydrogen detection means employed. It should be noted that to the best of the authors' knowledge, there are no electrocatalysts that are highly active for hydrogen oxidation and that are also inactive for oxygen and/or peroxide reduction. With the appropriate choice of catalyst and potential, a degree of selectivity may be possible, but not the absolute selectivity of silver shown in Figure 3. As a result, an electrochemical means of H₂ detection in the manner employed here for O₂/H₂O₂ is problematic.

These limitations, coupled with the fact that these limitations are not an issue when using a gas chromatograph

to analyze the contents of irradiated vials, show that the technique presented here should be complementary to, and not considered a replacement for, the techniques already known in the literature.

5. Conclusions

An electrochemical cell has been developed that allows for the rapid and exhaustive detection of oxygen and/or hydrogen peroxide produced during the radiolysis of aqueous solutions by alpha particle or proton beams. Short, 10–100 s, exposures were sufficient to yield steady-state electrochemical currents proportional to the radiolysis G-factor. The use of thin SiC windows provided a robust means of separating the vacuum environment of the ion-beam accelerator from the aqueous solution at atmospheric pressure with minimal energy loss. The primary advantage of this technique is in its rapid screening capability. Multiple solutions of interest can be analyzed, with repeat measurements for a high level of confidence in the results, in the time it would typically take to make one measurement on one sample using existing techniques. However, given the limitations imposed by the electrochemical detection of the radiolysis products (solutions must be ionically conductive, and the radiolysis products must be able to be selectively oxidized or reduced using a suitable combination of electrocatalyst and potential), this technique provides a complement to, but not a replacement for, the existing analytical methods.

Acknowledgments

Portions of this paper were funded by DARPA under AFRL Award FA8651-04-1-0005. J. E. Liedhegner was partially supported by an Innovation Incentive Fellowship Award granted by the State of Ohio, Department of Development under the Third Frontier Program, and by a Case Prime Fellowship from CWRU. The assistance of Mr. Alan McIlwain with the ion-beam experiments is greatly appreciated. Professors M. Mehregany and C. Zorman of the Department of Electrical Engineering at CWRU graciously provided the SiC windows and helpful suggestions as to their care and handling.

References

- [1] J. A. LaVerne and S. E. Tonnies, "H production in the radiolysis of aqueous SiO suspensions and slurries," *Journal of Physical Chemistry B*, vol. 107, no. 30, pp. 7277–7280, 2003.
- [2] A. L. Cecal, M. Goanta, M. Palamaru et al., "Use of some oxides in radiolytical decomposition of water," *Radiation Physics and Chemistry*, vol. 62, no. 4, pp. 333–336, 2001.
- [3] J. Bockris and S. Srinivasan, *Fuel Cells: Their Electrochemistry*, McGraw-Hill, New York, NY, USA, 1969.
- [4] M. Burton and J. L. Magee, *Advances in Radiation Chemistry*, vol. 1, Wiley-Interscience, New York, NY, USA, 1969.
- [5] A. O. Allen, *The Radiation Chemistry of Water and Aqueous Solutions*, D. Van Nostrand, Princeton, NJ, USA, 1961.
- [6] R. B. Peterson, B. K. Paul, T. Palmer et al., "Radiolytic microscale power generation based on single chamber fuel cell operation," *Journal of Micromechanics and Microengineering*, vol. 17, no. 9, pp. S250–S256, 2007.

- [7] J. Liedhegner, *Radiolytically Powered Micro Fuel Cell*, Ph.D. dissertation, Case Western Reserve University, Cleveland, Ohio, USA, 2008.
- [8] J. A. LaVerne and S. M. Pimblott, "New mechanism for H formation in water," *Journal of Physical Chemistry A*, vol. 104, no. 44, pp. 9820–9822, 2000.
- [9] M. V. Vladimirova and I. A. Kulikov, "Formation of H₂ and O₂ in radiolysis of water sorbed on PuO₂," *Radiochemistry*, vol. 44, no. 1, pp. 86–90, 2002.
- [10] J. A. La Verne and L. Tandon, "H production in the radiolysis of water on UO₂ and other oxides," *Journal of Physical Chemistry B*, vol. 107, no. 49, pp. 13623–13628, 2003.
- [11] S. Seino, T. A. Yamamoto, R. Fujimoto et al., "Enhancement of hydrogen evolution yield from water dispersing nanoparticles irradiated with gamma-ray," *Journal of Nuclear Science and Technology*, vol. 38, no. 8, pp. 633–636, 2001.
- [12] C. A. Zorman, S. Rajgopal, X. A. Fu, R. Jezeski, J. Melzak, and M. Mehregany, "Deposition of polycrystalline 3C-SiC films on 100 mm diameter Si(100) wafers in a large-volume LPCVD furnace," *Electrochemical and Solid-State Letters*, vol. 5, no. 10, pp. G99–G101, 2002.
- [13] M. Berger, J. Coursey, M. Zucker, and J. Chang, ESTAR, PSTAR, and ASTAR: Computer Programs for Calculating Stopping-Power and Range Tables for Electrons, Protons, and Helium Ions (version 1.2.3), National Institute of Standards and Technology, Gaithersburg, Md, USA, 2005, <http://physics.nist.gov/Star>.
- [14] Y. Wada, K. Kawaguchi, and M. Myouchin, "Decomposition of water and production of H using semiconductor-photocatalytic effect induced by gamma ray from high radioactive waste," *Progress in Nuclear Energy*, vol. 29, supplement, pp. 251–256, 1995.
- [15] T. A. Yamamoto, S. Seino, M. Katsura, K. Okitsu, R. Oshima, and Y. Nagata, "Hydrogen gas evolution from alumina nanoparticles dispersed in water irradiated with γ -ray," *Nanostructured Materials*, vol. 12, no. 5, pp. 1045–1048, 1999.
- [16] G. Merga, B. H. Milosavljevic, and D. Meisel, "Radiolytic hydrogen yields in aqueous suspensions of gold particles," *Journal of Physical Chemistry B*, vol. 110, no. 11, pp. 5403–5408, 2006.

Research Article

Cobalt Ferrite Nanocrystallites for Sustainable Hydrogen Production Application

Rajendra S. Gaikwad,¹ Sang-Youn Chae,¹ Rajaram S. Mane,^{1,2}
Sung-Hwan Han,³ and Oh-Shim Joo¹

¹ Clean Energy Research Centre, Korea Institute of Science and Technology, Seoul 130-650, Republic of Korea

² School of Physical Sciences, Swami Ramanand Teerth Marathwada University, Nanded 431 606, India

³ Inorganic Nanomaterials Laboratory, Department of Chemistry, Hanyang University, Seoul 133-791, Republic of Korea

Correspondence should be addressed to Oh-Shim Joo, joocat@kist.re.kr

Received 22 January 2011; Accepted 26 February 2011

Academic Editor: Bengi Uslu

Copyright © 2011 Rajendra S. Gaikwad et al. This is an open access article distributed under the Creative Commons Attribution License, which permits unrestricted use, distribution, and reproduction in any medium, provided the original work is properly cited.

Cobalt ferrite, CoFe_2O_4 , nanocrystalline films were deposited using electrostatic spray method and explored in sustainable hydrogen production application. Reflection planes in X-ray diffraction pattern confirm CoFe_2O_4 phase. The surface scanning microscopy photoimages reveal an agglomeration of closely-packed CoFe_2O_4 nanoflakes. Concentrated solar-panel, a two-step water splitting process, measurement technique was preferred for measuring the hydrogen generation rate. For about 5 hr sustainable, 440 mL/hr, hydrogen production activity was achieved, confirming the efficient use of cobalt ferrite nanocrystallites film in hydrogen production application.

1. Introduction

Special magnetic and electrical properties, high chemical, and mechanical hardness [1], in modern information technology, have made ferrite films significantly important while designing the electromagnetic devices including the memories [2], sensors [3], and microwaves [4]. In particular, spinel-type ferrites such as $M\text{Fe}_2\text{O}_4$ where $M = \text{Co, Ni}$ are among the most important magnetic materials which have been previously preferred over the past half century [5, 6]. On account of large magnetocrystalline anisotropy, high coercivity, moderate saturation magnetization, large magnetostrictive coefficient, chemical stability, and mechanical hardness, which generally are helpful for magnetic recording devices, magneto-optical recording, and electronic devices, cobalt ferrites are nowadays highly in demand. Currently, the well-known established techniques used for fabricating the ferrite films include pulsed laser deposition, rf-magnetron sputtering, electron beam evaporation, metal organic chemical vapour deposition, and molecular beam epitaxy [7–10]. Most of these techniques involve a two step process. In the first step, the desired ferrite material is

synthesized in the bulk form using conventional method, and in the second step, synthesized bulk material is used as a target for irradiation by high power laser, ion/electron beam, or rf source. The resultant plume is then captured on a cold substrate. These techniques require a high power source and/or an ultrahigh vacuum system, making them extremely capital and energy intensive. These techniques are also not suited to obtain conformal coatings on curved substrates. Furthermore, these techniques are inapplicable when the target material is maintained at low-temperatures, as an irradiation would lead to instantaneous decomposition of the target material [11]. There is, therefore, a need to develop simple and inexpensive wet chemical approach for synthesizing ferrite nanostructures on variety of substrates at ambient temperature. Different chemical methods such as ferrite plating [12, 13], sol-gel [14], spin spray ferrite plating [15], and modified ferrite plating [16], spray pyrolysis [17], and the thin liquid film method [18] have been documented in the literature for depositing ferrite nanostructures in the films form. The multicomponent, nanocrystalline, active redox water splitting cobalt ferrite films can be fabricated using electrostatic spray pyrolysis (ESP) electronic method.

Cobalt ferrite films, synthesized using this method, could offer several advantages, for example, synthesis at low temperatures, especially, below 150°C that would be environmentally benign for hydrogen production application [19]. Secondly, available conventional methods such as electrodeposition or normal spray pyrolysis are facing serious large area uniform deposition problem that can be easily solved in ESP method as ESP is a simple chemical synthesis technique in which the high potential field is applied between the substrate and spray nozzle for acceleration.

Chemical synthesis of cobalt ferrite nanocrystalline films using $\text{Co}(\text{CH}_3\text{COO})_2 \cdot 2\text{H}_2\text{O}$ and $\text{Fe}(\text{NO}_3)_3 \cdot 9\text{H}_2\text{O}$ is quite known [20, 21]; however, its direct implication in hydrogen production application is quite unknown. Therefore, in the present paper, we report the synthesis of smooth and uniform cobalt ferrite nanocrystallites films using ESP method. Various parameters including the substrate temperature, carrier gas flow rate, solution flow rate, droplet size, nozzle-to-substrate distance, were optimized for acquiring adherent and high quality films. The X-ray diffraction (XRD) analysis, X-ray photoelectron spectroscopy (XPS), the scanning electron microscopy (SEM), and atomic force microscopy (AFM) techniques were preferred for the structural elucidation and surface morphological evolution confirmation. Cobalt ferrite films deposited onto a glass substrate were employed for an optical and surface hydrophilicity studies using Uv-Vis spectrophotometry and water contact angle techniques, respectively. For an optical absorption measurement, deposited onto glass substrate, Cranx 100 UV-Vis spectrophotometer was preferred. Finally, cobalt ferrite films deposited onto stainless substrate of about $9 \times 9 \text{ cm}^2$ surface area were utilized in hydrogen production activity. During old fashion of hydrogen production, photoelectrochemical (PEC) cell system was used in water splitting process which mainly preferred semiconductor materials photoelectrode, for generating electron-hole pairs [22].

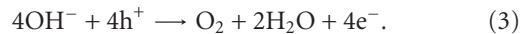
In the relatively new system, silicon solar cell and electrolytic cell are used as active components wherein, for water electrolysis, silicon solar cell provides biasing current to the cathode-anode electrode assembly in an electrolytic cell. The water electrolysis in this system is expected through three steps. The incident solar energy generates electron-hole pairs due to silicon solar cell, in a first step. In a second step, these electron-hole pairs flow through the cathode-anode electrolyte assembly followed by water electrolysis in a third step,



at cathode



and at anode



2. Experimental Details

The ESP technique feasibly facilitates the formation of cobaltite films onto commonly available and inexpensive

glass and stainless steel substrates. These substrates were well cleaned (glass: deionized water, isopropanol, acetone in ultrasonic bath; stainless steel: a zero polishing paper and then ultrasonication) prior to deposition process. For the cobalt ferrite deposition, the aqueous solutions of analytical reagent grade (with 99.99% purity) cobalt acetate hydrate ($\text{Co}(\text{CH}_3\text{COO})_2 \cdot 2\text{H}_2\text{O}$), and iron nitrate nanohydrate ($\text{Fe}(\text{NO}_3)_3 \cdot 9\text{H}_2\text{O}$) were mixed in ethanol and water mixture of 3:1 ratio. Each of the precursor concentration taken in 1:1 volume ratio was 0.2 M. The spraying operation was carried out under an electrostatic potential of 14 kV, at a steady temperature of 150°C by maintaining the substrate-to-spray nozzle distance of 18 cm with spray rate of 15 $\mu\text{L}/\text{min}$. After deposition, the films were annealed at 550°C for 2 h for obtaining cobalt ferrite phase and then used for the structural, morphological, and optical studies and hydrogen production application, respectively. Thickness, measured from the depth profilometer, was close to 100 nm. The X-ray diffractometer (Rigaku, RINT/PMAX 2500) with Cu-K α radiation wavelength of 1.5406 Å was used for the structural identification. The X-ray source was operated at 40 kV and 100 mA, with a drive axis in 2θ for a scan range from 20 to 80°. Surface morphology and surface topography and average roughness were confirmed from JEOL-JSM 5410 SEM and AFM photoimages, respectively. The sessile drop method was used to measure the contact angle by dropping a microlevel water droplet using fine syringe. The optical absorption measurement of cobaltite film, deposited onto glass substrate, was performed by using Cranx 100 UV-Vis spectrophotometer. The metal contents in cobalt ferrite films were determined by XPS using a Varian FT220s. For hydrogen production measurement, an electrolyser was fabricated with two electrodes (for oxidation and reduction reaction of H_2O). Electrolyte was 1 M NaOH, and Pt counter electrode was for H_2 evolution, and cobalt ferrite film was used for H_2O oxidation. The energy for water splitting can be gained from the photoelectrode located outside of the electrolyser. The areas of photoelectrode and active electrodes were 12.5×12.5 and $9 \times 9 \text{ cm}^2$, respectively. The light intensity was controlled to 100 mW/cm² using xenon lamp of 1.5 kW.

3. Results and Discussion

The XRD spectrum of cobalt ferrite film deposited onto glass substrates after annealing at 550°C is shown in Figure 1(a). The XRD spectrum consists of several low intensity peaks. Structure of cobalt ferrite was confirmed after correlating observed XRD peaks to that found in standard JCPDF data card (22-1086). Identical peaks, similar to reported elsewhere [20], were indexed to (220), (311), (400), and (440) diffraction planes. The peak intensity of (311) was relatively higher than others confirming the presence of single cobalt ferrite phase instead of mixed CoO and Fe_2O_3 phases. This higher intensity of (311) plane can be attributed to an annealing effect that boosts the crystallinity and specific orientation of crystallites. Using Scherrer's formula, crystallite size of about 50 nm was calculated. The SEM image

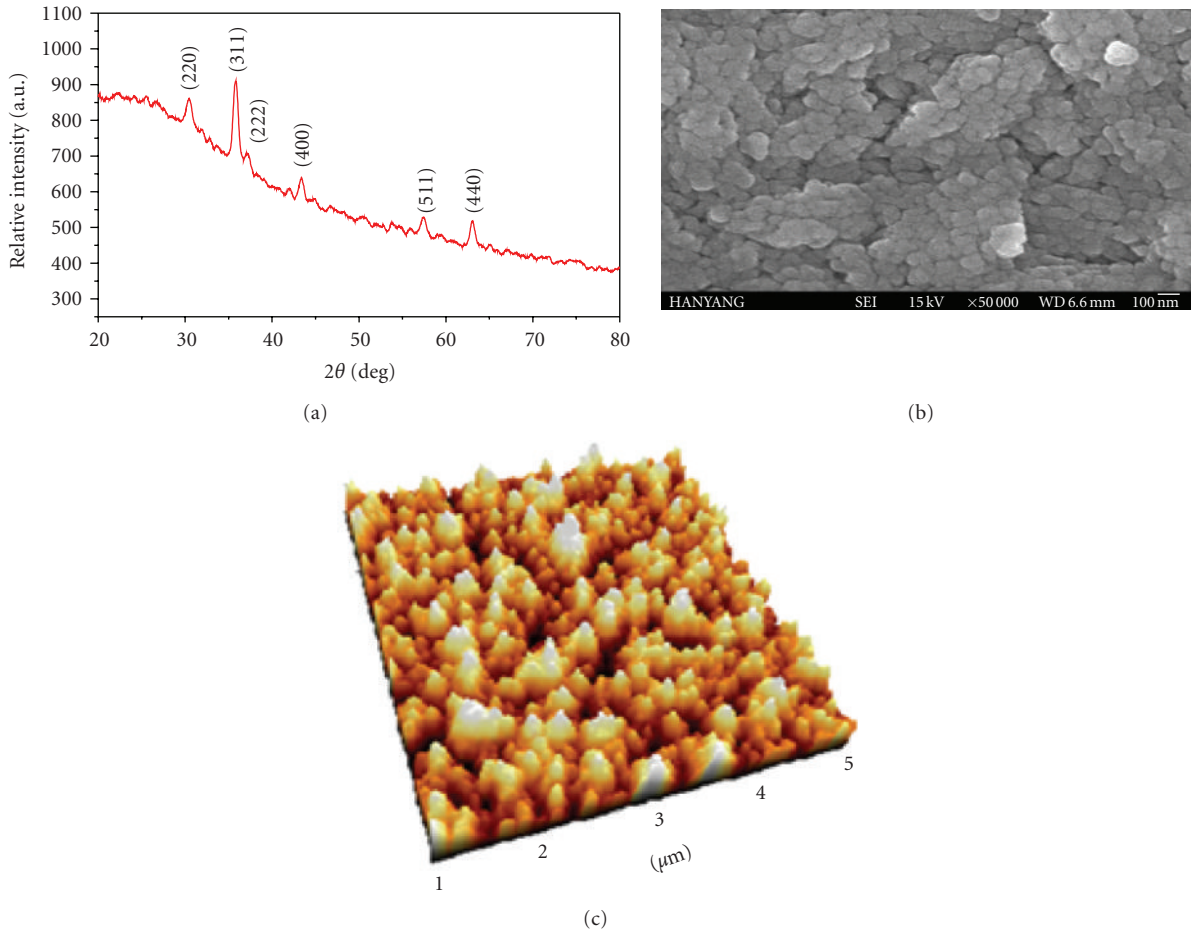


FIGURE 1: (a) Normalized XRD pattern, (b) SEM, and (c) 3D AFM image confirming the structural identification with spherical crystallites evolution of cobalt ferrite.

of cobalt ferrite film is presented in Figure 1(b). Within the scanned surface area, aggregated-type uniform coverage of cobalt ferrite nanoflakes was obtained which was free from the surface cracks or voids. It was found that these nanoflakes were made up of several oval-type elongated crystallites separated by fine and sharp grain boundaries. Each of these crystallites was 60–80 nm in width. However, due to their interpenetrating behaviour, it was difficult for us to measure exact individuals height. Similar type of morphology was also reported by others [21, 23]. We expect enhanced redox reactions, due to the large surface area of these nanoparticles, can be advantageous in hydrogen production activity application. The 3D surface topography image, scanned using noncontact mode of AFM, is presented in Figure 1(c). From 3D AFM image oval-type grain texture, which was actually missing in SEM image, was confirmed.

Figure 2(a) shows the contact angle measurement photo-image recorded with CCD camera. Surface wettability, an important parameter that enables to know the surface interaction of the metal oxide with given electrolyte, was important measurement during this study. The surface of cobalt ferrite was hydrophilic as water contact angle was less than 90° . Water-droplet was spread equally in all directions instead of forming hilly-like dome once water

droplet fixed on it [24]. In the present case, cobalt ferrite film showed hydrophilic surface with $41 (\pm 2)^\circ$ contact angle measurement. Hydrophilic cobalt ferrite could be useful for increasing the redox reactions due to relatively strong interfacial contact between the nanoparticles electrode and electrolyte [25]. The optical absorbance spectrum as a function of the photon energy in the wavelength range of 350–800 nm for cobalt ferrite film deposited onto glass substrate is shown in Figure 2(b). The band gap energy was estimated by using Tauc relation [26]. The film exhibited a strong band edge around 400 nm.

The overall chemical stoichiometry of cobalt ferrite in film was obtained from the XPS analysis. In the XPS analysis, the samples are generally exposed to the monochromatic X-radiation and the properties of the inner shell electrons are probed. Figures 3(a), 3(b), and 3(c) present the XPS spectra of synthesized cobalt ferrite film for Co 2p, Fe 2p and O 1s core levels. The film was composed of Co, Fe, and O with corresponding binding energies of 779.18 (Co 2p $3/2$), 794.60 (Co 2p $1/2$), 710.40 (Fe 2p $3/2$), 723.96 (Fe 2p $1/2$), and 529.61 eV (O 1s), respectively, and the values presented here belong to Co^{2+} , Fe^{3+} , and O^{2-} . The analysis of the Co 2p, Fe 2p, and O 1s peaks offered Co:Fe and Fe:O atomic ratios close to 1:2 and 1:2, respectively, as expected for

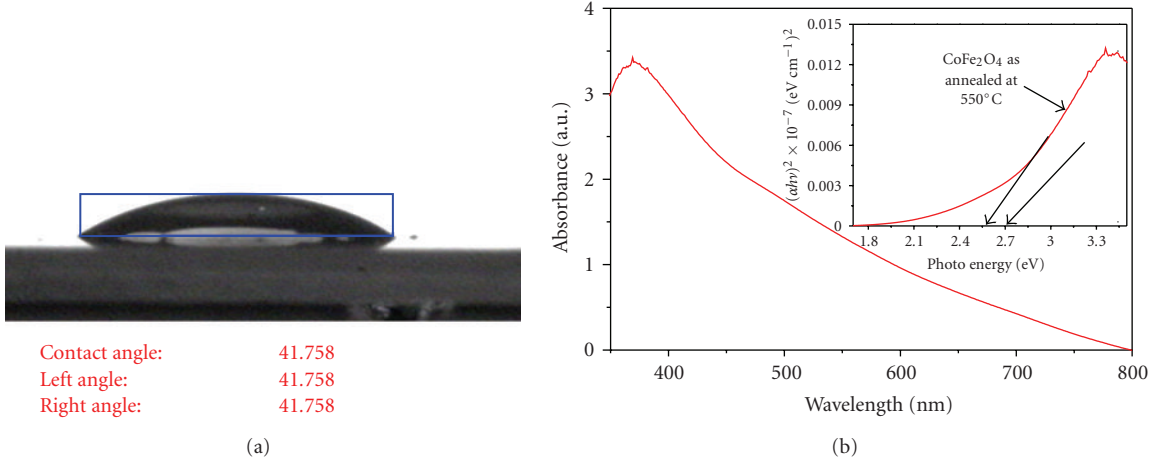
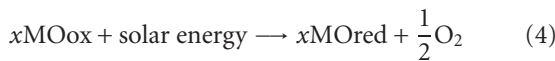


FIGURE 2: (a) Measurement of water contact angle, (b) Uv-Vis spectrum, and then corresponding direct band gap (inset, free arrow indicates the bulk band gap energy).

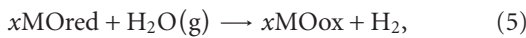
the stoichiometric composition of cobalt ferrite. The XPS measurement results were consistent to XRD observations, confirming the formation of single phase cobalt ferrite rather than mixed phases of CoO and Fe₂O₃. These observations suggest that annealing step played a key role during the process growth of cobalt ferrite nanoflakes. The nucleus of cobalt ferrite could be created by Co ions with the Fe³⁺ and O²⁻ on the surface of Fe₂O₄ as the Fe²⁺ could be easily interchanged into the Fe₂O₄ lattice by only electron transfer, Fe³⁺ might gather near the cobalt ferrite nucleus and became part of the ferrite lattice [27]. This could results the formation of Fe²⁺ rich phase left in the Fe₂O₄ among the reactions of the H₂O/CoFe₂O₄ system. To satisfy electronic neutrality, this Fe²⁺ rich phase could hold few O²⁻, so called as a cation-excess magnetite.

The cation-excess magnetite has the ability for sufficient water splitting in which some Fe²⁺ get oxidized to Fe³⁺ for H₂O/CoFe₂O₄ reaction operation. The production of pure hydrogen is based on splitting and regeneration rates. In general, the regeneration rate is temperature dependent. The most advantageous way to get such high temperature is exploitation of the photon energy of the sun which reduces the environmental utilization of polluting gases that does not cause immense and impact on the energetic and economics [3, 28]. The water-splitting process can produce H₂ gas, which is a promising solar fuel, and has the advantages that H₂ and O₂ gases can be separately recovered due to the two separated steps of the H₂ generation step and the O₂ releasing step. The two-step water-splitting processes that uses metal oxides, MOred/MOOx, as a redox pair utilizing the concentrated solar heat, can be presented using the following oxygen and hydrogen production steps:

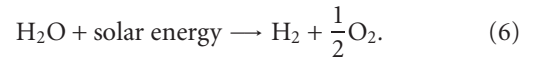
O₂ generation



H₂ generation



where MOred and MOox denote the reduced and oxidized states, respectively. The net reaction is



Iron oxides have a higher possibility for utilization in the two-step water-splitting system, as they are oxides with different oxidation states [29]. The practical operating temperature for the O₂ releasing step of the cobalt ferrite was quite unknown. Lowering the operating temperature for the O₂ generation step was an important step for the practical production of solar hydrogen. While the gas phase (Co, O₂) formation from CoO by the solar thermochemical process has been extensively studied [30, 31], but that from the CoFe₂O₄ phase has not yet been reported. In Figure 3(d), the amount of hydrogen production rate (L/hr) with time showed the stability of the system wherein the water-splitting conversion was totally depending upon product characteristics. Cobalt ferrite film synthesized on stainless steel substrate using electrostatic spray pyrolysis showed comparable water-splitting activity when compared with zinc ferrite films (450 mL/hr) [32]. Water splitting rate, that is, hydrogen production rate was almost the same during the total time span. It is noteworthy that there was no chemical dissociation or degradation of photoanode, cobalt ferrite electrode during the oxidation-reduction process, which, in fact, was advantageous in long-run hydrogen production application due to good chemical stability of cobalt ferrite electrode.

4. Conclusions

In summary, the present work deals with an electrochemical synthesis of cobalt ferrite films and its sustainable hydrogen production application. Cobalt ferrite films, deposited onto both conducting steel and glass substrates, were uniform and free from the pinholes or cracks. Films obtained onto glass substrates were examined for structural, morphological, optical, and surface wettability characteristics whereas those

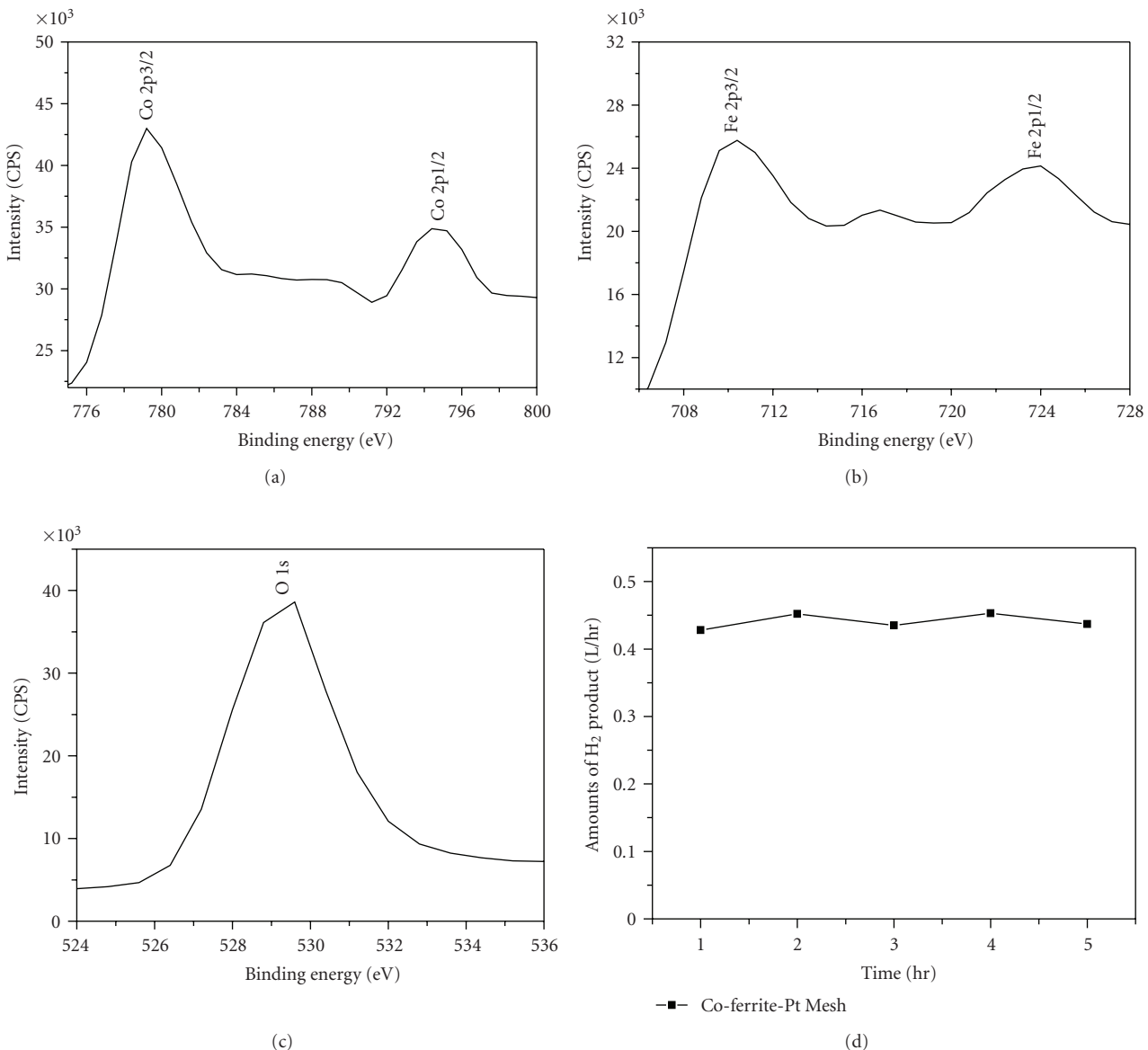


FIGURE 3: The XPS spectra of (a) Co 2p, (b) Fe 2p, (c) O 1s core levels, and (d) quantitative measurement of hydrogen production rate using cobaltite films.

onto stainless steel were used for hydrogen production activity application. The XRD and XPS measurements proved the formation of single phase of CoFe_2O_4 instead of mixed phased. The SEM image showed agglomeration of closely packed nanoflakes with a direct band gap energy of 2.57 eV and water contact angle of $41 (\pm 2)^\circ$. Finally, about 440 mL/hr hydrogen generation activity for more than 5 hr was obtained.

Acknowledgment

The authors appreciate the financial support from the Hydrogen Energy R & D Centre, one of the 21st century frontiers R & D program funded by Ministry of Science and Technology of Korea.

References

- [1] Z. Wu, M. Okuya, and S. Kaneko, "Spray pyrolysis deposition of zinc ferrite films from metal nitrates solutions," *Thin Solid Films*, vol. 385, no. 1-2, pp. 109–114, 2001.
- [2] H. Kaneko, N. Gokon, N. Hasegawa, and Y. Tamaura, "Solar thermochemical process for hydrogen production using ferrites," *Energy*, vol. 30, no. 11-12, pp. 2171–2178, 2005.
- [3] S. Lorentzou, C. C. Agrafiotis, and A. G. Konstandopoulos, "Aerosol spray pyrolysis synthesis of water-splitting ferrites for solar hydrogen production," *Granular Matter*, vol. 10, no. 2, pp. 113–122, 2008.
- [4] C. Agrafiotis, M. Roeb, A. G. Konstandopoulos et al., "Solar water splitting for hydrogen production with monolithic reactors," *Solar Energy*, vol. 79, no. 4, pp. 409–421, 2005.

- [5] M. Roeb, C. Sattler, R. Klüser et al., "Solar hydrogen production by a two-step cycle based on mixed iron oxides," *Journal of Solar Energy Engineering*, vol. 128, no. 2, pp. 125–133, 2006.
- [6] S. Zhang, J. Liu, Y. Han, B. Chen, and X. Li, "Formation mechanisms of SrTiO_3 nanoparticles under hydrothermal conditions," *Materials Science and Engineering B*, vol. 110, no. 1, pp. 11–17, 2004.
- [7] C. Inui, Y. Tsuge, H. Kura, S. Fujihara, S. Shiratori, and T. Sato, "Preparation of one-dimensional photonic crystals by sol-gel process for magneto-optical materials," *Thin Solid Films*, vol. 516, no. 9, pp. 2454–2459, 2008.
- [8] Y. C. Wang, J. Ding, J. B. Yi, B. H. Liu, T. Yu, and Z. X. Shen, "High-coercivity Co-ferrite thin films on (100)- SiO_2 substrate," *Applied Physics Letters*, vol. 84, no. 14, pp. 2596–2598, 2004.
- [9] P. D. Thang, G. Rijnders, and D. H. A. Blank, "Stress-induced magnetic anisotropy of CoFe_2O_4 thin films using pulsed laser deposition," *Journal of Magnetism and Magnetic Materials*, vol. 310, no. 2, pp. 2621–2623, 2007.
- [10] C. Araújo, B. G. Almeida, M. Aguiar, and J. A. Mendes, "Structural and magnetic properties of CoFe_2O_4 thin films deposited by laser ablation on Si (001) substrates," *Vacuum*, vol. 82, no. 12, pp. 1437–1440, 2008.
- [11] M. Lie, K. B. Klepper, O. Nilsen, H. Fjellvåg, and A. Kjekshus, "Growth of iron cobalt oxides by atomic layer deposition," *Dalton Transactions*, no. 2, pp. 253–259, 2008.
- [12] J. X. Wang, H. Inada, L. Wu et al., "Oxygen reduction on well-defined core-shell nanocatalysts: particle size, facet, and Pt shell thickness effects," *Journal of the American Chemical Society*, vol. 131, no. 47, pp. 17299–17302, 2009.
- [13] N. Gupta, A. Verma, S. C. Kashyap, and D. C. Dube, "Microstructural, dielectric and magnetic behavior of spin-deposited nanocrystalline nickel-zinc ferrite thin films for microwave applications," *Journal of Magnetism and Magnetic Materials*, vol. 308, no. 1, pp. 137–142, 2007.
- [14] A. Kleiman-Swarsctein, M. N. Huda, A. Walsh et al., "Electrodeposited aluminum-doped $\alpha\text{-Fe}_2\text{O}_3$ photoelectrodes: experiment and theory," *Chemistry of Materials*, vol. 22, no. 2, pp. 510–517, 2010.
- [15] P. S. Anil Kumar, J. J. Shrotri, S. D. Kulkarni, C. E. Deshpande, and S. K. Date, "Low temperature synthesis of $\text{Ni}_{0.8}\text{Zn}_{0.2}\text{Fe}_2\text{O}_4$ powder and its characterization," *Materials Letters*, vol. 27, no. 6, pp. 293–296, 1996.
- [16] J. G. Barbosa, M. R. Pereira, J. A. Mendes, M. P. Proença, J. P. Araújo, and B. G. Almeida, "Cobalt ferrite thin films deposited by electrophoresis on p-doped Si substrates," *Journal of Physics: Conference Series*, vol. 200, Article ID 072009, 2010.
- [17] Z. Gu, XU. Xiang, G. Fan, and F. Li, "Facile synthesis and characterization of cobalt ferrite nanocrystals via a simple reduction-oxidation route," *Journal of Physical Chemistry C*, vol. 112, no. 47, pp. 18459–18466, 2008.
- [18] M. Endo, H. Nakane, and H. Adachi, "Field emission from transition metal nitride," *Applied Surface Science*, vol. 100-101, pp. 378–382, 1996.
- [19] R. J. McQueeny, M. Yethiraj, S. Chang et al., "Zener double exchange from local valence fluctuations in magnetite," *Physical Review Letters*, vol. 99, no. 24, Article ID 246401, 2007.
- [20] F. Cheng, Z. Peng, Z. Xu, C. Liao, and C. Yan, "The sol-gel preparation and AFM study of spinel CoFe_2O_4 thin film," *Thin Solid Films*, vol. 339, no. 1-2, pp. 109–113, 1999.
- [21] M. Aronniemi, J. Lahtinen, and P. Hautojärvi, "Characterization of iron oxide thin films," *Surface and Interface Analysis*, vol. 36, no. 8, pp. 1004–1006, 2004.
- [22] T. Bak, J. Nowotny, M. Rekas, and C. C. Sorrell, "Photo-electrochemical hydrogen generation from water using solar energy. Materials-related aspects," *International Journal of Hydrogen Energy*, vol. 27, no. 10, pp. 991–1022, 2002.
- [23] A. G. King and S. T. Keswani, "Colloid mills: theory and experiment," *Journal of the American Ceramic Society*, vol. 77, no. 3, pp. 769–777, 1994.
- [24] Z. Zhang, H. Chen, J. Zhong, G. Saraf, and Y. Lu, "Fast and reversible wettability transitions on ZnO nanostructures," *Journal of Electronic Materials*, vol. 36, no. 8, pp. 895–899, 2007.
- [25] H. Aoki, H. Kaneko, N. Hasegawa, H. Ishihara, A. Suzuki, and Y. Tamura, "The $\text{ZnFe}_2\text{O}_4/\text{(ZnO+Fe}_3\text{O}_4)$ system for H_2 production using concentrated solar energy," *Solid State Ionics*, vol. 172, no. 1–4, pp. 113–116, 2004.
- [26] G. P. Joshi, N. S. Saxena, R. Mangal, A. Mishra, and T. P. Sharma, "Band gap determination of Ni-Zn ferrites," *Bulletin of Materials Science*, vol. 26, no. 4, pp. 387–389, 2003.
- [27] M. Aronniemi, J. Lahtinen, and P. Hautojärvi, "Characterization of iron oxide thin films," *Surface and Interface Analysis*, vol. 36, no. 8, pp. 1004–1006, 2004.
- [28] Y.-Q. Chu, Z.-W. Fu, and Q.-Z. Qin, "Cobalt ferrite thin films as anode material for lithium ion batteries," *Electrochimica Acta*, vol. 49, no. 27, pp. 4915–4921, 2004.
- [29] T. Sano, M. Kojima, N. Hasegawa, M. Tsuji, and Y. Tamura, "Thermochemical water-splitting by a carbon-bearing Ni(II) ferrite at 300°C," *International Journal of Hydrogen Energy*, vol. 21, no. 9, pp. 781–787, 1996.
- [30] T. Tsurumi, T. Suzuki, M. Yamane, and M. Daimon, "Fabrication of barium titanate/strontium titanate artificial superlattice by atomic layer epitaxy," *Japanese Journal of Applied Physics, Part 1*, vol. 33, no. 9B, pp. 5192–5195, 1994.
- [31] C. C. Agrafiotis, C. Pagkoura, S. Lorentzou, M. Kostoglou, and A. G. Konstandopoulos, "Hydrogen production in solar reactors," *Catalysis Today*, vol. 127, no. 1–4, pp. 265–277, 2007.
- [32] R. S. Gaikwad, S. Y. Chae, R. S. Mane, Cai-Gangri, S. H. Han, and O. S. Joo, "Large area ($9 \times 9 \text{ cm}^2$) electrostatically sprayed nanocrystalline zincite thin films for hydrogen production application," *International Journal of Hydrogen Energy*, vol. 35, no. 13, pp. 6549–6553, 2010.

Research Article

Kinetics of Hydrogen Evolution on Copper Electrode Involving Organic Acids as Proton Donors

A. Survila, S. Kanapeckaitė, J. Pilekienė, and J. Būdienė

Center for Physical Sciences and Technology, Institute of Chemistry, A. Goštauto 9, 01108 Vilnius, Lithuania

Correspondence should be addressed to A. Survila, arvydass@ktl.mii.lt

Received 10 March 2011; Accepted 17 May 2011

Academic Editor: Bengi Uslu

Copyright © 2011 A. Survila et al. This is an open access article distributed under the Creative Commons Attribution License, which permits unrestricted use, distribution, and reproduction in any medium, provided the original work is properly cited.

Linear potential sweep (LPS) voltammetry was applied to study the kinetics of hydrogen evolution in solutions containing glycolic, malic, tartaric, and gluconic acids. The CE mechanism of hydrogen evolution was analyzed invoking the 2nd Fick's law equations supplemented by terms that account for chemical interactions between diffusing particles. Acids are considered as components that are capable of releasing hydrated protons taking part in the charge-transfer step. Current peaks observed on LPS voltammograms are in linear dependence on \sqrt{v} (v is the potential sweep rate). They obey well-known relationships obtained for simple redox processes, provided that the concentration of oxidant is treated as total concentration of proton donors. Determination of surface concentrations as current density functions makes it possible to transform LPS voltammograms into linear Tafel plots normalized with respect to the surface concentration of hydronium ions. Similar kinetic parameters ($\alpha \approx 0.6$ and $i_0 \approx 10 \mu\text{A cm}^{-2}$) obtained at pH 3 for all OA solutions indicate that the nature of OA has no noticeable influence on the charge-transfer process.

1. Introduction

Organic acids containing OH groups are often used as ligands capable of forming quite stable coordination compounds with different metals including copper. Due to their environmental compatibility, most of them have found use in various industrial applications. Tartaric and citric acids are used in plating baths as additives producing compact, fine-grained copper coatings. Besides, electroless plating of dielectrics involving Cu(II)-tartrate complexes is also worthy of mention.

Hydrogen evolution often attends the electrodeposition of metals. This side reaction should be taken into account when the main process is studied. Often the reduction of hydronium ions can be complicated and involves some chemical steps. In the case of CE mechanism (chemical + electrochemical step), electroactive particles are formed in a chemical reaction that precedes the electron transfer step. Components that produce hydronium ions are often referred to as proton donors. Aforementioned organic acids, which are commonly added to improve the coatings, can also play such a role.

Fundamentals of CE processes, that have been substantially elaborated for present (see, e.g., [1–3]), can serve as a basis for studies of hydrogen evolution. However, some difficulties emerge, when a wide range of proton donors is considered; then, certain extensions and generalizations are desirable. The literature data on this problem show that the knowledge in this area is not sound. Therefore, the investigations of kinetics and mechanism of hydrogen evolution in such systems still remain an actual problem. In this connection, we referred to some concepts [4] that have been applied by us for reduction of metal complexes. This paper presents the main characteristics of the processes occurring on the copper electrode in solutions containing some organic acids that act as proton donors.

2. Experimental Details

Solutions under investigation contained 0.04 M analytical grade glycolic, malic, or tartaric acid (Reakhim, Russia), 0.02 or 0.05 M sodium gluconate (Sigma-Aldrich, 99% purity), 0.3 M Na_2SO_4 or K_2SO_4 (Reakhim, Russia, high purity) and 0.5 M Na_2SO_4 (Lach-Ner, Czech Republic, 99% purity)

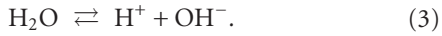
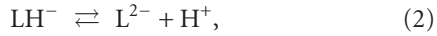
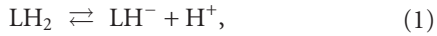
served as supporting electrolytes. Some experiments were carried out with addition of 0.01 M CuSO₄ (Mallinckrodt, USA). Specified values of pH were adjusted by addition of H₂SO₄ or KOH. Twice-distilled water was used to prepare solutions. A pure argon stream was passed through solutions for 0.5 h prior to measurements. All experiments were carried out at 20°C.

To prepare a working electrode, a platinum disc was coated with a 5–7 µm thick copper layer in the solution containing (g dm⁻³): CuSO₄·5H₂O–200, H₂SO₄–50 at 10 mA cm⁻². Electrode potentials were measured with respect to the Ag|AgCl|KCl (sat) reference electrode and were converted to the standard hydrogen scale.

Voltammograms were recorded under linear potential sweep (LPS) conditions using a potentiostat PI-50-1 (Belorussia). Potential sweep rates ν ranged from 10 to 200 mV s⁻¹. Some supporting experiments were carried out using a conventional RDE technique.

3. A Quantitative Model

Let us assume that an aqueous solution of weak acid LH₂ is prepared and an excess of indifferent (supporting) electrolyte is added. The main reversible processes occurring in such a system can be depicted as follows:



Let us suppose that these equilibria are initially established.

When the reduction of hydronium ions, abbreviated as H⁺, starts, their surface-concentration decreases. This results in the onset of mass transport of reacting substances. To describe the latter process quantitatively, we invoke the second Fick's law supplemented by terms that account for chemical interactions between diffusing particles. Then, a set of differential equations should be written for each component, except the water that is present in a large excess. In the case of linear diffusion, these relationships take the following form:

$$\begin{aligned} \frac{\partial[\text{LH}_2]}{\partial t} &= D \frac{\partial^2[\text{LH}_2]}{\partial x^2} - k_2[\text{LH}_2] + k_{-2}[\text{LH}^-][\text{H}^+], \\ \frac{\partial[\text{LH}^-]}{\partial t} &= D \frac{\partial^2[\text{LH}^-]}{\partial x^2} + k_2[\text{LH}_2] - k_{-2}[\text{LH}^-][\text{H}^+] \\ &\quad - k_1[\text{LH}] + k_{-1}[\text{L}^-][\text{H}^+], \\ \frac{\partial[\text{L}^{2-}]}{\partial t} &= D \frac{\partial^2[\text{L}^{2-}]}{\partial x^2} + k_1[\text{LH}^-] - k_{-1}[\text{L}^{2-}][\text{H}^+], \\ \frac{\partial[\text{H}^+]}{\partial t} &= D \frac{\partial^2[\text{H}^+]}{\partial x^2} + k_2[\text{LH}_2] - k_{-2}[\text{LH}^-][\text{H}^+] + k_1[\text{LH}] \end{aligned}$$

$$\begin{aligned} &- k_{-1}[\text{L}^-][\text{H}^+] + k_w[\text{H}_2\text{O}] - k_{-w}[\text{H}^+][\text{OH}^-], \\ \frac{\partial[\text{OH}^-]}{\partial t} &= D \frac{\partial^2[\text{OH}^-]}{\partial x^2} + k_w[\text{H}_2\text{O}] - k_{-w}[\text{H}^+][\text{OH}^-]. \end{aligned} \quad (4)$$

Here and below, the rate constants of forward reactions (1), (2), and (3) are specified as k_2 , k_1 , and k_w , respectively. Similarly, the rate constants of reverse processes are denoted by the respective negative subscripts.

Simple linear operations, applied to (4), yield the relationships that contain no kinetic terms:

$$\frac{\partial c_{\text{ac}}}{\partial t} = D \frac{\partial^2 c_{\text{ac}}}{\partial x^2}, \quad (5)$$

$$\frac{\partial c_{\text{H}}}{\partial t} = D \frac{\partial^2 c_{\text{H}}}{\partial x^2}, \quad (6)$$

where the total (analytical) concentration of acid

$$c_{\text{ac}} = [\text{LH}_2] + [\text{LH}^-] + [\text{L}^{2-}], \quad (7)$$

and the total concentration of proton donors and acceptors

$$c_{\text{H}} = 2[\text{LH}_2] + [\text{LH}^-] + [\text{H}^+] - [\text{OH}^-]. \quad (8)$$

A more extensive analysis shows that similar equations are obtained in the case of systems containing any number of proton donors.

Prior to further dealing with the problem, some points should be discussed. Firstly, it should be noted that the same effective diffusion coefficient D is attributed to all species, despite the fact that the individual mobilities of various particles can be rather different. Previously, it has been shown [5–7] that such an assumption is admissible in the case of labile systems, that is when the abovementioned chemical interactions are fast enough. Specifically, Kačena and Matoušek [5] elaborated the mechanism that gives rise to the apparent equalization of diffusion coefficients.

The second remark concerns the total concentrations that are defined by (7) and (8). Whereas c_{ac} has a clear physical meaning, the second one, c_{H} , looks as made-up quantity. Moreover, c_{H} can turn negative at sufficiently high pH, but then the hydrogen evaluation involving hydronium ions becomes unfeasible. Notice that a similar approach, constructed in such a way and involving c_{H} values, was successfully used for analysis of electrochemical processes occurring in the systems containing metal complexes and protonated ligands [4].

The certain gradient of c_{H} developed in the diffusion layer is determined by the relationship following from the first Fick's law:

$$i = -nFD \frac{\partial c_{\text{H}}}{\partial x} \Big|_{x=0}, \quad (9)$$

where $n = 1$ is a charge number of the electrode reaction.

For as much as an acid itself is assumed to be an electrically inactive substance, the c_{ac} quantity should be constant over the entire range of diffusion layer. Solution of

the differential equation (6) in combination with common initial conditions and boundary condition (9) yields the result:

$$\Delta c_H(t) = -\frac{1}{nF\sqrt{\pi D}} \int_0^t \frac{i(t-u)}{\sqrt{u}} \Psi(u) du, \quad (10)$$

where $\Delta c_H(t)$ is the difference between the bulk and surface concentrations of proton donors and u is an auxiliary variable having dimension of time. Thus, the variable t in $i(t)$ -function should be replaced by $(t-u)$ when (10) is used. The function

$$\Psi(u) = 1 + 2 \sum_m^{\infty} (-1)^m \exp\left(-\frac{m^2 \delta^2}{Du}\right) \quad (11)$$

accounts for the existence of δ -thick diffusion layer. Hence, the foregoing shows that the variations of c_H are rather similar to those established for the oxidized form in the case of simple redox processes (see, e.g., [2]).

The next problem consists in determination of the interrelation between the current density i and overvoltage η (or electrode potential E). This can be performed by means of the proper modification of Butler-Volmer equation that also contains the surface concentrations of oxidant and reductant as well as kinetic parameters of the charge-transfer step. Notice that the above equations (5)–(10) operate with total concentrations only. Then, to determine the amount of concrete particles, the certain interrelations between concentrations of different species should be formulated. This can be done in a simple way, when chemical interactions are sufficiently fast. Then, it is reasonable to suppose that the deviations from chemical equilibria are negligible and the well-known material balance equations, involving respective equilibrium constants, may be used for estimation of bulk or surface concentrations of every component. Otherwise, when the above assumption is not acceptable, (5) and (6) lose their significance and initial equations (4) involving kinetic terms should be solved.

4. Results and Discussion

Voltammetric experiments were carried out with solutions containing different organic acids (OA) and an excess of supporting electrolyte. The presence of the latter substance made it possible to minimize the effect of migration on the mass-transport processes. Besides, some data were obtained with similar solutions containing Cu(II). The acids under study are listed in Table 1; their symbols LH or LH₂ render a number of mobile protons (H^+ ions) that can be splitted out in acidic water solutions. Hereinafter, equilibrium characteristics of dissociation processes involving OA are presented quantitatively by cumulative stability constants (reciprocals of dissociation constants) defined as follows:

$$\beta_1 = \frac{[LH]}{[L^-][H^+]}, \quad (12)$$

$$\beta_2 = \frac{[LH_2]}{[L^-][H^+]^2}, \quad (13)$$

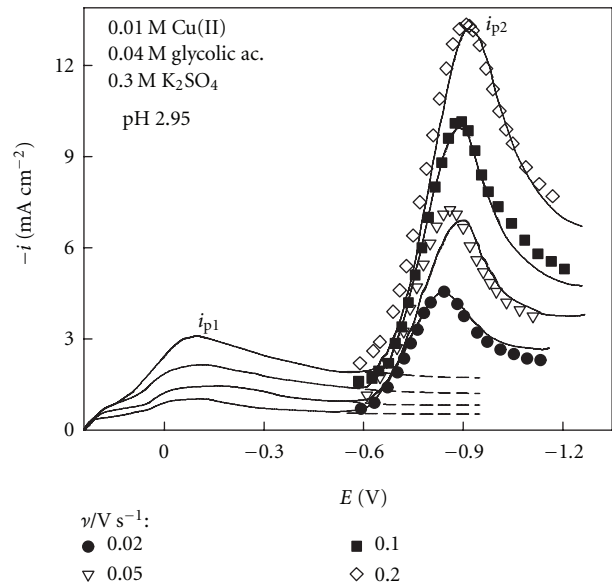


FIGURE 1: Comparison of voltammetric data obtained at different potential sweep rates ν for Cu(II)-containing (solid lines) and Cu(II)-free (symbols) solutions. The latter data are superimposed on the limiting currents of Cu(II) reduction (dotted lines).

(in the case of dibasic acid LH₂, the stability of intermediate anion LH⁻ is also characterized by the relationship similar to (12)).

Due to a sufficiently high difference between the standard potentials of Cu | Cu²⁺ and H₂ | H⁺ electrodes, partial processes of Cu(II) reduction and hydrogen evolution are well-separated, unless very stable Cu(II) complexes are formed. This can be seen from a typical example shown in Figure 1. Experimental voltammograms contain two well-defined maxima that are indicative of two different cathodic processes. The first current peak (i_{p1}) observed at a relatively low cathodic polarization ($E_{p1} \approx -0.1$ V) results from Cu(II) reduction. A further increase in cathodic polarization gives rise to the second process with a distinctive current peak (i_{p2}) observed at $E_{p2} \approx -0.9$ V. This maximum may be conditioned by different reasons, such as Cu₂O reduction or hydrogen evolution [12]. EQCM investigations of Cu(II)-glycolic acid solutions have shown [12] that no extra changes in copper electrode mass are observed in this region. Moreover, similar current peaks are also observed in Cu(II)-free solutions. The voltammograms obtained in the latter case and brought to the level of partial Cu(II) reduction current (dotted lines in Figure 1) coincide sufficiently well with the data recorded in the presence of Cu(II). This effect, as well as large difference between E_{p1} and E_{p2} , gives grounds to suppose that the two partial processes may be analyzed independently. The limiting current of Cu(II) reduction, specified by the relationship

$$i_{lim} = \frac{nFD}{\delta} c_{Cu(II)}, \quad (14)$$

could serve as the base line for hydrogen evolution. In this connection, it should be said, that the thickness, δ , of

TABLE 1: Selected stability constants of organic acids.

Substance	Formula	Symbol	Stability constant		Ref.
			Log β_1	Log β_2	
Glycolic acid	HO-CH ₂ -COOH	LH	3.63		[8, 9]
Malic acid	HOOC-CH ₂ -(CH-OH)-COOH	LH ₂	4.24	7.24	[8, 9]
Tartaric acid	HOOC-(CH-OH) ₂ -COOH	LH ₂	4.26	7.4	[8-10]
Gluconic acid	HO-CH ₂ -(CH-OH) ₄ -COOH	LH	3.7		[11]

the Nernst-type diffusion layer (that develops under the natural convection conditions) depends on the potential sweep rate ν . Voltammetric investigations of Fe(CN)₆⁴⁻/Fe(CN)₆³⁻ redox system have shown [13] that the empirical condition $\delta\sqrt{\nu} \approx \text{const}$ is obeyed in this case. According to the results of our further investigations, this relation is also valid for Cu(II) systems containing OA. The procedures used for estimation of δ values are described elsewhere [13].

Solution pH should be mentioned in the first place as a factor which determines the rate of hydrogen evolution. This can be clearly seen from the typical data shown in Figure 2. Naturally, current density significantly falls with increase in solution pH, that is, when the concentration of hydronium ions decreases. However, when pH is kept constant, the rate of the process under discussion increases with the total concentration of acid (c_{ac}). This effect will be analyzed below in more detail. Finally, the supporting electrolyte plays a part in these processes: the height of the second current peak decreases gradually when sulphate is replaced by perchlorate (Figure 3). Revealed experimental phenomena imply that not only LH⁻ or LH₂ but also HSO₄⁻ should be treated as a proton donor and should be included into (8).

The composition of solutions was calculated using modified material balance equations (7) and (8):

$$c_{ac} = [L^{2-}] \left(1 + \beta_1 [H^+] + \beta_2 [H^+]^2 \right), \quad (15)$$

$$c_H = [H^+] \left(1 + \beta_1 [L^{2-}] + 2\beta_2 [L^{2-}][H^+] \right. \\ \left. + K_{slf} [SO_4^{2-}] - [OH^-] \right), \quad (16)$$

and the expression written for total sulphate concentration:

$$c_{slf} = [SO_4^{2-}] (1 + K_{slf} [H^+]). \quad (17)$$

Stability constants β_1 and β_2 are listed in Table 1; a similar characteristic of hydrosulfate, $K_{slf} = 30$, was taken from a handbook [8, 9] as best-matched to the ionic strength of the solutions under discussion. To obtain the concentration of hydronium ions from pH measurements, the activity coefficient $\gamma_H = 0.7$ was used. It was obtained by empirical equations given in [14, 15]. The concentration of OH⁻ ions was obtained from the ion product of water. An example of the results obtained is given in Table 2. It can be seen that the amount of hydronium ions is not great in the solutions containing a large excess of sulphate. Thus, LH molecules and hydrosulphate anions are the species that should be related to predominating proton donors.

Most of the experimental data obtained are typical of every OA under investigation. Therefore, to minimize

TABLE 2: Distribution of different species in the solutions containing 0.02 M of gluconic acid and 0.5 M of Na₂SO₄ as a supporting electrolyte.

pH	H ₃ O ⁺ (mM)	L ⁻ (mM)	LH (mM)	HSO ₄ ⁻ (mM)	c _H (mM)
2.0	14.3	0.28	19.7	150	184
2.5	4.51	0.85	19.1	59.7	83.3
3.0	1.43	2.5	17.6	20.5	39.5
4.0	0.14	11.6	8.3	2.16	10.6

the size of this paper, we present below freely selected results obtained for either system. According to them, current peaks (that further are simply symbolized as i_p) increase with the potential sweep rate ν , and linear dependences between i_p and $\sqrt{\nu}$ are observed (Figures 4 and 5). The slopes of these lines, S , increase when the acidity of solutions grows (pH falls) and the acid concentration is increased. The observed phenomena are consistent with the aforesited assumptions concerning the mechanism of electrode reactions. Since the position of current peaks depends on ν (Figures 1 and 2 and the data given below), the cathodic process should be treated as irreversible. Then, the simplified kinetic equation is valid for sufficiently high overvoltages:

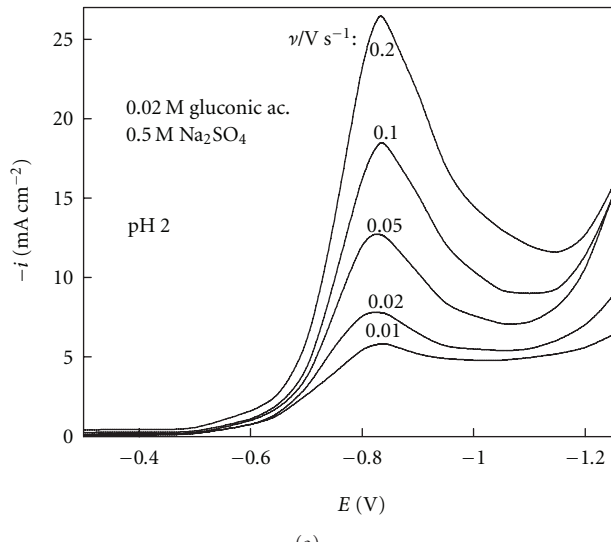
$$\log i_{\text{norm}} = \log i_0 - \frac{\alpha nF}{2.303RT} \eta, \quad (18)$$

where i_0 is an exchange current density, α is a cathodic charge-transfer coefficient, overvoltage $\eta = E - E_{\text{eq}}$, and E_{eq} is equilibrium potential. Normalized current density is defined by the relationship:

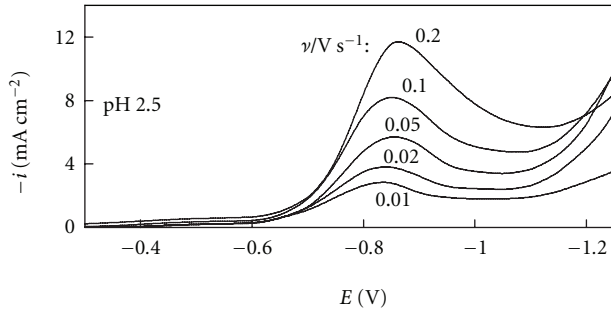
$$i_{\text{norm}} = \frac{|i|}{[H^+]_s/[H^+]_b}, \quad (19)$$

where subscripts s and b denote the surface and bulk concentrations of hydronium ions. Once the latter two quantities are determined, linear normalized Tafel plots (NTP) can be obtained.

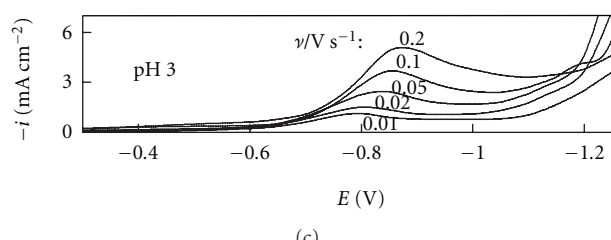
Procedures of data treatment might be as follows. Firstly, special integration of experimental voltammograms, transformed into $i - t$ functions, is performed (see (10)) and Δc_H quantities, as E functions, are obtained (Figure 6). The latter operation needs a certain diffusion coefficient to be used. Traditionally, it can be obtained from RDE data and tested for the condition according to which the limiting Δc_H value (see plateau in Figure 6) cannot exceed the bulk concentration of proton donors.



(a)



(b)



(c)

FIGURE 2: Voltammograms obtained for 0.02 M gluconic acid solutions containing 0.5 M Na_2SO_4 at different pH. Potential sweep rates are indicated at the respective curves.

The second step consists, in determination, of distribution of proton donors at the electrode surface under cathodic polarization conditions. For this purpose, (15)–(17) are used. The surface value of total concentration of proton donors, c_{Hs} , is decreased from the bulk value c_{H} (initial state) to zero (limiting current region) keeping c_{ac} and c_{slf} constant. It should be emphasized that the surface concentration of the electrically active substance (hydronium ions) does not fall to zero in contrast to common redox processes (see (8) or (16)). In the absence of proton donors, a neutral medium is created at the electrode surface ($[\text{H}^+]_s = [\text{OH}^-]_s$), otherwise alkalization occurs. An example of the data obtained is shown in Figure 7.

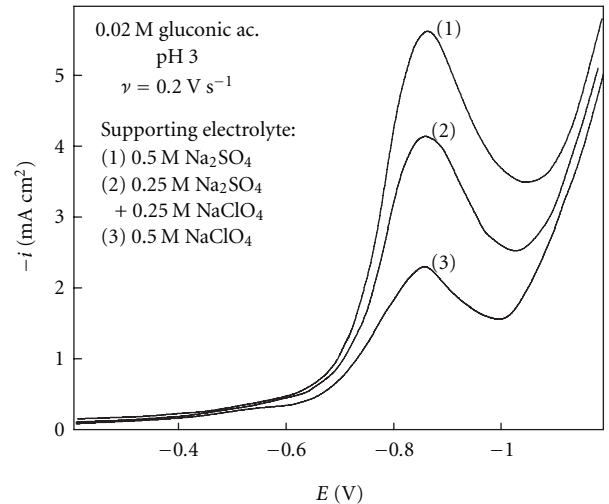


FIGURE 3: Comparison of voltammetric data obtained at $\nu = 0.2 \text{ V s}^{-1}$ for 0.02 M gluconic acid solutions containing different supporting electrolytes as indicated.

Notice that the same data can be presented as E functions, since the interrelation between c_{Hs} and E is easily obtained from Figure 6. This makes it possible to assign the value of $[\text{H}^+]_s$ at any potential of voltammograms and to transform them into normalized Tafel plots. Some results of the procedures performed are shown in Figure 8. The data obtained at different ν are very close and can be approximated by one average NTP. The kinetic parameters of charge-transfer process obtained by (18) are shown in Figure 8 and listed in Table 3. Though the equilibrium potential of $\text{H}^+ | \text{H}_2$ electrode is uncertain in H_2 -free solutions, the exchange of current density, named as “effective”, was determined by extrapolation of NTP to the theoretical quantity defined by the relationship:

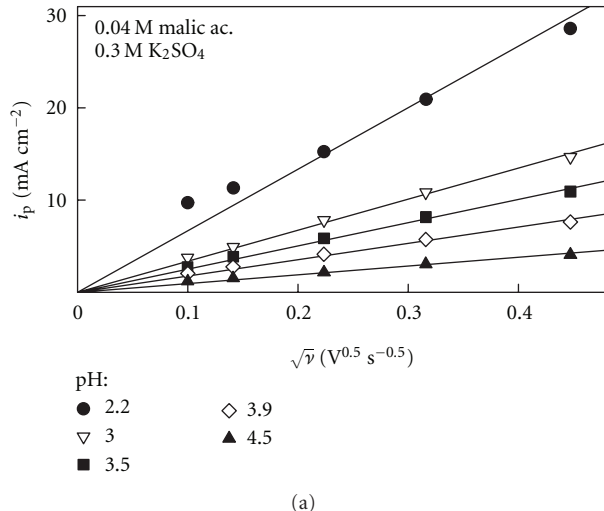
$$E_{\text{eq}} = -\frac{2.303RT}{F} \text{pH.} \quad (20)$$

Low i_0^{eff} values are responsible for a high overvoltage of hydrogen evolution: current densities are low over a wide initial range of potentials. The rise of voltammograms is observed at rather negative potentials ranging up to $\sim -0.6 \text{ V}$.

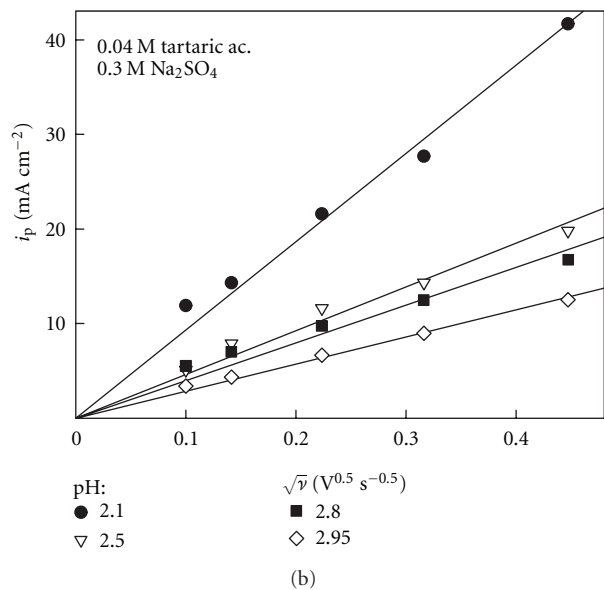
LPS voltammograms possess characteristic maxima, the coordinates of which are convenient to use in the kinetic analysis. At present, relationships for i_p and E_p are available for different mechanisms, including the case of simple redox processes that are controlled by the charge transfer and diffusive mass transport [1–3]. The latter case is somewhat similar to that presented here, but one peculiarity needs to be considered. When a simple redox process occurs, both current density and electrode potential depend on the concentration of the same electroactive species. However, the case under consideration offers the following distinctive feature: the electrode potential is determined by $[\text{H}^+]$, whereas the current density is determined by the total flux of all proton donors and is dependent on c_{H} . Keeping this in mind, we reasoned that the certain modification of common

TABLE 3: Equilibrium characteristics of OA solutions and the kinetic parameters of hydrogen evolution.

OA	c_{ac} (mM)	c_{slf} (M)	pH	c_H (mM)	$10^6 D$ ($\text{cm}^2 \text{s}^{-1}$)	α	i_0^{eff} ($\mu\text{A cm}^{-2}$)	S ($\text{mA cm}^{-2} \text{V}^{-0.5} \text{s}^{0.5}$)
								Equation (21)
Gluconic	40	0.3	2.95	43.3	6.8	0.61	10	26.9
Malic	40	0.3	3.0	76.2	3.1	0.64	8	32.7
Tartaric	40	0.3	2.9	85.0	2.1	0.64	9	30.1
Gluconic	20	0.5	3.0	39.5	1.5	0.60	8	11.4



(a)



(b)

FIGURE 4: Peak current densities versus \sqrt{v} obtained at different pH for 0.04 M malic and tartaric acid solutions.

relationships, with c_H in place of c , is permissible. Then, the current peak expression takes the following form:

$$i_p = 0.282nF\sqrt{\frac{\pi F}{RT}}\alpha\nu D c_H. \quad (21)$$

To check the correctness of this equation, the slopes $S \equiv \partial i_p / \partial \sqrt{v}$ of linear “ $i_p - \sqrt{v}$ ” plots were analyzed with the

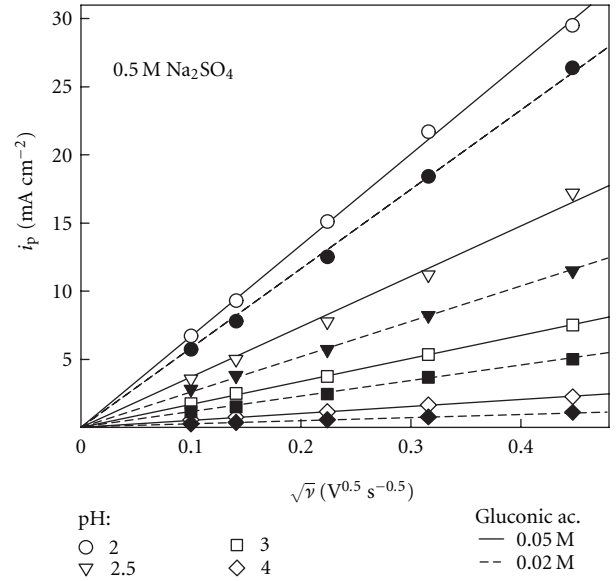
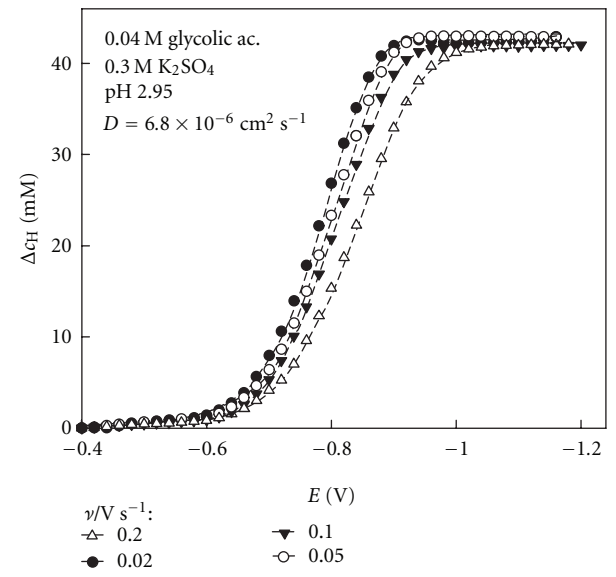
FIGURE 5: Peak current densities versus \sqrt{v} obtained at different pH for 0.02 M (dashed lines) and 0.05 M (solid lines) gluconic acid solutions.

FIGURE 6: Changes in the surface concentration of proton donors calculated by (10) from voltammetric data obtained for 0.04 M glycolic acid solution at different potential sweep rates.

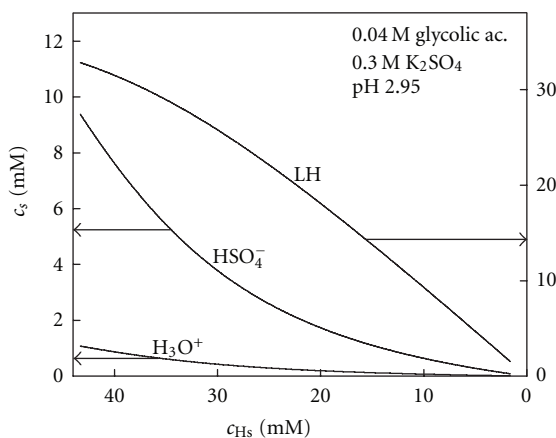


FIGURE 7: Distribution of proton donors at the electrode surface during the electrolysis of 0.04 M glycolic acid solution. Cathodic current density increases from left to right.

values of α , D , and c_H taken from the foregoing analysis. According to the results obtained, experimentally determined slopes are in a good agreement with the quantities that follow from (21) (Table 3).

It can be also seen from these data that the kinetic parameters of the charge-transfer step, obtained for different OA, are quite similar. Then, according to (21), the linear interrelation between S and c_H should be governed only by the equilibrium and mass transport parameters. In this regard, all experimental data, obtained for different OA solutions at various c_{ac} and pH, were generalized and collected in Figure 9. It can be seen that a satisfactory approximation can be performed by single general regression line. The results obtained show that the processes of hydrogen evolution, proceeding in the systems under consideration, possess very similar features, and the same theoretical model is acceptable for their description.

It is of interest to view the data concerning the position of current maxima in the scale of potentials. The model presented above supposes a linear dependence between E_p and $\log \nu$, the slope of which is determined by the relationship:

$$\frac{\partial E_p}{\partial \log \nu} = -\frac{2.303RT}{2\alpha F}. \quad (22)$$

This regularity is consistent with the most experimental data obtained for moderately acidic Cu(II)-free solutions. For instance, the average slope of lines, presented in the lower part of Figure 10, is ca 50 mV/decade; then, the value $\alpha \approx 0.6$ that follows from (22) is in agreement with the experimental data listed in Table 3. However, E_p ceases to depend on ν in more acidic (pH 2.0) 0.02 M gluconic acid solutions, this is indicative of the reversible character of the charge-transfer process. When pH of such solutions was increased, a tendency for a certain increase in $\partial E_p / \partial \log \nu$ magnitudes was observed, but this was not the case for more concentrated (0.05 M) solutions.

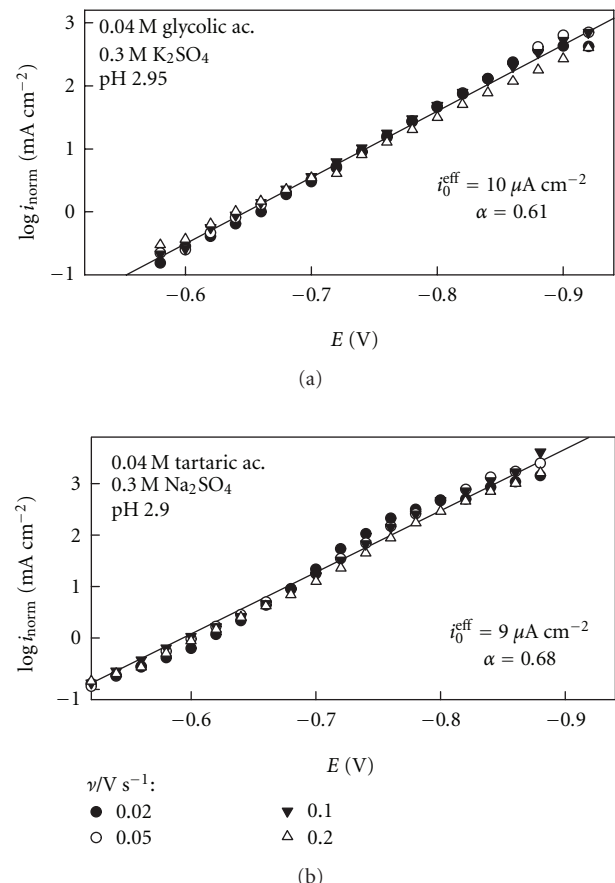


FIGURE 8: Normalized Tafel plots obtained at different potential sweep rates for 0.04 M glycolic (a) and tartaric (b) acid solutions. Indicated kinetic parameters are calculated from general regression lines.

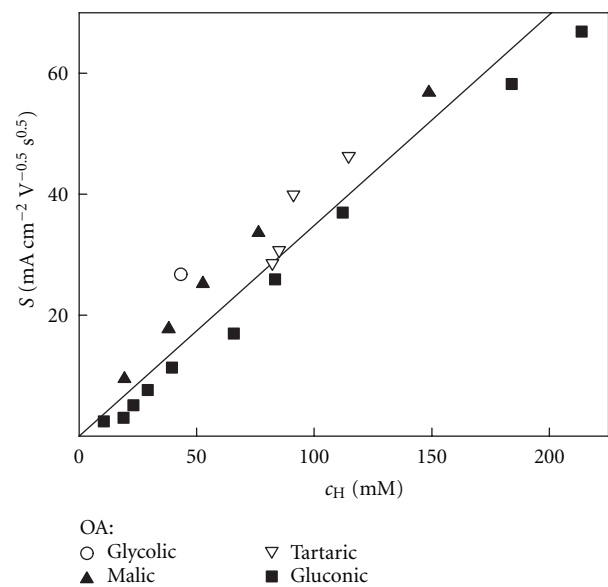


FIGURE 9: Experimental slopes $S \equiv \partial i_{p2} / \partial \sqrt{\nu}$ versus total concentration of proton donors. Summation of the data obtained for different solutions at $2.5 < \text{pH} < 4.0$.

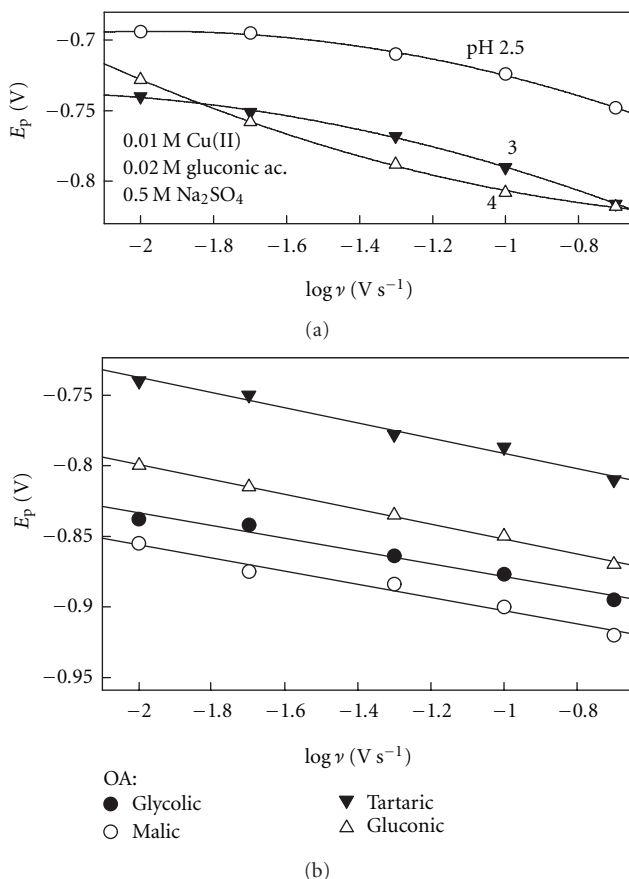


FIGURE 10: Dependencies of peak potentials on potential sweep rate presented in semilogarithmic coordinates. The data are obtained for 0.02 M gluconic acid solutions containing Cu(II) (a) and for Cu(II)-free solutions (b), the composition of which is given in the Table 3.

Nonlinear E_p dependences on $\log \nu$ are observed in the case of Cu(II)-containing solutions (Figure 10(a)). It is necessary to point out that the situation at the electrode surface is not exactly the same as that in identical Cu(II)-free solutions containing the same c_{ac} and pH. As what was stated above, hydrogen evolution starts in the region of limiting current, where the surface concentration of Cu(II) approaches zero but c_{ac} and c_H remain unchanged. However, a certain amount of OA anions is released from the reduced Cu(II)-OA complexes. This results in the shift of chemical equilibria and in the relevant increase in surface pH. Again, simultaneous deposition of copper can also modify the properties of original coatings that were prepared as working electrodes (see Section 2).

The kinetic parameters listed in Table 3 have been determined using not only experimental, but also the literature data. It is common knowledge that stability constants expressed in concentration terms depend on the ionic strength of solutions and on the nature of supporting electrolyte. Unfortunately, data given in different handbooks concern, as a rule, perchlorate or nitrate media and the certain problems arise when fitting such data for sulphate media. Therefore, the reliability of the parameters established here also depends on the reliability of the data selected from

the literature. Nevertheless, it can be stated that the kinetic parameters of hydrogen evolution, occurring on the same copper substrate, are very similar in the case of all the systems under investigation. Organic acids seem to be of minor importance for the charge-transfer process and act in general as sufficiently labile proton donors.

5. Conclusions

The CE mechanism of hydrogen evolution occurring in organic acids (OAs) solutions was analyzed invoking the 2nd Fick's law equations supplemented by terms that account for chemical interactions between diffusing particles. OA are considered as components that are capable of releasing hydrated protons (hydronium anions) taking part in the charge-transfer step. Simple equations containing no kinetic terms were obtained for total concentration of proton donors and acceptors, c_H . When the dissociation of OA is sufficiently fast, the surface concentrations of species can be obtained from the material balance equations involving the stability constants of proton donors.

Linear potential sweep (LPS) voltammetry was applied to study the kinetics of hydrogen evolution in the solutions containing glycolic, malic, tartaric, and gluconic acids. Current peaks observed on LPS voltammograms are in a linear dependence on $\sqrt{\nu}$ (ν is the potential sweep rate). They obey well-known relationships obtained for simple redox processes, provided that the concentration of oxidant is treated as c_H .

Determination of surface concentrations as current density functions makes it possible to transform LPS voltammograms into linear Tafel plots normalized with respect to the surface concentration of hydronium ions. Similar kinetic parameters ($\alpha \approx 0.62$ and $i_0 \approx 10 \mu\text{A cm}^{-2}$) obtained at pH 3 for all OA solutions indicate that the nature of OA has no noticeable influence on the charge-transfer process.

References

- [1] D. D. Macdonald, *Transient Techniques in Electrochemistry*, Plenum Press, New York, NY, USA, 1977.
- [2] A. J. Bard and L. R. Faulkner, *Electrochemical Methods: Fundamentals Applications*, John Wiley & Sons, New York, NY, USA, 2nd edition, 2001.
- [3] Z. Galus, *Fundamentals of Electrochemical Analysis*, John Wiley & Sons, New York, NY, USA, 2nd edition, 1994.
- [4] A. Survila, *Electrode Processes in Systems of Labile Metal Complexes*, Mokslas, Vilnius, Lithuania, 1989.
- [5] V. Kačena and L. Matoušek, "Proteins and aminoacids. XVI-II. The effect of electrolytes on proteins," *Collection of Czechoslovak Chemical Communications*, vol. 18, p. 294, 1953.
- [6] F. Hilbert, *Die elektrolytische abscheidung von eisen und wasserstoff*, Habilitations, Schrift Universität Graz, 1969.
- [7] Y. Miyoshi and W. J. Lorenz, "Zum Protonentransport in schwefelsauren Lösungen," *Berichte der Bunsengesellschaft für Physikalische Chemie*, vol. 74, no. 4, pp. 412–416, 1970.
- [8] L. G. Sillen and A. E. Martel, *Stability Constants Metal-Ion Complexes*, no. 17, Chemical Society, London, UK, 1964.
- [9] L. G. Sillen and A. E. Martel, *Stability Constants Metal-Ion Complexes*, no. 25, Chemical Society, London, UK, 1971.

- [10] E. P. Serjeant and B. Dembsey, *Ionisation Constants of Organic Acids in Aqueous Solutions*, Pergamon Press, Oxford, UK, 1979.
- [11] "Gluconic acid and derivatives," SIDS Initial Assessment Report for SIAM 18, SIAM, Paris, France, 2004.
- [12] A. Survila, A. Survilienė, S. Kanapeckaitė et al., "Oxide layers developed on copper solutions containing electrodes in Cu(II) ligands," *Journal of Electroanalytical Chemistry*, vol. 582, no. 1-2, pp. 221–229, 2005.
- [13] A. Survila, P. V. Stasiukaitis, and S. Kanapeckaitė, "Concept of Nernst-type diffusion layer in linear potential sweep voltammetry," *Chemija*, vol. 2, pp. 138–142, 1998.
- [14] J. N. Butler, *Ionic Equilibrium (A Mathematical Approach)*, Addison-Wesley, Reading, Mass, USA, 1964.
- [15] C. W. Davies, *Ion Association*, Butterworths, London UK, 1962.

Research Article

Electrochromism and Swelling of Polypyrrole Membranes: An Electrochemical and Ellipsometric Study

J. O. Zerbino,¹ M. G. Sustersic,² C. Falivene,² N. Avaca,² and A. Maltz³

¹ Instituto de Fisicoquímica, INIFTA, CIC, Suc. 4, C.C. 16, 1900 La Plata, Argentina

² Facultad de Ingeniería, FICES, UNSL, 25 de Mayo 384 C.P. 5730. Villa Mercedes, San Luis, Argentina

³ Departamento de Matemática, Facultad de Ciencias Exactas, UNLP, Calle 115 y 50, 1900 La Plata, Argentina

Correspondence should be addressed to J. O. Zerbino, jzerbino@inifta.unlp.edu.ar

Received 18 March 2011; Accepted 16 May 2011

Academic Editor: Bengi Uslu

Copyright © 2011 J. O. Zerbino et al. This is an open access article distributed under the Creative Commons Attribution License, which permits unrestricted use, distribution, and reproduction in any medium, provided the original work is properly cited.

The growth of polypyrrole (Ppy) layers on gold electrodes in nearly neutral pH solutions is analysed using “in situ” voltammetric and ellipsometric techniques. Different film structures are obtained depending on the potentiodynamic programme and the composition of the electrolyte. More compact dodecylsulphate-(DS) doped Ppy layers were grown at 1.2 V versus RHE than those obtained by applying a higher potential. The more compact layers correspond to the growth of an oxidised Ppy/DS layer that shows low pseudo capacity behaviour. After dipping, the doped Ppy/DS film in KCl solution—significant variations in optical indices and thickness are detected as a function of the applied potential. Higher electrochromism as well as decrease in film thickness after cathodisation is achieved. The optical indices and the thickness of the Ppy layer formed under different applied potential/time programmes are estimated.

1. Introduction

Conducting polymers and particularly polypyrrole, Ppy, is extensively used in sensors, oxygen sensing, microelectronic mechanical systems MEMS, metal-insulator-semiconductor field effect transistors, drug release, actuators, water treatment, protective coatings against corrosion, and analytical displays [1–13].

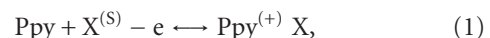
Polypyrrole (Ppy) shows high permeability and selectivity for the detection of catecholamines in different electrolytes owing to anionic species exclusion by the interaction with negative charges into the film [14–18].

The kinetics of growth and the final structure of the Ppy layers depend on the potential programme, the anodic limit, and on the cycling time [19–22]. On the other hand, the presence of different ions in the electrolyte modifies the layer growth rate, the voltametric response, and the interfacial capacity. These effects are related to variations in pyrrole absorption, concentration of radicals, structure of the oligomers initially formed during anodisation, and partial water exchange taking place together with ion’s uptake processes into the membrane [23–25].

Oxidation of Ppy yields positive fixed charges on the polymer networks. Commonly prepared Ppy layers exhibit anion exchange during the oxidation cycle. The Ppy matrix in the reduced state is electroneutral and a poor ionic and electronic conductor.

The properties of these membranes can be modified by doping the Ppy with large and bulky shaped anions such as dodecylsulphate, dodecylsulphonate, paratoluensulphonate, and so forth. This has been achieved by electrooxidation in solutions containing the large anions, which are thereby incorporated into the film as fixed charges. In electroanalysis, these membranes offer good selectivity and high stability during prolonged switching conditions.

Cation exchange takes place on these PPY modified layers due to the high immobility of these ions through the PPY chain [26, 27].



the superscript “S” indicates that the species is in the electrolyte.

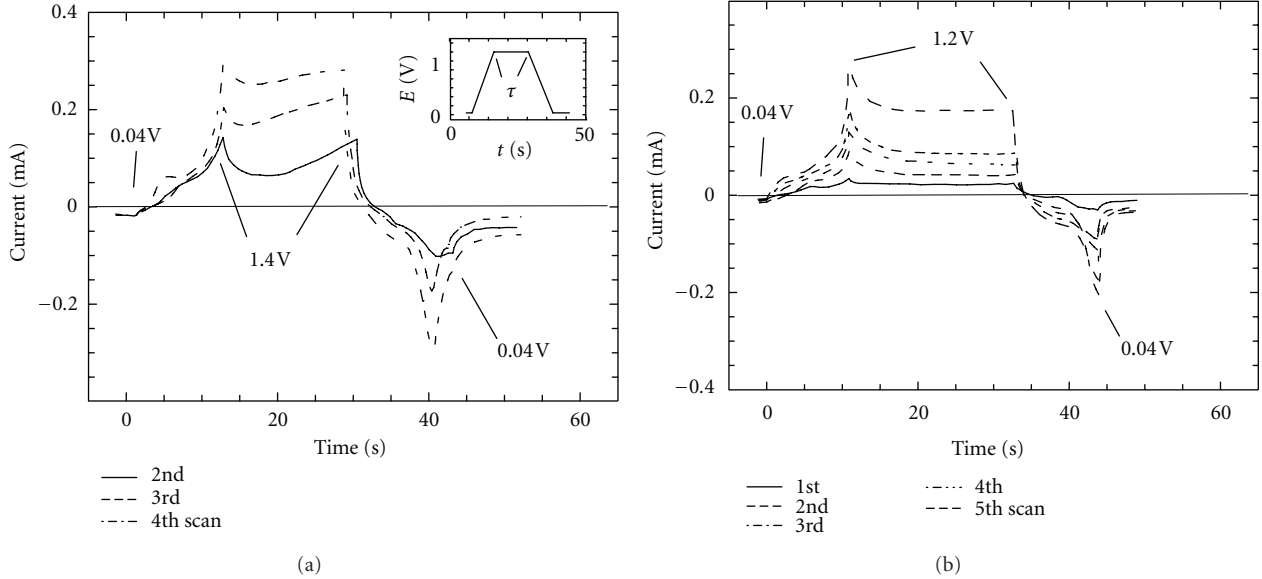


FIGURE 1: Potential/time programmes used in polypyrrole layer growth. Potential sweep in 0.1 M SDS, 0.1 M Py solution from $E_c = 0.04\text{ V}$ to E_a followed by a holding time τ at E_a and consecutive cathodic scan to E_c . Scan rate 100 mV/s. The different curves show the evolution of current/potential/time profiles for successive cycling using either (a) $E_a = 1.4\text{ V}$ with $\tau = 15\text{ s}$ or (b) $E_a = 1.2\text{ V}$ with $\tau = 20\text{ s}$.

Ellipsometry can be applied “in situ” to characterise the layer structure seeing that the optical signal is very sensitive to the modifications produced by the polarisation of the electrode. Recent work has investigated the characteristics of electrodeposited Ppy on gold in buffer phosphate solution [15].

In this work, cyclic voltammetry and ellipsometry were used to investigate the effect of the potential on the growth of doped Ppy/DS layers.

2. Experimental

Experimental conditions were similar to those described in previous work [28, 29]. The gold electrode was made by axially fitting a polycrystalline gold plaque (99.99% purity, 1.5 mm thick) into a Teflon sheath. It was polished to a mirror finish with 1.0, 0.3 and 0.05 μm alumina powders. The electrode, horizontally placed in the cell, had a total area of 0.55 cm^2 and an area sampled by ellipsometry of about 2 mm^2 . All experiments were performed under nitrogen bubbling. The potentials were referred to the reversible hydrogen electrode (RHE) in the same solution.

The freshly polished metal was pretreated by scanning five cycles in the potential region $0.1\text{ V} < E < 1.70\text{ V}$.

For the ellipsometric measurements, the light wavelength was selected by interposing adequate filters in the range $405 < \lambda < 580\text{ nm}$. The on manual ellipsometer, Rudolph Research Fairfield, NJ, USA, type 43702-200E, Serial No 4210, takes about 1 min to measure the Δ/Ψ parameters. The electrode was illuminated through optically polished glass lateral windows 20 mm in diameter using an incident angle of 69° . The optical indices of the substrate were obtained at open circuit in the aqueous electrolyte, from the ellipsometric parameters of the polished gold electrode. The resulting

values were in good agreement with previously reported data [15, 28, 29].

The Ppy films were anodically grown in the cell containing 0.1 M Pyrrole, Py, Sigma Aldrich (SAFC: W338605), 0.1 M sodium dodecylsulphate, SDS, Riedel-de Haen, and aqueous solution. After polymerisation, the electrolyte of the cell was replaced by a new SDS solution free of pyrrole.

The changes in the ellipsometric parameters Δ and Ψ after successive deposition cycles of Ppy were measured using the following potential/time programme: the potential was scanned at 100 mV/s between the cathodic potential limit $E_c = 0.1\text{ V}$ and the anodic limit E_a followed by a holding time, τ , at E_a . Next, a cathodic scan at 100 mV/s was applied between E_a and E_c , and then successively measured values of Δ and Ψ were taken at E_c with intervals of 2 min.

3. Calculations

The simplest model assumes a single homogeneous film. The real part of the refraction index of the film, n , the imaginary part of the refraction index or absorption coefficient, k , and the thickness, d , are calculated using the gradient technique [28, 29].

In the case of inhomogeneous layers, the high number of parameters makes the determination of the structure very cumbersome. However, the single homogeneous film model is a good first approximation in the description of the interface, and these indices correspond to effective optical indices for the composite fibre/occluded electrolyte layer [28, 29]. In the case of composite materials, the effective medium theory using either Maxwell Garnett or Bruggeman formalisms relates the optical constant of the polymeric fibre phase and that of the electrolyte with the volume fraction of

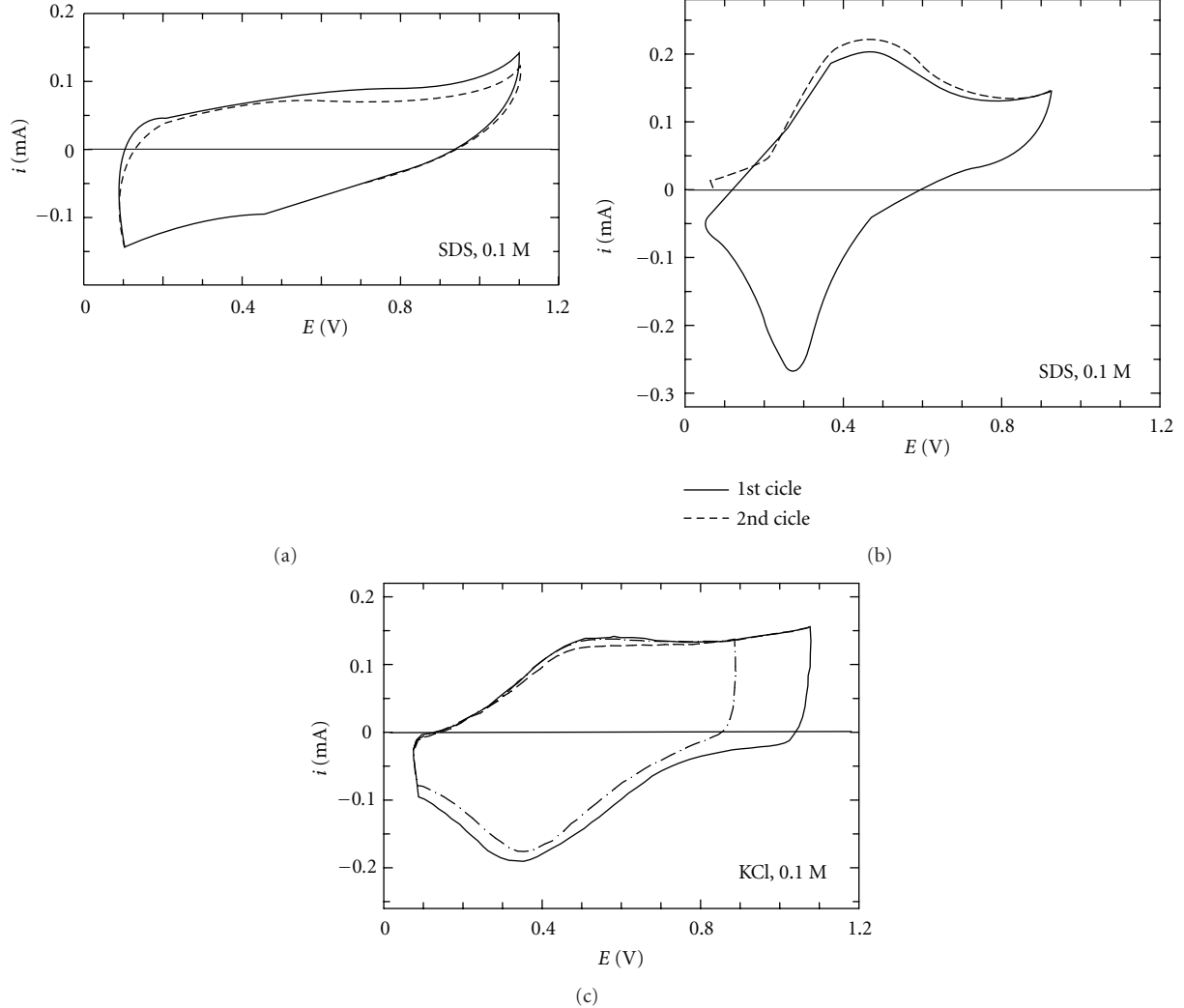


FIGURE 2: Current/potential voltammograms obtained scanning at 100 mV/s between $E_c = 0.04$ V and either $E_a = 0.9$ V or $E_a = 1.1$ V. Pseudocapacitive response observed after five anodic cycles using (a) $E_a = 1.2$ V with $\tau = 20$ s, and (b) $E_a = 1.4$ V with $\tau = 15$ s. (a) and (b) in SDS solution free of Py, (c) the same electrode shown in Figure 2(a) and after immersion in 0.1 M KCl.

the components providing the effective optical constants for the composite polymer/electrolyte.

The fitting procedure minimises the function G :

$$G = \sum \left(\Delta_{ij}^{\text{ex}} - \Delta_{ij}^{\text{the}} \right)^2 + \left(\Psi_{ij}^{\text{ex}} - \Psi_{ij}^{\text{the}} \right)^2, \quad (3)$$

where the subindex i corresponds to the optical data measured at different λ_j , and the sub index j corresponds to different cycling deposits or thicknesses d_i .

In the simplest process, the layer grows in thickness with constant compactness and composition bearing stable n and k values. In many cases, the fitting of the n , k , and d values for a sequential set of thicknesses allows to evaluate variations in the compactness of the film as a function of the distance to the electrode. In this procedure, it is very important to use accurate initial values in the fitting, which can usually be found fitting the complete set of thicknesses. Another possibility is to increase the amount of optical data for a given layer measuring the Δ and Ψ data at different λ_j . This allows

increasing the amount of experimental data to find univocal values of thicknesses and optical constants.

The optimisation method converges after m iterations, to theoretical Δ_{ij}^{the} , Ψ_{ij}^{the} values. The convergence is fulfilled after m iterations when (a) the Euclidean norm of the arrangement $p_m - p_{m+1}$ tends to 0, (b) $G(p_m) > G(p_{m+1}) > G(p_{m+2})$, and (c) $\partial G_m / \partial p$ tends to 0.

4. Results and Discussion

Several electrochemical perturbations are customarily employed for the deposition process of Ppy layers. Potentiodynamic polymerisation (cyclic voltammetry) probably favours the formation of disordered chains [30] just because the continuous change between its neutral (insulating) and its doped (conducting) state usually involves compaction and opening of the polymeric network. On the other hand, galvanostatic pulses applied during relatively long periods of polarisation produce thick and porous deposits due to the

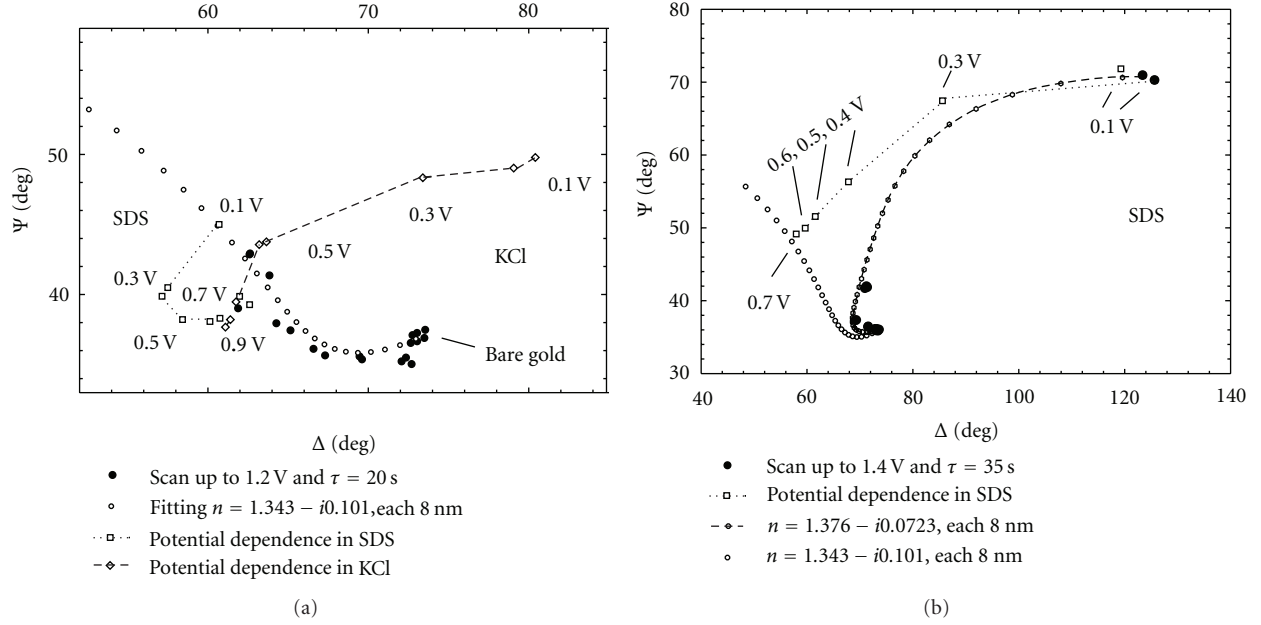


FIGURE 3: (•) Evolution of the experimental parameters Δ and Ψ after successive cycles in the condition of Figure 1, namely, (a) $E_a = 1.2$ V and $\tau = 20$ s, (b) $E_a = 1.4$ V and $\tau = 15$ s. The figures correspond to number of cycles. Evolution of the thicker film changing the potentials in both (□): SDS and (◊): after immersion in KCl. (○): Theoretical values corresponding to a layer of optical index n and increasing the thickness, d , every 8 nm. The film obtained at $E_a = 1.2$ V fits $n = 1.343 - i0.101$ and that obtained at $E_a = 1.4$ V fits $n = 1.3476 - i0.0723$. Owing of the change in the Δ/Ψ plot scale, both fitted curves are plotted in (b) for comparison.

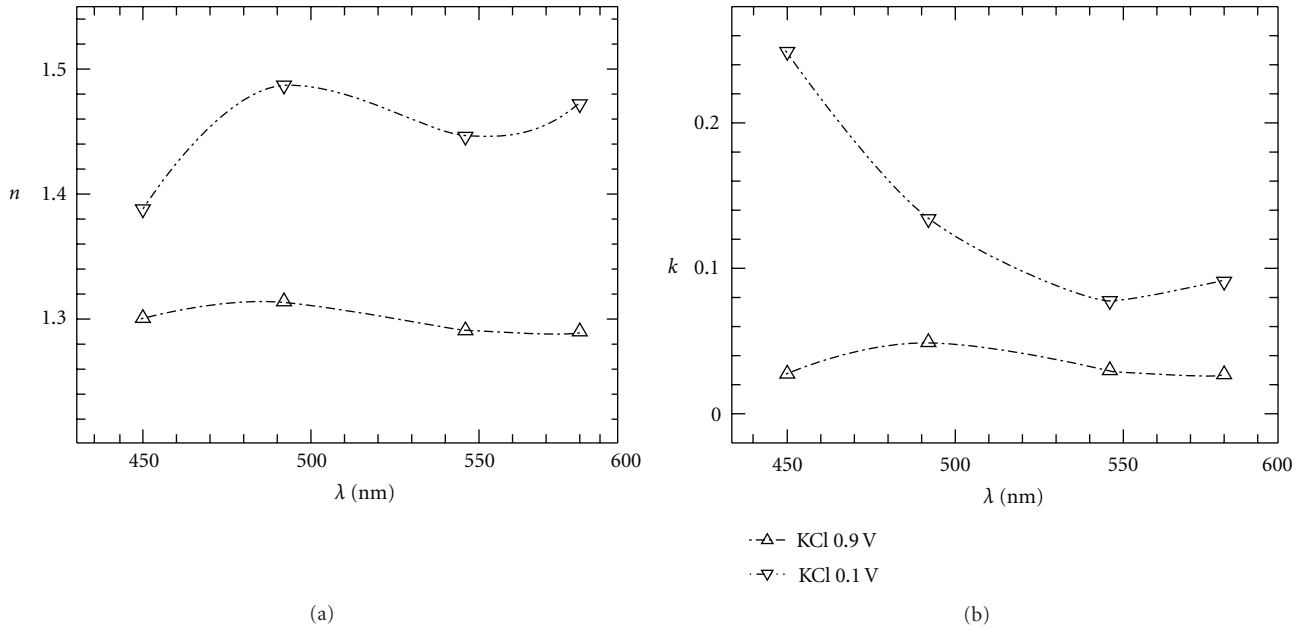


FIGURE 4: Calculated refractive index n and absorption index k for illuminating light beam in the region $450 < \lambda < 580$, for the film obtained after five cycles with $E_a = 1.2$ V and $\tau = 20$ s after immersion in KCl.

deflection of the monomer concentration near the vicinity of the electrode.

Figure 1 shows the current potential profile obtained after applying successive anodic cycles at 1.2 V and 1.4 V in 0.1 M Pyrrole, 0.1 M SDS solution. For $E_a = 1.2$ V, a continuous decrease on the current during the anodising time τ is

observed. Moreover, the anodic scans show a peak at 0.45 V that increases with the successive cycles. This evidences the electrooxidation of the Ppy deposited in the previous cycles, and the increasing cathodic peak currents highlights its reduction. Figure 1(b) shows similar current/time profiles. However, a current increase occurs at $E_a = 1.4$ V after about

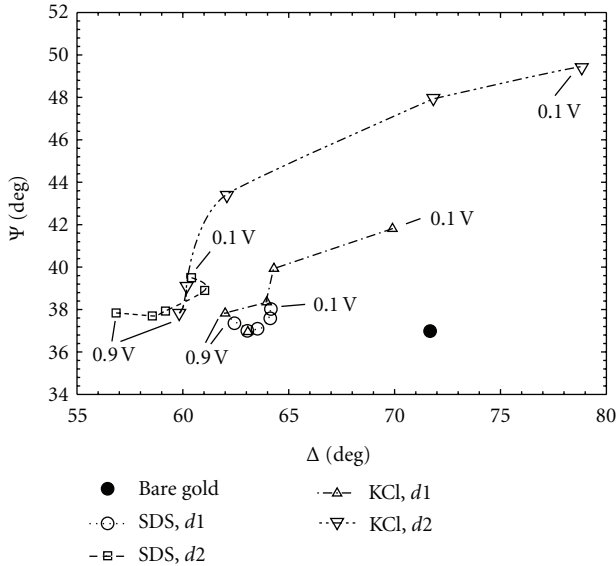


FIGURE 5: Evolution of the experimental parameters Δ and Ψ as a function of the applied potential for Ppy film grown in SDS, after applying both four or five successive cycles and using $E_a = 1.2$ V, $\tau = 20$ s. (○) in SDS and (□) after immersion in KCl.

$\tau = 5$ s. This effect probably stems from the anodic oxidation of the Py dissolved in the SDS micelles, which can solvate part of the reaction intermediates (free radicals) as well as the resulting Ppy oligomers. DS has a charged, polar end and a hydrophobic end. The charged end facing out into the solution can be maintained during polymerisation, even though the negative group is being incorporated into the polymer as a counter ion. Alternatively, the polymer, which is deposited subsequently, could also develop polar surface properties [31].

Figures 2(a) and 2(b) shows voltammetric scans at 100 mV/s obtained from Ppy electrodeposited either at 1.2 or at 1.4 V. The plot of Figure 2(a) shows a small anodic peak at 0.68 V and another cathodic one at 0.48 V. On the other side, Figure 2(b) shows very well-defined peaks at 0.45 V and 0.38 V. The cathodic charge that involves in the cathodic scan is $Q_{2a} = 0.58$ mC and $Q_{2b} = 0.70$ mC. Nevertheless, the current jump at potentials near the sweep inversion shows that the double layer capacity for the film grown at 1.2 V is higher than that grown at 1.4 V, Figures 2(a) and 2(b). After immersion in 0.1 M KCl solution, the film grown in the experiment of Figure 2(a) has a remarkably high pseudocapacitive charge ($Q_{2c} = 0.73$ mC).

Voltammograms with a relatively high double layer capacity have been previously reported in the case of Ppy films doped with PSS [32]. Three forms of Ppy has been reported, Ppy(I) the regular polymer, contains longer chains, (with length up to 64 units), Ppy(II) containing short oligo pyrrole units (with length between 12 and 16 units), while a cross-linked material referred to as Py-III is generated at high potentials. The oxidation peak at more negative potentials may indicate the presence of Ppy(II) [30, 33]. However, other factors may influence the polymerisation processes and the redox capacity, such as different solvents,

additives, and electrolytes. The concentration of SDS trapped in the network may regulate the redox properties of the layer. In the case of Ppy/SDS films subjected to a very thin polystyrene coverage, used to increase the hydrophobicity of the polymer/electrolyte interface, the voltammogram shows a cathodic shift of about 0.5 V of the redox couple, related to the Ppy layer free of SDS, for the electrode switching in 0.1 M KCl [34].

Figure 3 shows the evolution of the ellipsometric parameters Δ/Ψ during the layer growth. After each potential cycle, three successive measures at 0.1 V are taken with intervals of 2 min. Figure 3(a) shows for both the 3rd and the 4th cycle a small increase in the Δ values during the holding time at 0.1 V. After 2 min at 0.1 V, the data of the third measure practically reproduces the second one. In the case of the 5th cycle, the opposite tendency occurs and the Δ/Ψ values show some instability. According to the calculation procedure mentioned above, the whole set of experimental Δ/Ψ values corresponding to the five cycles were fitted for common n and k parameters and different d . For the obtained fitted n and k values, the theoretical Δ/Ψ curve was plotted. A maximum thickness d of about 122 nm, and $n = 1.343 - i0.101$ was obtained. Using the same procedure, the fitting corresponding to the deposit obtained at 1.4 V values of $n = 1.376 - i0.0723$ and a maximum $d = 254$ nm was obtained.

Likewise, Figure 3(b) shows the potential dependence of the experimental Δ/Ψ values in 0.1 M SDS solution, free of pyrrole, corresponding to the film grown at 1.4 V.

In the experiment of the Figure 3(a), the Δ/Ψ measurements in SDS shows low dependence with the potential and some instability during the holding time and the successive cycles. Otherwise, a very large and reproducible change in Δ/Ψ occurs, after dipping in KCl.

On the other side, Figure 3(b) shows that, for the film grown at 1.4 V after oxidation at 0.7 V, the Δ/Ψ values fit the theoretical curve $n = 1.343 - i0.101$. Then, a thickness of 164 nm is obtained. This theoretical curve is shown in Figure 3(a), and it is transferred to the plot scale of Figure 3(b) for comparison.

Figure 4 shows the calculated optical indices at 0.1 and 0.9 V for the film grown at 1.2 V and dipped in KCl solution. In this fitting, the optical data taken at 450, 492, 546, and 580 nm are fitted independently at both potentials and thickness d_{ox} and d_{red} corresponding to the oxidised and the reduced state are obtained. This way, values of $d_{\text{ox}} = 165$ and $d_{\text{red}} = 120$ nm, which show a swelling of the film after reduction, are obtained. The k increase observed for $\lambda = 400$ nm agrees with reported spectroelectrochemical measurements [22]. The optical indices of the film in SDS solution corresponding to the anodic and the cathodic potential limit are very similar to that corresponding to the oxidised state in KCl [35].

Moreover, the Ppy/SDS electrode recently dipped in KCl solution adjusts spontaneously to an open circuit potential of about 0.88 V. These results show that even polarised at 0.1 V the Ppy/SDS layer grown at 1.2 V remains highly oxidized, and the cycling in Figure 2(a) corresponds to a switching between highly oxidized states with a scarce Ppy network

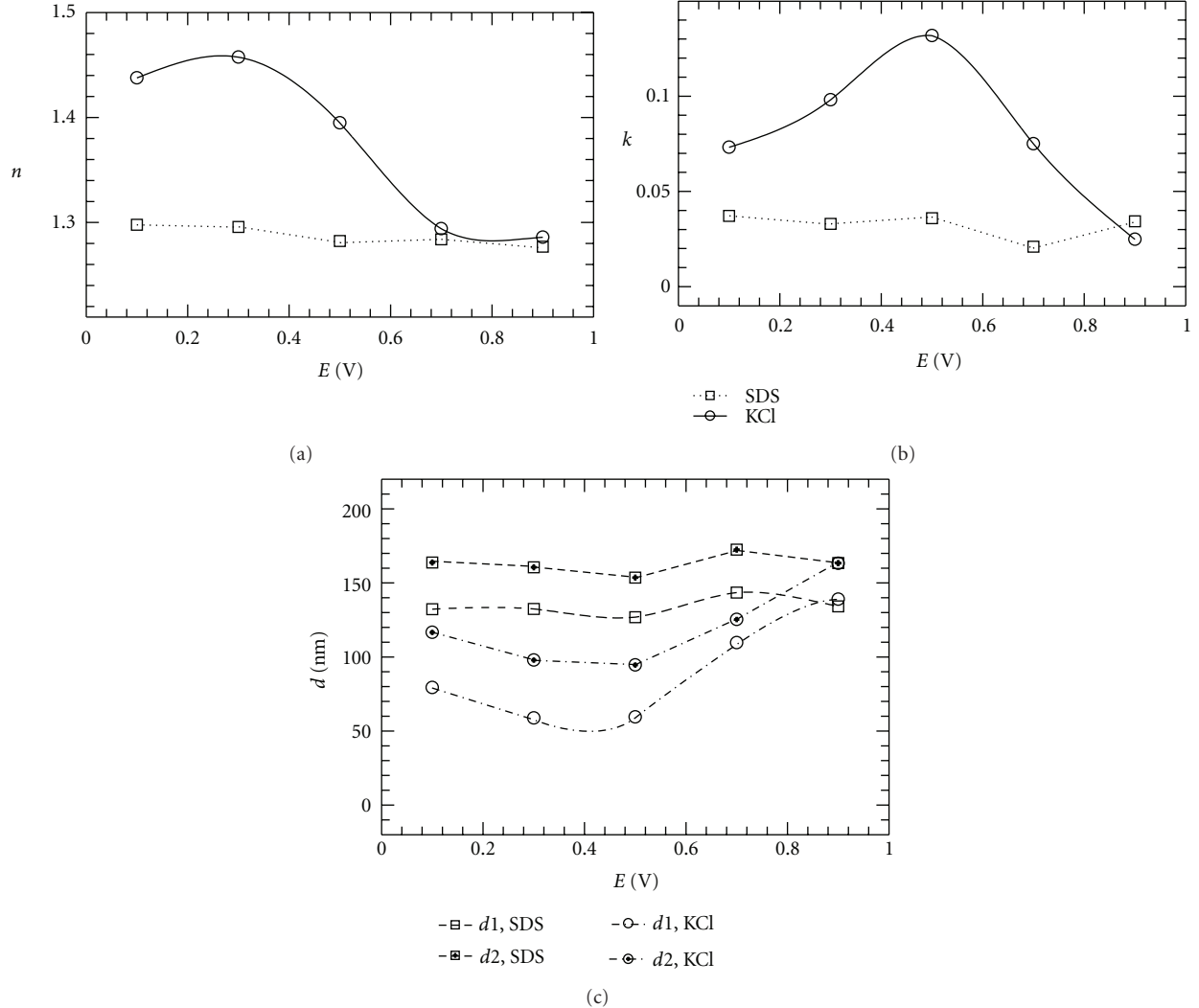


FIGURE 6: Calculated thickness, d , and optical indices, n , k , for the Ppy layers already described in Figure 5 and for an illuminating light beam of $\lambda = 546$ nm. (○) in SDS and (□) after immersion in KCl.

reduction. The higher values of n at 0.1 V correspond to the shrinking of the layer with exchange of cations and expulsion of solvent.

The Δ/Ψ values that correspond to two Ppy/SDS-independent experiments obtained at 1.2 V applying four and five cycles are plotted in Figure 5. The optical data in the SDS solution free of pyrrole show a potential evolution, in the region of $0.1 < E < 0.9$ V stepping every 0.2 V. They display a small clockwise arch. After changing the electrolyte with new KCl solution, the switching shows a counterclockwise and higher potential dependence. Assuming common optical indices at each fixed potential for both deposited films, univocal values of n , k , and d are obtained. The n , k , and d fitted values are plotted as a function of the potential in Figure 6. In the case of SDS solution, very small n , k , and d dependencies on E are noticed. However, a shrinking in the thickness results during the progressive cathodisation in KCl solution, which is the maximum for about 0.4 V. The k versus E plot shows a maximum value in k for about 0.5 V.

The shrinking of the membrane may partially increase the values of the optical constants. For a pure substance, n and k are independent of the thickness but Maxwell Garnett and Bruggeman predict an increase of the effective n and k indices for a composite due to the extraction of water [36]. However, the increase in k is so significant that it shows a structural change in the Ppy phase.

The chain structure, compactness of both the bulk and the surface of the composite Ppy/electrolyte, as well as the concentration and mobility of counter anions become critical factors in the behaviour of the membrane. Bipolarons are equivalent to di ionic states of a system generated after oxidation of the neutral state initiated through the polaron state monocation. In the oxidation process, the structural relaxation causes a local distortion of the chain in the vicinity of the charge, and the twisted benzoid-like network turns into a quinoid-like structure. The extraction of the second electron produces the bipolaron instead of two polarons, to which structural relaxations larger than those corresponding

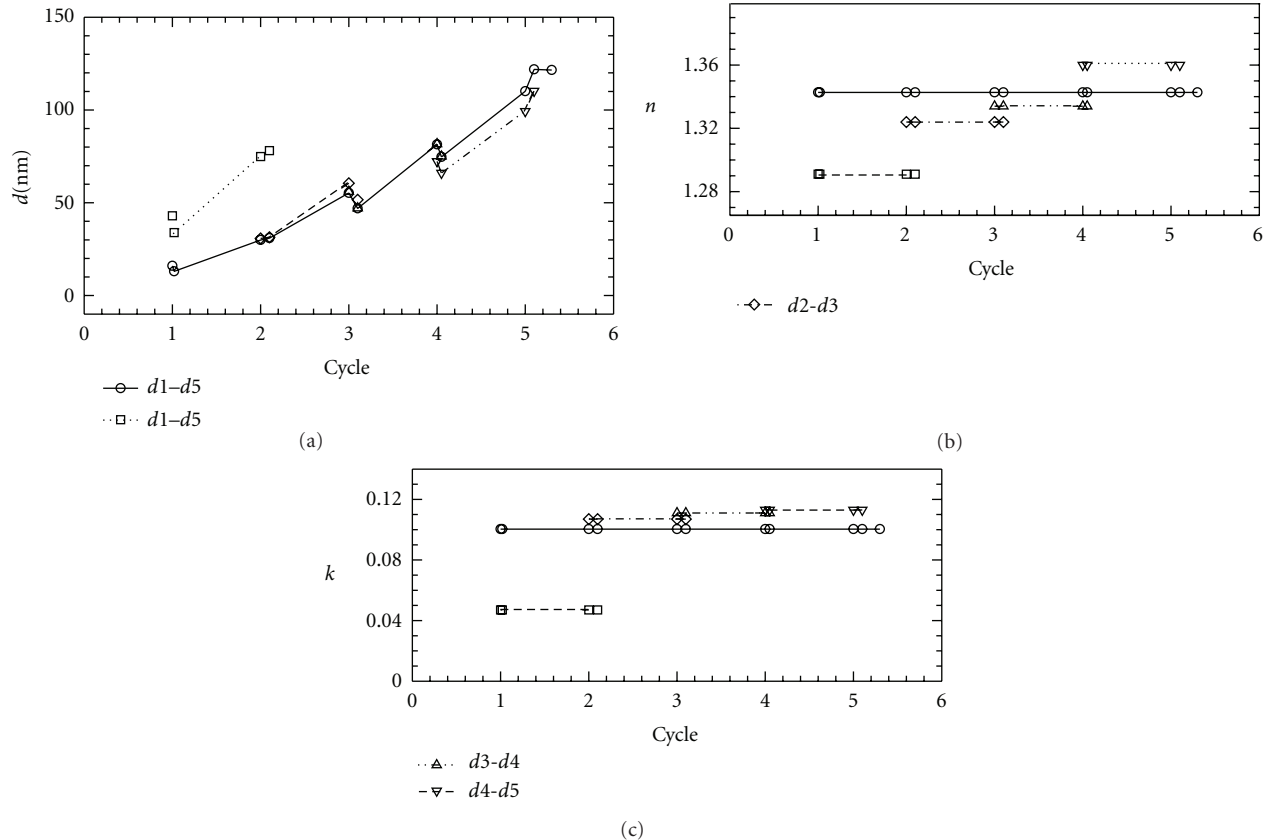


FIGURE 7: Calculated thickness, d , and optical indices, n , k , for the Ppy layers already described in Figure 3(a), $E_a = 1.2$ V, $\tau = 20$ s. SDS solution, $\lambda = 546$ nm. The different values n and k correspond to the resulting fitted values for different set of thicknesses.

to the polarons occur. Several $\pi-\pi^*$ transitions and polarons band are reported for different Ppy/doped layers [37, 38]. A band at 584 nm may be surmised as an antipolaron to a bipolaron band transition.

The experiment in Figure 5 shows a probable maximum polaron effect at the equilibrium potential E_{eq} corresponding to 50% oxidation of the chains. On the other side, these kinds of experiments show that E_{eq} which is associated with the voltametric peak potentials and the amenable maximal reduction state depends on the structure, compactness, and electronic conductivity of the network and the characteristic of the counterions than spreads through the membrane.

Moreover during Ppy reduction, the penetration of the cation into the membrane may flatten the smaller indentations [39]. Furthermore, overoxidation produces a decrease in conductance and probably in the concentration of the polaron after effect of the disruption of the conjugated doubled bond structure [40].

Figures 7 and 8 correspond to the plot of the fitted n , k , and d values taking either the complete or smaller sets of successive thicknesses. Common values for n and k are assumed as a boundary condition. A linear increase of d is observed starting from the second cycle together with a small increase in the values of n and k . The initial thickness of the oligomers attached to the surface in the first and the second cycle can be estimated of about 40 nm. After an initial deposit of 40 nm, the second cycle produces the compactness of the

first deposited layer with practically no change in thickness. In these calculations, n and k are considered as independent parameters. However they become related parameters using a more exhaustive analysis of Kramers-Kronig. In this case the optical data should be measured in a wide range of wavelengths. On the other side, the Maxwell Garnett and Bruggeman formalisms predict that both n and k must increase for a more compacted composite material, in the conditions of decreasing the volume fraction corresponding to the electrolyte [36]. In Figure 7, a small decrease in thickness during the successive optical measures taken at 0.1 V with intervals of 1 min that corresponds to the aging or the so-called first cycle or memory effect in the Ppy layer also can be noticed after each cycle.

In the case of the experiment using $E_a = 1.4$ V, Figure 8, the scheme corresponding to a film increasing in compactness at constant thickness prevails up to the third cycle with a thickness of about 100 nm. After the third cycle, the layer starts to thicken with practically fixed n and k values.

Figure 9 shows the Δ/Ψ evolution during the first deposition cycles. In the graphics, theoretical curves corresponding to the film increasing in thickness each 8 nm with constant n and k values, namely, $n = 1.343 - i0.100$, $1.291 - i0.047$, and $1.376 - i0.0723$, corresponding of the fitted values obtained taking the complete set of cycles are also plotted. Likewise, the theoretical Δ/Ψ corresponding to films of either 130, 100, 70, or 40 nm whose optical indices decrease progressively

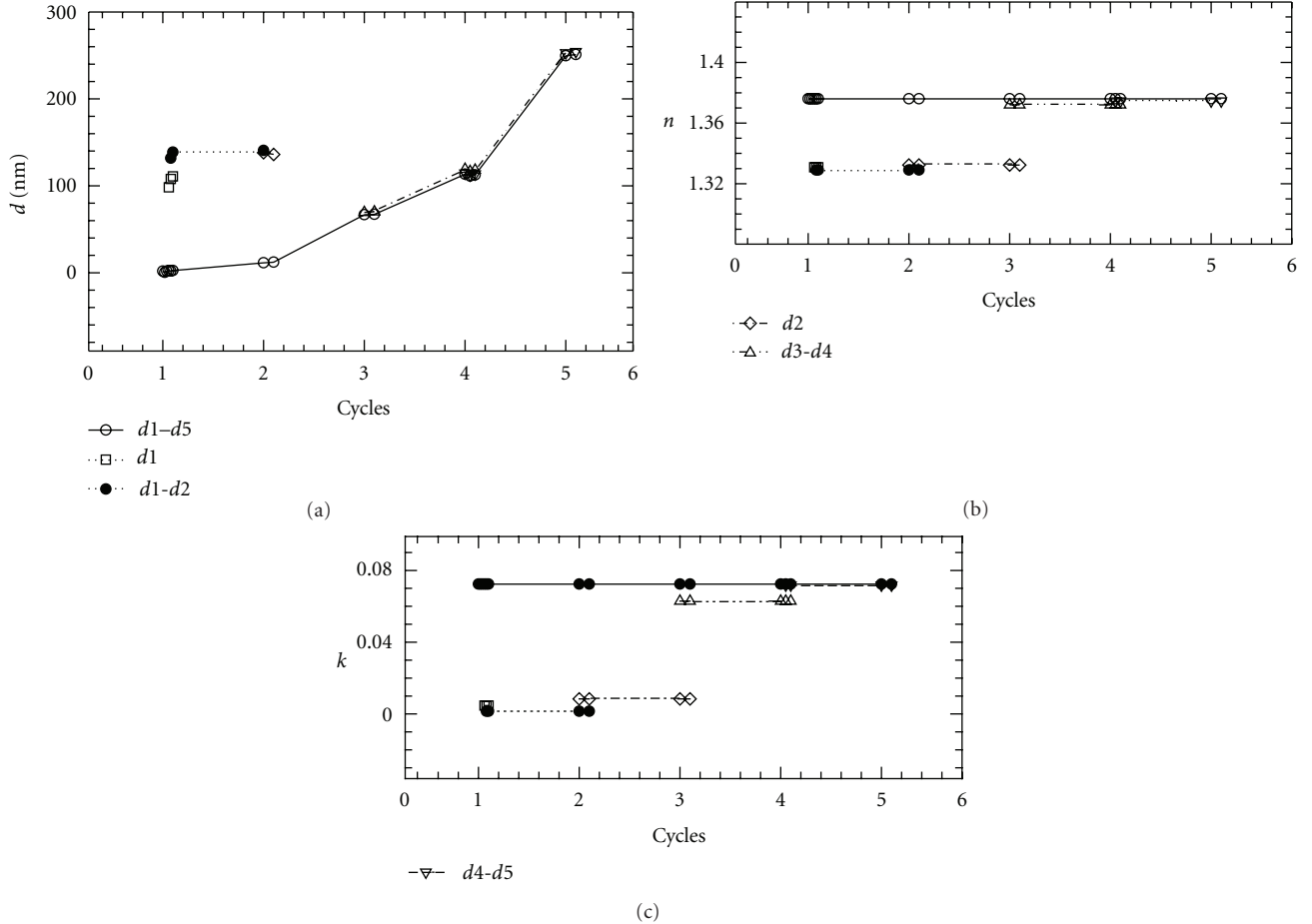


FIGURE 8: Calculated thickness, d , and optical indices, n , k , for the Ppy layers already described in Figure 3(b). $E_a = 1.4$ V, $\tau = 15$ s. SDS solution, $\lambda = 546$ nm. The different values n and k correspond to the resulting fitted values for different set of thicknesses.

according to the Bruggeman relationship starting from the mentioned $n - ik$ values to the values of $n = 1.332$ and $k = 0$ corresponding to the electrolyte are plotted. Figure 9 shows similar calculations to that described in Figures 7 and 8. It states as for films of low thickness very similar evolution in Δ/Ψ results for both (I) d increasing with constant n and k indices or (II) n and k increasing at constant d values.

In the case of the films formed using 5 cycles at 1.4 V and 1.2 V and assuming average values for the oxidised and the reduced state, the calculated d versus Q rate is equal to 1 μm for 7.3 mC/cm² and 1 μm for 11.6 mC/cm² of cathodic charge, respectively. This charge is similar to the reported for other thin films and about twenty times lower than the anodic charge used in the deposition process [8, 28]. The deposited layer at 1.4 V is obtained with a higher water contents. The currents of the peaks corresponding to the oxidation and the reduction of the deposited Ppy, Figure 1, indicate higher swelling and shrinking in the case of the film formed at 1.4 V than in the case of that formed at 1.2 V.

Divers articles had reported the swelling and shrinking process in several systems.

The mechanism of swelling can be originated by (1) insertion and extraction of bulky ions, (2) conformation change of a structure due to the delocalisation of π -electrons

and formation of polarons and bipolarons, (3) electrostatic repulsion between charges of the same sign [41]. Classical molecular dynamic simulation of Ppy/water interface holds that Ppy/Ppy interaction prevail over Ppy/water interactions in the reduced state, while the oxidised state induces more favourable Ppy/water interactions. The high hydrophobicity of the reduced Ppy expels the water from the bulk polymer. A density of 70 atoms/nm³ was estimated for the reduced state [42].

Nevertheless, different mechanisms can prevail, and diverse effects have been reported

Ppy/PPS network expands due to the insertion of anions in the oxidation and shrinks (extraction of anions) in the reduction [41]. Ppy/PTS swells on reduction and shrinks on oxidation. Charge compensation is probably accomplished by the cation transport rather than anion expulsion from the polymer matrix [43].

In Ppy/ClO₄⁻ is reported 30% decrease in thickness during oxidation. This seems strange with the expansion due to anion incorporation and electrostriction is considered as the controlling mechanism. Ppy/DBS expands about 61% by reduction [23, 25].

In the case of Ppy/SDS film, the deposition at 1.2 V forms compact layers where SDS stabilise the Ppy in the

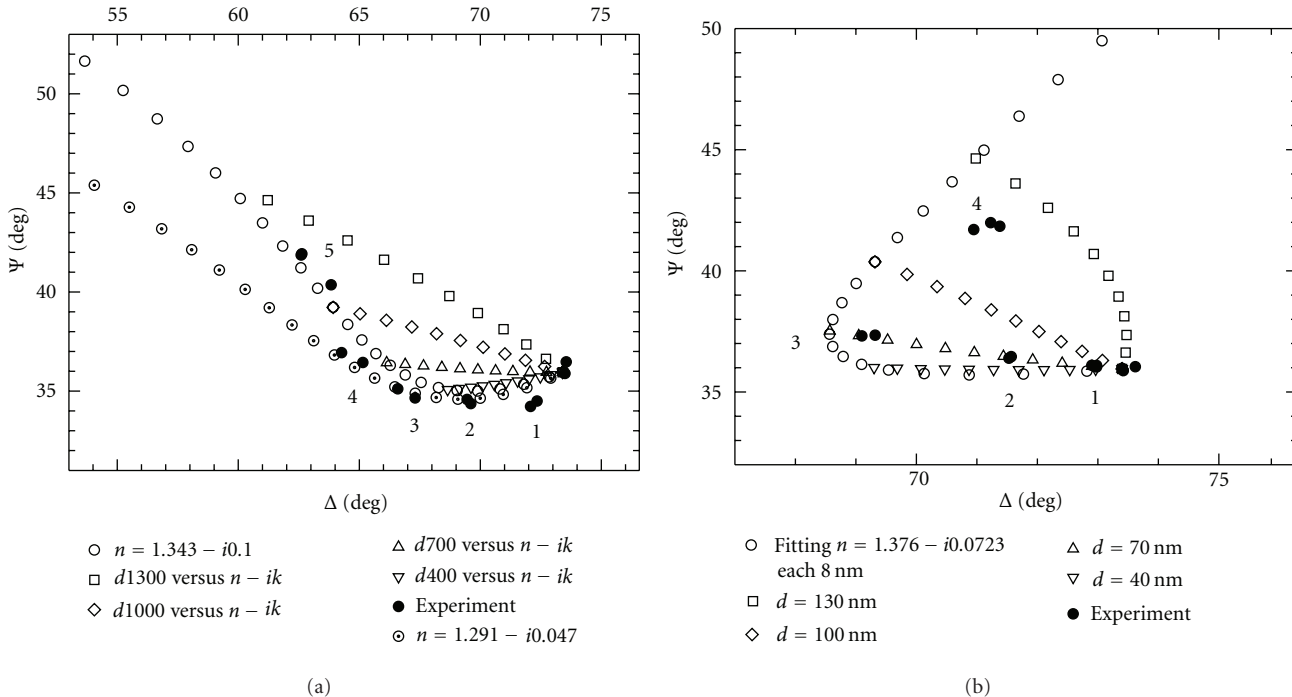


FIGURE 9: Enlarged plots of Ppy layers showing Δ/Ψ values corresponding to the first cycles shown in Figure 3. (●) experimental points, (a) $Ea = 1.2$ V, (b) $Ea = 1.4$ V. The figures correspond to number of cycles. Open points corresponds to different growing models: (○, ○) increasing d holding n and k fixed; (□, △, ▽) decreasing both n and k for different d fixed values, namely $d = 130, 100, 70$ and 40 nm, respectively.

high oxidised state. In KCl solution, Ppy shrinks showing an increasing polaronic effect for middle oxidation charge, water expulsion, and cation insertion. The high sensibility and reproducibility of the process may indicate the presence of a composite gel/electrolyte [30, 44, 45].

The Ppy/PO₄⁻³ electrodeposited at $Ea = 1.2$ V and 1.4 V in phosphate buffer show higher optical indices, $n = 1.50 - i0.07$, and an increase of d for the successive cycles starting from the second one, holding n and k quasi constants. On the other side, at a relatively very low potential, $Ea = 0.9$ V, a thick Ppy layer grows. Its thickness is about 80 nm and an initial very low optical density similar to that of the electrolyte increases with the number of cycles [15]. In the case of Ppy/SDS, the initial cycles show a very low optical density at $Ea = 1.2$ V, and the mean thickness of the initial dispersed attached oligomer increases for increasing $Ea = 1.4$ V. In this electrolyte, the monomer is extensively dissolved into the SDS micelles, and the electro polymerisation leads towards an initially more dispersed film than in PO₄⁻³ solution. The surfactant may also modify the growing process, induce the formation of ion pairing, and promote the Py polymerisation [46, 47].

5. Conclusions

The Ppy/SDS layer grown by successive potential pulses shows an initially low optical index $n - ik$, and thickness d_i of about 100 nm. The density and optical indices $n - ik$ of the layer increase after the successive pulses up to a maximum

value $n - ik$, holding constant d , after which the film grows in thickness holding constant density and $n - ik$ indices.

The fitted d depends on the anodic limit Ea , increasing with Ea , and $d_i = 40$ nm and $d_i = 100$ nm result from anodic polarisation at $Ea = 1.2$ V and $Ea = 1.4$ V, respectively.

The film grown at $Ea = 1.2$ V is more compact, shows low pseudocapacity, and stays in a high oxidation state, even under cathodic polarisation. After dipping in KCl solution, significant increases in pseudocapacity and electrochromism come out.

The Ppy/SDS layer grown at $Ea = 1.4$ V shows swelling under cathodic polarisation in SDS and KCl solutions. The Ppy/SDS layer grown at $Ea = 1.2$ V is very inert under switching in SDS solution. However, it shows significant shrinking under cathodic polarisation in KCl solution.

Acknowledgments

Authors are grateful to the “Comisión de Investigaciones Científicas de la Prov. de Bs. As.” (CIC) and the Universidad Nacional de San Luis (UNSL) for their grants to support this work. J. O. Z is member of the Research Career of CIC and M. G. S. of the Research Career of CONICET.

References

- [1] S. Barnoss, H. Shanak, C. C. Bof Bufon, and T. Heinzel, “Piezoresistance in chemically synthesized polypyrrole thin films,” *Sensors and Actuators A*, vol. 154, no. 1, pp. 79–84, 2009.

- [2] K. S. Teh, Y. Takahashi, Z. Yao, and Y. W. Lu, "Influence of redox-induced restructuring of polypyrrole on its surface morphology and wettability," *Sensors and Actuators A*, vol. 155, no. 1, pp. 113–119, 2009.
- [3] M. M. Chehimi, M. L. Abel, Z. Sahraoui, K. Fraoua, S. F. Lascelles, and S. P. Armes, "Time-dependent variation of the surface energy of conducting polypyrrole," *International Journal of Adhesion and Adhesives*, vol. 17, no. 1, pp. 1–8, 1997.
- [4] D. Ge, X. Tian, R. Qi et al., "A polypyrrole-based microchip for controlled drug release," *Electrochimica Acta*, vol. 55, no. 1, pp. 271–275, 2009.
- [5] X. Luo and X. T. Cui, "Sponge-like nanostructured conducting polymers for electrically controlled drug release," *Electrochemistry Communications*, vol. 11, no. 10, pp. 1956–1959, 2009.
- [6] J. K. Lim, J. W. Ciszek, F. Huo, J. W. Jang, S. Hwang, and C. A. Mirkin, "Actuation of self-assembled two-component rodlike nanostructures," *Nano Letters*, vol. 8, no. 12, pp. 4441–4445, 2008.
- [7] G. S. Gohil, V. V. Binsu, and V. K. Shahi, "Preparation and characterization of mono-valent ion selective polypyrrole composite ion-exchange membranes," *Journal of Membrane Science*, vol. 280, no. 1-2, pp. 210–218, 2006.
- [8] D. O. Flamini and S. B. Saidman, "Electrodeposition of polypyrrole onto NiTi and the corrosion behaviour of the coated alloy," *Corrosion Science*, vol. 52, no. 1, pp. 229–234, 2010.
- [9] G. Paliwoda-Porebska, M. Rohwerder, M. Stratmann, U. Rammelt, L. M. Duc, and W. Plieth, "Release mechanism of electrodeposited polypyrrole doped with corrosion inhibitor anions," *Journal of Solid State Electrochemistry*, vol. 10, no. 9, pp. 730–736, 2006.
- [10] M. Rohwerder and A. Michalik, "Conducting polymers for corrosion protection: what makes the difference between failure and success?" *Electrochimica Acta*, vol. 53, no. 3, pp. 1301–1314, 2007.
- [11] S. de Marcos and O. S. Wolfbeis, "Optical sensing of pH based on polypyrrole films," *Analytica Chimica Acta*, vol. 334, no. 1-2, pp. 149–153, 1996.
- [12] A. Riul, A. M. G. Soto, S. V. Mello, S. Bone, D. M. Taylor, and L. H. C. Mattoso, "An electronic tongue using polypyrrole and polyaniline," *Synthetic Metals*, vol. 132, no. 2, pp. 109–116, 2003.
- [13] Y. C. Liu and B. J. Hwang, "Mechanism of conductivity decay of polypyrrole exposed to water and enhancement of conductivity stability of copper(I)-modified polypyrrole," *Journal of Electroanalytical Chemistry*, vol. 501, no. 1-2, pp. 100–106, 2001.
- [14] A. Gratton, B. J. Hoffer, and G. A. Gerhardt, "In vivo electrochemical studies of monamine release in the medial prefrontal cortes of the rat," *Neuroscience*, vol. 29, no. 1, pp. 57–64, 1989.
- [15] J. O. Zerbino, L. J. H. Pesetti, and M. G. Sustersic, "Electrochemical and ellipsometric study of polypyrrol films in solutions containing ascorbic acid," *Journal of Molecular Liquids*, vol. 131–132, pp. 185–189, 2007.
- [16] J. Bobacka, A. Ivaska, and A. Lewenstam, "Potentiometric ion sensors," *Chemical Reviews*, vol. 108, no. 2, pp. 329–351, 2008.
- [17] Z. Gao, Z. Minxian, and C. Beshen, "The influence of overoxidation treatment on the permeability of polypyrrole films," *Journal of Electroanalytical Chemistry*, vol. 373, no. 1-2, pp. 141–148, 1994.
- [18] Z. Gao and A. Ivaska, "Electrochemical behaviour of dopamine and ascorbic acid at overoxidized polypyrrole(dodecyl sulphate) film-coated electrodes," *Analytica Chimica Acta*, vol. 284, no. 2, pp. 393–404, 1993.
- [19] F. Beck, P. Braun, and M. Oberst, "Organic electrochemistry in the solid state-overoxidation of polypyrrole," *Berichte der Bunsengesellschaft für Physikalische Chemie*, vol. 91, no. 9, pp. 967–974, 1987.
- [20] W. J. Plieth, J. Zerbino, C. Lahmann, and G. Kossmehl, "Examination of electrically conducting films of poly(2,5-thiophenediyl) by cyclic voltanometry and ellipsometry. Part II," *Journal of Electroanalytical Chemistry*, vol. 274, no. 1-2, pp. 213–224, 1989.
- [21] J. O. Zerbino, W. J. Plieth, and G. Kossmehl, "Optical properties of electrically conducting films formed by anodic oxidation of 1,2-di(2-thienyl)ethylene," *Journal of Applied Electrochemistry*, vol. 21, no. 10, pp. 935–940, 1991.
- [22] E. Kriván, C. Visy, and J. Kankare, "Deprotonation and dehydration of pristine PPY/DS films during open-circuit relaxation: an ignored factor in determining the properties of conducting polymers," *Journal of Physical Chemistry B*, vol. 107, no. 6, pp. 1302–1308, 2003.
- [23] E. Smela and N. Gadegaard, "Volume change in polypyrrole studied by atomic force microscopy," *Journal of Physical Chemistry B*, vol. 105, no. 39, pp. 9395–9405, 2001.
- [24] P. A. Christensen and A. Hamnett, "In situ spectroscopic investigations of the growth, electrochemical cycling and overoxidation of polypyrrole in aqueous solution," *Electrochimica Acta*, vol. 36, no. 8, pp. 1263–1286, 1991.
- [25] A. Hamnett, P. A. Christensen, and S. J. Higgins, "Analysis of electrogenerated films by ellipsometry and infrared spectrometry," *The Analyst*, vol. 119, no. 5, pp. 735–747, 1994.
- [26] S. Li, Y. Qiu, and X. Guo, "Influence of doping anions on the ion exchange behavior of polypyrrole," *Journal of Applied Polymer Science*, vol. 114, no. 4, pp. 2307–2314, 2009.
- [27] C. Zhong, K. Doblhofer, and G. Weinberg, "The effect of incorporated negative fixed charges on the membrane properties of polypyrrole films," *Faraday Discussions of the Chemical Society*, vol. 88, pp. 307–316, 1989.
- [28] J. O. Zerbino, M. I. Florit, and A. Maltz, "Voltammetric and ellipsometric study of electrically conducting films of poly(o-toluidine) in different acid media," *Electrochimica Acta*, vol. 44, no. 12, pp. 1973–1979, 1999.
- [29] J. O. Zerbino and M. G. Sustersic, "Ellipsometric and electrochemical study of dopamine adsorbed on gold electrodes," *Langmuir*, vol. 16, no. 19, pp. 7477–7481, 2000.
- [30] J. Heinze, B. A. Frontana-Uribe, and S. Ludwigs, "Electrochemistry of conducting polymers-persistent models and new concepts," *Chemical Reviews*, vol. 110, no. 8, pp. 4724–4771, 2010.
- [31] P. R. Teasdale and G. G. Wallace, "In situ characterization of conducting polymers by measuring dynamic contact angles with Wilhelmy's plate technique," *Reactive Polymers*, vol. 24, no. 3, pp. 157–164, 1995.
- [32] H. Yamato, M. Ohwa, and W. Wernet, "Stability of polypyrrole and poly(3,4-ethylenedioxythiophene) for biosensor application," *Journal of Electroanalytical Chemistry*, vol. 397, no. 1-2, pp. 163–170, 1995.
- [33] I. L. Lehr, O. V. Quinzani, and S. B. Saidman, "Comparative study of polypyrrole films electrosynthesized in alkaline and acid solutions," *Materials Chemistry and Physics*, vol. 117, no. 1, pp. 250–256, 2009.
- [34] C. Zhong and K. Doblhofer, "Polypyrrole-based electrode coatings switchable electrochemically between the anion- and cation-exchanger states," *Electrochimica Acta*, vol. 35, no. 11–12, pp. 1971–1976, 1990.

- [35] J. O. Zerbino, C. Falivene, A. Maltz, and M. G. Sustersic, “Polypyrrole films electropolymerised in sodium doedecylsulphate solution,” *Avances en Ciencias e Ingenieria*, vol. 1, no. 4, pp. 23–32, 2010.
- [36] M. E. Vela, J. O. Zerbino, and A. J. Arvia, “Ellipsometric study of hydrous gold oxide layers and gold surfaces resulting from their electroreduction,” *Thin Solid Films*, vol. 233, no. 1-2, pp. 82–85, 1993.
- [37] S. Little, S. F. Ralph, C. O. Too, and G. G. Wallace, “Solvent dependence of electrochromic behaviour of polypyrrole: re-discovering the effect of molecular oxygen,” *Synthetic Metals*, vol. 159, no. 19-20, pp. 1950–1955, 2009.
- [38] S. Chakrabarti, D. Banerjee, and R. Bhattacharyya, “Enhancement of room temperature electrical conductivity of polypyrrole by chemical modification,” *Journal of Physical Chemistry B*, vol. 106, no. 12, pp. 3061–3064, 2002.
- [39] Y. W. Lu, Y. Takahashi, and K. S. Teh, “Wettability switching technique of a biocompatible polymer for protein adhesion control,” in *Proceedings of the 22nd Annual IEEE International Conference on Micro Electro Mechanical Systems (MEMS '09)*, Sorrento, Italy, January 2009.
- [40] T. F. Otero, P. Herrasti, P. Ocón, and C. R. Alves, “Electrogeneration of polypyrrole-carboxymethylcellulose composites: electrochemical, microgravimetric and morphological studies,” *Electrochimica Acta*, vol. 43, no. 9, pp. 1089–1100, 1998.
- [41] M. Fuchiwaki, W. Takashima, S. S. Pandey, and K. Kaneto, “Proposal of novel actuators using conducting polymer laminates,” *Synthetic Metals*, vol. 135–136, pp. 135–136, 2003.
- [42] J. J. López Cascales, A. J. Fernández, and T. F. Otero, “Characterization of the reduced and oxidized polypyrrole/water interface: a molecular dynamics simulation study,” *Journal of Physical Chemistry B*, vol. 107, no. 35, pp. 9339–9343, 2003.
- [43] M. F. Suárez and R. G. Compton, “In situ atomic force microscopy study of polypyrrole synthesis and the volume changes induced by oxidation and reduction of the polymer,” *Journal of Electroanalytical Chemistry*, vol. 462, no. 2, pp. 211–221, 1999.
- [44] E. Ruckenstein and J.-H. Chen, “Polypyrrole conductive composites prepared by coprecipitation,” *Polymer*, vol. 32, no. 7, pp. 1230–1235, 1991.
- [45] K. Aoki and M. Kawase, “Introduction of a percolation threshold potential at polyaniline-coated electrodes,” *Journal of Electroanalytical Chemistry*, vol. 377, no. 1-2, pp. 125–129, 1994.
- [46] G. Zotti, G. Schiavon, S. Zecchin, F. Sannicolo, and E. Brenna, “Anion-assisted anodic coupling of 2,2'-bipyrrole. Role of tosylate anion in the electrochemical synthesis of polypyrrole,” *Chemistry of Materials*, vol. 7, no. 8, pp. 1464–1468, 1995.
- [47] L. M. Abrantes and J. P. Correia, “On the initiation and growth of polymer films onto electrode surfaces,” *Electrochimica Acta*, vol. 44, no. 12, pp. 1901–1910, 1999.

Research Article

False Oxygen Consumption Effect and Factors Causing It

M. V. Miniaev, M. B. Belyakova, N. V. Kostiuk, and D. V. Leshchenko

Department of Biochemistry and Research Center, Tver State Medical Academy, 4 Sovetskaya Street, Tver 170100, Russia

Correspondence should be addressed to M. B. Belyakova, mayabe@yandex.ru

Received 24 February 2011; Revised 28 April 2011; Accepted 29 April 2011

Academic Editor: Sibel A. Ozkan

Copyright © 2011 M. V. Miniaev et al. This is an open access article distributed under the Creative Commons Attribution License, which permits unrestricted use, distribution, and reproduction in any medium, provided the original work is properly cited.

False oxygen consumption effect characterized by a decrease of the polarographic sensor readings by the introduction of neutral microadditives into the incubation medium was modeled and tested. These neutral microadditives neither consume oxygen nor cause its consumption by other components of the medium. It is shown that microadditives less than 3% of the volume of incubation medium can cause statistically significant effect of false oxygen consumption more than 4% of the initial oxygen content. The effect can reach more than 15% at higher volumes of additives. The most important properties of additives enhancing the effect are low oxygen content, low temperature, and low concentration of oxygen salting out components.

1. Introduction

The introduction of reagents in the incubation medium is obligatory operation for the polarographic study of oxygen consumption. Additives such as ADP, substrate, or uncoupler precisely start the process of consumption. Even at constant oxygen content in the reaction mixture, the peculiarities of additives capable to decrease the readings of the measuring equipment are neglected. In the best case, this should lead to a distortion of measurement results, and in worst case would ascertain the consumption of oxygen where it is actually not. Under such circumstances, the result appears to be more significant than expected. Here, this phenomenon would be called “false oxygen consumption effect.”

The most common properties of the additives, which can cause false oxygen consumption, include: (1) absence or low content of dissolved oxygen, (2) low temperature, (3) low levels of oxygen salting-out components, and (4) high viscosity.

The introduction of microadditives (10–500 μL) that have at least one of the above listed properties should lead to a noticeable reduction in either the concentration or partial pressure of oxygen in medium. Moreover, viscous additives would increase the thickness of the diffusion layer of the measuring electrodes. This would result in the reduction of polarographic oxygen sensor readings, which

could be incorrectly interpreted as oxygen consumption by the biological object of study.

The effect of false oxygen consumption accompanies almost every study of respiration in liquid incubation media, whereas in the literature there are separate efforts to identify the effect and to understand its mechanisms [1–5]. So a simple system was used as a model where certain parameters of microadditives were manipulated. This demonstrated the quantitative aspect of false oxygen consumption, achieving the aim of the study.

2. Methods

2.1. Measuring Cell. A measuring cell of volume 4 mL (Figure 1), was equipped with silver-zinc polarographic oxygen sensor, a Clark electrode [6] in the modification of Mancy [7], and thermostabilized at 37°C ($\pm 0.1^\circ\text{C}$). Sensor readings were recorded by an oximeter N5221 (Poland). To reduce the gas exchange between the incubation medium and atmosphere, floating plastic lid was placed on the surface of the medium. This allowed addition of any volume to cell without loss of fluid. However, the lid did not completely stop the diffusion of oxygen from the atmosphere into the incubation medium. Therefore, the raw data were corrected as published previously [8].

TABLE 1: Parameters of oxygen-free additives used in the study of the factors causing false oxygen consumption.

no.	Investigated factor	Salt concentration	Thickener	$t^{\circ}\text{C}$
1	Oxygen concentration	KCl, 60 g/L	—	37
2	Temperature	KCl, 60 g/L	—	0
3	Salting out	0 g/L (H_2O)	—	37
4	Salting out	KCl, 120 g/L	—	37
5	Viscosity	KCl, 60 g/L	starch (10%)	37

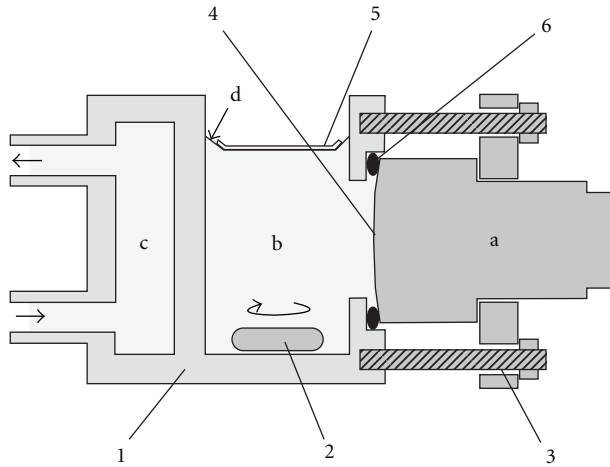


FIGURE 1: Thermostated measuring cell. (a) oxygen sensor, (b) the incubation medium, (c) water jacket, and (d) a place to introduction of additives. (1) the cell body (PMMA), (2) magnetic stirrer, (3) sensor mount, (4) sensor membrane (Teflon, 20 μm), (5) floating lid (polyethylene), and (6) gasket (rubber).

2.2. Model of the Incubation Medium. To exclude the osmotic effects on the membrane of the oxygen sensor and to facilitate the calculation, instead of the real incubation medium, a simple model was used. This model was a solution of KCl with a concentration of 60 g/L, which had the same composition and osmotic pressure as the sensor electrolyte. It allowed to calculate the concentration of oxygen basing on reference data. This solution was saturated with oxygen by continuous flow of atmospheric air enriched with water vapor in a thermostated flask at 37°C. The concentration of O_2 in the medium was 1.54×10^{-7} mol/mL at 37°C and atmospheric pressure 760 mmHg.

2.3. Oxygen-Free Additive. Solutions for taking of additives were prepared by blowing the mixtures with water vapor saturated nitrogen, which was begun an hour before and continued throughout the experiment (Table 1).

Mixtures were heated in thermostat at 37°C or cooled by immersing the flask on melting ice. A thickening solution was prepared by dissolving of KCl in 10% starch solution up to a concentration 60 g/L. After mixing 3.5 mL of the medium with various volumes of thickening additives, the relative viscosity was detected by viscosimeter VK-4 (Russia) in fivefold replicates at 20°C (Table 2).

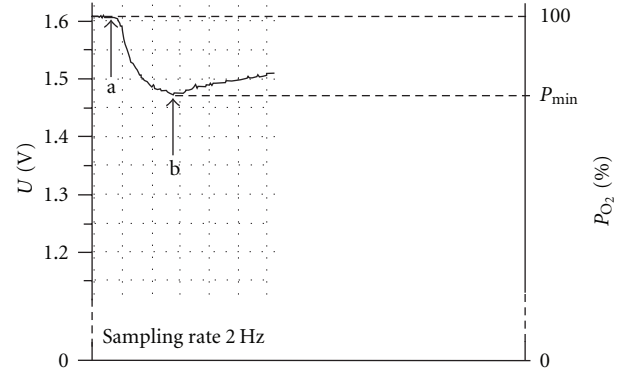


FIGURE 2: Typical registration curve of false oxygen consumption. (a) the time of additive introduction and (b) the minimal value of oxygen partial pressure (P_{\min}). Recorded by ADC L-154 (L-Card, Russia), application PowerGraph (D. Izmailov, Russia). Curve demonstrates a distinct change in the partial pressure of oxygen in the medium in which the proper content of oxygen was not changed. However, the result of such measurement seems to be oxygen consumption and can be interpreted as a consumption of oxygen by the investigated objects under the influence of additives (“false consumption”).

TABLE 2: Dependence of viscosity on the volume of thickening additive at 20°C (mean and coefficient of variation for $n = 5$).

V additive (μL)	Relative viscosity of mixture	C_V (%)
0	1.06	5.2
100	1.16	4.7
200	1.28	3.5
300	1.36	4.0
400	1.50	0.0

2.4. Scheme of the Experiment. Once incubation medium was oxygen-saturated at 37°C, then 3.5 mL of medium was placed in a thermostated measuring cell and covered with a floating lid (Figure 1). This was left aside for 5–15 minutes to stabilize oximeter readings. The recording was turned on. Then, anoxic additive was introduced into the medium by a micropipette through a notch in the lid. Registration curve is shown in Figure 2.

The value of the false oxygen consumption effect ΔN was determined by the minimum P_{\min} of registration curve (Figure 2)

$$\Delta N = \frac{5.373 \times 10^{-7} \cdot P_A \cdot (100 - P_{\min})}{760 \cdot 100}, \quad (1)$$

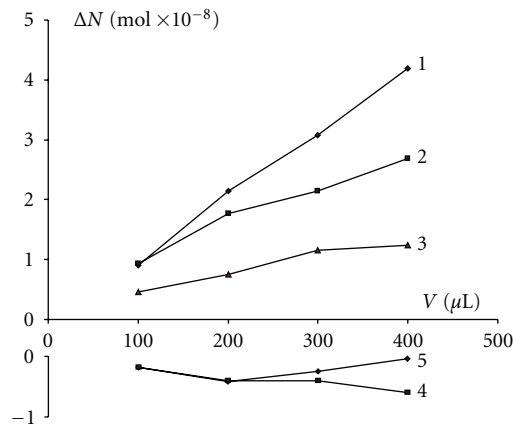


FIGURE 3: The dependence of false oxygen consumption caused by various factors on the volume of additives. (1) oxygen-free additive, (2) cooled additive, (3) absence of salts in the additive, (4) high concentration of salt in the addition, and 5: high viscosity of additive.

where 5.373×10^{-7} (mol): the content of O_2 in 3.5 mL of medium ($37^\circ C$, 760 mmHg),

100 (%): initial reading of oximeter, P_{\min} (%): oximeter reading at the minimum, 760 (mmHg): standard atmospheric pressure, and P_A (mmHg): atmospheric pressure at the time of measurement.

After each measurement, the cell was filled with a fresh portion of solution saturated with atmospheric oxygen at $37^\circ C$ and kept for 20 minutes for the restoration of initial readings. Additives of 100, 200, 300, and $400 \mu L$ were used in all cases. Accordingly, 10 readings were obtained for each volume.

In order to determine the spread of viscosity, the coefficient of variation C_V was calculated. Furthermore, for the statistical evaluation of study results, the average mean and standard error were also calculated. To demonstrate the statistical significance of false oxygen consumption, t -test was used. This test statistically compared the results obtained by the introduction of additives no. 2–5 with the records of additive no. 1 (volume to volume).

3. Results

Table 3 represents the mean value of false oxygen consumption ΔN , at the introduction of oxygen free additives. A distinct effect was observed in all cases even for additive of $100 \mu L$, which is less than 3% of the incubation medium volume.

Maximum effect was achieved with the introduction of oxygen-free additive cooled to $0^\circ C$ (additive no. 2) and the minimum—by using of additive containing 120 g/L KCl (additive no. 4).

In all experiments, the effect develops in the absence of oxygen in the additives. Therefore, individual contributions of other factors were calculated as differences between the effect developed under simultaneous action of two factors (for additives no. 2–5) and the effect of the oxygen-free

additive, which did not differ from the medium by other parameters (additive no. 1). Results are presented in Table 4.

As the table shows, absence of oxygen (additive no. 1), low temperature of additive (additive no. 2), and an absence of the dissolved compounds salting out the oxygen (additive no. 3) caused a statistically significant, but nevertheless a false reduction of oxygen content in the incubation medium. This happened even when the volume of the additive was $100 \mu L$. Excess of salts in the additive (additive no. 4) caused reliable, but an opposite effect. A more complicated picture was created when thickening additives were used (additive no. 5). Therefore, the effect of the viscous additives on the value of false oxygen consumption is presented in graphic form (Figure 3). For comparison, the influence of other factors is shown also.

According to the published data [2], an increase in the viscosity should lead to reduction of the measuring equipment readings and thereby cause the effect of false consumption. However, introduction of viscous additive led to opposite effect (Figure 3). Moreover, statistically confirmed minimum was noted in the curve.

4. Discussion

In the present study, by appropriate methods using generally accepted schemes of statistical analysis for biological experiment it was demonstrated that introducing additives, which neither consumed oxygen nor initiated its consumption by other components of the medium, may cause a reproducible and statistically significant decrease in partial pressure of oxygen. Although the content of oxygen in the medium does not change, a decline of partial pressure does not eliminate a possibility of ambiguous interpretation of obtained results [4, 9–11].

False oxygen consumption turned out to be not only reproducible, but also quite significant. For example, under combined effects of the factors, even if the additive does not exceed 3% ($100 \mu L$) of incubation medium volume, there can be statistically significant “consumption” of more than 4% of the initial amount of oxygen. With the increase in volume of additive to 11% ($400 \mu L$), the false consumption exceeds 15%. This is quite comparable with the real oxygen consumption by objects such as mitochondria in biological experiments [9, 11, 12].

There are different reasons for the fall of oxygen partial pressure depending on the types of additives. Absence of oxygen in additive (additive no. 1) leads to a dilution of oxygenated medium with pure solvent [1, 4]. As a result the concentration, but not quantity, of oxygen decreases, leading to a drop in partial pressure. If the additive has a lower temperature than the medium (addition no. 2), its introduction leads to temporary cooling of the mixture. Hence, the solubility of oxygen in the medium increases [5], and the partial pressure decreases. Absence or lower content of oxygen salting out components in the additive (additive no. 3) causes a reduction in concentrations of these components in the incubation medium. It also leads to an

TABLE 3: False oxygen consumption ΔN ($\text{mol} \times 10^{-8}$), caused by the introduction in the incubation medium of various oxygen-free additives (mean \pm SE, $n = 10$).

V additive (μL)	Type of additive (Table 1)				
	no. 1	no. 2	no. 3	no. 4	no. 5
100	0.91 \pm 0.05	1.84 \pm 0.05	1.37 \pm 0.03	0.72 \pm 0.03	0.72 \pm 0.09
200	2.15 \pm 0.03	3.92 \pm 0.03	2.91 \pm 0.04	1.74 \pm 0.07	1.73 \pm 0.06
300	3.08 \pm 0.05	5.23 \pm 0.07	4.23 \pm 0.04	2.68 \pm 0.03	2.83 \pm 0.08
400	4.20 \pm 0.06	6.89 \pm 0.06	5.44 \pm 0.01	3.59 \pm 0.03	4.16 \pm 0.13

TABLE 4: Individual contributions of separate factors to the total value of false oxygen consumption ΔN ($\text{mol} \times 10^{-8}$), $n = 10$.

V additive (μL)	Oxygen concentration	Temperature	Acting factor		
			Salting out (no. 3)	Salting out (no. 4)	Viscosity
100	0.91 \pm 0.05	0.93***	0.46***	-0.19**	-0.19*
200	2.15 \pm 0.03	1.77***	0.76***	-0.41***	-0.42***
300	3.08 \pm 0.05	2.15***	1.15***	-0.40***	-0.25**
400	4.20 \pm 0.06	2.69***	1.24***	-0.60***	-0.03

* $P \leq .05$; ** $P \leq .01$; *** $P \leq .001$. Significant difference in comparison with oxygen-free additive of the same volume.

increase in oxygen solubility [13, 14] and a decrease in its partial pressure.

Thus, the additives with high oxygen content, high temperature, or high salt content should cause the opposite effect. However, oversaturated with oxygen and high temperature additives are not commonly used in a biological experiment. The tests were only carried out with additives of salt concentration twofold higher than that of the medium (additive no. 4). The obtained result, as expected, was a statistically significant increase in oxygen partial pressure, which may easily mask the actual oxygen consumption observed in biological study.

The most difficult for interpretation was the experiment with the use of thickening additive (additive no. 5). The increase in viscosity should cause an increase in thickness of electrode diffusion layer [2] and consequently reduce the oxygen sensor readings (the apparent decrease in the partial pressure of oxygen), but the result obtained was the opposite. Moreover, for thickening additives dependence of false consumption effect on the volume of additive has significant minimum, corresponding to volume 200 μL (Figure 3). The most probable explanation for this fact may be the simultaneous effect of two factors that have opposite effects on readings of oxygen sensor.

The factor contributing to the reduction of false oxygen consumption effect is the salting-out effect of additive. It contained not only 60 g/L KCl (about 6%), but also 10% of starch as a thickener. Their total concentration in the additive was considerably higher than the concentration of solutes in the incubation medium. As a result, the influence of additive no. 5 up to the volume of 200 μL was quite similar to the action of additive no. 4 (KCl, 120 g/L).

The factor contributed to the enhancing of the effect was the increase of viscosity. The diffusion layer of the closed oxygen sensor was large enough, as it included the thickness of the membrane. A slight increase in viscosity of the solution could not have significant influence on its work. The effect

began to appear only when the growth of diffusion layer thickness due to the increase in viscosity was comparable to the thickness of the membrane. It is assumed that this occurred when the amount of additive reached 300 μL , and the relative viscosity of the mixture increased up to 1.36 at 20°C. Starting from this volume, viscosity determined the character of dependence (Figure 3).

5. Conclusion

Thus, we can conclude that introduction of any additive to the incubation medium, which differs from medium in composition, temperature, or viscosity, will unavoidably lead to changes in oxygen sensor readings. These changes can be large enough to cause a significant increase in measurement error, and also an appearance of well-reproducible artifact. This is identified as the false oxygen consumption effect. Under certain conditions, this effect can reach high percentage of the oxygen content in the incubation medium.

Exclusion of such distortions is not possible, because additives will always be different from the incubation medium by various parameters. Nevertheless, it is necessary to minimize the effect. For this purpose, reagent solutions saturated with atmospheric oxygen at the temperature of incubation medium should be used. When the reagents with low concentrations are prepared, water should be substituted by incubation medium. If these recommendations are difficult to fulfill, additives should be introduced with control measurements of oxygen partial pressure changes in the conditions that prevent real consumption of oxygen in the incubation medium.

References

- [1] B. Chance and G. R. Williams, "Respiratory enzymes in oxidative phosphorylation. I. Kinetics of oxygen utilization,"

- The Journal of Biological Chemistry*, vol. 217, no. 1, pp. 383–393, 1955.
- [2] A. A. Shpakov and L. F. Panchenko, “Nature of the effect “rapid oxygen consumption” during the introduction of tissue homogenate or a mitochondrial suspension into the polarographic cell,” *Biofizika*, vol. 20, no. 3, pp. 467–472, 1975.
 - [3] E. N. Kotova and I. S. Rotenberg, “Nature of rapid oxygen consumption by mitochondria following their placement in a polarography,” *Biofizika*, vol. 22, no. 4, pp. 746–747, 1977.
 - [4] E. Gnaiger, “Bioenergetics at low oxygen: dependence of respiration and phosphorylation on oxygen and adenosine diphosphate supply,” *Respiration Physiology*, vol. 128, no. 3, pp. 277–297, 2001.
 - [5] A. Barrientos, “In vivo and in organello assessment of OXPHOS activities,” *Methods*, vol. 26, no. 4, pp. 307–316, 2002.
 - [6] L. C. Clark Jr., R. Wolf, D. Granger, and Z. Taylor, “Continuous recording of blood oxygen tensions by polarography,” *Journal of Applied Physiology*, vol. 6, no. 3, pp. 189–193, 1953.
 - [7] K. H. Mancy, D. A. Okun, and C. N. Reilley, “A galvanic cell oxygen analyzer,” *Journal of Electroanalytical Chemistry*, vol. 4, no. 2, pp. 65–92, 1962.
 - [8] M. V. Miniaev and L. I. Voronchikhina, “Ambient air interference in oxygen intake measurements in liquid incubating media with the use of open polarographic cells,” *Aviakosmicheskaya i Ekologicheskaya Meditsina*, vol. 41, no. 2, pp. 64–68, 2007.
 - [9] A. Barrientos, L. Kenyon, and C. T. Moraes, “Human xenomitochondrial cybrids: cellular models of mitochondrial complex I deficiency,” *Journal of Biological Chemistry*, vol. 273, no. 23, pp. 14210–14217, 1998.
 - [10] C. Pourplanche, V. Larreta-Garde, and D. Thomas, “Comparison of polarographic and chemical measurements of oxygen uptake in complex media: the example of lipoxygenase reaction,” *Analytical Biochemistry*, vol. 198, no. 1, pp. 160–164, 1991.
 - [11] E. P. Dassa, E. Dufour, S. Goncalves, H. T. Jacobs, and P. Rustin, “The alternative oxidase, a tool for compensating cytochrome c oxidase deficiency in human cells,” *Physiologia Plantarum*, vol. 137, no. 4, pp. 427–434, 2009.
 - [12] C. J. Kay and J. M. Palmer, “Solubilization of the alternative oxidase of cuckoo-pint (*Arum maculatum*) mitochondria. Stimulation by high concentrations of ions and effects of specific inhibitors,” *The Biochemical Journal*, vol. 228, no. 2, pp. 309–318, 1985.
 - [13] J. Mexal, J. T. Fisher, J. Osteryoung, and C. P. Reid, “Oxygen availability in polyethylene glycol solutions and its implications in plant-water relations,” *Plant Physiology*, vol. 55, no. 1, pp. 20–24, 1975.
 - [14] A. M. Klibanov, N. O. Kaplan, and M. D. Kamenhy, “A rationale for stabilization of oxygen labile enzymes: application to a clostridial hydrogenase,” *Proceedings of the National Academy of Sciences of the United States of America*, vol. 75, no. 8, pp. 3640–3643, 1978.

Research Article

Fabrication of Hybrid Diamond and Transparent Conducting Metal Oxide Electrode for Spectroelectrochemistry

Jingping Hu, James Hodge, Arthur J. Boff, and John S. Foord

Chemistry Research Laboratory, Department of Chemistry, University of Oxford, Mansfield Road, Oxford OX1 3TA, UK

Correspondence should be addressed to John S. Foord, john.foord@chem.ox.ac.uk

Received 10 February 2011; Accepted 24 February 2011

Academic Editor: Bengi Uslu

Copyright © 2011 Jingping Hu et al. This is an open access article distributed under the Creative Commons Attribution License, which permits unrestricted use, distribution, and reproduction in any medium, provided the original work is properly cited.

A novel diamond transparent electrode is constructed by integrating conductive diamond film and transparent conducting metal oxide to combine the superior electrochemical properties of diamond and the electrical conductivity of transparent metal oxide (TCO). Direct growth of diamond on indium tin oxide (ITO) and aluminium doped zinc oxide (AZO) was explored, but X-ray photoelectron spectroscopy measurement reveals that both substrates cannot survive from the aggressive environment of diamond growth even if the latter is regarded as one of the most stable TCO. As a second route, a diamond membrane in silicon frame was prepared by selective chemical etching, and a diamond optically transparent electrode (OTE) was constructed by assembling the diamond membrane on the top of an ITO-coated substrate. The resulting device exhibits a high optical transparency and quasireversible electrochemical kinetics, which are competitive to other diamond OTEs reported previously. Its application in UV-Vis spectroelectrochemical studies on the oxidisation of 4-aminophenol was demonstrated.

1. Introduction

The development of optically transparent electrodes (OTEs) for electrochemical and particularly spectroelectrochemical studies has received considerable attention for investigation of electrochemical reaction mechanism and electroanalytical applications [1]. By measuring the transmission or reflection of UV, visible, or IR light through the electrode, the spectra of electrogenerated species can be characterised directly. In addition to the cell design, the choice of OTE is a focus of investigation. Conventionally, the OTEs are consisted of metal (Au, Pt) [2, 3] or metal oxide thin films deposited on transparent substrates (such as glass or quartz). The use of metal micromech and minigrid was also reported [4, 5].

Boron doped diamond (BDD) shows a combination of unique properties, such as a wide potential window, a low background current, mechanical and chemical stability, and resistance to fouling [6]. The application of BDD as OTEs in spectroelectrochemical studies was reported previously. Zak and Haymond et al. demonstrated the concept using a mechanical polished free-standing diamond of 0.38 mm thickness for the detection of ferricyanide, methyl viologen [7], and ferrocene [8]. BDD thin films of 0.5 μm and 1 μm

thickness were deposited on quartz from microwave-assisted chemical vapour deposition (MWCVD) and used to characterise the electrochemical responsiveness of $\text{Ru}(\text{NH}_3)_6^{3+}$, $\text{Fe}(\text{CN})_6^{3-}$, and chlorpromazine [9]. A 100-mesh platinum grid was coated with BDD thin film as an OTE, and applied to the chronoabsorptometry measurement of the redox couples, $\text{Rb}(\text{bpy})_3^{3+}$ and $\text{Fe}(\text{phen})_3^{3+}$ [10]. The application of BDD OTE requires two seemingly contradictory features, optical transparency and electrical conductivity. Higher boron doping is desired to increase electrical conductivity, but the boron inclusion creates electronic and vibrational states within the bandgap, leading to strong light absorption. So, a compromise must be reached to balance the doping levels required for electrical conductivity (R_s) while maintaining sufficient optical transparency (T), which is described by the figure of merit $\Phi_{\text{TC}} = T/R_s$ [11].

To achieve a good transparency as well as an improved electrical conductivity, we report a novel approach to fabricate diamond OTEs by integrating diamond thin film with a more conductive transparent substrate, such as indium tin oxide (ITO) and aluminium doped zinc oxide (AZO). The underlying conductive substrate will carry the majority of the currents, and the device resistance is mediated by

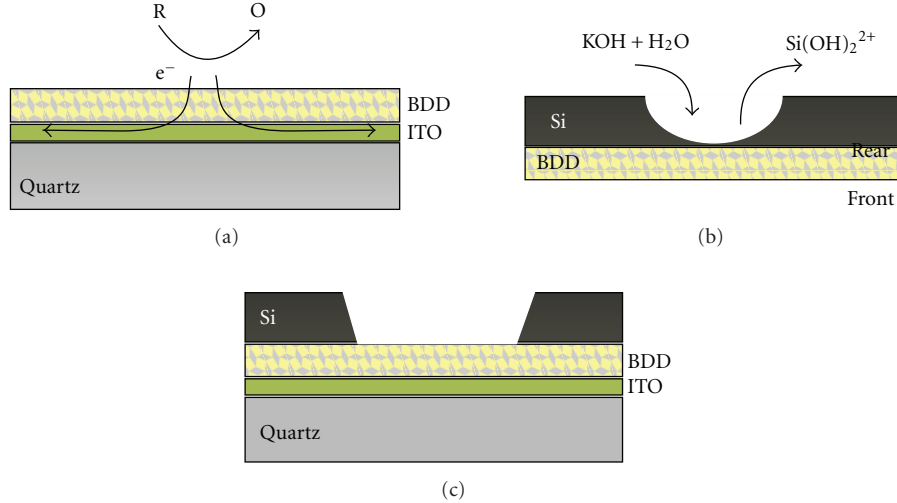


FIGURE 1: (a) Redox reaction on BDD surface and electron transfer through BDD membrane and along ITO film. (b) Chemical etching of silicon support to prepare free-standing BDD membrane. (c) Hybrid structure of diamond membrane—ITO electrode.

the resistance through the thin diamond film and the sheet resistance of the underlying highly conductive ITO substrate, which is much more conductive than the large sheet resistance along the diamond film in the conventional structure. This hybrid structure also permits the BDD thin film to be only lightly doped and hence highly transparent. In this work, two approaches were explored to fabricate this hybrid OTE, direct CVD deposition of BDD film on top of ITO or AZO thin films, or integration of a frame-supported diamond membrane with an ITO electrode. The feasibility of the former method was explored by investigating the chemical stability of ITO and AZO film in harsh diamond growth conditions. The device from the latter route was characterised by spectroscopic, optical, and electrochemical measurements, and its application in UV-Vis spectroelectrochemical studies on 4-aminophenol was also demonstrated.

2. Experimental

2.1. Fabrication of Diamond/ITO or AZO OTEs. An ITO film of 400 nm thickness was deposited on fused silica quartz substrate by electron beam evaporation of premixed powder of In_2O_3 with 10% SnO_2 in 1.5×10^{-4} mbar of oxygen. The deposition was followed by annealing in ambient conditions at 400°C for 2 hours. The metallic indium particles will be oxidised to In_2O_3 by atmospheric oxygen, and the associated defects are eliminated by annealing [12]. After annealing, the colour changed from dark grey to light green tint, and the transmission is over 90% between 450 nm and 900 nm in UV-Vis spectra. AZO film was prepared by the sol gel process [13]. A mixture of zinc acetate ($\text{Zn}(\text{CH}_3\text{CO}_2)_2 \cdot 2\text{H}_2\text{O}$) and aluminium nitrate ($\text{Al}(\text{NO}_3)_3 \cdot 9\text{H}_2\text{O}$, 0.8 at.%) was refluxed in 2-propanol with equimolar diethanolamine (DEA) and two molar equivalents of water at 78°C for 3 hours to get a clear solution, where DEA and added water acted as sol-stabiliser [14]. After aging for three days, the sol was used

for spin coating on fused silica quartz substrate. The AZO-coated samples were annealed at 530°C in air for 30 minutes to improve the crystallinity and performance [13].

The ITO- or AZO-coated quartz substrate was ultrasonically seeded in nanodiamond (3.5 nm, Yorkshire bioscience Ltd, UK) slurries for half an hour before diamond deposition. The diamond film was deposited by hot filament assisted chemical vapour deposition (HFCVD) from a mixture of hydrogen (99.3%) and methane (0.7%) gases. Boron doping was achieved by passing hydrogen gas through an ice-cooled bubbler containing trimethylborate (99%, Sigma-Aldrich Ltd). The HFCVD was conducted using a tungsten filament above 2200°C on a substrate heated to around 800°C in a vacuum chamber at around 33 mbar. The structure of the OTE with an electron transfer route is illustrated in Figure 1(a).

2.2. Fabrication of Diamond Membrane/ITO Composite OTEs. N-type (100) silicon substrate of 655 μm thickness was ultrasonically seeded in a mixture of 10 μm and 250 nm diamond suspension for one hour. A mixture of slurry was employed to enhance the nucleation due to “hammering effect” [15]. After seeding, the silicon substrate was rinsed with copious amounts of water to remove the excess diamond debris and dried with compressed air. Boron doped diamond was deposited from an HFCVD reactor under similar conditions for ITO and AZO substrates, except that the growth time is around 10 hours to achieve a mechanical robust diamond membrane. The diamond film coated silicon was sealed in a purposely built PTFE cell, leaving only a circular area in the rear side of Si substrate exposed. The exposed silicon was selectively chemical etched in 30% KOH held in a water bath of 80°C to prepare diamond membrane, as illustrated in Figure 1(b). The etching rate is around 67 μm per hour, and the etching time is around 10 hours. The membrane thickness is estimated to be 11.8 μm from the weight of delaminated BDD membranes.

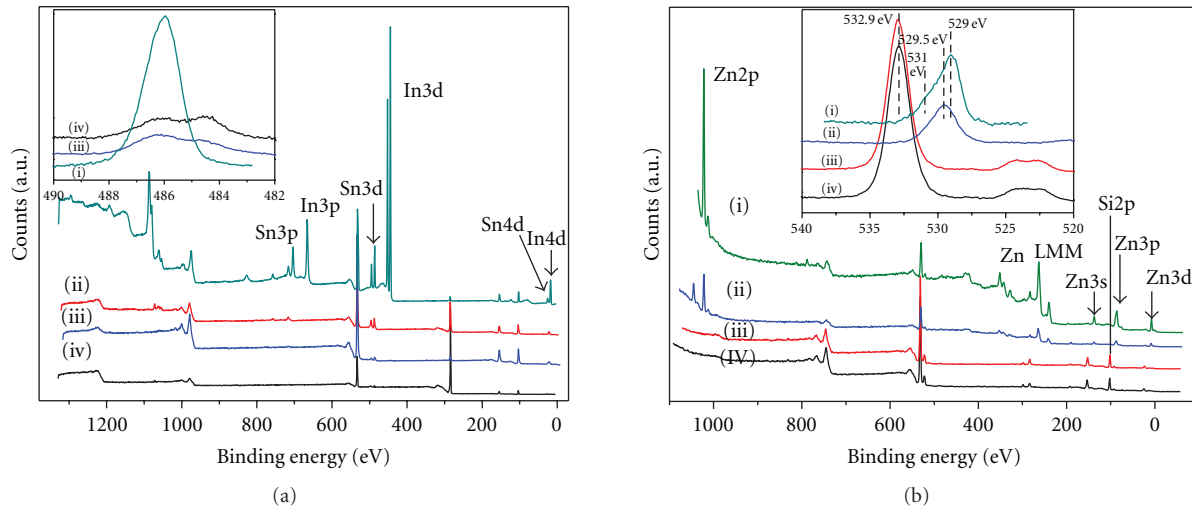


FIGURE 2: (a) XPS survey scan and Sn3d_{5/2} spectra (inset) of (i) as-grown ITO film, (ii) after 30 minutes diamond growth on ITO substrate, (iii) after 1 hour hydrogen plasma treatment at 800°C, (iv) after two hours diamond growth on ITO substrate. (b) XPS survey scan and O1s spectra (inset) of (i) as-prepared AZO film, (ii) after 5 minutes and (iii) 10 minutes hydrogen plasma treatment at 800°C in an HFCVD reactor, (iv) after 30 minutes diamond growth on AZO substrate.

The diamond membrane in silicon frame was assembled onto a 400 nm thick ITO film on fused silica quartz substrate, as shown in Figure 1(c). The device was further insulated with nail varnish and epoxy, and an electrical connection was made by attaching an aluminium foil on the edge of ITO film. The diamond membrane and ITO formed an electrical contact due to surface tension after a wetting and drying process.

2.3. Characterisation of Diamond OTEs. The surface chemical state was characterised by an in-house built X-ray photoelectron spectroscopy (XPS) with an Mg K_α X-ray source and a high resolution XPS system (Scienta ESCA 300) with an Al K_α X-ray source in National Centre for Electron Spectroscopy and Surface Analysis (NCESS) at Daresbury Laboratory, UK. The film morphology was measured by NanoScope MultiMode AFM (Digital Instrument) in contact mode, and Raman spectra were recorded using a Dilor Raman spectroscopy with an Ar laser source (514.5 nm). The optical transparency was characterised by a fibre optic UV-Vis spectrometer (USB2000, Ocean Optics Inc.) equipped with deuterium and halogen lamps and a Unicam UV2 scanning spectrophotometer.

Electrochemical experiments were performed using an Autolab PSTAT 10 bipotentiostat (EcoChemie, Netherlands) in a PTFE one-compartment electrochemical cell, incorporating the diamond OTE as a working electrode, a platinum counter electrode, and a standard calomel reference electrode. Spectroelectrochemical measurements were performed using a special designed thin-layer cell. Hexaamine-ruthenium ($\text{Ru}(\text{NH}_3)_6^{3+}$, 98%) and 4-aminophenol (98%) were ordered from Aldrich and used as redox couples without further purification. Acetate buffer of 0.1 M was used as supporting electrolyte for all electrochemical measurements and prepared using Milli-Q water (>18 MΩcm). All solutions

were freshly prepared and deaerated by bubbling with argon gas before each electrochemical experiment.

3. Results and Discussion

3.1. Direct CVD Growth of BDD on ITO or AZO Electrodes. BDD was grown directly on ITO-coated quartz substrate, and the deposition process was characterised by XPS, as shown in Figure 2(a). Before diamond deposition, the as-grown ITO film (Figure 2(a)(i)) shows intense and sharp peaks of In, Sn, and O 1s ascribed to indium oxide and tin oxide comprising the ITO film, together with weak peaks of Si 2p and Si 2s originated from the quartz substrate, confirming the phase purity of the film. After diamond growth or hydrogen plasma treatment, no indium peaks can be discernable from the background any more, and the Sn peaks diminishes drastically with longer treatment time, as seen from Figure 2(a)(ii)–(iv). Although the increase of C1s peak intensity with diamond growth time indicates the presence of diamond film on the surface, the absence and diminishing of In and Sn peaks are not attributed to the burying of ITO by diamond layer, as diamond layer is still incomplete which, is evidenced by the presence of Si 2p and Si 2s peaks from quartz substrate as presented in Figure 2(a)(ii).

The inset of Figure 2(a)(i, iii, iv) shows the Sn3d_{5/2} peaks of as-grown ITO, ITO after one hour hydrogen plasma treatment, and after two hours diamond growth, respectively. After plasma treatment and diamond growth, the sharp Sn 3d_{5/2} peak of SnO at 486.10 eV diminishes, accompanied by the appearance and growth of another peak attributed to elemental tin at 484.4 eV with longer treatment time. This reflects that both indium oxide and tin oxide were reduced to elemental metals in the HFCVD reactor by hydrogen plasma

due to high concentration of hydrogen radicals at elevated temperature. Most of the reduced elemental indium and tin evaporated rapidly at elevated substrate temperature under diamond growth conditions, and the former evaporated faster than the latter due to a lower melting temperature (156°C) and a higher vapour pressure. This explanation is consistent with the literature that metal agglomeration was observed by SEM after hydrogen plasma treatment, and the figure of merit decreases more than 80% after one minute treatment by hydrogen plasma at 200°C [16]. Similar phenomenon has been observed that the emergence of elemental Sn 3d_{5/2} peak was observed in XPS measurement after exposing in hydrogen plasma of 0.25 W/cm² rf power density at 250°C for 30 minutes [17]. It is also reported that annealing of reduced ITO films in air at 400°C for 1 hour can restore to a complete oxidised state, which is, however, not observed in our case as almost all the reduced indium and tin metals are evaporated due to the elevated temperature (800°C) and intense plasma power (100 W) in an HFCVD reactor.

Since ITO cannot survive from the aggressive diamond growth environment, a more stable substrate is preferred for the fabrication of a hybrid OTE. The previous study shows that zinc oxide is much more resistant to hydrogen plasma reduction, photodecomposition, and is more thermal stable at higher temperature than other TCOs [13, 17–19]. So a direct diamond growth on zinc oxide film was also explored. Figure 2(b) shows the XPS spectra of as-prepared AZO films from sol-gel process, and the XPS spectra after hydrogen plasma treatment of 5 and 10 minutes and after 30 minutes diamond growth, respectively. The as-prepared AZO film is characterised by strong Zn2p core lines and LMM Auger peaks in the survey spectrum (Figure 2(b)-i). The aluminium peak is so weak and not detectable due to a low doping level. It can be clearly seen that the zinc signal diminishes, and Si 2p core line from quartz substrate appears after exposure to hydrogen plasma at 800°C, indicating the decomposition of AZO film. The as-prepared AZO film shows a main peak at 529.0 eV, as shown in Figure 2(b), attributable to the O²⁺ ions of O-Zn bonding surrounded by Zn. The broad shoulder at higher binding energies can be attributed to the loosely bound oxygen species on the surface or hydrated oxides [20, 21], probably originating from acetate in the sol-gel process. During the hydrogen plasma treatment, hydrogen adsorbs on the surface forming Zn-H and OH bonds [22], and adsorbed hydrogen can also be bonded in bridged structures between two zinc (Zn-H-Zn) or oxygen atoms (OH···O). The formation of such surface bonds leads to surface passivation which makes ZnO stable towards thermal decomposition and hydrogen plasma reduction. The passivation layer has a slightly higher binding energy, which explains the shift of O1s peak towards higher binding energy after 5 minutes in hydrogen plasma, as presented in Figure 2(b). With a prolonged exposure to hydrogen plasma, the O1s peak shifts to a much higher binding energy of 532.9 eV which is attributed to SiO₂ from quartz substrate. We observed an unstable ZnO film under the harsh conditions for diamond growth, in contrary to the good stability of ZnO film upon mild hydrogen plasma treatment observed by Major et al. [17], probably due to

different experimental conditions such as temperature and plasmas power.

3.2. A Hybrid BDD OTE with a BDD Membrane on ITO. Since the first route of directly diamond deposition was undermined by the stability of ITO and AZO substrate, we explored an alternative method to circumvent the problem by preparing silicon frame-supported diamond membrane separately followed by integrating diamond membrane with an ITO conducting substrate to fabricate the OTE device.

The morphology of the as-prepared diamond membrane was examined by AFM in contact mode, as shown in Figures 3(a) and 3(b). Optical application of OTE requires a smooth surface with a grain size much smaller than the wavelength of incident light to eliminate light scattering. To achieve this, the silicon substrate was ultrasonic treated in mixed micro- and nanodiamond slurries to increase the nucleation density. Following the ultrasonic treatment, the deposited diamond film exhibits a surface root mean square (RMS) roughness of around 26 nm and a grain diameter between 50 to 100 nm, which corresponds to a nucleation density of 1×10^{10} to 4×10^{10} cm⁻². The features of surface morphology confirm the significance of the ultrasonic treatment process.

The diamond phase on both front and rear side of membrane was characterised by Raman spectroscopy, as presented in Figure 4(a). The characteristic peaks of sp³ carbon at 1333 cm⁻¹ are weak and broad in both spectra, indicating dense grain boundaries inherit to small diamond grains. The peaks at 1130 cm⁻¹ and around 1470 cm⁻¹ are most likely associated with transpolyacetylene at grain boundaries which is often observed in nanodiamond. The peak at 1130 cm⁻¹ is less pronounced on the rear side of membrane, probably due to the inclusion of SiC in the nucleation phase of diamond growth and the modification during chemical etching. The peaks centred at around 1345 cm⁻¹ and 1550 cm⁻¹ are attributed to sp² amorphous carbon which seems intense due to a resonant enhancement of sp² bonded portion by a factor of 50 to 200 [23].

The optical properties of the OTE fabricated from diamond membrane were characterised by UV-Vis spectroscopy measurement, as illustrated in Figure 4(b). The optical transmittance of the diamond OTE is around 27% between 600 and 850 nm. The falloff of transmission near and in the UV region is due to light scattering associated with surface roughness. This transmittance value is much higher than the free-standing diamond OTE reported by Zak et al. [7] which has best transmittance of 5% at around 300 nm and 1% at 600 nm, and comparable to the diamond coated quartz OTE and diamond membrane fabricated by Stotter et al. [9] and Michaelson et al. [24]. In comparison with the OTE, the ITO film is highly transparent and has marginal contribution to the absorption, with an average transmittance around 95% at the interference fringes. Besides absorption by diamond membrane, light reflection by the smooth diamond membrane and ITO film might also contribute to the transmission loss.

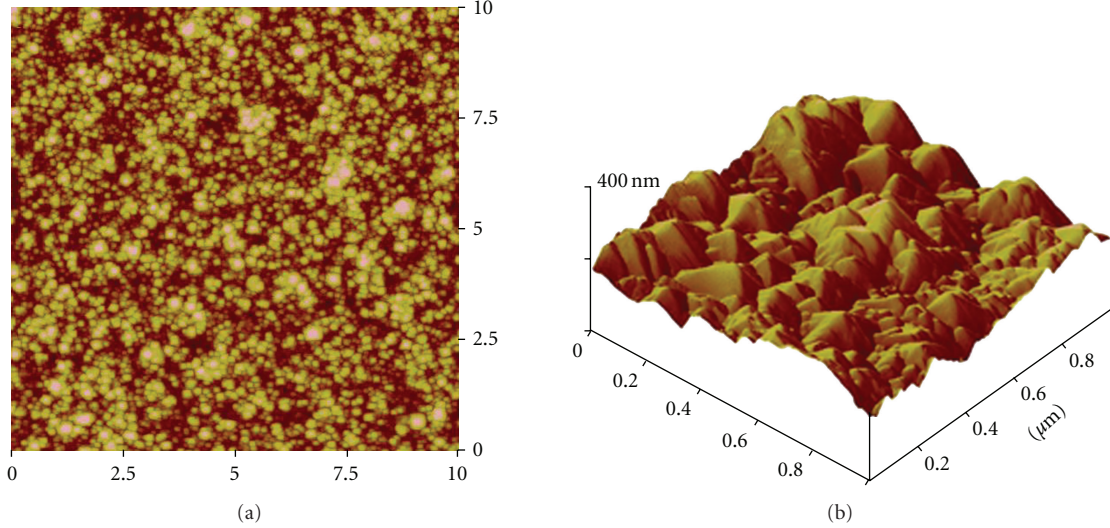


FIGURE 3: AFM images of diamond membrane, (a) $1 \times 1 \mu\text{m}$ and (b) $10 \times 10 \mu\text{m}$. The diameter of diamond grain is around 50 to 100 nm, and the root mean square (RMS) roughness is around 26 nm.

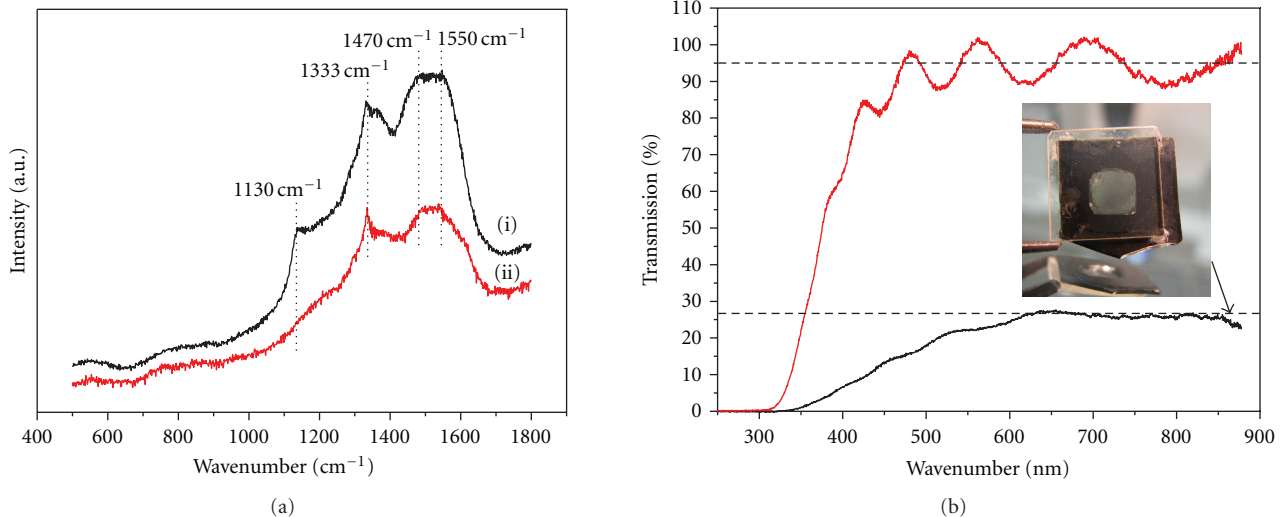


FIGURE 4: (a) The Raman spectra of (i) front side and (ii) rear side of diamond membrane. (b) The UV-Vis transmission spectra of ITO and fabricated OTE device consisting of a diamond membrane on an ITO substrate.

3.3. Electrochemical Properties of Hybrid OTE Device: BDD Membrane on ITO. The background corrected electrochemical response of the diamond OTE is measured by cyclic voltammetry in $\text{Ru}(\text{NH}_3)_6^{3+}$ of different concentrations in 0.1 M acetate buffer as a supporting electrolyte as shown in Figure 5(a). The voltammograms have well-defined redox peaks, and a wide potential window from -1.35 to 1.50 V (Figure 5(b)), which is consistent with the value reported for free-standing diamond and diamond/quartz OTEs [7, 9]. A small peak separation is a characteristic of fast and reversible electron transfer kinetics. The diamond hybrid OTE exhibits a peak separation of 100 to 170 mV depending on the analyte concentration (Figures 5(a)–5(c)), much

smaller than the value reported for free-standing diamond OTE of 0.38 mm thickness in 1 mM $\text{Fe}(\text{CN})_6^{4-}$ [7], and comparable to the value for diamond/quartz OTEs in 0.1 mM ferrocene and CPZ [8, 9]. The peak separation of diamond hybrid OTE increases, as shown in Figure 5(c), and the curve tends to converge to 77 mV at close to zero analyte concentration which is close to the typical value for Nernstian systems, demonstrating the quasireversible behaviour of our OTEs. The linear relationship between peak separation and analyte concentration also suggests that the uncompensated resistance is responsible for the relative large peak separation instead of sluggish electron transfer kinetics. Besides resistances from solution and electrical contacts, the

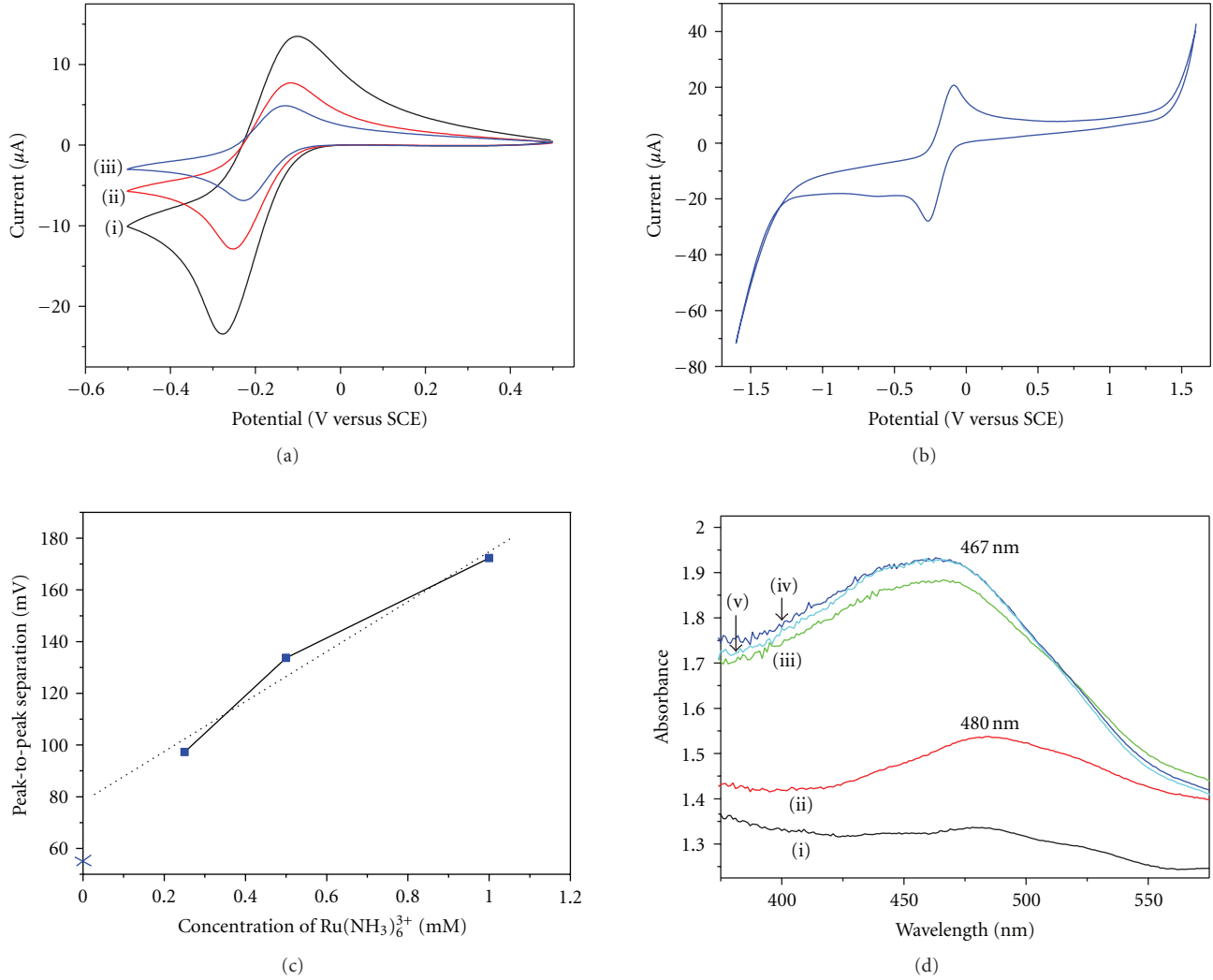


FIGURE 5: (a) Background corrected cyclic voltammograms of diamond hybrid OTE in $\text{Ru}(\text{NH}_3)_6^{3+}$ of different concentrations in 0.1 M acetate buffer: (i) 1000 μM , (ii) 500 μM , and (iii) 250 μM , with scan rate of 50 mV/s. (b) The cyclic voltammogram of diamond hybrid OTE in 1 mM $\text{Ru}(\text{NH}_3)_6^{3+}$ in 0.1 M acetate buffer, scan rate 50 mV/s, showing a wide potential window from -1.35 to 1.5 V. (c) The peak-to-peak separation in voltammograms with differing $\text{Ru}(\text{NH}_3)_6^{3+}$ concentrations for diamond hybrid OTE, with scan rate 50 mV/s. The ideal Nernstian system exhibits a peak separation of 59.2 mV which is marked as a crossing in the Y-axis. (d) UV-Vis spectroscopy of 1 mM 4-aminophenol in 0.1 M acetate buffer of pH 4.6 with a BDD OTE at differing applied potentials: (i) 0.1 V, (ii) 0.12 V, (iii) 0.14 V, (iv) 0.16 V, and (v) 0.18 V.

electrical contact between diamond membrane, and ITO film is probably the major source of uncompensated resistance which could be improved further by more careful assembly.

The oxidation of 4-Aminophenol to semiquinonimine was measured between 374 nm and 579 nm to demonstrate the spectroelectrochemical application of this diamond hybrid OTE, as depicted in Figure 5(d). The potential was stepped from 0.10 to 0.18 V in increments of 0.02 V, and the spectrum was collected after equilibrium for 60 s at each potential. As the potential stepped positive, the peak at around 460 to 480 nm, a characteristic peak of semiquinonimine [25], increases sharply until reaching saturation at 0.16 V. The spectra suggest a quantitative conversion of 4-Aminophenol at this potential, in good agreement with the potential reported in the literature [26, 27].

4. Conclusions

A novel approach to fabricate diamond OTE is explored by combining the outstanding electrochemical properties of diamond and the electrical conductivity and optical transparency of metal oxide films. Conductive diamond was deposited directly on ITO and AZO film. XPS spectra after diamond growth reveal a reduction of the oxides to elemental metals by the hydrogen plasma and a fast evaporation of the metals due to elevated temperature during diamond growth. Although AZO film is reported to have the highest resistance to thermal decomposition and hydrogen plasma, it still cannot survive in the harsh conditions of diamond growth.

An alternative approach was explored to circumvent the degradation of metal oxide by preparing free-standing

diamond membrane from diamond film on silicon wafer followed by selective chemical etching of silicon substrate, and integrating the membrane with an ITO substrate. AFM measurement shows a smooth surface with small diamond grain of 50 to 100 nm, and Raman spectroscopy confirms the diamond phase purity and the presence of nanodiamond. The resulting OTE device exhibits competitive optical transparency and electrochemical properties compared with the value reported previously. The diamond membrane—ITO device shows well-defined redox peaks with a narrow peak separation in cyclic voltammograms, suggesting a quasireversible electrochemical kinetics. The spectroelectrochemical application of this hybrid device in the oxidation of 4-Aminophenol was demonstrated, and the results agree with previous studies.

Acknowledgments

The authors would like to acknowledge the financial support from EPSRC with Grant no. EP/D504813/1. J. Hu acknowledges the financial support of Newton Abraham studentship.

References

- [1] W. Kaim and A. Klein, *Spectroelectrochemistry*, RSC Publishing, Cambridge, UK, 2008.
- [2] B. S. Pons, J. S. Mattson, L. O. Winstrom, and H. B. Mark, "Application of deposited thin metal films as optically transparent electrodes for internal reflection spectrometric observation of electrode solution interfaces," *Analytical Chemistry*, vol. 39, no. 6, pp. 685–688, 1967.
- [3] A. Yildiz, P. T. Kissinger, and C. N. Reilley, "Evaluation of an improved thin-layer electrode," *Analytical Chemistry*, vol. 40, no. 7, pp. 1018–1028, 1968.
- [4] H. B. Mark and B. S. Pons, "An in situ spectrophotometric method for observing the infrared spectra of species at the electrode surface during electrolysis," *Analytical Chemistry*, vol. 38, no. 1, pp. 119–121, 1966.
- [5] R. W. Murray, W. R. Heineman, and G. W. O'Dom, "An optically transparent thin layer electrochemical cell," *Analytical Chemistry*, vol. 39, no. 13, pp. 1666–1668, 1967.
- [6] R. G. Compton, J. S. Foord, and F. Marken, "Electroanalysis at diamond-like and doped-diamond electrodes," *Electroanalysis*, vol. 15, no. 17, pp. 1349–1363, 2003.
- [7] J. K. Zak, J. E. Butler, and G. M. Swain, "Diamond optically transparent electrodes: demonstration of concept with ferri/ferrocyanide and methyl viologen," *Analytical Chemistry*, vol. 73, no. 5, pp. 908–914, 2001.
- [8] S. Haymond, J. K. Zak, Y. Show, J. E. Butler, G. T. Babcock, and G. M. Swain, "Spectroelectrochemical responsiveness of a freestanding, boron-doped diamond, optically transparent electrode toward ferrocene," *Analytica Chimica Acta*, vol. 500, no. 1-2, pp. 137–144, 2003.
- [9] J. Stotter, J. Zak, Z. Behler, Y. Show, and G. M. Swain, "Optical and electrochemical properties of optically transparent, boron-doped diamond thin films deposited on quartz," *Analytical Chemistry*, vol. 74, no. 23, pp. 5924–5930, 2002.
- [10] Y. R. Zhang, Y. Kato, S. Yoshihara, and T. Watanabe, "A novel boron-doped diamond (BDD)-coated platinum mesh electrode for spectroelectrochemistry," *Journal of Electroanalytical Chemistry*, vol. 603, no. 1, pp. 135–141, 2007.
- [11] G. Haacke, "New figure of merit for transparent conductors," *Journal of Applied Physics*, vol. 47, no. 9, pp. 4086–4089, 1976.
- [12] F. Zhu, C. H. A. Huan, K. Zhang, and A. T. S. Wee, "Investigation of annealing effects on indium tin oxide thin films by electron energy loss spectroscopy," *Thin Solid Films*, vol. 359, no. 2, pp. 244–250, 2000.
- [13] M. J. Alam and D. C. Cameron, "Preparation and properties of transparent conductive aluminum-doped zinc oxide thin films by sol-gel process," *Journal of Vacuum Science and Technology a-Vacuum Surfaces and Films*, vol. 19, no. 4, pp. 1642–1646, 2001.
- [14] G. K. Paul and S. K. Sen, "Sol-gel preparation, characterization and studies on electrical and thermoelectrical properties of gallium doped zinc oxide films," *Materials Letters*, vol. 57, no. 3, pp. 742–746, 2002.
- [15] Y. Avigal and A. Hoffman, "A new method for nucleation enhancement of diamond," *Diamond and Related Materials*, vol. 8, no. 2–5, pp. 127–131, 1999.
- [16] L. Raniero, A. Gonçalves, A. Pimentel et al., "Influence of hydrogen plasma on electrical and optical properties of transparent conductive oxides," in *Proceedings of the Materials Research Society Symposium*, vol. 862, p. A21.10, April 2005.
- [17] S. Major, S. Kumar, M. Bhatnagar, and K. L. Chopra, "Effect of hydrogen plasma treatment on transparent conducting oxides," *Applied Physics Letters*, vol. 49, no. 7, pp. 394–396, 1986.
- [18] B. M. Ataev, A. M. Bagamadova, V. V. Mamedov, and A. K. Omaev, "Thermally stable, highly conductive, and transparent ZnO layers prepared in situ by chemical vapor deposition," *Materials Science and Engineering B*, vol. 65, no. 3, pp. 159–163, 1999.
- [19] R. G. Gordon, "Criteria for choosing transparent conductors," *MRS Bulletin*, vol. 25, no. 8, pp. 52–57, 2000.
- [20] J. Cho, KI. H. Yoon, M. S. Oh, and W. K. Choi, "Effects of H annealing treatment on photoluminescence and structure of ZnO:Al/AlO grown by radio-frequency magnetron sputtering," *Journal of the Electrochemical Society*, vol. 150, no. 10, pp. H225–H228, 2003.
- [21] J. Mass, P. Bhattacharya, and R. S. Katiyar, "Effect of high substrate temperature on Al-doped ZnO thin films grown by pulsed laser deposition," *Materials Science and Engineering B*, vol. 103, no. 1, pp. 9–15, 2003.
- [22] R. P. Eischens, W. A. Pliskin, and M. J. D. Low, "The infrared spectrum of hydrogen chemisorbed on zinc oxide," *Journal of Catalysis*, vol. 1, no. 2, pp. 180–191, 1962.
- [23] N. Wada, P. J. Gaczi, and S. A. Solin, "'Diamond-like' 3-fold coordinated amorphous carbon," *Journal of Non-Crystalline Solids*, vol. 35–36, no. 1, pp. 543–548, 1980.
- [24] S. Michaelson, R. Akhvlediani, and A. Hoffman, "Preparation and properties of sub-micron thick and free-standing diamond membranes," *Diamond and Related Materials*, vol. 11, no. 3–6, pp. 721–725, 2002.
- [25] J. Schwarz, W. Oelfner, H. Kaden, F. Schumer, and H. Hennig, "Voltammetric and spectroelectrochemical studies on 4-aminophenol at gold electrodes in aqueous and organic media," *Electrochimica Acta*, vol. 48, no. 17, pp. 2479–2486, 2003.
- [26] M. Goto, M. Kato, and D. Ishii, "Semidifferential electroanalysis with a solid working electrode," *Analytica Chimica Acta*, vol. 126, no. C, pp. 95–104, 1981.
- [27] M. Jamal, A. S. Sarac, and E. Magner, "Conductive copolymer-modified carbon fibre microelectrodes: electrode characterisation and electrochemical detection of p-aminophenol," *Sensors and Actuators B*, vol. 97, no. 1, pp. 59–66, 2004.